

The design and synthesis of potential acetylcholinesterase inhibitors and NMDA antagonists as neuroprotective agents

Sussan-Mari Botha

13032047

Submitted in partial fulfilment of the requirements for the degree

Master of Science

In the faculty of Natural & Agricultural Sciences

University of Pretoria

Pretoria

2020

Supervised by

Prof. D.L. Riley and Dr. J-L. Panayides

Declaration

I, Sussan-Mari Botha, declare that this dissertation, which I hereby submit for the degree of Master of Science at the University of Pretoria, is my own work and has not been previously submitted by me for a degree at this or any other tertiary institution.

Sussan-Mari Botha

Sussan-Mari Botha

1 February 2021

“Success is not final,

failure is not fatal:

It is the courage to continue that counts.”

-Winston Churchill

Financial Support

I am thankful and would like to give my sincerest gratitude to the National Research Foundation, my supervisor, Professor Darren Riley and the University of Pretoria for their financial assistance in enabling me to complete my master's degree in chemistry.

Acknowledgements

I would like to thank my supervisor, Professor Darren Riley, and my co-supervisor Dr Jenny-Lee Panayides for all their support and guidance throughout my master's degree.

I would like to thank my family, friends and colleagues for all their assistance, their time for lengthy discussions and most importantly their moral support these last few years.

Abstract

The envisaged project included the *in silico* assessment and synthesis of potential acetylcholinesterase inhibitors, structurally related to donepezil, and of *N*-methyl D-aspartate antagonists related to an active compound that was identified by the Liotta group. These inhibitors were hypothesised to act as neuroprotective agents targeting the symptomatic effects of Alzheimer's disease.

Three scaffolds were initially targeted. Scaffolds A and B, were based upon previous in-house work related to tricyclic thiazoles. These scaffolds would allow for the inhibition of acetyl cholinesterase at the catalytic anionic site (scaffold A), and at the catalytic anionic site and peripheral anionic site (scaffold B). The third, scaffold C, was envisaged to act as a potential dual neuroprotective agent inhibiting acetylcholinesterase and acting as an *N*-methyl D-aspartate antagonist.

Computational analysis for scaffolds A to C made predictions for each scaffold's ligand molecular docking scores (mimicking the ligands docked into the active site of acetylcholinesterase and providing an output as a negative score). The more negative the better the affinity the ligands have for acetylcholinesterase. The most potent inhibitors (docking scores < -13.000) included fifteen ligands out of the fifty-seven ligands under study. Further assessment of CYP2C9 inhibition suggested that only one of the compounds would not be a CYP2C9 inhibitor.

A Qikprop analysis, predicting the drug-likeness of the ligands under study, was also conducted. All the ligands obeyed the molecular weight, QPlogBB, number of H-donor or H-acceptor ranges for orally available drugs. However, all the ligands disobeyed the QPlogHERG rule which indicates that there is a significant difference in the dose response between acetylcholinesterase and hERG inhibition. Three ligands disobeyed the QPlogPo/w rule, while the total polar surface area rule was only broken by a single ligand. As a result, the potential drug-like molecules found in scaffolds A to C was limited to twelve ligands. Finally, SwissADME bioavailability analysis was also performed predicting that seventeen of the studied ligands would be bioavailable. Comparing both SwissADME and the Schrodinger analysis for drug-likeness a total of six ligands were identified for synthesis.

Ultimately, four ligands were targeted for synthesis, however, due to synthetic challenges these could not be accessed and a fourth, scaffold D, based upon an isoxazole core was identified. Scaffold D underwent a lower intensity computational analysis which included molecular docking, Qikprop analysis and CYP2C9 inhibition of fifty ligands which included twenty five α,β -unsaturated ketones and their respective cyclised

isoxazole forms. The *in silico* analysis identified four ligands that were considered as drug-like with a docking score within 1 log unit of donepezil. The Qikprop analysis indicated that all the ligands obeyed the molecular weight, QPlogPo/w, QPlogBB, H-donor, H-acceptor and total polar surface area rules for drug-likeness and only four ligands did not violate the QPlogHERG rule. The CYP2C9 inhibition study suggested that relative to donepezil, none of the ligands should cause adverse drug reactions.

Several cyclic and acyclic ketones were reacted with aldehydes affording a range of α,β -unsaturated ketones. A total of fourteen ligands were successfully synthesised in modest to good yields, however, we were unsuccessful in converting these to their related isoxazoles.

Biological activity studies between the successfully synthesised α,β -unsaturated ketones and acetylcholinesterase will be conducted in the future using the appropriate acetylcholinesterase electric eel enzyme in an enzymatic assay. This analysis will determine the inhibitory concentration of 50 % of the ligand (IC_{50}). Cytotoxicity studies will also be conducted and compared to donepezil which has an IC_{50} value of $0.05 \pm 0.06 \mu\text{M}$. The ligands falling below those values could then be considered as lead compounds in future studies.

Abbreviations

AD	-	Alzheimer's Disease
FTD	-	Frontotemporal Dementia
CJD	-	Creutzfeldt-Jakob Disease
A β	-	Amyloid β
AChEI	-	Acetylcholinesterase inhibitors
PSEN1	-	Presenilin-1
CDR	-	Clinical Dementia Rating
CDR-SOB	-	Clinical Dementia Rating – Sum of Boxes
MMSE	-	Mini-Mental State Examination
MRI	-	magnetic resonance imaging
PET	-	Positron emission tomography
FDG	-	[18F]-2-fluoro-2-deoxy-D-glucose
HKs	-	hexokinases
RT.LAT	-	Right lateral
LT.LAT	-	left lateral
RT.MED	-	right medial
LT.MED	-	left medial
SUVR	-	standardized uptake value ratio
CoA)		coenzyme A
ATP		adenosine triphosphate
CNS	-	central nervous system
GABA	-	γ -aminobutyric acid

EAA	-	excitatory amino acid
mAChRs	-	muscarinic receptors
nAChRs	-	nicotinic receptors
APP	-	β -amyloid precursor protein
SP	-	senile plaques
LTP	-	long-term potentiation
EGCG	-	Epigallo-catechin-3-gallate
ARIA-E	-	amyloid-related imaging abnormalities-edema
ARIA-H	-	amyloid-related imaging abnormalities-haemosiderin
MTs	-	microtubules
GOF	-	gain of function
LOF	-	loss of function
PHF	-	paired helical filaments
SF	-	straight filaments
NFTs	-	neurofibrillary tangles
FAT	-	fast axonal transport
BBB	-	blood brain barrier
ThS	-	thioflavine S
UPS	-	ubiquitin-proteasome system
Hsp90	-	heat shock protein
GSK-3	-	Glycogen synthase kinase 3
NMDA	-	<i>N</i> -methyl D-aspartate
ACh	-	acetylcholine
AChT	-	choline acetyl transferase
AChE	-	acetylcholinesterase

MPO	-	myeloperoxidase
PD	-	Parkinson's disease
CQ	-	Clioquinol
DFOA	-	Desferrioxamine
ROS	-	reactive oxygen species
ALS	-	amyotrophic lateral sclerosis
RNS	-	reactive nitrogen species
MDA	-	malondialdehyde
4-HNE	-	4-hydroxynonenal
GLT-1	-	glutamate transporter
SOD	-	superoxide dismutase
GSHRd	-	glutathione reductase
GSHPx	-	glutathione peroxidase
IL-1 α	-	interleukin 1 alpha
IL-1 β	-	interleukin 1 beta
IL-6	-	interleukin 6
IL-8	-	Chemotactic factor interleukin 8
MIP-1 α	-	Macrophage inflammatory protein-1 α
TGF- β	-	Transforming growth factor
TNF- α	-	Tumour necrosis factor alpha
MAC	-	membrane attack complex
α 1-ACT	-	α 1-antichymotrypsin
IL-1Ra	-	IL-1 receptor antagonist
COX	-	Cyclooxygenase
NSAIDs	-	non-steroidal anti-inflammatory drugs

COX-2	-	cyclooxygenase-2
nb	-	nucleus basalis
ms	-	medial septal nucleus
AChR	-	acetylcholine receptor
BuChE	-	butyrylcholine esterase
PAS	-	peripheral anionic site
CAS	-	catalytic site
PBS	-	peripheral binding site
α 7-nAChR	-	α -7 nicotinic acetylcholine receptor
AMPA	-	α -amino-3-hydroxy-5-methyl-4- isoxazolepropionic acid
AP-5	-	2-amino-5-phosphonovaleric acid
DQP	-	dihydroquinolone pyrazoline

Index

Declaration.....	i
Financial Support	ii
Acknowledgements.....	ii
Abstract.....	iii
Abbreviations	v
List of graphs.....	I
List of figures.....	II
List of schemes.....	V
List of tables	VI
Chapter 1 Introduction to Dementia and Alzheimer’s disease	1
1.1. Introduction to Dementia	2
1.1.1. Different types of Dementia	2
1.2. Introduction to Alzheimer’s disease	3
1.2.1. Prevalence and description of Alzheimer’s disease.....	3
1.2.2. Discovery of Alzheimer’s disease	4
1.3. Detection of Alzheimer’s disease.....	5
1.3.1. Clinical Dementia Rating – Sum of Boxes.....	5
1.3.2. Mini-Mental State Examination	6
1.3.3. Wechsler Memory Scale-Revised (Logical memory).....	6
1.3.4. Volumetric magnetic resonance imaging	6
1.3.5. Positron emission tomography	7
1.3.5.1. Fluorodeoxyglucose positron emission tomography	7
1.3.5.2. Pittsburg compound B.....	8
1.3.6. Biochemical analysis.....	10
1.4. The pathogenesis of the Alzheimer’s disease hypotheses	10
1.4.1. Amyloid cascade hypothesis	12
1.4.2. Hyperphosphorylated Tau protein.....	15

1.4.3. Cholinergic hypothesis	18
1.4.4. Metal ion hypothesis.....	19
1.4.5. Oxidative stress hypothesis.....	22
1.4.6. Inflammatory hypothesis	23
1.4.7. N-methyl D-aspartate hypothesis	26
Chapter 2 Cholinergic and N-methyl D-aspartate hypothesis	27
2.1. Cholinergic hypothesis	28
2.1.1. What is the cholinergic hypothesis?	28
2.1.2. Cholinergic cycle.....	29
2.1.3. Acetylcholine esterase	31
2.1.4. Attempts to target acetylcholine breakdown - acetylcholinesterase inhibitors	35
2.1.5. Examples of acetylcholinesterase inhibition – FDA approved drugs.....	36
2.1.6. Structural modification of Donepezil and related derivatives	37
2.1.6.1. Acetylcholinesterase inhibitions currently under trials	40
2.1.6.2. In-house development of acetylcholinesterase inhibitors in the Riley group	41
2.2. N-methyl D-aspartate hypothesis.....	45
2.3. Project background, aims and objectives	49
2.3.1. Potential acetyl cholinesterase inhibitors.....	49
2.3.1.1. Introduction.....	49
2.3.1.2. Aim one: <i>In silico</i> screening of scaffolds A, B and C	51
2.3.1.3. Aim two: Synthesis of scaffolds A, B and C.....	51
2.3.1.4. Aim three: <i>In vitro</i> activity assessment against acetyl cholinesterase.....	53
2.3.2. Potential N-methyl D-aspartate antagonists	54
2.3.2.1. Introduction.....	54
2.3.2.2. Aim one: <i>In vitro</i> activity assessment against NMDA.....	55
Chapter 3 Computational Analysis - Schrödinger and SwissADME	56
3.1. Introduction to docking analysis.....	57
3.2. Molecular docking.....	57
3.2.1. Introduction.....	57
3.2.2. Planned scaffolds	62
3.2.3. Molecular docking results and discussion.....	69
3.3. Qikprop analysis, results, and discussion	76

3.4. Pharmacophore model	83
3.5. SwissADME analysis	89
3.6. Cytochrome P450 isozyme CYP2C9 inhibition	96
3.6.1. Introduction.....	96
3.6.2. Results and discussion of CYP2C9 analysis.....	100
3.7. Conclusion.....	114
Chapter 4 Synthetic analysis and discussion of acetylcholinesterase inhibitors	116
4.1. Introduction	117
4.2. Attempted synthesis of scaffolds A and B	117
4.2.1. Preparation of diketoester (79).....	120
4.2.2. Attempted synthesis of ethyl 4 <i>H</i> -indeno[1,2- <i>c</i>]isoxazole-3-carboxylate (80).....	123
4.3. Scaffold C.....	126
4.3.1. Scaffold C1.....	127
4.3.1.1. Preparation of ethyl (2-aminophenyl)(pyridin-2-yl)methanone (87).....	128
4.3.1.2. Preparation of <i>N</i> -(2-picolinoylphenyl)acetamide (88)	130
4.3.1.3. Attempted synthesis of 2-(2-acetamidobenzoyl)-1-benzylpyridin-1-ium (89)	130
4.3.1.4. Benzylation of simplified pyridine rings	131
4.3.2. Scaffold C2.....	132
4.3.2.1. Preparation of ethyl 1-benzylpiperidine-3-carboxylate (104).....	132
4.3.2.2. Attempted synthesis of 1-benzyl- <i>N</i> -methoxy- <i>N</i> -methylpiperidine-3-carboxamide (105).....	133
4.3.2.3. Alternative Weinreb amide formation attempts	135
4.3.3. Scaffold C3.....	136
4.3.3.1. Attempted synthesis of 3-(pyridin-2-yl)-1 <i>H</i> -indazole (115)	137
4.3.3.2. Alternative attempted synthesis of 3-(pyridin-2-yl)-1 <i>H</i> -indazole (115).....	139
4.3.4. Scaffold C4.....	141
4.3.4.1. Synthesis of (2-aminophenyl)(pyridin-3-yl)methanone (117).....	141
4.3.5. Scaffold C5.....	143
4.3.5.1. Synthesis of compounds C5.1 - C5.13	143
4.4. Conclusion.....	145
Chapter 5 Computational Results - Schrödinger	146
5.1. Introduction	147
5.2. Molecular docking results and discussion	148

5.2.1 Molecular docking of α,β -unsaturated ketone scaffolds K_A_	155
5.2.2 Molecular docking of isoxazole scaffolds C.K_A_	156
5.3. Qikprop analysis, results, and discussion	162
5.4. Cytochrome P450 isozyme CYP2C9 inhibition	163
5.5. Conclusion	164
Chapter 6 Synthetic analysis and discussion of α,β -unsaturated compounds	165
6.1. Introduction	166
6.2. Scaffold D	166
6.3. Preparation of α,β -unsaturated compounds – method 1	167
6.3.1. (<i>E</i>)-3-(3-hydroxy-4-methoxyphenyl)-1-phenylprop-2-en-1-one (K4A5)	168
6.3.2. Unsuccessful reactions	168
6.4. Preparation of α,β -unsaturated compounds - method 2	169
6.4.1. (<i>E</i>)-3-(4-methoxyphenyl)-1-(naphthalen-2-yl)prop-2-en-1-one (K3A4)	169
6.4.2. Unsuccessful reactions	170
6.5. Synthesis of <i>N</i> -hydroxy-4-methylbenzenesulfonamide (131)	170
6.6. General procedure for the attempted formation of isoxazole ring systems from α,β -unsaturated ketones	171
6.7. Conclusion	172
Chapter 7 Conclusion and Future work	174
7.1. Conclusion	175
7.2. Future work	177
Chapter 8 Experimental	179
8.1. General experimental details	180
8.1.1. Purification of solvents	180
8.1.2. Experimental techniques and equipment used	180
8.1.3. Chromatographic separation	180
8.1.4. Spectroscopic and physical data	180
8.1.5. Nomenclature and numbering of compounds	181
8.2. Experimental details relating to scaffold A and B	181
8.2.1. Ethyl (<i>Z</i>)-2-hydroxy-2-(1-oxo-1,3-dihydro-2 <i>H</i> -inden-2-ylidene)acetate (79)	181
8.2.2. Ethyl 4 <i>H</i> -indeno[1,2- <i>c</i>]isoxazole-3-carboxylate (80)	182
8.2.2.1. General method 1:	182
8.2.2.2. General method 2:	182

8.2.3 Ethyl (<i>Z</i>)-2-(5,6-dimethoxy-1-oxo-1,3-dihydro-2 <i>H</i> -inden-2-ylidene)-2-hydroxyacetate (96)	183
8.2.4. Ethyl (<i>Z</i>)-2-hydroxy-2-(1-oxo-3,4-dihydronaphthalen-2(1 <i>H</i>)-ylidene)acetate (97)	183
8.2.5. Ethyl 6,7-dimethoxy-4 <i>H</i> -indeno[1,2- <i>c</i>]isoxazole-3-carboxylate (98)	184
8.2.5.1. General method 1:	184
8.2.5.2. General method 2:	184
8.3. Experimental details relating to scaffold C	186
8.3.1. (2-aminophenyl)(pyridin-2-yl)methanone (87)	186
8.3.2. <i>N</i> -(2-picolinoylphenyl)acetamide (88)	187
8.3.3. 2-(2-acetamidobenzoyl)-1-benzylpyridin-1-ium (89)	188
8.3.4. 1-benzylpyridin-1-ium (100)	189
8.3.5. 1-benzyl-2-bromopyridin-1-ium (102)	189
8.3.6. Ethyl 1-benzylpiperidine-3-carboxylate (104)	189
8.3.7. 1-benzyl- <i>N</i> -methoxy- <i>N</i> -methylpiperidine-3-carboxamide (105)	190
8.3.8. <i>N</i> -methoxy- <i>N</i> -methylpiperidine-3-carboxamide (112)	191
8.3.9. 3-(pyridin-2-yl)-1 <i>H</i> -indazole (115)	192
8.3.10. (2-aminophenyl)(pyridin-3-yl)methanone (117)	194
8.3.11. 2-methyl- <i>N</i> -(2-picolinoylphenyl)butanamide (C5.1)	196
8.3.12. 4-hydroxy- <i>N</i> -(2-picolinoylphenyl)benzamide (C5.2)	197
8.3.13. 4-nitro- <i>N</i> -(2-picolinoylphenyl)benzamide (C5.3)	197
8.3.14. 2-bromo-5-methyl- <i>N</i> -(2-picolinoylphenyl)benzamide (C5.4)	198
8.3.15. 2-fluoro- <i>N</i> -(2-picolinoylphenyl)benzamide (C5.5)	198
8.3.16. 4-fluoro- <i>N</i> -(2-picolinoylphenyl)benzamide (C5.6)	198
8.3.17. 3-fluoro- <i>N</i> -(2-picolinoylphenyl)benzamide (C5.7)	199
8.3.18. 2-iodo- <i>N</i> -(2-picolinoylphenyl)benzamide (C5.8)	199
8.3.19. <i>N</i> -(2-picolinoylphenyl)benzamide (C5.9)	200
8.3.20. 3,5-dinitro- <i>N</i> -(2-picolinoylphenyl)benzamide (C5.10)	200
8.3.21. <i>N</i> -(2-picolinoylphenyl)hexanamide (C5.11)	200
8.3.22. 6-bromo- <i>N</i> -(2-picolinoylphenyl)hexanamide (C5.12)	201
8.4. Experimental details relating to scaffold D	201
8.4.1. General procedure for the formation of α,β -unsaturated ketones with method 1:	201
8.4.1.1. (<i>E</i>)-3-(3-hydroxy-4-methoxyphenyl)-1-phenylprop-2-en-1-one (K4A5)	202
8.4.1.2. (<i>E</i>)-5,6-dimethoxy-2-(3-methoxybenzylidene)-2,3-dihydro-1 <i>H</i> -inden-1-one (K7A3)	202

8.4.1.3. (<i>E</i>)-5,6-dimethoxy-2-(4-methoxybenzylidene)-2,3-dihydro-1 <i>H</i> -inden-1-one (K7A4)	203
8.4.1.4. (<i>E</i>)-2-(3-hydroxy-4-methoxybenzylidene)-5,6-dimethoxy-2,3-dihydro-1 <i>H</i> -inden-1-one (K7A5)	203
8.4.1.5. (<i>E</i>)-2-(benzo[<i>d</i>][1,3]dioxol-5-ylmethylene)-5,6-dimethoxy-2,3-dihydro-1 <i>H</i> -inden-1-one (K7A8)	204
8.4.1.6. (<i>E</i>)-2-(3-methoxybenzylidene)-3,4-dihydronaphthalen-1(2 <i>H</i>)-one (K8A3)	204
8.4.1.7. (<i>E</i>)-2-(4-methoxybenzylidene)-3,4-dihydronaphthalen-1(2 <i>H</i>)-one (K8A4)	205
8.4.1.8. (<i>E</i>)-2-(3-hydroxy-4-methoxybenzylidene)-3,4-dihydronaphthalen-1(2 <i>H</i>)-one (K8A5)	205
8.4.1.9. (<i>E</i>)-2-(4-chlorobenzylidene)-3,4-dihydronaphthalen-1(2 <i>H</i>)-one (K8A7)	206
8.4.1.10. (<i>E</i>)-2-(benzo[<i>d</i>][1,3]dioxol-5-ylmethylene)-3,4-dihydronaphthalen-1(2 <i>H</i>)-one (K8A8)	206
8.4.1.11. Unsuccessful reactions using method 1:	207
8.4.2. General procedure for the formation of α,β -unsaturated ketones with method 2:	207
8.4.2.1. (<i>E</i>)-3-(4-methoxyphenyl)-1-(naphthalen-2-yl)prop-2-en-1-one (K3A4)	207
8.4.2.2. (<i>E</i>)-3-(benzo[<i>d</i>][1,3]dioxol-5-yl)-1-(naphthalen-2-yl)prop-2-en-1-one (K3A8)	208
8.4.2.3. (<i>E</i>)-3-(benzo[<i>d</i>][1,3]dioxol-5-yl)-1-phenylprop-2-en-1-one (K4A8)	208
8.4.2.4. (<i>E</i>)-2-(4-chlorobenzylidene)-5,6-dimethoxy-2,3-dihydro-1 <i>H</i> -inden-1-one (K7A7)	209
8.4.2.5. Unsuccessful reactions with Method 2:	210
8.4.3. Synthesis of <i>N</i> -hydroxy-4-methylbenzenesulfonamide (131)	210
8.4.4. General procedure for the attempted formation of isoxazole ring systems from α,β -unsaturated ketones	211
8.4.4.1. 3-(benzo[<i>d</i>][1,3]dioxol-5-yl)-4,5-dihydronaphtho[2,1- <i>d</i>]isoxazole (C.K8A8)	211
8.4.4.2. C.K7A8 3-(benzo[<i>d</i>][1,3]dioxol-5-yl)-6,7-dimethoxy-4 <i>H</i> -indeno[2,1- <i>d</i>]isoxazole	212
8.4.4.3. C.K4A5 2-methoxy-5-(5-phenylisoxazol-3-yl)phenol	213
8.5. Experimental details relating to other	213
8.5.1. (1-benzylaziridin-2-yl)methanol	213
8.5.2. Ethyl 2,4-dibromobutanoate	214
8.5.3. Ethyl 1-benzylazetidine-2-carboxylate	214
8.5.4. Ethyl 1-benzylpiperidine-2-carboxylate	215
8.5.5. (1-benzylpiperidin-2-yl)methanol	215
Chapter 9 Experimental Spectrums	217
9.1. Experimental details relating to scaffold A and B	218
9.1.1. Ethyl (<i>Z</i>)-2-hydroxy-2-(1-oxo-1,3-dihydro-2 <i>H</i> -inden-2-ylidene)acetate (79)	218
9.1.2. Ethyl (<i>Z</i>)-2-(5,6-dimethoxy-1-oxo-1,3-dihydro-2 <i>H</i> -inden-2-ylidene)-2-hydroxyacetate (96)	220

9.1.3. Ethyl (Z)-2-hydroxy-2-(1-oxo-3,4-dihydronaphthalen-2(1H)-ylidene)acetate (97)	222
9.2. Experimental details relating to scaffold C	223
9.2.1. (2-aminophenyl)(pyridin-2-yl)methanone (87).....	223
9.2.2. N-(2-picolinoylphenyl)acetamide (88)	225
9.2.3. Ethyl 1-benzylpiperidine-3-carboxylate (104).....	227
9.2.4. (2-aminophenyl)(pyridin-3-yl)methanone (117).....	229
9.2.5. 2-methyl-N-(2-picolinoylphenyl)butanamide (C5.1).....	231
9.3. Experimental details relating to scaffold D.....	232
9.3.1. (E)-3-(3-hydroxy-4-methoxyphenyl)-1-phenylprop-2-en-1-one (K4A5)	232
9.3.2. (E)-5,6-dimethoxy-2-(3-methoxybenzylidene)-2,3-dihydro-1H-inden-1-one (K7A3)	235
9.3.3. (E)-5,6-dimethoxy-2-(4-methoxybenzylidene)-2,3-dihydro-1H-inden-1-one (K7A4).....	238
9.3.4. (E)-2-(3-hydroxy-4-methoxybenzylidene)-5,6-dimethoxy-2,3-dihydro-1H-inden-1-one (K7A5)	241
9.3.5. (E)-2-(benzo[d][1,3]dioxol-5-ylmethylene)-5,6-dimethoxy-2,3-dihydro-1H-inden-1-one (K7A8) ..	244
9.3.6. (E)-2-(3-methoxybenzylidene)-3,4-dihydronaphthalen-1(2H)-one (K8A3)	247
9.3.7. (E)-2-(4-methoxybenzylidene)-3,4-dihydronaphthalen-1(2H)-one (K8A4)	250
9.3.8. (E)-2-(3-hydroxy-4-methoxybenzylidene)-3,4-dihydronaphthalen-1(2H)-one (K8A5).....	253
9.3.9. (E)-2-(4-chlorobenzylidene)-3,4-dihydronaphthalen-1(2H)-one (K8A7)	256
9.3.10. (E)-2-(benzo[d][1,3]dioxol-5-ylmethylene)-3,4-dihydronaphthalen-1(2H)-one (K8A8).....	259
9.3.11. (E)-3-(4-methoxyphenyl)-1-(naphthalen-2-yl)prop-2-en-1-one (K3A4)	262
9.3.12. (E)-3-(benzo[d][1,3]dioxol-5-yl)-1-(naphthalen-2-yl)prop-2-en-1-one (K3A8)	265
9.3.13. (E)-3-(benzo[d][1,3]dioxol-5-yl)-1-phenylprop-2-en-1-one (K4A8)	268
9.3.14. (E)-2-(4-chlorobenzylidene)-5,6-dimethoxy-2,3-dihydro-1H-inden-1-one (K7A7).....	271
9.3.15. TsNHOH: Synthesis of N-hydroxy-4-methylbenzenesulfonamide (131).....	274
9.4. Experimental details relating to other	277
9.4.1. (1-benzylaziridin-2-yl)methanol	277
9.4.2. Ethyl 1-benzylpiperidine-2-carboxylate	278
9.4.3. (1-benzylpiperidin-2-yl)methanol	280
Chapter 10 Appendix I – SwissADME data scaffolds A, B and C	282
Chapter 11 References.....	313

List of graphs

<i>Graph 1.1: A, B and C indicates the clinical and neurological impairments around the estimated year of symptomatic onset between carriers (orange) and non-carriers (blue) in the study done by Bateman and colleagues [15].</i>	6
<i>Graph 1.2: Change in the hippocampal volume and glucose metabolic levels around the estimated year of symptomatic onset between carriers (orange) and non-carriers (blue) in the study done by Bateman and colleagues [15].</i>	7
<i>Graph 1.3: Change in glucose metabolism around the estimated year of symptomatic onset of carriers (orange) and non-carriers (blue) in the study done by Bateman and colleagues [15].</i>	8
<i>Graph 1.4: Aβ deposits in the Precuneus around the estimated year of symptomatic onset between carriers (orange) and non-carriers (blue) in the study done by Bateman and colleagues [15].</i>	9
<i>Graph 1.5: A,B and C represents the CSF tau, CSF Aβ and plasma Aβ concentrations around the estimated year of symptomatic onset between carriers (orange) and non-carriers (blue) in the study done by Bateman and colleagues [15].</i>	10
<i>Graph 3.1: Docking score, QPlogPo/w and QPlogHERG of donepezil (25a – 25.d).</i>	78
<i>Graph 3.2: Total polar surface area of the ligands of scaffolds A-C5.</i>	82
<i>Graph 3.3: Comparison of the docking score and QPlogHERG values of the ligands for scaffolds A-C5.</i>	82
<i>Graph 3.4: CYP2C9 docking scores of scaffolds A, B, C1 and C2 compared to that of donepezil (25).</i>	101
<i>Graph 3.5: CYP2C9 docking scores of scaffolds C3, C4, and C5 compared to that of donepezil (25).</i>	101
<i>Graph 5.1: Docking score and Qikprop data, QPlogHERG and QPlogPo/w, for the α,β-unsaturated ketones forms of scaffold D.</i>	154
<i>Graph 5.2: Docking score and Qikprop data, QPlogHERG and QPlogPo/w, for the isoxazole forms of scaffold D.</i>	154
<i>Graph 5.3: Docking score and Qikprop data, QPlogHERG and QPlogPo/w, for the best ligands in the two data sets.</i>	160
<i>Graph 5.4: CYP2C9 docking scores for the α,β-unsaturated ketone and isoxazole forms of this data set.</i>	163

List of figures

Figure 1.1: Markers used for the detection of AD in the brain [21].	8
Figure 1.2: Cerebral metabolic reduction in confirmed AD patients. The statistical significance (Z-score) is color-coded, where red represents a more significant metabolic reduction. Sections of the brain are labelled as follows: Right lateral (RT.LAT) , left lateral (LT), right medial (RT.MED) and left medial (LT.MED). [21].	8
Figure 1.3: PIB-PET scans of A β deposition in Autosomal Dominant Alzheimer’s disease over twenty years before the onset of clinical symptoms – A indicates the difference in a carrier and non-carrier twenty years before the expected onset of symptoms. B indicates the difference in a carrier and non-carrier ten years before the expected onset of symptoms. C indicates the difference in carrier and non-carrier at the expected onset of symptoms. The SUVR indicates the binding of PIB to fibrillar A β , where high levels correlate to high SUVR (red) values, while low SUVR (blue) values indicate low levels of amyloid [14].	9
Figure 1.4: Visual differences between the brain of a healthy person and an AD patient – adapted from [28].	11
Figure 1.5: Normal neuron vs. AD neuron containing neurofibrillary tangles (tau hypothesis) and amyloid plaques (amyloid hypothesis) – adapted from [3].	13
Figure 1.6: Drugs synthesized for the treatment of AD with regards to the amyloid cascade [3].	14
Figure 1.7: Paclitaxel.	17
Figure 1. 8: Drugs used for the treatment of AD with regards to the tau hypothesis.	17
Figure 1.9: Illustration of the metallobiology of A β in AD – adapted from [50].	20
Figure 1. 10: Drugs used for the treatment of AD with regards to the metal ion hypothesis.	21
Figure 1.11: Drugs used for the treatment of AD with regards to the oxidative stress hypothesis.	23
Figure 1.12: Schematic representation of the inflammatory mechanism in AD – adapted from [58].	24
Figure 1.13: Drugs used for the treatment of AD with regards to the inflammatory hypothesis.	26
Figure 2.1: Choline transfer in the brain – adapted from [24].	28
Figure 2.2: ACh neurotransmission in the brain – adapted from [64].	30
Figure 2.3: Synthesis of ACh via ChAT and the breakdown of ACh via AChE – adapted from [29].	30
Figure 2.4: Schematic representation of the AChE active site – adapted from [24].	32
Figure 2.5: Torpedo AChE image illustrating the active site (yellow), anionic site (red) and PAS (green) – adapted from [64].	33
Figure 2.6: Torpedo AChE showing the PAS-associated omega loops. Omega loop 69-96, shown in green, including the two PAS residues Tyr 70 and Asp 72. Omega loop 274-308, shown in red, including the PAS residue Trp 279 – adapted from [64].	34
Figure 2. 7: FDA approved AChEIs (24-27).	36
Figure 2.8: Synthetic analysis of the development of the four parts of the indanone-piperidine derivative.	38
Figure 2.9: Four parts of 35 and compared to that of the four parts of donepezil (25).	38

Figure 2.10: Examples of donepezil derivatives as potential anti-Alzheimer's drugs.....	39
Figure 2.11: AChEI undergoing clinical trials.	40
Figure 2.12: Lead compound formed through the change of the donepezil scaffold part A (green) and B (red).	41
Figure 2.13: Linkers (A-green block) and R-groups (B-red block) involved in the synthesis of the different ligands to analyse the chemical space surrounding the donepezil scaffold.	42
Figure 2.14: Synthesis of different linkers and addition of the different R groups.	42
Figure 2.15: Improvement on previous lead compound (46) through changing part A and B.	43
Figure 2.16: Amide coupling reaction using the amine R-groups (70.1-70.15) which are attached to the final product (69).....	44
Figure 2.17: Lead compound (46) and its derivatives synthesized in the Riley group.	44
Figure 2.18: Schematic representation of an open NMDA receptor which is permeable to Ca^{2+} and blocked through memantine (73) and Mg^{2+} . – adapted from [63].	45
Figure 2.19: Schematic representation of long-term potentiation which involves the glutamate receptors AMPA and NMDA - adapted from [63].	46
Figure 2.20: The NMDA receptor antagonist, memantine (73).	47
Figure 2.21: Liotto group's lead compound (74) and its most potent derivative (75).	48
Figure 2.22: Comparison of donepezil (25), 76 and 77 to the targeted scaffolds A, B and C.	50
Figure 2.23: Comparison of the Dennis Liotta compound and the targeted scaffold C.....	55
Figure 3.1: Donepezil (25, purple ligand) docked into the active site of <i>Torpedo californica</i> AChE. -The 12 β - sheets (turquoise) are surrounded by 14 α -helices (red), the grey surface area represents the binding site. 59	
Figure 3.2: Donepezil (25, purple ligand) docked into the binding site (grey surface) of AChE.....	59
Figure 3.3: The 3D visual representation of donepezil (25) docked into the active site of AChE and the interactions involved. -Docking score of -14.470. Blue dashed lines indicate π - π stacking interactions, green dashed lines indicate π -cation interactions. The yellow dashed line indicates H-bonds.	60
Figure 3.4: The 2D visual representation of donepezil (25) docked into the active site of AChE and the interactions involved. -Docking score of -14.470. Green lines indicate π - π stacking interactions, red lines indicate π -cation interactions, and purple arrows indicate H-bonds with their arrow head indicating it as either being a H-acceptor or donor.....	61
Figure 3.5: Comparison of donepezil (25) and other compounds that led to scaffolds A and B backbone.	63
Figure 3.6: Scaffold C compared to the Dennis Liotta compound (93).	68
Figure 3.7: 3D representation of the interactions of C3.1.a with the active site of AChE with a docking score of -8.056. -Orange dashed lines indicate Van der Waals interactions.	75
Figure 3.8: Grey spheres represent the pharmacophore site hypothesis (APRR) with a tolerance of 2.00 Å around each site. -A1 indicates the acceptor atom (red sphere). P5 indicates the positive ionic atom (blue sphere). R7 and R9 indicates 2 aromatic ring pharmacophore sites (orange rings).	84
Figure 3.9: Active ligands A1.3.a (yellow), B1.1.a (green), and C1.3.a (turquoise) overlayed with the hypothesis APRR.....	84
Figure 3.10: Active ligands, C1.4.a (yellow), C1.4.b (green), C1.5.a (turquoise), C1.5.b (purple), and C1.6.a (pink) displayed with the hypothesis APRR.	85

Figure 3.11: Active ligands, C2.1.a (yellow), C2.4.a (green), C2.5.a (turquoise), and C2.6.a (purple) displayed with the hypothesis APRR.	86
Figure 3.12: Active ligands of donepezil 25.a (yellow) and 25.b (green) displayed with the hypothesis APRR.	87
Figure 3.13: Hypothesis generated from 25.a as reference ligand (H-25) with no excluded volumes shown. - Right-hand corner: Hypothesis APRR generated from scaffolds A, B, C and donepezil (25).	87
Figure 3.14: Inactive ligands with a partial match to hypothesis APRR, C3.1 (yellow), C3.2 (green), C4.2 (turquoise), C5.5 (purple), C5.9 (pink) and C5.10 (orange) displayed with the hypothesis APRR.	88
Figure 3.15: Ligands with no overlap with hypothesis APRR, C3.6 (yellow), C4.6 (green), C5.12 (turquoise), and C5.13 (purple).	89
Figure 3.16: Example of a data set generated by SwissADME for A1.1.	91
Figure 3.17: Boiled-egg plot for scaffold A compounds.	91
Figure 3.18: Bioavailability radar of the example molecule, A1.1.	92
Figure 3.19: Boiled egg diagram generated from SwissADME for scaffolds A-C5 in graphs A-F.	95
Figure 3.20: 3D X-ray crystallography of CYP2C9. - β -sheets (turquoise) and α -helices (red) arranged in a triangular protein. The heme group consisting of a porphyrin ring (green) and its central iron (Fe^{+3} , yellow sphere).	98
Figure 3.21: Donepezil (25, purple) docked into the active site of CYP2C9, allowing for the interaction with the heme domain.	99
Figure 3.22: Donepezil (25, purple) docked into the active site of CYP2C9 which interacts with the protein and the heme domain. -Green dashed lines indicate π -cation interactions. Blue dashed lines indicate π - π interactions. Yellow lines indicate hydrogen bonds. Purple lines indicate a salt bridge.	99
Figure 4.1: Comparison of donepezil (25) and other compounds that led to scaffold A and B backbone. ...	118
Figure 6.1: N-hydroxy-4-methylbenzenesulfonamide (TsNHOH; 131).	170
Figure 6.2: The α,β -unsaturated ketones targeted for use in the cyclisation reaction.	172
Figure 7.1: Alternative isoxazole formation.	177
Figure 7.2: Formation of β -lactams and γ -amino alcohols.	178

List of schemes

<i>Scheme 2.1: Proposed retrosynthesis of scaffold A.</i>	52
<i>Scheme 2.2: Retrosynthesis of scaffold B.</i>	52
<i>Scheme 2.3: Retrosynthesis of scaffold C.</i>	53
<i>Scheme 4.1: Synthesis of compounds A1.1 – A1.8.</i>	119
<i>Scheme 4.2: Synthesis of compounds B1.1 – B1.8.</i>	120
<i>Scheme 4.3: Mechanism for the synthesis of the isoxazole via the formation of an oxime intermediate under acidic conditions [91].</i>	124
<i>Scheme 4.4: Scaffold designed based on Liotta compound for scaffold C.</i>	127
<i>Scheme 4.5: Planned synthesis of scaffold C.</i>	128
<i>Scheme 4.6: The mechanism for the synthesis of 87 via the formation of an imine functional group [95, 96].</i>	129
<i>Scheme 4.7: Synthesis of 1-benzylpyridin-1-ium (100).</i>	131
<i>Scheme 4.8: Synthesis of 1-benzyl-2-bromopyridin-1-ium (102).</i>	131
<i>Scheme 4.9: Proposed retrosynthesis of scaffold C2.</i>	132
<i>Scheme 4.10: Reaction of an organometallic reactant with (a) and without (b) N,O-dimethylhydroxylamine hydrochloride.</i>	133
<i>Scheme 4.11: The mechanism for the synthesis of 106 via the formation of a Weinreb amide (105) [100, 101].</i>	134
<i>Scheme 4.12: Synthesis of N-methoxy-N-methylpiperidine-3-carboxamide (112).</i>	135
<i>Scheme 4.13: Synthesis of 1-benzyl-N-methoxy-N-methylpiperidine-3-carboxamide (114).</i>	136
<i>Scheme 4.14: Proposed retrosynthesis of scaffold C3.</i>	136
<i>Scheme 4.15: Mechanism of the forming of the nitrosonium ion [103].</i>	137
<i>Scheme 4.16: Mechanism for the synthesis of the 3-(pyridin-2-yl)-1H-indazole (115) via the formation of a diazonium salt through a Sandmeyer reaction [106].</i>	139
<i>Scheme 4.17: Mechanism for the synthesis of the isoxazole via the formation of a ketoxime intermediate in basic conditions [107].</i>	140
<i>Scheme 4.18: Proposed synthesis of scaffold C4.</i>	141
<i>Scheme 4.19: Proposed synthesis of scaffold C5.</i>	143
<i>Scheme 4.20: Mechanism for the adjusted Steglich-type esterification reaction [108].</i>	144
<i>Scheme 5.1: Planned synthesis of cyclised combinations of ketones and aldehydes (e.g., K3A3) for scaffold D.</i>	147
<i>Scheme 5.2: Mechanism for the planned synthesis of scaffold D [109].</i>	167
<i>Scheme 6.1: Mechanism of the cyclisation step involved in scaffold D [107, 112].</i>	171

List of tables

<i>Table 3.1: The 2D visual representation of donepezil (25b-25c) docked into the active site of AChE and the interactions involved. -Green lines indicate π-π stacking interactions, red lines indicate π-cation interactions, and purple arrows indicate H-bonds with their arrow head indicating it as either being a H-acceptor or donor.</i>	62
<i>Table 3.2: Docking score of donepezil (25) and scaffolds A – C5.</i>	64
<i>Table 3.3: Docking score and interactions of the best ten ligands across scaffold A-C.5.</i>	69
<i>Table 3.4: The π-π, π-cation and hydrogen interactions between the 10 best ligands and the amino acids involved (the distance of interactions measured in Å).</i>	72
<i>Table 3.5: Ligand descriptor values and their property values with their recommended limits.</i>	76
<i>Table 3.6: Docking score and Qikprop data of the conformations of the ligands in scaffolds A-C5.</i>	78
<i>Table 3.7: SwissADME parameter abbreviations.</i>	90
<i>Table 3.8: Permeability (BBB and GI) predictions, P-gp substrate, bioavailability parameter violations and CYP2C9 inhibitor predictions using SwissADME web tool. -All data can be seen in Appendix I under SwissADME data.</i>	93
<i>Table 3.9: The docking score, porphyrin interactions, amino acid and Van der Waal interactions involved between the good ligands and CYP2C9 causing different types of interactions.</i>	102
<i>Table 3.10: The docking score, porphyrin interactions, amino acid and Van der Waal interactions involved between the poor ligands and CYP2C9 causing different types of interactions.</i>	103
Table 3.11: <i>The overall SOM, Fe-accessibility and intrinsic reactivity of donepezil (25.a) and ligands of scaffolds A, B and C.</i>	105
<i>Table 4.1: Different reaction conditions for step (i) in both scaffold A and B.</i>	121
<i>Table 4.2: Illustrates the use of different starting materials for the Claisen reaction of scaffold A.</i>	122
<i>Table 4. 3: Different reaction conditions for step (i) in scaffold A and B when using excess acid.</i>	122
<i>Table 4.4: Reaction conditions for step (ii) in scaffold A for synthesising 80 and 98.</i>	125
<i>Table 4.5: Reaction conditions for step (ii) in scaffold C1. For the synthesis of 89.</i>	131
<i>Table 4.6: Different experimental conditions for the synthesis of 105.</i>	135
<i>Table 4.7: Different experimental conditions for the synthesis of 115.</i>	137
<i>Table 4.8: Alternative experimental conditions for the synthesis of 115.</i>	141
<i>Table 4.9: Different experimental conditions for the synthesis of 117.</i>	142
<i>Table 4.10: Carboxylic acid used in the Steglich-type esterification reaction.</i>	145
Table 5.1: <i>The ketones and aldehyde groups used in the synthesis of the α,β-unsaturated ketones of scaffold D.</i>	148
<i>Table 5.2: Docking score of α,β-unsaturated ketones (K_A_) and their isoxazole forms (C.K_A_) as part of scaffold D.</i>	149
<i>Table 5. 3: Docking score and Qikprop data of the conformations of the ligands in scaffold D.</i>	151

<i>Table 5.4: The π-π, π-cation and hydrogen interactions between the good and poor α,β-unsaturated ketones of scaffold D.</i>	<i>155</i>
<i>Table 5.5: The π-π, π-cation and hydrogen interactions between the good and poor isoxazole forms of scaffold D.</i>	<i>156</i>
<i>Table 5.6: Ligands where the α,β-unsaturated ketones had a higher docking score compared to their isoxazole forms.</i>	<i>158</i>
<i>Table 5.7: Docking score and interactions of the best 4 ligands in scaffold D.</i>	<i>162</i>
<i>Table 6.1: Crossed aldol condensation reaction using method 1 for the synthesis of K_A_.</i>	<i>168</i>
<i>Table 6.2: Crossed aldol condensation reaction using method 2 for the synthesis of K_A_.</i>	<i>169</i>

Chapter 1

Introduction to Dementia and Alzheimer's disease



1.1. Introduction to Dementia

Patients that struggle with at least two of the following: memory, communication and speech, focus and concentration, reasoning and judgment and visual perception have the syndrome called dementia. Dementia is difficult to diagnose due to the different forms of the diseases which often share common symptoms.

1.1.1. Different types of Dementia

1. Alzheimer's disease (AD) – Between 60 – 80 % of all the patients who have dementia are diagnosed with AD. It is a progressive degenerative disease of the brain and, in general, is characterized by nerve signals in the brain getting blocked by the accumulation of proteins and fibres (plaques and tangles). These blockages lead to the death of the nerve cells. Symptoms include confusion, mood swings and physical changes to the brain.
2. Vascular dementia – The amount of blood pumped to the brain is not sufficient, resulting in damaged or blocked blood vessels. These can cause mini-strokes or even brain bleeding. Symptoms are determined by the region of the brain affected.
3. Dementia with Lewy bodies – Clumps of alpha-synuclein proteins are deposited in the brain cortex. Symptoms can include loss of focus, insomnia, learning difficulties, hallucinations, slow and unbalanced movement and memory loss later in life.
4. Mixed dementia – A patient is diagnosed with mixed dementia when afflicted by several forms of dementia.
5. Frontotemporal Dementia (FTD) – Loss of nerve cells behind the forehead and ears. Symptoms include personality changes, behavioural changes and trouble with language. Writing and comprehension can also be affected.
6. Creutzfeldt-Jakob Disease (CJD) – A protein called a prion is folded into an abnormal shape and causes a cascade of prion formations. These prions damage brain cells and lead to rapid mental decline. Symptoms include mood swings, confusion, uncontrolled movement and trouble walking. The disease can be genetic or spread from cattle to people (mad cow disease).
7. Huntington's disease – It is a genetic mutation leading to uncontrolled upper body movements and affects the central part of the brain, which controls thought, action and emotion. Difficulty with depression is commonly noted in afflicted individuals.
8. Normal pressure hydrophalus – Spinal fluid gets built up inside the brain. Symptoms include slowed thought and decision-making capabilities, trouble concentrating, behavioural changes, loss of bladder control and difficulty walking [1].

1.2. Introduction to Alzheimer's disease

1.2.1. Prevalence and description of Alzheimer's disease

AD is the most common form of dementia. It is an irreversible, terminal and progressive neurodegenerative disease caused by a heterogeneous group of disorders of the human brain. The disorders include dysfunction of the amyloid β ($A\beta$) cascade, hyperphosphorylation of tau proteins, inflammation, the accumulation of toxic metals, oxidative stress and dysfunction of the central cholinergic activity in the brain. The disease influences the cognitive function (short- and long-term memory loss, loss in language skills, concentration and attention) and non-cognitive function (depression, agitation, personality changes, delusions and hallucinations) of patients. AD causes progressive memory loss and confusion, which eventually leads to the inability to communicate or take care of oneself [2-5]. There is no cure or effective treatment for the prevention or reversal of the progression of the disease [4]. The only FDA approved drugs on the market are used for the symptomatic relief of the disease [4].

Although AD is one of the senile diseases, there are cases where AD has manifested in presenile individuals who are younger than 70 years of age [6, 7]. The prevalence of AD increases with age, with only 10 % of AD cases occurring in individuals below 65 years of age; this then increases to 50 % by 85 years of age [8]. A definitive diagnosis of AD requires the identification of the histological changes caused by the disease. These include the abnormal accumulation of neurofibrillary tangles and senile plaques, primarily in the neocortex and hippocampus and although magnetic resonance screening can suggest these changes, a post-mortem examination is, unfortunately, the only way to obtain conclusive identification of the presence of these histological changes [7].

Healthy aging can also include signs of memory loss, impaired judgment, impaired language, inability to learn something new, or even reduced abstract thinking. Due to this relationship between healthy aging and AD, it is difficult to positively diagnose AD before it has already progressed to the severe stage. At this point, the most effective treatment involves the use of acetylcholinesterase inhibitors (AChEI) (see chapter 2) to manage the symptoms associated with the disease [6].

In the United States, AD is the 6th leading cause of death when considering all ages, and it is the 5th leading cause of death when considering individuals 65 and older. In 2019 there were nearly 5 million Americans that had developed AD. By the year 2050, the number of AD patients is expected to increase three-fold [4]. Currently, an estimated 46.8 million people are living with AD or other types of dementia and every 65 seconds, there is someone developing AD in America [4]. The increased prevalence of the disease is, in part,

linked to the fact that people are living longer as a result of better medical care and services [9].

1.2.2. Discovery of Alzheimer's disease

Alois Alzheimer (1864 – 1915) was a psychiatrist who investigated the relationship between brain disease and mental illness using microscopes [10]. Dr Alzheimer is best known for two landmark cases that he reported. He published the findings of his first case in 1907 as a summarized abstract of the case of Auguste Deter (August D.), aged 51. The second case was a detailed description of the clinical history and post mortem findings of a patient Johann F. who was 56 years of age [11].

Alzheimer first met Auguste Deter (August D.) in 1901. Her husband admitted her to the Community Hospital for Mental and Epileptic Patients in Frankfurt, Germany, after he noticed her increased memory problems over the course of a year, which led to paranoia, aggression and fearfulness [10]. Auguste D. was only 51 at the time of her admission. She died in 1906, whereafter Dr Emil Sioli (Alzheimer's previous boss at the Frankfurt Asylum) sent Alzheimer her brain material to examine [10]. Alzheimer examined her brain at the Munich Hospital microscopically using a new stain developed by Franz Nissl. The stain revealed structures in the brain's cells showing the presence of amyloid plaques and neurofibrillary tangles [12].

Johann F. was a 56-year-old male patient who over a period of six months began suffering from forgetfulness and the inability to do simple tasks. In 1907, he was admitted to the psychiatric clinic, and died in 1910. Post mortem brain examination revealed amyloid plaques but no neurofibrillary tangles in the cerebral cortex [11].

Alzheimer published these descriptions as well as those from several other patients in 1909. After that, Emil Kraepelin included Ms. Deter's case in his psychiatry textbook, '*Psychiatrie*', in 1910, being the first to call the disease Alzheimer's disease [11]. Alzheimer submitted a detailed description of the cellular pathology of Alzheimer's disease in 1911, and he also indicated that there might be little difference between the classical form of AD and senile dementia [3]. After the case of Johann, Alzheimer indicated that this case might belong to a subgroup of AD. Therefore the fact that Johann's brain revealed amyloid plaques but no neurofibrillary tangles in the cerebral cortex supported the fact that the disease is a heterogeneous group of disorders [11]. Neuritic plaques, neurofibrillary tangles and neurochemical deficits form part of the histological changes observed in AD. Notably, the cholinergic system is affected with the plaques and tangles disrupting the serotonergic and noradrenergic systems [12].

In 2011 a joint committee of experts redefined AD. They concluded after considering decades worth of evidence with biomarkers and neuroimaging that AD should not be considered a clinical syndrome of

dementia. AD should classify as a clinical disease that develops into a pathological process over the course of decades. They classify AD as having three stages. A first stage is a mild asymptomatic clinical phase, the second is a mild cognitive impairment phase, and the third is the neurocognitive disorder [10].

They indicate that the first phase is where AD has an initial, asymptomatic clinical phase, which can persist for years in which amyloid proteins accumulate. Neuroimaging techniques or the examination of cerebrospinal fluid can visualize these proteins. The second stage is where mild cognitive impairment and symptoms begin to appear. The performance of tasks begins being affected, but the patient is still generally independent. The third phase is dementia, where the patient's independence becomes challenged and their behavioural and cognitive function is affected [10].

1.3. Detection of Alzheimer's disease

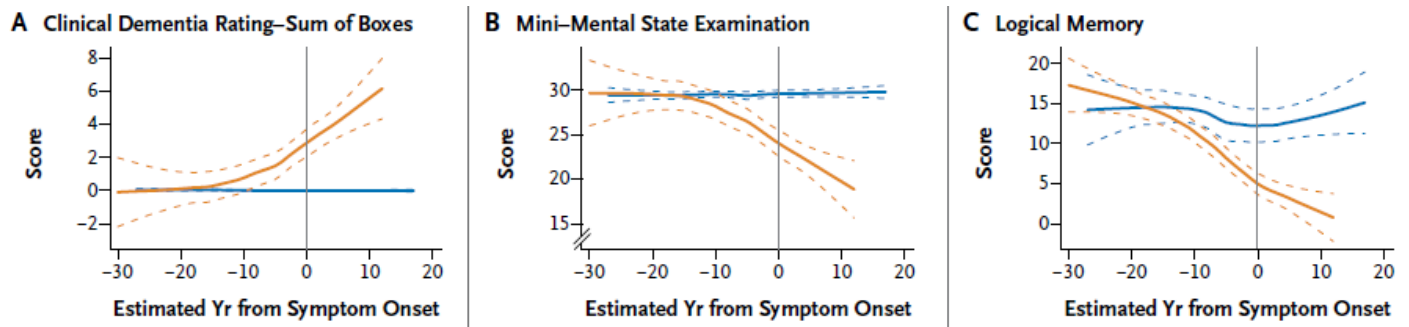
AD progresses over several years before symptoms reveal themselves. Currently there are clinical and neuropsychometric analyses used to provide a diagnosis of AD [13]. These involve studying the brain's atrophy, however, as noted above, a definitive diagnosis can only be performed by an autopsy after the patient's death.

A team of medical doctors conducted a study where they determined the clinical and biomarker changes in patients genetically identified, having autosomal dominant AD mutations. These include presenilin-1 (PSEN1), PSEN2 or APP, allowing them to predict the age of onset of the disease and therefore trace the sequence and the magnitude of the pathologies caused by the disease till the onset of symptoms. To follow will be the clinical and neurological impairment tests (1.4.1. – 1.4.3.), brain atrophy tests (1.4.4. – 1.4.5) and a biological marker test (1.4.6.), which the group performed [14].

1.3.1. Clinical Dementia Rating – Sum of Boxes

The Clinical Dementia Rating (CDR) is used by clinicians across the world to determine the severity of a patient's AD or other dementia [15, 16]. The 5-point scale ranges from 0 (normal) to 3 (severe) which is determined via an interview with the patient and a reliable personal associate of the patient. The areas of interest for analysis are memory, orientation, judgement and problem solving, community affairs, home and hobbies, and personal care [15, 16]. The CDR Sum of Boxes score (CDR-SOB) uses these six domains to sum up the score for each area and gives a total score of 0 (cognitive normality) to 18 (maximum cognitive impairment) [14, 16]. As seen in **Graph 1.1.A**, the non-carriers in their study indicated a score of 0 for all age groups, whereas the patients who were carriers the score increased as the age of the patient came closer to

the age of expected onset of symptoms [14].



Graph 1.1: A, B and C indicates the clinical and neurological impairments around the estimated year of symptomatic onset between carriers (orange) and non-carriers (blue) in the study done by Bateman and colleagues [15].

1.3.2. Mini-Mental State Examination

The Mini-Mental State Examination (MMSE) is a test used to determine the patient's abilities regarding orientation (time and place), memory (short and long term), registration, recall, constructional ability, language and the patient's ability to understand and follow commands through the use of questions [17]. The patient's level of education is used to adjust the test parameters [17]. The MMSE scores range from 0 (severe impairment) to 30 (no impairment) [14]. As seen in **Graph 1.1.B**, the score for the carriers decreased as they got closer to the age of expected onset to the disease, while non-carriers had a score of 30 throughout [14].

1.3.3. Wechsler Memory Scale-Revised (Logical memory)

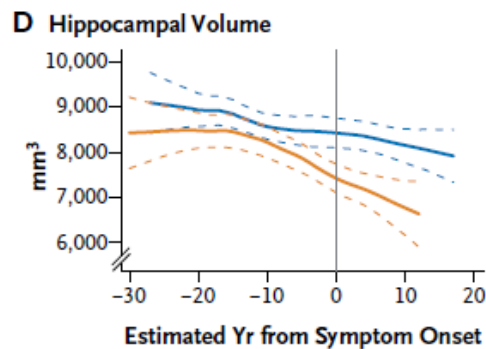
A story containing 25 bits of information was read to the patients and then again, after 30 min thereafter the patient had to recall the information where the patient receives a score which ranges from 0 (no recall) to 25 (complete recall) [14]. In their study, the results shown in **Graph 1.1.C** indicate that the non-carriers were steady until ten years before the expected onset. In contrast, the carriers had severe cognitive impairment and could not recall details from the story; the closer the symptom onset came [14].

1.3.4. Volumetric magnetic resonance imaging

Qualified 3-tesla scanners were used for the volumetric magnetic resonance imaging (MRI) to measure the hippocampal volume, which indicates the brain's atrophy (cell death) levels causing a decrease in

hippocampal volume as seen in **Graph 1.2** [14]. The non-carrier decrease is due to healthy aging and a corresponding steeper decrease is noted in that of the carriers [14].

1.3.5. Positron emission tomography



Graph 1.2: Change in the hippocampal volume and glucose metabolic levels around the estimated year of symptomatic onset between carriers (orange) and non-carriers (blue) in the study done by Bateman and colleagues [15].

1.3.5.1. Fluorodeoxyglucose positron emission tomography

Positron emission tomography (PET) can measure the cerebral glucose metabolic levels [18] by using a Siemens ECAT scanner following the intravenous injection of the tracer called [^{18}F]-2-fluoro-2-deoxy-D-glucose (FDG, 1 shown in **Figure 1.1**) [19]. It can move into cells via the glucose transporters, where it is then phosphorylated by hexokinases (HKs) to FDP-6-phosphate. It is then unable to proceed through the glycolytic pathway building up within intracellular cells [20]. In AD, the glycolysis pathway rates are elevated, which can be indicated by the glucose metabolism in the brain using FDG-PET by indicating the concentration of [^{18}F]FDG in the brain [14, 20]. The study performed by Bateman and colleagues indicated a steep decrease in the glucose metabolism shown in **Graph 1.3** in the previous ten years before the expected onset of symptoms [14].

The statistical map in **Figure 1.2**, representing the Z-score in colour (red – blue; significant metabolic reduction – no metabolic reduction), shows the results obtained from the study done by Minoshima and colleagues [21]. Post-mortem examination of an AD patient's brain confirms that there is a significant metabolic reduction in the temporal, lateral parietal and the associated frontal cortices of the AD patients. The arrows pointing towards the occipital cortex in the left and right medial views indicates that it is spared from glucose metabolism in AD [21].

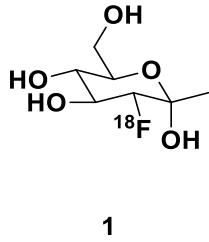
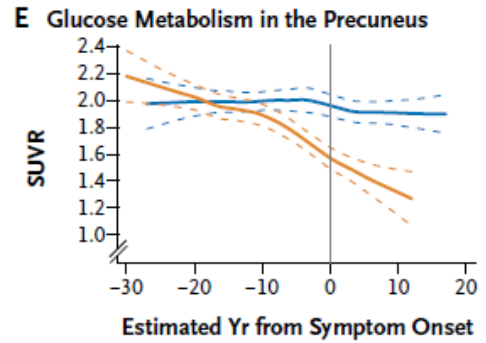


Figure 1.1: Markers used for the detection of AD in the brain [21].



Graph 1.3: Change in glucose metabolism around the estimated year of symptomatic onset of carriers (orange) and non-carriers (blue) in the study done by Bateman and colleagues [15].

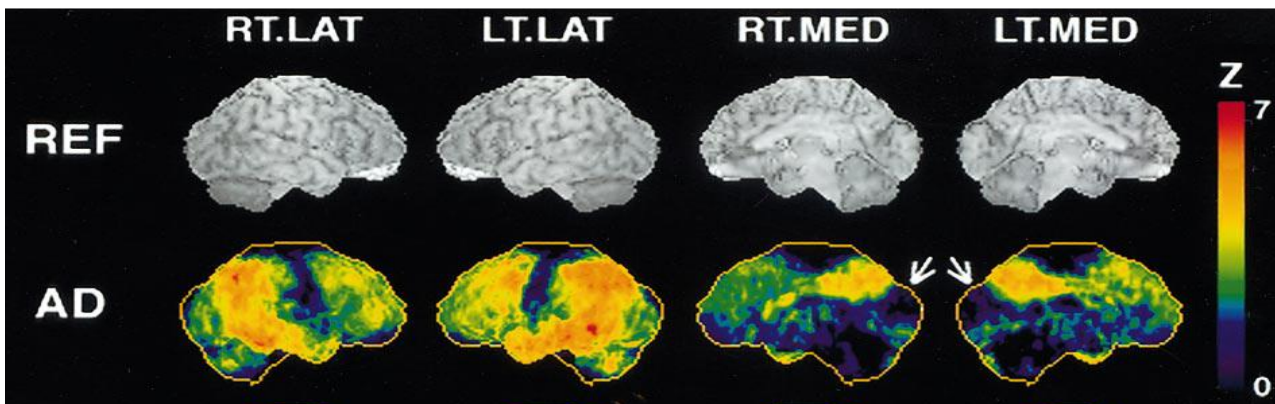


Figure 1.2: Cerebral metabolic reduction in confirmed AD patients. The statistical significance (Z-score) is color-coded, where red represents a more significant metabolic reduction. Sections of the brain are labelled as follows: Right lateral (RT.LAT) , left lateral (LT) , right medial (RT.MED) and left medial (LT.MED). [21].

1.3.5.2. Pittsburg compound B

The A β deposition measured with PET using the thioflavin T derivative called Pittsburg compound B [13] is called PIB-PET. By comparing it with FDG-PET and MRI images, the team used a program called FreeSurfer to determine regions of interest in AD patients and then determined the standardized uptake value ratio (SUVR) [14]. An increased A β deposition is indicated by an increase in the PIB SUVR, while a decreased metabolism indicates a decrease in the FDG SUVR [14]. **Figure 1.3** indicates the PIB-PET scans conducted by Bateman and colleagues comparing the A β deposits twenty years before, ten years before and at the

estimated year of symptomatic onset between carriers (orange) and non-carriers (blue) of autosomal dominant AD [14]. Already ten years before the onset of expected symptoms (B), there was a significant difference in the A β deposits in the caudate and cortex between the carriers and noncarriers. While C indicates an alarming increase in A β deposits at the expected time of symptomatic onset in carriers compared to non-carriers [14]. **Graph 1.4** indicates that there were no detectable A β deposits in the brain of non-carriers (scores of 0.88 or less), while carriers were already indicated to have A β deposits 15 years before the expected onset of symptoms [14].

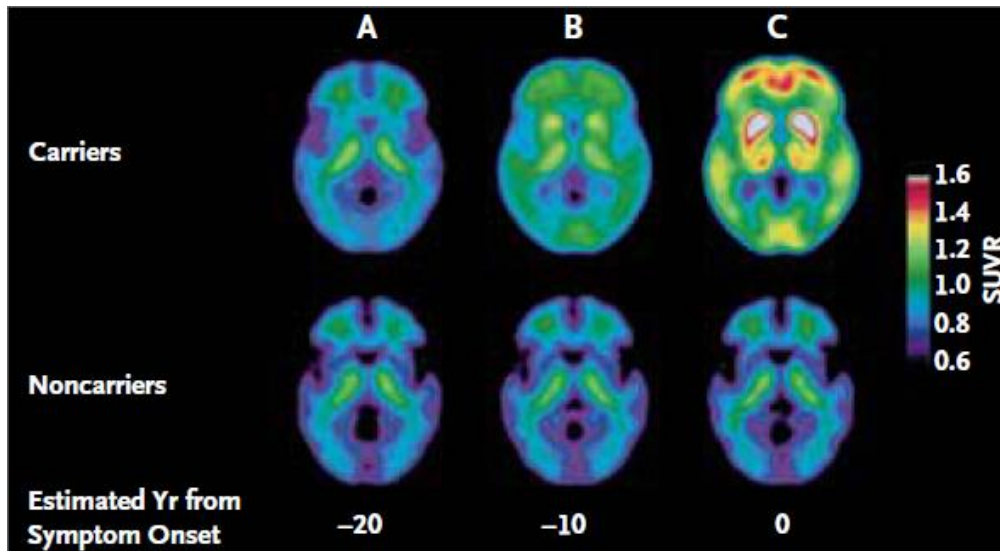
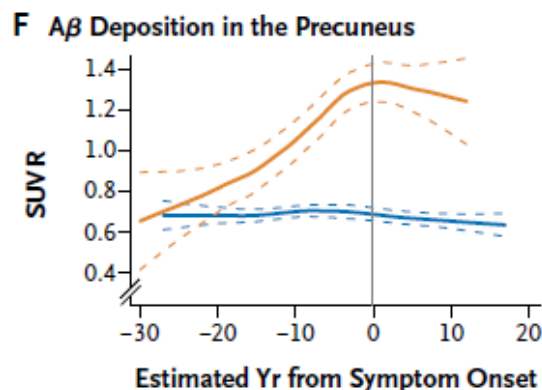


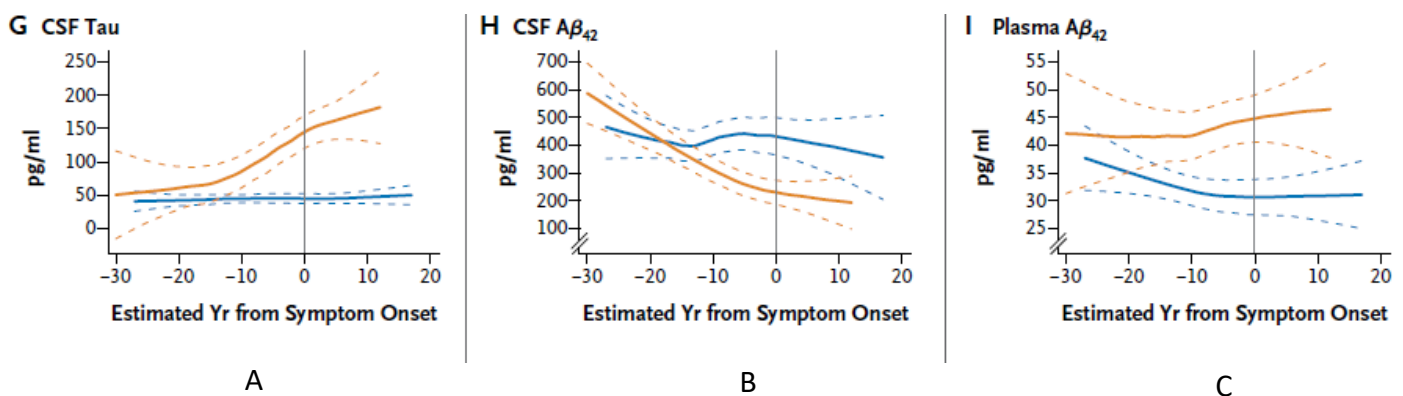
Figure 1.3: PIB-PET scans of A β deposition in Autosomal Dominant Alzheimer's disease over twenty years before the onset of clinical symptoms – A indicates the difference in a carrier and non-carrier twenty years before the expected onset of symptoms. B indicates the difference in a carrier and non-carrier ten years before the expected onset of symptoms. C indicates the difference in carrier and non-carrier at the expected onset of symptoms. The SUVR indicates the binding of PIB to fibrillar A β , where high levels correlate to high SUVR (red) values, while low SUVR (blue) values indicate low levels of amyloid [14].



Graph 1.4: A β deposits in the Precuneus around the estimated year of symptomatic onset between carriers (orange) and non-carriers (blue) in the study done by Bateman and colleagues [15].

1.3.6. Biochemical analysis

Through the use of robust immunoassays, which include INNOTEST β -Amyloid and INNO-BIA AlzBio3 or through the use of Innogenetics, the concentration of $A\beta$ total tau and phosphorylated tau at the threonine 181 amino acid in CSF can be determined [14]. The concentration of free $A\beta$ species which include $A\beta_{1-40}$, $A\beta_{1-42}$, $A\beta_{x-40}$ and $A\beta_{x-42}$ were determined using INNO-BIA Plasma $A\beta$ Forms Multiplex Assay and Innogenetics [14]. The work performed by Bateman and colleagues indicated that the carriers had an increase in tau 15 years prior to the onset of symptoms (**Graph 1.5 A**) and the $A\beta_{42}$ concentration in the central nervous system (CNS) started to increase ten years before the onset of symptoms (**Graph 1.5 B**). The $A\beta_{42}$ plasma concentration of carriers also appeared elevated (**Graph 1.5 C**) [14].



Graph 1.5: A,B and C represents the CSF tau, CSF $A\beta$ and plasma $A\beta$ concentrations around the estimated year of symptomatic onset between carriers (orange) and non-carriers (blue) in the study done by Bateman and colleagues [15].

1.4. The pathogenesis of the Alzheimer's disease hypotheses

AD has a mean average duration of 8.5 years between the onset of the clinical symptoms of the disease and death [22]. Different physiological processes related to AD cause damage to cells and ultimately lead to their destruction. Cells producing and using ACh are greatly affected [23], resulting in the apoptosis of basal forebrain nuclei resulting in fewer functioning cells available to carry out the messages sent from the brain leading to the cholinergic deficits observed in AD diagnosed patients [24]. Cholinergic hypofunction and AChE hyperactivity are responsible for early memory impairment in AD patients [10]. The degeneration of the medial-temporal-lobe memory system leads to explicit (conscious) memory loss [25] and the degeneration of cholinergic nuclei in the basal forebrain, synaptic loss and the neuronal apoptosis may also be associated with the reduction of the oxidative metabolism of glucose and the decrease in coenzyme A (CoA) and adenosine triphosphate (ATP) in AD patient's brains [26].

Biochemical evaluation of biopsy tissues from AD patients (three and a half years post diagnosis) shows a uniform reduction in the presynaptic markers of the cholinergic system. The reduction in ChAT activity and ACh synthesis correlates with the degree of cognitive impairment of AD patients. Slightly affected markers include other serotonergic and noradrenergic markers. Dopamine, γ -aminobutyric acid (GABA), and somatostatin are not affected. At more advanced stages of the disease, more neurotransmitter systems are affected [22]. The behavioural disturbance of AD, for example, depression, is expected to be due to the change in the serotonergic system [22].

By the time of a death, there is a loss of more than 75 % of the neurons in the basal forebrain nuclei. The remaining neurons in the brain contain an abundance of neurofibrillary tangles. The death of neurons in the brain causes an 80-90 % reduction in the hippocampus and temporal cortex and a 40-75 % reduction in the parietal cortex and frontal convexity [24]. **Figure 1.4** indicates the striking visual difference between the healthy brain and that of a patient who died due to AD. There is a sharp shrinkage in the cerebral cortex and hippocampus and a severe enlargement of the ventricles in the brain [27].

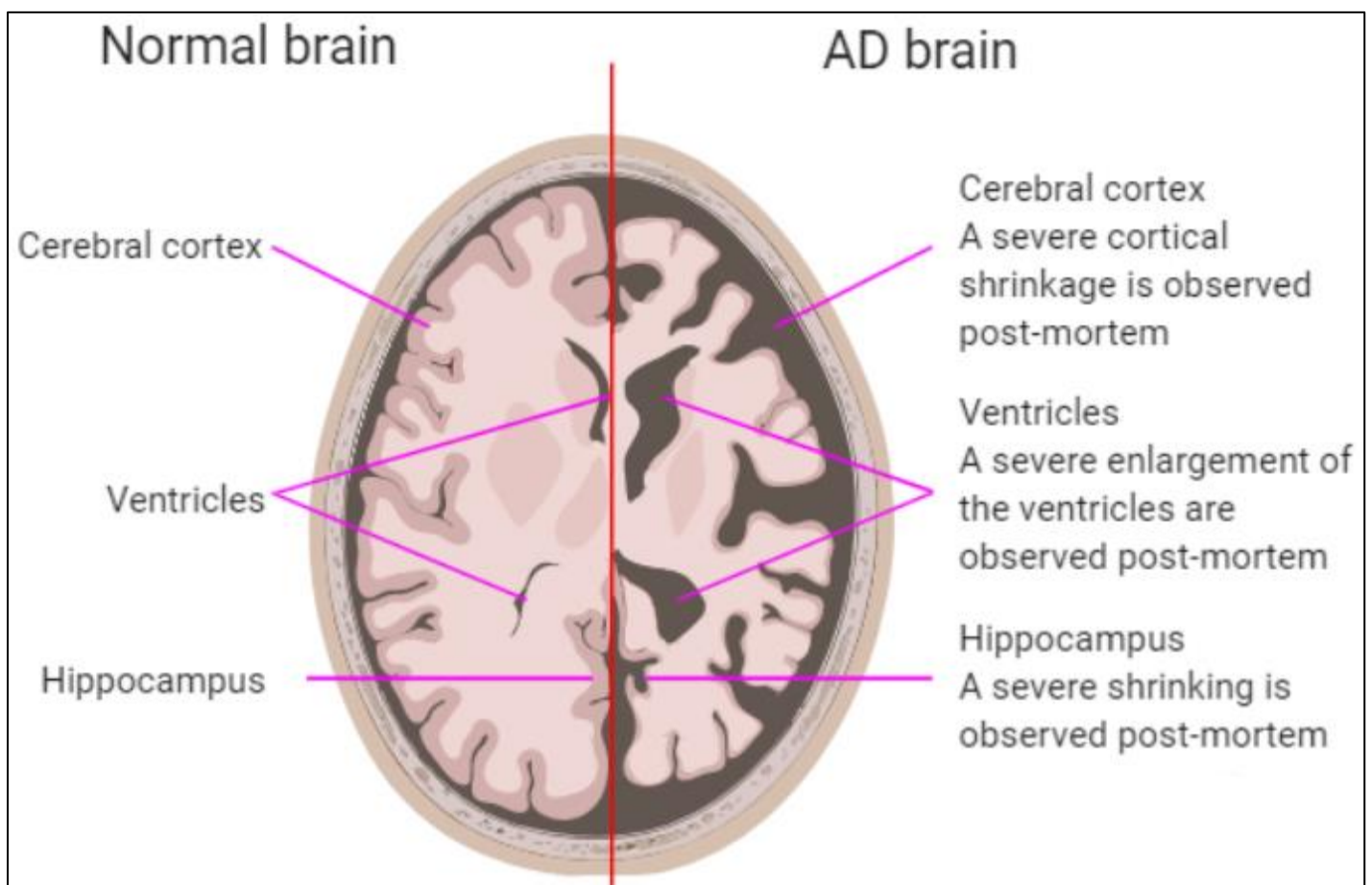


Figure 1.4: Visual differences between the brain of a healthy person and an AD patient – adapted from [28].

Typical cognitive functions in humans involve cortical pyramidal neurons. They get released by an excitatory amino acid (EAA) which activates postsynaptic cells that have a role in cholinergic function. They are cholinergic and their dysfunction strongly correlates to dementia. It is challenging to distinguish EAA neuron's metabolic pool from the aspartate and glutamate transmitter pool that function as transmitters for pyramidal neurons. They are, therefore, involved in the cognitive symptoms of AD. Samples taken from AD patients indicate a 14 % reduction in glutamate concentration in the temporal lobe biopsy. Regions enriched with EAA nerve terminals have an even more significant reduction in glutamate concentrations in post-mortem analyses. *In vivo* imaging studies indicate that a parallel exists between the pyramidal neurons and neuronal loss, tangle formation and reduced glutamate concentration [24, 28].

Binding of muscarine to the EAA neuron's muscarinic receptors (mAChRs) activates the neuron. Binding of the nicotinic receptors (nAChRs) also activates the EAA neurons [9, 22, 24, 29]. They are expressed in the hippocampus and could, therefore, affect learning and memory [28]. The mAChR is a G-protein coupled metabotropic receptor (membrane receptor acting through a second messenger) for signal transduction. A nAChR is a ligand-ion gated ion channel, therefore making them ionotropic [24, 28].

The mAChRs are involved in the regulation of ionic conductance, which results in a depolarization or hyperpolarization response. They cause the signal transduction in the hippocampal pyramidal cells and interneurons [28].

The most common muscarinic receptor is M₁, found in abundance in the cerebral cortex, are also located in the dentate gyrus, hippocampus, anterior olfactory nucleus, olfactory tubercle, olfactory bulb, nucleus accumbens and the amygdala. Different regions of the brain contain M₂, M₃, and M₄ receptors [24].

The binding of ACh to the nAChR induces the opening of the nicotinic channel to allow an influx of Ca²⁺ [28]. The ion concentration increases in the cell, affecting neurotransmission release, signal transduction and apoptosis. Other ions can cause cell depolarization inducing electrical firing. Activation of the nAChR blocks the release of the proinflammatory cytokines in the brain and inhibits the synthesis of cytokines in the periphery [28].

1.4.1. Amyloid cascade hypothesis

Amyloid proteins are formed by normal body processes, through the proteolytic processing of the β -amyloid precursor protein (APP) by α -secretase, β -secretase [3] and γ -secretase. In this process, a soluble protein called A β is produced in the neocortex of the brain [2, 30]. These proteins are then broken down and, in the case of healthy brains, eliminated. The APP metabolism process involves either cleavage of the N-terminus

of the A β sequence by β -secretase which is then processed by γ -secretase forming A β or by forming soluble APP α through the cleavage of the A β sequence with α -secretase [13].

In AD, however, A β self-aggregate and accumulate in the brain due to an imbalance between A β production and clearance. As a result, insoluble amyloid plaques accumulate in the brain, in between nerve cells, forming several toxic oligomers that can form protofibrils, fibrils and insoluble senile plaques (SP) (see **Figure 1.5**) [2, 3, 31]. The accumulated plaques further cause an inflammatory response and ultimately brain cell apoptosis [10]. The toxicity of these plaques was highlighted in a study by Christain and co-workers where it was concluded that significant levels of peptide aggregation causes β -amyloid-induced neurotoxicity [32]. In further studies it was suggested that the soluble forms of A β lead to even higher neurotoxicity levels [2].

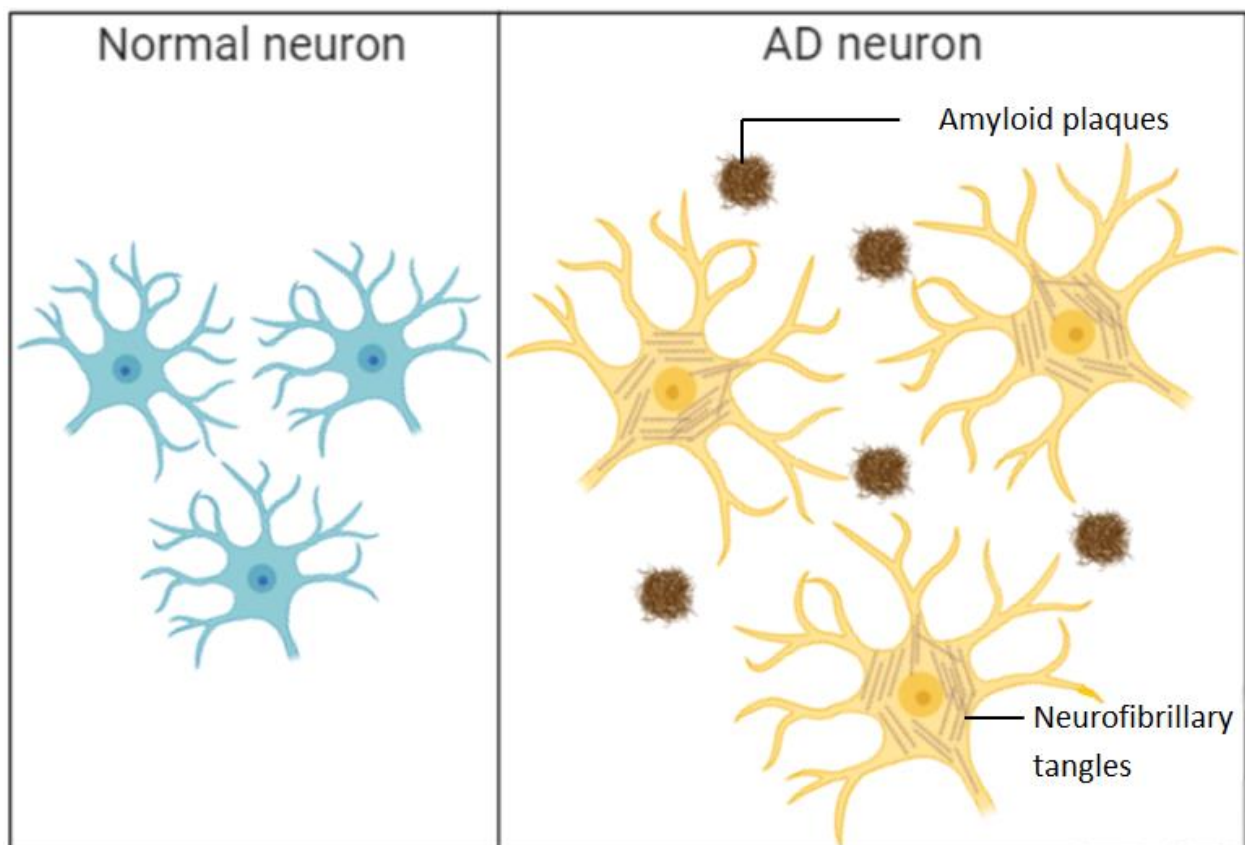


Figure 1.5: Normal neuron vs. AD neuron containing neurofibrillary tangles (tau hypothesis) and amyloid plaques (amyloid hypothesis) – adapted from [3].

A β oligomers impair the potentiation of long-term synaptic function but also synaptic structures like dendritic spines. The soluble oligomers of A β_{42} , isolated from the cortex of AD rats, indicated that the decrease in synaptic function and impaired memory depends on the concentration of these oligomers in the brain [13]. In rats, these A β_{42} oligomers decrease synaptic density, inhibit long-term potentiation (LTP),

enhancing long-term synaptic depression and impairment of memory [13].

Early-onset AD is typically the result of a missense mutation in presenilin 1 or presenilin 2. The mutation on the catalytic subunits of γ -secretase increases the hydrophobic species of $A\beta_{42/43}$ peptides that then self-aggregate to form $A\beta$ deposition, causing a progressive accumulation of neurofibrillary tangles [13].

$A\beta$ targeted therapies include attempts to decrease the $A\beta$ production by synthesizing β - and γ -secretase inhibitors and modulators as well as active AD immunotherapy, passive AD immunotherapy and the prevention of $A\beta$ aggregation by promoting the clearance of $A\beta$ [2].

To date there are no approved drugs which target the amyloid cascade, however, there are several inhibitors in clinical trials, see **Figure 1.6**. The β -secretase inhibitor, MK-8931 (**2**), is a BACE1 inhibitor and is currently in phase I clinical trials. It reduces the concentration of CSF $A\beta$ in patients with mild to severe AD. The drug shows limited adverse effects, good dose tolerance and reduced CNS $A\beta$ in both healthy and AD volunteers [2].

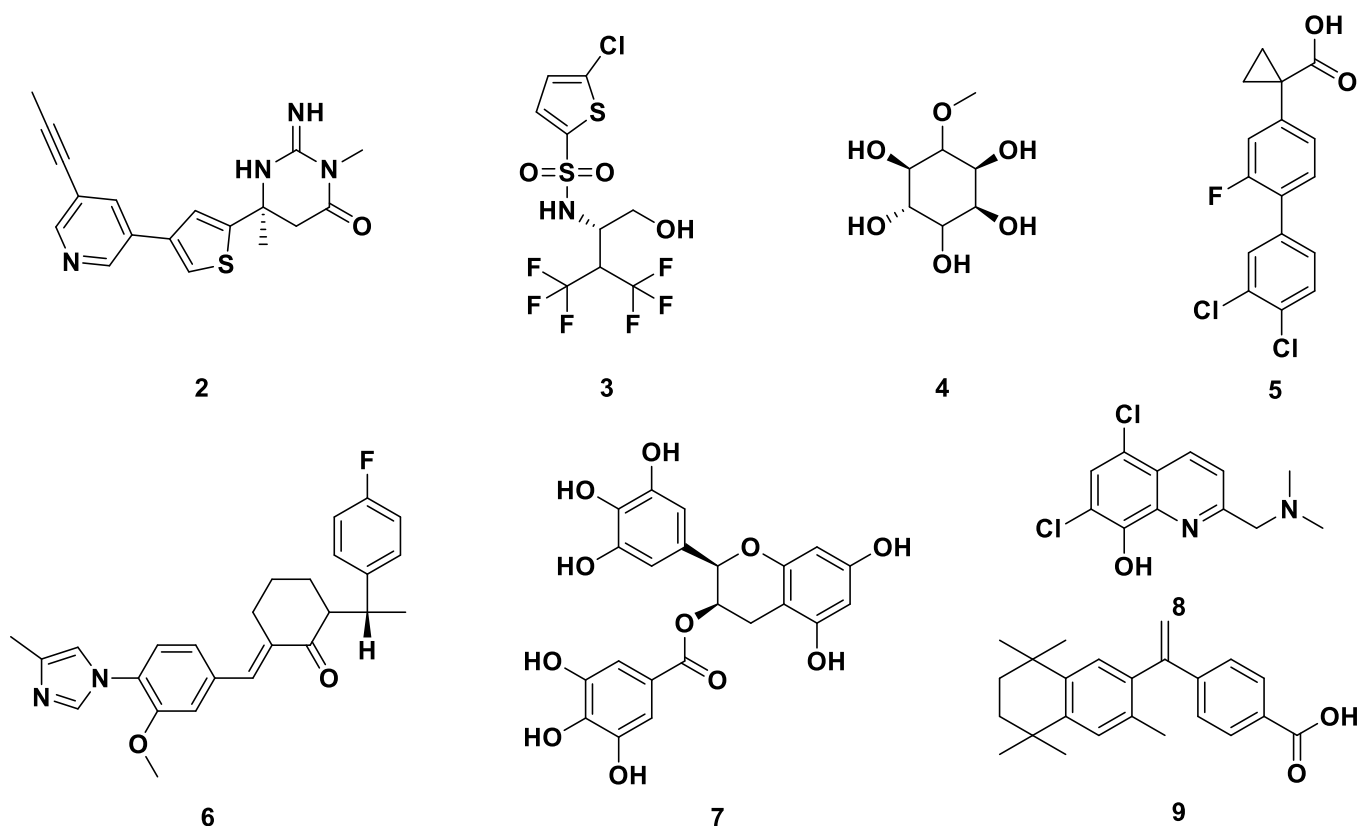


Figure 1.6: Drugs synthesized for the treatment of AD with regards to the amyloid cascade [3].

The γ -secretase inhibitor, Begacestat (**3**), inhibits APP cleavage and phase I clinical trials have shown promise. NIC5-15 (**4**) improves cognitive function by reducing $A\beta$ production through the modulation of γ -secretase

and it has excellent tolerability. The microglial modulator, CHF5074 (**5**), reduces brain A β and has been shown to enhance memory in transgenic AD mice. It is well tolerated in patients with mild to moderate AD and has dose-dependent effects on the central nervous system. E2012 (**6**) decreases the A β_{40} and A β_{42} concentration in rats in a dose-dependent manner without affecting notch cleavage [2]. Epigallo-catechin-3-gallate (EGCG; **7**) can bind to unfolded peptides, thereby preventing the formation of toxic A β oligomers. It can further improve the mitochondrial and cholinergic synaptic function. It acts as a modulator in cell signalling, reverse superoxide dismutase activity. It can also help with the damaging effects caused by AlCl₃ neurotoxicity [2]. PBT₂ (**8**) is a metal chaperone that can conduct A β oligomerization, decreasing the concentration of soluble and insoluble A β as well as decreasing the clearance of the A β oligomers [33, 34]. The phase II trial showed improved cognitive function, safety, tolerance and that the drug is able to reduce the concentration of A β_{42} in CSF [35]. Bexarotene (**9**) targets the primary nucleation step in the aggregation of A β_{42} , which then delays the formation of toxic species in neuroblastoma cells resulting in the suppression of A β_{42} deposits [2].

Active AD immunotherapy is the use of a vaccine or antibody that targets A β clearance. CAD106 reduces A β accumulation and has currently passed Phase II trials. ACI-24, an A β_{1-15} liposome-based vaccine, is currently undergoing Phase I/II clinical trials and has been shown to restore memory and reduce plaques in transgenic AD mice [2]. A synthetic peptide, UB-311, couples to the A β_{1-14} peptide and is currently being prepared for Phase II trials [2].

Passive AD immunotherapy makes use of humanized monoclonal antibodies that target A β clearance. PF-04360365 (Ponezumab) is an IgG2 δ A monoclonal antibody that binds to A β and therefore prevents A β deposition in a dose-dependent manner, improving the symptoms of AD [36]. A phase I trial indicated that there were no adverse effects observed and that it was well tolerated in the Japanese subjects involved in the study [37]. GSK-933776 is an Fc-inactivated anti-A β monoclonal antibody that showed pharmacological activity. The antibody targets A β found in plasma and lowers the free A β peptide concentration in plasma. There were no amyloid-related imaging abnormalities-edema (ARIA-E) or –haemosiderin (ARIA-H) abnormalities observed in patients with mild AD [2].

1.4.2. Hyperphosphorylated Tau protein

Tau proteins are microtubule-associated proteins that are responsible for the stability of microtubules (MTs). MTs in turn, are responsible for facilitating the transport of nutrients and other substances and are predominantly found in neurons [10, 31, 38]. There is a dynamic balance between the phosphorylation and dephosphorylation of tau proteins in the brain,[2] and when there is a change in the tau protein's ability to

bind extracellular cargo, there is a corresponding gain of function (GOF) or loss of function (LOF), resulting in possible pathogenesis [2, 38].

Hyperphosphorylated tau proteins are a network of insoluble twisted fibers resembling paired helical filaments (PHF), twisted ribbons and straight filaments (SF) [39, 40]. Microtubule binding involves the self-assembly of tau proteins in AD, causing intermolecular hydrophobic interactions. The binding occurs when the rest of the molecule, for example, the amino-terminal and carboxylic terminal of the protein, is neutralized by abnormal hyperphosphorylation [39]. **Figure 1.5** indicates these aggregates called neurofibrillary tangles (NFTs) which are formed within the neurons of AD patients. Phosphorylated tau proteins are also present as a non-filamentous form in the cytosol of AD brains [2, 10, 39, 40].

Hyperphosphorylated tau proteins have a reduced ability to bind to MTs, resulting in instability and ultimately the collapse of the said MTs [10, 31, 38]. The density of these NFTs has been correlated to the cognitive decline observed in AD patients [38]. The loss of normal tau leads to the death of neurons, which then leads to neurodegeneration, causing dementia [38, 39]. In addition, the concentration of acetyl-tubulin, an MT stabilizing marker, is shown to be low in concentration in AD patients [38].

Tau in AD patients are conformationally altered causing a LOF, however, this LOF can be compensated for by the MT associated proteins MAP1A/MAP1B and MAP2 [39]. Since it is the formation of toxic tau proteins that cause the collapse of the MT, there is no amount of compensation that will prevent the ultimate destruction of the neurons [39]. As more tau proteins are produced by the brain to battle the toxic tau aggregate and form these abnormally hyperphosphorylated tau as inert, insoluble polymers (neurofibrillary tangles) [39].

The protein phosphorylation is itself controlled by kinases; however, it has proven challenging to determine which kinases are involved in the tau protein's phosphorylation. To make matters worse, many kinase inhibitors target the ATP binding site, which is shared by many members of the kinase family, as a result, inhibitor selectivity is an issue [38].

Paclitaxel (**10**), an MT-stabilizing drug, facilitated improvement in fast axonal transport (FAT) and MT density in mice during a three month study (see **Figure 1.7**) [38]. The MT-stabilizing compounds are pumped out of the brain into the bloodstream due to poor blood brain barrier (BBB) penetration [38]. BBB penetration is critical because the concentration of the compound in the brain used for treatment needs to be high enough to serve its purpose, but be low enough not to cause side effects [38].

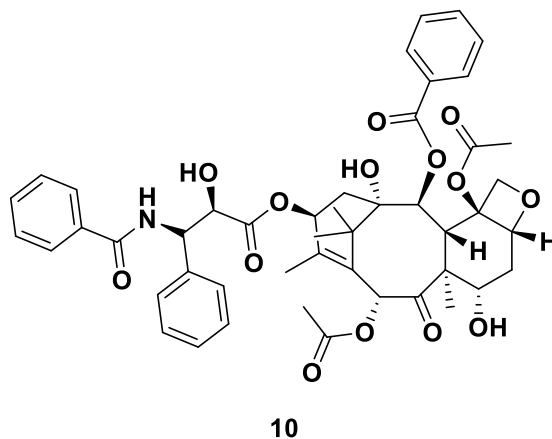


Figure 1.7: Paclitaxel.

Compounds used for the treatment of AD targeting the tau hypothesis can be seen in **Figure 1.8**. The dye, methylene blue (**11**), was the first compound reported inhibiting tau-tau interactions. The dye was shown to alter PHF, which was isolated from the brain. Phase II AD trials showed a positive treatment effect when using methylene blue, phase III trials are currently underway [38].

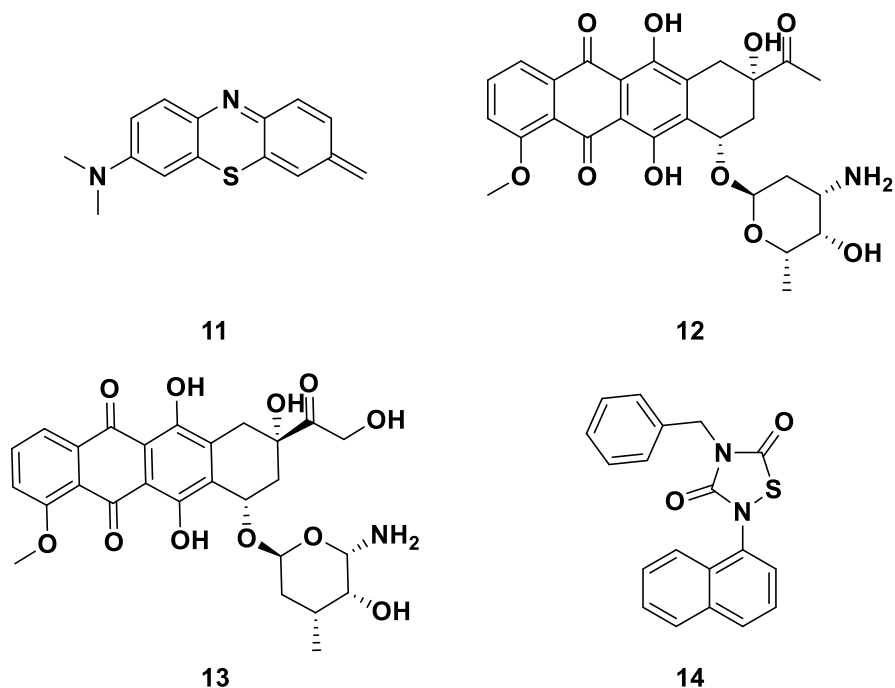


Figure 1. 8: Drugs used for the treatment of AD with regards to the tau hypothesis.

There have also been compounds identified that can prevent fibrillization of tau proteins and even dissolve existing ones. The use of thioflavine S (ThS) fluorescence can indicate drugs that inhibit the tau fibril

formation upon binding cross- β -fibril structures. Tau fibrils disaggregation come into effect when the concentrations that prevent fibrillization have been exceeded [38]. Compounds that can affect this include Daunorubicin (**12**) and Adriamycin (**13**) of the anthraquinone family. The two drugs were able to inhibit PHF formation with an IC_{50} value of 1-5 μ M and disassemble these PHFs at IC_{50} values of 2 – 4 μ M [41]

Free tau in the cytoplasm is readily phosphorylated when compared to the MT-bound tau and the membrane-bound tau proteins are effectively not involved in aggregation [39]. The ubiquitin-proteasome system (UPS) degrades phosphorylated tau proteins, however, hyperphosphorylated tau is resistant to protease activity causing the levels of tau in an AD brain to increase [39]. A potential therapeutic target is to up-regulate UPS through the inhibition of the heat shock protein (Hsp90) in an effort to lower the tau fibril concentration in the brain [38].

A high concentration of a suitable tau inhibitor compared to the free tau concentration is necessary for the inhibition of tau aggregation. Treatments that target the stabilization of MT, thereby compensating for the phosphorylated tau protein's LOF, are currently being researched [38]. Through the use of the MT-stabilizing agent, the octapeptide NAP (consists of the following amino acids: NAPVSIPQ), the loss of tau interactions can be compensated for, leading to an improved AD pathology [42].

Finally, glycogen synthase kinase 3 (GSK-3) is enriched in the brain and can phosphorylate multiple sites in the tau protein, affecting the APP processing and release of $A\beta_{1-42}$ peptides. Therefore the inhibition of GSK-3 will lead to lower $A\beta$ production and the number of phosphorylated tau proteins [43]. A small non-ATP competitive GSK-3 inhibitor called Tideglusib (NP-031112, **14**) is an irreversible, non-ATP-competitive GSK-3 β inhibitor and can prevent the overactivation of the *N*-methyl D-aspartate hypothesis (NMDA, discussed in chapter 2) receptors inducing cell death [44]. The inhibition of tau protein hyperphosphorylation leads to improved learning and memory, reduces brain amyloid plaque levels and prevents the loss of neurons [2, 45].

1.4.3. Cholinergic hypothesis

The dysfunction of cholinergic activity in the brain leads to memory loss and related cognitive impairments associated with dementia and AD. A neurotransmitter, specifically acetylcholine (ACh), is responsible for cognitive performance, learning and other memory processes. It operates by conducting electrical impulses from one nerve cell to another [10, 46]. ACh, choline acetyltransferase (AChT) and acetylcholinesterase (AChE) decreases readily as the disease progressed [2]. Chapter 2 covers the cholinergic hypothesis in more detail.

1.4.4. Metal ion hypothesis

Metal ion dyshomeostasis has a significant role in the development and progression of AD [47]. Transition metals (Cu, Fe and Zn) are critical as co-factors in metalloproteins (catalytic, transport, storage) involved in metabolism [2, 48]. The concentration of the metal ions and redox-active metals are normally regulated by the BBB, however, in the case of AD patients elevated levels of these species are commonly noted [48]. The BBB dysfunction and metal ion balance in the brain gets influenced causing neurodegeneration in AD patients [2]. The metal ion balance dysfunction also affects the oxidative stress response of mitochondria [2]. Finally, the accumulation of metals including Al, Zn, Cu and Fe all lead to changes in the A β protein leading to the folding of proteins into wrong conformations [2].

Studies have shown that there is a correlation to A β toxicity and their abnormal interaction with neocortical metal ions like Zn, Cu and Fe even though A β is involved in normal metal ion homeostasis [49]. Standard metal ion age-matched neuropil concentrations are Zn²⁺ (350 μ M), Cu²⁺ (70 μ M) and Fe³⁺ (340 μ M) compared to the levels in amyloid plaques having concentrations as follows Zn²⁺ (1055 μ M), Cu²⁺ (390 μ M) and Fe³⁺ (940 μ M). Therefore Bush suggested that Cu²⁺ and Fe³⁺ are co-precipitates with Zn²⁺ due to the presence of Cu²⁺ and Zn²⁺ binding sites on the A β [49]. Fe²⁺ is the principal chemical factor in the aggregation of A β and has 3.5 metal-ion-binding sites (as oligomers) with various affinities for A β . The highest being almost 100 nM for Zn²⁺ and only 8 nM for Cu²⁺ [49]. A β and tau protein accumulation in NFT-containing neurons involves Fe ion interaction, but in some cases, even the binding of Al ions can have the same effect [2, 48]. Al and Cu are also involved in nerve inflammation in the brain [2].

Figure 1.9 illustrates the relationship between metal ions in the brain and A β . The metal ion (Cu and Fe) concentration increases in the brain's neocortex with age. The brain responds to this increase in metal ion concentration by overproducing APP leading to an increased production of A β . The average pH in the brain is about 7.2. However, in the presence of mild acidosis (green background), the A β becomes hypermetallated, forming A β Fe and A β Cu₂ species if the metal ion levels keep increasing. The hypermetallated A β then uses oxygen and biological reducing agents to produce hydrogen peroxide catalytically via the Fenton reaction. Hydrogen peroxide then reacts with A β Cu₂ generating oxidized A β (now resistant to protease) and cross-linked forms of A β , freed from the membrane. The free oxidized A β peptides initiate microglial activation, which produces even more hydrogen peroxide and myeloperoxidase (MPO), favouring further crosslinking of A β and hydrogen peroxide outside the cell.

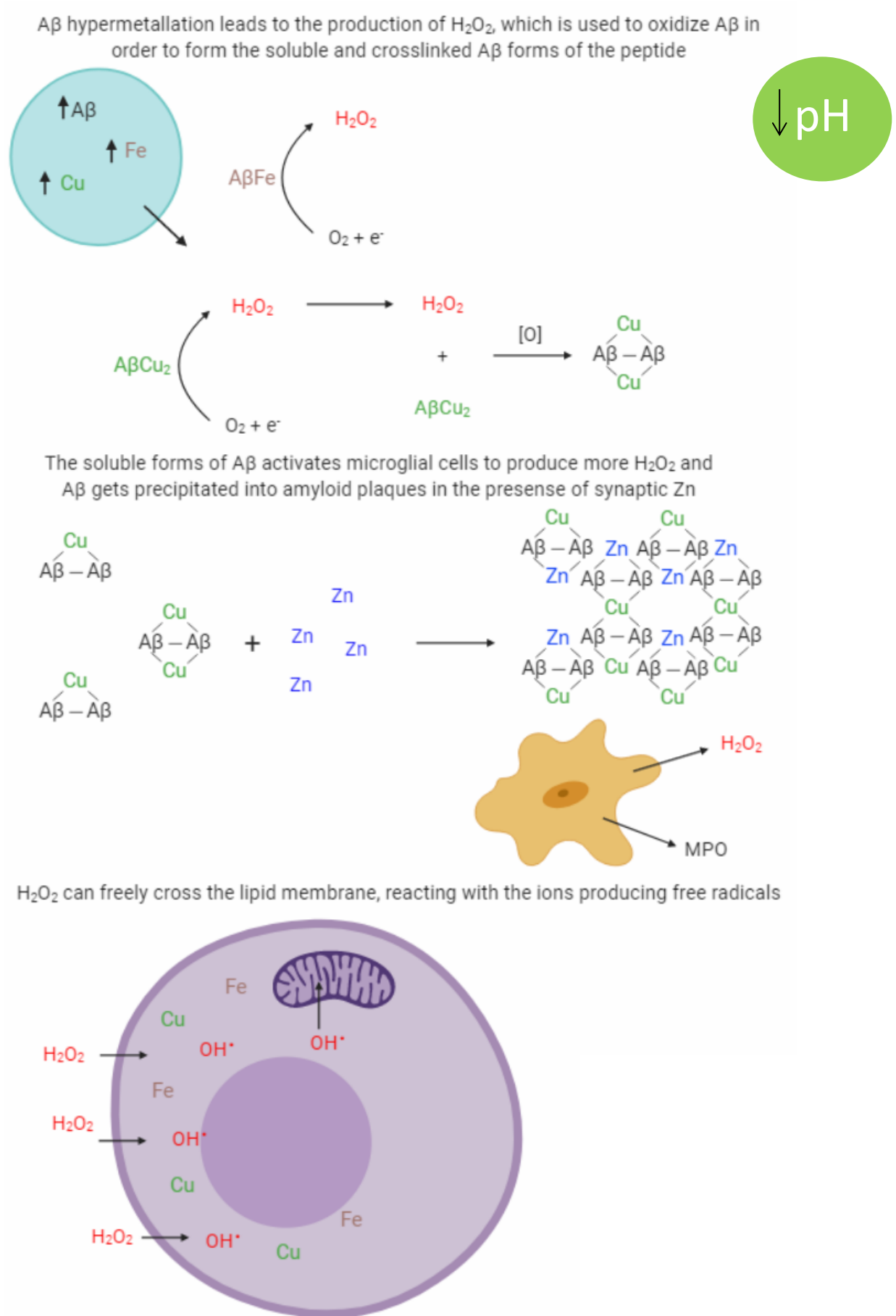


Figure 1.9: Illustration of the metallobiology of $A\beta$ in AD – adapted from [50].

The hydrogen peroxide can freely cross lipid membranes and further cross into cellular compartments. Inside the cellular compartments, it also reacts with Cu and Fe forming hydroxyl radicals ($\text{OH}\cdot$) and furthermore, leads to the oxidation of nucleic acids, proteins (for example, the tau protein) and lipids. Oxidized forms of $\text{A}\beta$, which form part of plaque deposits of $\text{A}\beta$, are found outside of cells that show signs of AD-affected brain tissue. The high concentration of Zn in the synaptic cleft indicates why there are high concentrations of Zn, Cu and Fe found in $\text{A}\beta$ plaques [49]. The transition metals (Cu, Fe and Zn) are also essential in biological reactions in the human body and, therefore, a deficiency could lead to disturbances in the CNS and even affect organ function [48].

Targeting the ion channels of $\text{A}\beta$ represents a possible means of treating AD as well as other disorders such as Jakob's disease, Parkinson's disease (PD), motor neuron disease and cataracts [49].

Compounds used for the treatment of AD targeting the metal ion hypothesis can be seen in **Figure 1.10**. Clioquinol (CQ; **15**) is a metal chelator, which can chelate Cu and has shown to inhibit β -amyloid accumulation by improving its deposition and can also prevent toxin-induced oxidative stress [50]. Another proposed mechanism of CQ (**15**) and PBT2 (**8**) suggests that the molecules enter the brain where they are attracted to and bind to the metals (Zn and Cu) that are in high concentrations with $\text{A}\beta$ [51]. The $\text{A}\beta$ then dissolve the aggregated $\text{A}\beta$ to their monomer forms that can be degraded. Copper levels in the cortex were lowered and maintained at normal levels in the blood through the use of the copper chelator Plerixafor (JKL169; **16**) [51]. Desferrioxamine (DFOA; **17**) was used in a treatment as a chelator of Al, but it also chelates Zn, Fe and Cu. A reduction in the rate of decline in the patient's living skills proved the possible positive effect of the use of DFOA [17, 51].

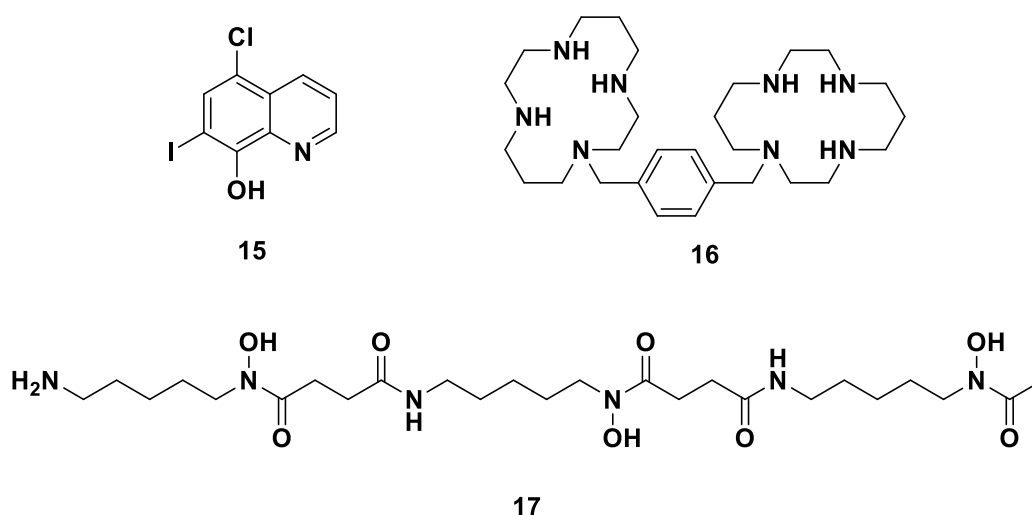


Figure 1. 10: Drugs used for the treatment of AD with regards to the metal ion hypothesis.

1.4.5. Oxidative stress hypothesis

Reactive oxygen species (ROS) found in AD, PD and amyotrophic lateral sclerosis (ALS) causes neurodegeneration [50]. In AD, the extreme levels of oxidative stress are due to increased levels of ROS and reactive nitrogen species (RNS), which are involved in the functioning of cellular signalling pathways and some deleterious processes in the body [2]. Disruption of these processes could lead to protein oxidation, advanced glycation end products, lipid peroxidation, 3-nitrotyrosine formation and DNA/RNA oxidation. Potential damage to cellular structures like the cell membrane, lipids, protein and DNA could occur [2, 52].

The brain is vulnerable to oxidative stress since neurons contain large numbers of polyunsaturated fatty acids forming lipid bilayers. Lipids can undergo lipid peroxidation, causing rearrangements of oxidized proteins. The rearrangement exposes hydrophobic amino acids and bulky aliphatic residues, which are recognized by the proteasome, followed by proteolytic degradation of these lipids [2, 53].

Oxidative stress influences the expression of superoxide dismutase. Malondialdehyde (MDA) and the lipid peroxidation marker 4-hydroxynonenal (4-HNE) are oxidative stress markers which increase in concentration in the cortex and hippocampus of AD patients [9, 50]. When a small hydrophobic aggregate of A β ₁₋₄₂ gets incorporated into the lipid bilayer, the lipid peroxidation marker forms as a result causing lipid peroxidation and indicates that free radicals are involved in the initiation of β -amyloid toxicity [54]. Another mode of action includes a Michael addition reaction where HNE and acrolein react with transmembrane proteins thereby causing a covalently modified structure disrupting the transmembrane's function leading to molecular apoptosis [2, 52]. The glutamate transporter (GLT-1) or the glutamate synthase enzyme regulates glutamate levels in cells. Changes that increase excitotoxic glutamate activity leads to neurodegeneration in AD [52].

Decreased neuronal glutathione levels cause a reduction in the activity of antioxidant molecules [2]. The activity of superoxide dismutase (SOD), glutathione reductase (GSHRd), glutathione peroxidase (GSHPx) and catalase decrease. These changes lead to oxidative stress injury [50]. Oxidative stress causes an increase in ceramides and cholesterol leading to synaptic dysfunction and neuronal degeneration. This dysfunction and degeneration have been noted in mild to moderate AD patients but not in healthy brains, suggesting that these abnormal lipid metabolisms occur early in the development of the disease [52, 55].

Nitration of the tau proteins is also elevated in the neocortex and hippocampus in the AD brain due to the reaction of NO with O₂⁻ resulting in the formation of ONOO⁻ which is cytotoxic when protonated [50, 56]. The nitration of the amino acid, tyrosine, has led to the inactivation of numerous proteins [56]. The formation of OH[·] (explained in detail in the metal ion hypothesis) also leads to the oxidation of nucleic acids, proteins

(for example, the tau protein) and lipids. Outside the cells, showing signs of AD-affected brain tissue, oxidized forms of A β form part of plaque deposits of A β (see **Figure 1.9**) [49].

Drugs used for the treatment of AD targeting the oxidative stress hypothesis can be seen in **Figure 1.11**. Vitamin E (**18**) is a free radical scavenger known as a hydrophobic chain-breaking antioxidant that prevents the formation of A β ₁₋₄₂-induced ROS, causing the neurodegeneration of AD [52]. Hydrogen atoms of adjacent lipid carbon atoms are vulnerable to free radical attack and, therefore, methionine (**19**) inserts into the lipid bilayer preventing the chain reaction of free radical attack causing subsequent membrane damage [52]. Met-35, which forms part of the A β ₁₋₄₂ peptide, is the key to the peptide's oxidative stress and neurotoxic properties, which gets entirely abolished by substituting the S atom with a methylene group (CH₂) (**20**) [52]. Julie Andersen's research group is concentrating on emulating the protective effect of enzymatic components that regulate oxidative stress by developing synthetic drugs or genetic therapies [50].

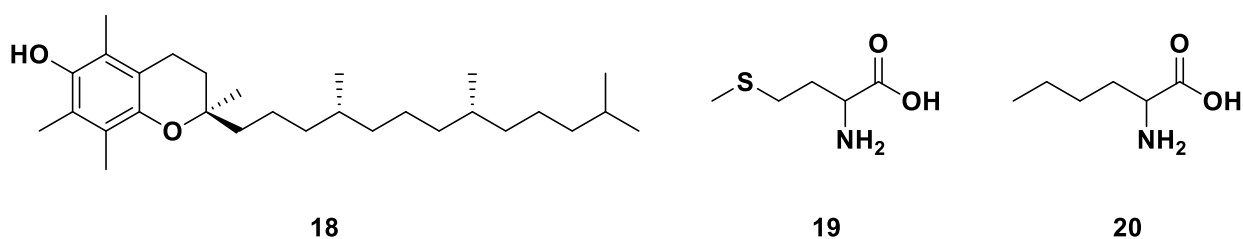


Figure 1.11: Drugs used for the treatment of AD with regards to the oxidative stress hypothesis.

1.4.6. Inflammatory hypothesis

In AD, there is an increase in inflammatory cytokines due to an oxidative stress response leading to the upregulation of MTs, which has the potential to lead to an increased level of Zn²⁺ in the intracellular space [47]. The inflammatory response is caused by activated microglia and astrocytes, which produce proinflammatory mediators that can kill neighbouring neurons. Inflammatory responses include changes in the concentration of interleukin one alpha (IL-1 α), interleukin one beta (IL-1 β), interleukin 6 (IL-6), chemotactic factor interleukin 8 (IL-8), macrophage inflammatory protein-1 α (MIP-1 α), the transforming growth factor (TGF- β), tumour necrosis factor-alpha (TNF- α), monocyte chemotactic protein-1 and macrophage inflammatory protein-1. Prostaglandins, leukotriene, coagulation factor, protease and protease inhibitors all lead to the neuronal apoptosis seen in AD (see **Figure 1.12**) [2, 57].

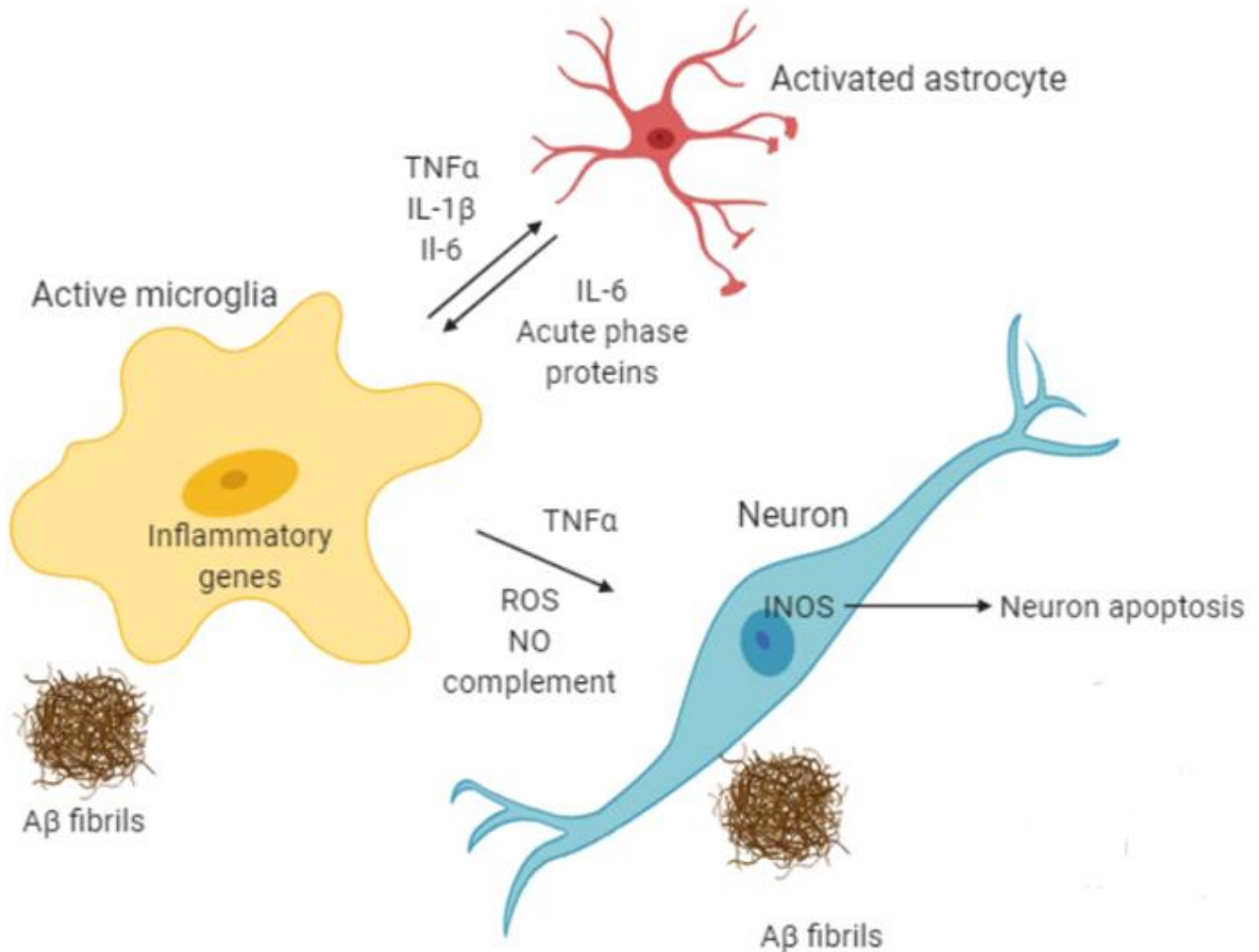


Figure 1.12: Schematic representation of the inflammatory mechanism in AD – adapted from [58].

A β peptides and tau NFTs activate the inflammatory response in the brain via the classical pathway, consisting of 20 or more serine protease components that can sequentially activate and function as an amplifying cascade. As a result, the cascade forms a membrane attack complex (MAC), which assembles on cell membranes, forming a transmembrane channel permitting the free diffusion of small molecules and ions (Ca^{2+}), disrupting the cell's homeostasis which can lead to cell death [57].

In AD, the A β stimulates the cytokines and chemokine processes in activated microglia, astrocytes, cerebrovascular endothelial cells, brain macrophages and T-cells [2, 57, 58]. The chemokines upregulate IL-1 α , IL-1 β , IL-6, IL-8, MIP-1 α , TGF- β , TNF- α , monocyte chemoattractant protein-1 and macrophage inflammatory protein-1 [57]. As a result, the astrocytes get stimulated to synthesize and secrete IL-6, acute phase proteins and other cytokines that stabilize microglia cells [58]. The autocrine-paracrine interactions in the brain between different cytokines and cells producing cytokines can either have an additive, inhibitory, synergistic or antagonistic effect [57].

The interaction of pro-inflammatory cytokines and chemokines is an example of an additive effect. It leads to the upregulation of APP and thereby increases A β peptides formation [57]. IL-1 and IL-5 are immunoregulatory cytokines that are overexpressed by activated microglia in the cerebral cortex, which promotes the synthesis of APP [57]. The increased IL-1 production also leads to the activation of astrocytes, which expresses A β binding proteins like α_1 -antichymotrypsin (α_1 -ACT), ApoE and complement protein C3, which are all found in elevated concentrations in A β plaques in AD patients [57]. IL-6 increases vascular permeability, and it activates lymphocytes and antibody synthesis. It acts as a significant pyrogen, which indicates that it mediates the CNS's immune and inflammatory response when it is expressed by microglia, astroglia and neurons in the brain, but where overexpression can cause CNS damage and even behavioural deficits in AD patients [57].

IL-8 and IL-10 are examples of chemokines that have cytokine-like activity and have leukocyte chemoattractant activity. They fulfil their biological activity through G-protein-coupled cell-surface receptors that can bind to different chemokines and are strictly regulated by inflammatory responses. The receptor's activity gets upregulated through activated microglia. These microglia produce MIP-1, MIP-1 α and MIP-1 β , though a dose-dependent interaction with A β [57].

Cytokines like IL-1 receptor antagonist (IL-1Ra), IL-10, IL-4 and TGF- β are examples of anti-inflammatory cytokines. The anti-inflammatory cytokines inhibit the production of pro-inflammatory cytokines. They are responsible for balancing in the brain's anti- and pro-inflammatory responses. An imbalance of this system causes deleterious amplification in cells, increases cytotoxicity and causes neuroinflammation [57]. Cyclooxygenase (COX) is a pro-inflammatory factor synthesizing prostaglandin, which is another inflammatory factor, where COX-2 is a potential risk factor for AD. COX-1 is produced by activated astrocytes, while COX-2 by astrocytes and neurons. An elevated level of COX-2 is present in NFT and damaged axons in the brain of AD patients. The selective inhibition of COX-2 with approved NSAID drugs (marketed for the treatment of arthritis) shows neuroprotective potential through the inhibition of prostaglandin production at the affected sites in the brain [57].

Other pathogenic AD pathways like the A β deposition and ACh dysfunction limits the efficacy of anti-inflammatory agents. ACh suppresses pro-inflammatory cytokines released from peripheral tissue-activated macrophages (as well as in microglia) [54]. TNF α and glutamate are both released from the activated microglial cells and can cause an increase in the likelihood of TNF α acting as neurotoxin provoking neuronal death [59].

Vitamin anti-oxidants, herbal extracts with antioxidant properties, and the use of non-steroidal anti-

inflammatory drugs (NSAIDs) have shown some protective effects against AD pathology [54]. NSAIDs used in anti-inflammatory therapy resulted in decreasing the patient's risk of developing or the onset of AD [54]. A 60 % reduction in the development of AD was observed together with the improvement of symptoms and slowing of the rate of the cognitive impairments caused due to AD. A 65 % decrease in the amount of A β -fibril associated microglia was also observed [54].

Drugs used for the treatment of AD targeting the inflammatory hypothesis can be seen in **Figure 1.13**. Rofecoxib (**21**) is a COX-2 NSAID, but has been shown to be ineffective for the treatment of AD [60]. Celecoxib (**22**) and naproxen (**23**) are COX inhibitors used in a study for the treatment of AD which both showed positive effects. However, the study was discontinued due to the cardiovascular concerns of using celecoxib (**22**) and the adverse reactions observed in the trial [57].

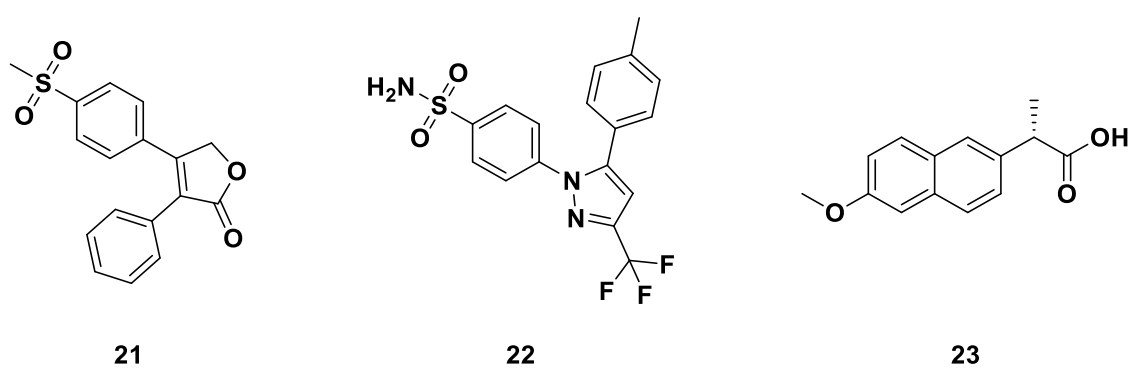


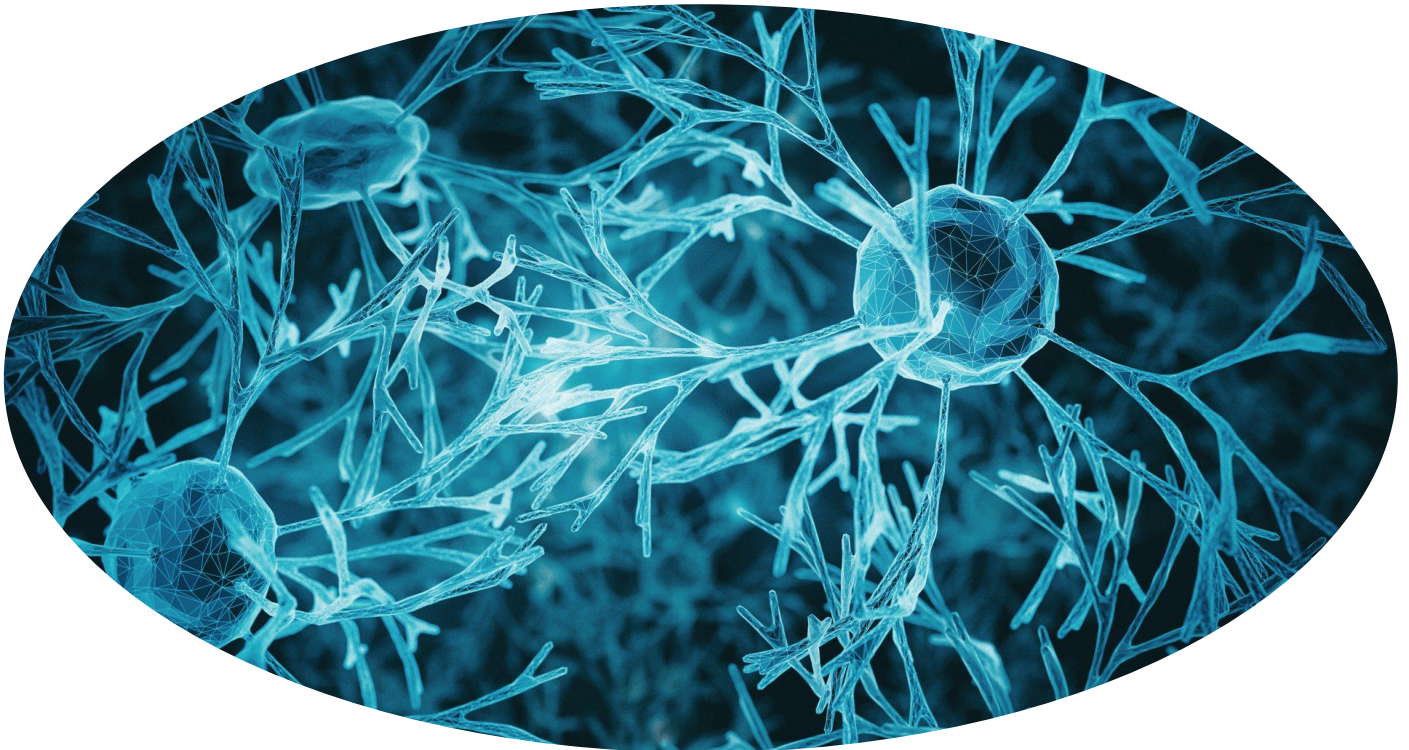
Figure 1.13: Drugs used for the treatment of AD with regards to the inflammatory hypothesis.

1.4.7. N-methyl D-aspartate hypothesis

NMDA is an ionotropic receptor (ion channel) found throughout the CNS which mediates the brain's neuroplasticity, the underlying mechanism of memory function and learning. NMDA binds glutamate and the co-factor glycine (or D-serine) causing the ion channel to open and allow the influx of only Na⁺, as Mg²⁺ blocks the influx of other ions [61]. The increased Na⁺ concentration forms an excitatory postsynaptic potential, which depolarizes the membrane. As a result, the Mg²⁺ ion gets removed, leading to the free movement of Ca²⁺ ions through the NMDA channel. The influx of these Ca²⁺ ions leads to several enzymatic processes involved in neuronal memory formation and the overactivation of the NMDA receptors results in the neural dysfunction and cell death in AD [61, 62]. Chapter 2 covers the NMDA hypothesis in more detail.

Chapter 2

Cholinergic and N-methyl D-aspartate hypothesis



2.1. Cholinergic hypothesis

2.1.1. What is the cholinergic hypothesis?

Researchers described the cholinergic hypothesis in the late 1970s. The dysfunction of cholinergic activity in the brain leads to the loss of memory and related cognitive impairments involved in dementia and AD. A small chemical messenger called a neurotransmitter, specifically ACh, is responsible for cognitive performance, learning and other memory processes acting by conducting electrical impulses from one nerve cell to another [10, 46]. Notably, ACh, ChAT and AChE levels have been shown to decrease steadily in patients afflicted with AD [2].

Interneurons and long-axon cholinergic pathways contain the primary neurotransmitter in the brain, ACh [6, 23]. The neurons containing ACh and glutamate are most widely affected in patients with AD and ACh is either found in neural synaptic spaces in their soluble form or the synaptic membrane in its membrane-bound form (see **Figure 2.1**) [9, 24].

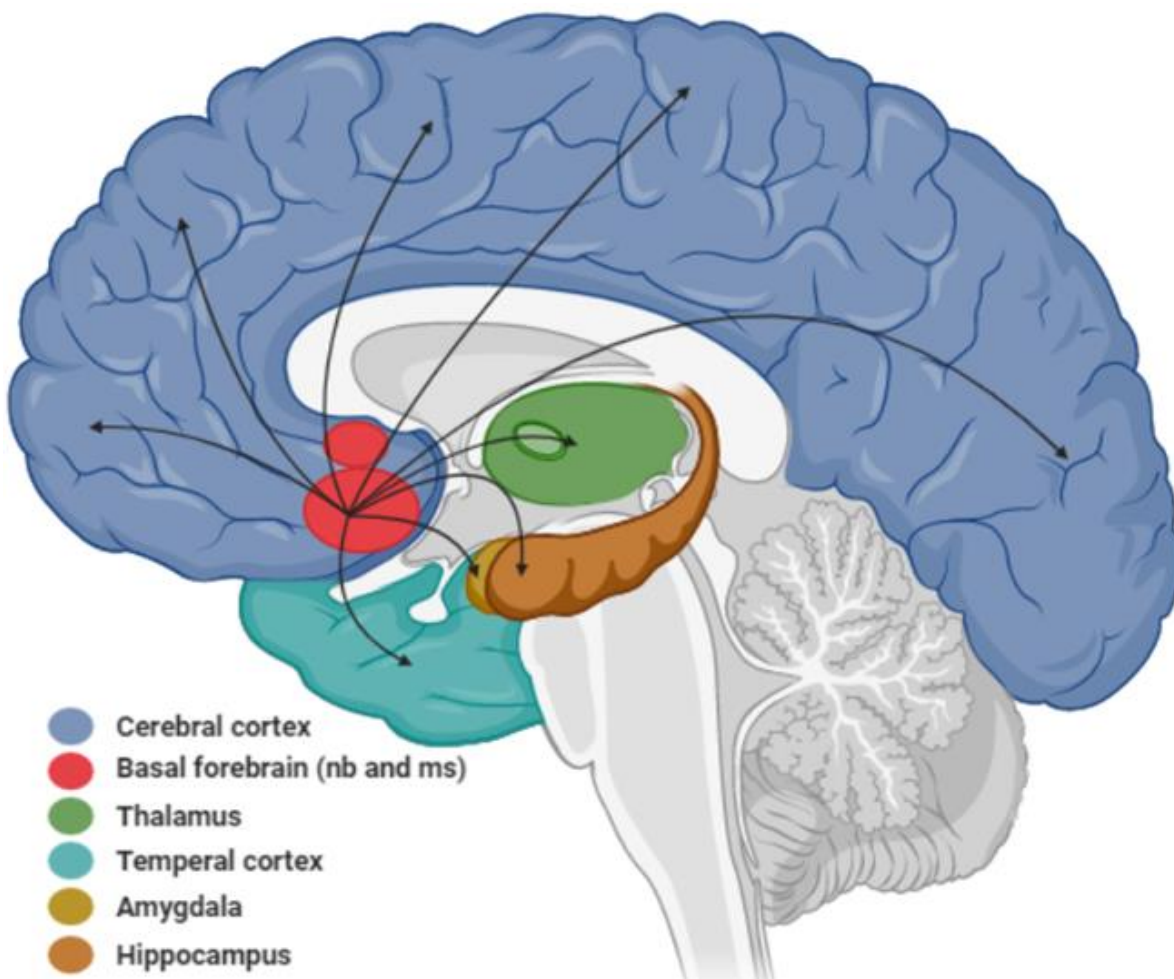


Figure 2.1: Choline transfer in the brain – adapted from [24].

ACh distributes in the brain through many different nuclei that fall under two groups, the basal forebrain and pedunculo-pontine. The group that has a pathological connection to AD is the movement of ACh from the *nucleus basalis* of Meynert (located in the basal forebrain) to the forebrain neocortex and associated limbic structures [25]. **Figure 2.1** represents this ACh movement from the basal forebrain, which consists of the nucleus basalis (nb) and the medial septal nucleus (ms) (red circles) to other regions of the brain. The largest ACh projection observed is to the limbic and the paralimbic regions which form part of the cerebral cortex. The thalamus, temporal cortex, amygdala and the hippocampus are other regions where choline is transported from [23]. In AD, a patient's selective attention, which is very low, is controlled by the cortex and thalamus ACh distribution levels, affect their conscious awareness and are linked to the cognitive and memory impairments observed [25].

2.1.2. Cholinergic cycle

Figure 2.2 illustrates how ACh in the brain is synthesized, transported and broken down. Near the presynaptic end of a neuron, ACh and CoA are synthesized through the catalysis of acetyl-CoA to choline through the enzyme ChAT (mechanism illustrated in **Figure 2.3**) [23, 29]. Most of the ACh molecules (approximately 10^4) formed through this process are stored and kept inside synaptic vesicles within presynaptic membranes. The synaptotagmin I protein found on the presynaptic membrane binds Ca^{2+} , resulting in an action potential forming across the presynaptic membrane. The Ca^{2+} channel on the presynaptic neuron, which forms part of the synaptic vesicle, opens, causing extracellular Ca^{2+} to influx into the membrane. The influx of Ca^{2+} into the cell results in the exocytosis of the synaptic vesicle, which releases ACh into the synaptic cleft [23, 29].

The ACh released into the synaptic cleft transmits nerve impulses across the synapses between certain types of nerve cells. They connect to the transmembrane acetylcholine receptor (AChR) on the postsynaptic membrane [29]. Binding of a second ACh molecule to the receptor induces the opening of a Na^+ channel in the postsynaptic membrane that allows for the diffusion of Na^+ ions into the cell for 1 to 2 ms releasing ACh as a result. An intracellular response causes the activation of the AChE membrane protein, situated on the surface of the postsynaptic membrane, to hydrolyse ACh into acetic acid and choline (see the mechanism in **Figure 2.3**) terminating the nerve impulse [29]. The choline is then taken up by the presynaptic cell via a choline channel and reused to form ACh [29].

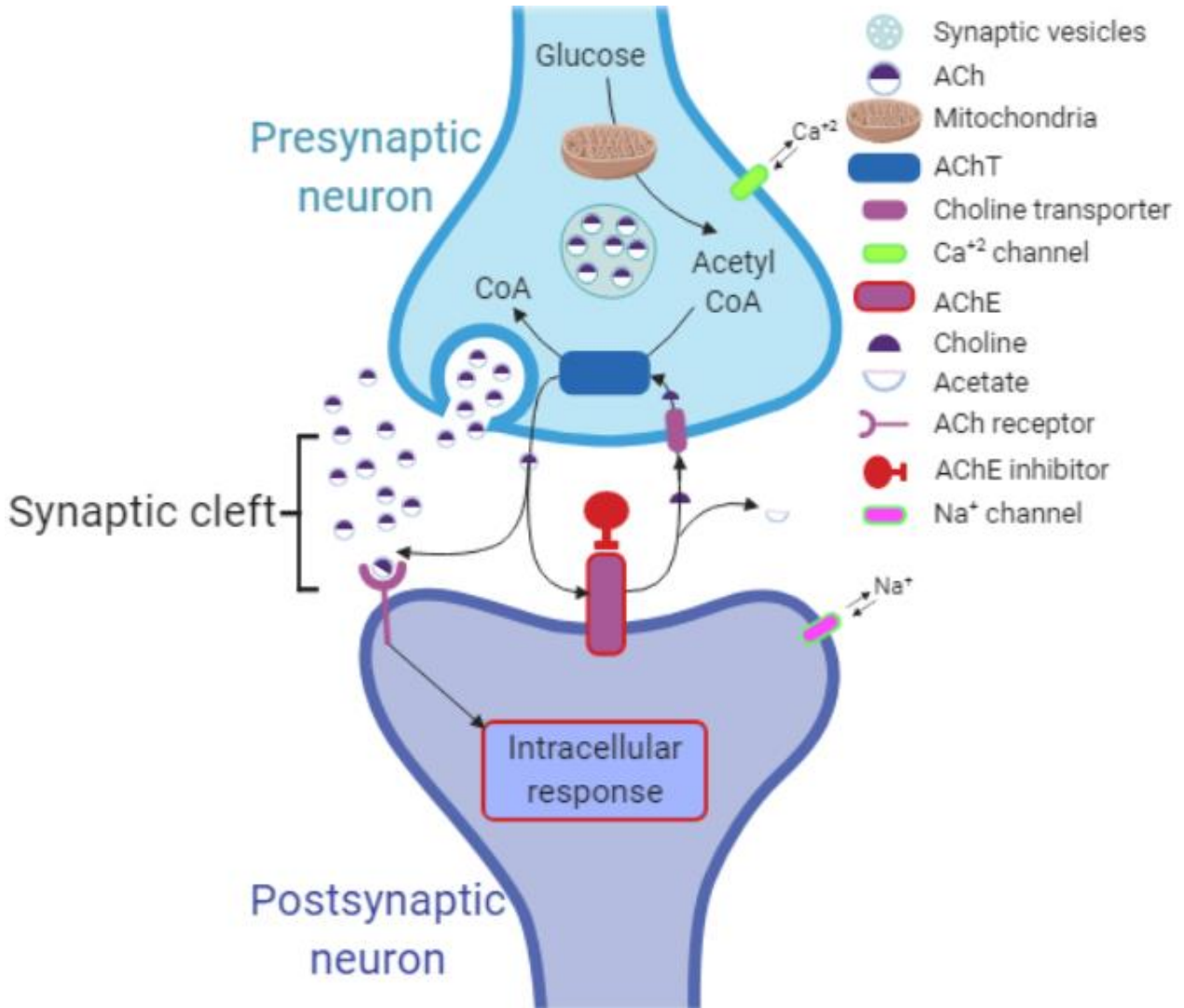


Figure 2.2: ACh neurotransmission in the brain – adapted from [64].

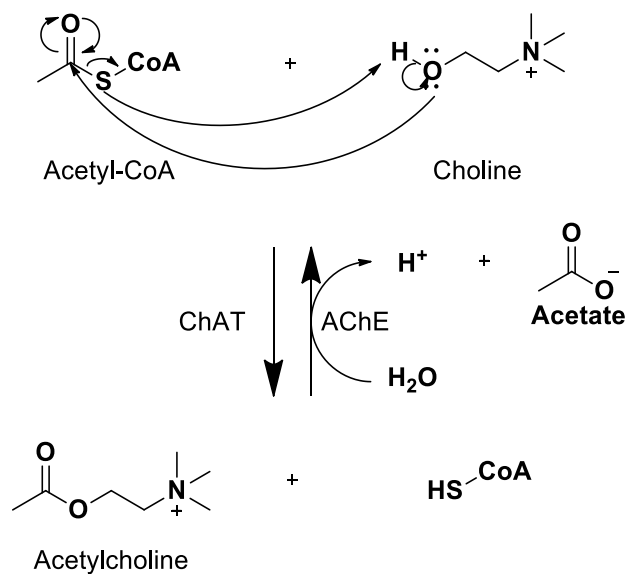


Figure 2.3: Synthesis of ACh via ChAT and the breakdown of ACh via AChE – adapted from [29].

By increasing the level of ACh in the brain through the improvement of the dysfunction of cholinergic activity could reduce the impairments caused in this system due to AD [10]. As a result the development of AChEIs became attractive as a means of increasing levels of ACh through the inhibition of its clearance [2, 10].

2.1.3. Acetylcholine esterase

Conducting tissue like nerve cells, muscle cells, central and peripheral tissue contain choline esterases of the CNS. They are also found in motor and sensory fibers, cholinergic and non-cholinergic fibers, and in blood cell membranes. The esterases provide a similar catalytic function. Structurally, they differ in their oligomeric assembly and mode of attachment to cell surfaces. The two classes of choline esterases are AChE and butyrylcholine esterase (BuChE). BuChE is primarily found in the liver but also occurs in plasma [23, 24]. AChE and BuChE hydrolyse ACh, but in AD patients, the activity of BuChE is 50 % up-regulated in the hippocampus and temporal cortex compared to people who do not have AD [46].

Figure 2.4 is a schematic representation of the enzyme, AChE, which is one of the α/β hydrolase protein subfamily and consists of 12 β -sheets that are surrounded by 14 α -helices (can be observed in **Figure 2.5**) and is the one that is most closely related to BuChE [23, 63]. It is a 45 Å x 60 Å x 65 Å ellipsoidal shaped serine hydrolase monomer containing 537 amino acids [23]. The enzyme contains a deep and narrow hydrophobic gorge (20 Å long), lined with fourteen aromatic amino acid residues, penetrating halfway into the enzyme, widening out close to the base [6, 23].

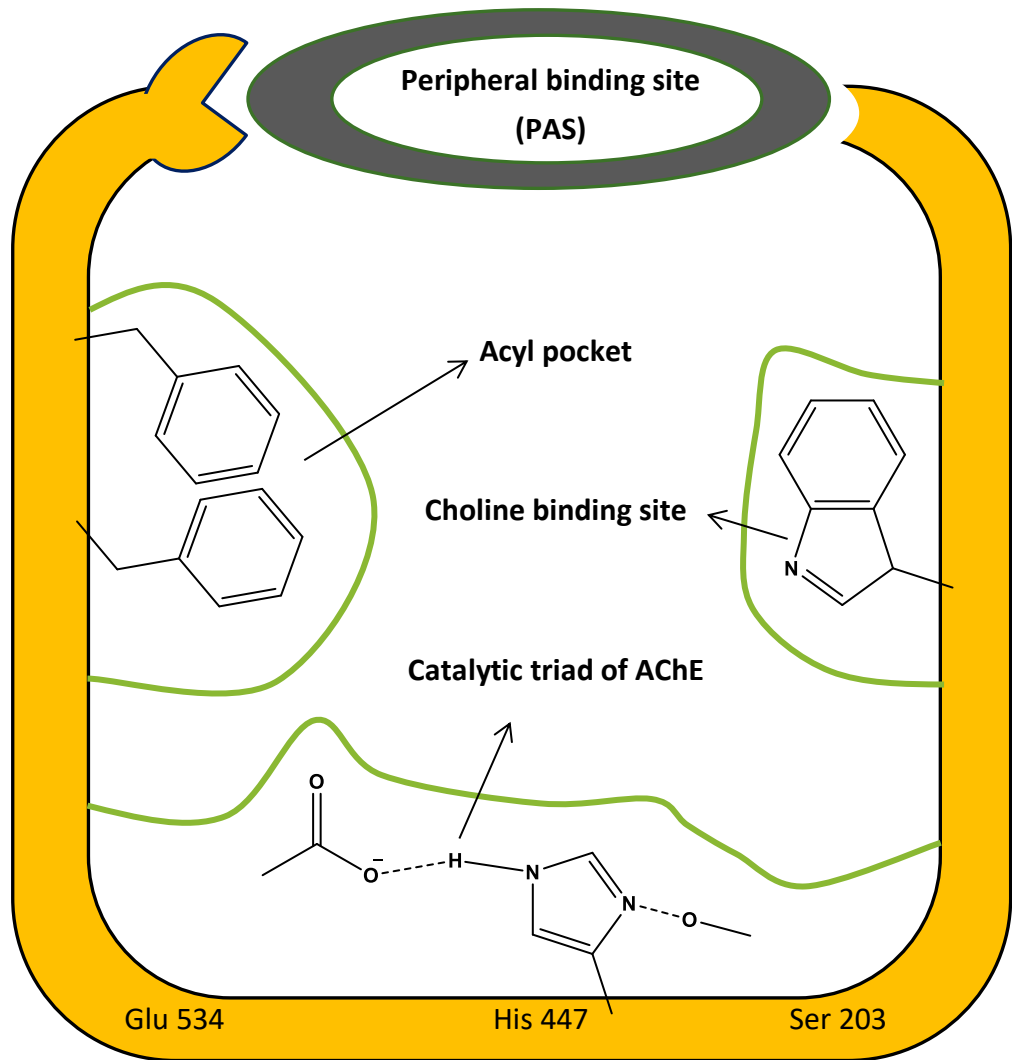


Figure 2.4: Schematic representation of the AChE active site – adapted from [24].

AChE contains a peripheral anionic site (PAS) (shown as green spheres in **Figure 2.5**) located at the entrance to the active site gorge, 20 Å from the active site. The PAS consists of 5 amino acid residues: Tyr 70, Asp 72, Tyr 121, Trp 279 and Tyr 334. The PAS serves as a binding site for ACh and acts as the binding site for other uncompetitive inhibitors of AChE and allosterically modulates the catalytic cycle [23, 64]. The PAS amino acids Tyr 70, Tyr 121 and Trp 279 have aromatic rings that interact with charged groups on ligands [63]. The Trp 279 and Asp 72 may have different interactions depending on the nature of the ligand introduced to the enzyme. Trp 279 can undergo stacking, aromatic-aromatic and π -cation interactions while the Asp 72 can have charge-charge interactions or hydrogen-bonded interactions with the ligand [63]. The PAS mode of action involves the short-lived initial binding of a substrate and then trapping it to improve catalytic efficiency as the substrate moves towards the active site. Once a substrate binds to the PAS it induces a conformational change in the enzyme's gorge, causing a change in the active site. This change causes an

accelerated carbamylation at the active site [63]. Cell adhesion, neurite outgrowth in both developing or transformed neural cells and amyloidosis are examples of non-cholinergic functions that the PAS obstructs [63].

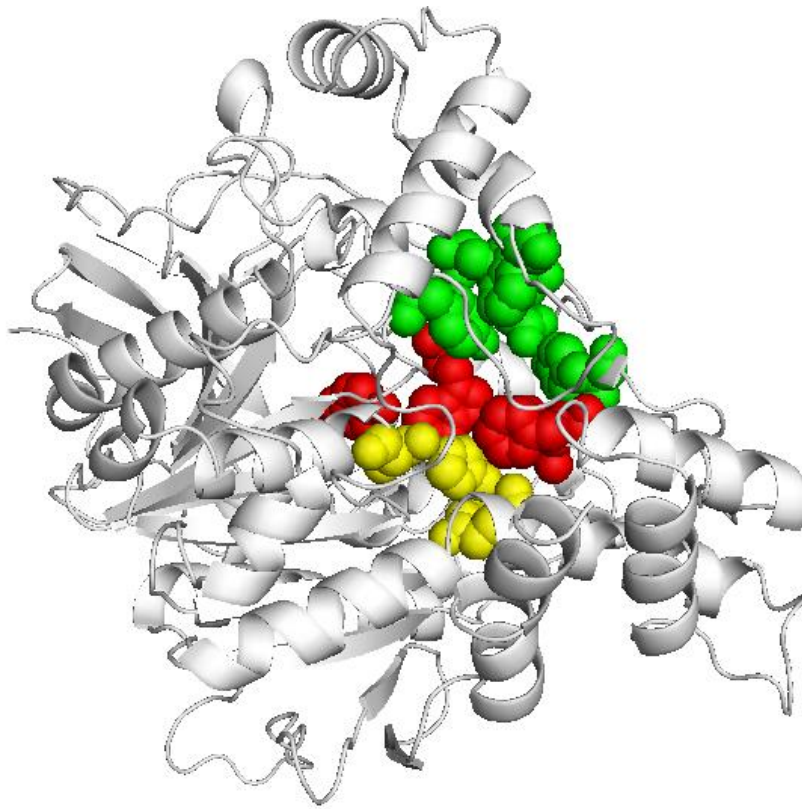


Figure 2.5: *Torpedo* AChE image illustrating the active site (yellow), anionic site (red) and PAS (green) – adapted from [64].

The active site, 4 Å above the bottom of the gorge, consists of two subunits called the anionic subsite (shown as red spheres in **Figure 2.5**) and the catalytic site (CAS) (shown as yellow spheres in **Figure 2.5**) [23, 64]. The anionic site corresponds to the catalytic machinery of the enzyme, which consists of Trp 84, Tyr 130, Tyr 330 and Phe 331. These amino acids are involved in π stacking interactions between the enzyme and the substrate [63]. These amino acids are uncharged, lipophilic and bind to the amine moiety of ACh, forming the acyl pocket seen in **Figure 2.4**. The CAS corresponds to the choline-binding pocket where ACh is hydrolysed and is located at the base of the 20 Å gorge containing a catalytic triad of three amino acids: Ser 200, His 440 and Glu 327 [6, 23, 63].

The area surrounding the PAS consists of ten acidic residues, called an annular electrostatic motif, and is not shared with BuChE [63]. As a result, AChE can funnel polar substances to their active site through interactions on the surface of the enzyme [29]. **Figure 2.6** indicates the two surface loops that are associated with the

PAS and the CAS of the enzyme. The large omega loop, Cys 69 – Cys 96 (**Figure 2.6** loop shown in green), is associated with Tyr 70 and Asp 72 of the PAS [63]. The Cys 96 section of the omega loop, forming the outer wall of the gorge, is associated with Trp 84 from the anionic site [63]. These loops contribute to the conformational flexibility of the enzyme [63].

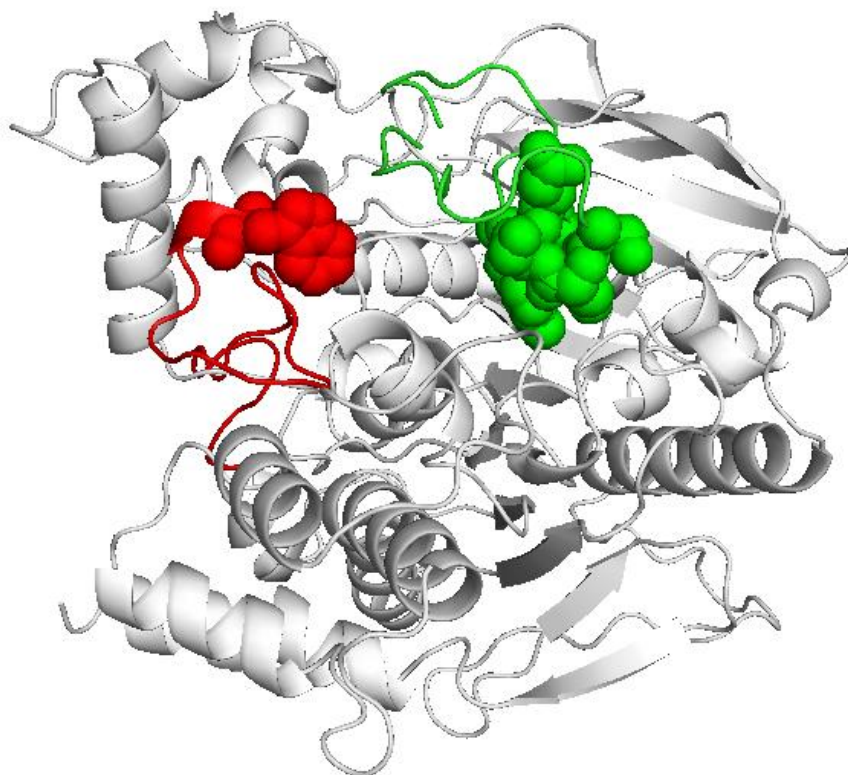


Figure 2.6: *Torpedo* AChE showing the PAS-associated omega loops. Omega loop 69-96, shown in green, including the two PAS residues Tyr 70 and Asp 72. Omega loop 274-308, shown in red, including the PAS residue Trp 279 – adapted from [64].

Hydrophobic binding of residues 275 – 305 through the surface loop of AChE allows for binding to A β -peptides and actively promotes the amyloid fibril formation resulting in senile plaques in AD [46, 63]. Due to their affiliation with A β -peptide formation and the fact that the concentration of ACh in the brain of AD patients is so low resulted in the development of AChEIs and other cholinergic receptor modulators to increase the ACh concentration in the brain [2, 10, 63].

AChEIs are only one of six classes of drugs developed to enhance the decrease of ACh in AD patients. These include the increased bioavailability of choline through choline precursors, wherein, ACh is released at presynaptic end terminals through choline releasers, increasing the amount of ACh released will increase the ACh concentration in the cells. Designing M1 and M3 receptor agonists that interact with postsynaptic

end terminal receptors just like ACh. M2 and M3 receptor agonists, which are presynaptic receptors, regulate the ACh concentration via negative feedback. Nicotinic agonists or substances can also enhance ACh release through the nicotinic effect [6]. Overall, AChEIs have proven to be the most effective in reducing symptoms through the improvement of the cholinergic deficit shown in patients suffering from AD [6].

2.1.4. Attempts to target acetylcholine breakdown - acetylcholinesterase inhibitors

AChEIs are reversible inhibitors that prevent the rapid breakdown of ACh and allow normal signalling of nerve impulses, thereby maintaining a steady level of functioning brain cells in regions of the brain involved in learning, memory, behaviour and emotional responses [2, 23, 29, 46, 65]. Inhibiting AChE decreases the effect of neural damage as a result of the cytotoxic effects of AD [9].

AChEIs act by either restoring the amount of ACh available in the synaptic cleft, decreasing A β deposition, protecting against free radical toxicity and β -amyloid induced injury, preventing increased production of antioxidants, inhibiting the release of cytokines from monocytes and microgli, functioning as an anti-inflammatory agent or leading to the hyperstimulation of nAChRs and mAChRs [23, 46, 54, 66].

AChEIs relieve not only cognitive symptoms but they also improve neuropsychiatric symptoms that include hallucinations, apathy, fear, sadness and anxiety [24, 25]. Neuropsychological deficits can improve through the functional restoration of the limbic and paralimbic cortices. This in turn leads to an increased score or a superior performance on a patient's cognitive subscale of the Alzheimer's disease Assessment Scale, Mini-Mental State examination, and the Clinician Interview-Based Impression [24].

The AD symptoms (cognitive and behavioural) can only be improved in a dose-dependent manner when using AChEIs and only to a certain extent due to the limited efficacy of these drugs [2, 5, 46]. As AChEIs do not affect disease progression itself but rather provide symptomatic relief of the disease, researchers have concluded that the cholinergic system is only a downstream mechanism involved in AD [10].

Side effects of using AChEIs include nausea, vomiting and diarrhoea. However, a higher dose during clinical trials indicated an increase in the mentioned symptoms but additionally included muscle cramps and fatigue [5]. That being said, in some patients, cognitive improvement is noted and in most there are observable emotional benefits, suggesting that the use of AChEIs although not a cure can still be beneficial in patients afflicted with AD [24].

2.1.5. Examples of acetylcholinesterase inhibition – FDA approved drugs

See **Figure 2.7** for FDA approved AChEIs. Tacrine (Cognex; $IC_{50} = 167 \text{ nM}$; **24**) is a reversible inhibitor and was approved by the FDA in 1993 for the treatment of mild to moderate AD [2, 6]. It can slow down the decline of cognitive function and memory loss of patients if sufficient doses are given for 3 – 6 months. [26]. Due to hepatotoxicity as a severe side effect, the drug was withdrawn from the market [6, 46]. There have been several attempts to lower the toxicity of tacrine by changing the ring structures, however, a suitable alternative which maintains the activity of tacrine has not yet been reported [46]. Another option considered was forming more active dual inhibitors, one inhibiting the active site and the other inhibiting the peripheral binding site (PBS) of AChE by forming dimers, substituted dimers and changing the linker group between dimers [46].

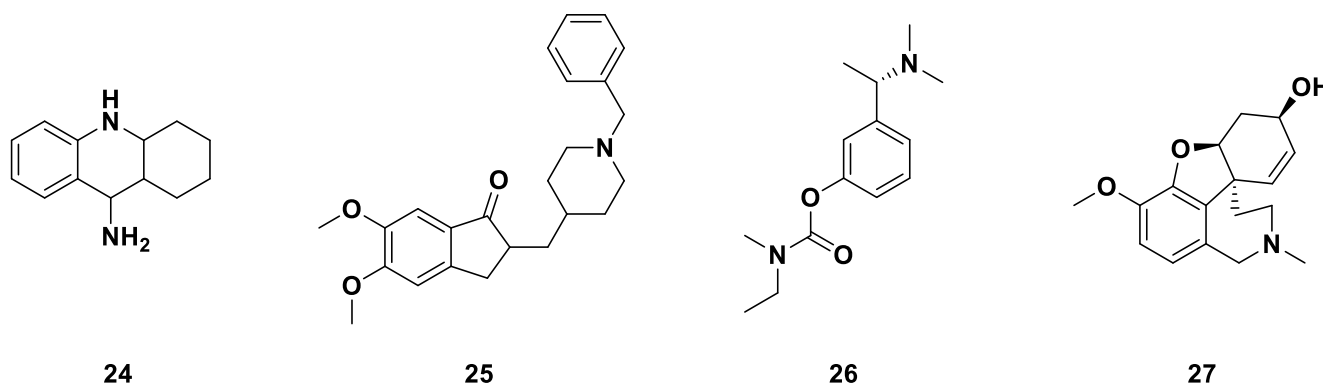


Figure 2. 7: FDA approved AChEIs (**24-27**).

Donepezil (Aricept; $IC_{50} = 5.7 \text{ nM}$; **25**) has reversible activity, it was FDA approved in 1996 and is prescribed for the treatment of mild to moderate AD symptoms [2, 5, 6, 23, 24, 46]. Donepezil (**25**) interacts with the CAS and the PAS of AChE, affords a dose-dependent improvement in cognitive function and only requires a once daily dose as donepezil (**25**) has a half-life ($t_{1/2}$) of 70 h [5, 9, 23, 46]. It is 100 % oral bioavailable, crosses the BBB with ease, and is excreted via the renal and cytochrome P450 (CYP450) system [5, 23].

Rivastigmine (Exelon; $IC_{50} = 4.150 \text{ nM}$; **26**) was FDA approved in 2000 and it contains a carbamate moiety that reacts covalently with the active site of the enzymes and carbamylates the serine residue of the catalytic triad in a pseudo irreversible manner [2, 6, 46]. Side effects include nausea, vomiting, diarrhea, loss of appetite, dizziness, and fatigue [6].

Galantamine (Razadyne, Nivalin; $IC_{50} = 800 \text{ nM}$; **27**), a natural product, was first synthesized chemically in 1960 and subsequently received FDA approval for the treatment of AD in 2001 [2, 6]. It is a reversible inhibitor of AChE, has a dual mechanism binding to the cholinergic system's CAS and PAS, increasing the release of ACh [2].

2.1.6. Structural modification of Donepezil and related derivatives

Figure 2.8 indicates the process of how the four parts of the indanone-piperidine derivative of donepezil (**25**; **Figure 2.9**) were synthesized by testing numerous options and finding the best-balanced compound in terms of activity and pharmacokinetics. The synthesis started with a random screening performed by the Sugimoto group, which then led to the discovery of **28** which was synthesized in a separate study for anti-arterial sclerosis. The IC_{50} value for **28** was found to be 12'600 nM in rat brain homogenate when screened against AChE. Replacing the *N*-benzylpiperazine with *N*-benzylpiperidine afforded an increase in the anti-AChE activity for **29** with an IC_{50} value of 340 nM. The ether moiety was replaced by an amide moiety giving **30** further improving the IC_{50} value to 55 nM. The functional group on the para-position of the benzamide group caused either an increase or decrease in the potency of the compound, with the most potent derivative being **31**, with an IC_{50} value of 0.6 nM. Unfortunately, **31** had a reduced bioavailability rate. Further examination used **32** ($IC_{50} = 560 \text{ nM}$) as a parent molecule for the development of potential AChEIs. Their next attempt involved using a ketone to replace the amide group affording **33** with an IC_{50} value of 530 nM. Cyclizing the amide derivative gave **34** with an IC_{50} value of 98 nM. Thereafter, incorporating both the ketone and the five-membered ring, forming an indanone moiety, gave **35** with an IC_{50} value of 230 nM. Although less active, **35** showed a longer duration of action [6].

The group then synthesised different indanone derivatives, evaluating each part of **35** separately to generate the best AChEI, ultimately replacement of the indanone ring system with a dimethoxy indanone ring system (section 1 of **35**, **Figure 2.9**) and the ethyl linker with a methyl linker (section 2 of **35**, **Figure 2.9**) afforded the best-balanced compound, donepezil (**25**) [6].

In the case of part one of **35**, the five-membered ring portion of the indanone moiety, was replaced with larger cyclic systems, leading to a decrease in activity. However, the introduction of methoxy groups onto the indanone moiety increases the activity, and the addition of the methoxy groups at the 5th and 6th carbon increased the activity 25-fold seen in part 1 of **25**. The ketone carbonyl group was indicated to be essential for the activity of the inhibitor and was kept in further analysis.

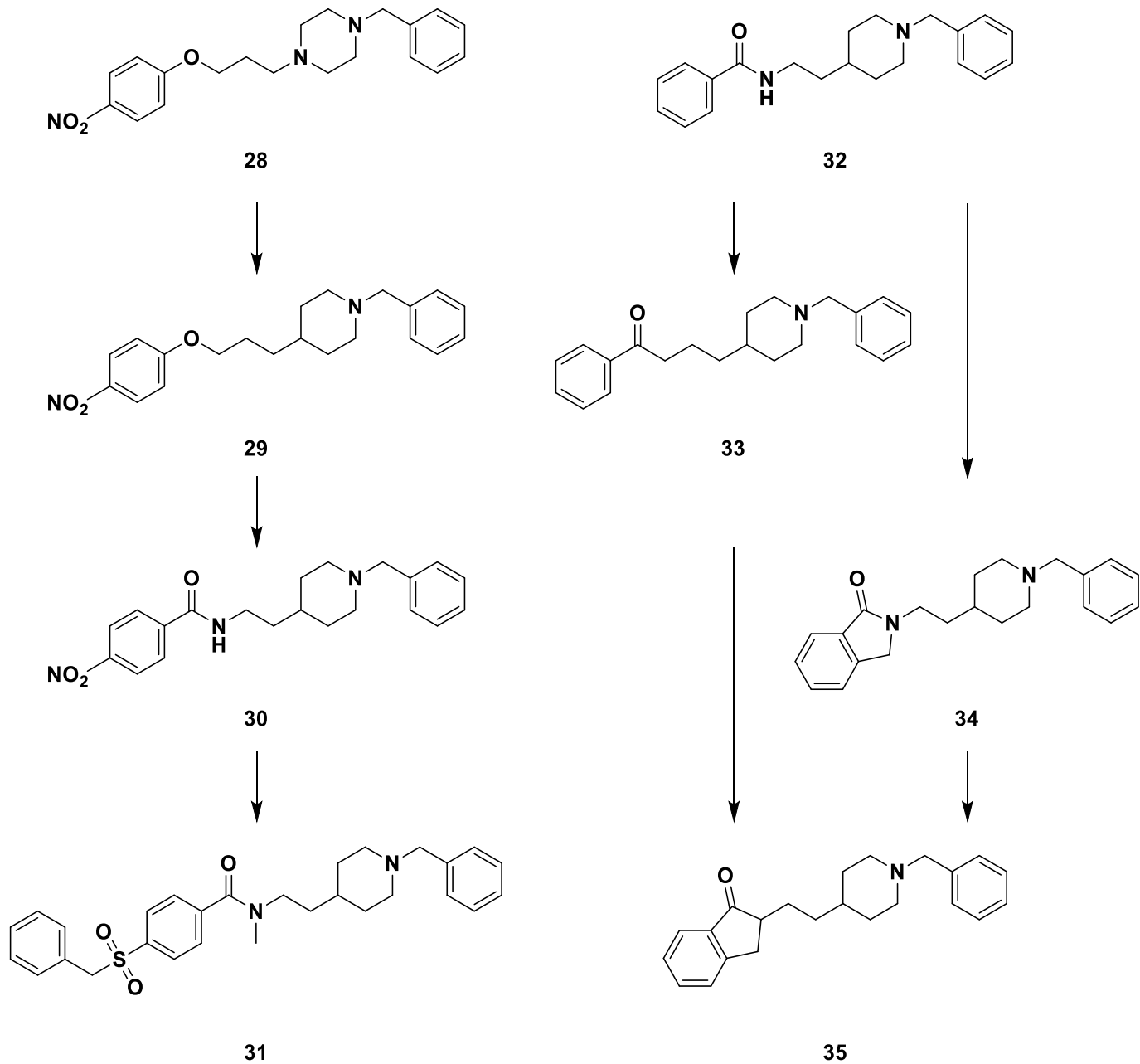


Figure 2.8: Synthetic analysis of the development of the four parts of the indanone-piperidine derivative.

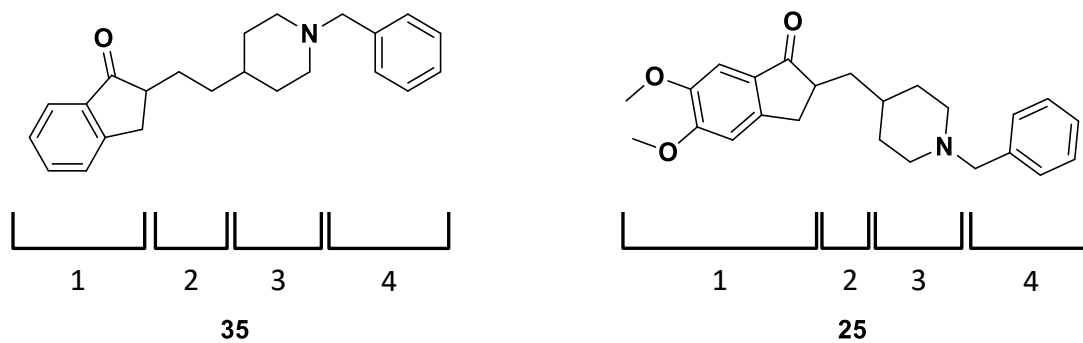


Figure 2.9: Four parts of 35 and compared to that of the four parts of donepezil (25).

Change in the linker length (part 2 of **35**) leads to a range of inhibitions with a propyl linker giving the best results, followed by the methyl linker. The methyl linker in part 2 for **25** was used in further analysis by the group. Part 3 of **35** was changed by having the *N*-atom at different positions or increasing the number of nitrogen's in the ring. Ultimately, retaining the original piperidine moiety proved to be the best option and was kept in further analysis.

Replacement of part 4 with different benzyl groups (2- / 3- / 4-benzyl) and substituted benzyl groups or even larger conjugated systems resulted in a range of suitable ligands, however, the simple unsubstituted benzyl system proved best. Ultimately, donepezil (**25**) is one of the most potent compounds developed for AChE inhibition, having an IC_{50} value of 5.7 nM [6].

In subsequent years, further development of donepezil-like drugs, resulted in the development of more active derivatives as potential anti-Alzheimer's drugs (see **Figure 2.10**) [46]. Icopezil (**36**; IC_{50} = 0.33 nM) has more than a 10'000-fold selectivity towards AChE over BuChE. Substituting the indanone ring with an indole or pyrrole ring led to more compact AChEIs such as **37** (IC_{50} = 6000.00 nM), but their rigid structures resulted in reduced penetration into the AChE gorge thereby decreasing their AChE inhibitory capabilities. TAK-147 (**38**; IC_{50} = 51.20 nM) has a higher selectivity for AChE versus BuChE (518-fold) due to dual binding characteristics to the PAS and CAS site of AChE. A donepezil-tacrine hybrid (**39**; IC_{50} = 90.00 μ M) interacts with the PAS, active, and mid-gorge binding site of AChE. The compound **40** which shares several structural features with donepezil **25** showed an IC_{50} value of 0.0018 μ M.

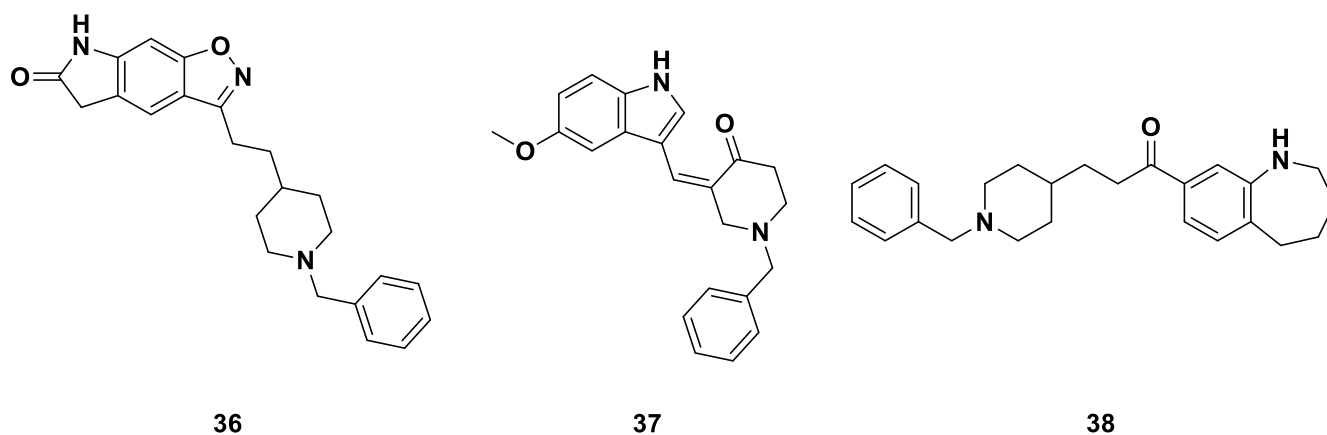


Figure 2.10: Examples of donepezil derivatives as potential anti-Alzheimer's drugs.

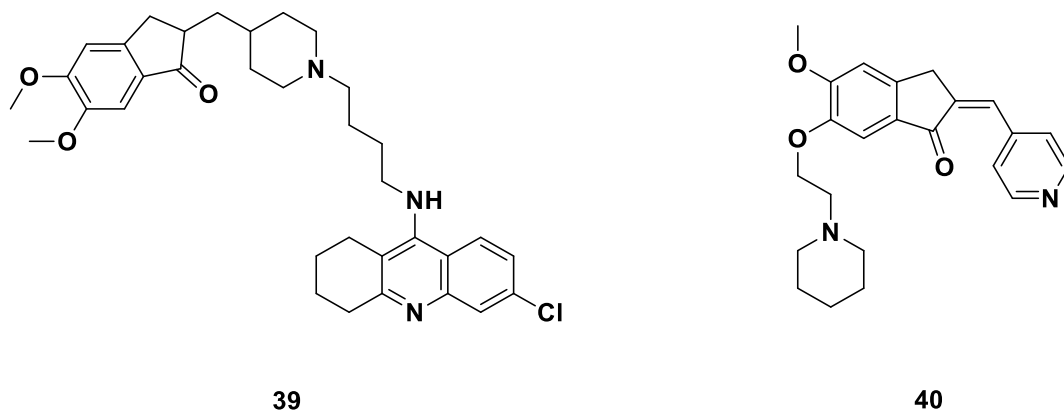


Figure 2.10: Examples of donepezil derivatives as potential anti-Alzheimer's drugs

2.1.6.1. Acetylcholinesterase inhibitions currently under trials

The AChEI currently in clinical trials can be seen in **Figure 2.11**. In the case of (-)-phenserine (**41**), cognitive impairment and a reduction in the translation of APP to reduce the A β concentration is noted [2]. Ladostigil (**42**) shows scopolamine-induced impairment relief in spatial memory and it increases brain cholinesterase activity. It is anti-apoptotic, neuroprotective, can regulate the APP process, facilitates the activation of protein kinase C and even regulates the mitogen-activated protein kinase signalling pathways in rats. NGX267 (**43**) is an M1-selective muscarinic agonist that can enhance cognitive abilities and was shown to reduce A β ₁₋₄₂ and tau hyperphosphorylation in AD transgenic mice [2]. EVP-6124 (**44**) is a partial selective α -7 nicotinic acetylcholine receptor (α 7-nAChR) agonist currently in phase III trials. It increases the patient's ACh response and, in turn, improves cognitive deficits [2]. The selective agonist, GTS-21 (**45**), of the α 7-nAChR is currently in Phase II AD treatment and had indicated a significant cognitive enhancement with regards to attention, working memory and episodic secondary memory through the activation of the cholinergic receptor and blocking neurodegeneration [2, 67].

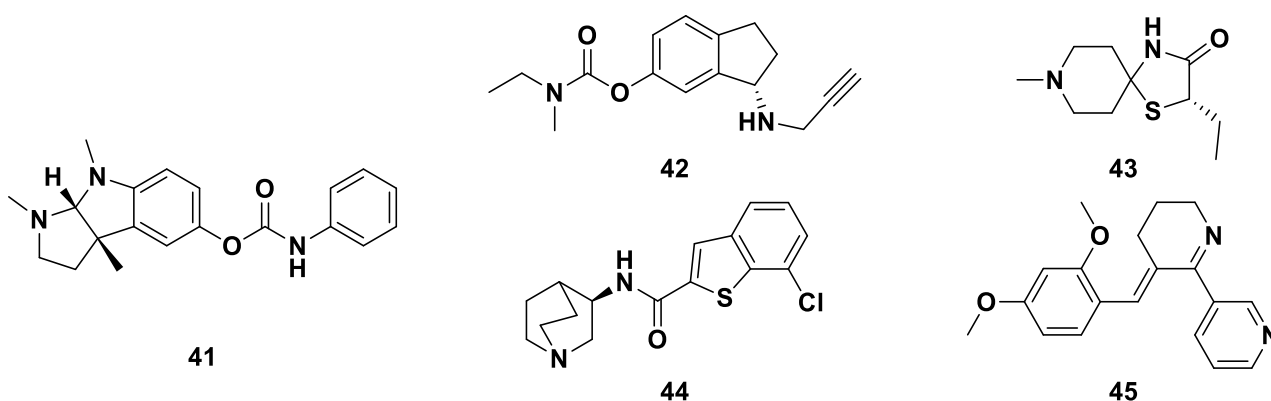


Figure 2.11: AChEI undergoing clinical trials.

2.1.6.2. In-house development of acetylcholinesterase inhibitors in the Riley group

Recently we have developed several neuroprotective hits and leads in-house. Lead compound, 5,6-dimethoxy-1-oxo-2,3-dihydro-1*H*-inden-2-yl 1-benzylpiperidine-4-carboxylate (**46**, see **Figure 2.12**), with an IC_{50} value of $0.03 \pm 0.07 \mu\text{M}$ was synthesized as part of a library of 27 AChEIs. The design process focused on probing the chemical space surrounding the donepezil scaffold (**25**), in particular, the methyl linker moiety (**A** in **47**, in **Figure 2.12**; part 2 of the donepezil scaffold) was replaced with a methylene, ester, reverse ester or ketone linker (see **Figure 2.13**: **48-51**) and the piperidine ring (**B** in **47**, in **Figure 2.12**; part 3 of the donepezil scaffold) was exchanged for 3-6 membered saturated *N*-containing ring systems (see **Figure 2.13**: **52.1-60.2**) [68].

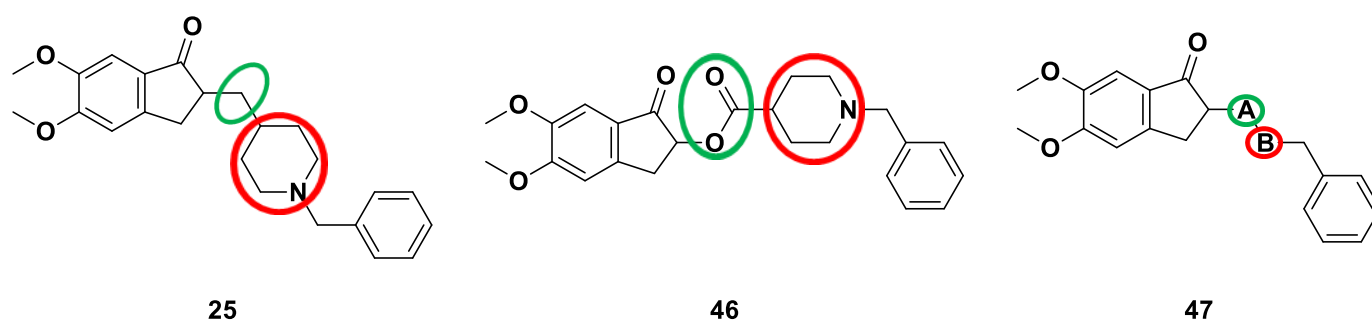


Figure 2.12: Lead compound formed through the change of the donepezil scaffold part A (green) and B (red).

The methylene linked ligands (**62**, see **Figure 2.14**) were accessed by an aldol condensation with dimethoxyindanone **61** and appropriate aldehydes after which hydrogenation afforded the methyl linked ligands **63**. In almost all instances compounds containing the methylene and methyl linkers showed better activity compared to the FDA approved drug galantamine (3.57 mM) [68].

The incorporation of an ester linker (**49**) was achieved through the carboxylation of **61** forming **64** (see **Figure 2.15**) and then transesterification with various alcohols to access scaffold **65**. The ester linked ligands resulted in loss of activity for all systems with the exception of **60.2**. Interestingly, reversing the orientation of the ester linker, forming a reverse ester linker, through the bromination of **61** followed by S_N2 displacement with the carboxylic acid (of **59.1**) resulted in **46** which increased activity dramatically, affording an IC_{50} value of $0.03 \mu\text{M}$, versus that of donepezil (**25**) which has an IC_{50} value $0.05 \mu\text{M}$. The replacement of this reverse ester with a ketone linker (**51**) also indicated a good AChE inhibition of $0.66 \mu\text{M}$ [68].

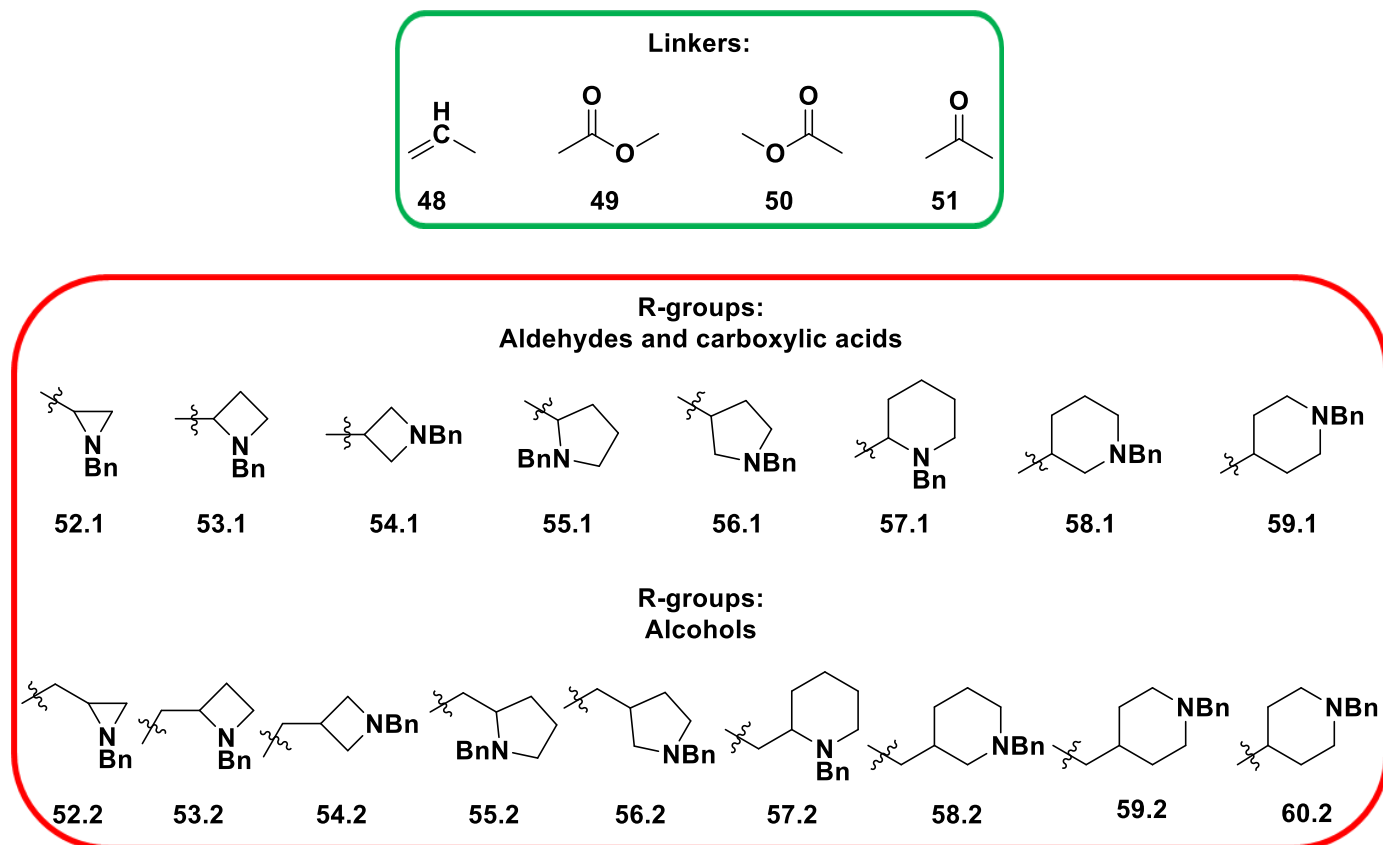


Figure 2.13: Linkers (A-green block) and R-groups (B-red block) involved in the synthesis of the different ligands to analyse the chemical space surrounding the donepezil scaffold.

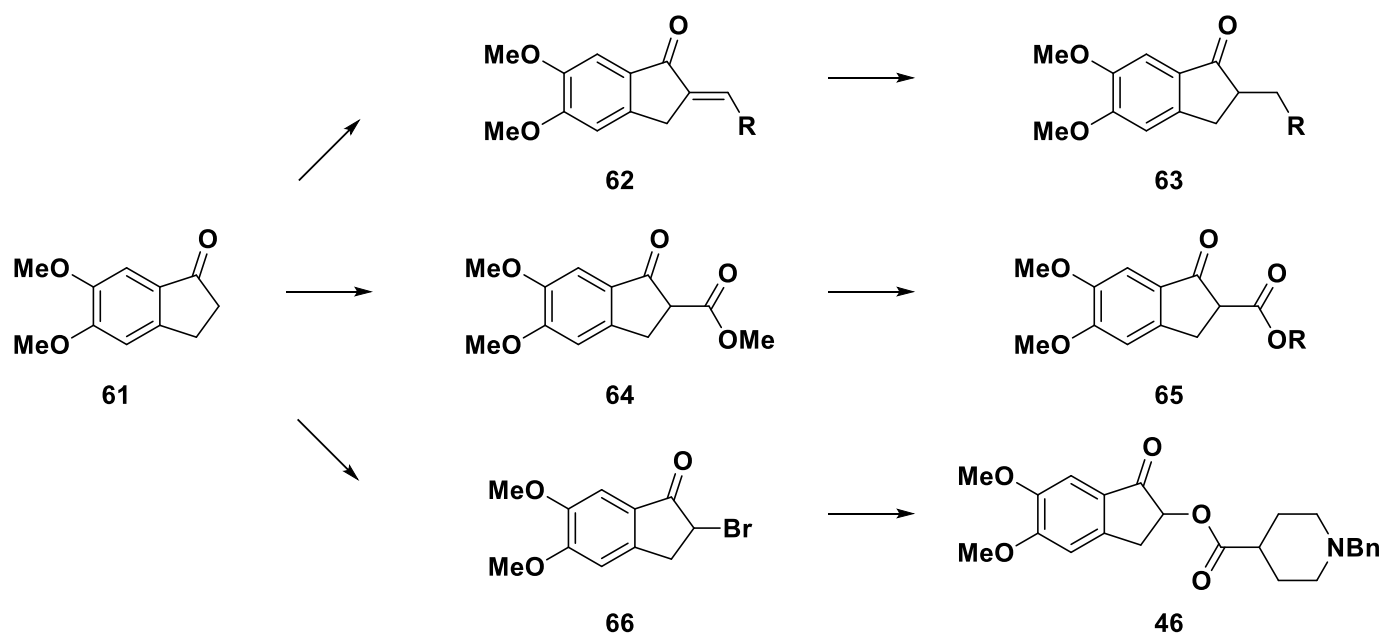


Figure 2.14: Synthesis of different linkers and addition of the different R groups.

The reverse ester containing compound (**46**) was thereafter further modified in **Figure 2.15** by exchanging the ester linker (**B** in **46**), which represented a metabolic liability in the lead compound, with a more stable amide linker (**B** in **67**) and the indanone-moiety (**A** in **46**) with a range of aromatic heterocycles (**A** in **67**).

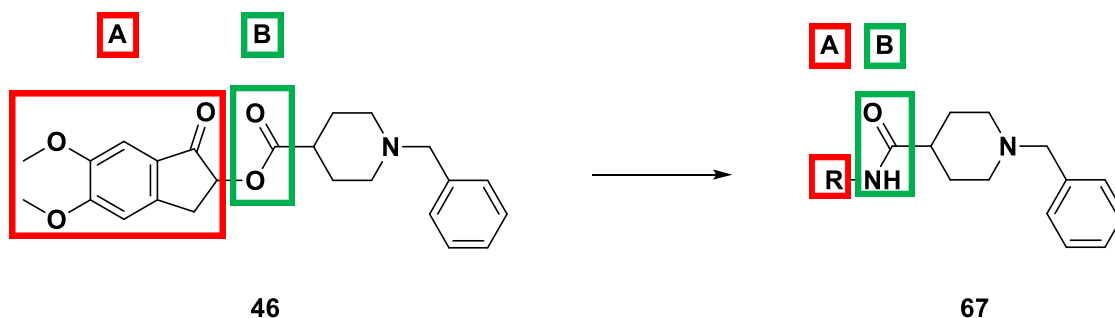


Figure 2.15: Improvement on previous lead compound (**46**) through changing part **A** and **B**.

The amide linker was accessed in **Figure 2.16** by coupling *N*-benzylpiperidine imidazole (**68**) with commercial and synthetic heterocyclic amines (**70.1-70.15**) in the presence of catalytic amounts of 4-(dimethylamino)pyridine (4-DMAP) affording amide coupled products **69**.

Two promising compounds in **Figure 2.17** were identified namely, 1-benzyl-*N*-(1-methyl-3-oxo-2-phenyl-2,3-dihydro-1*H*-pyrazol-4-yl) piperidine-4-carboxamide (**71**) with an IC_{50} value of $5.94 \pm 1.08 \mu\text{M}$ and 1-benzyl-*N*-(5,6-dimethoxy-8*H*-indeno[1,2-*d*]thiazol-2-yl)piperidine-4-carboxamide (**72**) with an IC_{50} value of $0.41 \pm 1.25 \mu\text{M}$ [69]. In both instances there is a loss in AChE inhibition activity when compared to **46**, however, it is important to note that these amide linkers reduce the metabolic liability associated with the ester in **46**. Compound **72** was ultimately selected for continued in-house development due to superior pharmacokinetic parameters and predicted BBB permeability.

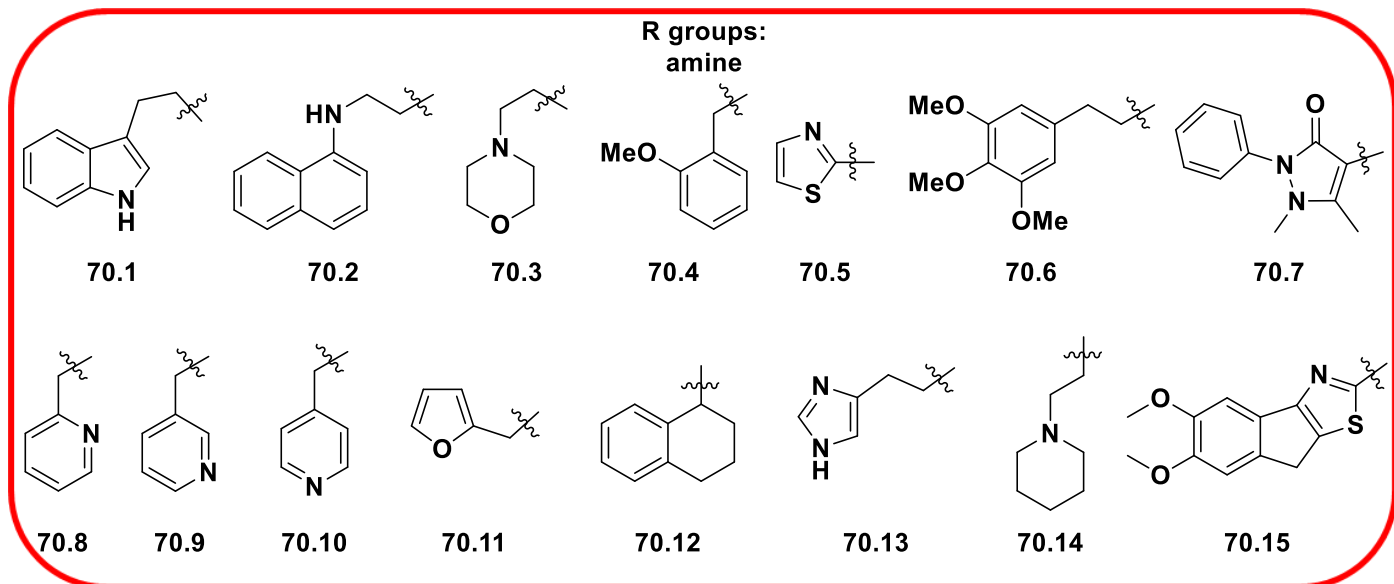
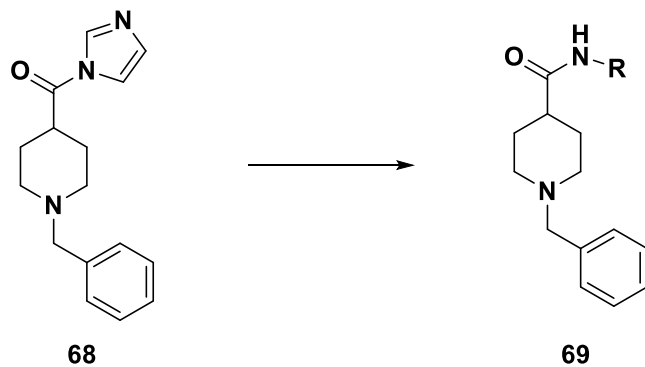


Figure 2.16: Amide coupling reaction using the amine R-groups (70.1-70.15) which are attached to the final product (69).

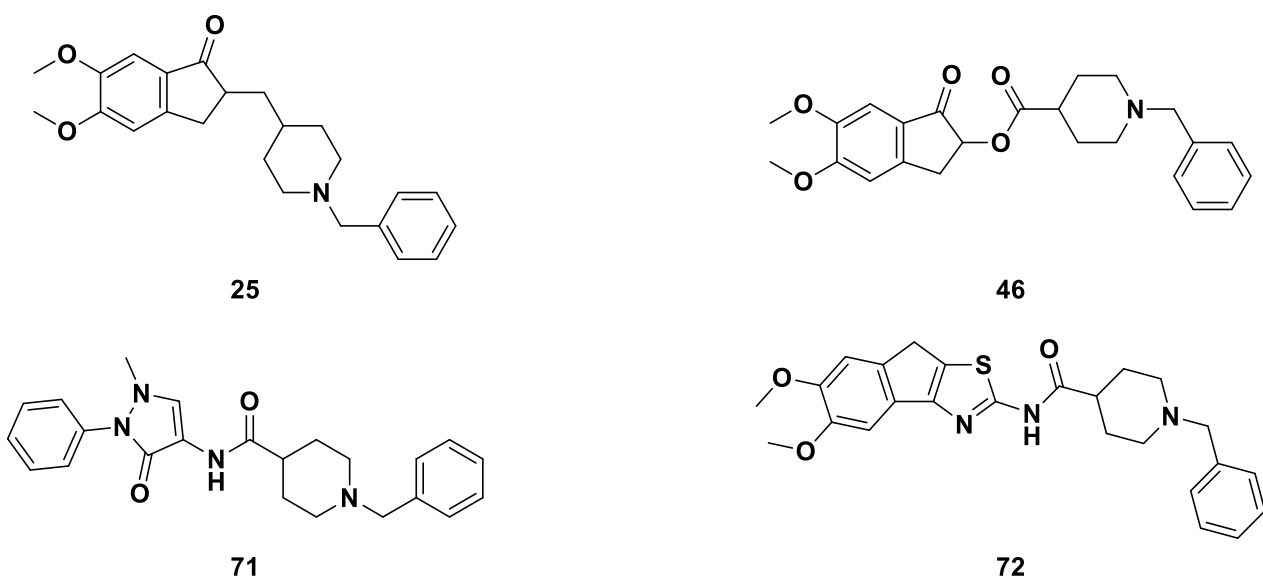


Figure 2.17: Lead compound (46) and its derivatives synthesized in the Riley group.

2.2. N-methyl D-aspartate hypothesis

The NMDA hypothesis is linked to moderate to severe AD, VD, PD, Huntington's disease, stroke, schizophrenia and treatment-resistant depression. These symptoms can be treated with NMDA antagonists [61, 70].

Glutamic neurons are the brain's primary excitatory system in all mammals [61, 62]. The neurotransmitter, glutamate, produced by the presynaptic glutamic neurons activates several metabotropic receptors. Glutamate activates three types of ionotropic receptors. They are all ligand-gated channels on postsynaptic glutamic neurons. The three types include the kainate activated receptor, the α -amino-3-hydroxy-5-methyl-4-isoxazole propionic acid (AMPA) receptor, and the NMDA receptor. The AMPA receptor is mostly impermeable to Ca^{2+} ions but is involved in the quick transport of Na^+ ions [62]. The NMDA receptor (shown in **Figure 2.18**) is a subtype of AMPA, which is highly permeable to Ca^{2+} ions. It has slow gating kinetics and can be blocked by Mg^{2+} ions, which are regulated by the membrane's potential [62].

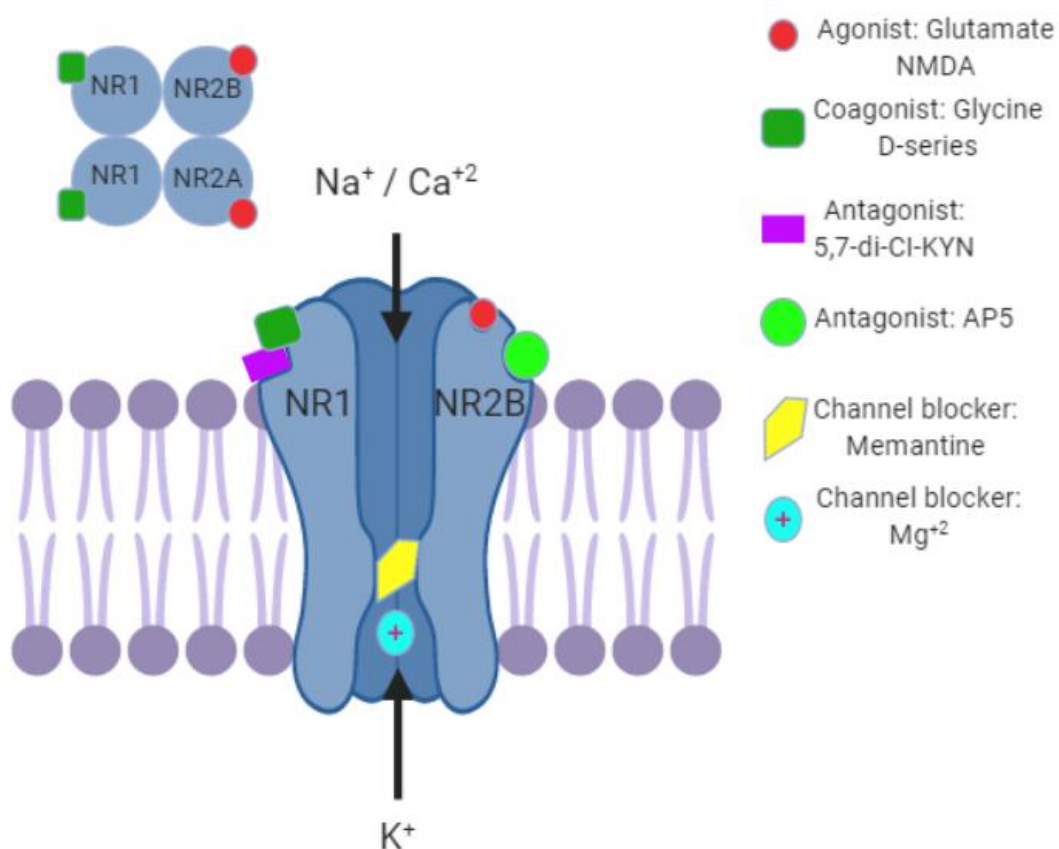


Figure 2.18: Schematic representation of an open NMDA receptor which is permeable to Ca^{2+} and blocked through memantine (**73**) and Mg^{2+} . – adapted from [63].

The NMDA receptor is a tetrameric complex (see **Figure 2.18**) that is composed of two NR1 subunits that form the ion channel itself. The two subunits of NR2A, NR2B, NR2C or NR2D, are found throughout the CNS and mediate the brain's neuroplasticity. Plastic changes, for example, in long term potentiation, form the underlying mechanism of memory function and learning. In **Figure 2.19**, glutamate gets released from the presynaptic glutamergic neuron due to a high-frequency signal. Glutamate then crosses the glutamatergic synapse. Together with the co-factor glycine (or D-serine) (see **Figure 2.18**), they bind and activate NMDA and AMPA receptors on the postsynaptic glutamergic neuron causing the ion channels to open [61]. Due to the NMDA channel being blocked by a Mg^{2+} ion, which cannot pass the narrow region of the NMDA receptor channel, it only allows for the influx of Na^+ ions into the postsynaptic glutamergic neuron. The increased Na^+ concentration forms an excitatory postsynaptic potential, which depolarizes the membrane. As a result, the Mg^{2+} ion gets removed from the NMDA receptor leading to the free movement of Ca^{2+} ions through the NMDA channel. The influx of these Ca^{2+} ions leads to several enzymatic processes involved in neuronal memory formation [61, 62].

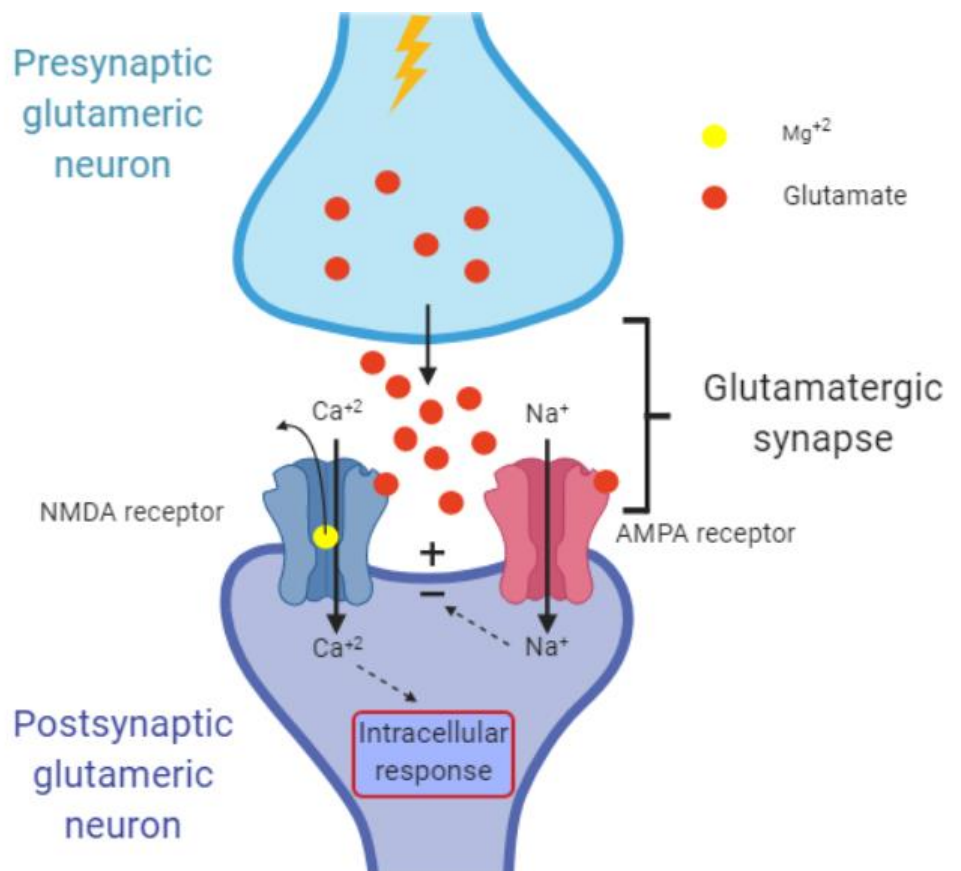
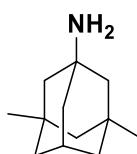


Figure 2.19: Schematic representation of long-term potentiation which involves the glutamate receptors AMPA and NMDA - adapted from [63].

Neural dysfunction and cell death in AD results from the overactivation of the NMDA receptors and the fact that Mg^{2+} ions are too weak to keep blocking the NMDA receptor under such conditions. Acute insults such as stroke and trauma result due to the influx of excessive amounts of Ca^{2+} ions into the cell [62]. As a result of the neuron death in AD, there is a 60 % decrease observed in NMDA receptors in the neocortex and hippocampus of AD patients showing a 35–40 % decrease in glutamate binding [70]. The fact that Mg^{2+} has strong voltage-dependency and very low affinity for NMDA, leading to its fast-blocking kinetics, leads to the search for an alternative to Mg^{2+} . The discovery of the inhibitor called memantine (**73**, **Figure 2.20**), which is strong enough to block the NMDA receptor during the abnormal continuous production of glutamate resulted from the search.



73

Figure 2.20: The NMDA receptor antagonist, memantine (**73**).

Memantine (**73**) was FDA approved for the treatment of moderate-to-severe AD [54]. It is an uncompetitive NMDA receptor antagonist that shows deficient receptor activity in normal neurological function. Receptor activity increases as the levels of glutamate increase due to the overactivation of NMDA receptors. As a result, the ion channel stays open long enough for memantine (**73**) to block the receptor [61]. Memantine (**73**) acts by stabilizing the function of the glutamatergic system by blocking the NMDA receptor as Mg^{2+} would under normal conditions [2, 62]. Memantine (**73**) allows for normal physiological function, due to it having rapid kinetics and a high voltage dependency [61]. Since NMDA receptors are inhibited 3-fold better in the hippocampus than in striatal neurons it provides neuroprotection of the synaptic plasticity of the brain when using NMDA antagonists for the treatment of AD [2, 10, 71].

In PD, treatment using 2-amino-5-phosphonovaleric acid (AP-5), which is a competitive NMDA receptor antagonist or memantine (**73**), indicated an increased inhibition of NMDA ion channel activity. It also resulted in the inhibition of NMDA-stimulated ACh release causing an anticholinergic activity in rat/rabbit striatum [71]. The use of memantine (**73**) for VD treatment might even slow down the neurodegeneration caused by the disease [71].

Memantine (**73**), in combination with AChEIs, was shown to lead to a synergistic effect for the treatment of AD [61]. Memantine (**73**) has a modest effect and is therefore used as a lead compound to synthesize second-generation compounds for the treatment of AD [61].

Four distinct genes are encoding the NMDA subunit GluN2 (GluN2A-D), which causes a difference in function and pharmacological effects and also has an effect on the blocking and unblocking kinetics of Mg^{2+} ions at the NMDA receptor [72]. The development of NMDA inhibitors, which can target specific subunits, could lead to fewer side effects and can lead to the selective treatment of neurological disorders, including schizophrenia and treatment-resistant depression [72].

The Liotta group synthesized a lead compound (**74**, see **Figure 2.21**) which forms part of the dihydroquinolone pyrazoline (DQP) class of GluN2C/D subunit selective antagonists which showed an IC_{50} value of 2.7 μM and 41-fold selectivity for NMDA receptors that had a GluN2-D subunit [72, 73]. The work done by the same group on the lead compound resulted in the synthesis of an S-enantiomer (**75**) shown in **Figure 2.21**, which is 11-fold more potent than its R-enantiomer (IC_{50} value of 0.17 μM vs. 1.9 μM). These compounds are highly selective towards binding GluN2C and GluN2D containing NMDA receptors and the potential of using them for the study of the role of these receptors in diseases is high [72]. The GluN2D expressed in subthalamus neurons involved in PD could, therefore, be studied and the blocking of these NMDA receptors in the substantia nigra pars compacta neurons could have a positive effect on neuronal death caused by the disease [72]. The cerebellum contains NMDA receptors containing GluN2C, which influences learning and is involved in schizophrenia [72]. Therefore, the blocking of overactivated NMDA receptors causing neural dysfunction and cell death due to AD are a potential target for the treatment of AD.

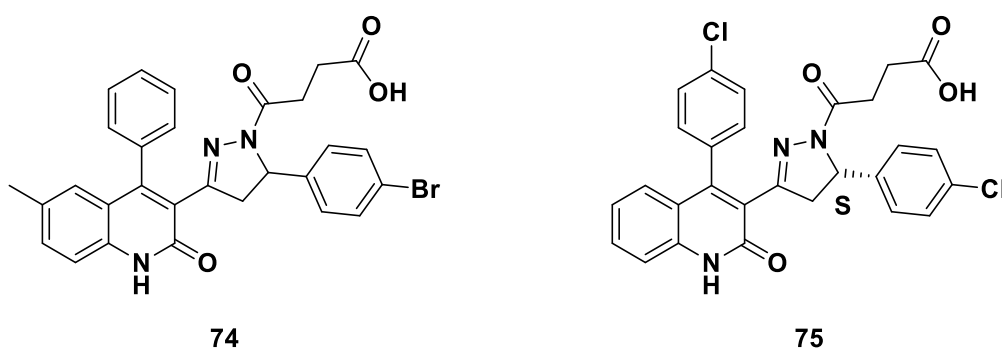


Figure 2.21: Liotta group's lead compound (**74**) and its most potent derivative (**75**).

2.3. Project background, aims and objectives

The envisaged project has two principle aims namely: i) the *in silico* assessment and synthesis of potential AChEIs that are structurally related to the FDA approved drug donepezil (**25**) and ii) The *in silico* assessment of potential NMDA antagonists related to the active compound (**75**) identified by the Liotto group at Emory University.

2.3.1. Potential acetyl cholinesterase inhibitors

2.3.1.1. Introduction

The crucial interactions of donepezil (**25**) with the catalytic triad of AChE (Ser 200, His 440, and Glu 327) located in the active site gorge and to the PAS at the entrance of the binding pocket, located near Trp 279 were described earlier. **Figure 2.22** indicates the different parts of donepezil (**25**; parts 1 – 4). The phenyl rings in sections 1 and 4 result in π - π stacking between the ligand and the enzyme at Trp 84 and Trp 279 respectively. There are also H-bonding interactions with the positively charged *N*-atom (part 3) of donepezil (**25**). We initially proposed to target the development of compounds that will afford novel inhibitors that retain these critical interactions; as a result, the assessment of a virtual library of compounds was envisaged using *in silico* approaches, thereafter, promising hits would be prepared synthetically for biological evaluation.

Initially, two target scaffolds A and B were selected based upon previous in-house experience on related tricyclic thiazole scaffolds [69]. As highlighted in **Figure 2.22**, in both instances, the indanone ring system and methyl linker (parts 1 and 2) present in donepezil (**25**) are replaced by a tricyclic isoxazole ring system. It was anticipated that heterocyclic nitrogen and oxygen would offer similar interactions as the carbonyl group in the aforementioned indanone ring system. Thereafter, scaffold A would allow us to explore the CAS site through functionalisation of an exocyclic ester (parts 3 and 4). In the case of scaffold B, a triazole ring was selected as a replacement for the piperidine ring in donepezil (**25**) (part 3). Furthermore, this would be readily accessed using Click chemistry, affording a convenient handle for adding functionality that would interact with the CAS (part 4). Scaffold B has longer molecules, which are particularly attractive as its length would lend itself well to the development of dual inhibitors that can access both the CAS and PAS sites of AChE.

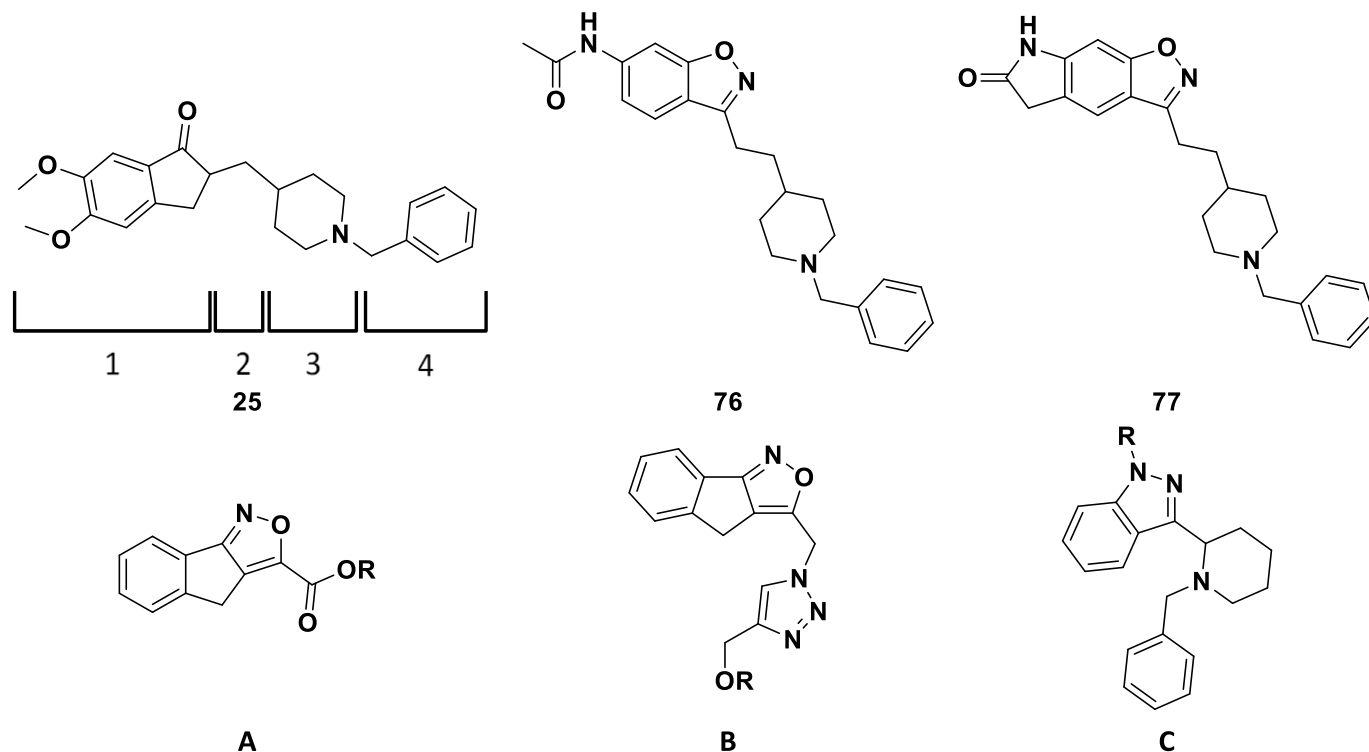


Figure 2.22: Comparison of donepezil (**25**), **76** and **77** to the targeted scaffolds A, B and C.

The use of an isoxazole ring system in AChEIs has previously been reported by Villalobos *et al.* In this instance the group replaced the indanone moiety of donepezil (**25**, part 1) with a benzisoxazole moiety and the methyl linker (part 3) with an ethyl linker which leads to a higher selective for AChE over BuChE (3 200 fold for **76**, and >10 000 fold for **77**) [74, 75]. These compounds are highly potent inhibitors, affording IC_{50} 's of 2.8 nM and 0.22 nM for **76** and **77** respectively [74]. Compound **76** is unfortunately rapidly hydrolysed under biological conditions, however, restricting the *N*-acetyl group in **76** by replacing it with a 5-membered heterocyclic ring system greatly improved the metabolic stability. We felt that in light of these positive results it would be worthwhile to explore chemical space surrounding the isoxazole ring system by swapping the relative positions of the 5 and 6-membered rings, present in **77** thereby still allowing the important π - π stacking between the ligand and the enzyme at Trp 84 and Trp 279.

Alternatively scaffold C incorporates the six and five membered rings corresponding to **76**, and the hope is that if these compounds are biologically active against AChE they could be further functionalised. The only functionalisation being targeted in this work is incorporating different R groups and determining if these are active compounds. The only setback for scaffold C is that the backbone of the scaffold is smaller compared to that of scaffold A and B, but it is believed that important conclusions about AChE activity could be discovered computationally and *in vitro*.

2.3.1.2. Aim one: *In silico* screening of scaffolds A, B and C

2.3.1.2.1. Objective one: Docking studies of scaffolds A, B and C

A virtual library of compounds based upon scaffolds **A**, **B** and **C** will undergo docking studies by using the program **Maestro** which forms part of the **Schrödinger** suite. The program will indicate the number, type, and distance of interactions present between the ligand and the active site of AChE. A resultant docking score will indicate the ligand's ability to bind to the active site of AChE, while biological prediction studies will be used to predict the ligand's ability to function as a pharmaceutical.

2.3.1.2.2. Objective two: *Qikprop* and enzymatic studies of scaffolds A, B and C

The **Qikprop** task on **Maestro** will be used to predict some physical properties of ligands, which include molecular weight (MW), QPlogPo/w, QPlogBB, QPlogHERG, the number of hydrogen donors and acceptors present in the ligands and the ligand's total polar surface area (TPSA). These properties must adhere to specific ranges to be classified as drug-like. These ligand's QPlogHERG values will predict if these ligands will inhibit the hERG K⁺ channel, while another study will predict the ligand's ability to inhibit the CYP450 isozyme CYP2C9.

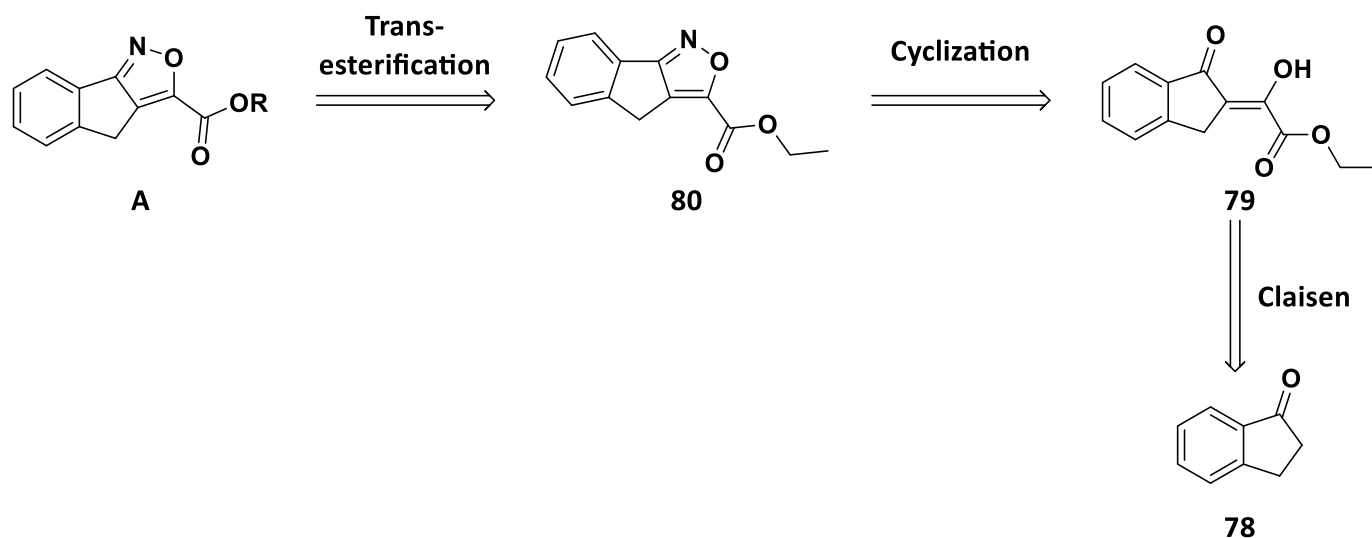
The *in silico* screening will indicate if the scaffolds are suitable for further development and if so two to three ligands will be selected to progress to aim two.

2.3.1.3. Aim two: Synthesis of scaffolds A, B and C

The second aim of the project is to synthesise scaffolds A, B and C, focusing on the best three ligands determined from the *in silico* studies of each scaffold.

2.3.1.3.1. Objective one: Synthesis of scaffold A

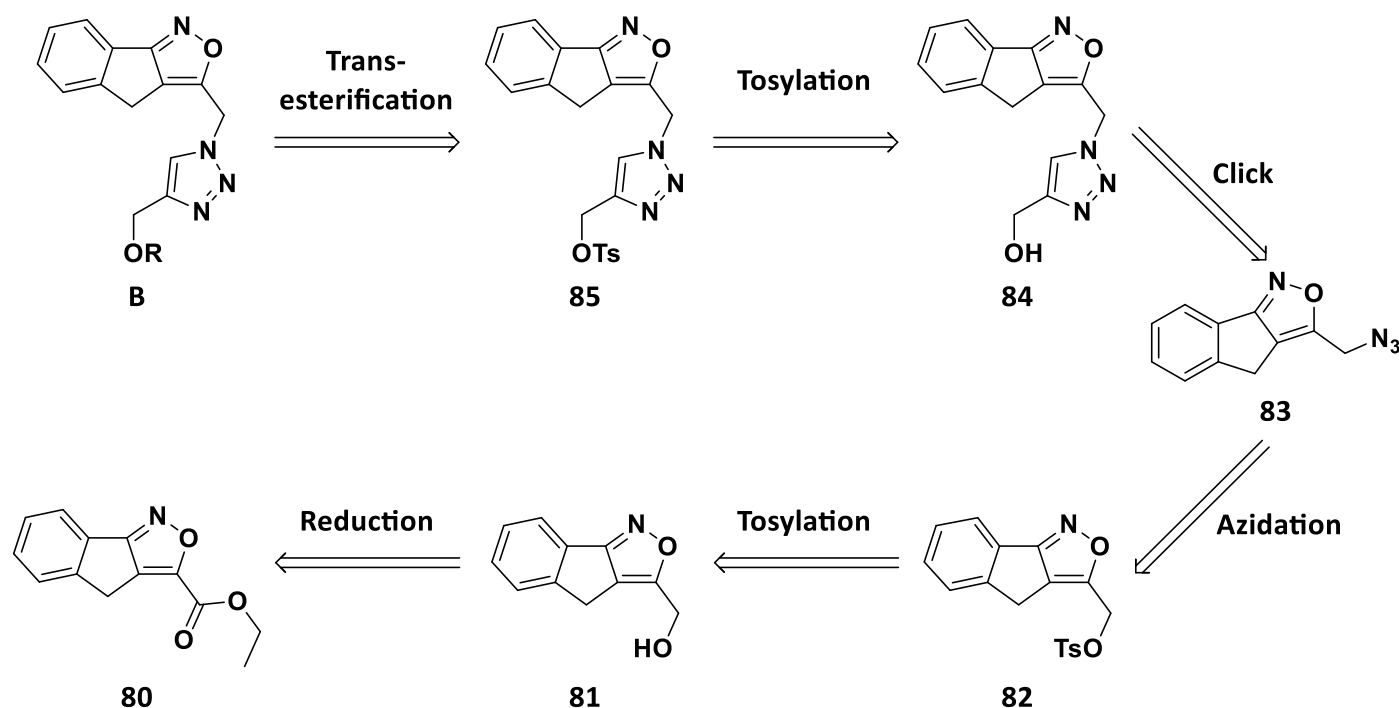
Scheme 2.1 represents the retrosynthesis to access scaffold A. Initially, a retro-transesterification of **A** back to isoxazole (**80**) is envisaged. This would then be followed by a retro-cyclization step to form the α,β -unsaturated system (**79**), and finally, a retro-Claisen condensation to indanone (**78**).



Scheme 2.1: Proposed retrosynthesis of scaffold A.

2.3.1.3.2. Objective two: Synthesis of scaffold B

Scheme 2.2 indicates the envisaged retrosynthesis of scaffold B. An initial S_N2 displacement of tosylated compound, **85**, is planned as a diversification point. Thereafter retro-activation to alcohol **84** as a tosylate and Click chemistry is planned starting from azide **83**. Azide **83** would then be accessible from **80** via an ester reduction to afford **81** followed by tosylation of the resulting alcohol to afford **82**.

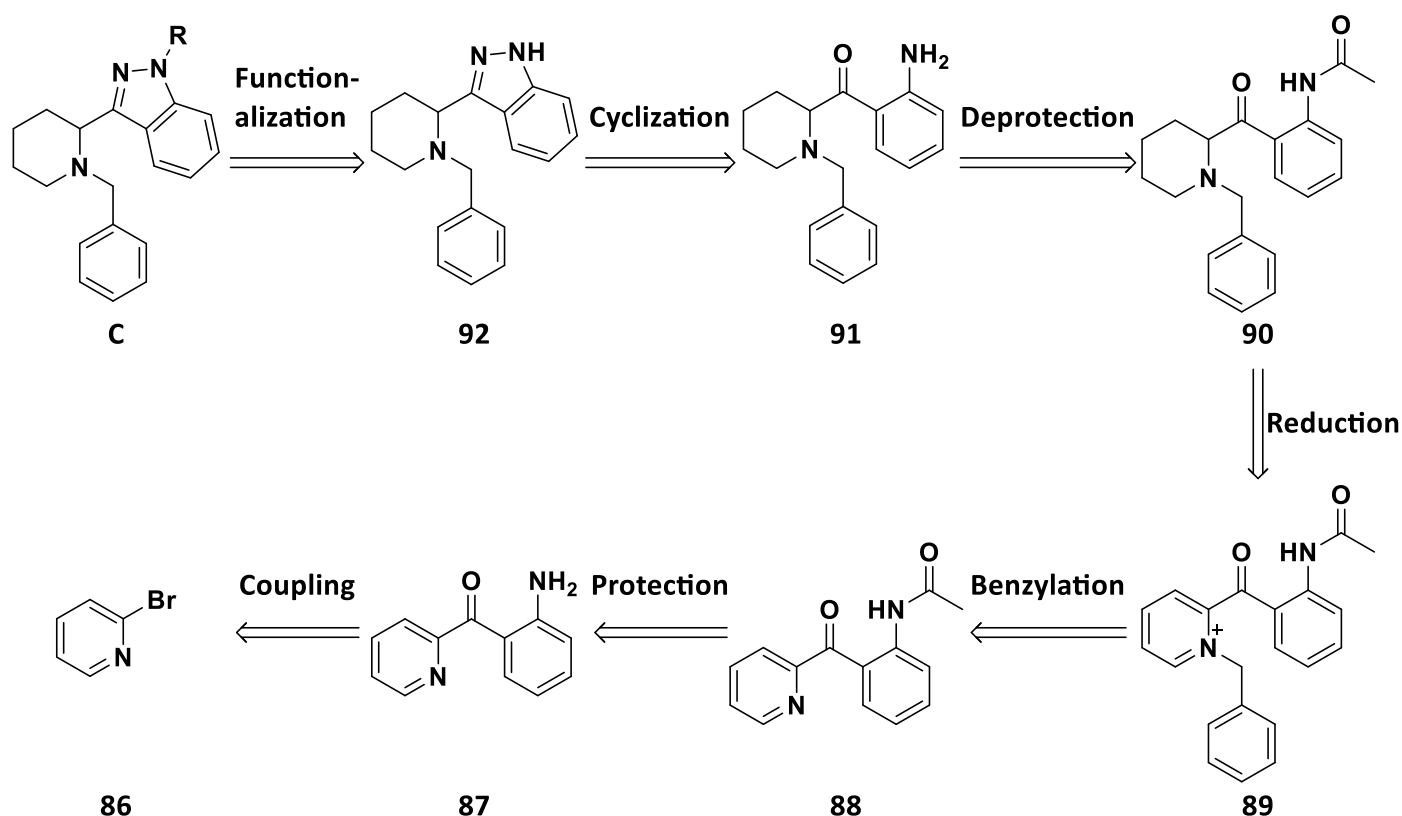


Scheme 2.2: Retrosynthesis of scaffold B.

The triazole containing compound (**85**) is the precursor of scaffold B, which will be transesterified with different sized *N*-containing alcohols in order to access promising ligands identified during the *in silico* analysis.

2.3.1.3.3. Objective three: Synthesis of scaffold C

Scheme 2.3 represents the retrosynthesis involved in scaffold C. We initially envisaged a simple functionalisation of the pyrazole NH group of **92** as a diversification point. Prior to this, we planned on accessing the pyrazole from **91** utilising a cyclisation with hydrazine. Thereafter a retro-deprotection to **90** is followed by a retro-reduction of the pyridine ring to **89**. Compound **89** could then be prepared in three steps from 2-bromopyridine **86** employing a coupling with anthranilic acid to afford **87**, followed by amine protection to give **88**.



Scheme 2.3: Retrosynthesis of scaffold C.

2.3.1.4. Aim three: *In vitro* activity assessment against acetyl cholinesterase

2.3.1.4.1. Objective one: Biological activity and cytotoxicity studies of scaffold A, B and C

Successfully synthesised compounds will be analysed for biological activity against AChE using the

appropriate AChE electric eel enzyme in an enzymatic assay, which will determine the inhibitory concentration of 50 % of the ligand (IC_{50}). Cytotoxicity studies will also be conducted on these ligands and compared to the results obtained from donepezil (**25**). Donepezil (**25**) has an IC_{50} value of $0.05 \pm 0.06 \mu\text{M}$, and those ligands falling below those values shown for donepezil (**25**) can be used as lead compounds in future studies.

2.3.2. Potential N-methyl D-aspartate antagonists

2.3.2.1. Introduction

N-methyl D-aspartate (NMDA) have recently been shown to be a promising target in the development of neuroprotective agents and can be seen as a new target in the battle against AD. Such agents can influence the blocking and unblocking of the NMDA receptors by Mg^{2+} ions. These NMDA antagonists can be synthesised in such a way that they only target specific subunits, which could lead to a decrease in ADR generally associated with the ingestion of NMDA drugs.

Previously, the Liotta group synthesized compounds that can interact with the GluN2C and GluN2D subunits. These subunits contain NMDA receptors and are bound to the membrane-proximal lobe of the GluN2 glutamate binding domain [72]. Several of the Liotta group's compounds have IC_{50} values between 100 – 500 nM and show 50 - 200-fold selectivity for GluN2A and GluN2B containing receptors, however, the lead compound **93** suffers from several undesirable characteristics most notably a high MW and poor predicted BBB penetration [72].

Analysis of scaffold C suggested that in addition to being potential AChEIs these could potentially also act as NMDA receptor agonists. As such, as a fortuitous side project, we envisaged the synthesis of a series of pyrazole-based pharmacophores based on scaffold C that mimicked the skeleton of **93** and account for the undesirable characteristics of **93** (**Figure 2.23**) [72]. We planned on modifying the Liotta scaffold by i) reducing the topological polar surface area (TPSA) by removing one or more O-atoms to increase potential BBB permeation, ii) increasing the flexibility by allowing for rotation at the pyrazole ring and benzyl group, and iii) reducing the MW of the Liotta compound by combining the 5 and 6-membered rings by replacing the quinoline ring with a pyrazole ring.

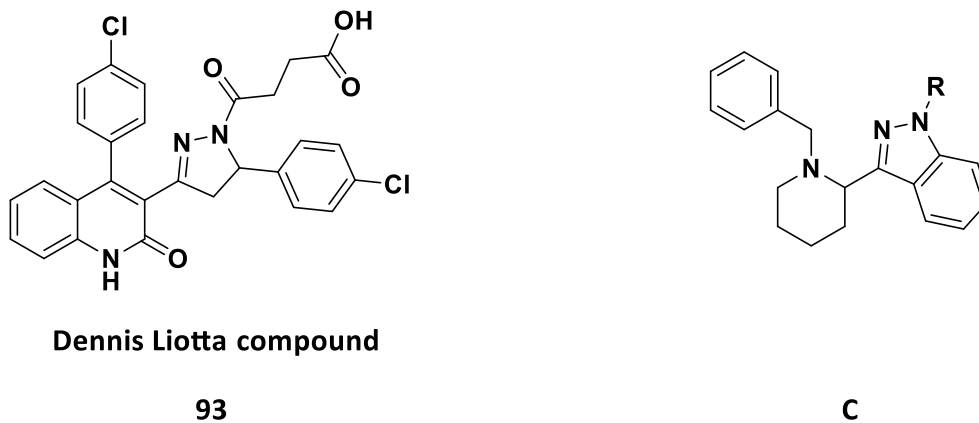


Figure 2.23: Comparison of the Dennis Liotta compound and the targeted scaffold C.

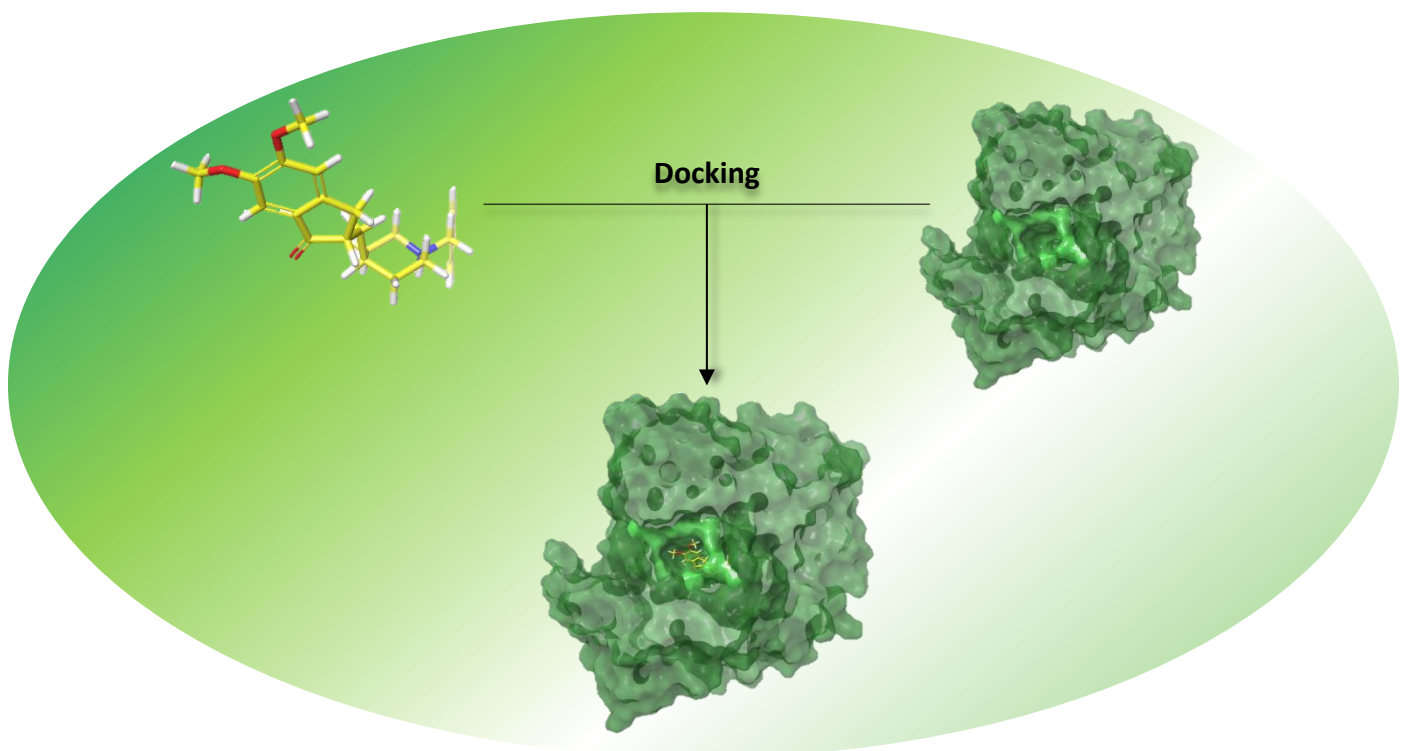
2.3.2.2. Aim one: *In vitro* activity assessment against NMDA

2.3.2.2.1. Objective one: Biological and cytotoxicity analysis studies of scaffold C

The *in silico* screening and enzymatic studies will yield several promising ligands with high docking scores to choose from, where at least 3 will be selected as targets to be synthesised from each scaffold. These will then be used in further studies.

Chapter 3

Computational Analysis - Schrödinger and SwissADME



3.1. Introduction to docking analysis

Ideally, to save both costs and time, *in silico* structure-based drug design or rational drug design is performed before synthesising compounds in the lab. In this study, *in-silico* assessments were performed in order to predict potential inhibition of the targeted scaffolds. The computational analysis conducted predicted and assessed the effectiveness of these compounds, however, one should be cognisant of the limitations on the accuracy of molecular docking. In practice the use of such *in silico* assessment can allow one to distinguish between good or poor inhibitors but it is not yet accurate enough to rank compounds in terms of their IC₅₀ values.

Structural drug design makes use of X-ray crystallography, which provides a three-dimensional (3D) structure of a ligand-enzyme complex revealing the receptor-binding site and other cavities within the enzyme. They guide the development of more active compounds targeting a specific protein. In the project in hand, the X-ray crystal structure, *Tetronarce californica* AChE enzyme (PDB code: 1EVE), was used for the analysis of the targeted ligands.

3.2. Molecular docking

3.2.1. Introduction

Computational docking analysis made use of the 3D structure of the anti-Alzheimer drug, donepezil (**25**), complexed with its target, *Tetronarce californica* AChE. The graphical user interface of **Maestro** is a molecular modelling tool that makes it possible to visualize the protein and ligand interactions and structures. **Maestro** is a suite from **Schrödinger**, which was used to prepare the protein by removing the ligand, donepezil (**25**), from the active site of AChE. This process results in a 3D conformation of the active site of AChE with no enzyme docked. The ligands under study can then be prepared and docked into the empty binding site for analysis.

The **Protein Preparation Wizard** was used to prepare the enzyme, 1EVE, by predicting the presence of amino acids that are missing in the 3D structure. The program predicts and inserts highly mobile amino acids, which are not present in the X-ray crystallogram as well as missing loops which replace chain breaks. The program settings removed water molecules found beyond 5 Å from the active site, and any remaining waters that did not bind to at least two non-waters. The water molecules remaining have significant binding interactions to the binding site, which could either help or hinder the binding of ligands to the receptor-binding site, as such their inclusion is critical. The resulting protein is now ready for the docking of new ligands after donepezil

(25) is removed from the active site.

The **Receptor Grid Generation** defines the active site area using the docked ligand, donepezil (25), present in the PDB. The program then excludes the ligand from the receptor grid calculation. The size of the ligand grid was increased to 24 Å, making it possible to dock ligands that are larger than donepezil (25) into the active site.

The new ligands are drawn using **2D Sketch**, whereafter **Ligprep** is used to generate their 3D forms, which are needed for the docking calculations. **Ligprep** generates all the possible stereoisomers of each ligand. Therefore, an increased number of chiral centres will lead to an increased number of ligands. The ligands generated were minimized to 32 stereoisomers per ligand.

Ligand docking uses the receptor grid generated to dock all the prepared ligands. The docking method used was extra precision, XP, to kick out false positives that might have been produced if the SP (standard precision) setting was used. XP focuses on the ligand shape complementarity, which gives higher scores for ligands that have better interaction with the binding site.

Figure 3.1 indicates the enzyme, AChE, as an α/β hydrolase protein that consists of 12 β -sheets (turquoise) surrounded by 14 α -helices (red) [63]. The enzyme contains a deep and narrow hydrophobic gorge (20 Å long), lined with 14 aromatic amino acid residues, represented by the grey surface area [6]. The gorge penetrates halfway into the enzyme, widening out close to the base [23]. The ligand, donepezil (25), is docked into the active site and can be seen as the purple ligand.

Maestro uses quantum mechanical calculations, which provide essential information about the ligands under investigation. These calculations predict the conformation of each ligand with the minimum energy required to interact with the enzyme's active site. The program can predict the optimal charge distribution of the new ligands docked into the enzyme and can indicate the number and type of interactions involved between the ligand and the enzyme.

An increased number of interactions between a ligand and the enzyme's active site suggests a potential candidate for the inhibition of AChE. The **Ligand docking** task estimates the potential inhibition of a ligand, which is represented by a docking score (the more negative the value, the higher the ligands inhibition). We first redocked donepezil (25) into the prepared protein (see **Figure 3.2**) to generate a baseline docking score value functioning as a comparison for the data generated from all new ligands. The docking scores, type of interactions, and the distance of these interactions in the active site are all considered when looking at the targeted ligands.

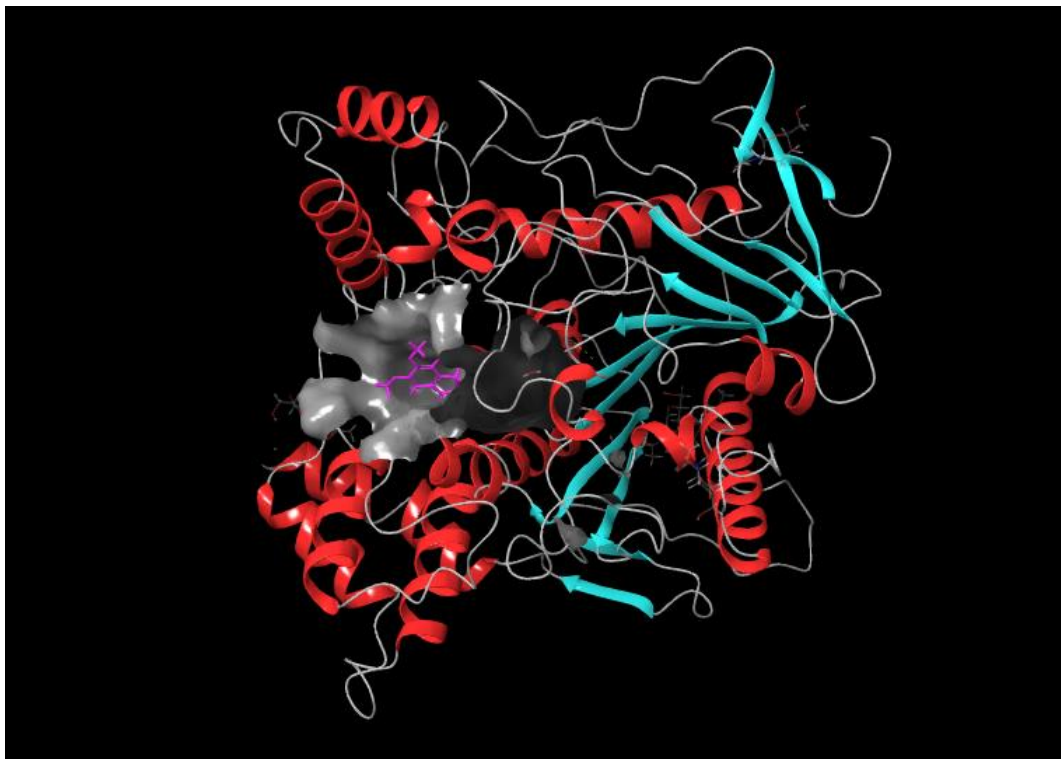


Figure 3.1: Donepezil (**25**, purple ligand) docked into the active site of *Torpedo californica* AChE. -The 12 β -sheets (turquoise) are surrounded by 14 α -helices (red), the grey surface area represents the binding site.

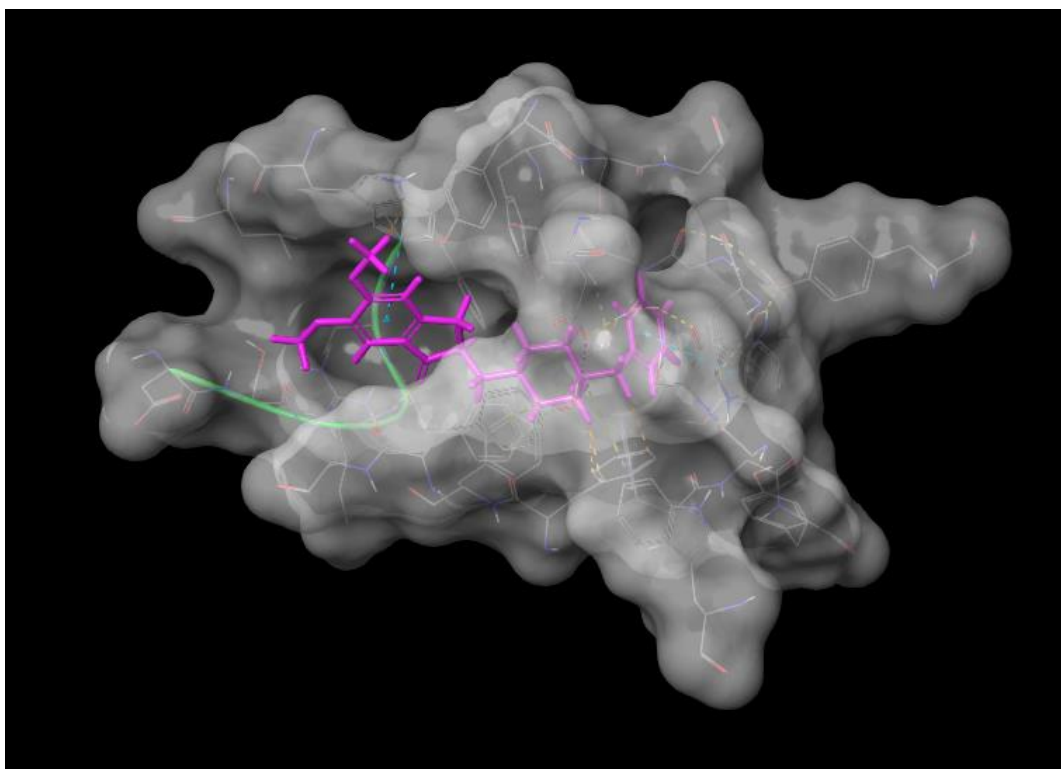


Figure 3.2: Donepezil (**25**, purple ligand) docked into the binding site (grey surface) of AChE.

The best docking score calculated for donepezil (**25**) docked into the active site of AChE is -14.470. Critical interactions of donepezil (**25**) are observed between the benzyl ring forming a π - π interaction with the active site gorge at the amino acid Trp84 and the positively charged *N*-atom forming a π -cation interaction with the active site gorge's Trp84, Tyr334 and Phe330 which form part of the CAS. The carbonyl *O*-atom forms a H-bond bridge with the amino acids Phe288 and Phe331 found in the active site gorge while the indanone ring forms a π - π interaction with the amino acid Trp279 found at the mouth of the gorge forming part of the PAS, see **Figure 3.3** and **3.4**. The result correlated well with those previously reported by Kryger and co-workers indicating the same interactions, including π - π stacking interactions, π -cation interactions and H-bonding interactions [76].

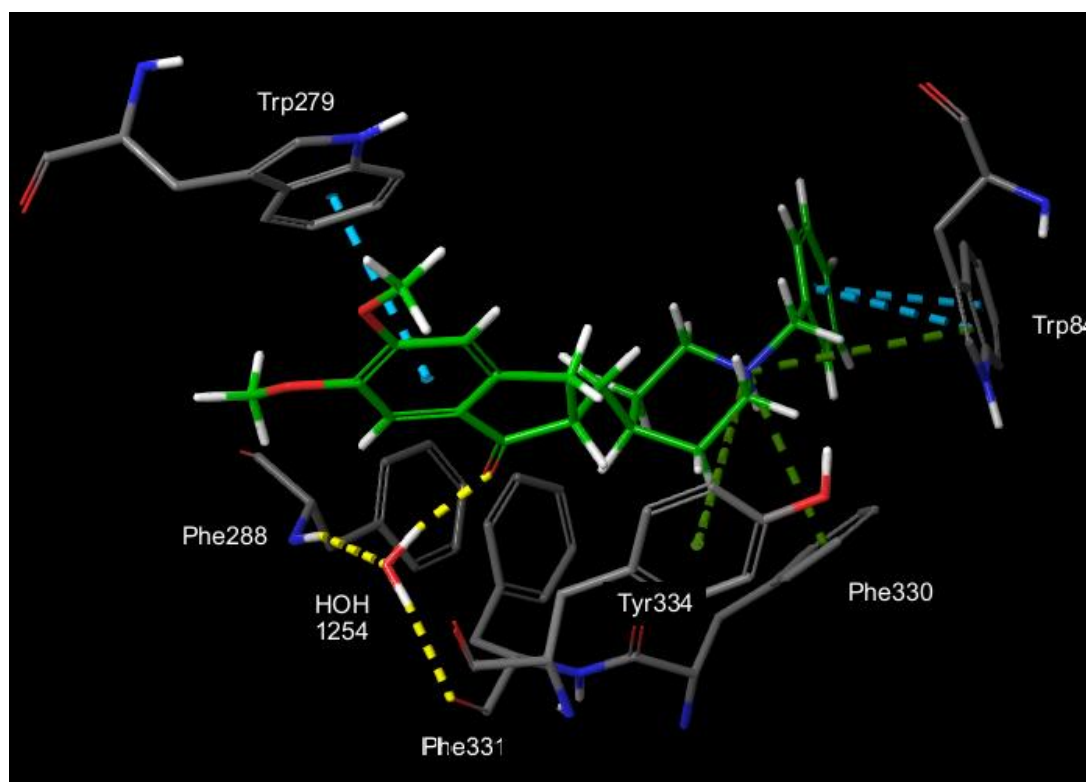


Figure 3.3: The 3D visual representation of donepezil (**25**) docked into the active site of AChE and the interactions involved. -Docking score of -14.470. Blue dashed lines indicate π - π stacking interactions, green dashed lines indicate π -cation interactions. The yellow dashed line indicates H-bonds.

A π - π stacking interaction takes place when aromatic rings interact causing them to stack on top of each other. Blue dashed lines in **Figure 3.3**, and the green lines in **Figure 3.4** represent these π - π stacking interactions. The first is between the indanone moiety's aromatic six-membered ring and Trp279. The second and third are between the benzene ring and Trp84.

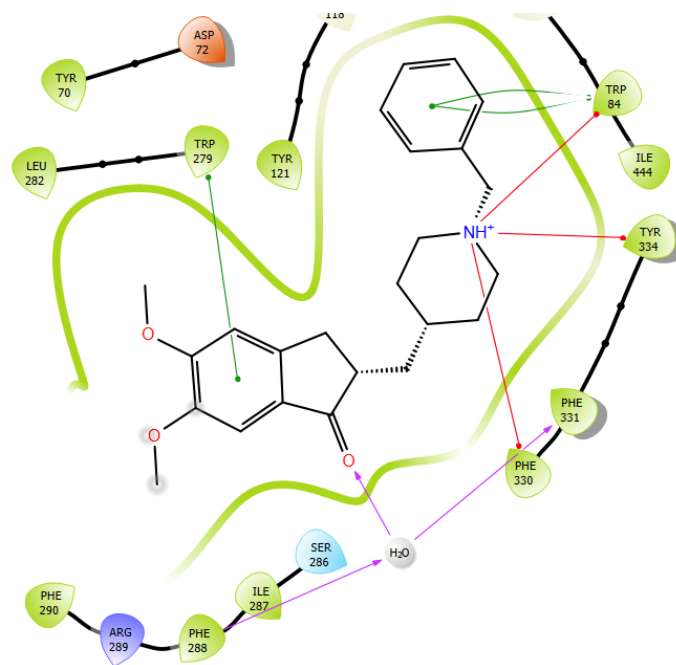


Figure 3.4: The 2D visual representation of donepezil (**25**) docked into the active site of AChE and the interactions involved. -Docking score of -14.470. Green lines indicate π - π stacking interactions, red lines indicate π -cation interactions, and purple arrows indicate H-bonds with their arrow head indicating it as either being a H-acceptor or donor.

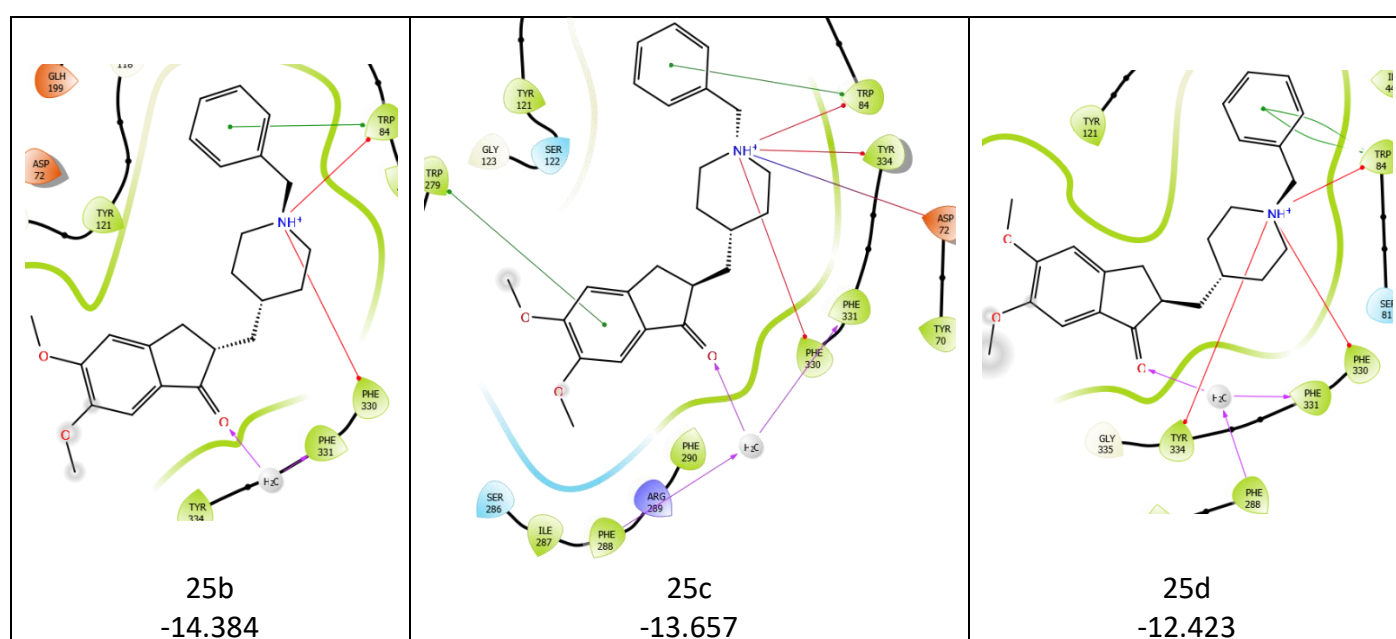
A π -cation interaction involves an aromatic ring interacting with a positively charged atom. Green dashed lines in **Figure 3.3** and red lines in **Figure 3.4**, indicate the π -cation interaction between donepezil's (**25**) positively charged piperidine *N*-atom to the aromatic rings of Tyr334, Trp84, and Phe330.

A hydrogen bond (H-bond) is formed when a hydrogen atom interacts with a water molecule or a more negative atom close to it, which forms part of an amino acid in the enzyme's active site. H-bonds can be either donating (arrow pointing away from the ligand in the 3D diagrams) or accepting (pointing towards the ligand atom in the 3D-diagram). These H-bonds form between the docked ligand and the ligand-binding site, or alternatively form bridging H-bonds by interacting with two other amino acids that are close to one another. In **Figure 3.3** and **Figure 3.4**, the H-bond formed between the ketone's oxygen atom and a hydrogen atom from a water molecule (HOH1254) is 1.8 Å away, represented by a yellow dashed line in **Figure 3.3** and a purple arrow in **Figure 3.4**. The water bridge (H-bridge) formed between donepezil (**25**), Phe288, and Phe331 is an essential contributor to its overall high docking score.

Table 3.1 indicates the rest of the orientations of donepezil (**25**, from now on designated as **25a**) docked into the active site of AChE. The orientation of **25d**, which has the weakest docking score (-12.423), is predicted

to have the same interactions as **25a** (see **Figure 3.4**), which has the strongest docking score of -14.470. However, **25a** has an extra π - π interaction to Trp279 which does not seem to be of great importance since **25b** does not show this interaction but still indicates a good docking score of -14.384. As this interaction is present in **25c** which has a docking score of -13.657, the distance of the interactions involved in **25d** should be considered. The interactions to Trp84 are much closer for **25a** than those in **25d** which indicates that this amino acid interaction is of importance for high docking scores. Overall, when considering the chiral centre it can be said that the *S*-configuration of donepezil (**25a** and **b**) is preferred over the *R*-configuration of donepezil (**25c** and **d**) considering the stronger docking scores (> -14.000) for **25a** and **b**.

Table 3.1: The 2D visual representation of donepezil (**25b-25c**) docked into the active site of AChE and the interactions involved. -Green lines indicate π - π stacking interactions, red lines indicate π -cation interactions, and purple arrows indicate H-bonds with their arrow head indicating it as either being a H-acceptor or donor.



3.2.2. Planned scaffolds

The computational analysis was conducted on a number of ligands planned for scaffolds A, B and C. We hypothesised using chemical intuition that these scaffolds would indicate good activity against AChE, and the computational analysis would hopefully verify this prior to attempting their synthesis in the lab. Ultimately, promising ligands, based on the *in silico* studies from each scaffold would be selected for synthesis and biological assessment.

We envisaged the replacement of the indanone ring and methyl linker of donepezil (blue circle, **25**, **Figure 3.5**) with a common isoxazole scaffold (blue circle, **A** and **B**) to afford the backbone of scaffolds A and B.

These scaffolds could be readily diversified through the replacement of the ester or ether R groups (red circles, **A** and **B**).

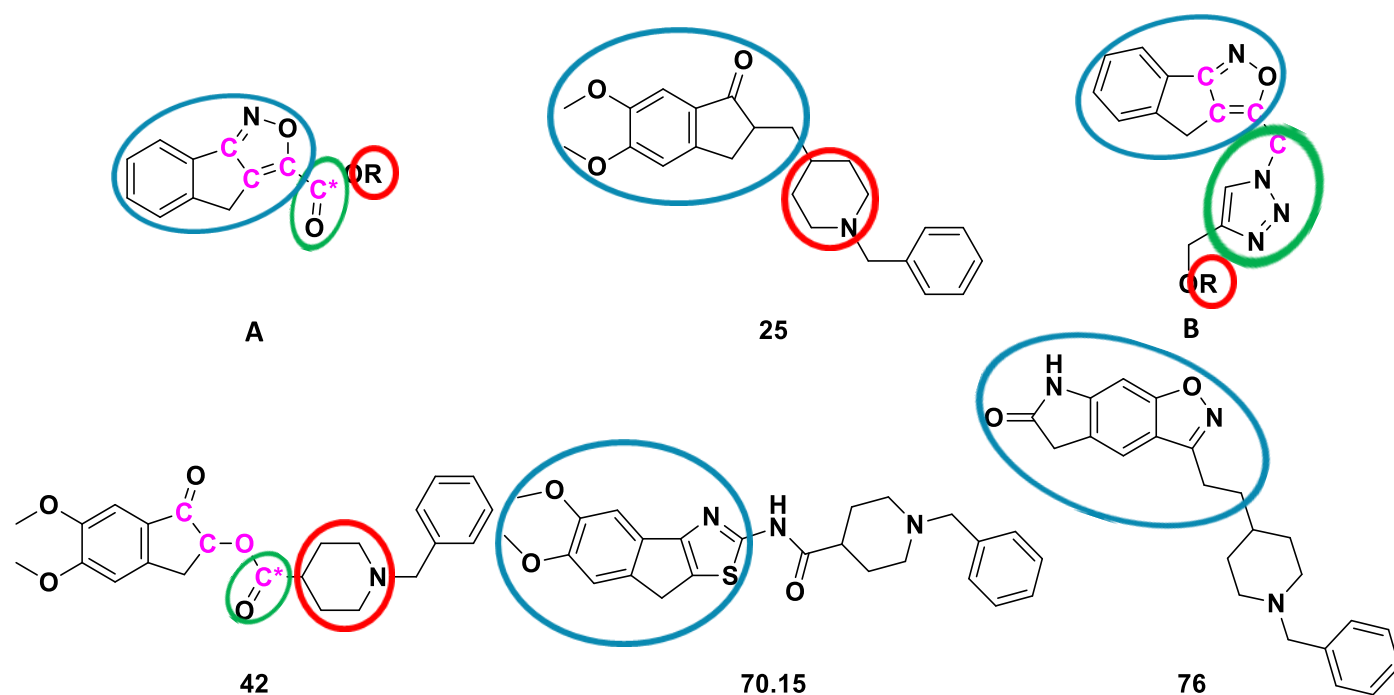


Figure 3.5: Comparison of donepezil (**25**) and other compounds that led to scaffolds **A** and **B** backbone.

The indanone ring and methyl linker (blue circle, **25**) and the tricyclic isoxazole ring system (blue circle, **A**) are structurally similar to tricyclic thiazole scaffold previously identified in-house (blue circle, **70.15**) as such one might expect similar interactions and binding affinities [69]. In addition, the isoxazole ring system proposed in scaffold **A** was also attractive considering the findings reported by Villalobos *et al* on similar systems where they identified **76** with a high activity against AChE (IC₅₀ value of 0.33 nM) with excellent selectivity for AChE over BuChE [74, 75].

In-house computational work performed previously indicated that compound **42**'s carbonyl carbon (green circle, C*), forming part of a “reverse” ester linker, led to extra water bridges when compared to donepezil (**25**) [69]. This carbonyl O-atom's position in the backbone of the molecule (green circle, C*, **42**) and its orientation correlates well to the ester linker's carbonyl carbon present in **A** (green circle, C*). As such one might expect comparable interactions in scaffold **A** and compound **42**.

The structure of scaffold **A** allows for the exploration of the CAS site of AChE through the functionalisation of an exocyclic ester (red circle, **A**). Following previous in-house work performed, we planned to assess scaffolds **A** and **B** by replacing the R group with 3-6 membered saturated nitrogen containing ring systems [69]. See **Table 3.2** for their structures.

Table 3.2: Docking score of donepezil (**25**) and scaffolds A – C5.

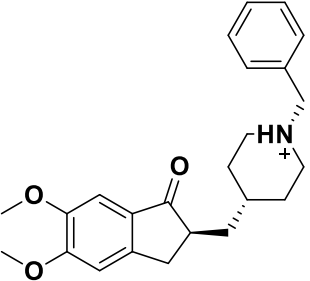
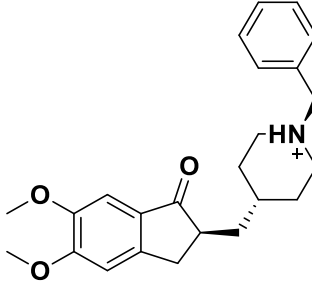
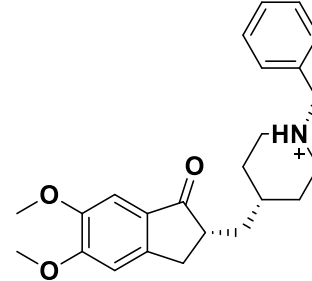
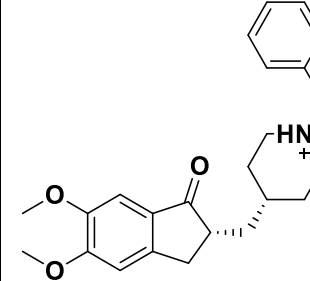
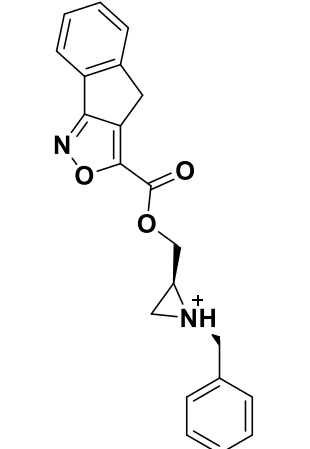
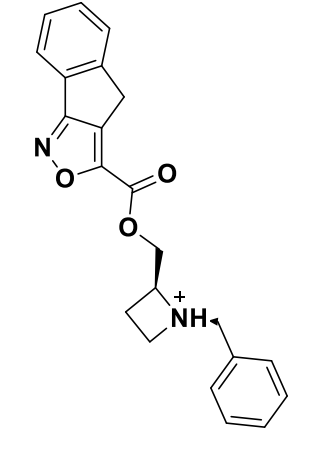
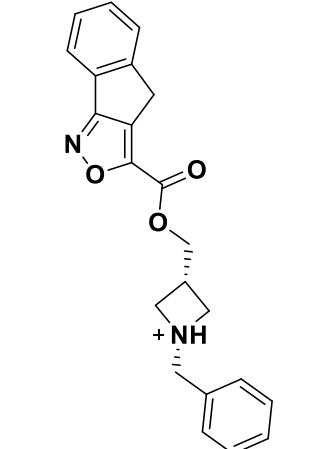
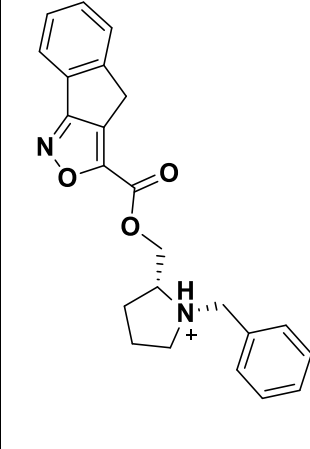
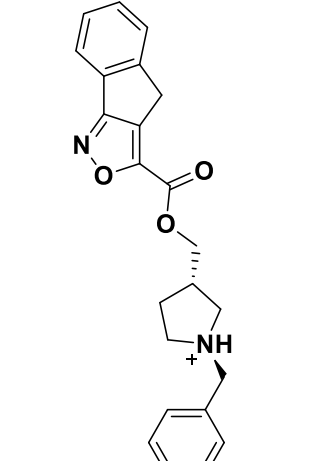
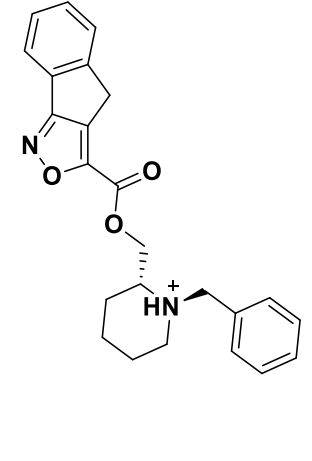
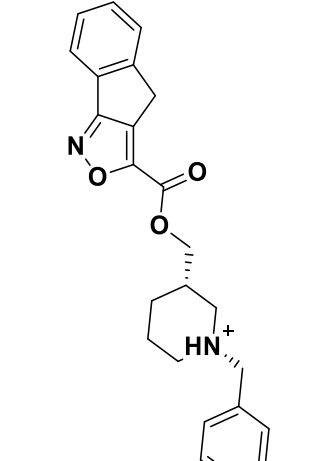
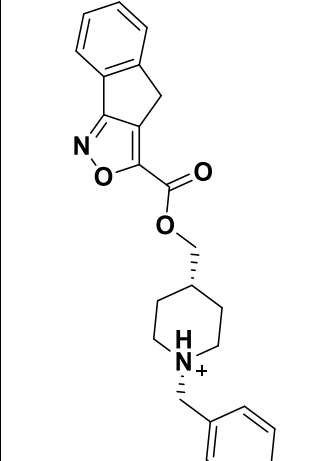
 <p>25 -14.470</p>	 <p>25 -14.384</p>	 <p>25 -13.657</p>	 <p>25 -12.423</p>
 <p>A1.1.a -12.926</p>	 <p>A1.2.a -13.076</p>	 <p>A1.3.a -14.017</p>	 <p>A1.4.a -12.706</p>
 <p>A1.5.a -13.021</p>	 <p>A1.6.a -12.929</p>	 <p>A1.7.a -12.997</p>	 <p>A1.8.a -13.147</p>

Table 3.2: Docking score of donepezil (25) and scaffolds A – C5 - continued.

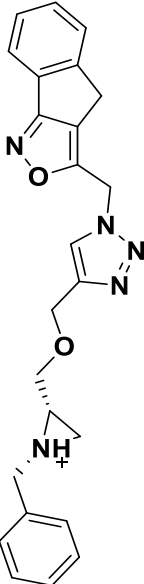
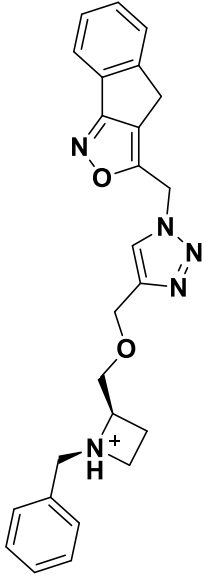
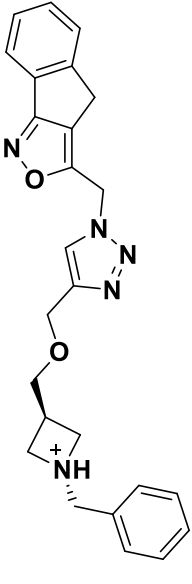
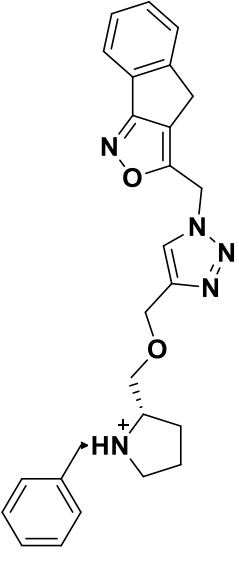
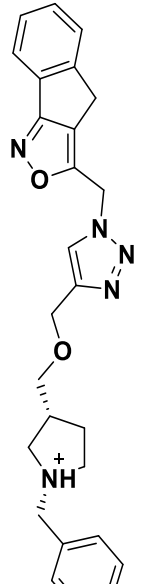
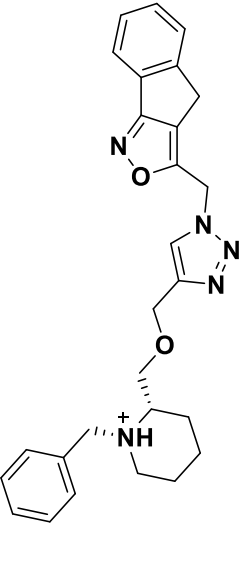
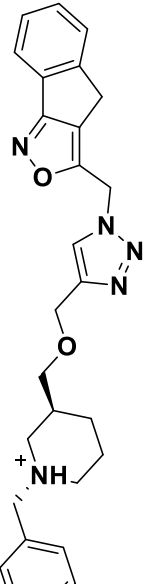
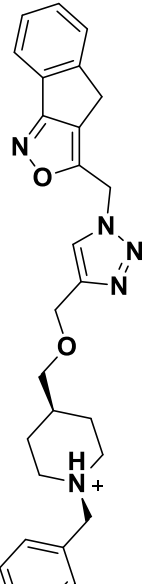
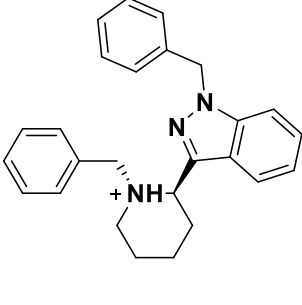
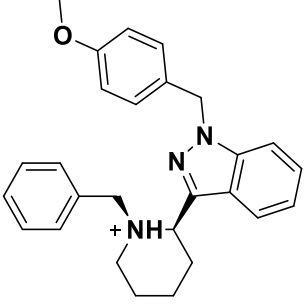
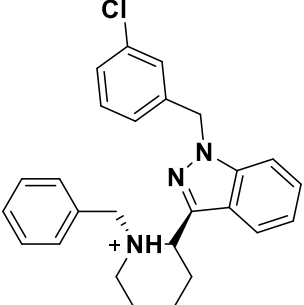
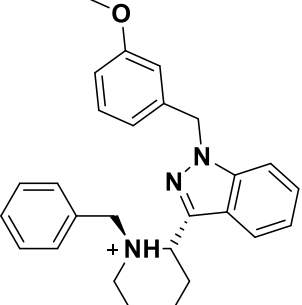
 <p>B1.1.a -14.264</p>	 <p>B1.2.a -10.829</p>	 <p>B1.3.a -11.521</p>	 <p>B1.4.a -12.114</p>
 <p>B1.5.a -12.162</p>	 <p>B1.6.a -11.699</p>	 <p>B1.7.a -11.133</p>	 <p>B1.8.a -10.843</p>
 <p>C1.1.a -13.094</p>	 <p>C1.2.a -13.254</p>	 <p>C1.3.a -13.341</p>	 <p>C1.4.a -13.948</p>

Table 3.2: Docking score of donepezil (25) and scaffolds A – C5 - continued.

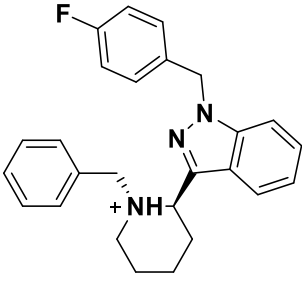
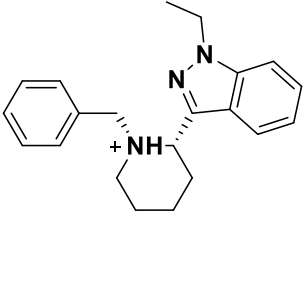
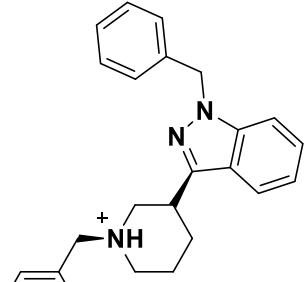
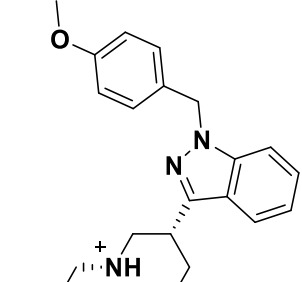
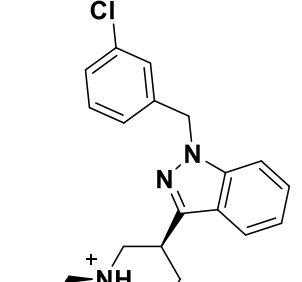
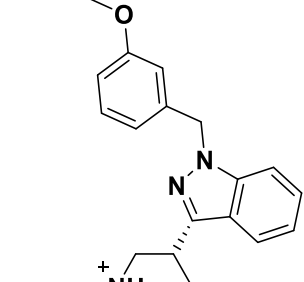
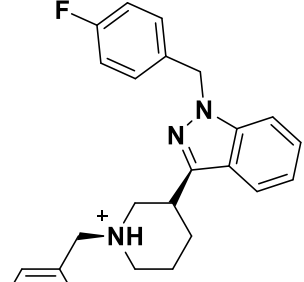
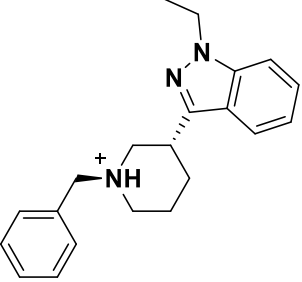
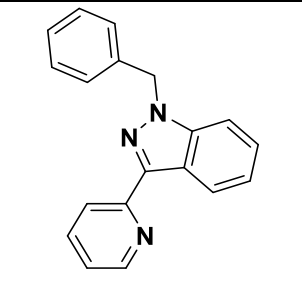
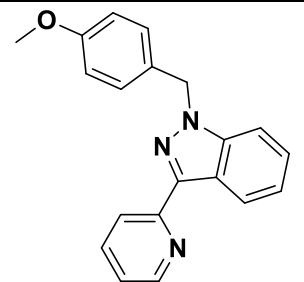
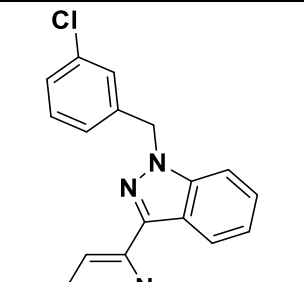
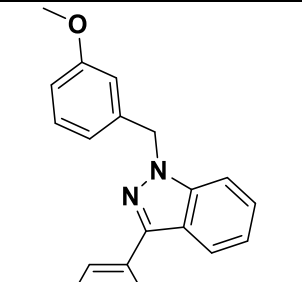
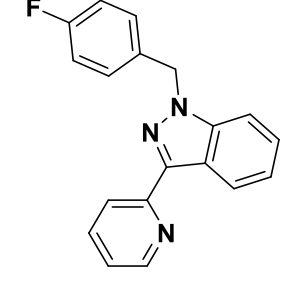
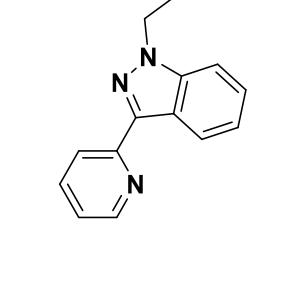
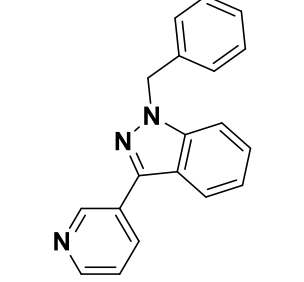
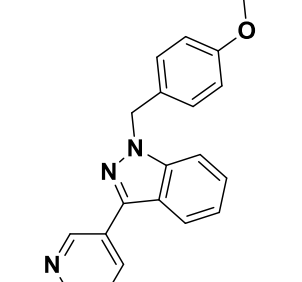
 <p>C1.5.a -13.483</p>	 <p>C1.6.a -13.431</p>	 <p>C2.1.a -13.964</p>	 <p>C2.2.a -12.856</p>
 <p>C2.3.a -12.688</p>	 <p>C2.4.a -13.340</p>	 <p>C2.5.a -13.596</p>	 <p>C2.6.a -13.445</p>
 <p>C3.1 -8.056</p>	 <p>C3.2 -7.861</p>	 <p>C3.3 -9.332</p>	 <p>C3.4 -8.390</p>
 <p>C3.5 -8.845</p>	 <p>C3.6 -6.186</p>	 <p>C4.1 -8.667</p>	 <p>C4.2 -8.061</p>

Table 3.2: Docking score of donepezil (25) and scaffolds A – C5 - continued.

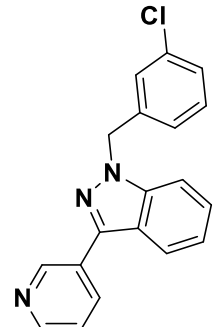
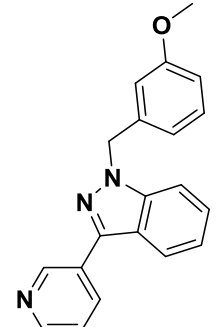
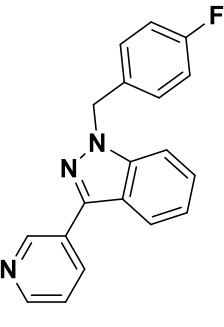
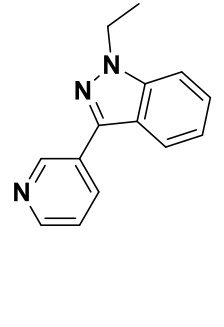
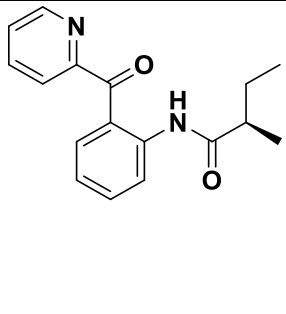
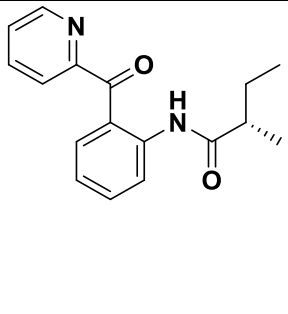
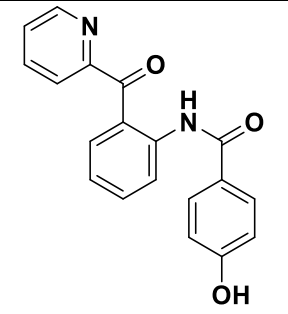
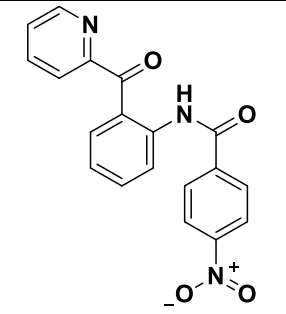
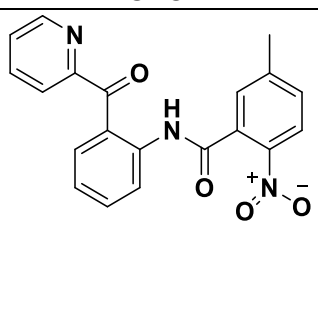
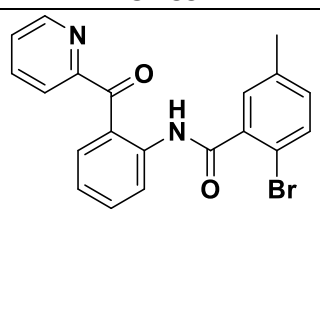
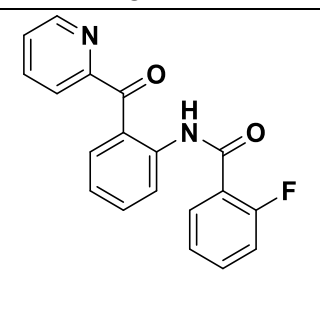
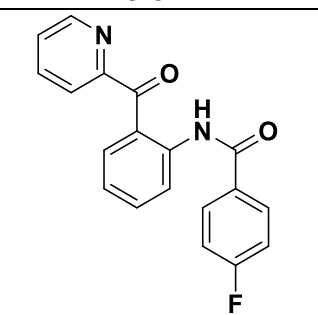
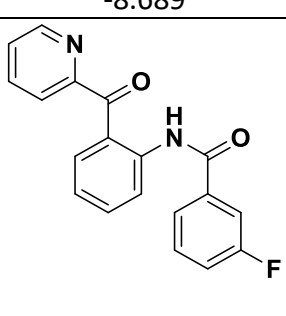
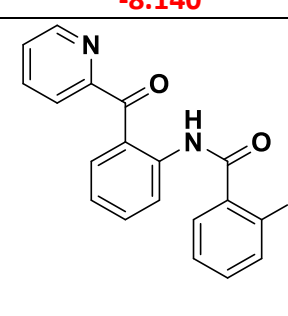
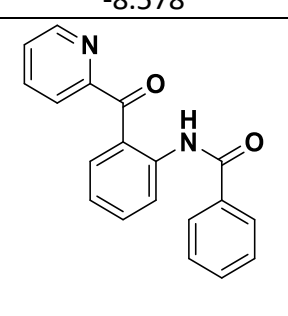
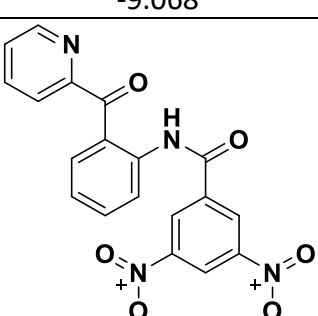
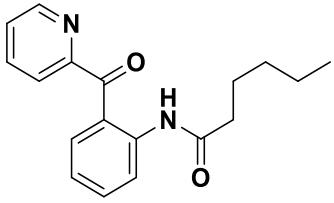
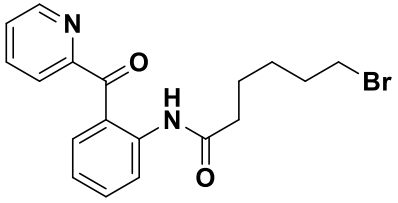
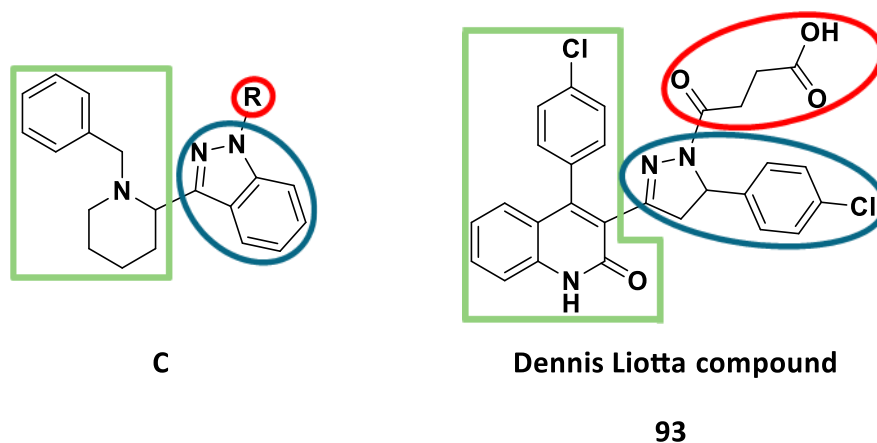
 <p>C4.3 -9.186</p>	 <p>C4.4 -8.468</p>	 <p>C4.5 -9.250</p>	 <p>C4.6 -6.820</p>
 <p>C5.1.a -8.754</p>	 <p>C5.1.b -8.439</p>	 <p>C5.2 -9.174</p>	 <p>C5.3 -9.047</p>
 <p>C5.4 -8.689</p>	 <p>C5.5 -8.140</p>	 <p>C5.6 -8.578</p>	 <p>C5.7 -9.068</p>
 <p>C5.8 -8.318</p>	 <p>C5.9 -8.159</p>	 <p>C5.10 -8.194</p>	 <p>C5.11 -8.899</p>

Table 3.2: Docking score of donepezil (25) and scaffolds A – C5 - continued.

 <p>C5.12 -7.977</p>	 <p>C5.13 -8.233</p>
---	--

Scaffold C incorporates a fused six and five membered ring which can structurally be compared to **76**, the scaffold therefore targets a series of pyrazole-based ligands which also incorporates the benzylated piperidine ring present in **25**, **42**, **70.15** and **76**. It was also noted that scaffold C relates well to a neuroprotective NMDA agonist (**93**) reported by the Liotta group, see **Figure 3.6** [73].

Scaffold C therefore presented a unique opportunity to develop dual neuroprotective agents targeting both AChE and NMDA. With regards to the Liotta compound although highly active (2.7 μM) it suffered from a higher than desired MW and TPSA for a drug that would need to cross the BBB. **Figure 3.6** highlights the similarities and differences between scaffold C and compound **93**. Scaffold C would afford a more rigid pyrazole ring system with reduced MW. The incorporation of the benzylpiperidine ring in scaffold C replaces the quinoline-2(1*H*)-one ring and the chlorobenzene group attached to it (shown in green), this represents a decrease in the MW of 80.426 g/mol also leading to a decrease in the TPSA. The incorporation of the different R groups (substituted benzene rings) was envisaged as replacements for the aryl chain containing the 3 O-atoms (**93**) (shown in red) again significantly decreasing the MW of the ligands for scaffold C and lowering the molecules TPSA to more acceptable levels.

**Figure 3.6:** Scaffold C compared to the Dennis Liotta compound (**93**).

Overall, it was hoped that scaffolds A, B and C would have some biological activity against AChE, affording hits that could then be further functionalised and refined. In the case of scaffold C, an added bonus would be if NMDA agonist activity were also noted.

3.2.3. Molecular docking results and discussion

Table 3.2 indicates all the docking scores of the assessed scaffolds in their best configuration of the ligands docked within the active site of AChE. Those highlighted in green in **Table 3.2** represent the ligands with the ten best docking scores, while those shown in red are the ligands with the ten worst docking scores. The 2D-images of the ten best ligands indicate the interactions they make to the active site of AChE (see **Table 3.3**). It is important to note that the more negative the docking score the higher the predicted inhibition of AChE. The 2D-images in **Table 3.3** highlight the ten best ligands found across the assessed scaffolds, these images indicate the type of interactions that can be found between the ligands and the active site. The interactions involved (π - π interactions, π -cation interactions and the H-bridges formed to specific amino acids) and distance (in Å) of these interactions are tabulated in **Table 3.4**.

Table 3.3: Docking score and interactions of the best ten ligands across scaffold A-C.5.

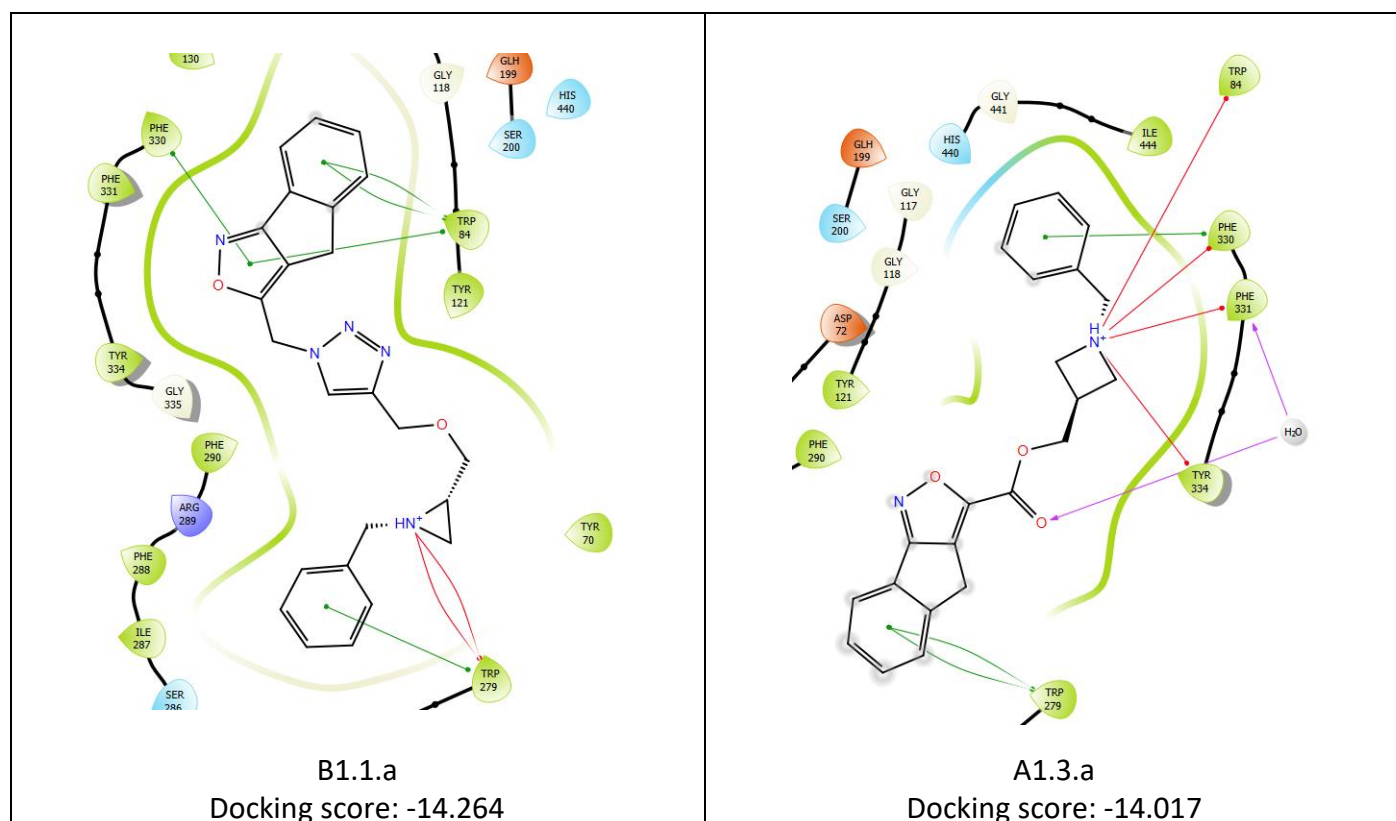


Table 3.3: Docking score and interactions of the best ten ligands across scaffolds A-C.5 -continued:

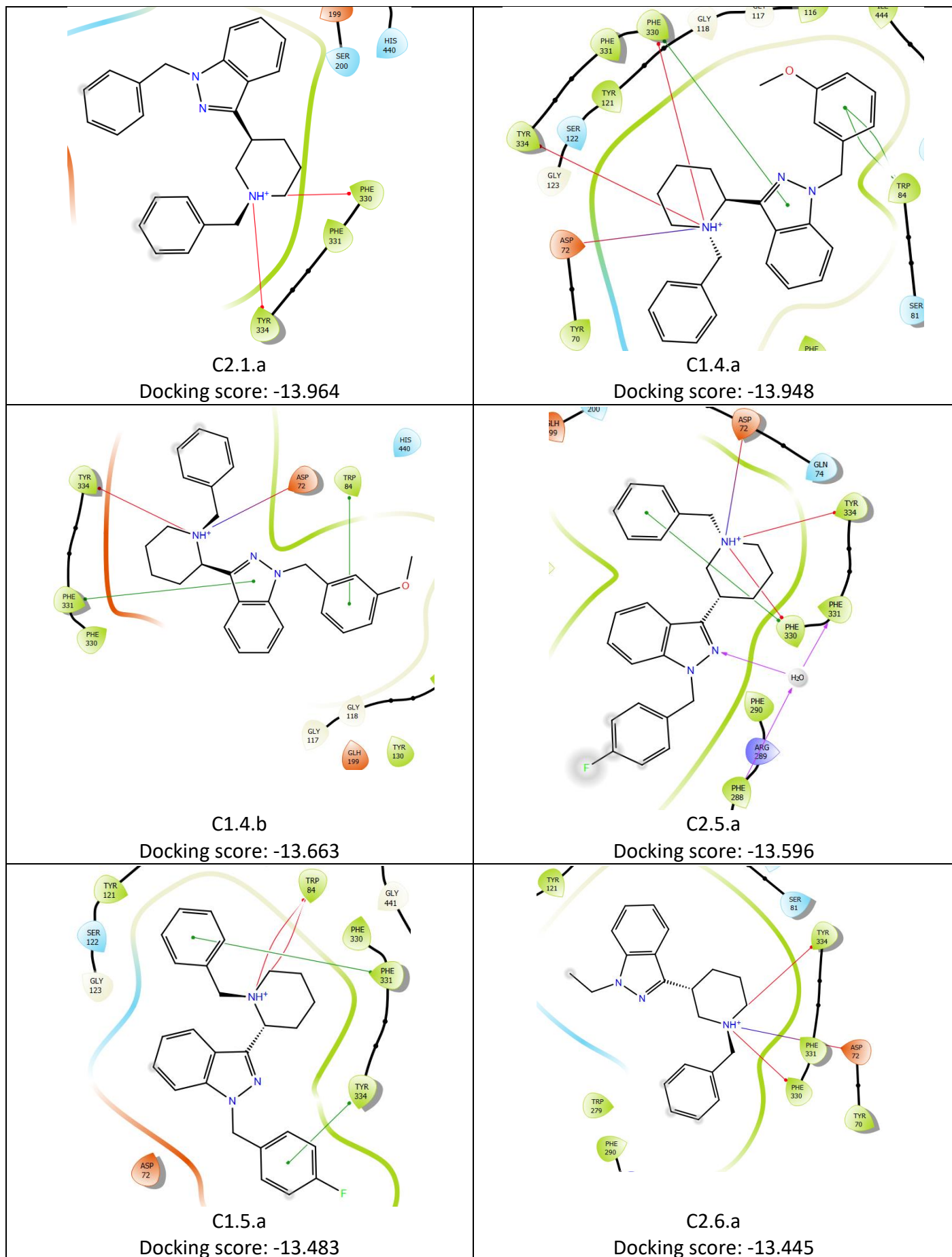
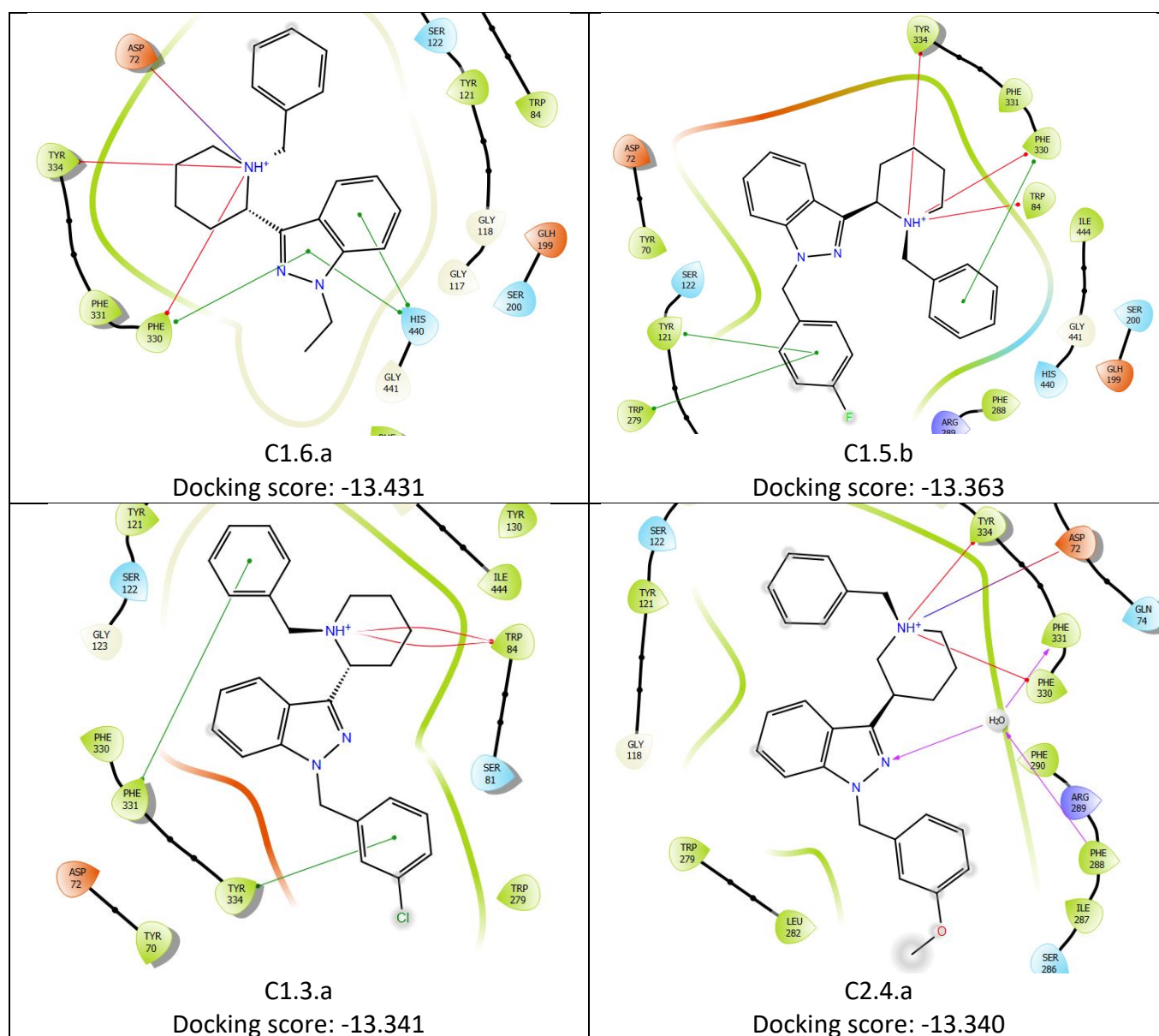


Table 3.3: Docking score and interactions of the best ten ligands across scaffolds A-C.5 -continued:

The ligands were divided into three distinct groups. Those considered good ligands that have docking scores ranging from -12.000 to -15.000 which corresponds well with the FDA approved drug donepezil (**25**) that has a docking score of -14.470. Thereafter, ligands with a docking score of -10.000 to -12.000 were considered fair with the potential to have activity improved through appropriate functionalisation. Finally, ligands that fall above -10.000 were considered to be poor ligands and would not be considered good options for future development.

From **Table 3.4** the most crucial amino acid interactions involved in the binding of ligands to the active site of AChE for the best 10 ligands are π - π interactions with Phe330, Trp84, and Trp279, and π -cation interactions with Phe330, Trp279 and Tyr334. Bridged H-bond interactions formed between the ligand and a water molecule between both Phe331 and Phe288 are also shown to be favourable.

Table 3.4: The π - π , π -cation and hydrogen interactions between the 10 best ligands and the amino acids involved (the distance of interactions measured in Å).

Ligand	Docking Score	π - π bonds (green bonds)							π -cation bonds (red bonds)						H ₂ O Bridge	
		His 440	Phe 330	Phe 331	Trp 84	Trp 279	Tyr 121	Tyr 334	Asp 72	Phe 330	Phe 331	Trp 84	Trp 279	Tyr 334		
25	-14.470				3.7 4.1	4.2				4.1			5.0		6.5	1.8 Phe331 Phe288
B1.1.a	-14.264		3.7		5.0 5.1 5.5	5.3							3.5 3.8			
A1.3.a	-14.017		5.4			4.1 4.1				3.4	6.2	5.3			5.4	2.0 Phe330
C2.1.a	-13.964									4.8					4.7	
C1.4.a	-13.948		4.5		3.6 4.2				4.3	5.9					4.6	

Table 3.4: The π - π , π -cation and hydrogen interactions between the 10 best ligands and the amino acids involved (the distance of interactions measured in Å – continued).

Ligand	Docking Score	π - π bonds (green bonds)							π -cation bonds (red bonds)						H ₂ O Bridge	
		His 440	Phe 330	Phe 331	Trp 84	Trp 279	Tyr 121	Tyr 334	Asp 72	Phe 330	Phe 331	Trp 84	Trp 279	Tyr 334		
C1.4.b	-13.663			5.3	4.1				4.7						3.8	
C2.5.a	-13.596		5.0						4.9	4.44					4.8	2.5 Phe331 Phe288
C1.5.a	-13.483			4.7				3.74				4.4 4.5				
C1.6.a	-13.431	4.6 5.3	5.3						4.1	4.1					4.6	
C2.6.a	-13.445								4.8	4.8					4.4	
C1.5.b	-13.363		5.2			4.4	5.2			3.9		6.1			5.6	
C1.3.a	-13.341			4.7				3.8				4.3 4.5				
C2.4.a	-13.34								4.7	3.8					4.5	4.32 Phe331 Phe288

Scaffold A's computational results indicate that all the planned ligands are considered good ligands as their docking scores are found to be between -12.000 and -15.000. The ligand considered to be the best of the

scaffold is **A1.3.a** (see **Table 3.3** and **Table 3.4**) and falls within the best 10 ligands overall. It has two π - π interactions with Trp279 and has both a π - π and a π -cation interaction with Phe330. Donepezil (**25**) and **A1.3.a** have corresponding π -cation interactions to Tyr334, Phe330, and Trp84, however, **A1.3.a** has an extra π -cation interaction with Phe331 and an additional π - π interaction with Phe330. Donepezil (**25**) has 2 π - π interactions with Trp84, whereas **A1.3.a** has none, which leads to donepezil's (**25**) higher docking score. Another essential interaction might be the H-bridge present in both donepezil (**25**) and **A1.3.a**. The water molecule is 1.8 Å from donepezil (**25**) and bridged between Phe330 and Phe228. However, **A1.3.a**'s water molecule is 2.0 Å away and is only bridged with Phe330, which could lead to a smaller contribution on the overall docking score of **A1.3.a** when compared to donepezil (**25**).

The other ligands in scaffold A are all considered to be good ligands and therefore have some similarities and some differences to **A1.3** (please see **Table 3.3** for detailed 2D-diagram interactions for scaffold A). The π - π interactions with Trp279 include ligands **A1.1**, **A1.4**, **A1.5**, **A1.6**, **A1.7** and **A1.8** where the number of interactions seem to be of importance. **A1.3** indicates a π - π interaction to Phe330 while the other ligands of scaffold A have π - π interactions with His440, Trp84, Tyr334, Tyr70, or Tyr121. The π -cation interactions in the rest of scaffold A contain two or more of the interactions present in **A1.3** which include amino acids Phe330, Phe331, Trp84, Tyr334. The only additional π -cation interaction present is Phe310 in **A1.4**. The ligands in scaffold A range from having one to two amino acids bridging the H-bond interaction which predominantly include Phe288 and Phe331.

Scaffold B's computational results indicate that only three ligands (**B1.1**, **B1.4** and **B1.5**) can be classified as good ligands with docking scores found between -12.000 and -15.000, while the rest of the ligands can be considered as having fair docking scores that fall between -10.000 and -12.000. The distance and number of interactions in scaffold B separating good ligands from the fair ligands indicates that the more interactions they make, especially those that include π - π interactions to Trp279, Trp84, Phe330 influence the ligand's docking score. Other π - π interactions involved in scaffold B include, Tyr121 and Tyr 334. The important π -cation interactions are found bonded to Trp279, Tyr334 and Phe330, but also include Trp84, Phe331. **B1.5**, **B1.7** and **B1.8** contained one or more donating groups from the following amino acids Arg289 and Phe288. Three of the fair ligands (**B1.2**, **B1.3** and **B1.1**) formed bridged H-bond interactions to both Phe331 and Phe288.

During this project, scaffold C underwent several redesigns driven primarily by synthetic difficulties experienced (see chapter 4), ultimately five sub-scaffold derivatives C1 to C5 were investigated computationally. In practice we cycled between synthesis and computational modelling from each sub-scaffold, however, for brevity and to facilitate ease of comparison we have elected to show and discuss all

five sub-scaffolds in this chapter ahead of providing a detailed overview of the synthetic difficulties experienced and how this drove the design of C2 to C5 (see chapter 4).

The computational results for scaffold C indicate that the ligands forming part of scaffolds C1 and C2 are all classified as good ligands with docking scores falling between -12.000 and -15.000, while the rest of the scaffolds (C3 to C5) are all poor ligands with docking scores higher than -10.000.

The ligands in scaffolds C1 and C2 all contain a benzyl group at either the 1,2 (C1) or 1,3 (C2) position relative to the piperidine *N*-atom. The ligand orientation of all these ligands differs enormously and most of the interactions are similar due to the presence of either 3 or 4 aromatic rings that can form π - π interactions or π -cation interactions. The π - π interactions listed under the C1 and C2 ligands in **Table 3.4** which fell under the best 10 ligands include Phe330, Tyr130, Trp84, Phe331, Tyr334 and His440. Other π - π interactions included, which formed part of the lowest docking scores in the set, are Tyr121 and Trp279.

The π -cation interactions that interacts with Trp84, Tyr334, Asp72 and Phe330 were present in most of the ligands in scaffolds C1 and C2, while an interaction with Phe331 was only observed with **C2.3**. The number and distance of these interactions are of importance. H-bridged interactions with Phe288 and Phe331 are observed only in ligands **C2.2**, **C2.3** and **C2.5**.

Scaffolds C3 and C4 were all classified as poor ligands, and this is caused directly by the absence of the benzyl group found in C1 and C2. The π - π interactions still contain the same interactions to amino acids like Trp84, Tyr334, His440, Phe330, Phe331 and the π -cation interactions still involve amino acids Phe331 and Tyr121. There are only three ligands, **C4.1**, **C4.3** and **C4.5** that indicate amino acids Phe288, and, or Arg289 acting as donors to the ligand. There are two ligands (**C3.1** and **C4.4**) that indicate no interactions and their docking scores are solely due to Van der Waals interactions across the surface of the ligands.

Scaffold C5 ligands contain two to four aromatic rings that could form interactions with amino acids, but only some sections of the ligands seem to interact, depending on the orientation of the ligand in the active site. All the ligands in scaffold C5 are arguably poor ligands with docking scores above -10.000. The functional groups like halide atoms which include I and Br are all interacting with amino acids that can donate an electron which includes **C5.5**, **C5.9** and **C5.13** which interact with Glh199. The ligands with a NO₂ functional group interact via two π -cation interactions with Trp279 and one with Tyr70 in the case of **C5.3** and in the case of **C5.4** only interacts with Arg289 which donates an electron to **C5.4**'s NO₂ group. While **C5.11** indicates two π -cation interactions with Trp279 and one amino acid donor Arg289.

The π - π interactions present in the ligands of scaffold C5 include Tyr121, Tyr334, Trp279, Trp84, Phe331 and His440. While the π -cation interactions are only present in two ligands (**C5.3** and **C5.11**) which are bonded

to Trp279 and Tyr70. H-donors and H-acceptors are found at carbonyl groups, pyridine group, an NH group, at NO₂ groups and halides which include Br and I. There are bridged H-bonds with Phe331 and Phe288 found in **C5.1**, **C5.2**, **C5.4**, **C5.5**, **C5.8**, **C5.9** and **C5.12**. There are also H-bridges found that are only bridged with Phe288 (**C5.3**) or Phe331 (**C5.7**).

From the scaffolds discussed we can conclude that the benzene rings found in the backbone of each scaffold are essential as they are involved in the π - π interactions with Trp279 and Phe330 which are found most frequently in the “good” ligands identified in the study. Other amino acids that seem to interact with the benzene rings include His440, Trp84 and Tyr334. A positively charged benzylated *N*-atom was also shown to be of great importance as it allows for π -cation interactions predominantly with Phe330, Phe331, Trp84 and Tyr334. It is considered that the functional groups which include carbonyl groups, pyridine rings, an NH group, NO₂ groups and halides are important as donor or acceptor groups which influence the docking scores of the respective ligands. It appears as if H-bridges bonded to 2 amino acids also have a good effect on the docking scores of the ligands under study, the two amino acids involved in the double bridged H-bonds seem to involve Phe331 and Phe288. Van der Waals interactions have not been discussed in detail above as all of the ligands do contain them, however, there are a few ligands that only contain these interactions (see **Figure 3.7**), and as such performed poorly.

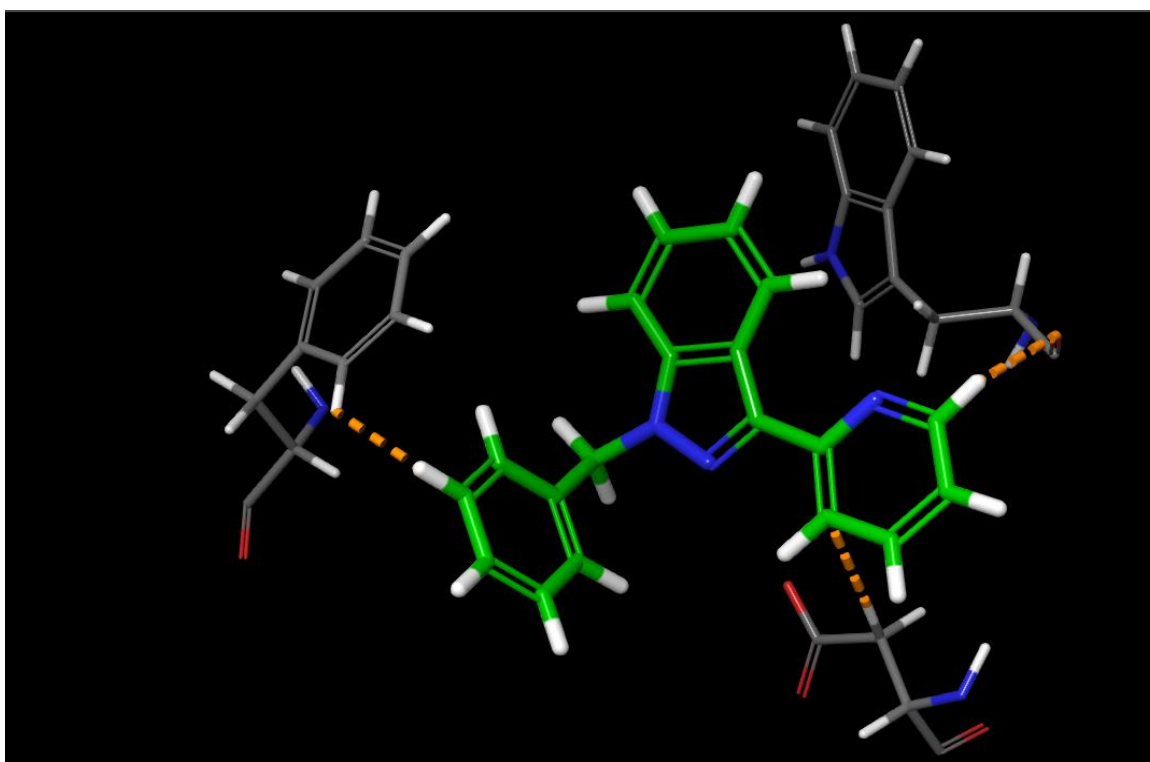


Figure 3.7: 3D representation of the interactions of C3.1.a with the active site of AChE with a docking score of -8.056. -Orange dashed lines indicate Van der Waals interactions.

3.3. Qikprop analysis, results, and discussion

The **Qikprop** task in **Maestro** provides absorption, distribution, metabolism, and excretion (ADME) predictions for each ligand. The program also includes other descriptors and properties with recommended ranges [77]. Lipinski's rule of five is a guide, indicating that ideally an orally available drug should adhere to all the rules before the ligand can be classified as drug-like. Ideally, the MW should be less than 500 g/mol, QPlogPo/w must be lower than 5, H-bond donors must be less than or equal to 5, and H-bond acceptors must be less than or equal to 10 [77, 78].

Table 3.5 indicates the docking score and Qikprop results for all conformers of donepezil (**25a-d**). As donepezil (**25**) is currently the FDA approved gold standard AChEI one would ideally want ligands with similar or lower docking scores. Although we previously grouped ligands with docking scores below -12 as "good" ligands while assessing the binding modes and interactions, we elected to further constrain the cut-off for a "good" ligand to a score of -13.000 (highlighted in green) moving forward so as to hopefully only identify ligands within 1 log unit difference to donepezil (**25**).

Table 3.5: Ligand descriptor values and their property values with their recommended limits.

Title	Docking score	MW	QPlogPo/w	QPlogBB	QPlogHERG	H-donor	H-acceptor	TPSA
Limit	-13.000	500.00	-2 to 6.5	-3 to 1.2	> -5.000	< 3	< 8.0	< 76.00
25.a	-14.470	379.50	4.453	0.099	-6.825	0	5.5	50.14
25.b	-14.384	379.50	4.429	0.099	-6.748	0	5.5	50.17
25.c	-13.657	379.50	4.406	0.116	-6.750	0	5.5	50.12
25.d	-12.423	379.50	4.386	0.117	-6.669	0	5.5	50.186

The Qikprop property called QPlogPo/w predicts the octanol/water partition coefficient, where the recommended value needs to fall between -2.0 to 6.5 [77]. The Qikprop property, QPlogBB, is the predicted brain/blood partition coefficient for orally delivered drugs, and the recommended range is -3.0 to 1.2 [77].

The cardiotoxicity screening property, QPlogHERG, predicts if a drug has the potential of interrupting the K⁺ current, which is encoded by the human ether-à-go-go gene, hERG. The blockage of the K⁺ channel can induce long QT syndrome (LQTS), which can lead to torsades de pointes that could degenerate into ventricular fibrillation and cause sudden death. QPlogHERG is measured as an IC₅₀ value representing the blockage of the hERG K⁺ channels indicating the cardiac toxicity of the drugs under study [77]. Concerns are raised when the value falls below -5.000, which are displayed as red blocks in the table above [77].

The number of hydrogen bonds present in the ligand that would be donated (H-donors) to the solute in

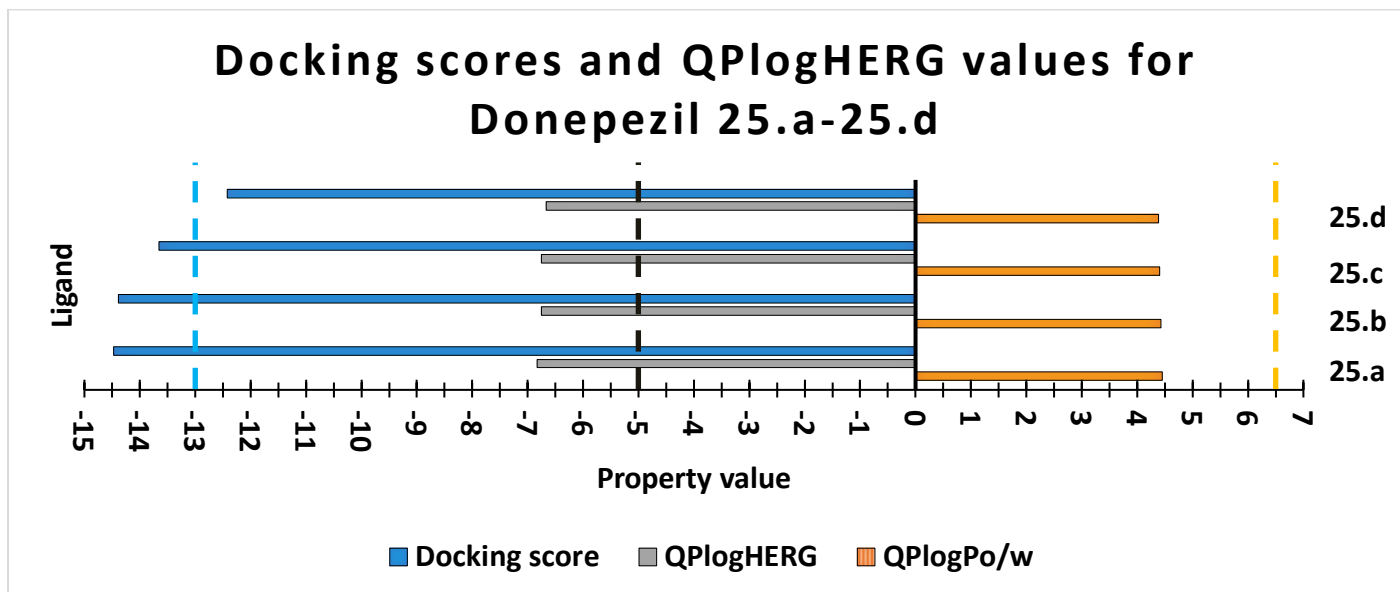
water molecules in an aqueous solution is limited to 6.00 [77]. However, this value was lowered to 5 by Lipinski's rules and then further reduced to 3 as the qualifying upper limit in a list of computed physiochemical qualifying ranges determined from already approved CNS oral drugs [78, 79]. The hydrogen acceptor (H-acceptor) limit was determined to be 8.3 as the qualifying range for CNS oral drugs [79]. The TPSA represents the Van der Waals surface area of the polar *N*- and *O*-atoms present in the ligand, the range was determined to be between 7 and 200 Å [77]. The TPSA limit was further lowered to 76 Å for the design of CNS lead compounds [79].

Table 3.5 indicates the docking score and some Qikprop results for all the possible conformers of donepezil (**25.a-25.d**) when interacting with the active site of AChE. The best docking score value is that of donepezil (**25.a**), which has a docking score of -14.470; it has a MW of less than 500.00 g/mol, QPlogPo/w less than 6.500 and a QPlogBB that falls between the range limits. These results indicate that the drug will be able to cross the BBB. It has no H-donors, but 5.5 H-acceptors and a TPSA of 50.16 Å.

The QPlogHERG value for donepezil (**25.a**), however, falls below the recommended -5.000 limit which indicates that at low concentrations it will cause a reduction in the hERG channel protein traffic [80]. While an increased concentration of donepezil (**25.a**) in the plasma membrane could cause a decrease in the channel protein expression through the inhibition of the K⁺ channel [80]. A suprathreshold concentration will be reached, where the effective concentration of the drug against AD reaches the levels whereby the drug will endanger a patient's health. As a result, it is of importance to have a low inhibition concentration for these drugs; otherwise, the hERG K⁺ channel could be blocked.

The visual representation of the limits of three of these descriptors can be seen in **Graph 3.1** for the donepezil conformers (**25.a-25.d**). As can be seen the docking score (blue) is close to or exceeds a value of -13.000 (blue dashed line) which we selected as the predictive cut-off for good inhibitors, as such compounds with comparable or better docking scores could potentially inhibit AChE within the same range as donepezil (**25**). The orange dashed line indicates QPlogPo/w (orange) upper limit for BBB penetration; in all instances **25.a-25.d** is lower than the upper limit. Finally, QPlogHERG (grey) limit is indicated by the black dashed line, which is exceeded by **25.a-25.d** and, therefore, indicates that donepezil (**25**) may block the hERG K⁺ channel in the heart if the drug concentration exceeds its effective concentration.

The program **Maestro** was used to calculate all the possible conformations for each ligand docked into the active site of AChE, which results in a docking score, and the Qikprop data seen in **Table 3.6**. The Qikprop data includes the molecular MW, QPlogPo/w, QPlogBB, QPlogHERG, H-donors, H-acceptors, and the TPSA of each ligand under study.



Graph 3.1: Docking score, QPlogPo/w and QPlogHERG of donepezil (25a – 25.d).

Table 3.6: Docking score and Qikprop data of the conformations of the ligands in scaffolds A-C5.

Title	Docking score	MW	QPlogPo/w	QPlogBB	QPlogHERG	H-donor	H-acceptor	TPSA
Limit	-13.000	500.00	-2 to 6.5	-3 to 1.2	> -5.000	< 3	< 8.0	< 76.00
A1.1.a	-12.926	346.385	4.783	-0.907	-6.635	0.0	3.5	72.61
A1.2.a	-13.076	360.412	4.796	-0.957	-6.417	0.0	3.5	72.07
A1.3.a	-14.017	360.412	5.195	-0.903	-6.887	0.0	3.5	70.78
A1.4.a	-12.706	374.438	3.940	-0.225	-7.263	0.0	5.5	65.56
A1.5.a	-13.021	374.438	4.025	-0.059	-6.955	0.0	5.5	67.61
A1.6.a	-12.929	388.465	4.314	-0.231	-7.158	0.0	5.5	66.86
A1.7.a	-12.997	388.465	4.320	-0.378	-7.679	0.0	5.5	66.28
A1.8.a	-13.147	388.465	4.309	-0.320	-7.528	0.0	5.5	67.07
B1.1.a	-14.264	413.478	4.889	-0.980	-6.564	0.0	5.7	78.62
B1.2.a	-10.829	427.505	5.565	-1.038	-7.275	0.0	5.7	72.73
B1.3.a	-11.521	427.505	5.369	-0.975	-7.061	0.0	5.7	73.17
B1.4.a	-12.114	441.532	3.485	-0.527	-6.288	0.0	7.7	70.56
B1.5.a	-12.162	441.532	3.852	-0.870	-7.847	0.0	7.7	75.09
B1.6.a	-11.699	455.558	4.167	-0.536	-7.673	0.0	7.7	72.15
B1.7.a	-11.133	455.558	4.386	-0.548	-7.495	0.0	7.7	71.42
B1.8.a	-10.843	455.558	4.421	-0.810	-8.009	0.0	7.7	73.47
C1.1.a	-13.094	381.519	6.030	0.651	-6.674	0.0	3.0	14.50
C1.2.a	-13.254	411.546	5.940	0.550	-6.925	0.0	3.8	26.69
C1.3.a	-13.341	415.964	6.599	0.807	-6.799	0.0	3.0	14.87
C1.4.a	-13.948	411.546	6.616	0.526	-7.513	0.0	3.8	25.05

Table 3.6: Docking score and Qikprop data of the conformations of the ligands in scaffolds A-C5 – continued.

Title	Docking score	MW	QPlogPo/w	QPlogBB	QPlogHERG	H-donor	H-acceptor	TPSA
C1.4.b	-13.663	411.546	6.093	0.548	-7.275	0.0	3.8	25.99
C1.5.a	-13.483	399.510	6.436	0.755	-7.239	0.0	3.0	14.63
C1.5.b	-13.363	399.510	6.303	0.779	-7.482	0.0	3.0	13.63
C1.6.a	-13.431	319.449	4.913	0.771	-5.713	0.0	3.0	16.83
C2.1.a	-13.964	381.519	6.112	0.630	-7.222	0.0	3.0	15.65
C2.2.a	-12.856	411.546	6.320	0.534	-7.688	0.0	3.8	29.15
C2.3.a	-12.688	415.964	6.680	0.766	-7.418	0.0	3.0	20.76
C2.4.a	-13.340	411.546	6.436	0.535	-7.889	0.0	3.8	28.11
C2.5.a	-13.596	399.510	6.237	0.696	-7.528	0.0	3.0	20.57
C2.6.a	-13.445	319.449	4.960	0.747	-6.386	0.0	3.0	18.90
C3.1	-8.056	285.348	5.118	0.323	-6.263	0.0	2.0	22.72
C3.2	-7.861	315.374	5.095	0.239	-6.299	0.0	2.8	32.87
C3.3	-9.332	319.793	5.476	0.455	-6.284	0.0	2.0	23.83
C3.4	-8.390	315.374	5.118	0.147	-6.367	0.0	2.8	33.44
C3.5	-8.845	303.338	5.311	0.413	-6.378	0.0	2.0	21.70
C3.6	-6.186	223.277	3.699	0.267	-5.301	0.0	2.0	27.14
C4.1	-8.667	285.348	4.501	0.094	-5.899	0.0	2.5	28.59
C4.2	-8.061	315.374	4.802	0.068	-6.220	0.0	3.3	33.69
C4.3	-9.186	319.793	5.077	0.222	-6.232	0.0	2.5	28.90
C4.4	-8.468	315.374	4.820	0.067	-6.379	0.0	3.3	33.80
C4.5	-9.250	303.338	4.819	0.171	-5.966	0.0	2.5	29.47
C4.6	-6.820	223.277	3.423	0.205	-5.150	0.0	2.5	27.51
C5.1.a	-8.754	282.341	3.312	-0.344	-5.358	0.0	4.5	67.65
C5.2	-9.174	318.331	2.937	-1.084	-6.226	1.0	5.3	92.32
C5.3	-9.047	347.329	2.686	-1.574	-6.368	0.0	5.5	114.91
C5.4	-8.689	361.356	3.233	-1.428	-6.536	0.0	5.5	109.99
C5.5	-8.140	395.255	4.586	-0.166	-6.626	0.0	4.5	65.06
C5.6	-8.578	320.322	3.690	-0.539	-6.547	0.0	4.5	71.73
C5.7	-9.068	320.322	3.740	-0.426	-6.418	0.0	4.5	70.29
C5.8	-8.318	320.322	3.569	-0.379	-5.799	0.0	4.5	70.27
C5.9	-8.159	428.228	4.021	-0.157	-5.702	0.0	4.5	68.71
C5.10	-8.194	302.332	3.707	-0.391	-6.716	0.0	4.5	67.43
C5.11	-8.899	392.327	1.963	-2.270	-5.688	0.0	6.5	160.80
C5.12	-7.977	296.368	3.721	-0.710	-5.815	0.0	4.5	70.91
C5.13	-8.233	375.264	4.288	-0.351	-5.542	0.0	4.5	64.49

Docking scores lower than the lower limit set at -13.000, are indicated in green blocks in **Table 3.6**; these ligands are identified as having the potential to be potent AChEIs in light of the fact that they display

comparable binding scores to the known inhibitor donepezil (**25**). In the case of scaffold A, five ligands surpassed the docking score lower limit including; **A1.2.a**, **A1.3.a**, **A1.5.a**, **A1.8a** and **A1.8.b**., however, there was only a single ligand in scaffold B that surpassed the lower limit, and that was **B1.1.a**. Interestingly, scaffold C performed better with fourteen ligands (**C1.1.a**, **C1.2.a**, **C1.3.a**, **C1.3.b**, **C1.3.c**, **C1.4.a**, **C1.4.b**, **C1.5.a**, **C1.5.b**, and **C1.6.a**, **C2.1.a**, **C2.4.a**, **C2.5.a** and **C2.6.a**) having a docking score of -13.000 or lower. A total of twenty ligands were identified as potential AChEIs when considering the docking score values. Furthermore, **Table 3.6** indicates that all the ligands assessed fall under the limit of 500 g/mol for the MW and fall between the lower limit (-3) and upper limit (1.2) for QPlogBB, therefore indicating that these ligands can be classified as drug-like and will potentially be able to cross the BBB. The only red flags noted are for **C1.3.a**, **C1.4.b** and **C2.3.a** which narrowly fall outside of the ideal range for lipophilicity (QPlogPo/w).

Unfortunately, all the ligands indicate QPlogHERG values falling below the recommended -5.000 lower limit (highlighted in red in **Table 3.6**). As such, low concentrations of these ligands in the plasma membrane might only result in a reduced hERG channel protein traffic. In contrast, an increased concentration can possibly cause a decrease in the channel protein expression through the inhibition of the K⁺ channel [80]. For these ligands, a supratherapeutic concentration will be reached when the effective concentration of the drug against AD reaches levels where it will be dangerous to your health. Therefore, these ligands if used for the treatment of AD, would need to be administered at low enough dosages to maintain activity but not cause significant inhibition of the hERG channel.

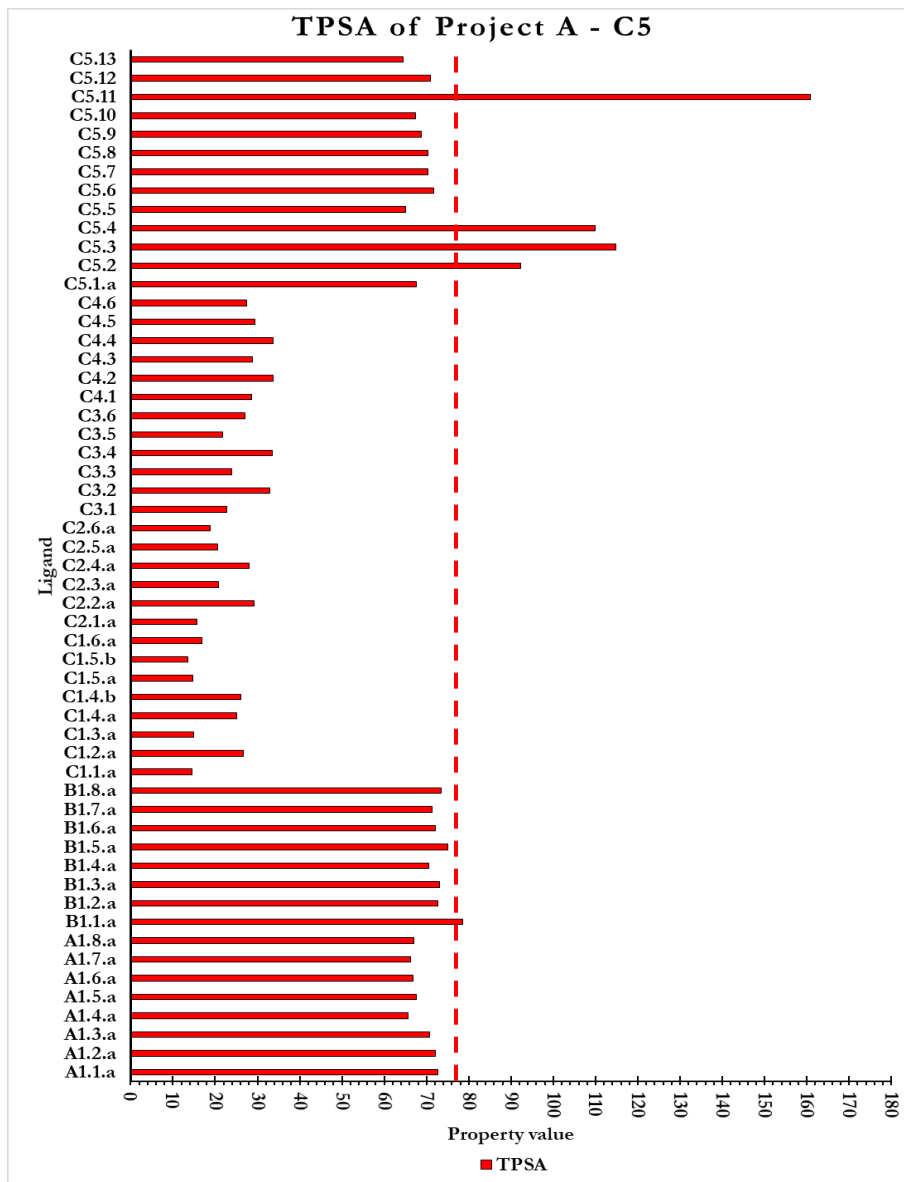
Table 3.6 indicates the number of H-donors that are present in ligands of scaffolds A-C5, which all meet the recommended maximum of 3 H-donors requirement. Additionally, the number of H-acceptors for all the studied ligands are lower than the recommended maximum of 8 H-acceptors.

The data generated for the entire virtual library is represented visually in **Graphs 3.2** and **3.3**, highlighting the values for the docking scores, QPlogHERG, QPlogPo/w and TPSA and their respective cut-off points.

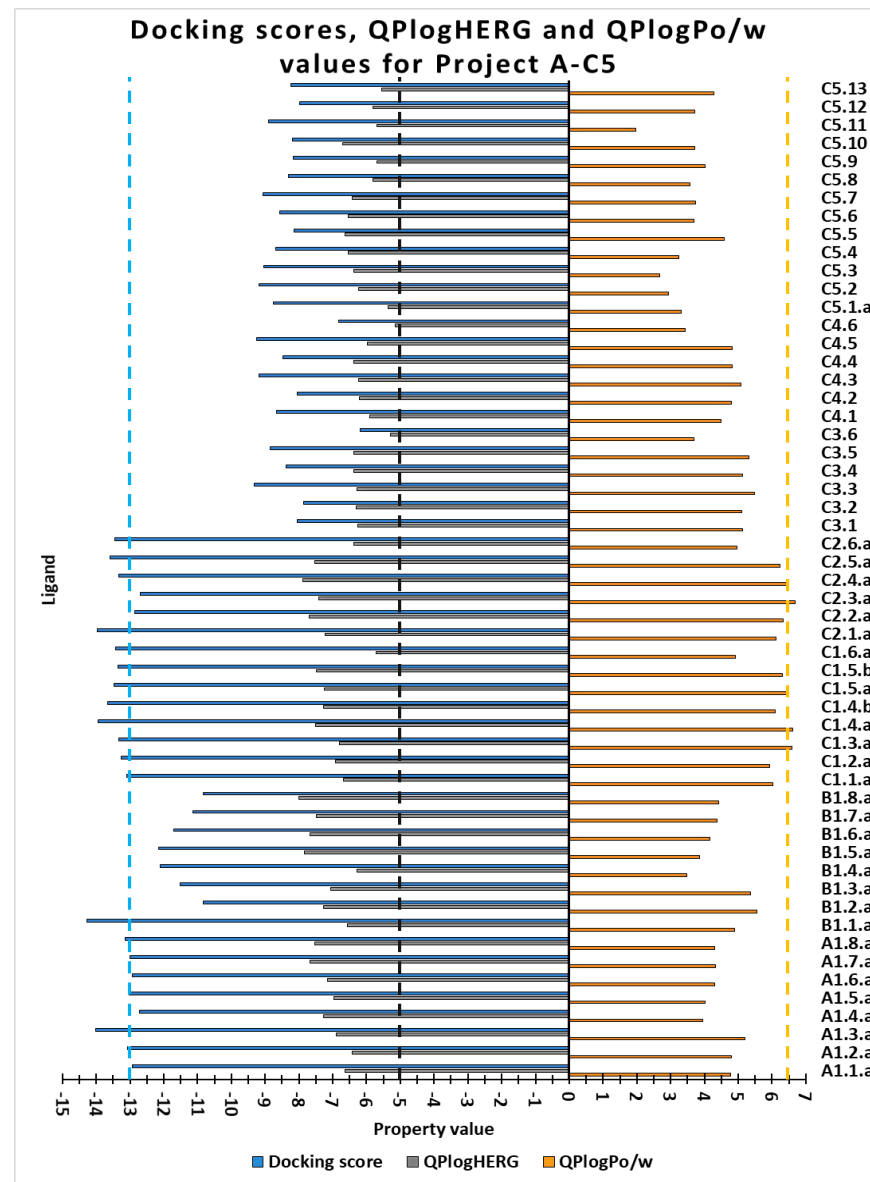
In terms of drug absorption, although all ligands are predicted to fall within the range for BBB penetration, the lipophilicity (QPlogPo/w) and TPSA values should also ideally be less than 6.500 and 76.00 Å respectively to ensure good absorption, in the case in hand only **B1.1.a** fell outside of this range.

A total of sixty-five ligands were studied which resulted in fifty-seven ligands with potential drug-like properties. A docking score of less than -13.000 was used as a further selection criterium which gave a total of seventeen ligands as potential AChEI hits. In addition, even though ligand **B1.1.a** was classified as non-drug-like, it had a very attractive docking score value of -14.264 and as such it was included with the other seventeen virtual hits as a viable synthetic target.

Ligands **A1.3.a**, **C1.6.a** and **C2.6.a** are the three ligands classified as the most promising drug-like molecules of the scaffolds according to their docking scores -14.017, -13.431 and -13.445 respectively. These three drugs all obeyed Lipinski's rules and other important drug requirements which included QPlogBB, QPlogPo/w and TPSA. As an AD drug targeting the brain, they are predicted to be able to cross the BBB and the QPlogHERG property, being disobeyed, can be regulated via dosages.



Graph 3.2: Total polar surface area of the ligands of scaffolds A-C5.



Graph 3.3: Comparison of the docking score and QPlogHERG values of the ligands for scaffolds A-C5.

3.4. Pharmacophore model

To gain further insight into the virtual ligands the program, *Phase* in *Maestro*, was used to develop a pharmacophore model from the 3D-docked ligands of scaffolds A, B and C. In this instance the ligands were split into active and inactive ligands again using the docking score of -13.000 as a cut-off between actives and in-actives.

The chemical structure pattern of all the ligands was then used to determine the pharmacophore features, which were then displayed graphically in the workspace as specific shapes. Hydrogen acceptors are displayed as red spheres, positive ionic atoms as a blue spheres and aromatic rings as orange rings.

A generated hypothesis had to match with at least 60 % of the twenty-one actives (ligands having a docking score below -13.000), therefore, decreasing the number of hypotheses being generated but still allowing for the variation in the degree of motion represented by the grey spheres around the pharmacophore features. Furthermore, the number of features in the hypothesis was limited to between 4 and 7 pharmacophore sites.

The difference allowed between hypotheses criterion was set as 0.5, which specifies that two hypotheses might be the same in every configuration of the ligands (e.g., as APRR, which indicates the presence of an acceptor atom, the positively charged ionic atom, and two aromatic rings). As a result, only the best-scored hypothesis is kept and available for analysis. The hypotheses were ranked using a scoring function in *Maestro* called *Phase Hypo Score*, which generates a score based on the ligand's alignment to the hypothesis and to each other.

An excluded volume shell was also generated, which is represented by the light blue spheres. These spheres are found surrounding the hypothesis and are placed in all regions where the in-actives had atoms while the actives did not. A total of 11 hypotheses were generated with four pharmacophore sites each. The hypothesis with the highest score, called APRR, is discussed below.

Figure 3.8 indicates the pharmacophore sites involved in hypothesis APRR. The pharmacophore sites have a tolerance of 2.00 Å around each site, which is represented by the grey spheres. The pharmacophore site A1 indicates the acceptor atom (red sphere) and a vector indicating the general location of the donating atom. P5 represents a positive ionic atom, while R7 and R9 indicate the presence of two aromatic ring pharmacophore sites. The light blue spheres indicate the excluded volumes.

Figure 3.9 indicates the overlap of active ligands **A1.3.a** (yellow), **B1.1.a** (green), and **C1.3.a** (turquoise) with the pharmacophore hypothesis APRR. All four pharmacophore sites are overlapping with each ligand,

indicating that these ligands are potential actives having some resemblance at these essential interactions.

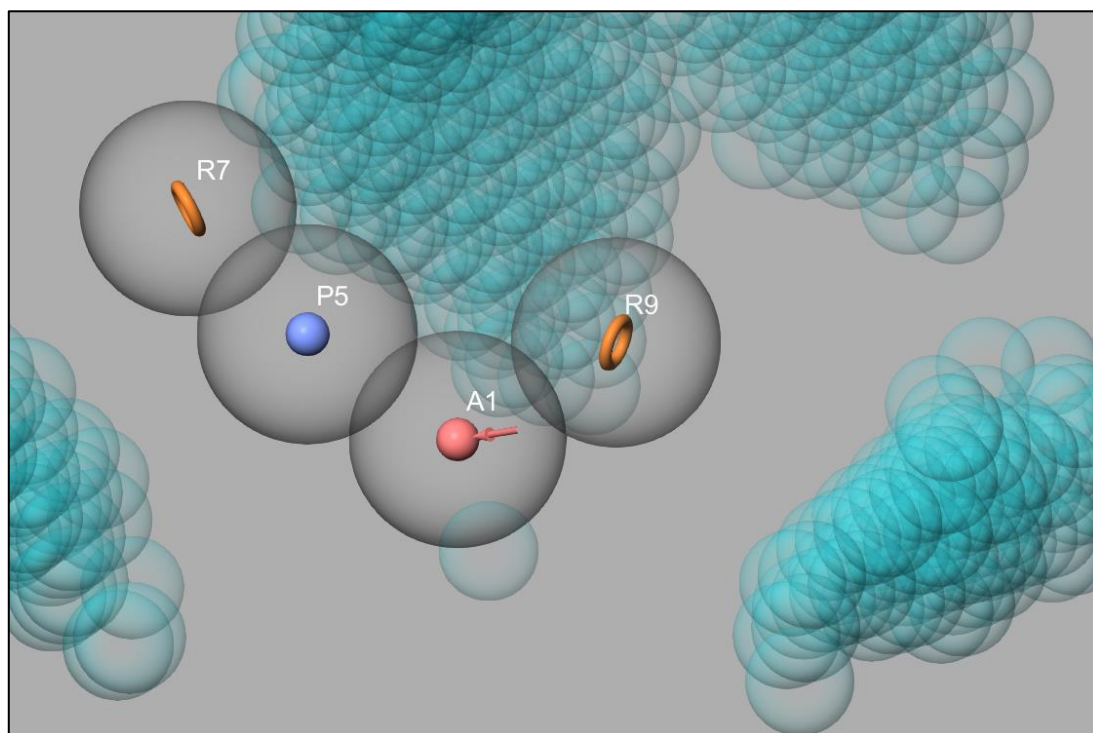


Figure 3.8: Grey spheres represent the pharmacophore site hypothesis (APRR) with a tolerance of 2.00 Å around each site. -A1 indicates the acceptor atom (red sphere). P5 indicates the positive ionic atom (blue sphere). R7 and R9 indicates 2 aromatic ring pharmacophore sites (orange rings).

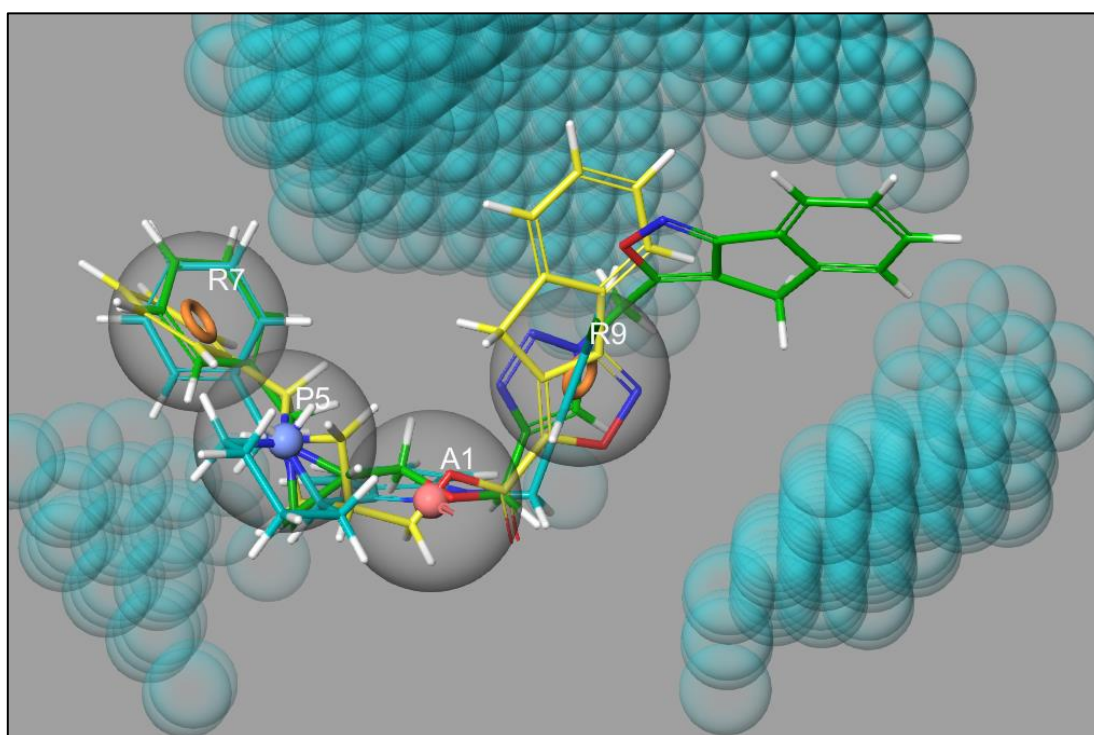


Figure 3.9: Active ligands **A1.3.a** (yellow), **B1.1.a** (green), and **C1.3.a** (turquoise) overlaid with the hypothesis APRR.

Figure 3.10 indicates the overlap of ligands **C1.4.a** (yellow), **C1.4.b** (green), **C1.5.a** (turquoise), **C1.5.b** (purple), and **C1.6.a** (pink) with the hypothesis APRR. The pair of conformers (**C1.4.a** and **C1.4.b**; **C1.5.a** and **C1.5.b**) orientate themselves in such a way that in all instances they overlap with these critical interaction sites.

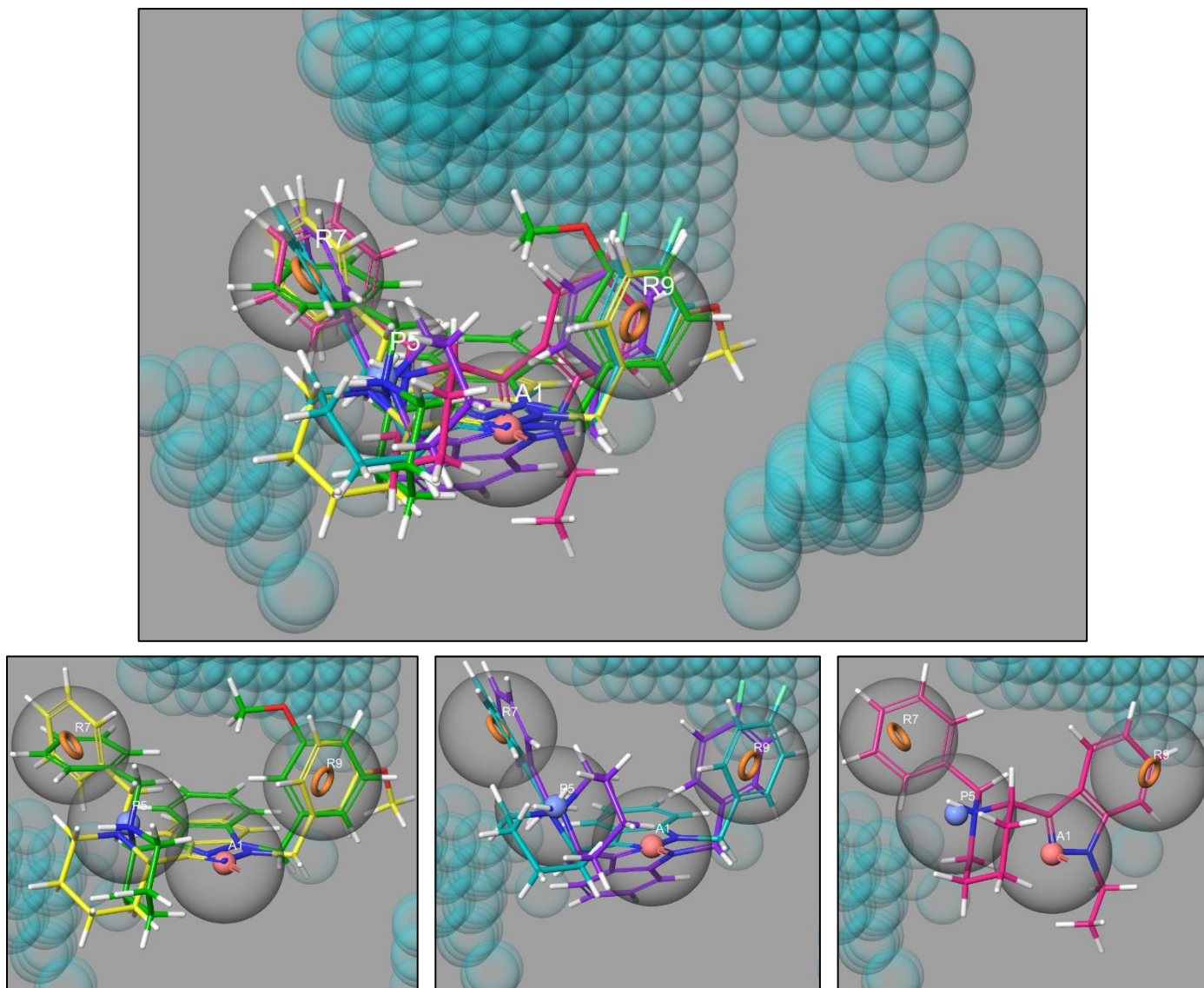


Figure 3.10: Active ligands, **C1.4.a** (yellow), **C1.4.b** (green), **C1.5.a** (turquoise), **C1.5.b** (purple), and **C1.6.a** (pink) displayed with the hypothesis APRR.

Figure 3.11 indicates the overlap of ligands **C2.1.a** (yellow), **C2.4.a** (green), **C2.5.a** (turquoise), and **C2.6.a** (purple) with the hypothesis APRR, indicating that these ligands orientate themselves in close proximity to the pharmacophore sites. Their docking scores are also similar, but their difference was more due to the interaction with Van der Waals forces than the interaction via other π -cation interactions, which did not form part of the pharmacophore sites generated by the best hypothesis. See **Chapter 4, section 4.2**, for more information.

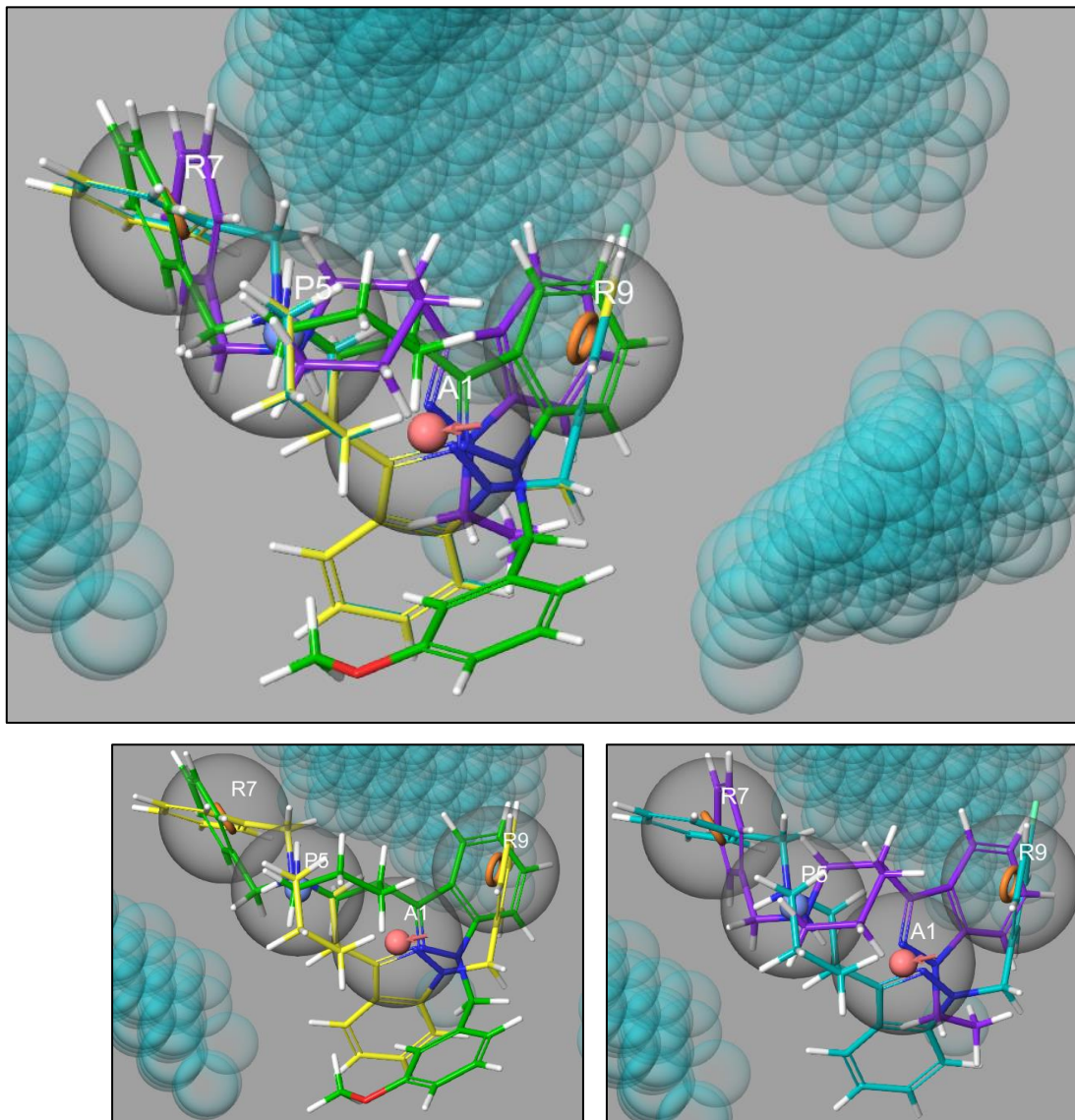


Figure 3.11: Active ligands, **C2.1.a** (yellow), **C2.4.a** (green), **C2.5.a** (turquoise), and **C2.6.a** (purple) displayed with the hypothesis APRR.

Figure 3.12 indicates the overlap of the conformers of donepezil **25.a** (yellow) and **25.b** (green) with the hypothesis APRR. The overlap with the pharmacophore sites was not ideal, but still fell within the tolerance of 2.00 Å. The high docking score of **25.a** and **25.b** is therefore in part due to their overlap with the identified pharmacophore sites when considering the similarity to the hypothesis generated from only **25.a** (see **Figure 3.13**; H-25). The high docking score for **25.a** is also due to other favourable interactions discussed earlier in this chapter.

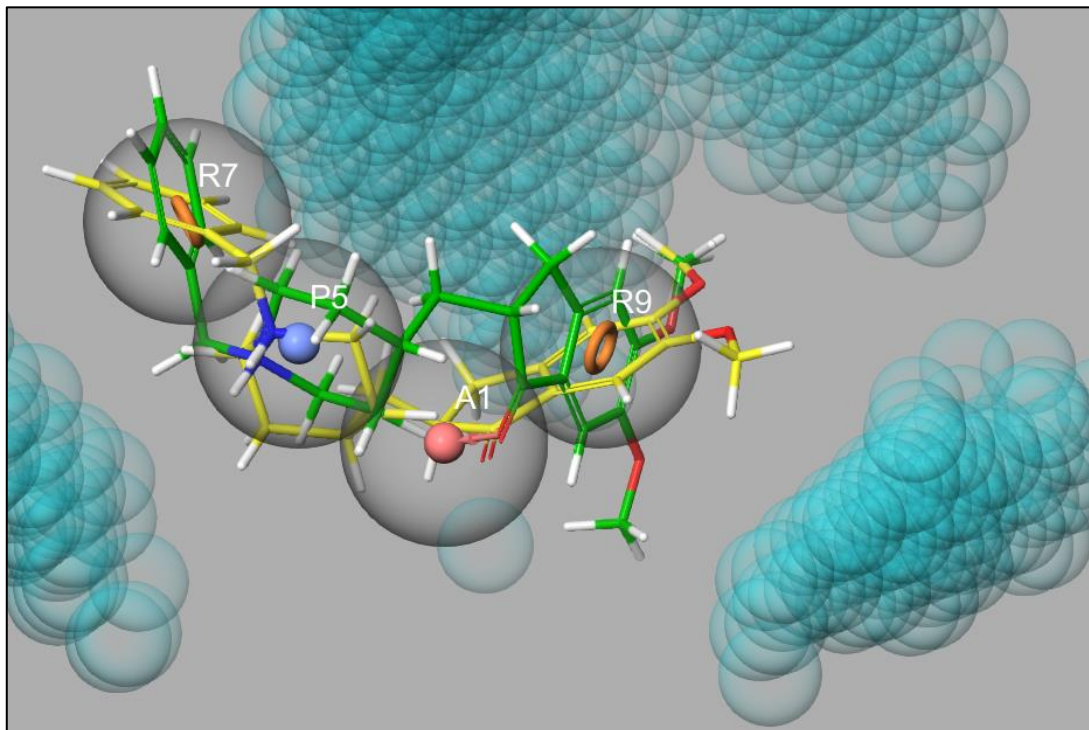


Figure 3.12: Active ligands of donepezil **25.a** (yellow) and **25.b** (green) displayed with the hypothesis APRR.

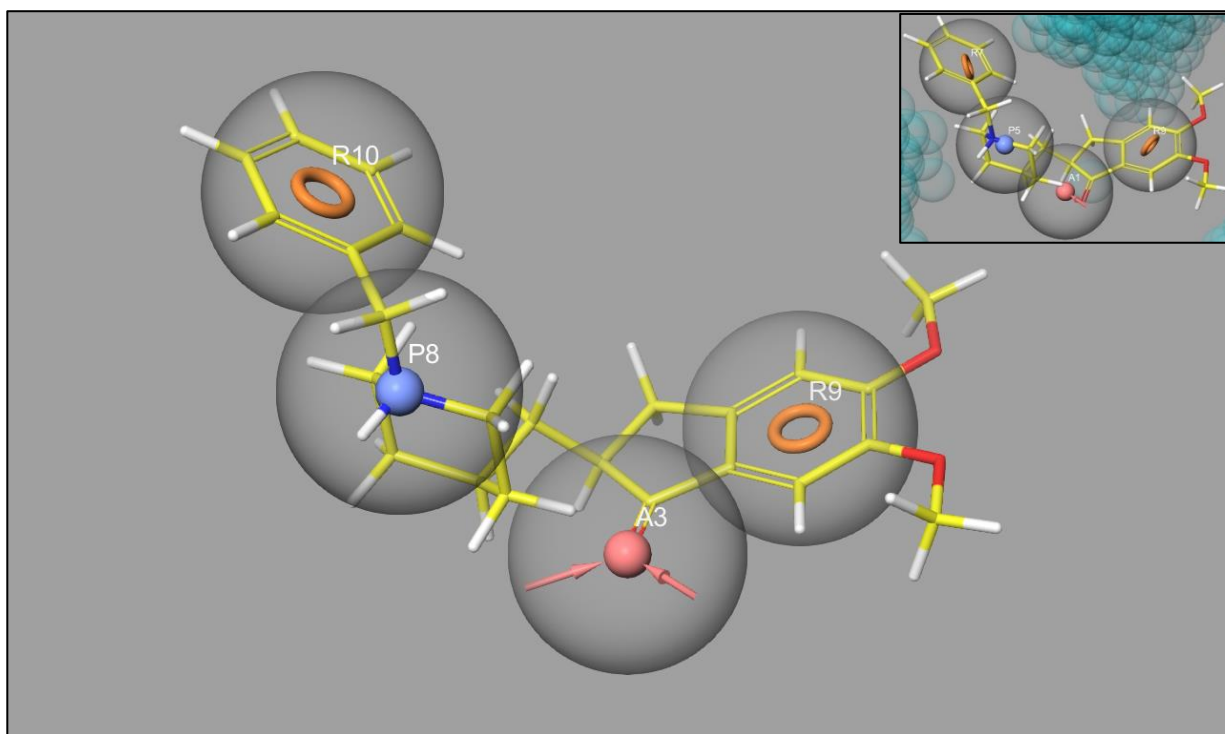


Figure 3.13: Hypothesis generated from 25.a as reference ligand (H-25) with no excluded volumes shown. - Right-hand corner: Hypothesis APRR generated from scaffolds A, B, C and donepezil (**25**).

See **Figure 3.13** for the pharmacophore sites of the hypothesis generated from donepezil (**25.a**), designated H-25. H-25 would in turn indicate that there would be less overlap with the ligands from scaffolds A-C as their structures differ somewhat from that of donepezil (**25**). The pharmacophore sites of H-25's aromatic

rings are slightly angled compared to the original hypothesis, while the location of the acceptor (red sphere) and positively charged atom (blue sphere) has moved slightly.

The pharmacophore sites generated were also overlapped with the ten worst performing ligands in **Figure 3.14** and **Figure 3.15**. **Figure 3.14** indicates the inactive ligands that only partially overlap with the pharmacophore sites. The crucial pharmacophore site where overlap is largely missing is at P5 which ideally requires the presence of a suitable H-bond acceptor, a feature which is absent in these ligands (**C3.1**, **C3.2**, **C4.2**, **C5.5**, **C5.9** and **C5.10**). **Figure 3.15** highlights the remaining worst performers (**C3.6**, **C4.6**, **C5.12** and **C5.13**) showing completely different orientations and little to no-overlap with the pharmacophore model.

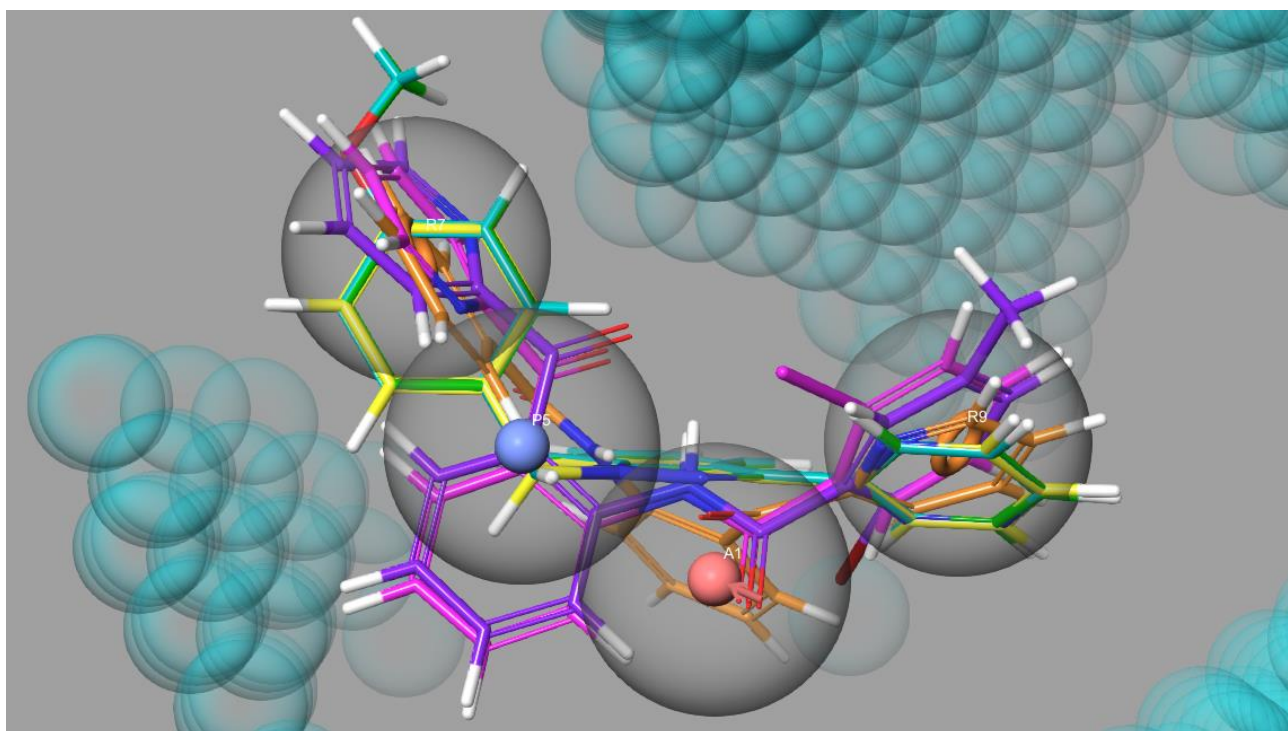


Figure 3.14: Inactive ligands with a partial match to hypothesis APRR, **C3.1** (yellow), **C3.2** (green), **C4.2** (turquoise), **C5.5** (purple), **C5.9** (pink) and **C5.10** (orange) displayed with the hypothesis APRR.

The pharmacophore sites generated for scaffolds A to C can be used in future studies as a template for assessing both real and virtual compound libraries. One should of course be cognisant of the fact that in a real-world dynamic system the enzyme can adopt different conformational arrangements whereas in the *in silico* model employed in this study the enzyme is regarded as a static entity based upon a crystal structure in which donepezil (**25**) was bound. The docking and pharmacophore models developed will as a result, have a bias towards donepezil (**25**) like compounds and one may miss novel actives that are structurally different from donepezil (**25**). That being said, the pharmacophore model generated will be useful for probing

unexplored chemical space surrounding donepezil (**25**).

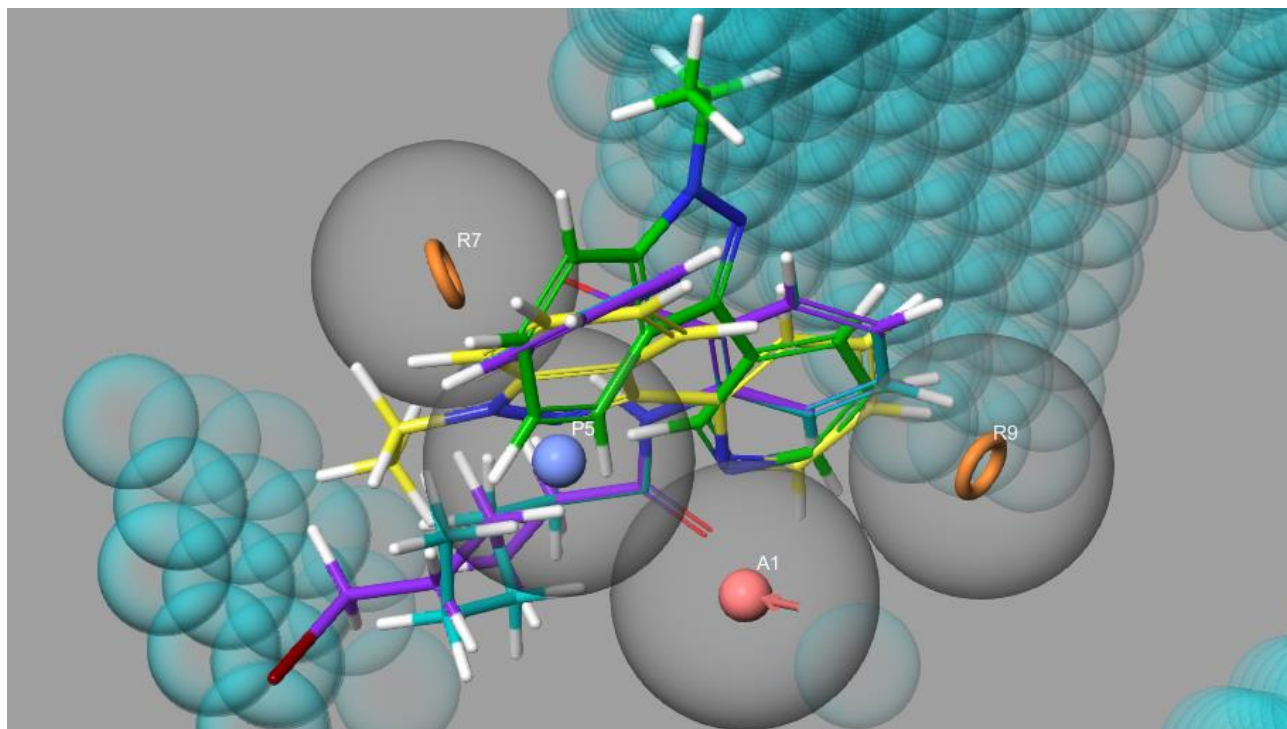


Figure 3.15: Ligands with no overlap with hypothesis APRR, **C3.6** (yellow), **C4.6** (green), **C5.12** (turquoise), and **C5.13** (purple).

3.5. SwissADME analysis

The program, **SwissADME**, was used to assess scaffolds A-C in terms of their physiochemical descriptors, predictive ADME parameters and their pharmaco-kinetic properties. The program was developed by the Swiss Institute of Bioinformatics as a free to use online webtool [81]. The parameter descriptions assessed can be seen in **Table 3.7**, and an example of the data generated can be seen in **Figure 3.16**. The complete dataset for scaffolds A – C5 can be seen in **Appendix I**.

Figure 3.17 highlights a “Boiled-egg” plot generated by the program for scaffold A, the plot depicts the predicted BBB permeants (yellow area) and gastrointestinal (GI) permeants (yellow and white areas) based upon the compounds lipophilicity (WlogP) and TPSA. The blue circles represent compounds that are P-gp substrates and which can be actively transported out of the brain across the BBB. The red circle indicates that the compound is not predicted to be a P-gp substrate and, therefore may potentially lead to accumulation in the brain if initial passage across the BBB into the brain is realized [81]. Therefore, all the compounds in scaffold A are predicted to be able to cross the GI tract and the BBB. Ligand **A1.1** is not a P-gp

substrate and may accumulate in the brain.

Table 3.7: SwissADME parameter abbreviations.

Parameter abbreviation	Description
TPSA	Total Polar Surface Area
Log P_{o/w}	Partition coefficient between octanol and water
Log S	Water solubility: insoluble < - 10 < poorly < - 6 < moderately < - 4 < soluble < - 2 < very < 0 < highly
Gi absorption	Gastrointestinal absorption (egg white in the boiled egg diagram)
BBB permeant	Blood-brain barrier penetration (egg white in the boiled egg diagram)
P-gp substrate	P-glycoprotein substrate which is responsible for the efflux of xenobiotics out of the cell
CYP inhibitor	CYP450 isozyme inhibition in the liver Isozymes include: CYP1A2, CYP2C9, CYP3A4, CYP2C19, CYP2D6
Log K_p	Partition coefficient through the skin
Lipinski	Meet the Lipinski's rule of five: MW ≤ 500; MLOGP ≤ 4.15; HBD (N and O-atoms) ≤ 10; HBA (NH or OH groups) ≤ 5
Ghose	Meet the following Ghose rules: 160 ≤ MW ≤ 480; -0.4 ≤ WLOGP ≤ 5.6; 40 ≤ MR ≤ 130, 20 ≤ atoms ≤ 70
Veber	Meet the following Veber rules: Rotatable bonds ≤ 10; TPSA ≤ 140
Egan	Meet the following Egan rules: WLOGP ≤ 5.88; TPSA ≤ 131.16
Muegge	Meet the following Muegge rules: 200 ≤ MW ≤ 600; -2 ≤ XLOGP ≤ 5; TPSA ≤ 150; Num. rings ≤ 7; Num. carbon > 4; Num. heteroatoms > 1; Num. rotatable bonds ≤ 15; H-bonds acceptors ≤ 10; H-bond donors ≤ 5
Bioavailability Score	Probability of F > 10 % in rat
PAINS	Pan Assay Interference Structures (False positives)
Brenk	Structural alert
Leadlikeness	The likeliness that the compound will be a lead compound: 250 ≤ MW ≤ 350; XlogP ≤ 3.5; Num. rotatable bonds ≤ 7
Synthetic accessibility	Synthetic accessibility score: 1 (easy) – 10 (very difficult)

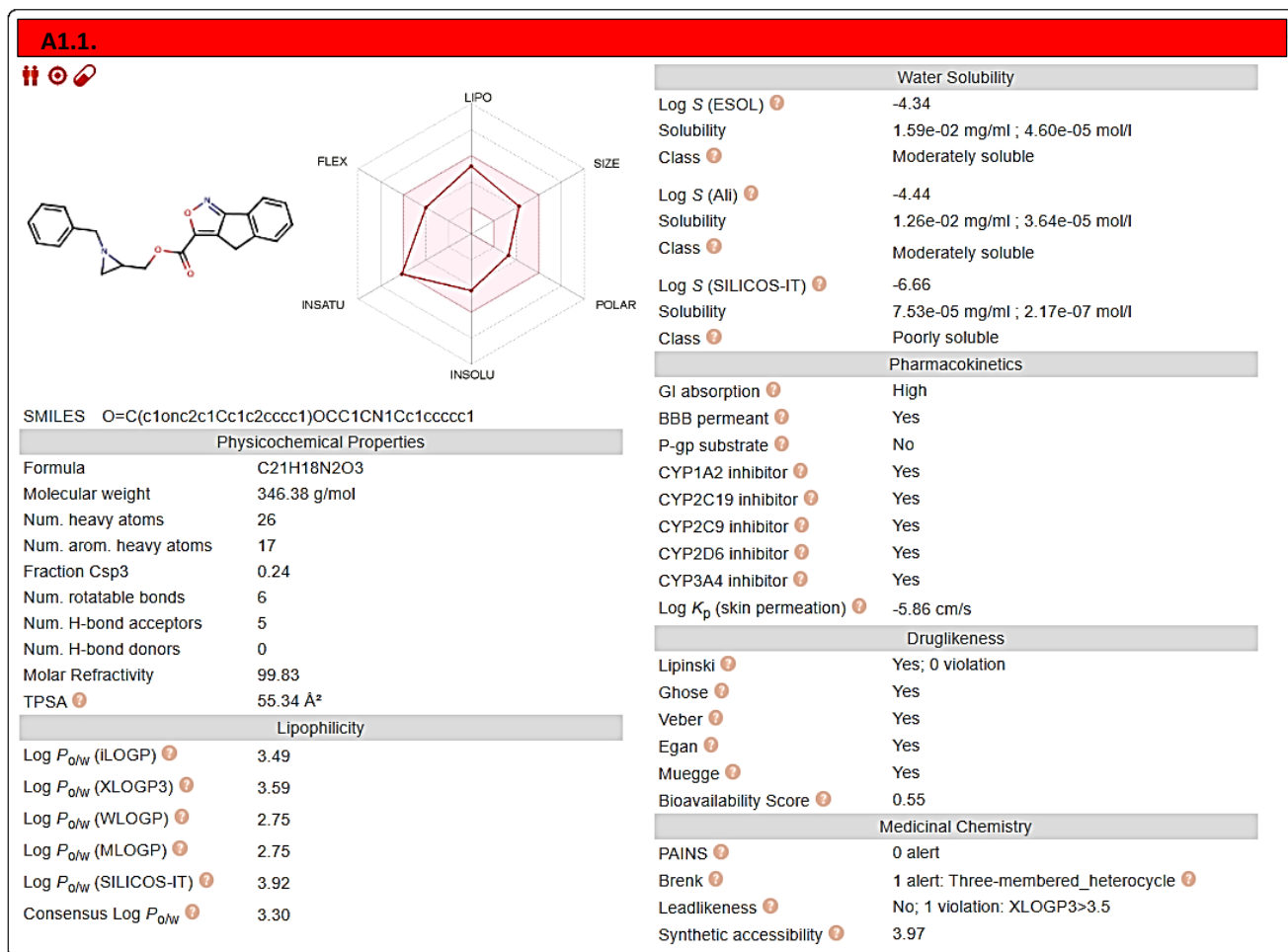


Figure 3.16: Example of a data set generated by SwissADME for A1.1.

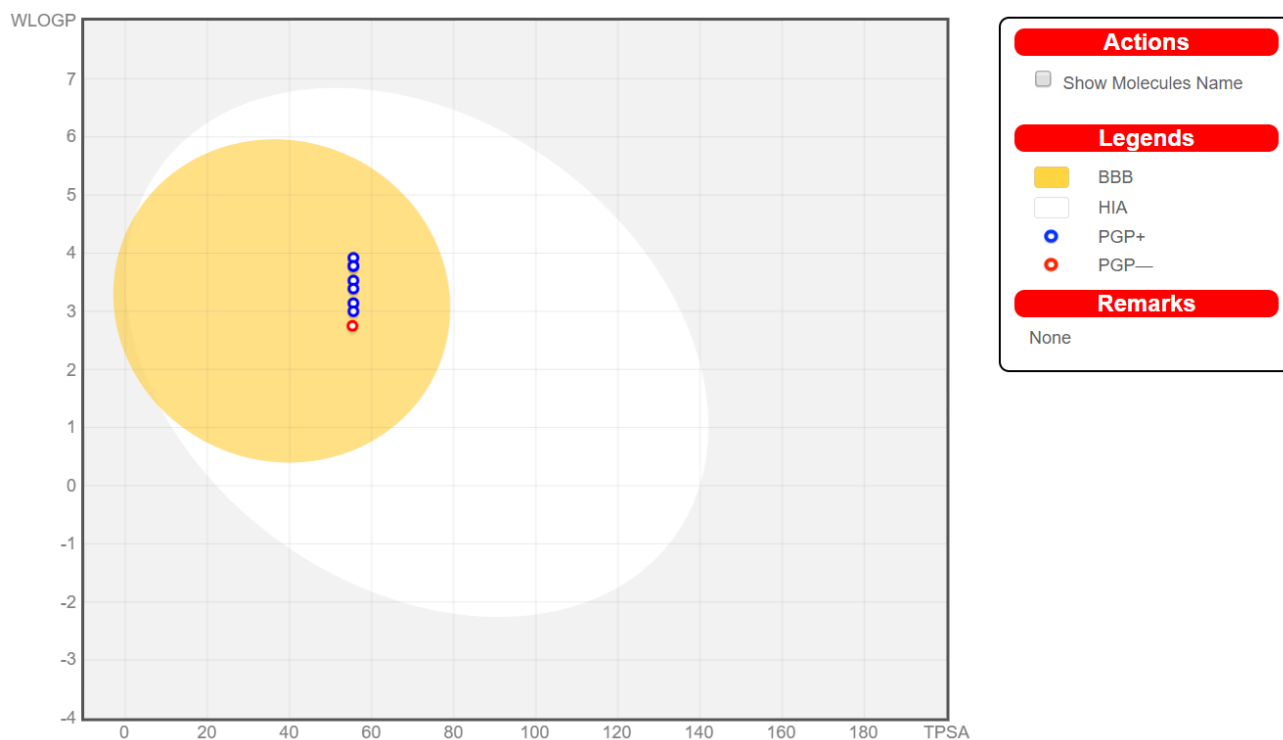


Figure 3.17: Boiled-egg plot for scaffold A compounds.

Figure 3.18 depicts an example of a bioavailability radar diagram representing the molecule's drug-likeness. The diagram for compound **A1.1** highlights six fundamental physiochemical properties that include lipophilicity, polarity, solubility, saturation, and flexibility. The diagram also displays the physical property, molecular weight (MW).

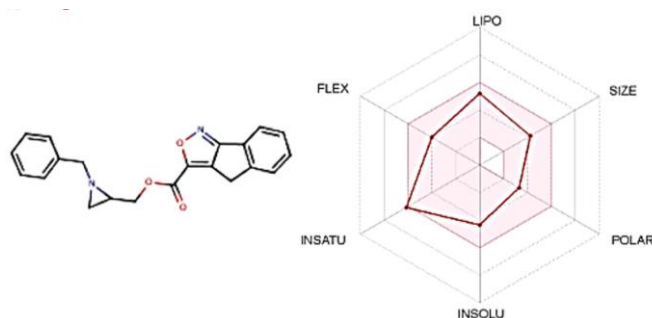


Figure 3.18: Bioavailability radar of the example molecule, **A1.1**.

The book, *Reviews in Computational Chemistry*, defines lipophilicity as the logarithm of the partition coefficient ($\log P$) of a solute between two essentially immiscible solvents [82]. The partition coefficient is a ratio of concentrations at equilibrium ($P = C_{\text{organic solute}} / C_{\text{water solute}}$). SwissADME calculates the partition coefficient between n-octanol and water, the program makes use of five freely available predictive models (XLOGP3, WLOGP, MLOGP, SILICOS-IT, and iLOGP), which are used to calculate the arithmetic mean of these values and determine a drug's lipophilicity [81]. The lipophilicity of drugs using the XLOGP3 must be in the range -0.7 to 6.0.

MW is represented by the axis called SIZE in the bioavailability graph in **Figure 3.18**. In regards to SwissADME predictions, if a drug is bioavailable, the MW of the drug needs to be between 150 and 500 g/mol, which also follows Lipinski's rule of five [78, 81].

The molecule's polarity in the form of its TPSA on the axis called POLAR, should have a value between 20 and 130 Å. These values were determined through calculations strictly based on the fragmental system provided by Ertl and co-workers [83].

Solubility calculations, $\log S$, were calculated using the ESOL model, which indicates that the value may not exceed 6. In the bioavailability graph, the solubility of the given structure is on the axis called INSOLU [81].

The saturation refers to the value given by the fraction C_{sp^3} , which is the ratio of sp^3 hybridized carbons to the total number of carbons in the drug. The fraction C_{sp^3} must be at least 0.25, and its axis is called INSATU in the bioavailability radar [81].

Flexibility in a drug in the SwissADME analysis is that drugs may not exceed 9 rotatable bonds (represented by the pink zone on the FLEX axis). If surpassed, it indicates a suboptimal physicochemical property for oral bioavailability [81].

The pink area of the SwissADME's bioavailability radar in **Figure 3.18** indicates the range into which a molecule must fall to be considered drug-like. Therefore, in conclusion, the example ligand may have bioavailable issues due to the molecule being too unsaturated, as seen in the data point which falls outside of the pink area on the INSATU axis [81].

Table 3.8 indicates if the ligands from scaffolds A to C are BBB permeants, GI permeants and if the ligands are P-gp substrate or not. The table also indicates the bioavailability parameter violations and if the ligand is a CYP450 inhibitor of CYP2C9 (which will be discussed in **section 3.6**).

Table 3.8: Permeability (BBB and GI) predictions, P-gp substrate, bioavailability parameter violations and CYP2C9 inhibitor predictions using SwissADME web tool. -All data can be seen in Appendix I under SwissADME data.

	BBB permeant	GI absorption	P-gp substrate	Bioavailability parameter violations	CYP2C9 inhibitor
A1.1	Yes	High	No	INSATU	Yes
A1.2	Yes	High	Yes	-	Yes
A1.3	Yes	High	Yes	-	Yes
A1.4	Yes	High	Yes	-	Yes
A1.5	Yes	High	Yes	-	Yes
A1.6	Yes	High	Yes	-	Yes
A1.7	Yes	High	Yes	-	Yes
A1.8	Yes	High	Yes	-	Yes
B1.1	Yes	High	Yes	-	Yes
B1.2	Yes	High	Yes	-	Yes
B1.3	Yes	High	Yes	-	Yes
B1.4	Yes	High	Yes	-	Yes
B1.5	Yes	High	Yes	-	Yes
B1.6	Yes	High	Yes	-	Yes
B1.7	Yes	High	Yes	-	Yes
B1.8	Yes	High	Yes	-	Yes
C1.1	Yes	High	Yes	LIPO	Yes
C1.2	Yes	High	Yes	LIPO	Yes
C1.3	Yes	High	Yes	LIPO, INSOLU	Yes
C1.4	Yes	High	Yes	LIPO	Yes
C1.5	Yes	High	Yes	LIPO	Yes
C1.6	Yes	High	Yes	-	Yes
C2.1	Yes	High	Yes	LIPO	Yes

Table 3.8: Permeability (BBB and GI) predictions, P-gp substrate, bioavailability parameter violations and CYP2C9 inhibitor predictions using SwissADME web tool – continued.

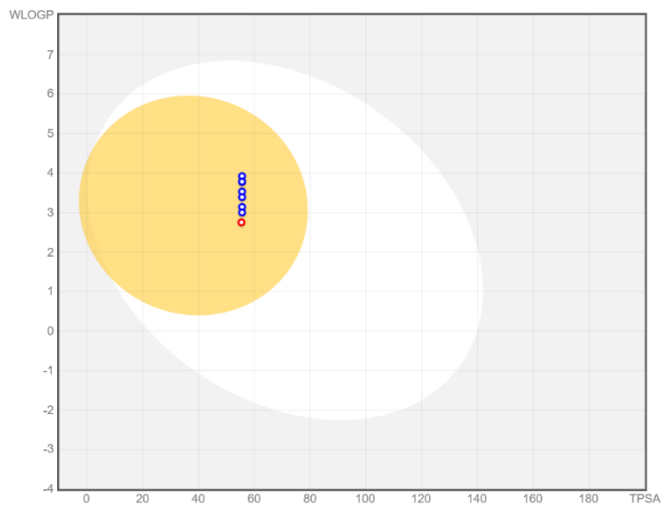
	BBB permeant	GI absorption	P-gp substrate	Bioavailability parameter violations	CYP2C9 inhibitor
C2.2	Yes	High	Yes	LIPO	Yes
C2.3	Yes	High	Yes	LIPO, INSOLU	Yes
C2.4	Yes	High	Yes	LIPO	Yes
C2.5	Yes	High	Yes	LIPO	Yes
C2.6	Yes	High	Yes	-	Yes
C3.1	Yes	High	Yes	INSATU	Yes
C3.2	Yes	High	Yes	INSATU	Yes
C3.3	Yes	High	Yes	INSATU	Yes
C3.4	Yes	High	Yes	INSATU	Yes
C3.5	Yes	High	Yes	INSATU	No
C3.6	Yes	High	Yes	INSATU	No
C3.7	Yes	High	Yes	INSATU	No
C4.1	Yes	High	Yes	INSATU	Yes
C4.2	Yes	High	Yes	INSATU	Yes
C4.3	Yes	High	Yes	INSATU	Yes
C4.4	Yes	High	Yes	INSATU	Yes
C4.5	Yes	High	Yes	INSATU	No
C4.6	Yes	High	Yes	INSATU	No
C4.7	Yes	High	Yes	INSATU	No
C5.1	Yes	High	No	INSATU	Yes
C5.2	No	High	No	INSATU	Yes
C5.3	No	High	No	INSATU	Yes
C5.4	No	High	No	INSATU	Yes
C5.5	Yes	High	No	INSATU, LIPO	Yes
C5.6	Yes	High	No	INSATU	Yes
C5.7	Yes	High	No	INSATU	Yes
C5.8	Yes	High	No	INSATU	Yes
C5.9	Yes	High	No	INSATU	Yes
C5.10	Yes	High	No	INSATU	Yes
C5.11	No	Low	No	INSATU, POLAR	Yes
C5.12	Yes	High	No	-	Yes
C5.13	Yes	High	No	-	Yes

Figure 3.19 indicates the only ligands that are predicted not to cross the BBB are **C5.2**, **C5.3**, **C5.4**, and **C5.11**. These ligands fall outside the yellow section of the boiled egg diagrams while all the other ligands are found in the yolk of the egg, indicating that they can cross the BBB. Compound **C5.11** is the only ligand that is not predicted to be able to cross the GI tract, falling outside the white area of the boiled egg plot (see Figure 3.19, scaffold C5). The ligands predicted not to be P-gp substrates include **A1.1** and all C5 compounds.

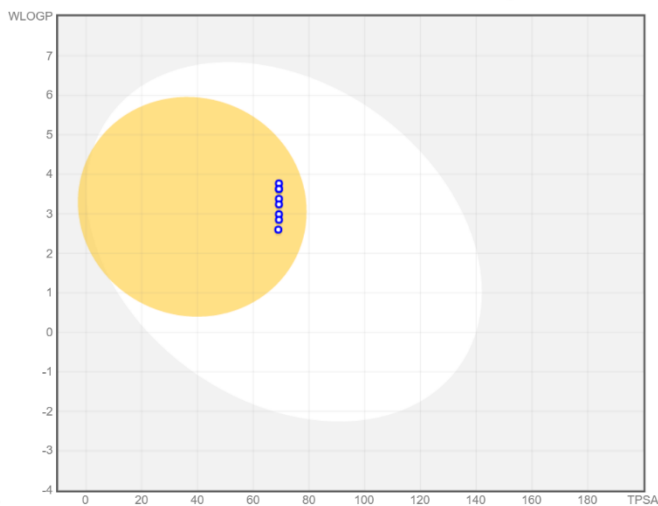
Legends

- BBB
- HIA
- PGP+
- PGP-

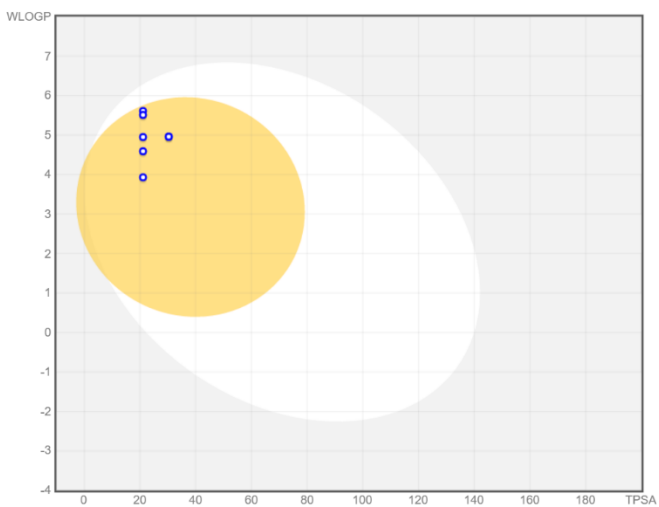
Scaffold A



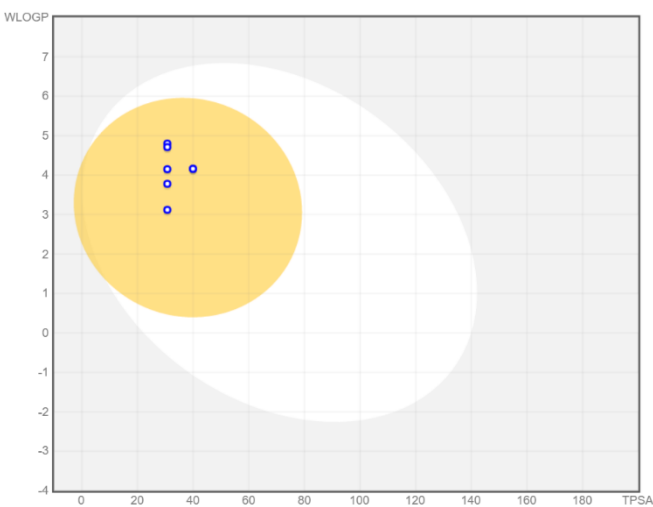
Scaffold B



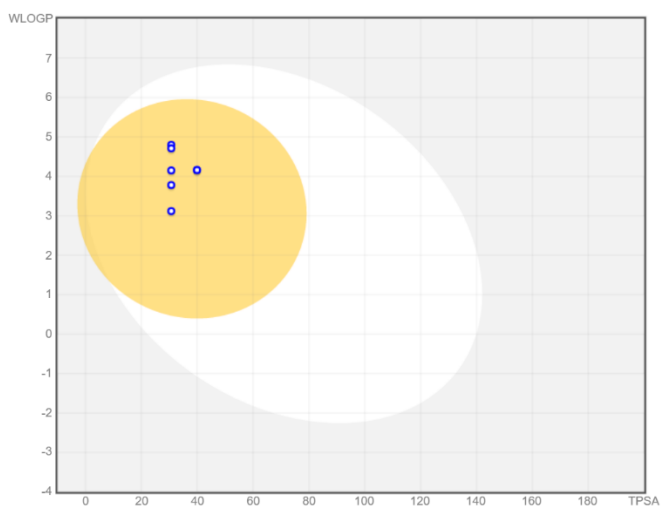
Scaffold C1 and C2



Scaffold C3



Scaffold C4



Scaffold C5

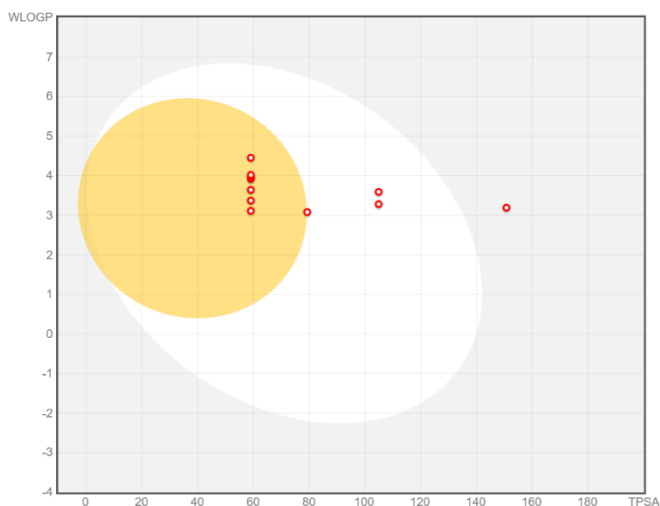


Figure 3.19: Boiled egg diagram generated from SwissADME for scaffolds A-C5 in graphs A-F.

The bioavailability radar violations present in **Table 3.8** of some of these ligands include INSATU, which represents the C_{sp^3} fraction that falls below 0.25, these include **A1.1** and ligands **C3.1-C5.11**. LIPO bioavailability radar violations, where the ligand's lipophilicity fell outside of the -0.7 to 6.0 range, included **C1.1-C1.5**, and **C2.1-C2.5**. INSOLU bioavailability radar violations, which refer to those ligands whose solubility calculations ($\log S$) exceeded 6, included **C1.3**, and **C2.3**. Ligand **C5.11** was the only ligand that contains the POLAR bioavailability radar violation, having a TPSA value falling outside the 20 to 130 Å range. These ligands are therefore predicted to be non-bioavailable. SwissADME analysis predicts that 17 ligands may be useful AChEIs.

Table 3.8 also indicates which ligands are CYP2C9 inhibitors. Ligands **C3.5**, **C3.6**, **C3.7**, **C4.5**, **C4.6**, and **C4.7** are the only ligands predicted to not be CYP2C9 inhibitors. The CYP2C9 inhibition potential was more comprehensively analysed using the program **Schrödinger** (see **section 3.6**).

3.6. Cytochrome P450 isozyme CYP2C9 inhibition

3.6.1. Introduction

The CYP450 enzymes are oxygen-activating enzymes, which are O_2 -mediated catalysts containing a b-type heme coordination complex with an Fe^{3+} centre that coordinates to a porphyrin ring, and forms part of the enzymes active site [84]. The microsomal cytochromes are found anchored in the endoplasmic reticulum (ER) and are responsible for $\pm 75\%$ of metabolic reactions of endogenous and exogenous substrates [85]. The effect of the metabolism of these drugs can either be beneficial or deleterious to the body [85]. They are responsible for the detoxification of xenobiotics, including pharmaceuticals [84].

The different isozymes of CYP450 are responsible for various types of catalytic reactions, which include oxidative ester cleavage or ring coupling. They can be responsible for the expansion or formation of rings; aromatic ring dehalogenation, de-aromatisation, dealkylation, hydroxylation, diarylation, and isomerization [84].

There are a total of 57 P450 genes in humans, but only a few are important in the hepatic clearance of drugs [84]. The CYP2C8, CYP2C18, CYP2C19, and CYP2C9 are functional CYP2C genes that form part of the isoforms of the CYP2C subfamily, which can be found on the long arm of chromosome 10 [86]. The most substantial microsomal P450 content in the liver is contributed by the membrane-anchored CYP2C9 isoform. It metabolises anti-inflammatory drugs, oral hypoglycemics, hypo anticoagulants, anticancer agents, and many more compounds, causing adverse drug reactions (ADR) during the metabolic process [86].

Patients that have mutations on their CYP2C9 gene, which encodes for defective functional forms of the isoform leads to more severe ADRs, as they are more active towards substrates that were initially classified as having low margins of safety [86]. In these patients, the drugs accumulate inside the body due to the drug being metabolized at a slower rate, causing toxicity which leads to more severe ADRs and as such the drug dosage prescribed to these patients must be adjusted accordingly [85]. However, the accumulation of the drug in the body can also be caused by dietary constituents that inhibit the P450 enzymes, e.g. the consumption of grapefruit has been shown to inhibit the breakdown of terfenadine [85, 87].

The bioavailability of a drug is determined by its microsomal stability, which determines if most of the molecules will be eliminated rapidly within the body and if the parent compound will cause any side effects when consumed by the patient. The prevention of side effects or limiting these effects is regulated by using as low a dose as possible of the drug to cause the desired effect [85].

The program **P450 Site of Metabolism** in **Schrödinger** was used to performed docking analysis of the ligands under study through the use of a computational approach called **IDSite**. The program models induced fit effects of docked ligands into the active site of the CYP isoform CYP2C9 through first sampling the conformational space with flexed docking, through **Glide** calculations. The ligands are then subjected to two refinement stages through the use of a program called the **Protein Local Optimization Program (PLOP)**.

There is a final docking score calculated which represents the binding of the ligand to the active site of CYP2C9, indicating the ligand's ability to inhibit CYP2C9. If the inhibition is high (low docking scores), the metabolism of the drug will be low, when increasing its concentration in the body it could lead to increased toxicity causing a ADRs. The data also provides the type of interactions between the ligand and CYP2C9 protein active site or the heme domain, which can be viewed in the workspace of **Maestro** in **Schrödinger**. This prediction will therefore be helpful in early drug development, indicating which parts of the drug interacts with the CYP2C9 active site.

The 3D X-ray crystal structure of CYP2C9 displays the structural information of the enzyme, shown in **Figure 3.20**, which indicates that it contains only a few β -sheets (turquoise), while the rest of the protein consists of α -helices (red), which are arranged in such a way that the enzyme looks triangular. The heme domain is located in the core of the protein with an Fe^{3+} ion (yellow sphere) in the centre of the porphyrin ring (green).

Donepezil (**25**) gets metabolized via the CYP450 system, where it interacts with CYP2C9's active site, disrupting its activity, and causing ADRs linked to GI side-effects like diarrhoea [86, 88]. The use of donepezil (**25**) has also been shown to cause nausea, malaise, dizziness, and insomnia [86, 88]. It is advised from literature to make sure that potential drugs must not contain aryl acetic acid or aryl propionic acids since

CYP2C9 exhibits selectivity for these groups and could therefore cause severe ADRs [86].

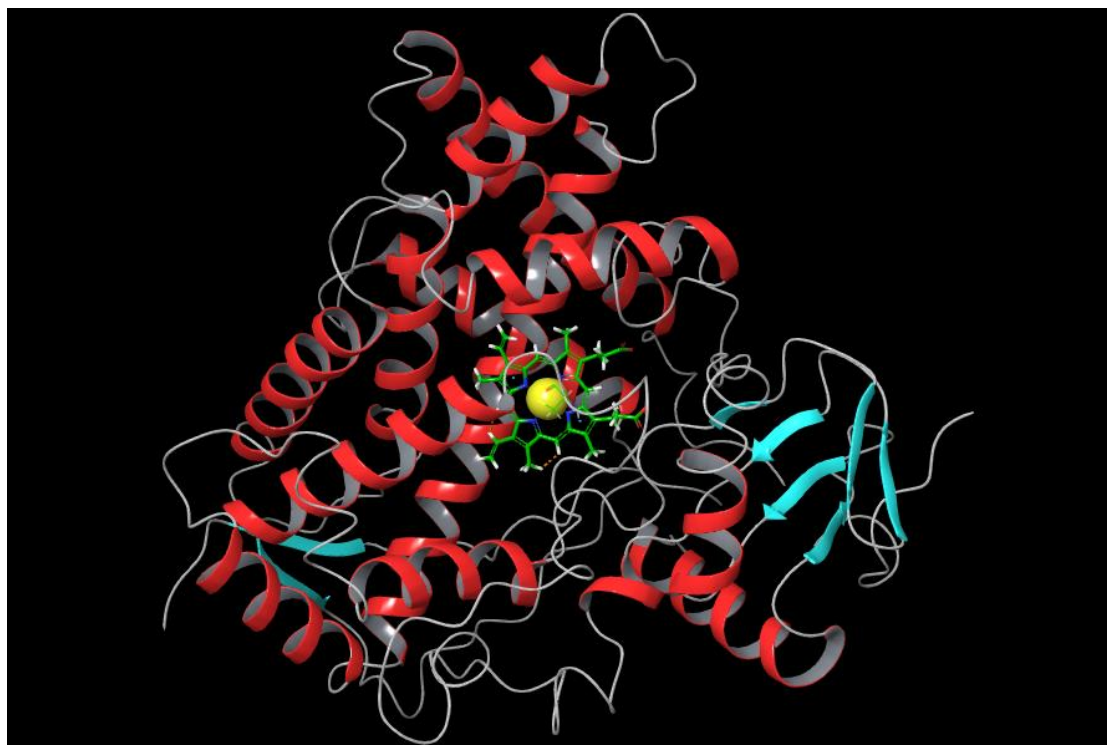


Figure 3.20: 3D X-ray crystallography of CYP2C9. β -sheets (turquoise) and α -helices (red) arranged in a triangular protein. The heme group consisting of a porphyrin ring (green) and its central iron (Fe^{+3} , yellow sphere).

The interactions between the heme domain, the CYP2C9 protein's active site, and donepezil (**25**) can be seen in **Figure 3.21**, while the specific interactions involved can be seen in **Figure 3.22**. The interactions include 3 π - π interactions (blue dashed lines) and 2 π -cation interactions (green dashed lines) with the porphyrin ring of the heme domain. A H-bond (yellow dashed lines) can be observed with Arg108, which forms part of the CYP2C9 enzyme, while a salt bridge (purple dashed lines) is formed between the porphyrin ring's OH group oxygens and Arg97's NH_2 hydrogen atoms.

The program, **Site of Metabolism – Examine Results**, needs to be used to view the sites of metabolism (SOM) results. These SOM results are represented by numerical scores that indicate the potential of each specific atom in the ligand that interacts with the catalytic Fe^{3+} centre (heme) of the enzyme with an overall SOM score represented by green spheres surrounding specific atoms. SOM data generated can identify the regions of a ligand that will potentially undergo CYP2C9 metabolism, therefore the data can be used to target these sites and adjust the structure of the ligand to minimize metabolism of the ligand by CYP2C9.

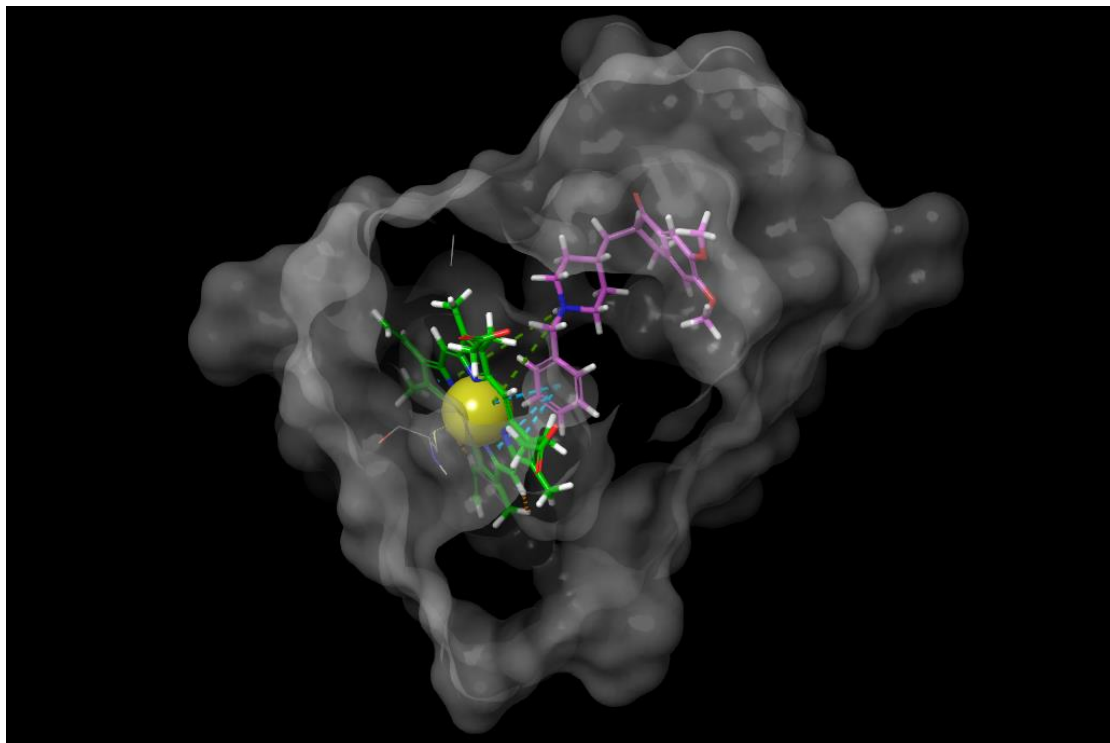


Figure 3.21: Donepezil (**25**, purple) docked into the active site of CYP2C9, allowing for the interaction with the heme domain.

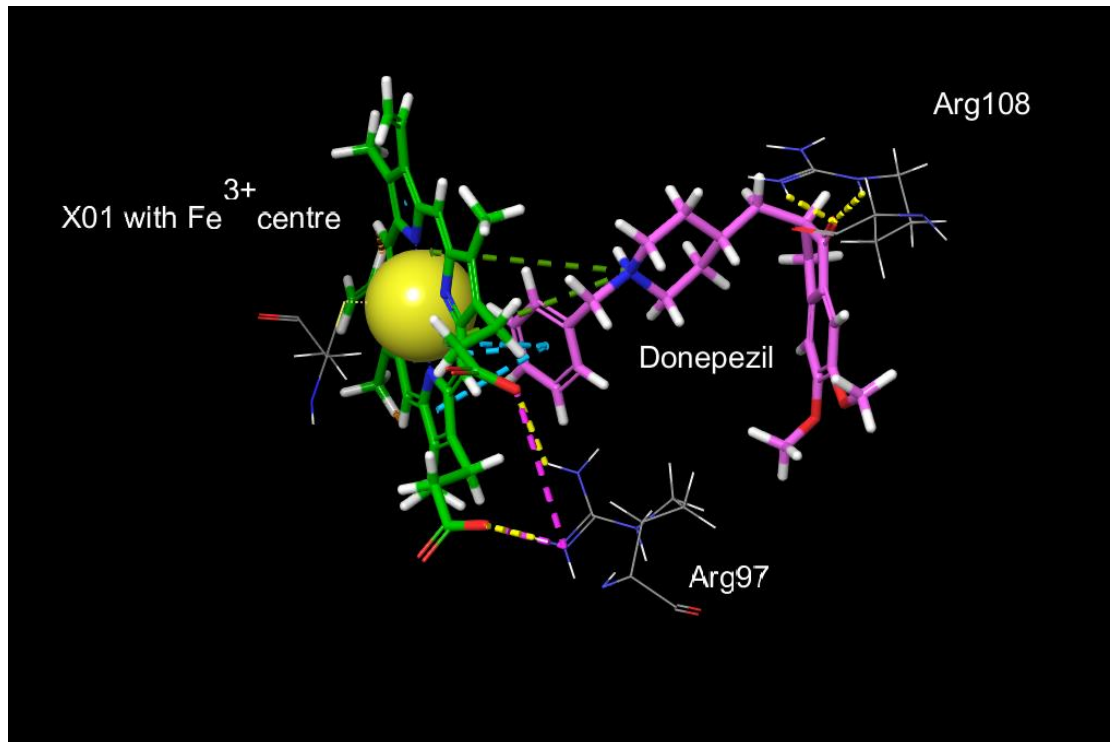


Figure 3.22: Donepezil (**25**, purple) docked into the active site of CYP2C9 which interacts with the protein and the heme domain. -Green dashed lines indicate π -cation interactions. Blue dashed lines indicate π - π interactions. Yellow lines indicate hydrogen bonds. Purple lines indicate a salt bridge.

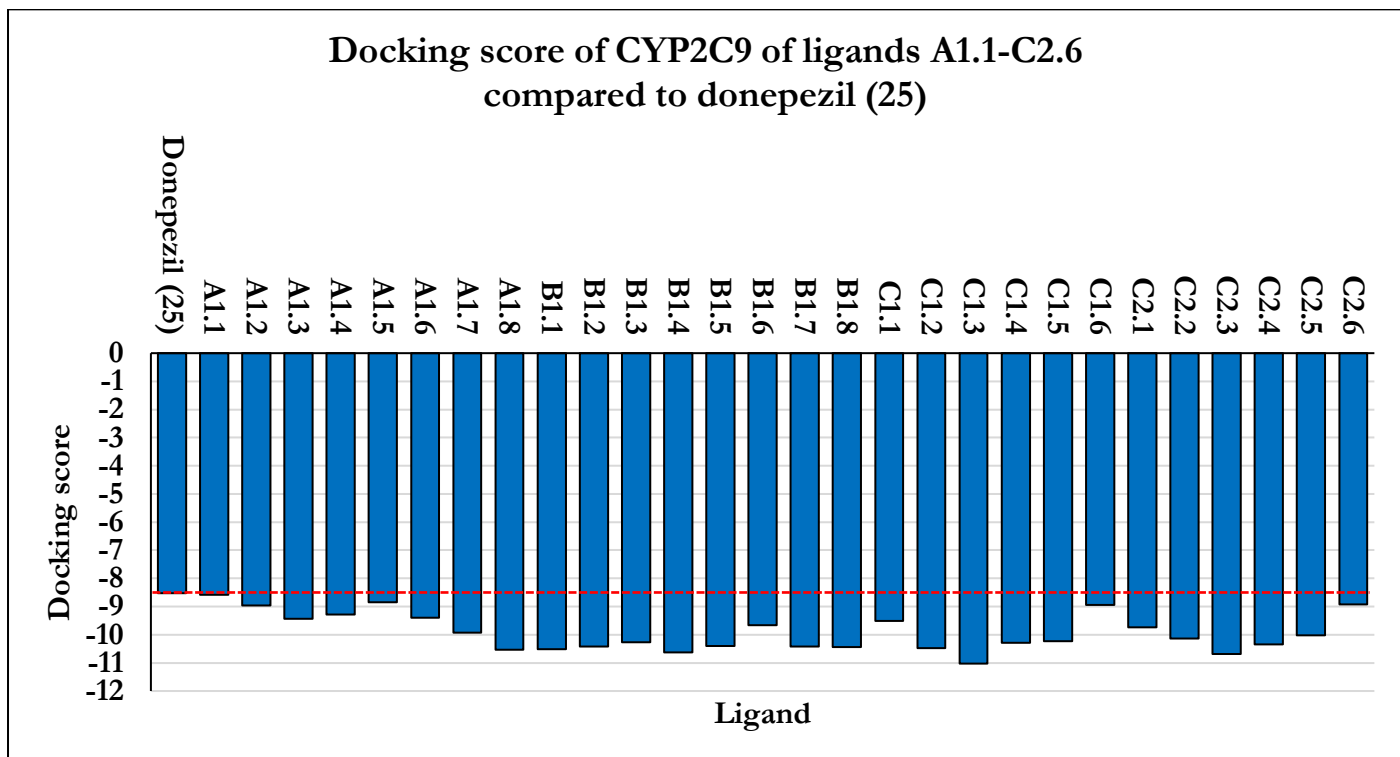
3.6.2. Results and discussion of CYP2C9 analysis

Both **Graph 3.4** and **Graph 3.5** indicate the CYP2C9 docking score of the ligands from scaffolds A, B and C compared to that of donepezil (**25**) that has a docking score of -8.518 (red dashed line for comparison). Donepezil's (**25**) docking score was utilised as the cut-off point as it is an FDA approved drug. CYP2C9 docking scores that indicate a higher docking score (more negative docking score value) than that of donepezil (**25**) are not considered to be good candidates for AChEIs, because a higher CYP2C9 inhibition indicates that the drug could lead to more severe ADRs.

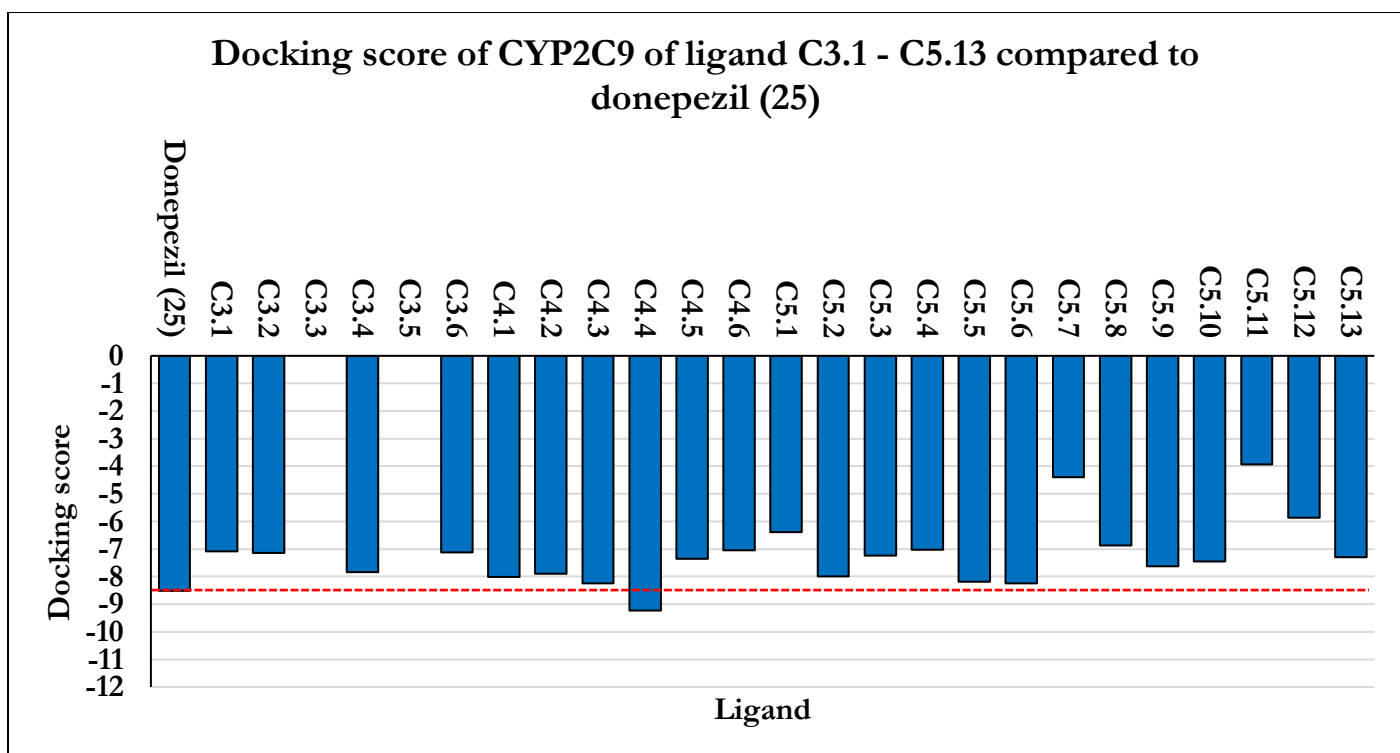
A docking scores > -9.000 are classified as poor ligands while the ligands falling within -9.000 to -10.000 are classified as fair ligands. The good CYP2C9 inhibitors have a docking score of < -10.000 since they are predicted to inhibit the CYP2C9 active site more and will potentially cause the most severe ADRs within the data set compared to that of donepezil (**25**). The best ligands under study must be a good AChEI but a poor CYP2C9 inhibitor.

All ligands in **Graph 3.4** and ligand **C4.4** in **Graph 3.5** have a higher inhibition of CYP29C compared to donepezil (**25**), indicating that they may cause more severe ADRs when metabolised. Except for donepezil (**25**), there are only 5 ligands (**A1.1**, **A1.2**, **A1.5**, **C1.6**, and **C2.6**) that can be classified as poor CYP2C9 inhibitors in **Graph 3.4**, while all the ligands in **Graph 3.5** (except **C4.4**) can all be classified as poor CYP2C9 ligands. The fair ligands include **A1.3**, **A1.4**, **A1.6**, **A1.7**, **B1.6**, **C1.1**, **C2.1**, and **C4.4** while the good ligands, which are predicted to cause the most severe ADRs, are **A1.8**, **B1.1**, **B1.2**, **B1.3**, **B1.4**, **B1.5**, **B1.7**, **B1.8**, **C1.2**, **C1.3**, **C1.4**, **C1.5**, **C2.2**, **C2.3**, **C2.4**, and **C2.5**.

The diversity in the ligand docking scores is determined to be dependent on ligand orientation within the active site of CYP2C9, allowing for porphyrin ring interaction with the functional groups present on the ligand. The importance of specific functional groups has been proven to be of interest in the inhibition of AChE and therefore the differentiation between good and poor CYP2C9 inhibition are important in the development of good AChEIs by determining which functional groups causes poor ligands in regards to CYP2C9 inhibition.



Graph 3.4: CYP2C9 docking scores of scaffolds A, B, C1 and C2 compared to that of donepezil (25).



Graph 3.5: CYP2C9 docking scores of scaffolds C3, C4, and C5 compared to that of donepezil (25).

The interactions involved in the good and poor CYP2C9 ligands can be seen in **Table 3.9** and **3.10**. The orientation of specific functional groups (benzene ring, aziridine ring, azetidine ring, phenyl ring, pyrrolidine ring, methyl, piperidine ring, or pyrazole ring) causes either π - π interactions, π -cation, or salt bridge interactions to the porphyrin ring located in the active site of CYP2C9. Some ligands indicate no interaction with the porphyrin ring system, while some only indicate Van der Waals (V.d.W) interactions.

Table 3.9: The docking score, porphyrin interactions, amino acid and Van der Waal interactions involved between the good ligands and CYP2C9 causing different types of interactions.

	Docking score	Porphyrin ring interaction		Phe 100	Phe 114	Phe 476	Arg 108	Asn 204	V.d.W.
		With	Type						
A1.8	-10.533	Benzene ring	4 π - π		π - π		H-bond		
B1.1	-10.510	Benzene ring Aziridine	4 π - π π -cation	π - π				H-bond	
B1.2	-10.429	Azetidine ring	2 π -cation salt bridge		π - π	π - π	π -cation	H-bond	
B1.3	-10.275	Phenyl ring	4 π - π	π - π		π - π π -cation	H-bond		
B1.4	-10.629	Pyrrolidine ring	4 π -cation				π -cation	H-bond	
B1.5	-10.410	Benzene ring Pyrrolidine ring	π - π π -cation	π - π			H-bond		
B1.7	-10.411	None	-				π -cation	H-bond	3
B1.8	-10.429	Benzene ring	4 π - π	π - π	π - π		H-bond		
C1.2	-10.483	None							14
C1.3	-11.025	Benzene ring	5 π - π V.d.W.	π - π		π - π			6
C1.4	-10.295	Benzene ring	V.d.W.			π - π	π -cation	H-bond	
C1.5	-10.240	Benzene ring	π - π						
C2.2	-10.129	Methyl	3 V.d.W.	π - π		π -cation			7
C2.3	-10.690	Benzene ring Piperidine ring	π - π 2 π -cation	π - π					8
C2.4	-10.351	Piperidine ring	3 π -cation salt bridge			π - π			
C2.5	-10.024	Benzene ring	2 π -cation						

Table 3.10: The docking score, porphyrin interactions, amino acid and Van der Waal interactions involved between the poor ligands and CYP2C9 causing different types of interactions.

	Docking score	Porphyrin ring interaction		Phe 100	Phe 476	Arg 108	Arg 97	Thr 301
		With	Type					
25	-8.518	Benzene ring Piperidine ring	3 π - π 2 π -cation			H-bond		
A1.1	-8.584	Aziridine ring	2 π -cation	π - π	π - π			
A1.2	-8.960	Azetidine ring	4 π -cation	2 π - π				
A1.5	-8.854	Benzene ring	4 π - π	π -cation	π -cation	π -cation		
C1.6	-8.938	Benzene ring	4 π - π		π - π			
C2.6	-8.918	Pyrazole	π - π					
C3.1	-7.085	Benzene	4 π - π					
C3.2	-7.144					π -cation H-bond		
C3.6	-7.126	Benzene	4 π - π					
C4.2	-7.889	Benzene	4 π - π				π -cation	
C4.5	-7.351	Benzene	4 π - π	π - π			π - cation	
C4.6	-7.039	Benzene	3 π - π					
C5.7	-4.407	Benzene	4 π - π		π - π			
C5.11	-3.935	Benzene	4 π - π	π - π				
C5.12	-5.865				π - π			H-bond

The CYP2C9 computational results of scaffold A indicates that only **A1.8** can be considered a good ligand, ligands **A1.1**, **A1.2** and **A1.5** are considered the poor ligands while the rest of the ligands are considered fair ligands as their CYP2C9 docking scores fall within -9.000 to -10.000. From the data provided in the tables, **A1.8** would not be considered as being a better ligand than those in **Table 3.10**, but the distance of the interactions involved in **A1.8** is much closer than those indicated in **A1.1**, **A1.2** and **A1.3**, leading to a higher docking score of -10.533 for **A1.8**. The Phe114 π - π interaction in **A1.8** seems to be of importance as this interaction is not present in any one of the poor ligands.

The computational results for the CYP2C9 data for scaffold B indicate that most of the ligands can be considered as good ligands while only ligand **B1.6** can be considered a fair ligand. The important amino acid interactions that drive the higher docking scores of scaffold B include Phe110, Phe114, Phe476, Arg108 and Asn204. The number and type of interactions between a functional group (benzene ring, aziridine ring, azetidide ring, phenyl ring, pyrrolidine ring) and the porphyrin ring of the CYP2C9 active site is shown to be of some importance but might not be that important when considering the interactions for **B1.7** which only indicates a π -cation bond to Arg108, a H-bond to Asn204 and interestingly the three Van der Waals interactions which are not present in any of the other ligands in the scaffold indicating it is of some importance in the metabolism of the ligand.

The ligands in scaffold C are spread across the three levels and only some are tabulated in each scaffold class which focuses on the “best” good ligands and the “worst” poor ligands in each scaffold group in order to determine the importance of the interactions at these two levels. For the good ligands in scaffold C the Van der Waals interactions are shown to be of some importance in **C1.2**, **C1.3**, **C2.2** and **C2.3**. The H-bond to Asn204 in **C1.4** seems to lead to an increased docking score as Arg108 does not seem to affect the docking score that much when compared to the other ligands in the scaffold. Phe476 and Phe100 seems to be important interactions as seen from **Table 3.9** listing the good ligands. The Phe114 interaction is not present in the poor ligands, indicating its importance yet again. The amino acid Thr301, does not seem important as it is only present in **C5.12** in **Table 3.10**. A wide range of functional groups interact with the porphyrin ring and only the distance from the ring determines the larger effect on the docking scores among these ligands in scaffold C.

In conclusion to the docking analysis of CYP2C9 the number, distance, and the type of interactions to the porphyrin ring are of importance, but also the amino acid interactions involved. The important π - π interactions include Phe100, Phe114, and Phe476, while π -cation interactions are found to be important when interacting with Phe476 and Arg108. Important H-bond interactions, are found to be involved with the amino acids Arg108 and Asn204. The functional groups that are found to be of great importance for interaction with the porphyrin ring and the rest of the active site of CYP2C9 are *N*-containing ring systems and benzene rings, unfortunately these functional groups are also important in the interactions involved in AChE inhibition and the following results could help in determining why these functional groups are of importance in CYP2C9 inhibition and what can be done in future work to decrease inhibition and lead to the formation of poor CYP2C9 inhibitors but still good AChEIs.

Schrodinger's program, **Site of Metabolism**, uses induced-fit docking to assess the ligand's ability to interact with the active site of CYP2C9 using a rule-based approach to intrinsic reactivity. The initial sampling of each ligand is enhanced by generating a more extensive range of ligand conformers found in the general docking stage. Side-chain predictions are performed on those ligands that have been selected during the refining stage, called **Prime**, which selects all the ligands that have atoms within 5 Å from any ligand pose. The next minimization step includes the ligand and its side chains to be redocked into the active site of CYP2C9. Atoms still found within 5 Å from the heme iron are classified as SOM regions, represented by the green spheres around the atoms in the 2D-images displayed under the overall SOM in **Table 3.11**.

Table 3.11: The overall SOM, Fe-accessibility and intrinsic reactivity of donepezil (**25.a**) and ligands of scaffolds A, B and C.

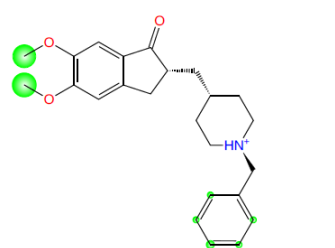
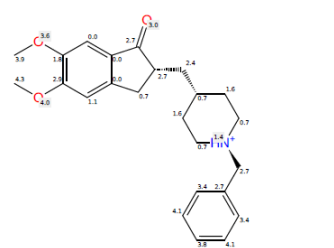
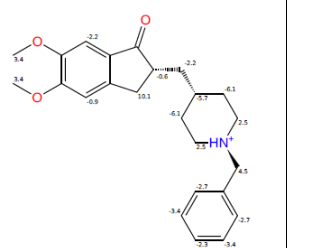
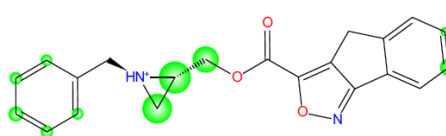
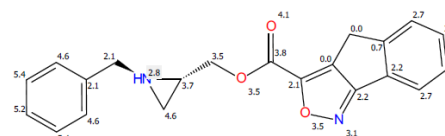
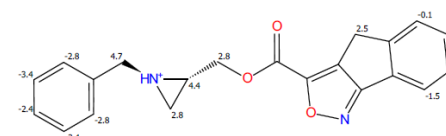
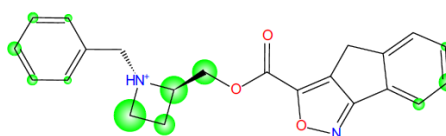
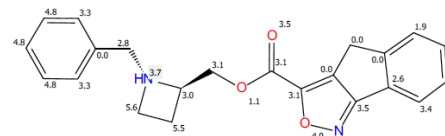
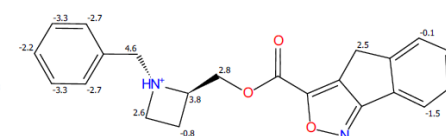
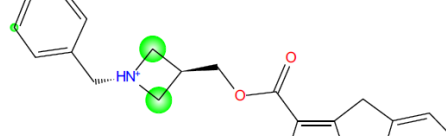
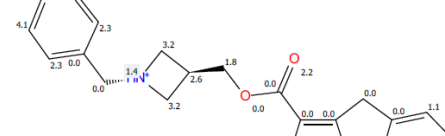
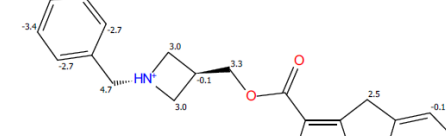

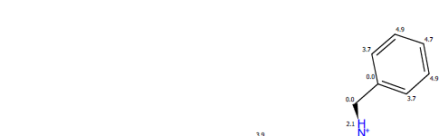

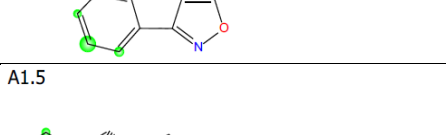
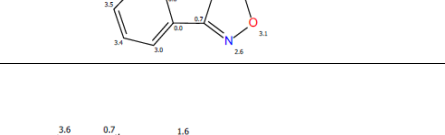
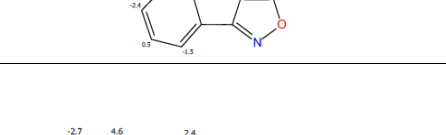

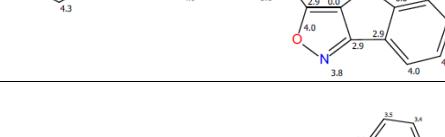
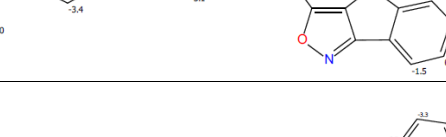
Overall SOM	Fe-accessibility	Intrinsic reactivity	
			
A1.1			
A1.2			
A1.3			
A1.4			
A1.5			
A1.6			

Table 3.11: The overall SOM, Fe-accessibility and intrinsic reactivity of donepezil (**25.a**) and ligands of scaffolds A, B and C -continued.

Overall SOM	Fe-accessibility	Intrinsic reactivity
<p>A1,7</p>		
<p>A1.8</p>		
<p>B1.1</p>		
<p>B1.2</p>		
<p>B1.3</p>		
<p>B1.4</p>		
<p>B1.5</p>		

Table 3.11: The overall SOM, Fe-accessibility and intrinsic reactivity of donepezil (**25.a**) and ligands of scaffolds A, B and C -continued.

Overall SOM	Fe-accessibility	Intrinsic reactivity
B1.6 		
B1.7 		
B1.8 		
C1.1 		
C1.2 		
C1.3 		
C1.4 		

Table 3.11: The overall SOM, Fe-accessibility and intrinsic reactivity of donepezil (**25.a**) and ligands of scaffolds A, B and C -continued.

	Overall SOM	Fe-accessibility	Intrinsic reactivity
C1.5			
C1.6			
C2.1			
C2.2			
C2.3			
C2.4			

Table 3.11: The overall SOM, Fe-accessibility and intrinsic reactivity of donepezil (**25.a**) and ligands of scaffolds A, B and C -continued.

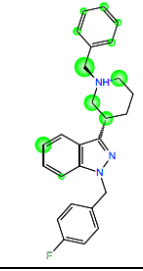
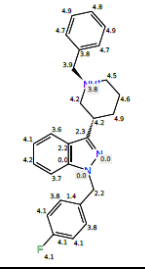
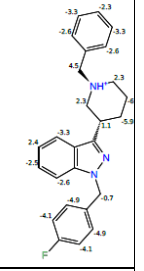
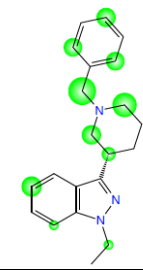
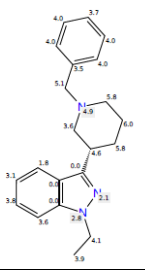
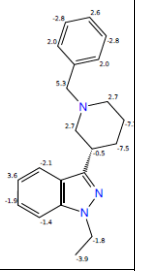
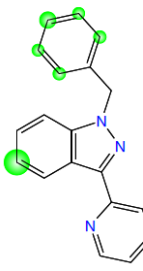
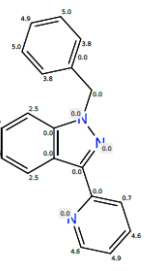
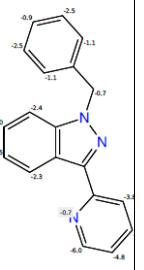
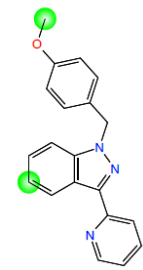
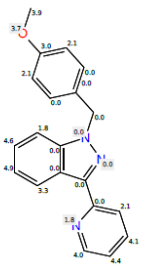
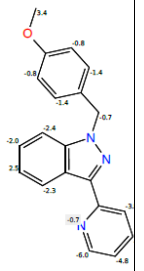
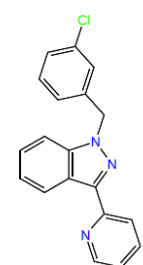
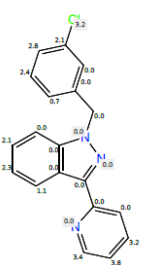
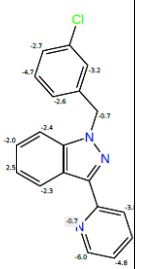
Overall SOM	Fe-accessibility	Intrinsic reactivity
C2.5 		
C2.6 		
C3.1 		
C3.2 		
C3.3 		

Table 3.11: The overall SOM, Fe-accessibility and intrinsic reactivity of donepezil (**25.a**) and ligands of scaffolds A, B and C -continued.

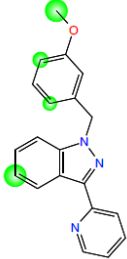
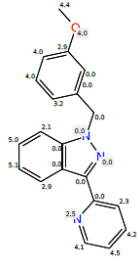
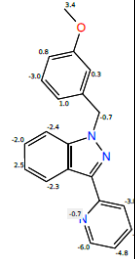
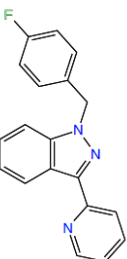
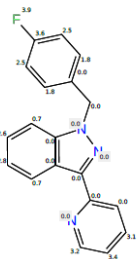
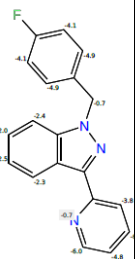
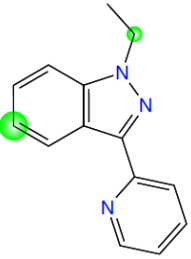
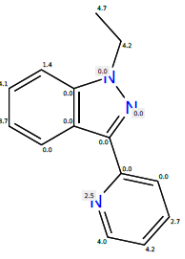
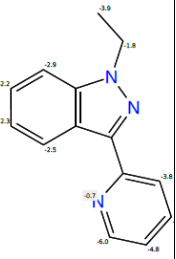
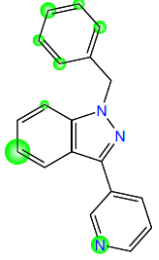
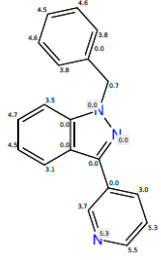
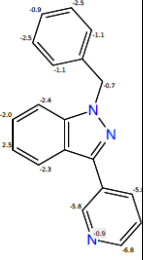
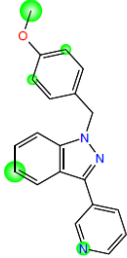
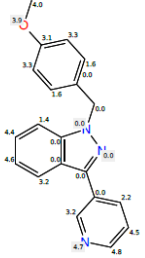
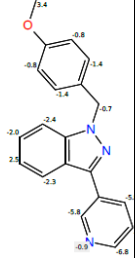
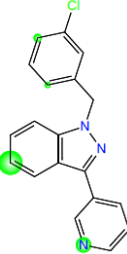
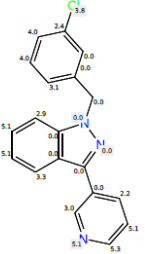
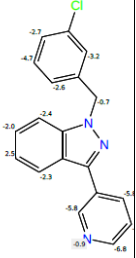
Overall SOM	Fe-accessibility	Intrinsic reactivity
C3.4 		
C3.5 		
C3.6 		
C4.1 		
C4.2 		
C4.3 		

Table 3.11: The overall SOM, Fe-accessibility and intrinsic reactivity of donepezil (**25.a**) and ligands of scaffolds A, B and C -continued.

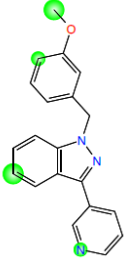
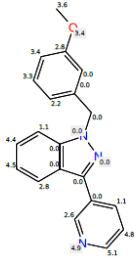
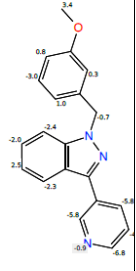
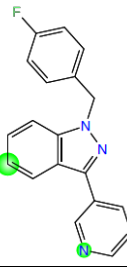
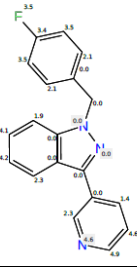
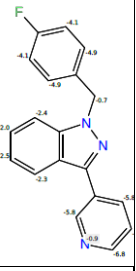
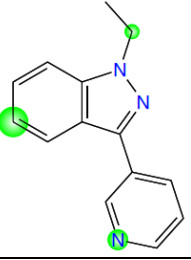
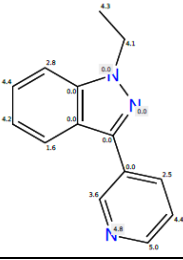
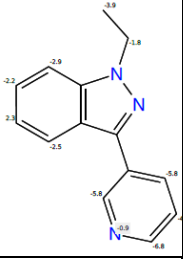
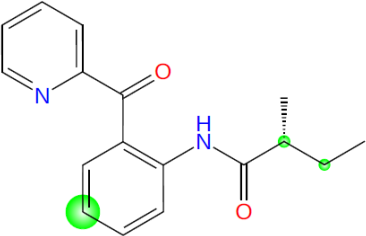
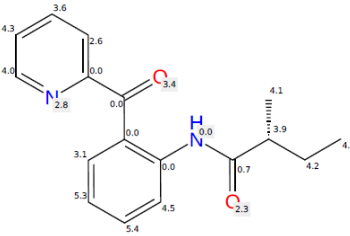
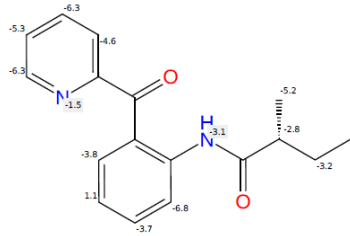
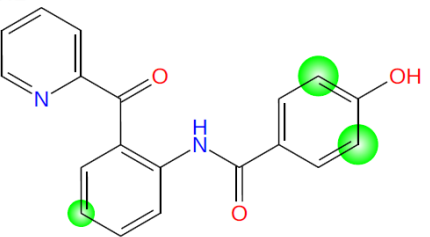
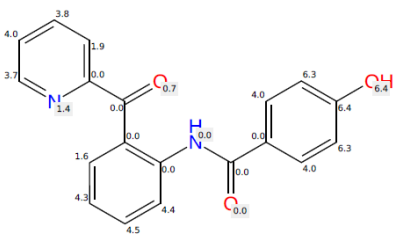
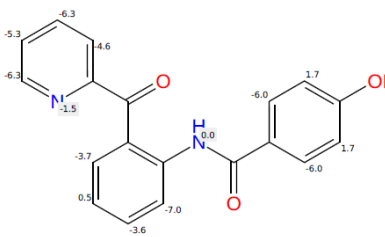
Overall SOM	Fe-accessibility	Intrinsic reactivity
C4.4 		
C4.5 		
C4.6 		
C5.1 		
C5.2 		

Table 3.11: The overall SOM, Fe-accessibility and intrinsic reactivity of donepezil (**25.a**) and ligands of scaffolds A, B and C -continued.

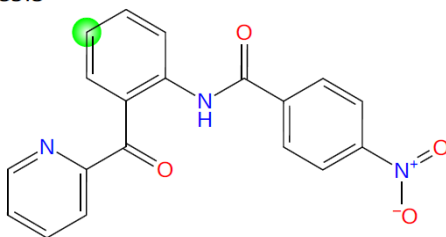
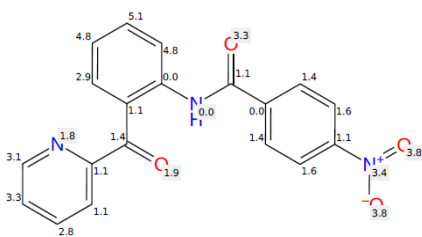
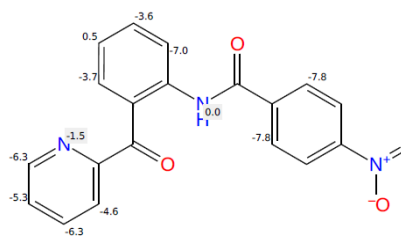
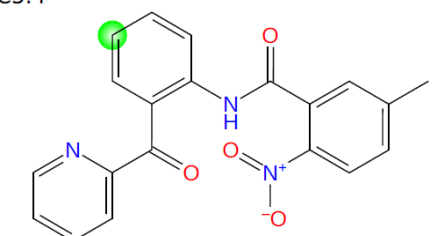
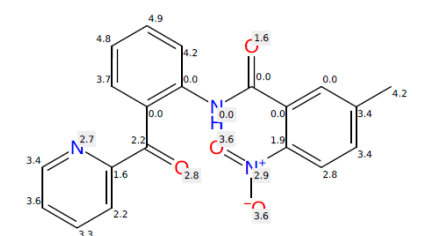
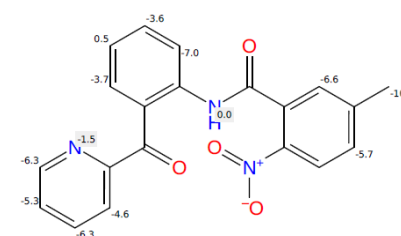
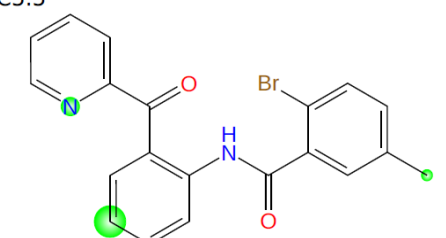
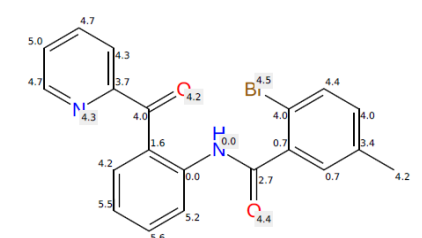
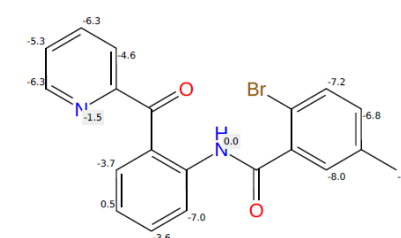
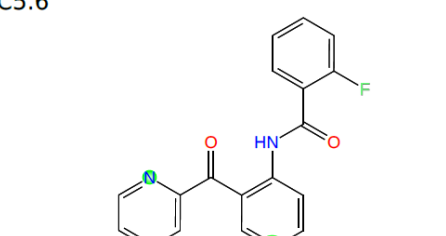
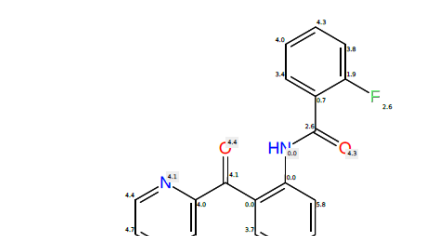
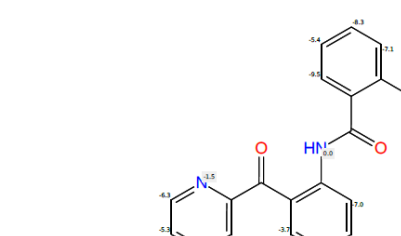
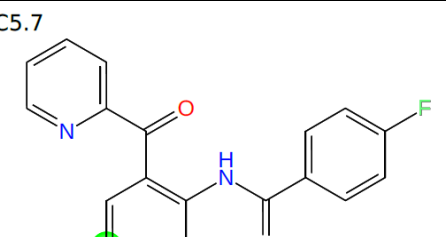
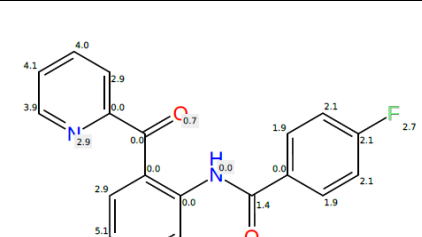
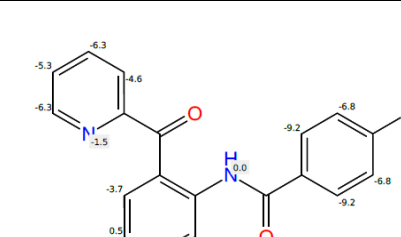
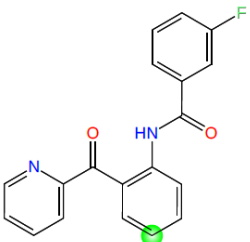
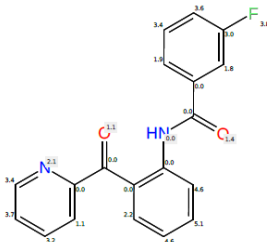
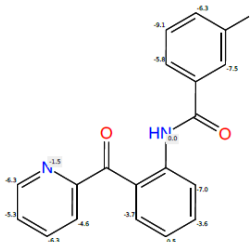
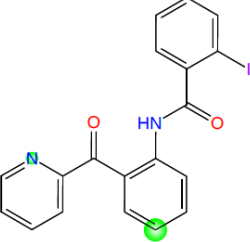
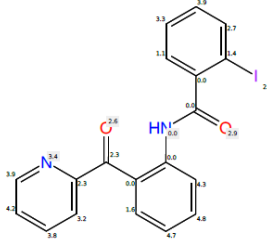
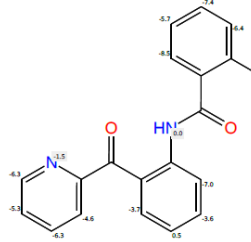
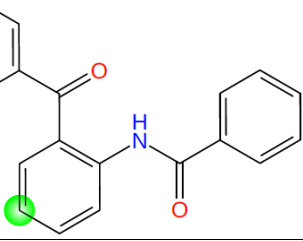
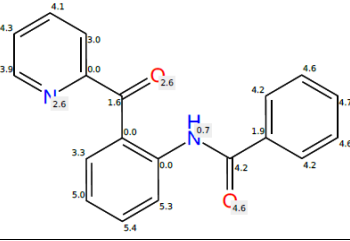
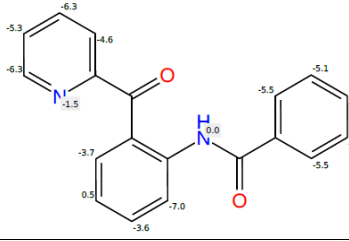
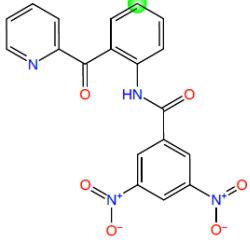
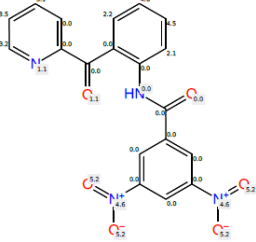
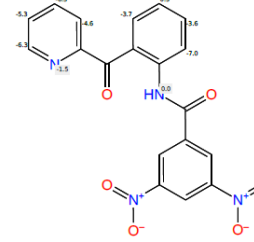
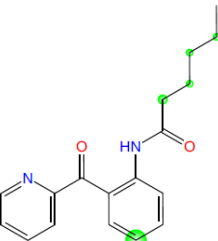
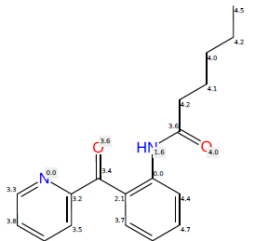
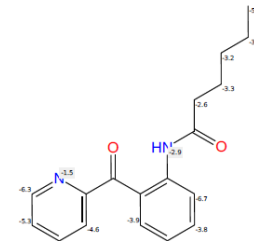
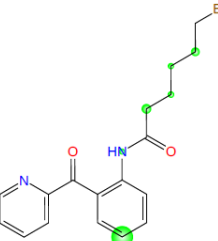
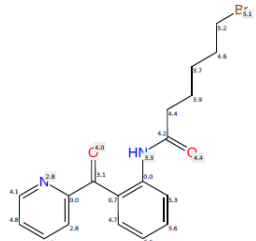
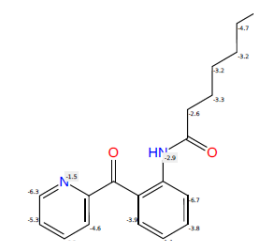
Overall SOM	Fe-accessibility	Intrinsic reactivity
<p>C5.3</p> 		
<p>C5.4</p> 		
<p>C5.5</p> 		
<p>C5.6</p> 		
<p>C5.7</p> 		

Table 3.11: The overall SOM, Fe-accessibility and intrinsic reactivity of donepezil (**25.a**) and ligands of scaffolds A, B and C -continued.

Overall SOM	Fe-accessibility	Intrinsic reactivity
C5.8 		
C5.9 		
C5.10 		
C5.11 		
C5.12 		
C5.13 		

The SOM for the CYP2C9 enzyme targeted ligands must have some activity even in the absence of the enzyme, and at the same time, have access to the heme Fe³⁺ centre. These 2 factors compete and result in an overall SOM of each atom. Each atom's Fe-accessibility, defined as the natural logarithm of the number of poses for each atom found within 5 Å from the Fe³⁺ centre can be seen in **Table 3.11**. The larger the Fe-accessibility value, the greater accessibility the atom has to the Fe³⁺ centre. The positive intrinsic reactivity values indicate more reactivity, while negative values indicate less reactivity, which is also displayed in **Table 3.11**. The overall SOM score is a linear combination of these two parameters. The radius of the green spheres is proportional to the SOM score. The larger the SOM sphere, the higher the reactivity of the atom (see **Table 3.11**).

SOM could cause any number of the following reactions, which could lead to the inactivation of the active ligands. The hydroxylation of a benzene ring or the benzylic demethylation can occur when the benzene ring is close to the heme group, *N*-dealkylation, or demethylation of methoxy groups are also possible. An alkyl chain could undergo an oxidation reaction resulting in a secondary alcohol, or an amine group can be turned into an amide group. A primary alcohol can also be turned into a carboxylic acid. Further, *in vivo* studies and analysis will be necessary to verify these predictions and be kept in mind for future work.

The SwissADME data indicated that ligands **C3.5**, **C3.6**, **C3.7**, **C4.5**, **C4.6**, and **C4.7** would not inhibit CYP2C9. The docking analysis for CYP2C9 inhibition indicates that only ligands **C3.3** and **C3.5** do not have any overall SOM and are therefore not CYP2C9 inhibitors. In conclusion, **C3.5** is the only ligand that can be classified as not an inhibitor of CYP2C9 in the data set even though many of the other ligands are considered to still be under acceptable CYP2C9 inhibition levels when compared to donepezil (**25**).

3.7. Conclusion

The computational work reported in this chapter covered the molecular docking, Qikprop analysis, pharmacophore analysis, SwissADME analysis and CYP2C9 inhibition of a total of sixty-five ligands from scaffolds A, B and C. The molecular docking indicated that fifty-seven ligands could be classified as drug-like but when a lower docking score limit of -13.000 was applied, only fifteen ligands passed the mark, which included **A1.2.a**, **A1.3.a**, **A1.5.a**, **A1.8.a**, **B1.1.a**, **C1.1.a**, **C1.2.a**, **C1.3.a** (and **C1.3.b**, **C1.3.c**), **C1.4.a** (and **C1.4.b**), **C1.5.a** (and **C1.5.b**), **C1.6.a**, **C2.1.a**, **C2.4.a**, **C2.5.a** and **C2.6.a**.

The Qikprop analysis indicated that all sixty-five ligands fell within the MW, QPlogBB, the number of H-donor or H-acceptor ranges for orally available drugs. The QPlogHERG rule was violated by all the ligands suggesting that early screening against hERG inhibition may be warranted to determine if there is a significant enough difference in the dose response between AChE and hERG. Only 3 ligands (**C1.3.a**, **C1.4.b** and **C2.3.a**) violated

the rule for QPlogPo/w and only **B1.1.a** violated the TPSA rule. This limited the potential drug-like molecules in the scaffolds to twelve ligands **A1.2.a**, **A1.3.a**, **A1.5.a**, **A1.8.a**, **C1.1.a**, **C1.2.a**, **C1.5.a** (and **C1.5.b**), **C1.6.a**, **C2.1.a**, **C2.4.a**, **C2.5.a** and **C2.6.a**.

Additional work conducted with pharmacophore studies generated from the ligands that had docking scores of less than -13.000 could potentially be used in future studies to target scaffolds that overlap with the resultant hypotheses. The bioavailability radar violations using SwissADME analysis indicated the following ligand violations, INSATU included **A1.1** and **C3.1-C5.11**, LIPO included **C1.1-C1.5**, and **C2.1-C2.5**, INSOLU included **C1.3**, and **C2.3**, while POLAR was only violated by **C5.11**. Therefore, the SwissADME analysis only predicts that seventeen of the ligands will be bioavailable, lowering the number of drug-like compounds that incorporates both Schrodinger and SwissADME analysis results to six ligands (**A1.2.a**, **A1.3.a**, **A1.5.a**, **A1.8.a**, **C1.6.a**, **C2.6.a**). Both Schrodinger and SwissADME were used to indicate which ligands would be CYP2C9 inhibitors which in the end only excluded **C3.5**.

From the results above, excluding the CYP2C9 results, ligands **A1.3.a**, **C1.6.a** and **C2.6.a** are the three ligands classified as the most promising drug-like molecules. These three ligands, together with the non-drug-like molecule, **B1.1.a**, were therefore identified as most important for progression to the synthesis stage.

Chapter 4

Synthetic analysis and discussion of acetylcholinesterase inhibitors



4.1. Introduction

In the previous chapter we identified three promising scaffolds A, B and C with good, predicted binding affinity for AChE and good drug-likeness. The molecular docking analysis identified the most crucial AChE interactions involving specific amino acids and indicated the importance of the spread of Van der Waals interactions across the surface of the ligand. The **Qikprop** data results limited the targeted ligands to twelve promising ligands, the selection was further refined with the SwissADME bioavailability web-based tool kit to six ligands. These ligands might be useful AChEIs, but the data of course needed to be verified through the synthesis of the targeted ligands of scaffolds A, B and C followed by biological assessment. The parent targets identified for synthesis are **A1.3.a**, **B1.1.a**, **C1.6.a**, and **C2.6.a**.

To summarise, the project's targeted scaffolds were designed by considering the interactions observed between the FDA approved drug donepezil (**25**) and AChE as well as the publication by Villalobos with regards to compounds **75** and **76** [74, 75]. The targeted scaffolds were designed to retain the critical interactions observed in donepezil (**25**) and allow for the exploration of the CAS site of AChE with scaffold A, B and C. In the case of scaffold B as it is somewhat longer it was particularly attractive as its length would lend itself well to the development of dual inhibitors that can bind to both the CAS and PAS sites of AChE. We initially envisaged the synthesis of scaffolds A, B and C with a focus on the preparation of **A1.3.a**, **B1.1.a**, **C1.6.a**, and **C2.6.a**.

4.2. Attempted synthesis of scaffolds A and B

Scaffolds A and B are based on a common isoxazole core (blue circle in **Figure 4.1, A and B**). Diversification of scaffold A was planned by simply transesterification of the ester moiety (red circle, **A**). In the case of scaffold B, we envisaged a series of transformations following the isoxazole formation to afford an azide which could be diversified by Click type chemistry leading to a triazole functional group (green circle, **B**) with a range of different ethers (red circle, **B**). The replacement of the indanone ring of donepezil (**25**) with an isoxazole ring system appeared to be promising based upon both the *in silico* studies conducted (chapter 3) as well as reports by Villalobos *et al.* who showed that similar systems had high activity against AChE as well as high selectivity for AChE over BuChE (compound **76**) [74, 75].

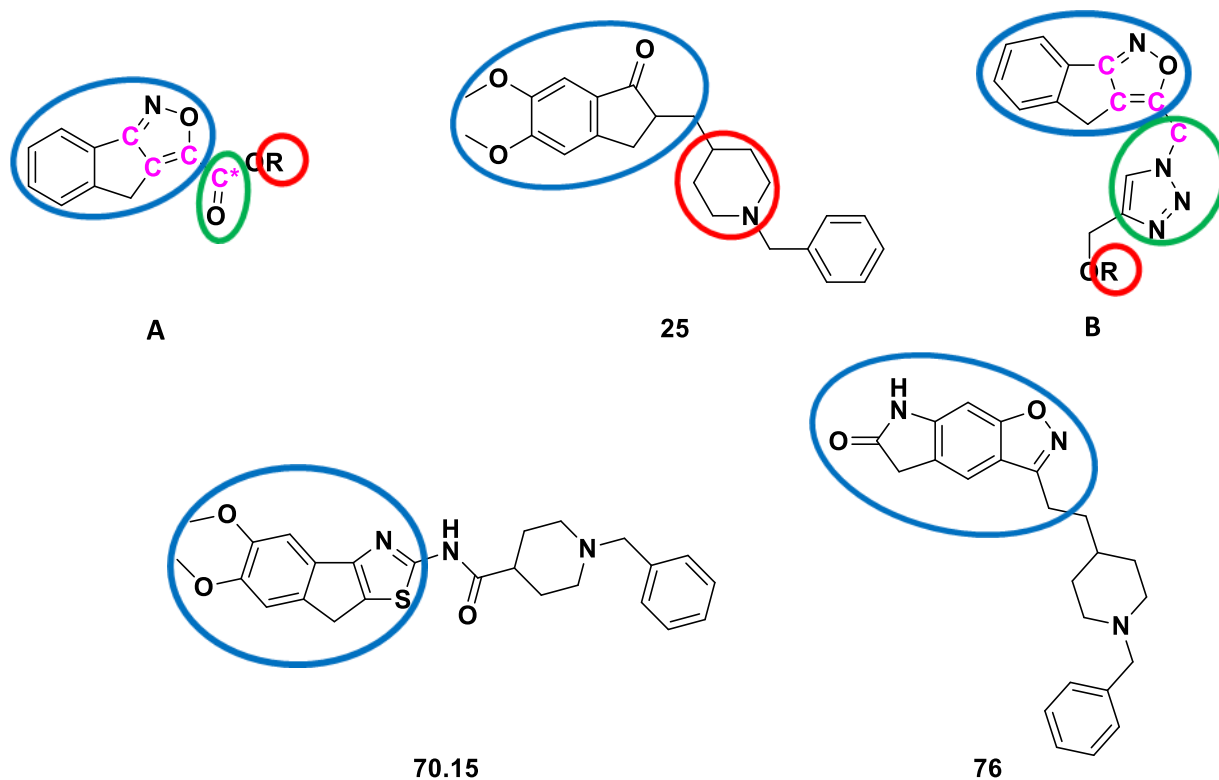
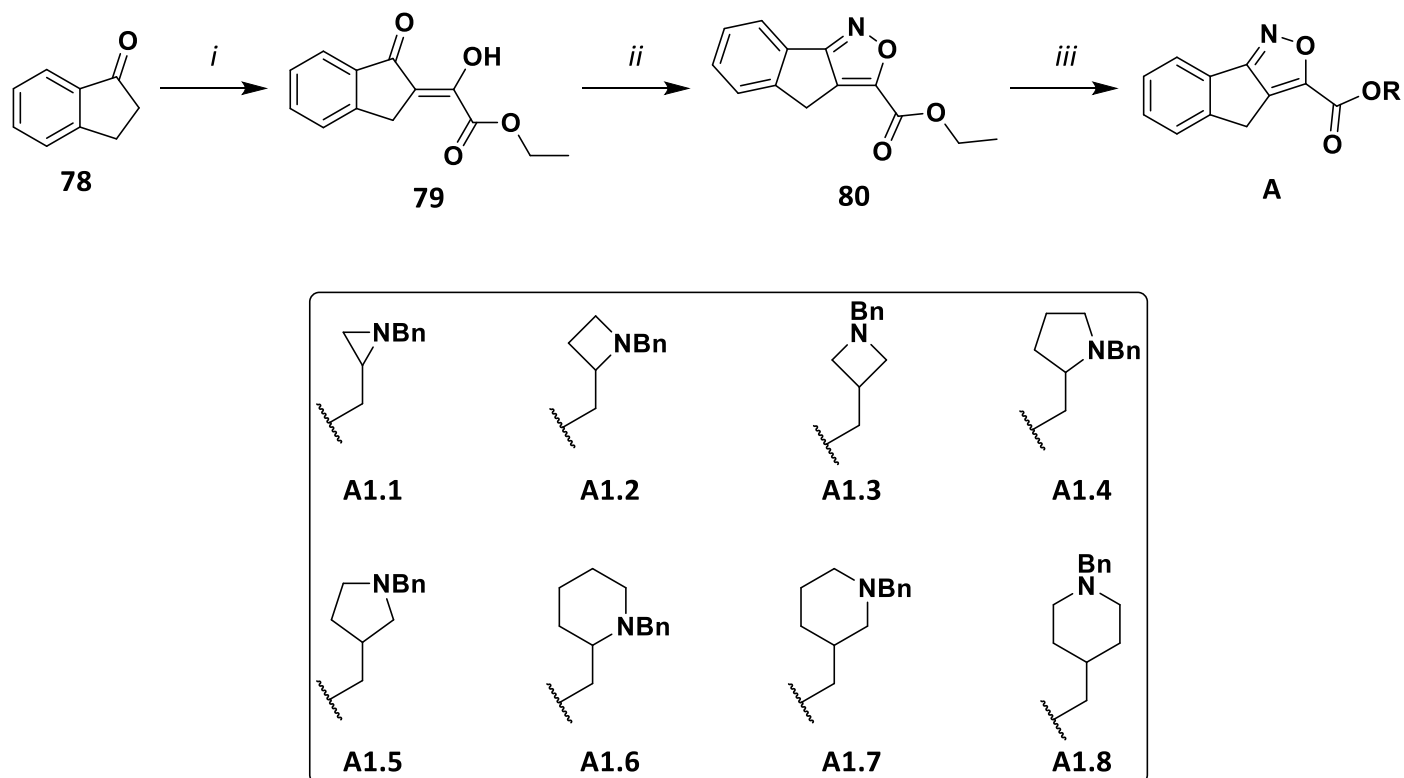


Figure 4.1: Comparison of donepezil (25) and other compounds that led to scaffold A and B backbone.

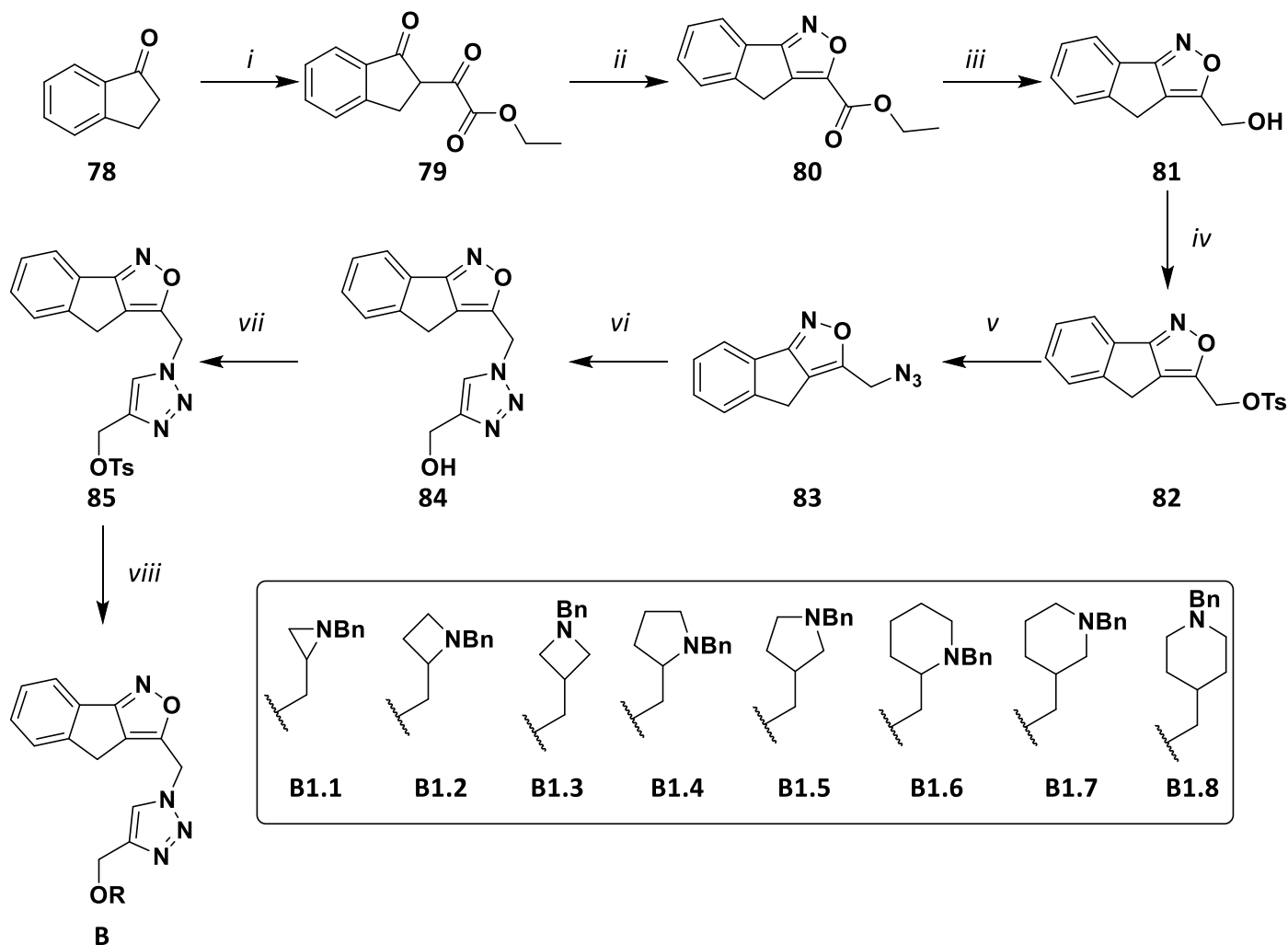
The structure of scaffold A allows for the exploration of the CAS site of AChE through the functionalisation of an exocyclic ester (red circle, **A**), which in the *in-silico* investigations showed promise as potential AChEIs. Following previously reported in-house work which contains a tricyclic thiazole scaffold (blue circle, **70.15**) and the *in silico* studies reported in chapter 3, we elected to focus on the functionalisation of the R-group in scaffold A as various saturated *N*-benzylated ring systems [69].

The synthesis of scaffold A was planned to start from indanone (**78**) which would undergo an aldol condensation reaction (step *i*) with the ester, diethyl oxalate, allowing for the formation of a diketoester (**79**) (**Scheme 4.1**). Thereafter the isoxazole ring (**80**) would be formed by treatment with hydroxylamine hydrochloride under acidic conditions (step *ii*). Finally, diversification can then be achieved through transesterification with different *N*-benzylated saturated ring systems (step *iii*) with a focus on the preparation of **A1.3** which showed the most promise after the *in silico* studies.



Scheme 4.1: Synthesis of compounds **A1.1 – A1.8**.

The envisaged approach to scaffold B diverged from scaffold A from after step *ii* (see **Scheme 4.2**). The ester group would be reduced to the primary alcohol (**81**). The alcohol would then be converted to a tosyl group (**82**) which in turn could then be converted to an azide group (**83**). Click chemistry would then be used to form the triazole functional group (**84**) using an alcohol containing alkyne and copper catalyst. The alcohol group can then be tosylated and then diversified through the addition of a range of different ethers (scaffold B).



Scheme 4.2: Synthesis of compounds **B1.1** – **B1.8**.

4.2.1. Preparation of diketoester (**79**)

Diketoester (**79**), **Scheme 4.2**, was prepared via a Claisen condensation reaction, which forms a new carbon-carbon bond between a ketone and an ester group through a process where the ketone is deprotonated to form an enolate that then condenses with the ester. The Claisen condensation reaction is an equilibrium process that requires the deprotonation of the indanone ring's α -H by treatment with sodium ethoxide, once reacted the resulting diketoester is again deprotonated at the α -position. At this point the reaction is irreversible and as such the use of equimolar or excess base is required to ensure that the reaction goes to completion [89].

Unfortunately, although well known and extensively reported, the reaction proved to be problematic (**Table 4.1**) affording no conversion to the desired diketoester (**79**). Initially the starting material (**78**) and the diethyl oxalate were kept at an equimolar ratio in an effort to minimise the amount of unreacted diethyl oxalate left

in solution, which is not easily removed in post reaction purification steps. The solvent used was absolute ethanol unless stated otherwise and the alkoxide base was generated *in situ* by addition of sodium metal (2.2 - 3.0 eq.) to the protic solvent system.

Table 4.1: Different reaction conditions for step (i) in both scaffold A and B

Entry	78 (eq.)	Solvent	Na (s) (eq.)	Diethyl Oxalate (eq.)	Reflux	2M HCl (eq.)	% Yield 79
1	1.0	96.0 % EtOH	3.0	1.0	No	0.1	-
2	1.0	99.9 % EtOH	2.5	1.0	No	1.5	-
3	1.0	99.9 % EtOH	2.5	1.0	Yes	0.1	-
4	1.0	99.9 % EtOH	2.2	1.0	No	0.4	-
5	1.0	99.9 % EtOH	2.2	1.0	No	7.7	-

We initially performed the reaction at ambient temperature (**entries 1-2**) to no success. When increased to a refluxing temperature (**entry 3**) we again observed no product formation. We briefly explored the effect of reducing the base to 2.2 eq. (**entry 4**) and increasing the acid added post reaction to 7.7 equivalents still to no avail.

In an effort to ascertain if the failure was substrate dependant, we elected to try the reaction using a range of different ketones (**Table 4.2**). To our pleasant surprise we were able to prepare the corresponding diketones when starting from **94** and **95** when adding 8.6 eq. of acid. We then revisited indanone (**78**) and were able to prepare the desired **79** in a 65 % yield under the same conditions.

Comparatively, the six-membered ring of tetralone (**95**) seemed to allow for better reactivity compared to the five-membered ring moiety of indanone (**78**) and 5,6-dimethoxy indanone (**94**), evident by the high yield displayed in **Table 4.2**. This relationship may be explained by the more flexible tetralone six-membered ring being more accessible for the removal of the α -proton and the subsequent addition of diethyl oxalate. In hindsight, the stabilised enol needs an acid source to ensure that it is protonated post reaction, as such initially observed poor reactivity may have resulted from simply losing the unprotonated equivalent of the desired product to the aqueous waste when worked-up. We subsequently upscale the reaction by 50-fold, which resulted in a modest 6 % decrease in yield (**Table 4.3, entry 2**).

Table 4.2: Illustrates the use of different starting materials for the Claisen reaction of scaffold A.

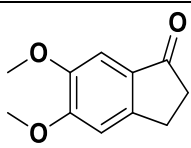
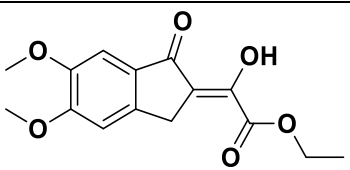
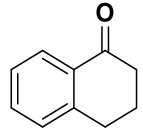
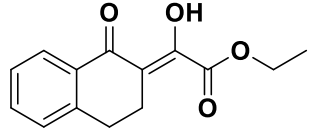
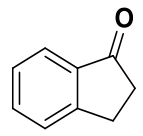
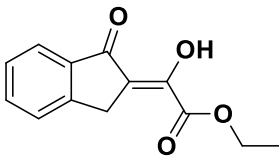
Starting material	Product	Yield
 94	 96	70 %
 95	 97	95 %
 78	 79	65 %

Table 4.3: Different reaction conditions for step (i) in scaffold A and B when using excess acid.

Entry	78 (eq.)	Solvent	Na (s) (eq.)	Diethyl Oxalate (eq.)	Reflux	2M HCl (eq.)	% Yield 51
1	1.0 (0.15g)	99.9 % EtOH	2.5	1.0	No	8.6	65 %
2	1.0 (5.0 g)	99.9 % EtOH	2.5	1.0	No	8.6	59 %

The formation of **96** was verified through the analysis of its ^1H NMR spectrum which correspond to the predicted NMR spectrum using Advanced Chemistry Development, Inc. (ACD/Labs) Software V11.01 (© 1994-2021 ACD/Labs). Interestingly, the NMR spectrum indicated the presence of a very deshielded proton at 13.23 ppm, as a broad singlet integrating for one proton suggesting the presence of a hydroxy group, suggesting further, that the middle carbonyl group is actually a stabilised enol, this is of course not unexpected as the enol is resonance stabilised through conjugation with the other two carbonyls. The characteristic singlet peak representing the indanone ring's CH_2 group is present at 3.87 ppm and the two methoxy groups are seen at 4.00 ppm and 3.94 ppm, both integrating for three protons. Finally, the ethyl ester group is present and found as the quartet peak for the $-\text{CH}_2$ at 4.41 ppm and a triplet peak representing the $-\text{CH}_3$ at 1.43 ppm. Analysis of the ^{13}C NMR spectrum further supported the proposed enol structure with

only two carbonyl peaks being noted, the enol is confirmed by the presence of two alkene carbons at 162.92 ppm and 117.25 ppm. The FTIR spectrum shows the two ketone C=O stretch bands at 197.74 cm^{-1} and 151.52 cm^{-1} . The enol is confirmed by the presence of alkene stretches at 1600 – 1800 cm^{-1} and the -OH functional group at 2700 – 3200 cm^{-1} . Finally, MS data supports the formation of the product with an (M-H)⁺ mass ion at 291.114 ($\text{C}_{15}\text{H}_{16}\text{O}_6$ requires 291.087).

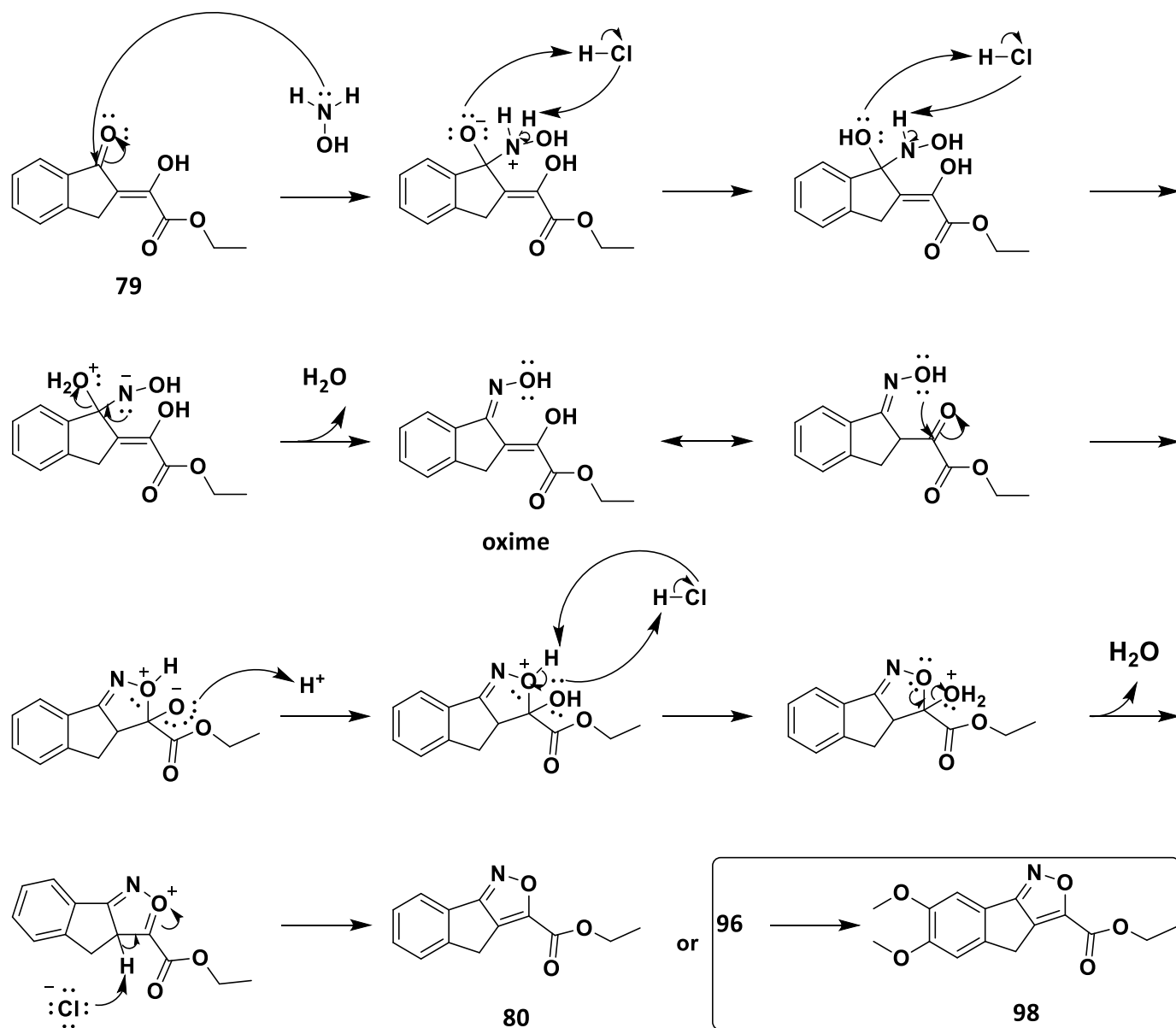
In the case of **97** the NMR spectrum also indicated the presence of a very deshielded proton at 15.80 ppm, as a broad singlet integrating for one proton again suggesting the presence of a hydroxy group from the stabilised enol. The ethyl ester group is found as the quartet peak for the -CH₂ at 4.38 ppm and a triplet peak representing the -CH₃ at 1.40 ppm. The multiplet at 2.97 – 2.83 ppm integrating for four protons indicates the two -CH₂ groups of the dihydronaphthalene ring system. The ¹³C NMR spectrum further supported the proposed enol structure with the presence of only two carbonyl peaks being noted at 186.98 ppm and 162.99 ppm and the presence of two alkene carbons at 169.78 ppm and 108.83 ppm.

Finally, the formation of **79** was also verified through the analysis of its ¹H NMR spectrum which is comparable to previously published results [90]. The NMR spectrum indicated the presence of the now expected deshielded proton as a broad singlet at 13.02 ppm integrating for one proton. The stabilised enol is therefore verified. The CH₂ group, characteristic of the indanone ring, is present at 3.95 ppm as a singlet integrating for two hydrogen atoms. Finally, the ethyl ester group is present and found as the quartet peak for the CH₂ at 4.41 ppm and a triplet peak representing the CH₃ at 1.43 ppm. Analysis of the ¹³C NMR spectrum further supported proposed enol structure formation also indicating the presence of only two carbonyl peaks being noted at 198.74 ppm and 153.96 ppm. The enol is further confirmed by the alkene carbons at 162.69 ppm and 116.41 ppm. The peaks corresponding to the alkene carbons and carbonyl carbons are further evidenced by their disappearance in the Dept 135 spectrum. The FTIR spectrum shows the two ketone C=O stretch bands and the enol's alkene stretches are found at 1600 – 1800 cm^{-1} and the -OH functional group at 2800 – 3200 cm^{-1} . Finally, MS data supports the formation of the product with an (M-H)⁺ mass ion at 231.084 ($\text{C}_{13}\text{H}_{11}\text{O}_4$ requires 231.066).

4.2.2. Attempted synthesis of ethyl 4*H*-indeno[1,2-*c*]isoxazole-3-carboxylate (**80**)

The second step in the proposed synthetic route involved the formation of the isoxazole ring by treatment with NH₂OH under acidic conditions, shown mechanistically in **Scheme 4.3** [91]. The NH₂OH acts as a nucleophile (Nu⁻), attacking the carbonyl carbon of the starting material [91]. As a result, a zwitterion is formed with a positively charged *N*-atom and negatively charged *O*-atom. The negatively charged *O*-atom

attacks the H-atom of the HCl molecule, kicking off the Cl-atom which in turn abstracts a proton from the positively charged N-atom, forming a neutral species. These two steps then repeat to form the oxime group and are followed by an intramolecular cyclisation involving the oxime moiety's O-atom and the carbonyl carbon atom. Finally, HCl then dehydrates the intermediate species and residual Cl⁻ removes the α-H to form **80**.



Scheme 4.3: Mechanism for the synthesis of the isoxazole via the formation of an oxime intermediate under acidic conditions [91].

The reaction conditions attempted are tabulated in **Table 4.4**, however, as the quantity of **79** available was limited, we elected to use **96** as a model system for determining the optimal conditions for this reaction. The

α,β -unsaturated ketone was kept as the limiting reagent while the equivalents of NH_2OH were screened from 1.5 to 3.0 equivalents. Two known methods were tested.

Table 4.4: Reaction conditions for step (ii) in scaffold A for synthesising **80** and **98**.

Entry	79 (eq.)	NH_2OH (eq.)	Solvent	Stirred at	Added	Reflux	% Yield 80
1	1.0	3.0	EtOH 99 %	Room temp.	-	Yes, overnight	-
Entry	79 (eq.)	NH_2OH (eq.)	Solvent	Stirred at	Added	Reflux	% Yield 80
2	1.0	3.0	EtOH 99 %	Room temp.	-	Yes, overnight	-
3	1.0	3.0	EtOH 99 %	Room temp.	-	Yes – 5 h	-
4	1.0	2.0	MeOH; NaOH H_2O	at - 70 °C	12M HCl	Yes - overnight	-
5	1.0	2.0	EtOH; NaOH H_2O	at - 60 °C	cHCl (1ml)	Yes - overnight	-
6	1.0	1.5	MeOH; NaOH H_2O	at - 40 °C	X	No Room temp. 2 days	-
7	1.0	1.5	MeOH; NaOH H_2O	at - 40 °C	X	No Room temp. 3 days	-
8	1.0	2.2	MeOH; K_2CO_3 H_2O	at - 40 °C	X	Yes, 2h Room temp. 1 day	-

The first method (**entries 1 and 2**) adopted an approach by Andrzejak and co-workers [92]. To the stirring solution of the starting material (**79** or **96**) in EtOH was added 3.0 eq. of NH_2OH which from the mechanism above indicated it will react with the ketone carbonyl carbon. This part of the reaction was allowed to react at room temperature for 2 hours whereafter it was refluxed overnight instead of just 5 hours as the method suggested. Unfortunately, we only observed degradation of the starting material or product as observed by TLC. We initially thought that this may have been due to the extended heating period. As such the same method was repeated with **96** as starting material, but now only allowing the reaction to reflux for 5 hours. In this instance no degradation was apparent, but again no product formed was observed.

According to the mechanism shown in **Scheme 4.3** HCl seems to have an important role for picking up the H⁺-atoms in solution, which leads to the use of the method described by Clausen and co-workers [93]. The NH₂OH equivalence was decreased to 2.0 equivalents and methanol was used as a solvent. The reaction was dosed with aqueous sodium hydroxide in an attempt to drive the reaction forward due to it dissociating the HCl (either 12 M or concentrated HCl) which deprotonates the NH₂OH that was attached to the α,β -unsaturated ketone. Unfortunately, this approach also proved unsuccessful.

We then investigated the effect of reducing the temperature (**entries 4-8**), reducing the equivalents of NH₂OH and exchanging the base (NaOH **entries 4-7**) for potassium carbonate (**entry 8**) however in all instances no product was observed.

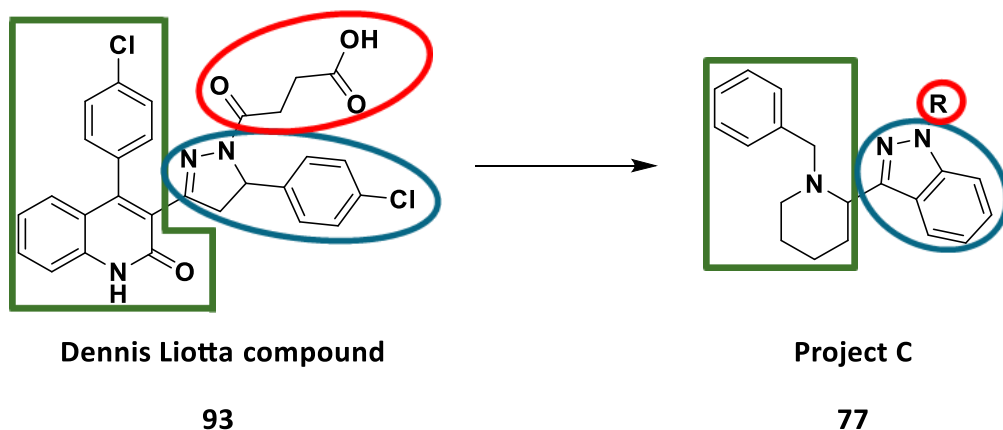
Despite several attempts we were unable to detect any of the desired product, in hindsight, the issue may be that the formation of isoxazoles using NH₂OH is typically performed between two ketones in a 1,3 relationship or an α,β -unsaturated system. In the case in hand the ester group stabilizes the one “carbonyl” as an enol and the keto-enol tautomerism to access the required carbonyl functionality appears to lie completely to the enol side as evidenced by NMR analysis. Although disappointing, at this stage we realised that simple access to the desired isoxazole scaffolds A and B with the exocyclic ester group was not synthetically feasible. As such we elected to focus our synthetic efforts of scaffold C which arguably performed significantly better in the *in silico* studies.

4.3. Scaffold C

This section focuses on the synthesis of novel AChEIs based on scaffold C which fortuitously also resembled NMDA antagonists designed by Liotta and co-workers. As such the scaffold was proposed to potentially afford dual targeting neuroprotective agents. We proposed to synthesise a series of pyrazole-based pharmacophores that in addition to acting as AChEIs would also mimic the skeleton of the Liotta NMDA antagonist (**93**), with improved drug-likeness (see **Scheme 4.4**) [72]. The Liotta compound, although potent, suffers in terms of drug-likeness due to a high MW (534.393 g/mol) and TPSA both of which fall outside the ideal limits for an orally available drug that is required to cross the BBB. As such we envisaged plans to reduce the MW and TPSA, the latter through the reduction of the number of H-donors and acceptors. In addition, we also aimed to increase the potential BBB permeation and the flexibility of the compound.

Scaffold C was envisaged to exchange the pyrazole and chlorobenzene rings in the Liotta compound with an indazole ring providing a molecule that incorporates both the pyrazole and phenyl ring motifs (**Scheme 4.4**, blue). In doing so the MW is reduced by 26.03 g/mol. A benzylpiperidine ring was then proposed to replace the quinoline-2(1*H*)-one ring and the chlorobenzene group (**93**) attached to it (**Scheme 4.4**, green), this

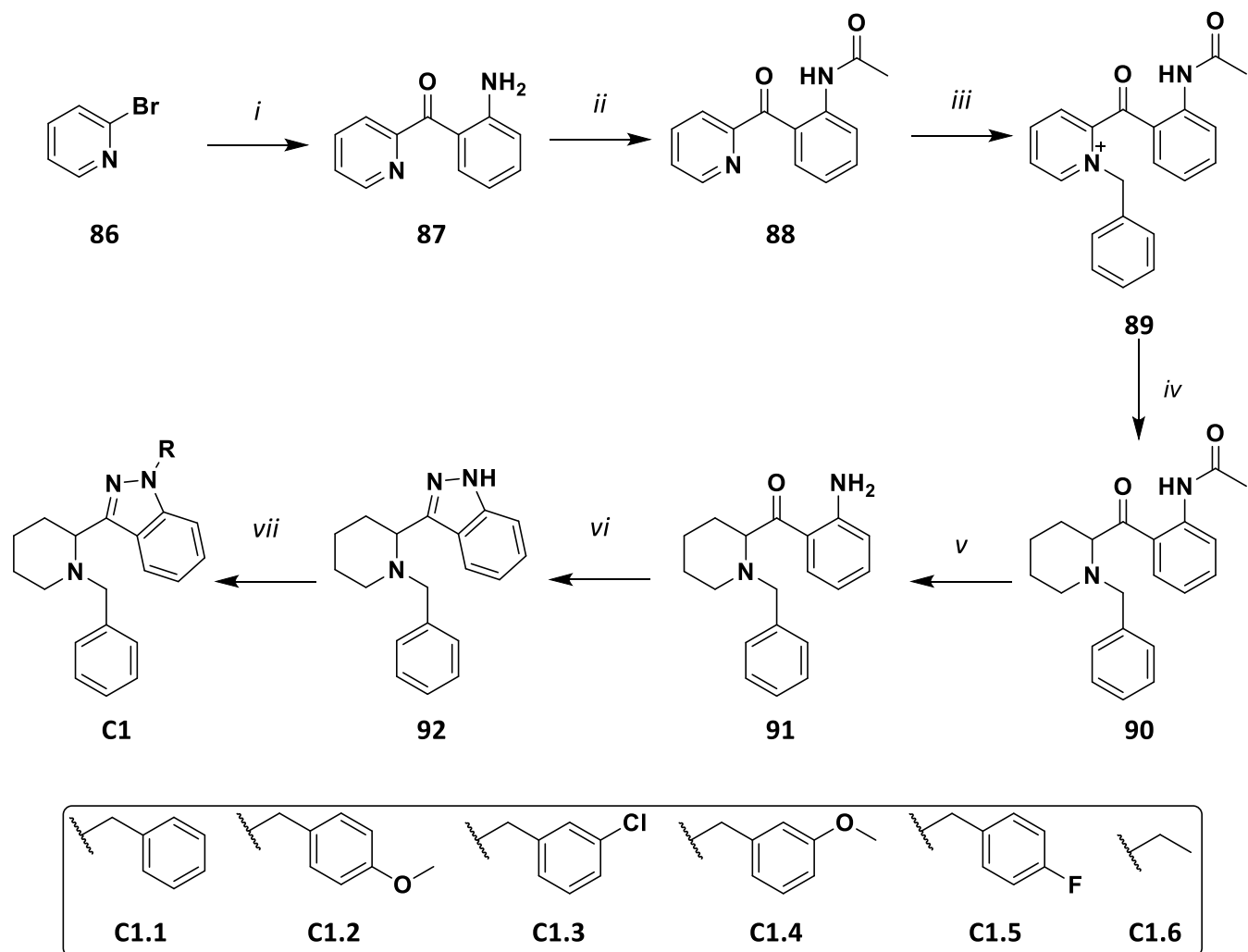
decreases the MW by a further 80.426 g/mol and also leads to a decrease in the TPSA. The incorporation of the different R groups (**Scheme 4.4**, red) would then also focus on decreasing the TPSA by replacing the aryl chain containing 3 O-atoms in the Liotta compound (**93**) with substituted benzene rings.



Scheme 4.4: Scaffold designed based on Liotta compound for scaffold C.

4.3.1. Scaffold C1

A retrosynthetic analysis of scaffold C is provided earlier in this chapter. The installation of the *N*-benzylated piperidine ring system was envisaged through the *N*-benzylation of pyridine **87** which in subsequent steps could then be reduced to afford the saturated piperidine ring system. To allow this, the NH_2 -group of **87** needs to be protected (**88**) prior to the benzylation step to afford **89**. Thereafter the envisaged reduction of the pyridine ring will afford **90** and after deprotection **91** which is required for the indazole formation of **92**. The indazole ring can then be diversified through the addition of different benzyl or aryl groups (see **Scheme 4.5**) to form **C1.1** to **C1.6**.



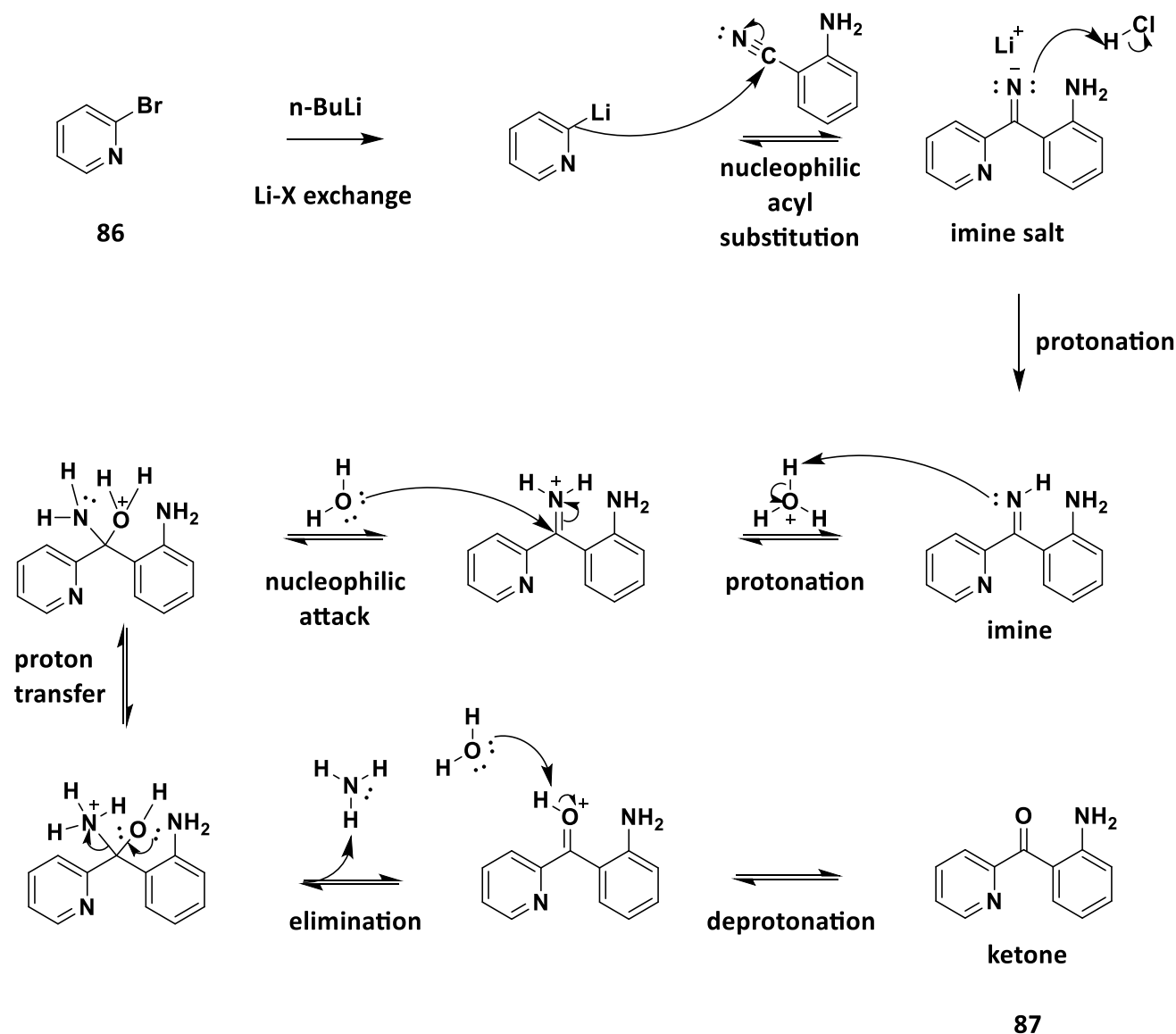
Scheme 4.5: Planned synthesis of scaffold C.

4.3.1.1. Preparation of ethyl (2-aminophenyl)(pyridin-2-yl)methanone (**87**)

A lithium-halogen exchange reaction initiates the preparation of scaffold C1, in which 2-bromopyridine (**86**) is lithiated and is then allowed to condense with the nitrile group of 2-aminobenzonitrile, forming the desired ketone (**87**). The reaction was conducted by adopting the method reported by Mizar and co-workers [94].

The mechanism of the lithium halogen exchange reaction can be seen in **Scheme 4.6** [95]. The lithium-halogen exchange reaction occurs between *n*-butyl lithium (*n*-BuLi) and 2-bromopyridine (**86**), forming 2-lithiopyridine. The nucleophilic carbon of 2-lithiopyridine adds to the electrophilic carbon of the nitrile group via a nucleophilic acyl substitution reaction, forming a new C-C bond. One of the π -bonds of the cyanide group breaks, causing the electrons to move to the *N*-atom forming the imine salt as an intermediate [95]. Thereafter acid mediated protonation of the imine salt affords the imine functional group which is subjected to nucleophilic addition of water which attaches at the carbonyl carbon to neutralise the positive *N*-atom

through the breakage of the π -bond of the imine functional group. The *O*-atom is left positively charged followed by a proton transfer causing the *N*-atom to be positively charged, and therefore converting it to a good leaving group (NH_3^+). Then the lone pair of electrons on the *O*-atom reforms the carbonyl group ejecting the NH_3 group. Another water molecule then deprotonates the positively charged *O*-atom resulting in the formation of the ketone functional group [96].



Scheme 4.6: The mechanism for the synthesis of **87** via the formation of an imine functional group [95, 96].

Using the approach by Mizar and co-workers, the preparation of **87** was readily achieved by initial treatment of 2-bromopyridine with $n\text{-BuLi}$ to afford the analogous lithiated pyridine, after which addition of 2-aminobenzonitrile afforded ketone **87** in an isolated yield of 77 %. Purification employing column chromatography proved challenging due to similar R_f values of the starting material and product and in addition, decomposition occurred on the column. This could however be mitigated by instead washing the crude reaction mixture with cold diethyl ether in which the starting material is soluble but ketone **87** is not,

employing this approach afforded **87** in a comparable yield to when purified by column chromatography. The formation of **87** was verified through the analysis of the ^1H NMR spectrum. The NMR spectrum indicated the presence of the NH_2 group at 6.42 – 6.18 ppm as a broad singlet. The analysis of the ^{13}C NMR spectrum supports the formation of the carbonyl group linker as noted by the carbonyl peak at 196.08 ppm. The FTIR spectrum shows the aromatic C-H bend regions at 744 cm^{-1} and 933 cm^{-1} and the band at 1148 cm^{-1} indicates the C=N stretch. The ketone C=O stretch band is at 1616 cm^{-1} and the peak for the aromatic C=C stretches are at 1450 cm^{-1} . The presence of the two distinct peaks at 3329 cm^{-1} indicate the presence of the two N-H stretches forming part of the amine functional group.

4.3.1.2. Preparation of *N*-(2-picolinoylphenyl)acetamide (**88**)

The next step in the formation of scaffold C1 was the protection of the amine group. The protection was required to prevent regioselectivity issues in step 3 which required the benzylation of the pyridine ring. The method used was a general protection group procedure published by Pranaya and co-workers [97].

The synthesis of **88** was achieved by the treatment with acetic anhydride under solvent free conditions. The solvent free conditions allowed for the reaction to be completed in a more environmentally friendly manner. A high temperature of $140\text{ }^\circ\text{C}$ contributed to a high yield where 1 hour and 30 min reaction time was sufficient affording a 99 % yield.

The formation of **88** was verified through the analysis of the ^1H NMR spectrum. The NMR spectrum indicated the presence of the NH group at 11.09 ppm as a broad singlet integrating for a single hydrogen atom. The methyl group is found at 2.24 ppm as a singlet that integrates for three hydrogen atoms. The analysis of the ^{13}C NMR spectrum supports the presence of two carbonyl groups at 169.26 ppm and 196.29 ppm. The methyl group is found at 25.44 ppm. The FTIR spectrum shows the aromatic C-H bend regions at 732 cm^{-1} and 931 cm^{-1} and the band at 1272 cm^{-1} indicates the C=N stretch. The ketone C=O stretch bands are found at 1642 and 1695 cm^{-1} and the peak for the aromatic C=C stretches are at $1450 - 1650\text{ cm}^{-1}$. The N-H stretch at 3306 cm^{-1} is represented as a small broad band.

4.3.1.3. Attempted synthesis of 2-(2-acetamidobenzoyl)-1-benzylpyridin-1-ium (**89**)

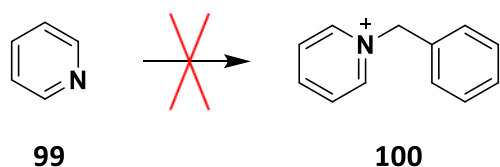
The attempted *N*-benzylation of the pyridine ring made use of a general method wherein **88** was treated with benzyl chloride (1.1 eq.) in the presence of triethylamine (4.0 eq.) and allowed to reflux overnight. Unfortunately, in this instance no product formation was observed (**Table 4.5, entry 1**). The reaction was repeated several times at reduced reflux (3 to 3.5 h) followed by stirring at ambient temperature overnight (**entries 2 and 3**) to no avail. Finally, decreasing the amount of triethylamine or increasing the amount of benzyl chloride and triethylamine (**entries 4 and 5**) also proved unsuccessful.

Table 4.5: Reaction conditions for step (ii) in scaffold C1. For the synthesis of **89**.

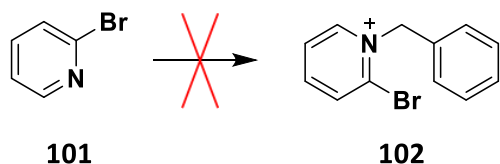
Entry	88 (eq.)	BnCl (eq.)	Et₃N (eq.)	Solvent	Refluxed	Yield (%)
1	1.0	1.1	4.0	Dry AcCN	Overnight	0
2	1.0	1.1	4.0	Dry AcCN	3h 30 min; RT overnight	0
3	1.0	1.1	4.0	Dry AcCN	3h; RT overnight	0
4	1.0	1.1	2.9	Dry AcCN	3h; RT overnight	0
5	1.0	1.1 (x2)	3.1 (x2)	Dry AcCN	3h; RT overnight (x2)	0

4.3.1.4. Benzylation of simplified pyridine rings

Due to the benzylation of **88** being unsuccessful we decided to use simpler model systems in an effort to ascertain if the lack of reactivity was linked to **88** or if it was a more general problem. We decided to attempt the benzylation using pyridine **99** and 2-bromopyridine **101**. In the case of pyridine (**99**), we employed solvent-free conditions adding 1.0 eq. of benzyl chloride to pyridine at 0 °C as described by Javed and co-workers (**Scheme 4.7**) [98]. Once again, we were unable to isolate any of the benzylated material.

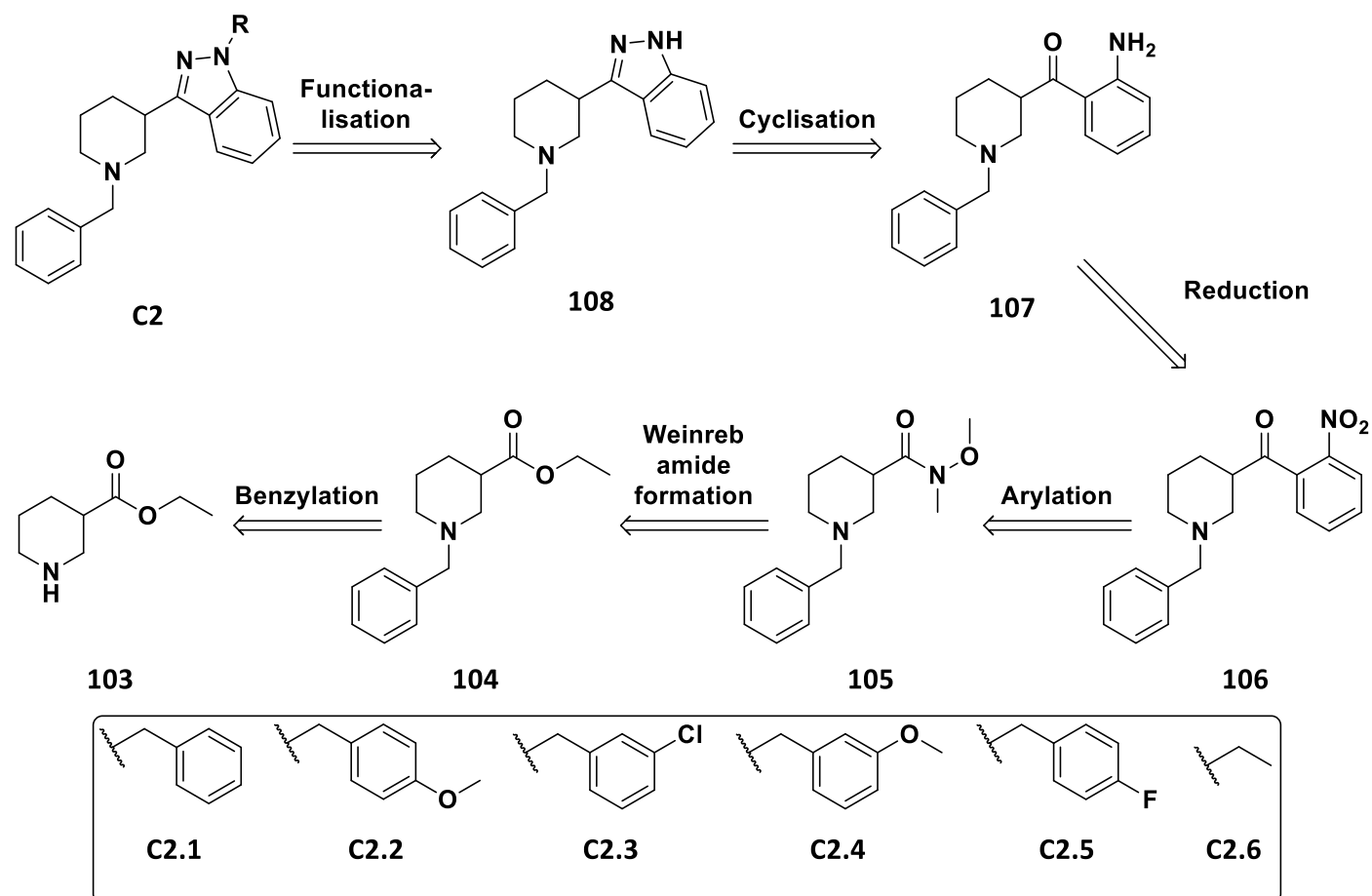
**Scheme 4.7:** Synthesis of 1-benzylpyridin-1-ium (**100**).

Alternatively 2-bromopyridine (**101**, **Scheme 4.8**) was dissolved in DCM and treated with 1.2 eq. of benzyl chloride which was sonicated at room temperature for 15 min using the method published by Ayman and co-workers [99]. Unfortunately, we were again not able to see any product formation. Despite several further attempts we were never able to benzylate the pyridine ring systems. As a result of these difficulties, we took the decision to modify the scaffold (C1) by shifting the attachment position of the indazole ring (scaffold C2).

**Scheme 4.8:** Synthesis of 1-benzyl-2-bromopyridin-1-ium (**102**).

4.3.2. Scaffold C2

Due to the difficulties experienced with the *N*-benzylation of pyridine **88** that we were faced with in the generation of scaffold C1, the retrosynthetic plan in **Scheme 4.9** was designed to incorporate a saturated piperidine ring from the start. The retrosynthesis envisaged the retro *N*-functionalisation of **108** which in turn would be prepared by the retro cyclisation of **107**. The preparation of ketone **107** was in turn envisaged through a retro reduction (**106**) and retro arylation of Weinreb amide **105**. Finally, **105** could be prepared in two steps involving a retro Weinreb amide formation (**104**) and retro benzylation of **103**.



Scheme 4.9: Proposed retrosynthesis of scaffold C2.

4.3.2.1. Preparation of ethyl 1-benzylpiperidine-3-carboxylate (**104**)

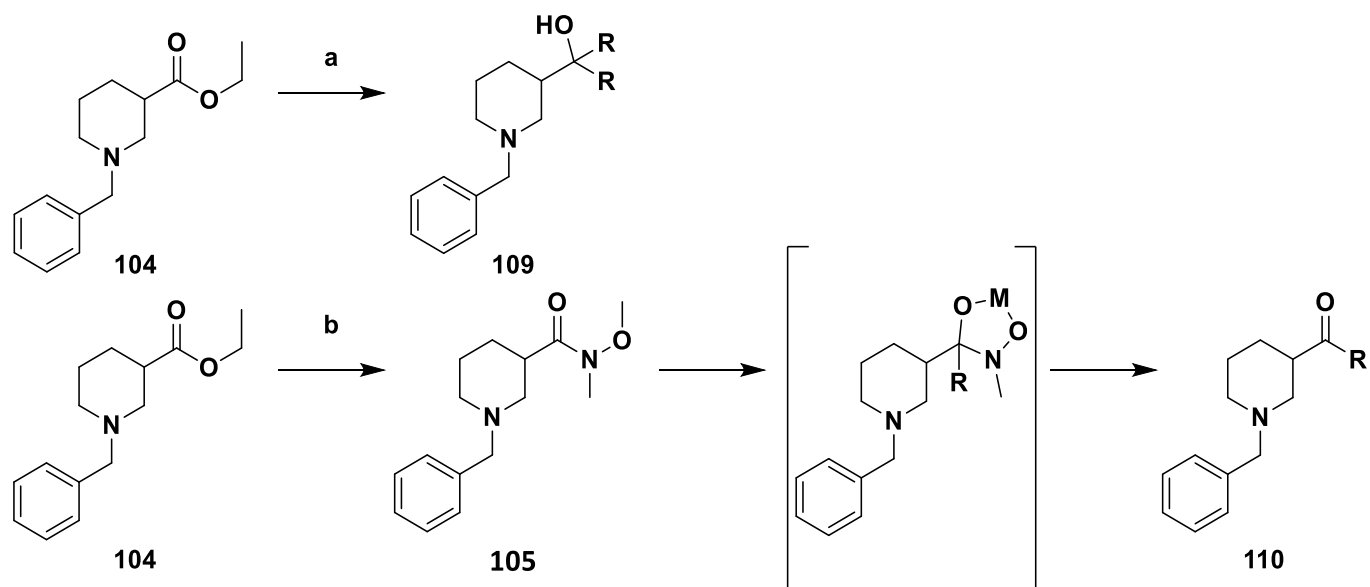
To avoid the difficulties associated with the benzylation of the pyridine ring system we instead elected to start with a piperidine system, in this instance with the point of functionalisation at the 3-position not the 2-position. In this instance a general benzylation reaction involving treatment with benzyl chloride and triethylamine was used affording **104** in 99 % yield.

The formation of **104** was verified through the analysis of the ¹H NMR spectrum. The NMR spectrum

indicated the addition of the benzyl group through the quartet peak representing the CH₂ group at 3.62 – 3.44 ppm and the five aromatic hydrogens (Ar H's) at 7.45 – 7.09 ppm. The ethyl group is also verified by the CH₂ group as the quartet found at 4.13 ppm and the CH₃ group as the triplet found at 1.25 ppm which integrates for two hydrogens and three hydrogens respectively. The ¹³C NMR spectrum supports the presence of the benzyl group's aromatic ring indicated by the four aromatic carbons at 138.40 ppm, 129.03 ppm, 128.19 ppm, and 126.97 ppm. The four deshielded CH₂ groups are found at 63.33 ppm, 60.23 ppm, 53.65 ppm and 55.46 ppm. The FTIR spectrum shows the aromatic C-H bend regions at 698 cm⁻¹ and 738 cm⁻¹. The band for the aromatic C=C stretches is at 1451 cm⁻¹, and the ketone C=O stretch band is at 1720 cm⁻¹. The presence of the sp³ and sp² C-H stretch bands are found in the 2700 - 3200 cm⁻¹ range.

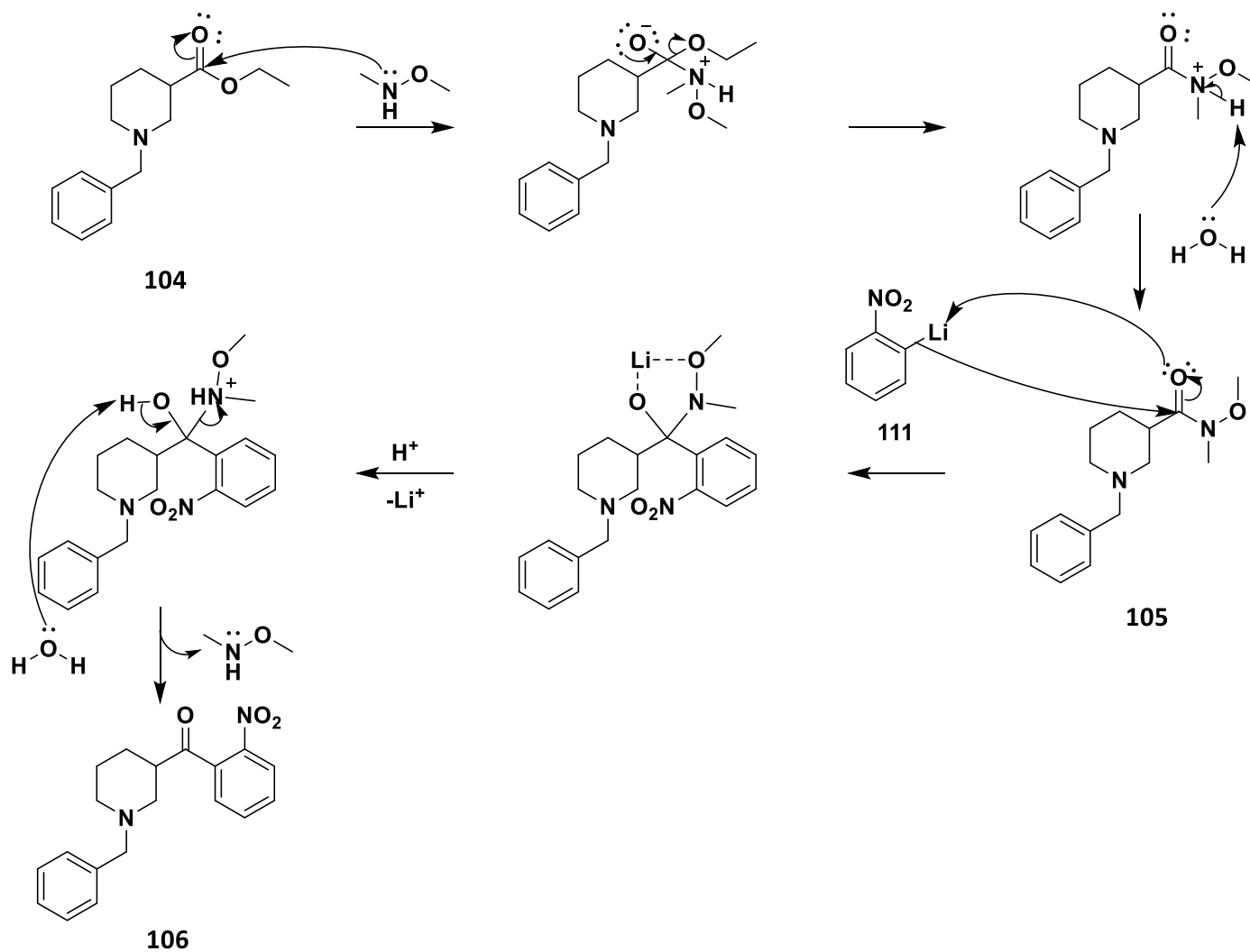
4.3.2.2. Attempted synthesis of 1-benzyl-N-methoxy-N-methylpiperidine-3-carboxamide (105)

The transformation of the ester group (104) to a Weinreb amide group (105) was targeted in the next step of the synthesis to be able to add the aryl group in the step that follows (106). The aryl group in this reaction is added as part of the organometallic compound, but this reagent would typically add twice (Scheme 4.10, a), producing a tertiary alcohol (109) and would therefore not form the targeted compound. The use of a Weinreb amide results in the formation a very stable metal-chelated intermediate when reacted with an organometallic compound (Scheme 4.10, b) which will prevent a second addition of the aryl group, hydrolysis of the chelate then affords the desired ketone (110).



Scheme 4.10: Reaction of an organometallic reactant with (a) and without (b) N,O-dimethylhydroxylamine hydrochloride.

Scheme 4.11 indicates the mechanism involved in the Weinreb amide formation which occurs through the reaction of *N,O*-dimethylhydroxylamine's *N*-lone pair attacking the partially positive carbonyl carbon of **104**. [100, 101]. The reaction results in a positively charged *N*-atom and a negatively charged *O*-atom, as an intermediate molecule. The good leaving group (ethoxy group; -OEt) gets kicked off when a lone pair on the *O*-atom reforms the carbonyl double bond. The positively charged *N*-atom gets hydrolysed by water, and results in the formation of the Weinreb amide (**105**) [100].



Scheme 4.11: The mechanism for the synthesis of **106** via the formation of a Weinreb amide (**105**) [100, 101].

The lithiated reagent's (**111**) Li-C bond breaks to form a C-C bond with the carbonyl carbon of **105**. As a result, the double bond breaks and transfers electrons to the *O*-atom, which in turn attacks the partially positive Li-atom. The Li-atom also interacts with the *O*-atom of the methoxy group. The addition of H-atoms and loss of the metal atom results in a positive charged *N*-atom and a neutral alcohol group. Water deprotonates the alcohol group resulting in the formation of the ketone functional group and removal of the *N,O*-dimethylhydroxylamine group.

The **entries 1** and **2** in **Table 4.6** were unsuccessful, but when considering the mechanism above, water is needed before the organo-lithium reagent is added, which was not the case as the method used was under inert conditions. This could have led to the addition of two propyl groups instead of forming the Weinreb amide. The reaction was repeated with the use of pyridine (**entries 3** and **4**) as a stronger base instead of water, no complex was added yet, but still the targeted Weinreb amide was not formed.

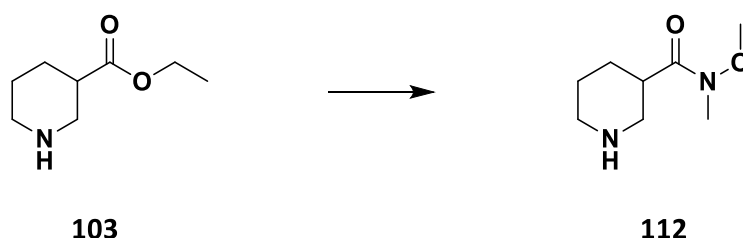
Table 4.6: Different experimental conditions for the synthesis of **105**.

Entry	Complex or base used	<i>N,O</i> -dimethylhydroxylamine hydrochloride (eq.)	Solvent	Temperature and reaction time	Yield
1	Propylmagnesium chloride	2.0	Ether	-20 °C; overnight	-
2	Trimethyl aluminium	1.5	DCM	0 °C; overnight	-
3	Pyridine	1.1	DCM	Room temperature; 20 h	-
4	Pyridine	1.1	DCM	Room temperature; 4 days	-

In hindsight as the mechanism suggests that water is necessary to form the Weinreb amide and that the organo-lithium reagent should be added afterwards, the reaction can be considered again in future work as a one pot synthesis. From the method done by Nahm and Weinreb it seems that a lower temperature of 0 °C might also be necessary for the formation of the product.

4.3.2.3. Alternative Weinreb amide formation attempts

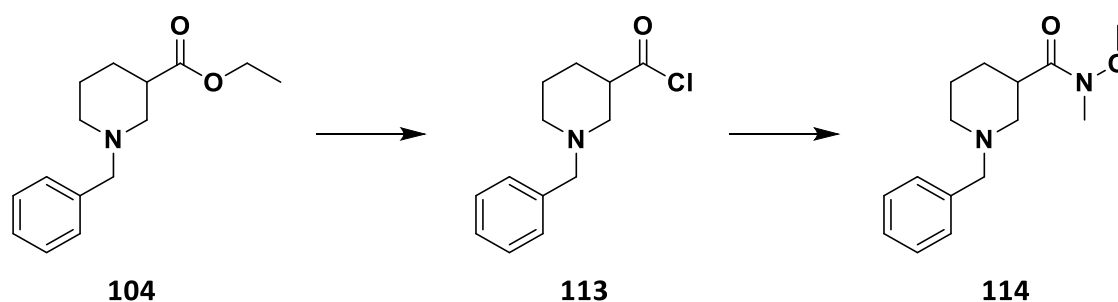
Due to the failure to prepare **105**, we wondered if the benzyl group might be inhibiting the formation of the Weinreb amide. As such, we attempted to prepare the Weinreb amide of the non-benzylated form of **104**, called ethyl piperidine-3-carboxylate (**103**). Unfortunately, this also proved unsuccessful (see **Scheme 4.12**)



Scheme 4.12: Synthesis of *N*-methoxy-*N*-methylpiperidine-3-carboxamide (**112**).

As an alternative we also considered the preparation of the analogous acid chloride **113** as a feedstock for the Weinreb amide formation as a one-pot synthesis. The approach seemed to be a feasible option as an ester can be easily converted to the acid chloride and then through the method described by Nahm and

Weinreb the acid chloride can be converted to the Weinreb amide [100, 102]. Unfortunately, once again the formation of the Weinreb amide (**114**) via this proposed one-pot synthesis also proved unsuccessful.

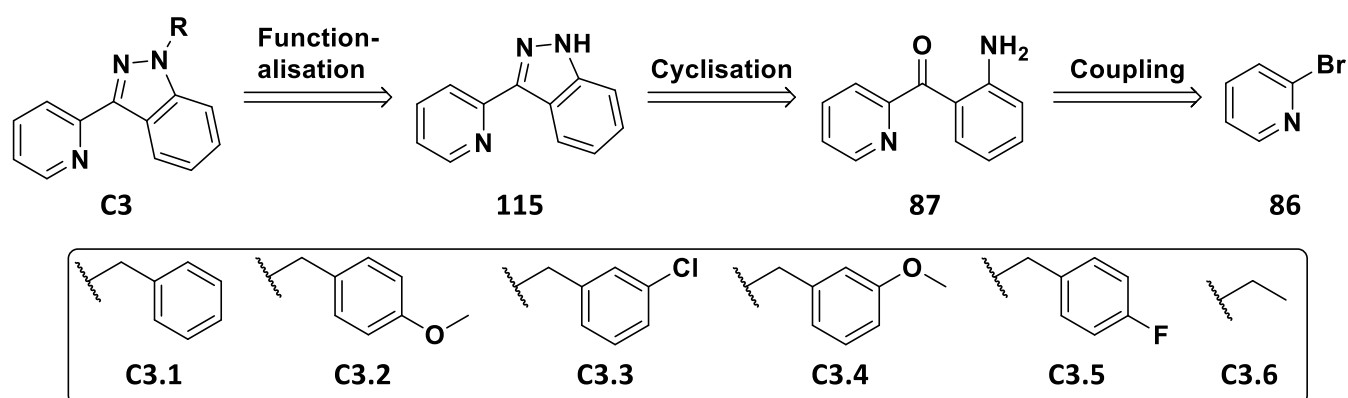


Scheme 4.13: Synthesis of 1-benzyl-N-methoxy-N-methylpiperidine-3-carboxamide (**114**).

Scaffold C2 seemed to be problematic with regards to the Weinreb amide formation, and due to time constraints we were forced to re-evaluate the scaffold. In this instance two structurally related scaffolds C3 and C4 were targeted in parallel.

4.3.3. Scaffold C3

In light of the synthetic difficulties experienced with scaffolds C1 and C2 and although not ideal, we again looked to modify the scaffold in hope of being able to prepare a somewhat simpler scaffold (C3). In this instance we selected to exchange the benzyl piperidine ring system for a simple pyridine ring system. The retrosynthesis in **Scheme 4.14** indicates the retro functionalisation of **115** which is followed by the cyclisation of **87** and the retro coupling of **86**.



Scheme 4.14: Proposed retrosynthesis of scaffold C3.

The synthesis of scaffold C3 would generate smaller compounds but would still hopefully indicate some good activities when considering the computational results from the previous chapter. As previously described, the lithium-halogen exchange and the nucleophilic acyl substitution reaction gave a 77 % yield for the synthesis of **87**.

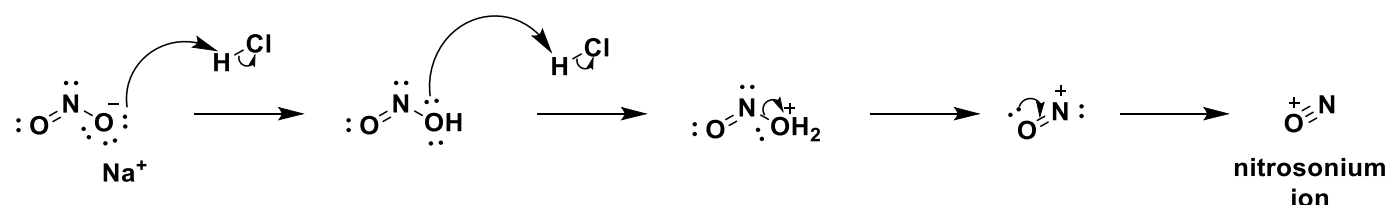
4.3.3.1. Attempted synthesis of 3-(pyridin-2-yl)-1H-indazole (115)

The cyclisation step forming **115** made use of multiple published methods but ultimately has proved to be unsuccessful [103-105]. The different reaction conditions attempted are tabulated in **Table 4.7**. The reaction was attempted under both acidic and basic conditions which were suggested by the different reported methods [103-105]. Different reagents were used as a *N*-source for this reaction which included isopentyl nitrite, NaNO_3 , NaNO_2 , $\text{NH}_2\text{OH}\cdot\text{HCl}$. The use of a reducing agent or transforming the leaving group into a better leaving group was also considered. The reaction times of these reactions were also varied. The potential causes of the reactions being unsuccessful is discussed below.

Table 4.7: Different experimental conditions for the synthesis of **115**.

Entry	87 eq.	Acid / base	<i>N</i> -source	Reducing agent	Better leaving group source	Reaction time	Yield
1	1.0	MeOH. HCl	isopentyl nitrite	-	-	overnight	-
2	1.0	6M HCl	NaNO_3	CaCl_2	-	30 min at 0 °C 30 min at 0 °C	-
3	1.0	H_2SO_4	NaNO_3	SnCl_2	-	1h at RT; 1h at 0 °C	-
4	1.0	cHCl	NaNO_2	SnCl_2	-	1h at 0 °C; 2h at 0 °C	-

Scheme 4.15 indicates the synthesis of the nitrosonium ion that is needed in the Sandmeyer reaction to form **115** [103]. Methanolic HCl was used instead of ethanolic HCl, as the method suggested in the literature. The reaction was unsuccessful, and since methanolic HCl and ethanolic HCl are not significantly different, there must be another reason for the failure of the reaction. It is suspected that the presence of the R group in isopentyl nitrite (**entry 1 in Table 4.7**), is not easily kicked off as compared to the removal of water in the mechanism shown in **Scheme 4.15** in order to form the nitrosonium ion.

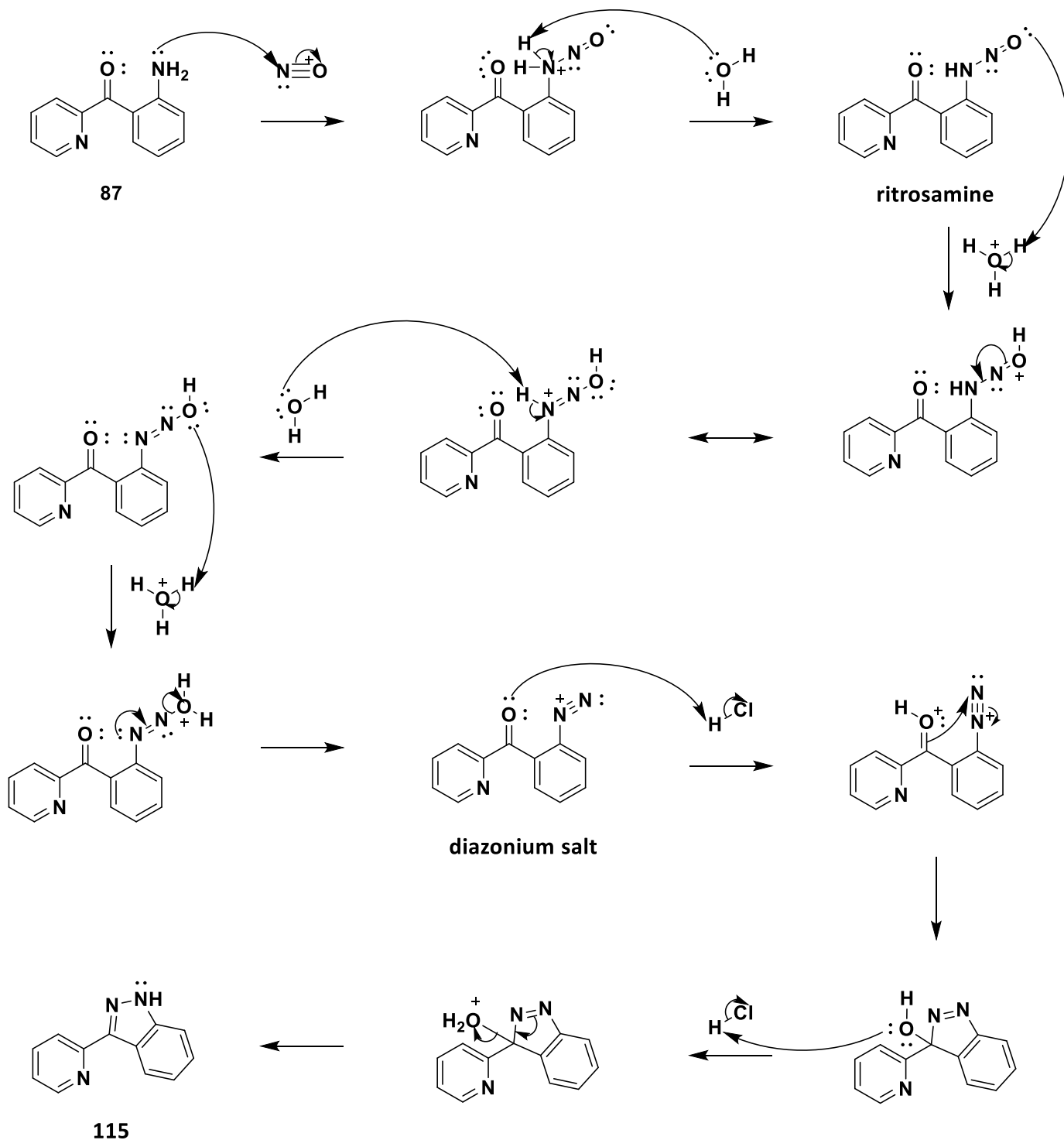


Scheme 4.15: Mechanism of the forming of the nitrosonium ion [103].

For **entry 2** and **3** in **Table 4.7**, it can be seen that nitrate (NO_3^-) instead of nitrite (NO_2^-) was used, which was done in error. That being noted, it is possible to form NO_2^- from NO_3^- , but high temperatures are needed, and as these reactions were done at 0 °C there was no possibility of forming NO_2^- in the altered method used. Unfortunately, **entry 4**, which makes use of NO_2^- , did not give a successful reaction when using acidic

conditions. Another way of forming the product was then considered.

Scheme 4.16 indicates the mechanism of adding the nitrosonium ion to **87** in order to form the diazonium salt via a Sandmeyer reaction under acidic conditions to form **115** [106]. The lone pair of electrons on **87** attacks the *N*-atom of the nitrosonium ion to force the one N-O double bond to break onto the *O*-atom. Water then takes up the H-atom on the positively charged *N*-atom resulting in a neutral ritosamine molecule. The lone pair on the *O*-atom then reacts with an H_3O^+ molecule leaving the *O*-atom positively charged and resulting in the resonance structure of the molecule where the charge is located in the *N*-atom instead of the *O*-atom. The positive charge gets neutralised through a water molecule taking up the H-atom and breaking the H-N bond onto the *N*-atom, resulting in a neutral molecule. The *O*-atom reacts with another H_3O^+ molecule leaving the *O*-atom positively charged. The movement of the lone pair from the *N*-atom, forms a triple bond, resulting in the water molecule getting kicked off and it leads to the formation of the diazonium salt. The carbonyl carbon double bond breaks and forms a bond with the *N*-atom with the lone pair in order for the triple bond to break onto the positively charged *N*-atom, resulting in a neutral molecule. The lone pair on the *O*-atom attaches another H-Cl bond and forms an excellent leaving group where the *O*-atom is positively charged. The double bond between the *N*-atoms moves in order to kick off the good leaving group as a water molecule resulting in the formation of **115**.



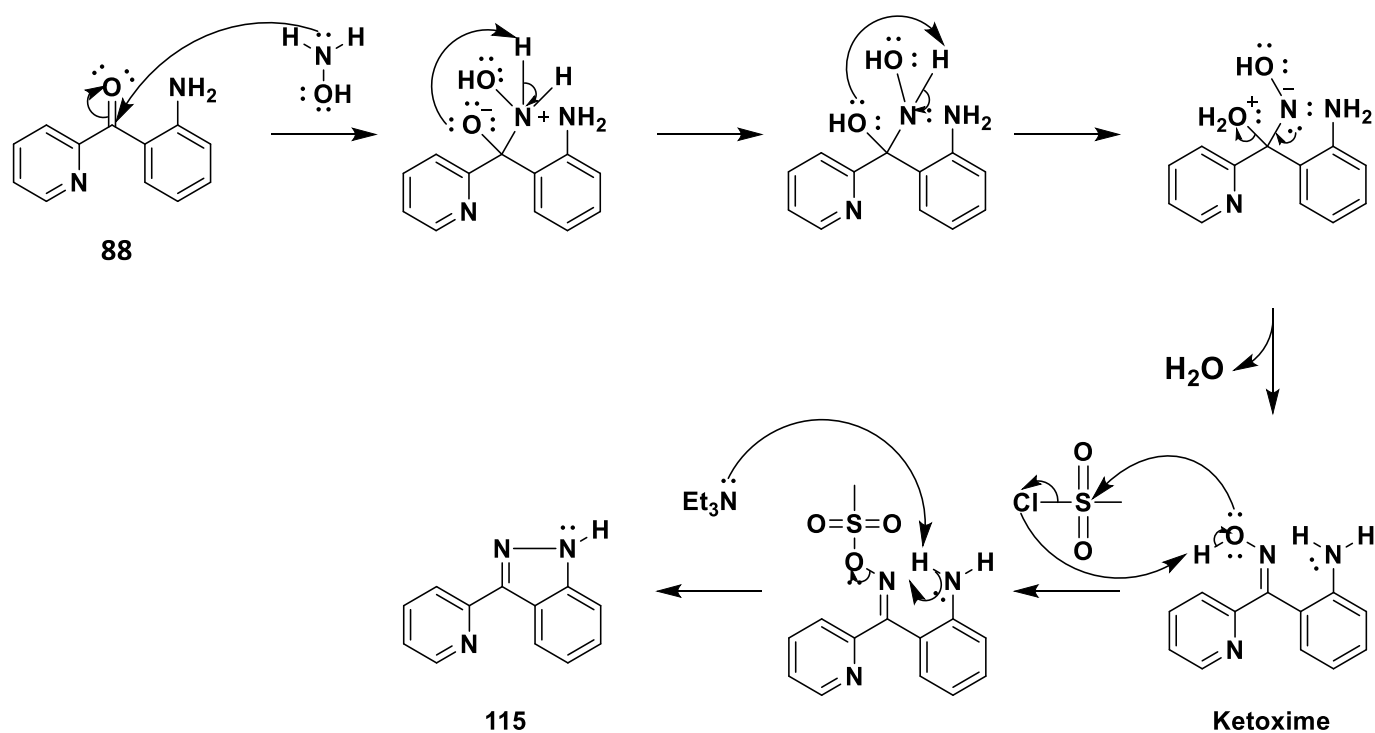
Scheme 4.16: Mechanism for the synthesis of the 3-(pyridin-2-yl)-1H-indazole (**115**) via the formation of a diazonium salt through a Sandmeyer reaction [106].

4.3.3.2. Alternative attempted synthesis of 3-(pyridin-2-yl)-1H-indazole (**115**)

Scheme 4.17 illustrates the mechanism of an alternative cyclisation step under basic conditions instead of acidic conditions [107]. It indicates how NH_2OH acts as a Nu^- , attacking the carbonyl carbon of the starting material. As a result, the *N*-atom gets positively charged (N^+) while the *O*-atom gets negatively charged (O^-).

The negatively charged *O*-atom attacking the H-atom of the positively charged *N*-atom will result in a neutral *N*-atom. The lone pair on the *O*-atom picks up a second H-atom, breaking the N-H bond onto the *N*-atom, leaving it negatively charged and the *O*-atom positively charged.

The one lone pair of electrons on the *N*-atom forms a C-N double bond, kicking off the good leaving group as a water molecule. A ketoxime functional group is formed as a result. The intramolecular cyclisation reaction will only be possible if the OH-group is converted into a good leaving group. This is achieved through the lone pair of electrons on the *O*-atom attacking a tosyl group, which loses a Cl-atom as a result. The Cl-atom will deprotonate the OH-group, leaving a neutral molecule containing an excellent leaving group. Et₃N acts as a base that deprotonates the NH₂-group, the N-H bond breaks and forms a bond between the two *N*-atoms kicking off the good leaving group, forming **115**.



Scheme 4.17: Mechanism for the synthesis of the isoxazole via the formation of a ketoxime intermediate in basic conditions [107].

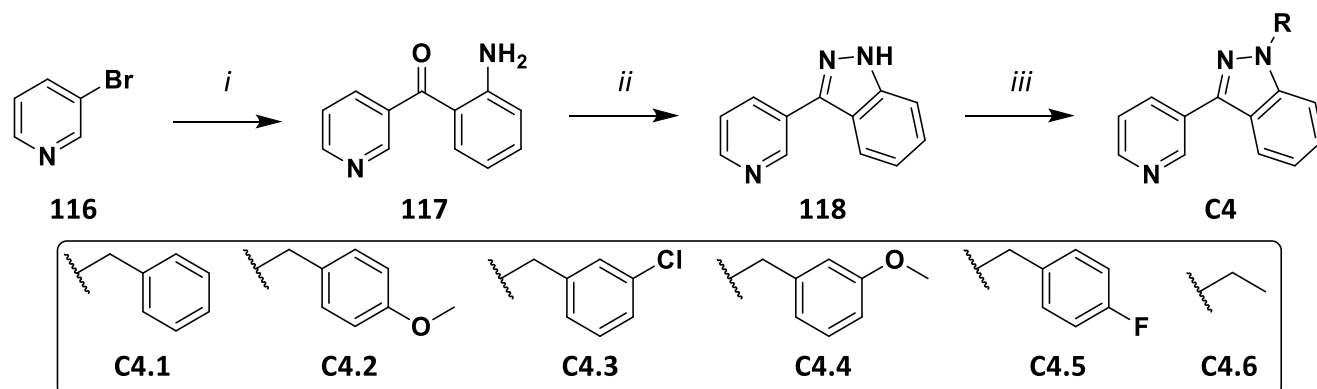
As seen above in **Scheme 4.17** a tosyl group acts as a good leaving group and therefore the addition of different tosyl groups to NH₂OH was attempted to determine if a specific tosyl group would result in the desired leaving group that will hopefully result in the cyclisation of the ketoxime molecule (see **entries 1-3** of **Table 4.8**). Unfortunately, all these reactions proved unsuccessful in the laboratory.

Table 4.8: Alternative experimental conditions for the synthesis of **115**.

Entry	87 eq.	Acid / base	N-source	Reducing agent	Better leaving group source	Reaction time	Yield
1	1.0	NaOH Et ₃ N	NH ₂ OH.HCl	-	methanesulfonyl chloride	reflux 2 h overnight at 0-5 °C	-
2	1.0	NaOH Et ₃ N	NH ₂ OH.HCl	-	thionyl chloride	reflux 2 h overnight at 0-5 °C	-
3	1.0	NaOH Et ₃ N	NH ₂ OH.HCl	-	tosyl chloride	reflux 2 h overnight at 0-5 °C	-

4.3.4. Scaffold C4

Scheme 4.18 represents the synthetic route of scaffold C4 which ran in parallel with scaffold C3. The position of the N-atom is altered through the use of 3-bromopyridine (**116**) instead of 2-bromopyridine (**86**). The lithium-halogen exchange reaction, and nucleophilic acyl substitution reactions were successful in forming **117** albeit in a low yield of 19 %. The reaction conditions used are tabulated in **Table 4.9**. The reaction conditions tested in order for the coupling reaction to be successful were: i) changing the temperature of the reaction from -50 °C to -70 °C in the hopes of keeping the temperature low enough to allow more time for the interaction between molecules to interact and combine to form **117** and ii) by changing the amount of n-BuLi used in the reaction in the hopes of pushing the reaction in the forward direction.

**Scheme 4.18:** Proposed synthesis of scaffold C4.

4.3.4.1. Synthesis of (2-aminophenyl)(pyridin-3-yl)methanone (**117**)

The synthesis of **117** made use of the previously discussed method used in C2 [94]. **Entry 1** in **Table 4.9** made use of the same conditions, but only a sample with an impure yield of 35 % was generated in the reaction. As a result of the low yield, THF and ether (**entries 2 and 3**) were considered as the solvent instead of toluene as they are more soluble than toluene and are also good options to use for dissolving organic compounds in

the reaction.

Table 4.9: Different experimental conditions for the synthesis of **117**.

Entry	Base	2-amino benzonitrile (eq.)	116 (eq.)	[n-BuLi]	Eq.	Stir at °C	Dry solvent	Yield %
1	3M NaOH	1.0	1.7	1.6M	2.5	-50 for 1h	Toluene	35 impure
2	3M NaOH	1.0	1.7	1.6M	2.5	-50 for 1h	THF	-
3	3M NaOH	1.0	1.7	1.6M	2.5	-50 for 1h	Ether	-
4	3M NaOH	1.0	1.7	1.6M	2.5	-70 for 1h	Toluene	-
5	3M NaOH	1.0	1.7	1.6M	2.5	-70 for 1h	THF	-
6	3M NaOH	1.0	1.7	1.6M	2.5	-70 for 1h	Ether	-
7	K ₂ CO ₃	1.0	1.7	1.6M	2.5	-50 overnight	Ether	-
8	K ₂ CO ₃	1.0	1.7	1.6M	3	-50 overnight	Ether	-
9	K ₂ CO ₃	1.0	1.7	1.6M	4	-50 overnight	Ether	-
10	K ₂ CO ₃	1.0	1.7	1.6M	5	-50 overnight	Ether	-
11	K ₂ CO ₃	1.0	2.0	1.6M	3	-50 3h	Ether	-
12	K ₂ CO ₃	1.0	1.8	1.6M	3	-50 3h	Ether	-
13	3M NaOH	1.0	1.7	1.6M	3	-50 3h RT - 6 days	Ether	-
14	6M NaOH	1.0	1.7	1.6M	2	Overnight	Toluene	19

For **entries 7-10** it was determined that the use of K₂CO₃ instead of NaOH, caused the degradation of the product before column chromatography. Degradation due to column chromatography was therefore avoided in the first entry in **Table 4.9** and is therefore recorded with an impure yield of 35 %. Unfortunately, we were unable to prepare sufficient material for analysis.

We attempted to lower the reaction time as it was suspected that the reaction might be degrading over time. **Entries 11-12** indicated that was not the case as no product formed from the reaction. **Entry 13** in **Table 4.9** was left to react for six days, but only degraded material was observed. The last entry in **Table 4.9** was the combined workup of two of these reactions on a 2.000 g scale of **116** used. A new bottle of 2-aminobenzonitrile was used in this reaction and resulted in a 19 % purified yield.

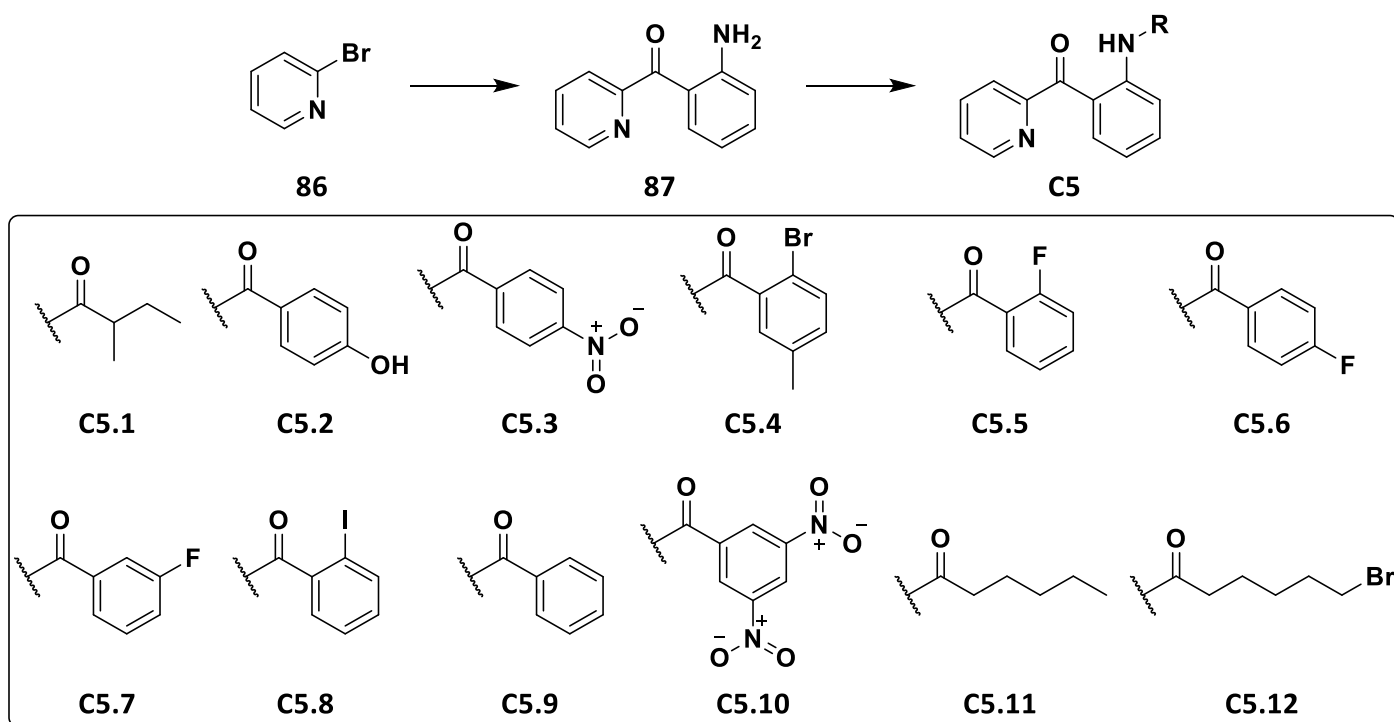
The formation of **117** was verified through the analysis of the ¹H NMR spectrum. The NMR spectrum indicated the presence of the NH₂ group at 6.32 ppm as a broad singlet integrating for two hydrogen atoms. The analysis of the ¹³C NMR spectrum supports the formation of the carbonyl group linker as noted by the carbonyl peak at 196.54 ppm. The deshielded carbon atom bonded to the NH₂-group is found downfield at 151.37 ppm. The FTIR spectrum shows the aromatic C-H bend regions at 727 cm⁻¹ and 927 cm⁻¹. The band at 1251 cm⁻¹ indicates the C=N stretch. The ketone C=O stretch band is at 1619 cm⁻¹, and the peak for the aromatic C=C stretches are at 1482 cm⁻¹. The presence of the two distinct peaks at 3347 cm⁻¹ and 3470 cm⁻¹

indicates the presence of the two N-H stretches forming part of the amine functional group.

Due to the starting material (**116**) being very expensive and the yield being meagre (19 % in **entry 14** of **Table 8.5.1.1**), as well as the fact that the cyclisation step continued to be problematic, we once again shifted focus in a final attempt to further simplify the scaffold to afford a synthetically accessible system.

4.3.5. Scaffold C5

Scaffold C5 skips the problematic cyclisation step entirely, and only focuses on the functionalisation of the NH₂-group of **87**. **Scheme 4.19** represents the synthetic route to scaffold C5. The lithium-halogen exchange and substitution reaction were discussed in section 4.4.1.1, forming **87**, which was now functionalised via an alkylation reaction to target **C5.1-C5.13**. As the scaffold now differed significantly from those proposed initially from the *in silico* studies, we elected to simply try functionalise the aniline amine through a series of amide couplings simply using carboxylic acids available in-house.



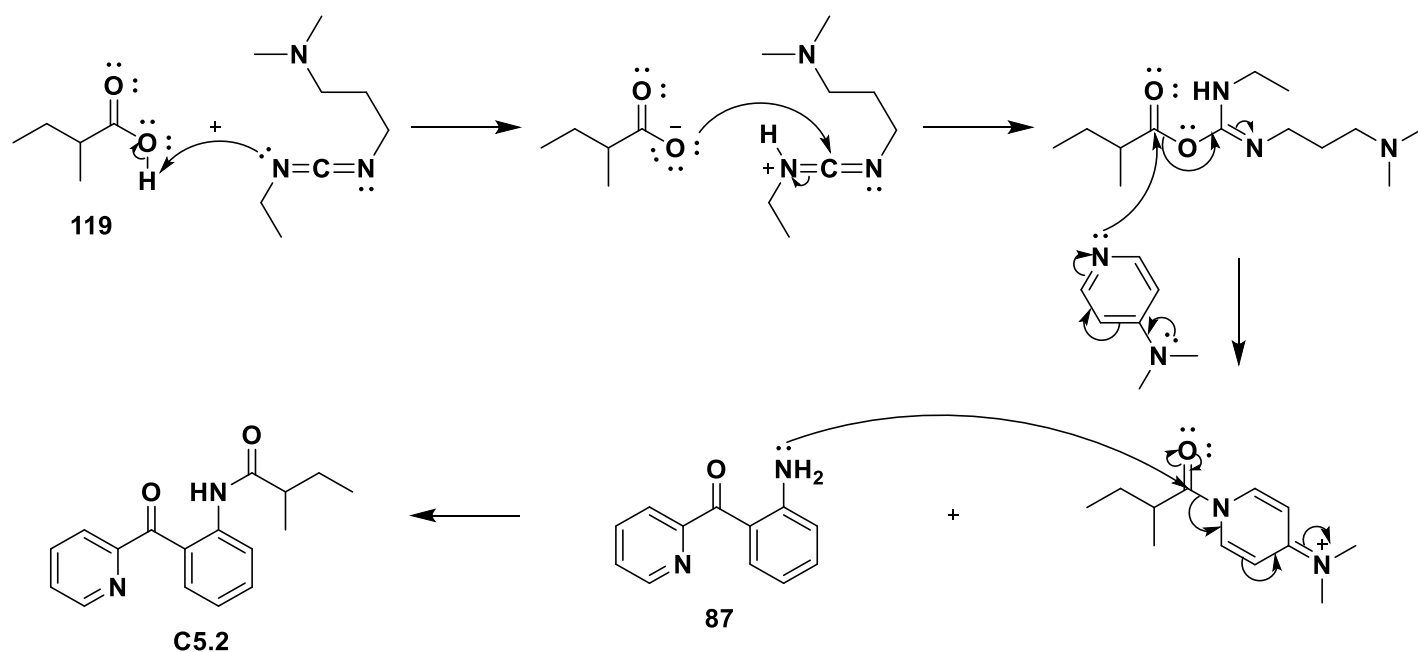
Scheme 4.19: Proposed synthesis of scaffold C5.

4.3.5.1. Synthesis of compounds C5.1 - C5.13

The alkylation reaction for scaffold C5 involved an adjusted Steglich-type esterification reaction which is mechanistically explained in **Scheme 4.20**, which illustrates the use of an amino group instead of an alcohol group as the electron donor group to incorporate the alkyl group [108].

Scheme 4.20 demonstrates that EDC-HCl acts as a base, picking up the H-atom of the carboxylic acid (**119**), leaving the O-atom negatively charged. The negatively charged O-atom condenses with the EDC molecule's

C-atom, with one pair of π -electrons neutralising the positively charged N-atom. DMAP's lone pair on the tertiary amine causes a delocalisation of electrons leading to the secondary amine's N-atom attacking the carbonyl carbon of the EDC coupled molecule, resulting in the C-O bond breaking and forming a new C-O bond. As a result, the ether bond breaks, and EDC gets kicked off. The nucleophilic N-atom on the amine molecule (**87**) attacks the carbonyl carbon of the DMAP coupled compound, resulting in DMAP being kicked off as a neutral molecule. The positively charged N-atom loses a proton, which is picked up by EDC, forming the desired product (**C5.2**).



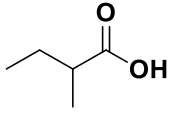
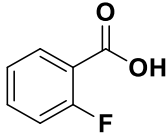
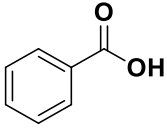
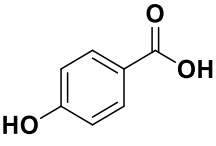
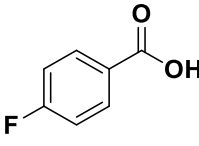
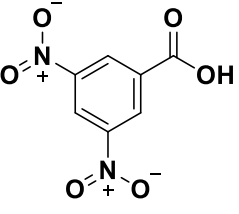
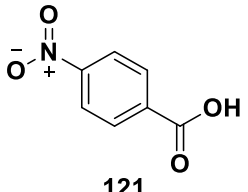
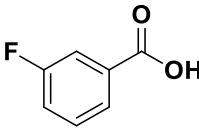
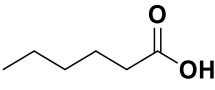
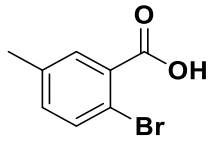
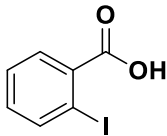
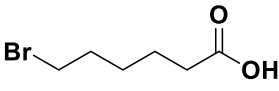
Scheme 4.20: Mechanism for the adjusted Steglich-type esterification reaction [108].

The carboxylic acids (**119-130**) listed in **Table 4.10** were added to a stirring solution of EDC-HCl (2.0 eq.) and left to stir at 0 °C for 1 hour 30 min, to form the negatively charged ester functional group. The amine was added to a stirring solution of DMAP (1.5 eq.) and left to stir until all the amine had dissolved. The EDC-HCl mixture was then added to the DMAP mixture and left to stir for 5 min before being allowed to warm to room temperature followed by stirring overnight.

The formation of **C5.1** was verified through the analysis of the ^1H NMR spectrum. The H-NMR spectrum indicated the presence of the NH group at 11.22 ppm as a broad singlet integrating for a single hydrogen atom. The methyl groups are found at 1.26 ppm (as a doublet) and 0.96 ppm (as a triplet peak) which both integrate for three hydrogen atoms. A multiplet peak integrating for a single hydrogen atom indicates the newly added CH group found at 2.40 ppm, and the two multiplets (at 1.87-1.71 ppm and 1.56 ppm), both integrate for one H-atom that each corresponds to the newly added CH_2 group. The analysis of the ^{13}C NMR spectrum supports the presence of two carbonyl groups at 197.36 ppm and 175.87 ppm and the methyl

groups are found at 17.32 ppm and 11.87 ppm.

Table 4.10: Carboxylic acid used in the Steglich-type esterification reaction.

Carboxylic acid	Yield	Carboxylic acid	Yield	Carboxylic acid	Yield
 119	22	 123	-	 127	-
 120	-	 124	-	 128	-
 121	-	 125	-	 129	-
 122	-	 126	-	 130	-

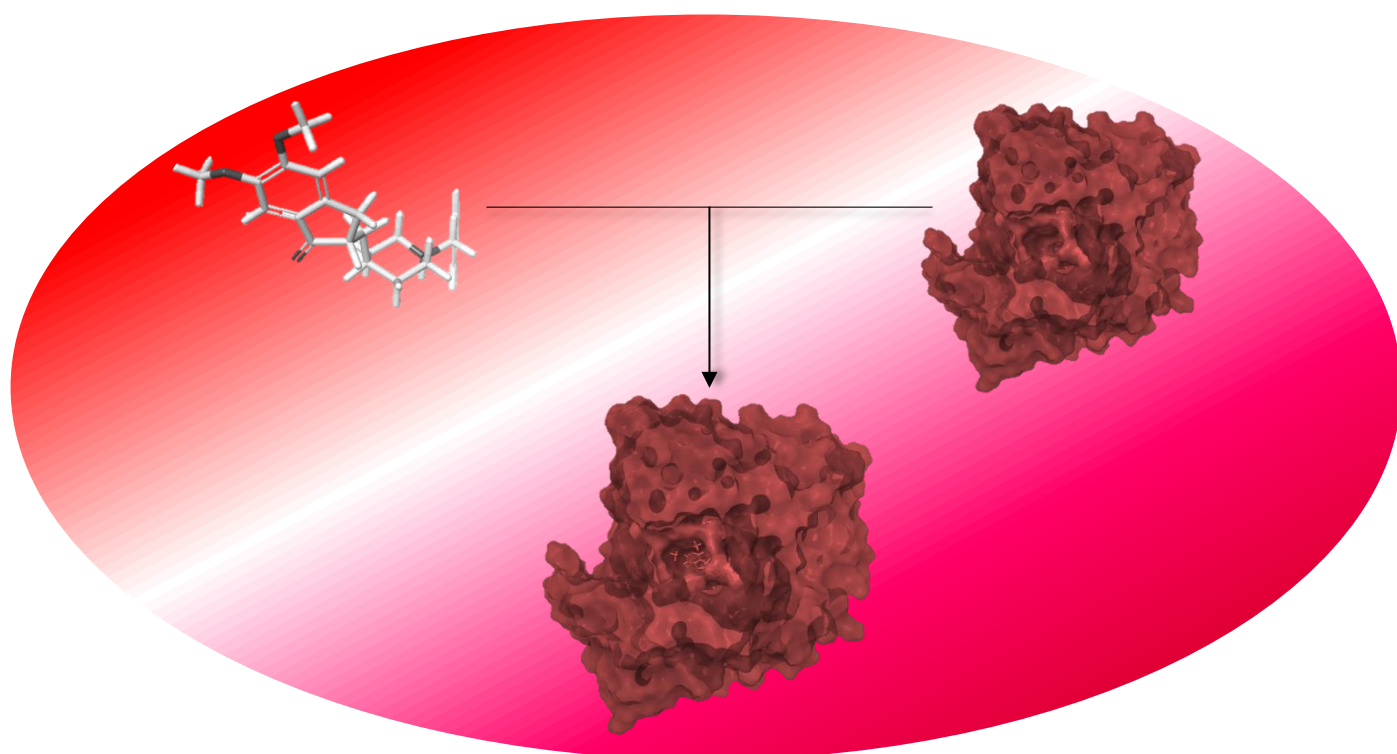
Disappointingly, the benzene containing carboxylic acids were not successful following this method. It is hypothesised that the benzene rings may be too bulky inhibiting easy approach and reaction of the acid and the amine.

4.4. Conclusion

Due to the synthetic challenges experienced we were unable to access scaffolds A and B and as such elected to target scaffold C. Unfortunately, in the case of scaffold C, several synthetic issues prevented the successful preparation of the initially proposed scaffold. We then elected to modify this scaffold, however after several iterations we ultimately elected to abandon these scaffolds as targets. As such, we elected to return to the computational drawing board so to speak to identify a new scaffold with potential to act as AChEIs.

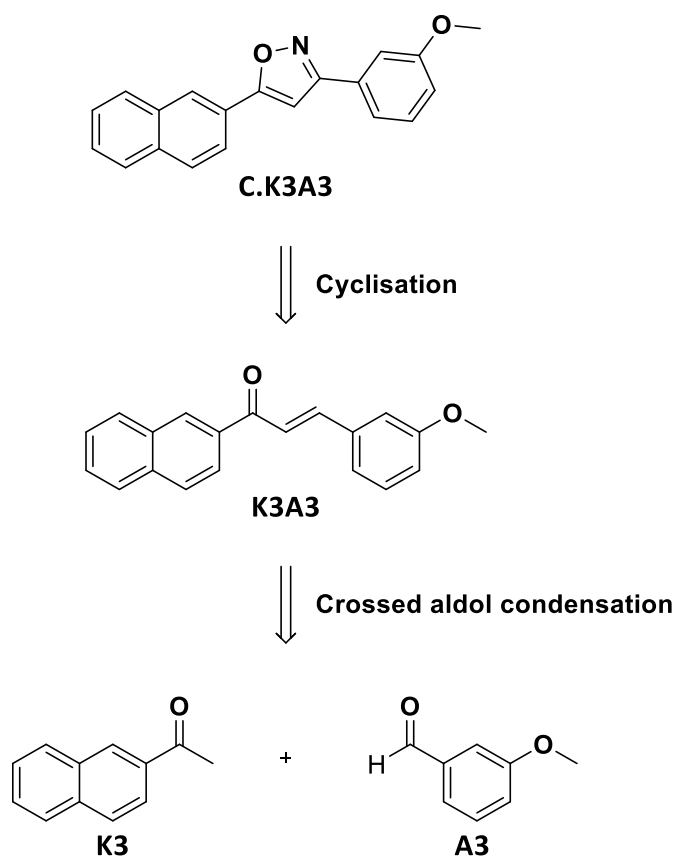
Chapter 5

Computational Results - Schrödinger



5.1. Introduction

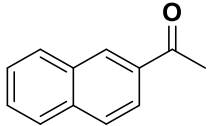
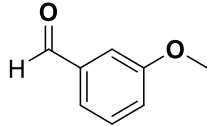
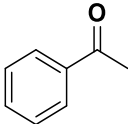
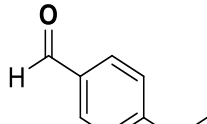
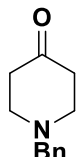
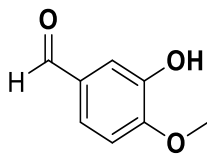
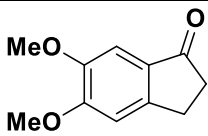
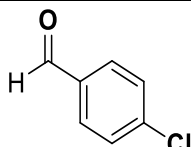
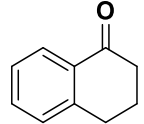
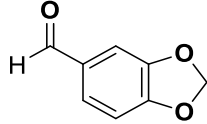
Due to the synthetic challenges associated with the preparation of scaffolds A, B and C we envisaged a new scaffold D containing an isoxazole core with aromatic pendants on the carbons adjacent to the oxygen and nitrogen atoms. The preparation of the scaffold was envisaged through the cyclisation of α,β -unsaturated ketones, which themselves could be prepared by crossed-aldol condensations (**Scheme 5.1**). Although we had previously failed with the cyclisation to form the isoxazole ring (scaffolds A and B) we suspected that the stabilised enol at the β -position was the root cause of this. In the case in hand the α,β -unsaturated ketones were hypothesised to act as good Michael-type acceptors and as such were more likely to cyclise. We anticipated that both the α,β -unsaturated ketones and the related isoxazoles would be potential AChEIs and as such elected to screen both of these cores computationally.



Scheme 5.1: Planned synthesis of cyclised combinations of ketones and aldehydes (e.g., **K3A3**) for scaffold D.

Table 5.1 indicates the ketones and aldehydes initially identified (based on chemical intuition) for the formation of the α,β -unsaturated ketone library (**K_A_**) and the isoxazole library (**C.K_A_**).

Table 5.1: The ketones and aldehyde groups used in the synthesis of the α,β -unsaturated ketones of scaffold D.

Ketone		Aldehyde	
K3		A3	
K4		A4	
K6		A5	
K7		A7	
K8		A8	

5.2. Molecular docking results and discussion

This chapter's computational analysis made use of the same conditions as the previous computational chapter (Chapter 3 Computational analysis – Schrödinger and SwissADME). The molecular docking scores and the structures of the targeted ligands can be seen in **Table 5.2**. The ligands labelled with a **C.K_A_** are the isoxazoles forms of the synthetic precursors and the α,β -unsaturated ketones are labelled as **K_A_**. Initial analysis highlighted that the best ligands in this study are those associated with ketone (**K6**), highlighted in green. The hope was that these ligands would produce good Qikprop data and then be successfully synthesised.

Table 5.2: Docking score of α,β -unsaturated ketones (**K_A_**) and their isoxazole forms (**C.K_A_**) as part of scaffold D.

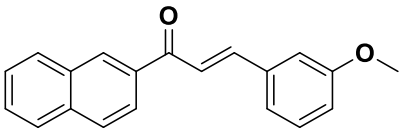
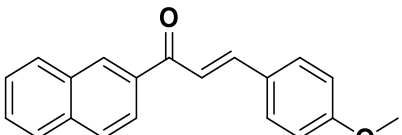
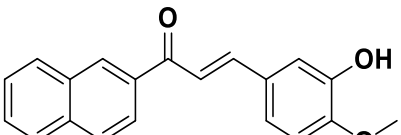
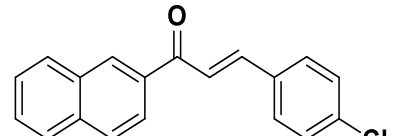
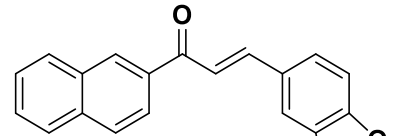
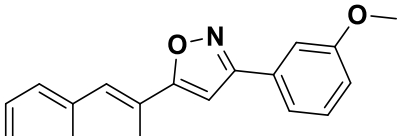
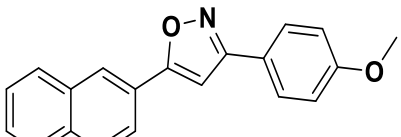
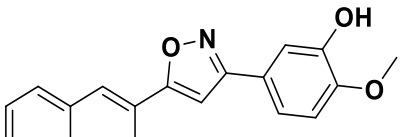
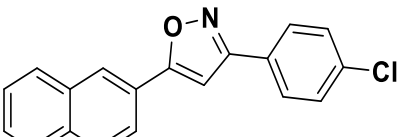
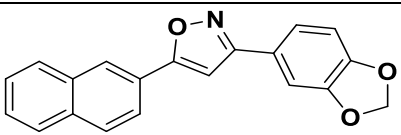
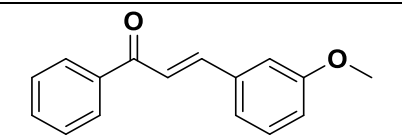
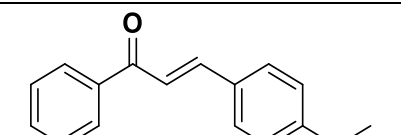
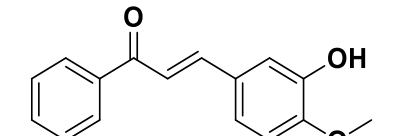
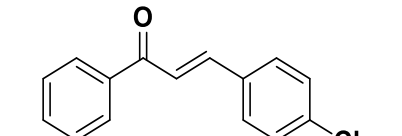
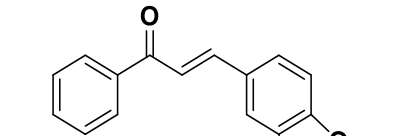
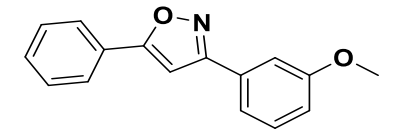
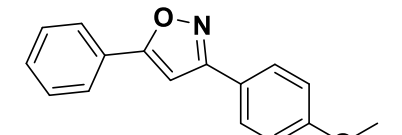
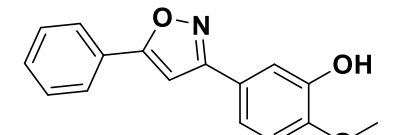
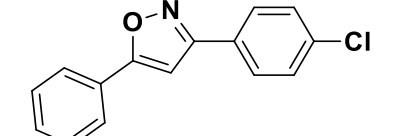
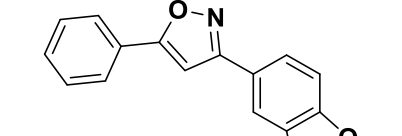
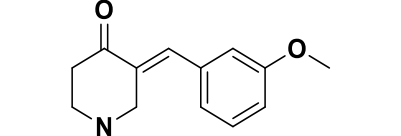
 K3A3 -8.058	 K3A4 -7.395	 K3A5 -9.519
 K3A7 -8.721	 K3A8 -8.232	 C.K3A3 -8.023
 C.K3A4 -8.312	 C.K3A5 -9.925	 C.K3A7 -7.510
 C.K3A8 -8.450	 K4A3 -7.181	 K4A4 -7.010
 K4A5 -8.551	 K4A7 -8.431	 K4A8 -8.684
 C.K4A3 -7.689	 C.K4A4 -7.753	 C.K4A5 -9.065
 C.K4A7 -7.147	 C.K4A8 -8.450	 K6A3 -11.942

Table 5.2: Docking score of α,β -unsaturated ketones (**K_A_**) and their isoxazole forms (**C.K_A_**) as part of scaffold D – continued.

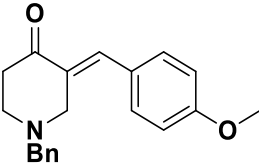
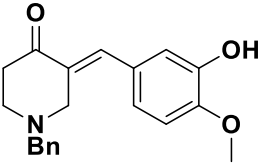
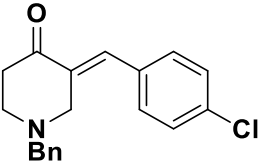
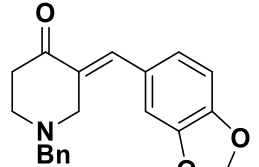
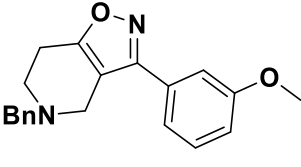
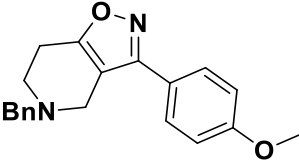
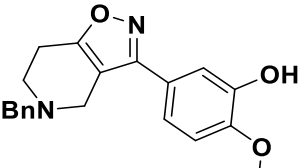
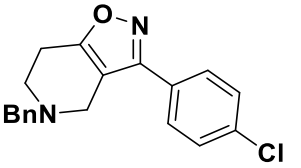
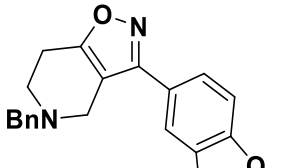
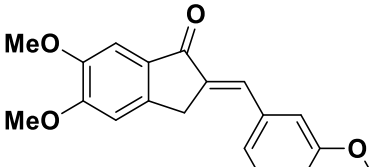
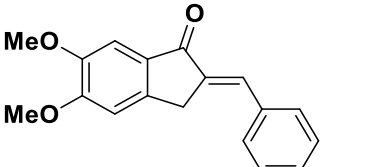
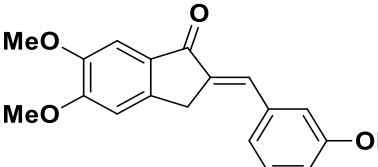
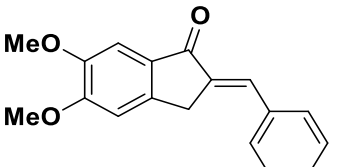
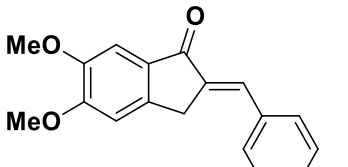
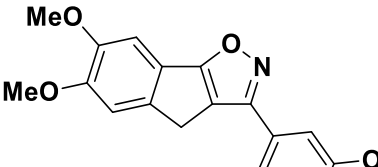
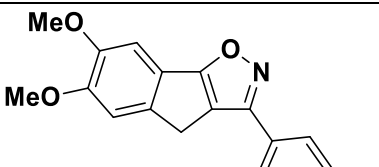
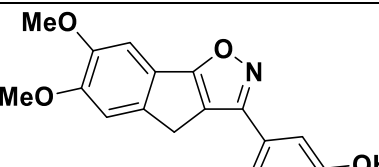
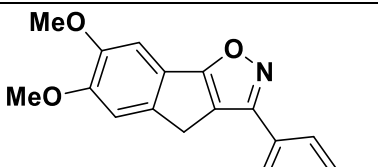
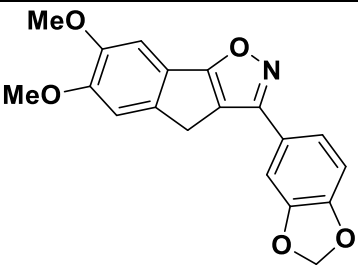
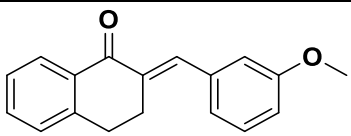
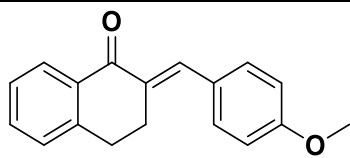
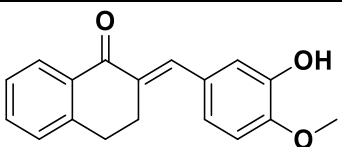
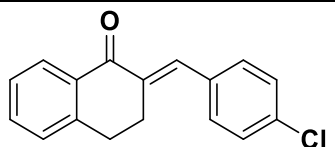
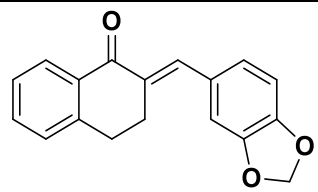
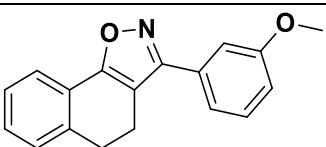
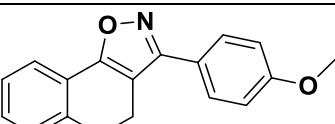
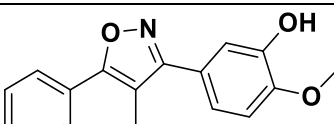
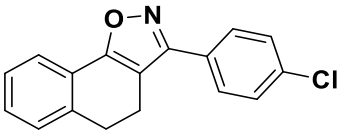
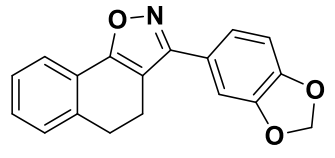
 K6A4 -12.199	 K6A5 -11.686	 K6A7 -11.762
 K6A8 -13.188	 C.K6A3 -13.073	 C.K6A4 -13.332
 C.K6A5 -13.323	 C.K6A7 -11.989	 C.K6A8 -12.587
 K7A3 -8.244	 K7A4 -8.831	 K7A5 -8.646
 K7A7 -8.333	 K7A8 -8.432	 C.K7A3 -9.057
 C.K7A4 -7.600	 C.K7A5 -9.028	 C.K7A7 -8.442

Table 5.2: Docking score of α,β -unsaturated ketones (**K_A_**) and their isoxazole forms (**C.K_A_**) as part of scaffold D – continued.

 C.K7A8 -6.481	 K8A3 -8.697	 K8A4 -8.386
 K8A5 -8.907	 K8A7 -8.444	 K8A8 -8.610
 C.K8A3 -7.868	 C.K8A4 -7.514	 C.K8A5 -9.252
 C.K8A7 -7.217	 C.K8A8 -8.819	

The Qikprop results for scaffold D can be seen in **Table 5.3** and in both **Graph 5.1** and **Graph 5.2**. The docking scores are represented graphically by the light blue data sets in the two graphs. As in chapter 3 we again selected -13.000 as the docking score cut-off for acceptable ligands (represented by a blue dashed lines).

Table 5.3: Docking score and Qikprop data of the conformations of the ligands in scaffold D.

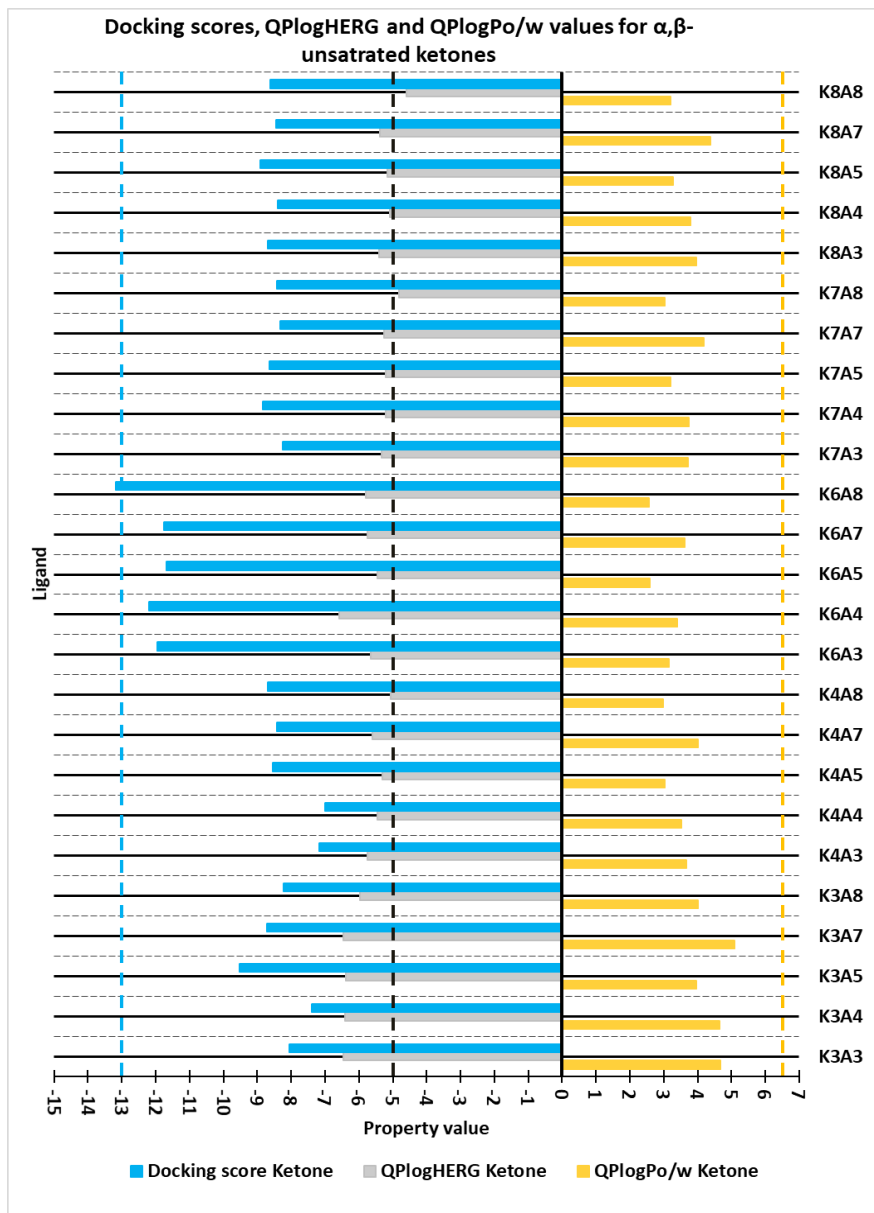
Title	Docking score	MW	QPlogPo/w	QPlogBB	QPlogHERG	H-donor	H-acceptor	TPSA
Limit	-13.000	500.000	6.500	(-3 – 1.2)	-5.000	3	8	76
C.K3A3	-8.023	301.344	4.951	0.113	-6.513	0.0	2.3	32.99
C.K3A4	-8.312	301.344	4.943	0.063	-6.534	0.0	2.3	34.67
C.K3A5	-9.925	317.343	4.316	-0.393	-6.329	1.0	3.0	54.44
C.K3A7	-7.510	305.763	5.580	0.264	-6.652	0.0	1.5	26.41
C.K3A8	-8.450	315.328	4.332	0.166	-6.076	0.0	3.0	44.32

Table 5.3: Docking score and Qikprop data of the conformations of the ligands in scaffold D- continued.

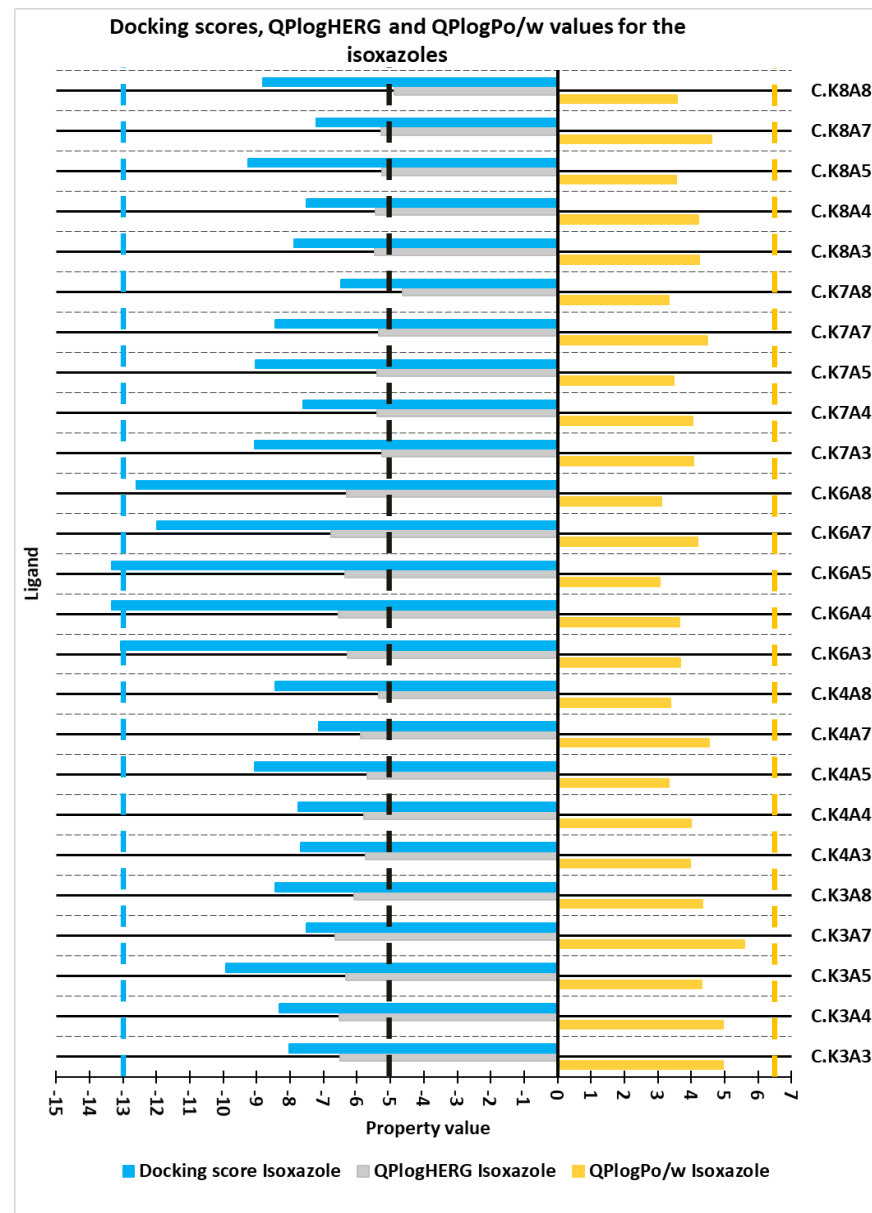
Title	Docking score	MW	QPlogPo/w	QplogBB	QPlogHERG	H-donor	H-acceptor	TPSA
Limit	-13.000	500.000	6.500	(-3 – 1.2)	-5.000	3	8	76
C.K4A3	-7.689	251.284	3.966	0.130	-5.736	0.0	2.3	33.34
C.K4A4	-7.753	251.284	3.981	0.135	-5.786	0.0	2.3	32.81
C.K4A5	-9.065	267.284	3.316	-0.402	-5.681	1.0	3.0	54.27
C.K4A7	-7.147	255.703	4.538	0.330	-5.899	0.0	1.5	25.83
C.K4A8	-8.450	265.268	3.373	0.190	-5.355	0.0	3.0	44.39
C.K6A3	-13.073	320.390	3.662	0.308	-6.273	0.0	4.3	39.41
C.K6A4	-13.332	320.390	3.643	0.269	-6.555	0.0	4.3	40.06
C.K6A5	-13.323	336.390	3.061	-0.272	-6.346	1.0	5.0	62.66
C.K6A7	-11.989	324.809	4.190	0.510	-6.779	0.0	3.5	31.65
C.K6A8	-12.587	334.374	3.117	0.368	-6.306	0.0	5.0	50.41
C.K7A3	-9.057	323.348	4.064	-0.106	-5.254	0.0	3.8	50.10
C.K7A4	-7.600	323.348	4.039	-0.123	-5.408	0.0	3.8	50.86
C.K7A5	-9.028	339.347	3.472	-0.743	-5.391	1.0	4.5	72.57
C.K7A7	-8.442	327.766	4.476	0.135	-5.354	0.0	3.0	42.24
C.K7A8	-6.481	337.331	3.321	0.028	-4.638	0.0	4.5	60.44
C.K8A3	-7.868	277.322	4.234	0.072	-5.458	0.0	2.3	35.04
C.K8A4	-7.514	277.322	4.212	0.078	-5.456	0.0	2.3	34.69
C.K8A5	-9.252	293.321	3.552	-0.398	-5.251	1.0	3.0	54.47
C.K8A7	-7.217	281.741	4.602	0.352	-5.269	0.0	1.5	25.60
C.K8A8	-8.819	291.306	3.571	0.180	-4.873	0.0	3.0	44.80
K3A3	-8.058	288.345	4.672	-0.174	-6.471	0.0	2.8	35.07
K3A4	-7.395	288.345	4.638	-0.175	-6.416	0.0	2.8	35.14
K3A5	-9.519	304.345	3.965	-0.810	-6.387	1.0	3.5	57.53
K3A7	-8.721	292.764	5.093	0.067	-6.462	0.0	2.0	26.71
K3A8	-8.232	302.329	4.014	-0.096	-5.977	0.0	3.5	45.89
K4A3	-7.181	238.285	3.663	-0.161	-5.737	0.0	2.8	35.51
K4A4	-7.010	238.285	3.526	-0.198	-5.457	0.0	2.8	36.20
K4A5	-8.551	254.285	3.023	-0.708	-5.310	1.0	3.5	58.18
K4A7	-8.431	242.704	4.005	0.041	-5.590	0.0	2.0	27.72
K4A8	-8.684	252.269	2.976	-0.122	-5.058	0.0	3.5	47.02
K6A3	-11.942	307.391	3.160	0.224	-5.660	0.0	4.8	39.91
K6A4	-12.199	307.391	3.391	0.154	-6.586	0.0	4.8	41.56
K6A5	-11.686	323.391	2.600	-0.318	-5.448	1.0	5.5	63.72
K6A7	-11.762	311.810	3.611	0.460	-5.744	0.0	4.0	33.51
K6A8	-13.188	321.375	2.572	0.271	-5.797	0.0	5.5	53.11
K7A3	-8.244	310.349	3.725	-0.240	-5.324	0.0	4.3	53.25
K7A4	-8.831	310.349	3.746	-0.229	-5.204	0.0	4.3	51.96
K7A5	-8.646	326.348	3.189	-0.842	-5.211	1.0	5.0	74.04

Table 5.3: Docking score and Qikprop data of the conformations of the ligands in scaffold D- continued.

Title	Docking score	MW	QPlogPo/w	QPlogBB	QPlogHERG	H-donor	H-acceptor	TPSA
Limit	-13.000	500.000	6.500	(-3 – 1.2)	-5.000	3	8	76
K7A7	-8.333	314.768	4.192	0.005	-5.260	0.0	3.5	44.48
K7A8	-8.432	324.332	3.019	-0.150	-4.807	0.0	5.0	63.85
K8A3	-8.697	264.323	3.951	-0.020	-5.411	0.0	2.8	35.16
K8A4	-8.386	264.323	3.795	-0.012	-5.080	0.0	2.8	35.88
K8A5	-8.907	280.323	3.268	-0.544	-5.154	1.0	3.5	56.69
K8A7	-8.444	268.742	4.376	0.221	-5.381	0.0	2.0	26.91
K8A8	-8.610	278.307	3.209	0.071	-4.590	0.0	3.5	46.16



Graph 5.1: Docking score and Qikprop data, QPlogHERG and QPlogPo/w, for the α,β -unsaturated ketones forms of scaffold D.



Graph 5.2: Docking score and Qikprop data, QPlogHERG and QPlogPo/w, for the isoxazole forms of scaffold D.

5.2.1 Molecular docking of α,β -unsaturated ketone scaffolds K_A_

The orientation of the *N*-containing ring system or aromatic ring systems towards amino acids Phe330 and Tyr334 allowing for π - π and π -cation interactions are especially prevalent in the α,β -unsaturated ketones that have the best overall docking scores (see **Table 5.4**) among the α,β -unsaturated ketones. The other amino acids seen to be of some interests are His440, Trp84, Tyr121, Phe331 and the amino acid Asp72 seems to be involved in a salt bridge interaction in **K6A7** and **K6A5** while H-bonds or H-bridges are predicted with Arg289, Glh199, Tyr130, Phe288, and Phe331 (see **Table 5.4**). As expected, the functional groups of importance are the *N*-containing ring system and the benzyl group attached to it. The ligands containing a substituted phenyl ring are indicated to only be of limited importance. The α,β -unsaturated ketones with the **K6** fragment are among the ligands with the highest predicted docking scores, mostly as a result of their piperidine ring system, again highlighting its importance in the inhibition of AChE.

Table 5.4: The π - π , π -cation and hydrogen interactions between the good and poor α,β -unsaturated ketones of scaffold D.

Ligand	Docking Score	Phe 330	Tyr 334	His 440	Trp 84	Tyr 121	Phe 331	Asp 72	H ₂ O Bridge
K6A8	-13.188	π - π π -cation	π -cation						Arg289
K6A4	-12.199	π - π π -cation	π -cation	π - π					Arg289
K6A3	-11.942	π - π π -cation			2 x π -cation	π - π	π - π		
K6A7	-11.762	π -cation	π -cation					Salt bridge	
K6A5	-11.686	π -cation	π -cation					Salt bridge	H-bond Glh199, Tyr130
K3A8	-8.232	2x π - π			2x π - π		π - π		H-bridge Phe288, Phe331
K3A3	-8.058				2x π - π				
K3A4	-7.395				π - π				
K4A3	-7.181	π - π		π - π					H-bridge Phe288, Phe331
K4A4	-7.010						π - π		

5.2.2 Molecular docking of isoxazole scaffolds C.K_A_

In the data tabulated in **Table 5.5** it can again be seen that the amino acids Phe330 and Tyr334 are of importance in their π -cation interactions with the positively charged *N*-containing ring systems and π - π interactions for the aromatic ring systems. The interactions that are found more frequent in the isoxazole forms when compared to the α,β -unsaturated ketones forms are the H-bonds to the different amino acids, Arg289 (**C.K6A4**, **C.K6A8**), Ser122 (**C.K6A5**) and Gly118 (**C.K6A3**), while for **C.K6A7** a salt bridge with Arg289 is observed. The other amino acids that are of importance in the isoxazole forms are His440, Trp84, Trp279 and Phe331. The ligand, **C.K8A7** displays no immediate relatable interactions, but upon closer inspection it was predicted that the ligand displays very weak H-bond interactions across its surface, but more interestingly the presence of two aromatic H-bonds were observed to Asp72 and Arg289. The computational data implies that the isoxazole functional group may result in extra π - π interactions not present in the corresponding α,β -unsaturated ketones forms.

Table 5.5: The π - π , π -cation and hydrogen interactions between the good and poor isoxazole forms of scaffold D.

Ligand	Docking Score	Phe 330	Tyr 334	His 440	Trp 84	Trp 279	Phe 331	H ₂ O Bridge
K6A4	-13.332	π -cation	π - π π -cation				π -cation	H-bonded: Arg289
K6A5	-13.323	π -cation	π -cation				π -cation	H-bonded: Ser122
K6A3	-13.073	π - π	π -cation	π - π	3X π - π			H-bonded: Gly118
K6A8	-12.587	π -cation	π -cation	π - π				H-bonded: Arg289
K6A7	-11.989	π -cation	π -cation		π - π			Salt bridge Arg289
K8A4	-7.514		π - π					

Table 5.5: The π - π , π -cation and hydrogen interactions between the good and poor isoxazole forms of scaffold D – continued.

Ligand	Docking Score	Phe 330	Tyr 334	His 440	Trp 84	Trp 279	Phe 331	H ₂ O Bridge
K3A7	-7.510	2X π - π		π - π			π - π	
K8A7	-7.217							Aromatic H-bonded to: Asp72, Arg289
K4A7	-7.147	π - π		π - π				
K7A8	-6.481					π - π		

The best-predicted ligands in the entire data set are shown to be **C.K6A3**, **C.K6A4**, **C.K6A5**, and **K6A8**. It is predicted that 60 % of scaffold D's isoxazole ligands exhibited higher docking scores, which indicate that they will likely have a higher activity for inhibiting AChE than their α,β -unsaturated ketones forms. The ligands that contradict this trend, include **K3A3**, **K3A7**, **K4A7**, **K4A8**, **K6A8**, **K7A4**, **K7A8**, **K8A3**, **K8A4**, and **K8A7**. The interactions involved in causing this trend are highlighted in **Table 5.6**.

In the cases where the α,β -unsaturated ketones scaffold performed better than the analogous isoxazole scaffold the interaction length of the π - π bonds are much shorter, see **K3A3**, **K3A7** and **K8A4**. In addition, **K3A7** and **K8A4** indicate an additional H-bond interaction to their carbonyl O-atom. This trend is also observed in **K4A7** where the number of π - π interactions are less than those present in **C.K4A7**.

C.K4A8 has a H-bond to one of its dioxole oxygen atom while **K4A8** has a H-bond to its carbonyl oxygen. The difference in their docking scores are likely due to the different number of π - π interactions to the benzo[*d*][1,3]dioxole ring of **K4A8** and the phenyl ring of **C.K4A8**. A similar trend is observed between **K6A8** and **C.K6A8**. The α,β -unsaturated ketones form of **K7A4** and **K7A8** indicates the presence of other interactions not present in their isoxazole forms, leading to the higher docking scores of their α,β -unsaturated ketones forms.

From **Table 5.6** it is expected that **C.K8A3** would have a higher docking score due to π - π interactions to its six-membered ring and the presence of shorter H-bonds compared to **K8A3**. Therefore it can be concluded that the undisplayed weak H-bond interactions to the α,β -unsaturated ketones are holding it in a more favourable position leading to the α,β -unsaturated ketones form's higher docking score.

The higher docking score of **K8A7**, is due to the H-bond interaction with the carbonyl O-atom, but also the π - π interaction to the phenyl ring. **C.K8A7** does not indicate any interactions, and it can, therefore, be concluded that its docking score is as a result of the weak H-bonds as mentioned above.

In conclusion, it seems that for these α,β -unsaturated ketones, the critical interaction is the H-bond to their carbonyl carbons and some additional π - π interactions which lead to a higher docking score. These observations can be used in the development of future ligands within the group.

The 4 ligands with the best docking scores (**K6A8**, **C.K6A3**, **C.K6A4**, and **C.K6A5**) are compared in **Graph 5.3** to that of donepezil (**25**), and the 5 best ligands from the previous computational chapter (Chapter 3). The graph indicates that all the docking scores surpass the lower limit of -13.000 and that only **C1.4.a** surpasses the upper limit of QPlogPo/w. All the ligands fall below the lower limit of QPlogHERG. Overall scaffold D's best performing ligands binding scores are approximately 1 log unit less than the best ligands identified in chapter 3.

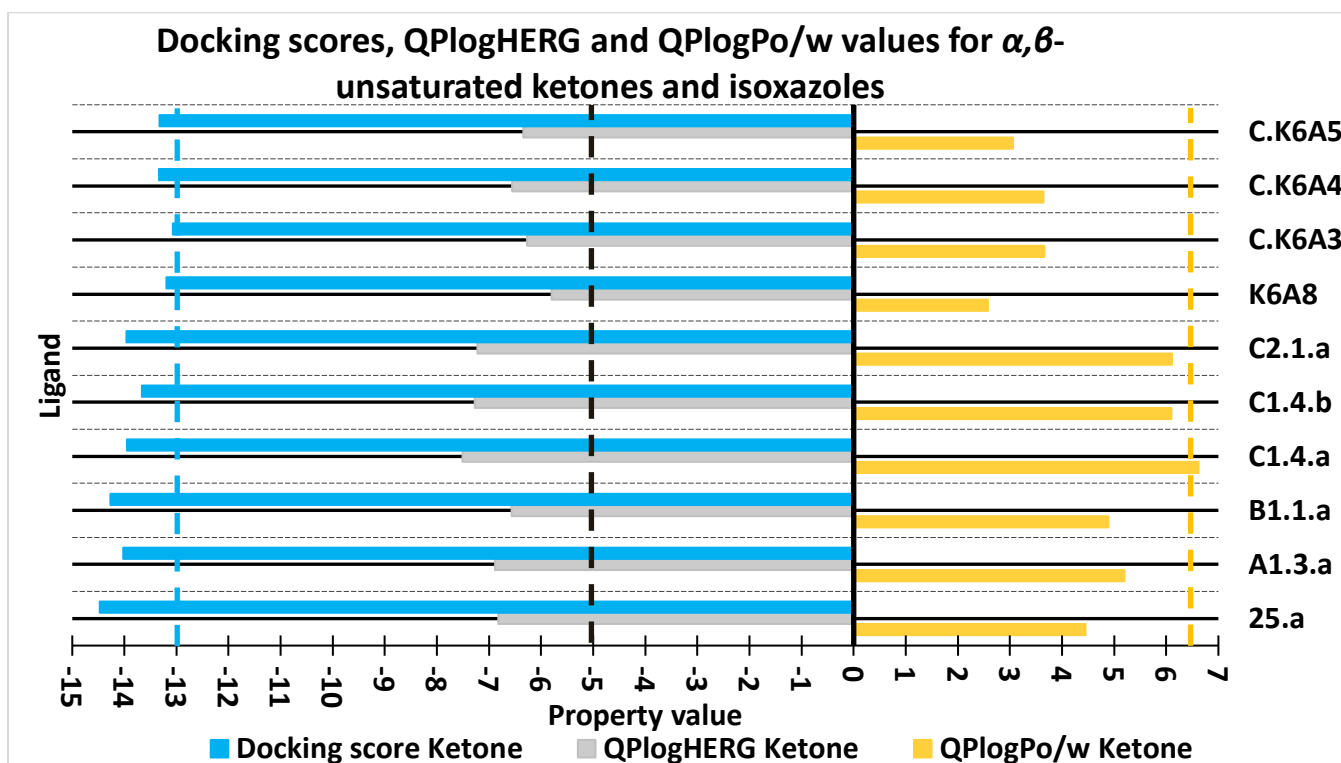
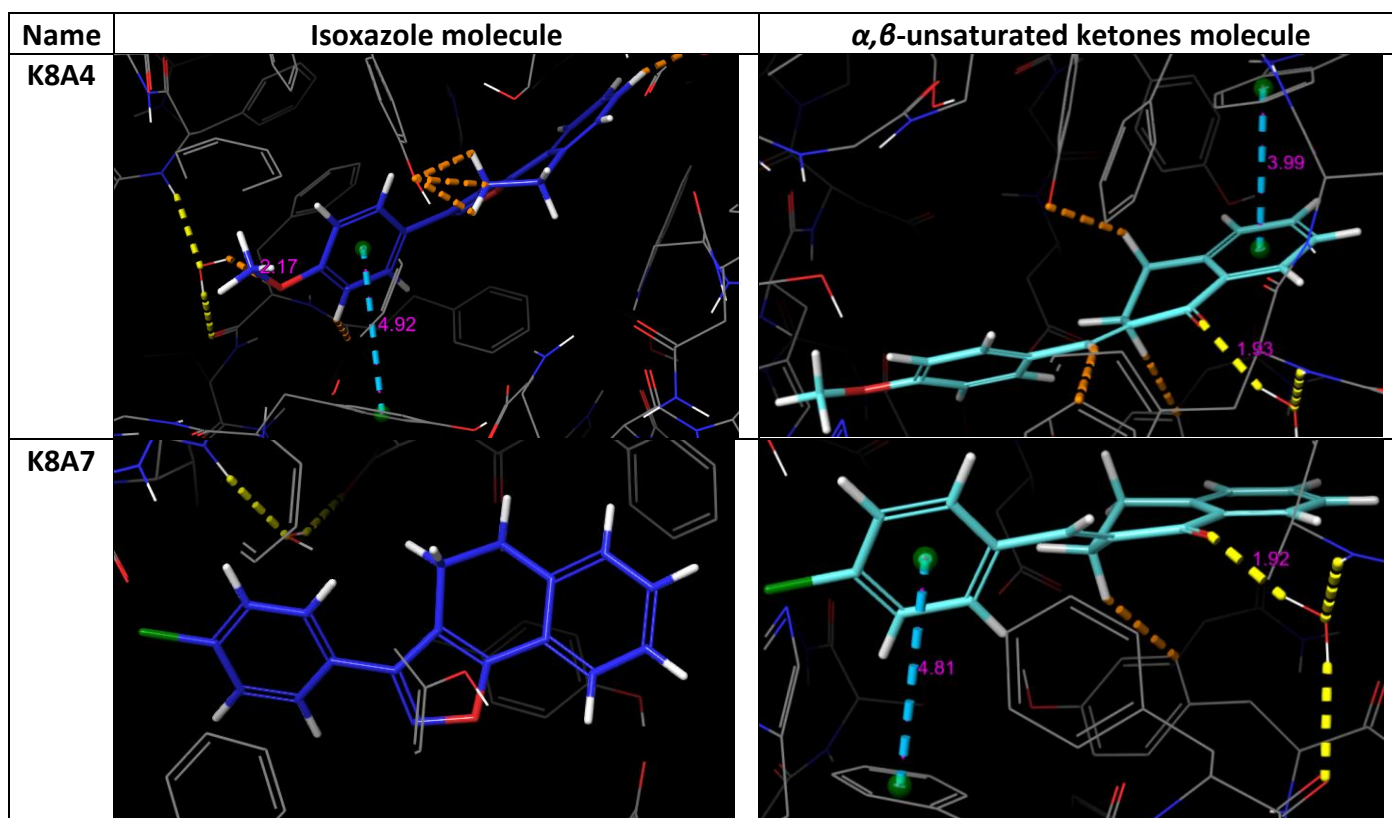
Table 5.6: Ligands where the α,β -unsaturated ketones had a higher docking score compared to their isoxazole forms.

Name	Isoxazole molecule	α,β -unsaturated ketones molecule
K3A3		
K3A7		
K4A7		
K4A8		

Table 5.6: Ligands where the α,β -unsaturated ketones had a higher docking score compared to their isoxazole forms – continued.

Name	Isoxazole molecule	α,β -unsaturated ketones molecule
K6A8 C.K6A8		
K7A4		
K7A8		
K8A3		

Table 5.6: Ligands where the α,β -unsaturated ketones had a higher docking score compared to their isoxazole forms – continued.

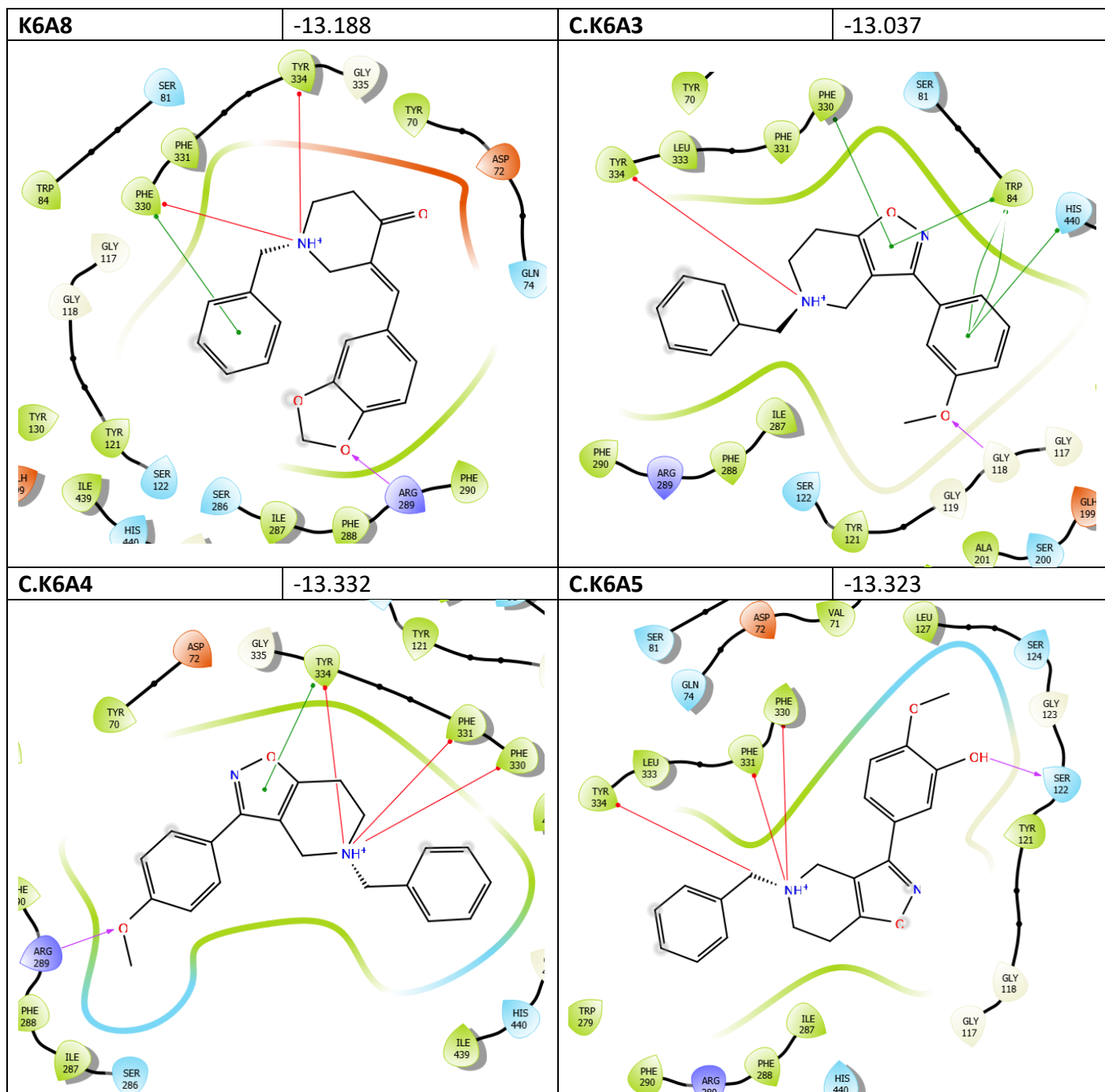


Graph 5.3: Docking score and Qikprop data, QPlogHERG and QPlogPo/w, for the best ligands in the two data sets.

In **Table 5.7**, the interactions involved in the four best ligands of scaffold D are compared. A conclusion can be drawn to the required functional groups that have to be present in a ligand for future work for the generation of good AChEIs. The positively charged *N*-atom, considered necessary in chapter 3, is again among all four of this chapter's best docking scores. Therefore, a *N*-containing ring system must be considered when planning a library for AChEIs. A π - π interaction with an isoxazole group in **C.K6A4** compared to **C.K6A5** also proves to be of some importance. The lack of the two π -cation interactions in **C.K6A3** compared to **C.K6A4** and **C.K6A5** could explain why **C.K6A3** has a high docking score. The importance of the benzyl π - π interactions could be considered as necessary when examining **K6A8** and **C.K6A4** since the only difference between their interactions is a π -cation interaction and to which type of ring the π - π interaction is formed.

Compared to the other three ligands in the table, **C.K6A3** has 5 π - π interactions, but still, it has the lowest docking score of the four ligands. Therefore, the purple arrow indicating a H-bond is of great importance. Since the H-bond is present in all four ligands, the conclusion can be made that a H-donor or acceptor is necessary in the structure of an AChEI. According to the previous chapter, the docking score will be significantly improved if this H-bond forms a bridged H-bond interaction like in donepezil (**25**).

In conclusion, the functional groups that should be considered when designing AChEIs from the results of these four ligands and the best ligands from the previous computational chapter suggest that i) benzyl rings or phenyl rings or other aromatic rings involved in π - π interactions or π -cation interactions should be considered which could potentially interact with Phe330, Trp84, Tyr334 and even His440, ii) a six-membered *N*-containing ring system which can be involved in π -cation interactions when positively charged is critical and binds to targeted amino acids like Phe330, Phe331, and Tyr334, and iii) the presence of H-bond acceptors such as *O*-atoms in carbonyl groups, isoxazoles or indazoles which interacts with Arg289, Gly118 or Ser122.

Table 5.7: Docking score and interactions of the best 4 ligands in scaffold D.

5.3. Qikprop analysis, results, and discussion

Table 5.2 indicates some Qikprop results, which were analysed to determine if the ligands from scaffold D follow Lipinski's rule of 5 and if they can be classified as drug-like. **Table 5.3**, indicates that the MW of all the ligands fall under 500.00 g/mol and QPlogBB falls between -3.0 and 1.2. These two parameters being met indicate that these drugs can be considered drug-like, and they are predicted to be able to cross the BBB if taken orally.

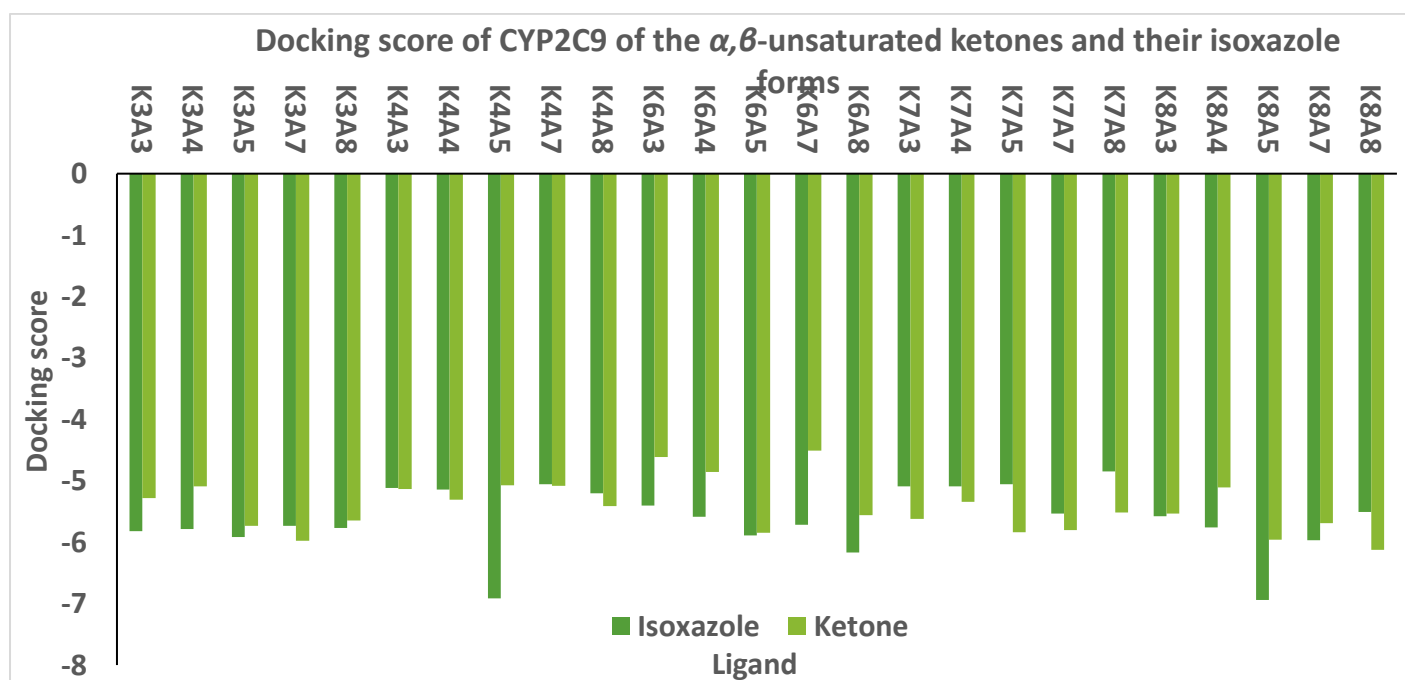
The partition coefficient Qikprop property, QPlogPo/w, can be seen in **Table 5.3** and in **Graphs 5.1** and **5.2**, which represents the upper limit as an orange dashed line. The graph indicates that all the ligands as orange data sets, all of which fall under the upper limit and are therefore considered to be drug-like.

Table 5.2 further indicates that only **C.K7A8**, **C.K8A8**, **K7A8**, and **K8A8** fall below the -5.000 lower limit of the QPlogHERG property. They are the only ligands in the data set that are predicted to not block the K⁺ channel, as seen in **Graphs 5.1** and **5.2**, which represents the QPlogHERG data graphically as the grey data sets. **Table 5.2** also indicates the H-donor, H-acceptors, and TPSA values for the data set. All the ligands fall within these designated property limits and are therefore considered drug-like.

The only rule that is broken by most of the ligands is that of the QPlogHERG rule, suggesting that the management of the compound's therapeutic dosage will be critical. Despite the hERG failure of most ligands, we felt that the entire range are arguably drug-like and have potential to be AChEIs. Critically, considering the hERG issue, one should invest in hERG screening earlier on in the developmental process rather than later in order to eliminate ligands wherein the difference in AChE inhibition and hERG inhibition is not sufficient to allow a dose-controlled use of the compounds.

5.4. Cytochrome P450 isozyme CYP2C9 inhibition

Graph 5.4 indicates the docking score of the ligands in this data set docked into the active site of the CYP2C9 enzymes. Donepezil (**25**) has a CYP2C9 docking score of -8.518 which, when compared to the data in **Graph 5.4** indicates that all the ligands are under acceptable CYP2C9 conditions.



Graph 5.4: CYP2C9 docking scores for the α,β -unsaturated ketone and isoxazole forms of this data set.

5.5. Conclusion

The computational results of scaffold D covered the molecular docking, Qikprop analysis and CYP2C9 inhibition of a total of fifty ligands. Of these ligands only **C.K6A3**, **C.K6A4**, **C.K6A5** and **K6A8** were considered drug-like when applying the lower docking score limit of -13.000. The Qikprop data of scaffold D indicated that all the ligands followed the MW, QPlogPo/w, QPlogBB, H-donor, H-acceptor and TPSA rules for drug-likeness. Ligands **C.K7A8**, **C.K8A8**, **K7A8** and **K8A8** were the only ligands under study that did not violate the QPlogHERG rule. From the CYP2C9 inhibition study it can be concluded that all the ligands in scaffold D would be good candidates for potential AChE inhibition as they would potentially cause less ADRs compared to that of donepezil (**25**) with a CYP2C9 inhibition of -8.518.

The ligands from scaffold D could be further functionalised in the future. These future targets could prove to be more potent than the current scaffold D and could then be more comparable to the larger ligands in scaffolds A and B.

The early QPlogHERG screening of potential future ligands would be a good start before complete synthesis as seen from the overwhelming number of QPlogHERG violations found in scaffolds A to C. The QPlogPo/w and TPSA must also be closely monitored as these rules can be more easily controlled among the Qikprop rules. Ultimately, we elected to target all the ligands in scaffold D synthetically in an attempt to have material available for future functionalisation of these targeted ligands.

Chapter 6

Synthetic analysis and discussion of α,β -unsaturated compounds



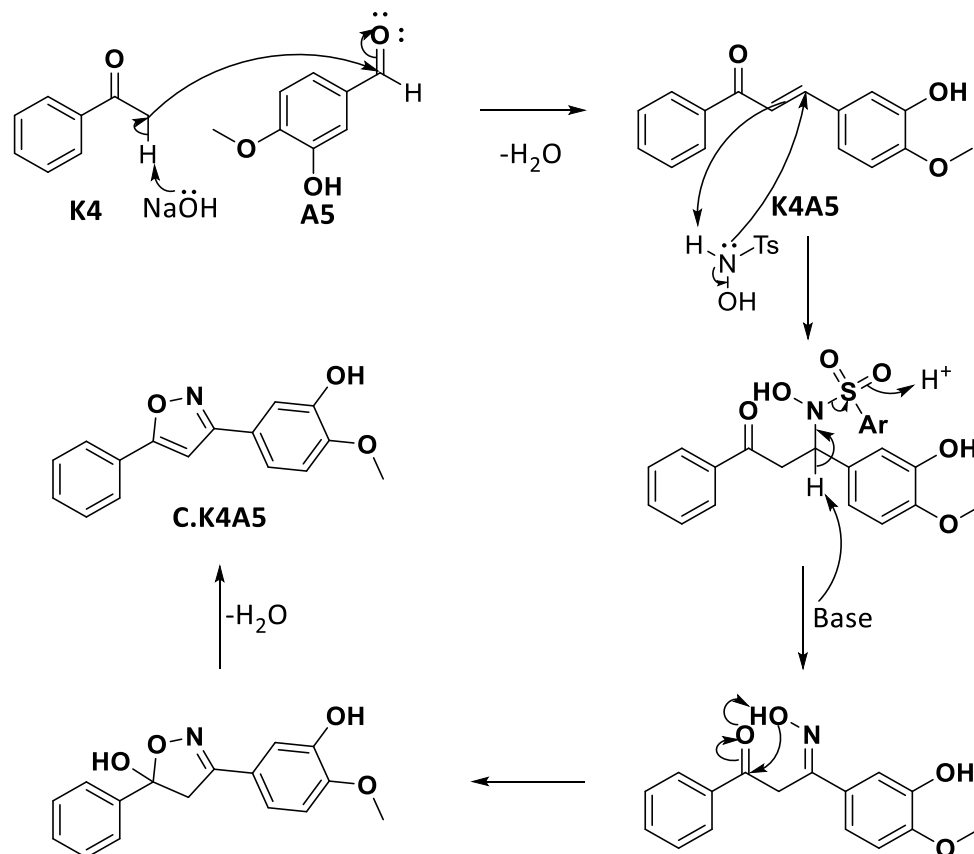
6.1. Introduction

In the previous chapter we indicated that all the scaffold D ligands would be synthesised as they have some affinity for AChE, they are classified as having good drug-likeness and structurally having the potential of being functionalised in future work within the group. The other target of this study is to determine if the isoxazole forms or the α,β -unsaturated ketone forms of the resultant synthesised ligands would provide similar results from biological studies than that predicted computationally with the limited studies conducted, discussed in Chapter 5.

6.2. Scaffold D

For the preparation of scaffold D, we identified five ketones and five aldehydes (**Table 5.1**) that could be used to generate a series of twenty five α,β -unsaturated compounds (see **Table 5.2**), formed through a crossed aldol condensation reaction. The successful crossed aldol products (**K_A_**) would then be cyclised, using TsNHOH to form their isoxazole forms (**C.K_A_**).

The mechanism for the preparation of scaffold D (exemplified by **K4A5**) can be seen in **Scheme 5.2** [109]. A general crossed aldol condensation reaction can be seen where the base (NaOH) deprotonates the ketone's (**K4**) α -carbon, allowing the negatively charged C to attack the carbonyl C-atom of the aldehyde (**A5**). The C-O bond breaks and forms an OH group, followed by dehydration to afford the α,β -unsaturated ketone (**K4A5**). In a second reaction the lone pair of electrons on TsNHOH adds to the β -position of **K4A5** (Michael type addition). The tosyl group (Ts) then gets kicked off, initiated by the deprotonation of the H-atom located alpha to the nitrogen to form an oxime group. Finally, the OH group's lone pair of electrons attacks the carbonyl carbon, which is followed by dehydration to afford the isoxazole **C.K4A5**.



Scheme 5.2: Mechanism for the planned synthesis of scaffold D [109].

6.3. Preparation of α,β -unsaturated compounds – method 1

In the first crossed aldol reaction sodium hydroxide pellets in methanol were stirred at room temperature until all the sodium hydroxide dissolved. The aldehyde was added to the solution and then left to stir at room temperature for 10 min, which can be done as the aldehyde would not react with itself, unlike the ketone. The ketone was thereafter added dropwise, while keeping the solution's temperature at 0 °C to minimise the formation of the aldol condensation reactions between two ketones. The solution was then left to stir overnight at room temperature and purified using column chromatography to yield a pure product.

The formation of the product was verified via their ^1H NMR where the alkene and aromatic peaks are identified, while in some cases an OH group can be easily identified. The ^{13}C NMR would indicate the presence of carbonyl groups in the ketone functional groups and methoxy groups where applicable. The DEPT spectrum was used to verify the identity of the carbon peaks on the ^{13}C NMR as the quaternary carbons disappear from the spectrum and the CH_2 groups have peaks going downwards. The FTIR spectrums were used to find and identify specific functional groups that was expected in the final product as the carbonyl group, alkene stretches and aromatic peaks. The MS spectrum were of great importance as the molecules

are large aromatic compounds where their peaks are all found in close proximity on their ^1H NMR spectrum and ^{13}C NMR spectrum. As an example of the classification, we included the analysis of **K4A5** while tabulating the rest of the crossed aldol reactions using method one in **Table 6.1**.

Table 6.1: Crossed aldol condensation reaction using method 1 for the synthesis of **K_A_**.

Product	Yield	Product	Yield	Product	Yield	Product	Yield	Product	Yield
K3A3	-	K4A3	-	K6A3	-	K7A3	40 %	K8A3	98 %
K3A4	-	K4A4	-	K6A4	-	K7A4	52 %	K8A4	91 %
K3A5	-	K4A5	63 %	K6A5	-	K7A5	77 %	K8A5	71 %
K3A7	-	K4A7	-	K6A7	-	K7A7	-	K8A7	93 %
K3A8	-	K4A8	-	K6A8	-	K7A8	95 %	K8A8	99 %

6.3.1. (*E*)-3-(3-hydroxy-4-methoxyphenyl)-1-phenylprop-2-en-1-one (**K4A5**)

The crossed aldol condensation reaction using 3-hydroxy-4-methoxybenzaldehyde (**A5**) and acetophenone (**K4**) was successful and gave a pure product (**K4A5**) with a 63 % yield. The formation of **K4A5** was verified through the analysis of ^1H NMR spectrum (which corresponded to literature) which indicate the presence of all the aromatic peaks including the alkene hydrogens [110]. The methoxy (CH_3) group integrates for three hydrogens and was found downfield at 3.84 ppm as a singlet. The OH group's H-atom is found downfield at 6.22 ppm as a singlet. The analysis of the ^{13}C NMR spectrum further supported the formation of **K4A5** through the single carbonyl carbon peak found at 190.65 ppm. The CH_3 group is found at 55.99 ppm while the deshielded alkene carbon is found at 149.06 ppm. The dept spectrum indicates the disappearance of five quaternary carbons which was expected. The FTIR spectrum indicates the presence of the methoxy group with a C-O stretch at 1263 cm^{-1} . The α,β -unsaturated ketone's C=O stretch band is found just over 1600 cm^{-1} , while the sp^3 C-H bonds are indicated by the range of $2750 - 3200\text{ cm}^{-1}$ which includes the OH peak that lays beneath it as a broad singlet peak. The MS spectrum indicated that the correct product did form with an $[\text{M}+\text{H}]^+$ ion at 255.118 ($\text{C}_{16}\text{H}_{15}\text{O}_3$ requires 255.102).

6.3.2. Unsuccessful reactions

Following this approach the following ketone and aldehyde combinations proved unsuccessful **K3A3**, **K3A4**, **K3A5**, **K3A7**, **K3A8**, **K4A3**, **K4A4**, **K4A7**, **K4A8**, **K6A3**, **K6A4**, **K6A5**, **K6A7**, **K6A8**, and **K7A7** [111]. We thought that the failure of these was linked to the structure of the ketones, where **K3**, **K4**, and **K6** all largely failing. As such we elected to employ a second method in the hope of getting these reactions to work [109].

6.4. Preparation of α,β -unsaturated compounds - method 2

The new method used added the ketone to a mixture of ethanol, sodium hydroxide and water. A very diluted solution of the aldehyde in ethanol was added dropwise to the mixture and then left to stir overnight instead of adding the ketone dropwise to the aldehyde.

The formation of the product was verified using the same approach as described previously. Again, as an example of the classification, we included the analysis of **K3A4** while tabulating the rest of the crossed aldol reaction using this method in **Table 6.2**.

Table 6.2: Crossed aldol condensation reaction using method 2 for the synthesis of **K_A_**.

Product	Yield	Product	Yield	Product	Yield	Product	Yield	Product	Yield
K3A3	-	K4A3	-	K6A3	-	K7A3	40 %	K8A3	98 %
K3A4	41 %	K4A4	-	K6A4	-	K7A4	52 %	K8A4	91 %
K3A5	-	K4A5	63 %	K6A5	-	K7A5	77 %	K8A5	71 %
K3A7	-	K4A7	-	K6A7	-	K7A7	39 %	K8A7	93 %
K3A8	41 %	K4A8	47 %	K6A8	-	K7A8	95 %	K8A8	99 %

6.4.1. (*E*)-3-(4-methoxyphenyl)-1-(naphthalen-2-yl)prop-2-en-1-one (**K3A4**)

Under the new conditions the combination of 2-acetonaphthone (**K3**) and 4-anisaldehyde (**A4**) was successful when making use of the second crossed aldol method and gave the pure product (**K3A4**) in a 41 % yield.

The formation of **K3A4** was verified through the analysis of its ^1H NMR spectrum which indicates the presence of all the aromatic peaks including the alkene hydrogens, while the methoxy CH_3 group's three hydrogens are found as a singlet at 3.81 ppm. The analysis of the ^{13}C NMR spectrum supported the formation of **K3A4** indicating the single carbonyl carbon peak found at 190.21 ppm. The presence of the CH_3 group is noted at 55.36 ppm. The shielded alkene is found at 144.64 ppm. The FTIR spectrum indicated the presence of the aromatic CH groups due to the presence of the C-H bend regions indicated by the sharp bands at 731 cm^{-1} and $1400 - 1600\text{ cm}^{-1}$. The aromatic C=C stretches are also found at $1450 - 1650\text{ cm}^{-1}$. The α,β -unsaturated ketone's C=O stretch is found just after 1600 cm^{-1} . The alkene C-H stretch is found within the range of $3100-3000\text{ cm}^{-1}$, which overlaps with the sp^3 C-H bond stretching peak. The MS spectrum indicates the presence of the $[\text{M}+\text{H}]^+$ mass ion at 289.140 ($\text{C}_{20}\text{H}_{17}\text{O}_2$ requires 289.123).

6.4.2. Unsuccessful reactions

After attempting method 2 in addition to method 1, the following eleven targets could not be synthesised, **K3A3**, **K3A5**, **K3A7**, **K4A3**, **K4A4**, **K4A7**, **K6A3**, **K6A4**, **K6A5**, **K6A7**, and **K6A8**. In conclusion the three ketones, **K3**, **K4** and **K6**, are considered to be very unreactive while it may also be concluded that out of all the aldehydes used, **A4**, **A5** and **A8** are the most active. The lower yields could be due to the ketone reacting with itself and therefore lowering the number of ketone molecules available in solution to undergo a crossed aldol condensation reaction in forming the desired product.

6.5. Synthesis of *N*-hydroxy-4-methylbenzenesulfonamide (**131**)

The next step in the synthesis of scaffold D, the cyclisation step, requiring the use of TsNHOH (**131**) as a reagent (see **Figure 6.1**) for the conversion of the α,β -unsaturated ketones to their cyclised forms. Although it is available commercially its high cost was prohibitive, as such we attempted to prepare the reagent in-house.

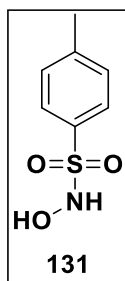


Figure 6.1: *N*-hydroxy-4-methylbenzenesulfonamide (TsNHOH; **131**).

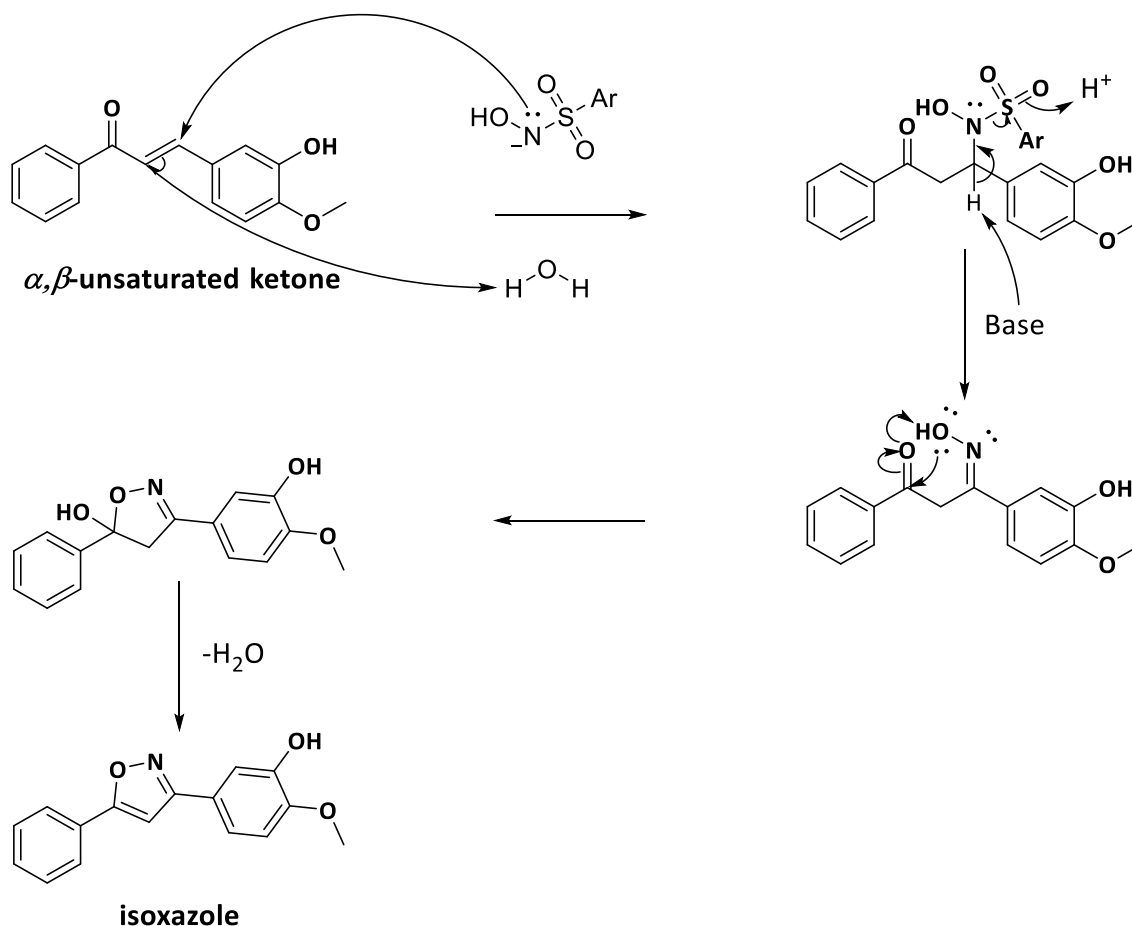
The general tosylation reaction conducted made use of either AlO_3 or Cr_2O_3 . The AlO_3 used afforded no product while the use of Cr_2O_3 afforded the tosylated material in an impure yield of 66 %, however, when increasing the reaction ten-fold the reaction was unsuccessful. Ultimately, we then elected to purchase the reagent.

The ^1H NMR spectrum of the tosylate material product (**131**) indicated a singlet peak at 10.35 ppm for both the NH and OH groups as it integrates for two hydrogens. The aromatic CH groups can be seen at 7.72 ppm as a doublet integrating for two hydrogens, and 7.24 ppm as a doublet integrating for a further two hydrogens. The CH_3 group can be seen at 2.38 ppm as a singlet integrating for three hydrogens. The ^{13}C NMR spectrum indicates the two quaternary carbons at 144.14 ppm and 134.23 ppm. The CH groups are found at 129.10 ppm, 129.04 ppm, 128.31 ppm, and 128.24 ppm. The CH_3 group is found at 20.23 ppm. The MS spectrum indicates the presence of the $[\text{M}-\text{H}]^+$ mass ion at 186.128 ($\text{C}_7\text{H}_8\text{NO}_3\text{S}$ requires 186.023).

6.6. General procedure for the attempted formation of isoxazole ring systems from α,β -unsaturated ketones

The reaction conditions used for the cyclisation reaction of an α,β -unsaturated ketone with TsNHOH being added to the β -position were reported by Tang and co-workers which they reported to have worked for a wide range of unsaturated ketones and aldehydes. Notably they did indicate that between the ketone and aldehyde's carbonyl groups, that the ketones do take longer to form the isoxazole product [107, 112].

The mechanism for the cyclisation reaction to afford the isoxazoles can be seen in **Scheme 6.1** [107, 112]. The deprotonated form of TsNHOH attacks the β -position via a 1,4-addition to the alkene, which then breaks onto the α -carbon followed by its protonation. The base will deprotonate the β -carbon atom which will lead to a C-N double bond, kicking off the tosyl group resulting in an oxime group. The lone pair of electrons on the O -atom acts as a nucleophile which attacks the partially positive carbonyl C-atom resulting in a breaking of the C-O double bond with the closing the ring system, allowing the O -atom to pick up a H-atom from the oxime group. The removal of water is then necessary to generate the targeted isoxazole product (scaffold D).



Scheme 6.1: Mechanism of the cyclisation step involved in scaffold D [107, 112].

During this cyclisation reaction the first step requires TsNHOH to be added to the β -carbon of an α,β -unsaturated ketone. We initially attempted the reaction with **K8A8** (see **Figure 6.2**). Unfortunately, the reaction was unsuccessful. In a second attempt more TsNHOH was added to the solution in the hope that having a more concentrated solution would allow for better interaction between the **K8A8** and TsNHOH molecules. The time allowed for the reaction was also increased to five days to allow for extra time for the reaction to take place since it was reported that this type of ketone would take much longer to react. Again, to our surprise no product formed. We then attempted to allow the reaction to not only have more time to react but to also increase the temperature of the reaction to 140 °C. In the end the reaction still proved unsuccessful.

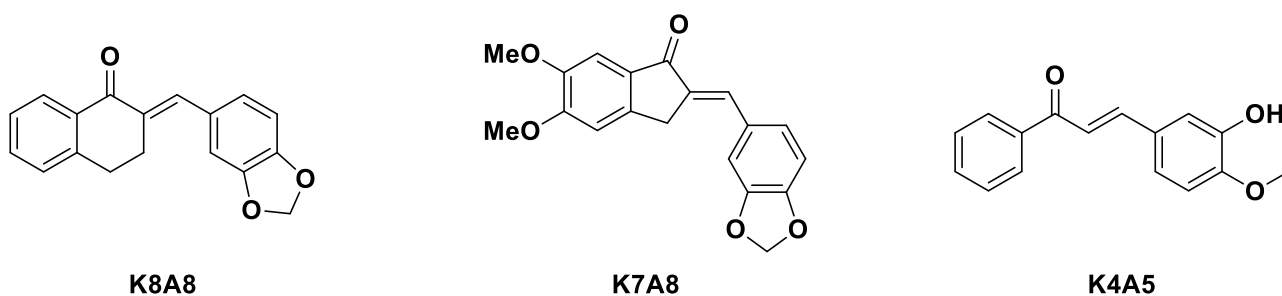


Figure 6.2: The α,β -unsaturated ketones targeted for use in the cyclisation reaction.

It was then considered that the six membered ring of the tetralone section of **K8A8** and the benzodioxole ring might be too rigid and does not allow for the cyclisation of **K8A8**. We therefore decided to exchange **K8A8** for **K7A8** which contains a five membered ring but retains the benzodioxole ring without success. Which could indicate that the benzodioxole ring could be inhibiting the addition of TsNHOH. We therefore attempted to exchanged **K8A8** with **K4A5** which does not contain a benzodioxole ring, but also keeping in mind that the ketone does not form part of a ring system which might also be preventing the cyclisation of these ligands. Unfortunately, the reaction was not successful and due to time constraints, we were unable to evaluate other approaches.

6.7. Conclusion

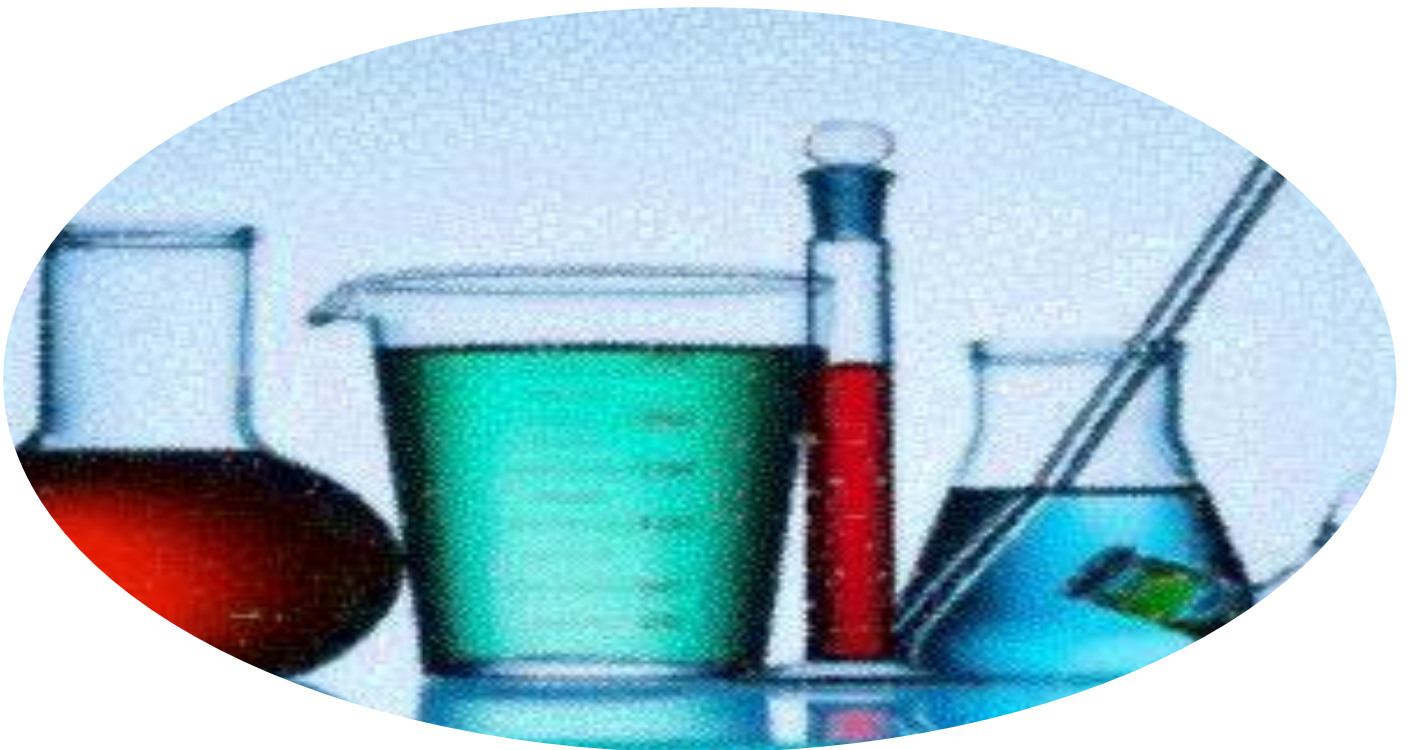
During the synthesis of scaffold D a set of novel α,β -unsaturated ketones were synthesised (see **Table 5.2**). The successful formation of these α,β -unsaturated ketones included fourteen out of the twenty five targets which incorporated different ketones and aldehydes. The ketone proved to be the most reactive was **K8** which is tetralone and gave yields in the range of 90 % with the exception of **K8A5** (71 %). The ketone containing an indanone ring and methoxy groups (**K7**) were also successful with yields of 39 – 95 %.

Unfortunately, the ketone (**K6**), containing a piperidone ring and which was computationally predicted to be the best ligands in scaffold D were all unsuccessful. While only some of the combinations with **K3** and **K4** proved successful with yields of 41 – 63 %, these ligands included **K3A4**, **K3A8**, **K4A5** and **K4A8**. Due to these results, it was concluded that **K3**, **K4** and **K6**, are very unreactive and that the aldehydes **A4**, **A5** and **A8** are the most reactive.

The next step in scaffold D was to cyclise these synthesised α,β -unsaturated ketones using TsNHOH. Unfortunately, when making use of either a six membered ring (**K8A8**), a five membered ring (**K7A8**) or an open chained ketone (**K4A5**) the desired isoxazole formation proved unsuccessful.

Chapter 7

Conclusion and Future work



7.1. Conclusion

The two main aims envisaged for the project included i) the *in silico* assessment and synthesis of potential AChEIs which are structurally related to donepezil (**25**) and ii) the *in silico* assessment of potential NMDA antagonists related to the active compound (**75**) that was identified by the Liotto group.

Scaffolds A and B were considered from previous in-house experience on related tricyclic thiazole scaffolds where scaffold A would undergo diversification upon functionalisation of an exocyclic ester allowing for the exploration of the CAS site inhibition of AChE [69]. Scaffold B would incorporate a step that adds functionality in scaffold B after the use of Click chemistry, making the ligands very long and leading to interactions at the CAS and PAS sites of AChE indicating that these ligands might function as dual inhibitors. Scaffold C focuses on novel AChEIs which resembles the NMDA antagonists designed by the Liotta group (**93**), which could potentially target both AChE and NMDA, and therefore function as potent dual action neuroprotective agents.

Computational analysis of scaffolds A to C made predictions for each scaffold's ligands regarding their molecular docking scores (mimicking the ligands docked into the active site of AChE), and CYP2C9 inhibition (which can predict how a ligand could cause severe adverse reactions). Additional predictive studies were conducted with Qikprop analysis predicting the drug-likeness of the ligands under study. Pharmacophore analysis of a set of the most potent ligands were analysed and the resultant hypothesis can be used in future predictions within the group for drug development against AChE. SwissADME analysis was also conducted for drug-likeness studies.

The molecular docking studies indicated that the lower limit of -13.000, which would identify the best ligands in scaffolds A to C, led to the identification of fifteen ligands from the initial fifty-seven ligands classified as drug-like. These ligands included **A1.2.a**, **A1.3.a**, **A1.5.a**, **A1.8.a**, **B1.1.a**, **C1.1.a**, **C1.2.a**, **C1.3.a** (and **C1.3.b**, **C1.3.c**), **C1.4.a** (and **C1.4.b**), **C1.5.a** (and **C1.5.b**), **C1.6.a**, **C2.1.a**, **C2.4.a**, **C2.5.a** and **C2.6.a**.

The Qikprop analysis, however, indicated that all the ligands obey the MW, QPlogBB, number of H-donor or H-acceptor ranges for orally available drugs and can therefore be classified as drug-like. Unfortunately, all the ligands disobeyed the QPlogHERG rule which suggests that there is a significant difference in the dose response between AChE and hERG inhibition. The QPlogPo/w rule was only disobeyed by three ligands (**C1.3.a**, **C1.4.b** and **C2.3.a**), while the TPSA rule was only broken by **B1.1.a**. These results limited the potential drug-like molecules in scaffolds A to C to twelve ligands **A1.2.a**, **A1.3.a**, **A1.5.a**, **A1.8.a**, **C1.1.a**, **C1.2.a**, **C1.5.a** (and **C1.5.b**), **C1.6.a**, **C2.1.a**, **C2.4.a**, **C2.5.a** and **C2.6.a**.

SwissADME results represented data in a bioavailability radar for each ligand under study which determines the bioavailability of ligands. The violations of the bioavailability radar included **A1.1** and **C3.1-C5.11** for the INSATU rule; **C1.1-C1.5** and **C2.1-C2.5** for the LIPO rule; **C1.3** and **C2.3** for the INSOLU rule; and **C5.11** violated the POLAR bioavailability radar rule. Overall, the SwissADME analysis only predicted that seventeen ligands will be bioavailable, and when comparing the results from both SwissADME and the Schrodinger analysis the drug-likeness of the ligands were lowered to only six ligands (**A1.2.a**, **A1.3.a**, **A1.5.a**, **A1.8.a**, **C1.6.a**, **C2.6.a**). With regards to the CYP2C9 predictions only **C3.5** was considered to not be a CYP2C9 inhibitor.

The second aim of the project was to synthesise the most promising ligands within scaffolds A, B and C which included **A1.3.a**, **C1.6.a**, **C2.6.a** and **B1.1.a** when considering the computational results. Synthetic challenges relating to scaffold A and B resulted in the abandonment of the scaffolds and a shift in focus to scaffold C, which unfortunately, also presented numerous synthetic challenges of its own. As the original synthesis of the originally proposed scaffold C proved impractical, we investigated approaches to several structurally similar scaffolds without luck. As a result, we opted to plan a new scaffold which would still target AChE but that would still have the capacity of being functionalised in future work within the group.

The resultant scaffold D underwent a lower intensity computational analysis which only included molecular docking, Qikprop analysis and CYP2C9 inhibition of fifty ligands which included an α,β -unsaturated ketone intermediates as well as their cyclised isoxazoles. In this instance the computed docking scores only identified four ligands when implementing the lower docking score limit of -13.000. These ligands include **C.K6A3**, **C.K6A4**, **C.K6A5** and **K6A8**. All the ligands obeyed the MW, QPlogPo/w, QPlogBB, H-donor, H-acceptor and TPSA rules for drug-likeness using Qikprop analysis. Ligands **C.K7A8**, **C.K8A8**, **K7A8** and **K8A8** were the only ligands under study that did not violate the QPlogHERG rule. The CYP2C9 inhibition study also indicated that all the ligands would not cause ADRs when compared to donepezil (**25**). The functionalisation of the ligands from scaffold D could have the potential to afford more potent inhibitors that could be more comparable to those ligands of scaffolds A to C. All the ligands in scaffold D were targeted for synthesis in an attempt to have material available for future functionalisation upon their successful synthesis.

Cyclic and heterocyclic ketones were selected to be reacted with different aldehydes leading to 25 α,β -unsaturated ketones and 25 related isoxazoles. Fourteen of these ligands were successfully synthesised which included the most reactive ketone option being tetralone (**K8**) that gave good yields. The indanone ring system (**K7**) gave yields of 39 – 95 %. **K3A4**, **K3A8**, **K4A5** and **K4A8** which incorporate either K3 or K4 ketone also proved successful with yields of 41 – 63 %. Indicating that the most reactive among the ketones are **K8** and **K7** and among the aldehydes are **A4**, **A5** and **A8**. The ketone containing the piperidone ring system (**K6**), which was predicted to all be among those ligands in the study to inhibit AChE the most, were all

unsuccessful.

The cyclisation of the successfully synthesised α,β -unsaturated ketones were then attempted in the following step where the incorporation of TsNHOH at the α,β -unsaturated ketone's β -position would result in the tosyl group being kicked off upon ring closure. The cyclisation of a six membered ring (**K8A8**), a five membered ring (**K7A8**) and an open chained ketone (**K4A5**) resulted in unsuccessful reactions. Due to time constraints, no further attempts were made to access the isoxazole core.

7.2. Future work

The successfully synthesised α,β -unsaturated ketones will be analysed for biological activity against AChE as part of the future work of the project using the appropriate AChE electric eel enzyme in an enzymatic assay. This analysis will determine the inhibitory concentration of 50 % of the ligand (IC_{50}). Cytotoxicity studies will also be conducted and compared to donepezil (**25**) which has an IC_{50} value of $0.05 \pm 0.06 \mu\text{M}$. The ligands with comparable or better values could be used as lead compounds in future studies.

Literature available where the cyclisation reaction can be attempted by making use of alternative methods resulting in comparable structures of the α,β -unsaturated ketones of scaffold D can be seen in **Figure 7.1** in an attempt to form isoxazoles [107]. Path c was followed in this thesis in order to generate the isoxazole rings where the *N*-atom is closer to R^1 group which predicted better computational results (not reported). The alternative methods using path a and b can be conducted in the future within the group.

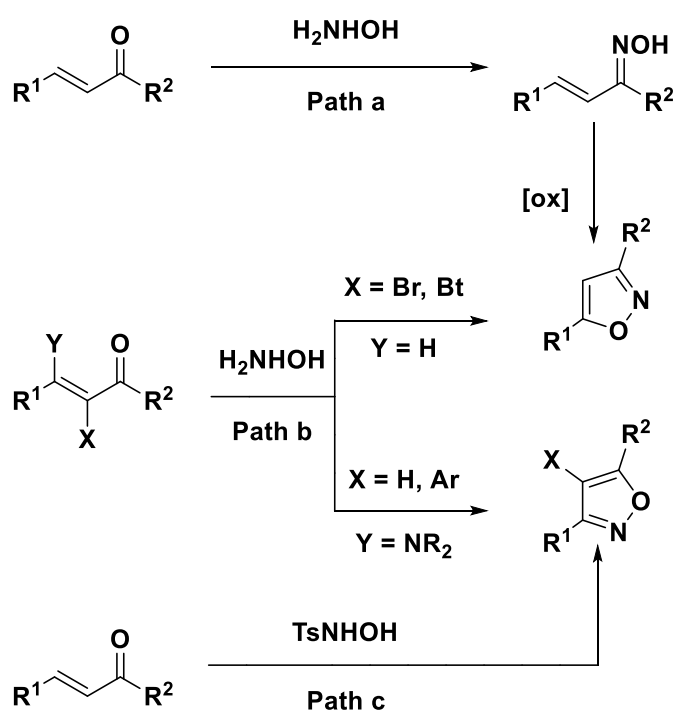


Figure 7.1: Alternative isoxazole formation.

If the successful formation of the isoxazole molecules from above is realised, the study could be extended to include the formation of β -lactams and γ -amino alcohols (see **Figure 7.2**) that makes use of work reported by Tang and co-workers which could also prove active against AChE [112].

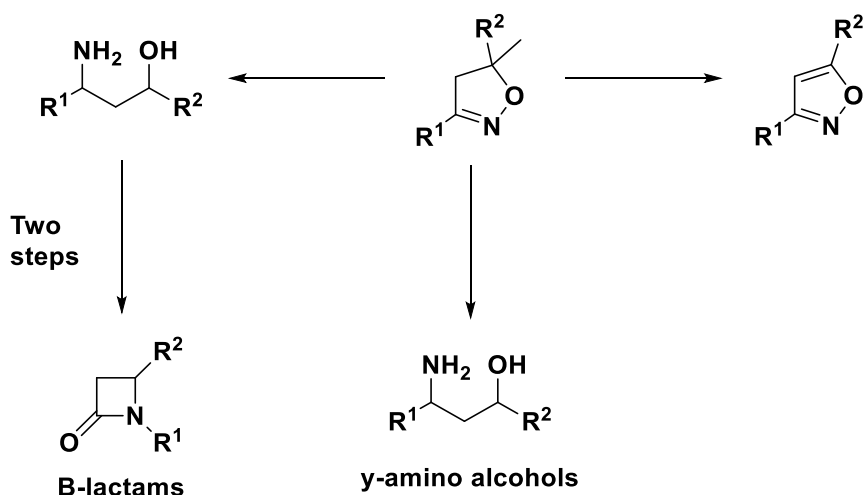


Figure 7.2: Formation of β -lactams and γ -amino alcohols.

The QPlogHERG screening of potential future ligands would be essential in predicting if targets would be worth synthesising and would therefore be a good starting point before commencing with their synthesis. A close eye must be kept on their QPlogPo/w and TPSA data as these rules can be more easily controlled among the Qikprop rules discussed.

Chapter 8

Experimental



8.1. General experimental details

8.1.1. Purification of solvents

Solvents used in reactions were all distilled over the appropriate drying medium under an argon atmosphere:

- Tetrahydrofuran (THF) and diethyl ether were distilled from sodium metal and benzophenone.
- Toluene was distilled from sodium metal lumps.
- Acetonitrile (AcCN) and dichloromethane (DCM) were distilled from calcium hydride.

Absolute ethanol (EtOH) was used without further purification.

8.1.2. Experimental techniques and equipment used

Most of the reactions performed were under inert conditions, using an argon atmosphere. Through the use of a standard manifold line connected to a vacuum pump. Reaction flasks which were connected to the manifold under inert conditions were flame-dried and then allowed to cool to room temperature.

Concentration or evaporation *in vacuo* refers to the removal of the solvent under reduced pressure (approximately 20 mmHg, 40 – 50 °C) on a rotary evaporator. The final drying of samples was dried under a “high vacuum” using an oil pump (approximately 1-2 mmHg). The yield of each product was calculated from the starting material used in the reaction.

8.1.3. Chromatographic separation

The retention factor (R_f) values given for the thin layer chromatography (TLC) on aluminium-backed Macherey-Nagel ALUGRAM Sil G/UV254 plates, pre-coated with 0.25 mm silica gel 60. Macherey-Nagel Silica gel 60 (particle size 0.063 – 0.200 mm) was used in the conventional preparative column chromatography as the adsorbent with silica to product ratio of 30:1. The silica was packed into a suitable sized column, the appropriate solvent to be used for the separation was pushed through the column twice using pressure or until all the air bubbles were forced out of the silica. The crude product was adsorbed onto silica, loaded onto the silica surface inside the column, and then plugged with a plug of cotton wool. The elution process was performed using the indicated solvent mixture under gravitation conditions.

8.1.4. Spectroscopic and physical data

Hydrogen nuclear magnetic resonance (^1H NMR) spectra were recorded on Bruker Avance-III-300 and Bruker Avance-III-400 spectrometers at 300.13 and 400.13 MHz respectively using standard pulse sequences. The temperature of the probe inside the NMR instrument was kept at 300 ± 1 K. All the spectra were recorded in deuterated chloroform (CDCl_3 at 7.26 ppm) or deuterated dimethylsulfoxide (d_6 -DMSO at 2.50 ppm) in a 5 mm NMR spectroscopy tubes. Chemical shifts, δ , are reported in parts per million (ppm) relative to

tetramethylsilane.

The ^1H NMR spectroscopy chemical shifts are reported as: values (number of hydrogens, description of the signal, coupling constants in hertz (Hz) where applicable, assignment). The abbreviations used included: s = singlet, d = doublet, t = triplet, q = quartet and m = multiplet.

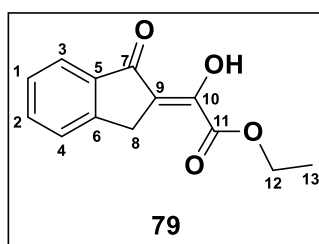
The ^{13}C NMR spectra were recorded on Bruker Avance-III-300 and Bruker Avance-III-400 spectrometers at 75.47 and 100.64 MHz respectively. Chemical shifts are reported on the scale relative to the central signal of deuterated chloroform (CDCl_3) (77.16). The ^{13}C NMR spectroscopy chemical shifts are reported: value (assignment). The infrared spectra (FTIR) were obtained on a Bruker ALPHA Platinum ATR spectrometer. The absorptions are reported on the wavenumber (cm^{-1}) scale, in the range 650 - 4000 cm^{-1} .

8.1.5. Nomenclature and numbering of compounds

The compounds prepared during this project are named in the following experimental sections by using ChemDraw Ultra (version 16.0). However, the numbering system used to illustrate the diagrams of these compounds is one adopted for convenience and is not meant to reflect the systematic numbering of these compounds.

8.2. Experimental details relating to scaffold A and B

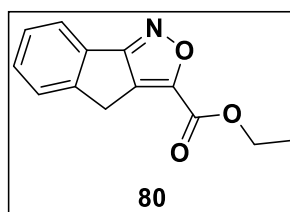
8.2.1. Ethyl (*Z*)-2-hydroxy-2-(1-oxo-1,3-dihydro-2*H*-inden-2-ylidene)acetate (**79**)



Sodium metal (22.99 g/mol, 0.0671 g, 2.89 mmol, 2.5 eq.) was added in small portions to dry EtOH (1.50 ml) at 0 °C, till all the sodium had reacted. Diethyl oxalate (146.14 g/mol, 0.16 ml, 1.18 mmol, 1.0 eq.) was then added and left to stir for 10 min. Indanone (132.06 g/mol, 0.1528 g, 1.16 mmol, 1.0 eq.) was added in small portions and left to stir for 10 min between additions. After complete addition, more EtOH was added and then left to stir overnight. HCl (2 M; 36.46 g/mol, 5.00 ml, 10.00 mmol, 8.6 eq.) was added to the solution in order to neutralize it. A precipitate formed as a result, which was filtered and then washed with water. The solids were washed with ethyl acetate (EtOAc), dried using anhydrous Na_2SO_4 , filtered and then evaporated *in vacuo*. The pure product was black solids with a yield of 65 % (0.1746 g). ^1H NMR (400 MHz, Chloroform-

d) δ 13.02 (s, 1H, OH), 7.84 (d, $J = 7.7$ Hz, 1H, C-1), 7.63 (td, $J = 7.5, 1.3$ Hz, 1H, C-4), 7.53 (dt, $J = 7.6, 1.0$ Hz, 1H, C-2), 7.42 (td, 1H, C-3), 4.41 (q, $J = 7.1$ Hz, 2H, CH_2CH_3), 3.95 (s, 2H, C-8), 1.43 (t, $J = 7.2$ Hz, 3H, CH_2CH_3).
 ^{13}C NMR (101 MHz, Chloroform-*d*) δ 198.74 (C-7), 162.69 (C-10), 153.96 (C-11), 150.46 (C-6), 137.03 (C-5), 135.04 (C-2), 127.68 (C-3), 126.15 (C-1), 123.93 (C-4), 116.41 (C-9), 62.27 (C-12), 31.52 (C-8), 14.19 (C-13).
 HRMS m/z (ESI) 231.084 ($[\text{M}-\text{H}]^+$ requires 231.066).

8.2.2. Ethyl 4*H*-indeno[1,2-*c*]isoxazole-3-carboxylate (**80**)



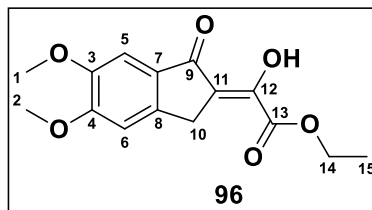
8.2.2.1. General method 1:

Hydroxylamine hydrochloride (69.49 g/mol, 0.1553 g, 2.23 mmol, 3.0 eq.) was added to ethyl 2-oxo-2-(1-oxo-2,3-dihydro-1*H*-inden-2-yl)acetate (232.07 g/mol, 0.5022 g, 2.16 mmol, 1.0 eq.) in dry EtOH (15.00 ml). After the solution was stirring for two hours at room temperature, the solution was refluxed overnight. The solvent was removed *in vacuo* and then partitioned between DCM and H_2O . The organic layer was dried, concentrated and columned. The product was not formed.

8.2.2.2. General method 2:

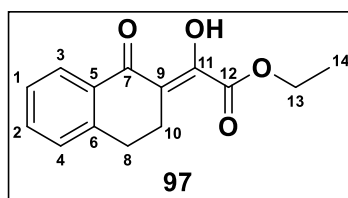
A mixture of ethyl 2-oxo-2-(1-oxo-2,3-dihydro-1*H*-inden-2-yl)acetate (10.40 mmol eq.) in MeOH (2.00 ml) was added in small portions to a stirring solution of NaOH (10.90 mmol), MeOH (7.00 ml) and H_2O (0.50 ml), while keeping the temperature at -70 °C. A solution of $\text{NH}_2\text{OH}\cdot\text{HCl}$ (21.00 mmol), NaOH (22.00 mmol), MeOH (8.00 ml) and H_2O (1.00 ml) was cooled to -70 °C before being added to the starting material stirring solution. The solution was allowed to slowly warm to 0 °C over the next 2 hours. Acetone (1.00 ml) was added to the mixture, which was then slowly added to a stirring 85 °C 12 M HCl (2.50 ml) solution. The mixture was refluxed for 1.5 hours. The solvent was removed *in vacuo*. Water (50.00 ml) and EtOAc (350.00 ml) was used to extract the mixture where the organic layer was collected, dried, filtered, concentrated and columned. The product did not form.

8.2.3 Ethyl (Z)-2-(5,6-dimethoxy-1-oxo-1,3-dihydro-2H-inden-2-ylidene)-2-hydroxyacetate (**96**)



Sodium metal (22.99 g/mol, 0.0473 g, 2.06 mmol, 2.5 eq.) was added in small portions to 99.9 % EtOH (2.00 ml) which was left to stir for 10 min whereafter diethyl oxalate (146.14 g/mol, 0.11 ml, 0.82 mmol, 1.0 eq.) was added, all at 0 °C, till all the sodium had reacted. After 15 min, 5,6-dimethoxyindanone (192.21 g/mol, 0.1581 g, 0.82 mmol, 1.0 eq.) was added in small amounts, leaving solution to stir for 10 min between additions. After complete addition the solution was left to stir overnight at room temperature. HCl (2 M; 36.46 g/mol, 3.50 ml, 6.58 mmol, 8.0 eq.) was added to the solution in order to neutralize it and left to stir for 2 hours. The resultant precipitate was filtered and then washed with a lot of water and then collected by washing the solids with EtOAc. This organic phase was dried using anhydrous Na₂SO₄, filtered and then evaporated *in vacuo*. The pure product was a light yellow solid with a yield of 70 % (0.1685 g). ¹H NMR (300 MHz, Chloroform-*d*) δ 13.23 (s, 1H, OH), 7.24 (s, 1H, C-5), 6.96 (s, 1H, C-6), 4.41 (q, *J* = 7.1 Hz, 2H, CH₂CH₃), 4.00 (s, 3H, C-2), 3.94 (s, 3H, C-1), 3.87 (s, 2H, C-9), 1.43 (t, *J* = 7.7, 6.5 Hz, 3H, CH₂CH₃). ¹³C NMR (75 MHz, CDCl₃) δ 197.74 (C-9), 162.92 (C-12), 156.03 (C-4), 151.52 (C-13), 149.73 (C-3), 146.35 (C-7), 129.96 (C-8), 117.25 (C-11), 107.20 (C-6), 104.30 (C-5), 62.10 (C-14), 56.41 (C-1), 56.12 (C-2), 31.21 (C-10), 14.18 (C-15). HRMS *m/z* (ESI) 291.114 ([M-H]⁺ requires 291.087).

8.2.4. Ethyl (Z)-2-hydroxy-2-(1-oxo-3,4-dihydronaphthalen-2(1H)-ylidene)acetate (**97**)

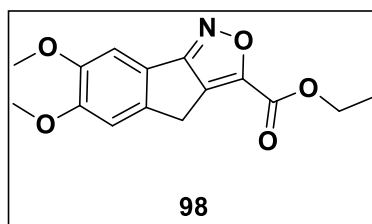


Sodium metal (22.99 g/mol, 1.1800 g, 51.35 mmol, 2.5 eq.) was added in small portions to 99.9 % EtOH (26.65 ml) which was left to stir for 10 min whereafter diethyl oxalate (146.14 g/mol, 2.78 ml, 20.54 mmol, 1.0 eq.) was then added, all at 0 °C, till all the sodium had reacted. After 15 min, tetralone (146.19 g/mol, 3.0027 g, 20.54 mmol, 1.0 eq.) was added in small amounts, leaving the solution to stir for 10 min between additions. After complete addition, the solution was left to stir for 3 days at room temperature. HCl (2 M;

36.46 g/mol, 82.20 ml, 164.32 mmol, 8.0 eq.) was added to the solution in order to neutralize it and left to stir for 3 hours. The resultant precipitate was filtered and then washed with water, collected by washing the solids with DCM. This organic phase was dried using anhydrous Na₂SO₄, filtered and then evaporated *in vacuo*. The pure product was a light yellow solid with a yield of 95 % (4.8267 g). **¹H NMR (300 MHz, Chloroform-*d*)** δ 15.80 (s, 1H, OH), 7.98 (dd, *J* = 7.8, 1.4 Hz, 1H, C-2), 7.46 (tdd, *J* = 7.5, 3.7, 1.5 Hz, 1H, C-4), 7.34 (td, *J* = 7.6, 1.3 Hz, 1H, C-3), 7.23 (dd, 1H, C-1), 4.38 (q, *J* = 7.1 Hz, 2H, C-13), 2.97 – 2.83 (m, 4H, C-8; C-10), 1.40 (t, *J* = 7.1 Hz, 3H, C-14). **¹³C NMR (75 MHz, CDCl₃)** δ 186.98 (C-7), 169.78 (C-11), 162.99 (C-12), 142.48 (C-5), 133.67 (C-6), 131.17 (C-2), 128.02 (C-4), 127.12 (C-3), 126.85 (C-1), 108.83 (C-9), 62.14 (C-13), 27.99 (C-8), 22.51 (C-10), 14.11 (C-14).

8.2.5. Ethyl 6,7-dimethoxy-4*H*-indeno[1,2-*c*]isoxazole-3-carboxylate

(98)



8.2.5.1. General method 1:

1.) Hydroxylamine hydrochloride (69.49 g/mol, 0.1553 g, 2.23 mmol, 3.0 eq.) was added to ethyl 2-oxo-2-(1-oxo-2,3-dihydro-1*H*-inden-2-yl)acetate (232.07 g/mol, 0.5022 g, 2.16 mmol, 1.0 eq.) in dry EtOH (15.00 ml). After the solution was stirring for 2 hours at room temperature, the solution was refluxed overnight. The solvent was removed *in vacuo* and then partitioned between DCM and H₂O. The organic layer was dried, concentrated and columned. The product was not formed.

2.) Hydroxylamine hydrochloride (69.49 g/mol, 0.0960 g, 1.34 mmol, 3.0 eq.) was added to ethyl 2-(5,6-dimethoxy-1-oxo-2,3-dihydro-1*H*-inden-2-yl)-2-oxoacetate (292.28 g/mol, 0.1307 g, 0.45 mmol, 1.0 eq.) in dry EtOH (6.00 ml). After the solution was stirring for 2 hours at room temperature, the solution was refluxed overnight. The solvent was removed *in vacuo* and then partitioned between DCM and H₂O. The organic layer was dried, concentrated and columned. The reaction was unsuccessful.

8.2.5.2. General method 2:

1.) A mixture of ethyl 2-oxo-2-(1-oxo-2,3-dihydro-1*H*-inden-2-yl)acetate (10.40 mmol eq.) in MeOH (2.00 ml) was added in small portions to a stirring solution of NaOH (10.90 mmol), MeOH (7.00 ml) and H₂O (0.50 ml), while keeping the temperature at -70 °C. A solution of NH₂OH.HCl (21.00 mmol), NaOH (22.00 mmol), MeOH

(8.00 ml) and H₂O (1.00 ml) was cooled to -70 °C before being added to the stirring solution. The solution was allowed to slowly warm to 0 °C over the next 2 hours. Acetone (1.00 ml) was added to the mixture, which was then slowly added to a stirring 85 °C 12 M HCl (2.50 ml) solution. The mixture was refluxed for 1.5 hours. The solvent was removed *in vacuo*. Water (50.00 ml) and EtOAc (350.00 ml) was used to extract the mixture where the organic layer was collected, dried, filtered and concentrated and columned. The product did not form.

2.) Hydroxylamine hydrochloride (69.49 g/mol, 0.7300 g, 10.51 mmol, 3.0 eq.) was added to ethyl 2-(5,6-dimethoxy-1-oxo-2,3-dihydro-1*H*-inden-2-yl)-2-oxoacetate (292.28 g/mol, 1.0234 g, 3.50 mmol, 1.0 eq.) in dry EtOH (17.13 ml). After the solution was stirring for 2 hours at room temperature, the solution was refluxed for 5 hours. The solvent was removed *in vacuo* and then partitioned between DCM and H₂O (50.00 ml : 50.00 ml). The organic layer was dried, concentrated and columned. The reaction was unsuccessful.

3.) At -70 °C a solution of (*Z*)-ethyl 2-(5,6-dimethoxy-1-oxo-1*H*-inden-2(3*H*)-ylidene)-2-hydroxyacetate (292.28 g/mol, 0.8105 g, 2.77 mmol, 1.0 eq.) in MeOH (1.60 ml) was carefully added to a mixture of NaOH (39.98 g/mol, 0.2326 g, 5.55 mmol, 2.0 eq.) in MeOH (3.50 ml) and H₂O (0.25 ml). A precooled (-70 °C) solution of NH₂OH-HCl (69.49 g/mol, 0.3892 g, 5.55 mmol, 2.0 eq.), NaOH (39.98 g/mol, 0.2278 g, 5.55 mmol, 2.0 eq.) in MeOH (4.00 ml) and H₂O (0.50 ml) was then added to the reaction flask. Over the next 2 hours, the solution was left to warm up to 0 °C. Acetone (0.50 ml) was added to the solution and then 12 M HCl, which was kept at 85 °C. The solution was then refluxed overnight. The solvent was removed *in vacuo*. Afterward, H₂O (10.00 ml) was added, extracted with EtOAc (3 x 10.00 ml). The organic layer was dried, filtered, evaporated and columned. The reaction was unsuccessful.

4.) To a solution of sodium hydroxide (39.98 g/mol, 0.1139 g, 2.85 mmol, 1.0 eq.) in EtOH (2.00 ml) and H₂O (1.00 ml), kept at -60 °C, was added NH₂OH-HCl (69.49 g/mol, 0.3944 g, 5.68 mmol, 2.0 eq.) in EtOH (2.00 ml) and H₂O (0.10 ml). The mixture was then filtered and cooled to -60 °C before being added to ethyl 2-(5,6-dimethoxy-1-oxo-2,3-dihydro-1*H*-inden-2-yl)-2-oxoacetate (292.28 g/mol, 0.8243 g, 2.82 mmol, 1.0 eq.) in EtOH (1.60 ml). The mixture was left to stir for 2 hours at -60 °C. Acetone (0.20 ml), CHCl₃ (1.00 ml; 80 °C), and H₂O (2.00 ml) were added to the mixture, which was then left to stir at 80 °C for 30 min and then left to reflux overnight. The solvent was removed *in vacuo* afterward H₂O (10.00 ml) was added, extracted with EtOAc (3 x 10.00 ml). The organic layer was dried, filtered, evaporated and columned. The reaction was unsuccessful.

5.) A mixture of sodium methoxide [Na(s) (22.99 g/mol, 0.0969 g, 4.21 mmol, 1.5 eq.) and MeOH (1.50 ml)] was added dropwise to a stirring mixture, kept at -40 °C, of NH₂OH-HCl (69.49 g/mol, 0.2928 g, 4.21 mmol, 1.5 eq.) in MeOH (3.00 ml). The mixture was then cooled to room temperature. A solution of ethyl 2-(5,6-dimethoxy-1-oxo-2,3-dihydro-1*H*-inden-2-yl)-2-oxoacetate (292.28 g/mol, 0.8209 g, 2.81 mmol, 1.0 eq.) and

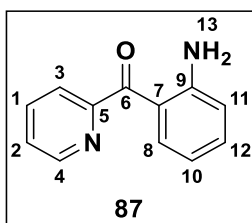
sodium methoxide [Na(s) (22.99 g/mol, 0.0969 g, 4.21 mmol, 1.5 eq.) and MeOH (1.50 ml)] was added to the mixture. The mixture was left to stir for 2 days. The mixture was cooled to 0 °C, whereafter a mixture of cHCl and MeOH was added until pH 4. The mixture was then left to stir for 2 hours at 0 °C. The solvent was removed *in vacuo* whereafter H₂O (10.00 ml) was added, extracted with EtOAc (3 x 10.00 ml). The organic layer was dried, filtered, evaporated and columned. The reaction was unsuccessful.

6.) A stirring solution of NH₂OH-HCl (69.49 g/mol, 0.3085 g, 4.44 mmol, 1.5 eq.) in MeOH (2.50 ml) was maintained at -40 °C, a solution of NaOMe, prepared from Na (s) (22.99 g/mol, 0.1021 g, 4.44 mmol, 1.5 eq.) and MeOH (1.30 ml), was added in a dropwise manner. The reaction mixture was warmed to room temperature, and a solution of ethyl 2-(5,6-dimethoxy-1-oxo-2,3-dihydro-1*H*-inden-2-yl-oxoacetate (292.28 g/mol, 0.8651 g, 2.96 mmol, 1.0 eq.) in MeOH (1.30 ml) was added. A solution of NaOMe, prepared from Na (s) (22.99 g/mol, 0.2042 g, 8.88 mmol, 3.0 eq.) and MeOH (2.60 ml), was added. The reaction mixture was left to stir for three days. The mixture was cooled to 0 °C before a solution of HCl in MeOH was added till pH 4. The mixture was then left to stir for 2 hours at 0 °C. The mixture was extracted with DCM (3 x 25.00 ml), concentrated *in vacuo* and columned. The reaction was unsuccessful and only left the starting material.

7.) A stirring solution of NH₂OH-HCl (69.49 g/mol, 0.1521 g, 2.19 mmol, 2.2 eq.) in MeOH (5.50 ml) was maintained at -40 °C, a solution of K₂CO₃ (138.21 g/mol, 0.1707 g, 1.24 mmol, 2.0 eq.) and MeOH (5.00 ml), was added in a dropwise manner. The reaction mixture was warmed to room temperature, and a solution of ethyl 2-(5,6-dimethoxy-1-oxo-2,3-dihydro-1*H*-inden-2-yl-oxoacetate (292.28 g/mol, 0.1521 g, 0.6176 mmol, 1.0 eq.) in MeOH (1.30 ml) was added. A solution of K₂CO₃ (138.21 g/mol, 0.2042 g, 8.88 mmol, 3.0 eq.) and MeOH (4.00 ml), was added. The reaction mixture was left to reflux for 2 hours and then left stir at room temperature overnight. The mixture was cooled to 0 °C before a solution of HCl in MeOH was added till pH 4. The mixture was then left to stir for 2 hours at 0 °C. The mixture was extracted with DCM (3 x 25.00 ml), concentrated *in vacuo* and columned. The reaction was unsuccessful.

8.3. Experimental details relating to scaffold C

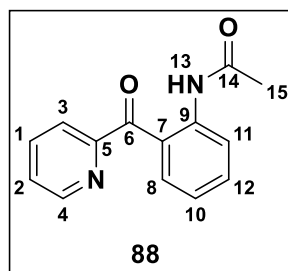
8.3.1. (2-aminophenyl)(pyridin-2-yl)methanone (**87**)



A mixture of 2-aminobenzonitrile (118.14 g/mol, 0.1535 g, 1.30 mmol, 1.0 eq.) and 2-bromopyridine (158.00 g/mol, 0.3490 g, 2.21 mmol, 1.7 eq.) in 26.00 ml dry toluene was kept under an argon atmosphere at -50 °C.

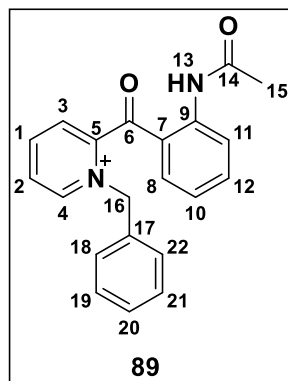
n-BuLi (2.5 M; 64.06 g/mol, 1.04 mL in hexanes, 11.03 mmol, 2.0 eq.) was added in a drop wise manner to the mixture and then left to stir for 3h at $-50\text{ }^{\circ}\text{C}$. The solution was then warmed to $0\text{ }^{\circ}\text{C}$ whereafter 3 M HCl (28.00 ml) was added to the solution, keeping the temperature below $10\text{ }^{\circ}\text{C}$. The organic layer was collected and extracted with 3 M HCl (2 x 25.00 ml). The combined aqueous fractions were basified to pH 10. The mixture was kept in the fridge overnight. The dark brown crystals were collected and dried. Yield 77 % (0.1972 g), R_f value of 0.19 (1:3; EtOAc: Hexane). $^1\text{H NMR}$ (300 MHz, Chloroform-*d*) δ 8.72 (dd, $J = 4.9, 1.7, 1.0\text{ Hz}$, 1H, C-4), 7.88 (td, $J = 7.7, 1.7\text{ Hz}$, 1H, C-1), 7.78 (dt, $J = 7.8, 1.2\text{ Hz}$, 1H, C-8), 7.66 (dd, $J = 8.2, 1.6\text{ Hz}$, 1H, C-3), 7.44 (ddd, $J = 7.5, 4.8, 1.3\text{ Hz}$, 1H, C-2), 7.36 – 7.25 (m, 1H, C-12), 6.74 (dd, $J = 8.3, 1.2\text{ Hz}$, 1H, C-10), 6.63 (dt, $J = 8.2, 7.0, 1.1\text{ Hz}$, 1H, C-11), 6.42 – 6.18 (s, 2H, N-13). $^{13}\text{C NMR}$ (75 MHz, CDCl_3) δ 196.08 (C-6), 157.49 (C-5), 151.80 (C-9), 148.47 (C-4), 136.92 (C-1), 135.04 (C-12), 134.84 (C-8), 124.98 (C-2), 123.91 (C-3), 117.03 (C-10), 116.77 (C-11), 115.62 (C-7).

8.3.2. *N*-(2-picolinoylphenyl)acetamide (88)



A mixture of (2-aminophenyl)(pyridine-2-yl) methanone (198.22 g/mol, 0.8156 g, 4.11 mmol, 1.0 eq.), anhydrous sodium acetate (82.03 g/mol, 0.5407 g, 6.59 mmol, 1.5 eq.) and acetic anhydride (102.09 g/mol, 1.56 ml, 16.50 mmol, 4.0 eq.) in toluene (60.00 ml) was heated to $110\text{ }^{\circ}\text{C}$ and left to react overnight. The reaction was then left to cool down and cold H_2O was added. The organic layer was extracted and washed with H_2O (20.00 ml), collected, dried with anhydrous sodium sulphate and then concentrated *in vacuo*. The product was a yellow oil with a yield of 98 % (0.9701 g), with an R_f value of 0.44 (3:1; EtOAc: Hexane). $^1\text{H NMR}$ (300 MHz, Chloroform-*d*) δ 11.09 (s, 1H, N-13), 8.78 – 8.59 (m, 2H, C-4, C-8), 7.97 – 7.82 (m, 2H, C-1, C-3), 7.77 (dd, $J = 8.0, 1.6\text{ Hz}$, 1H, C-2), 7.57 (dt, $J = 8.7, 7.3, 1.7\text{ Hz}$, 1H, C-11), 7.49 (dt, $J = 6.8, 4.8, 1.9\text{ Hz}$, 1H, C-12), 7.08 (dt, $J = 8.3, 7.4, 1.2\text{ Hz}$, 1H, C-10), 2.24 (s, 3H, C-15). $^{13}\text{C NMR}$ (75 MHz, CDCl_3) δ 196.29 (C-6), 169.26 (C-14), 155.94 (C-5), 148.77 (C-4), 141.54 (C-9), 137.14 (C-1), 135.05 (C-7), 134.69 (C-12), 126.02 (C-8), 124.58 (C-10), 122.01 (C-2), 121.47 (C-3), 121.05 (C-11), 25.44 (C-15).

8.3.3. 2-(2-acetamidobenzoyl)-1-benzylpyridin-1-ium (89)



1.) To a stirring solution of Et₃N (101.19 g/mol, 0.80 ml, 5.74 mmol, 4.0 eq.) in dry AcCN (20.00 ml) was added *N*-(2-picolinoylphenyl)acetamide (240.26 g/mol, 0.3286 g, 1.37 mmol, 1.0 eq.) and BnCl (126.59 g/mol, 0.18 ml, 1.56 mmol, 1.1 eq.). The mixture was refluxed overnight. The solvent was removed *in vacuo*. EtOAc (20.00 ml) was added to the flask and extracted using 3 M NaOH (3 x 10.00 ml) and H₂O (2 x 10.00 ml). The solvent was removed, and the mixture was purified using column chromatography using EtOAc: Hexane (1:3) as eluent. No product formed.

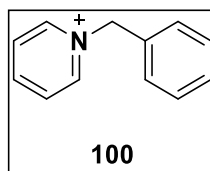
2.) The method is the same as in (1), except for the reaction time. The mixture was refluxed for 3 hours 30 minutes and then removed from heat. The mixture was then left to stir at room temperature overnight. There was also only degradation and no product formation observed on the NMR's.

3.) The method is the same as in (1), except for the reaction time. The mixture was refluxed for 3 hours whereafter it was removed from heat. The mixture was then left to stir at room temperature overnight. There was also only degradation and no product formation observed on the NMR's.

4.) The procedure was followed as in (2). After the addition of the EtOAc, before workup in (1.), Pd/C (106.42 g/mol, 0.0221 g, 0.21 mmol, 0.2 eq.) was added and was then connected to a hydrogenator with a H₂-gas cylinder attached at a pressure of 40 psi and left to react for 5 hours. The mixture was added onto celite and washed with MeOH in order to collect the organic fraction, unfortunately no product formed.

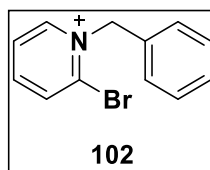
5.) The method is the same as in (3.). After the reaction was left to reflux for 3 hours, additional BnCl (1.1 eq.) and Et₃N (3.1 eq.) was added to the mixture. The mixture was then left to stir at room temperature overnight. Only degradation and no product formation observed upon the analysis of the NMR data.

8.3.4. 1-benzylpyridin-1-ium (100)



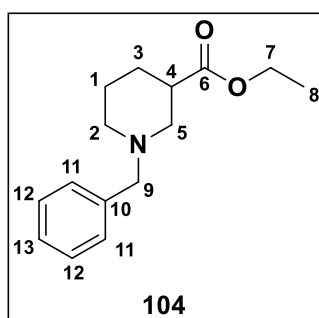
A mixture of pyridine (79.10 g/mol, 1.50 ml, 18.62 mmol, 1.0 eq.) and BnCl (126.59 g/mol, 2.20 ml, 19.12 mmol, 1.0 eq.) was stirred for 15 min at 0 °C, but no product formed yet. The mixture was left to stir at room temperature for 2 days. The solidification of a white and yellow precipitate formed. The mixture was extracted using DCM (3 x 5.00 ml), the organic layer was washed with H₂O (5.00 ml), dried over Na₂SO₄ and concentrated *in vacuo*. After column chromatography, it was determined through NMR analysis that the product did not form.

8.3.5. 1-benzyl-2-bromopyridin-1-ium (102)



BnCl (126.59 g/mol, 0.14 ml, 1.22 mmol, 1.2 eq.) was added to a stirring solution of 2-bromo-pyridine (158.00 g/mol, 0.12 ml, 1.24 mmol, 1.0 eq.) in 0.50 ml DCM. The mixture was left to stir at room temperature for 30 min but no product formed yet. The mixture was then left to stir at room temperature for 2 days. The mixture was extracted using DCM (3 x 5.00 ml), the organic layer was washed with H₂O (5.00 ml), dried over Na₂SO₄ and concentrated *in vacuo*. After column chromatography, it was determined through NMR analysis that the product did not form.

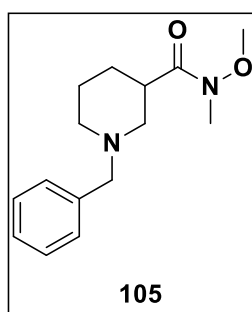
8.3.6. Ethyl 1-benzylpiperidine-3-carboxylate (104)



To a stirring mixture of Et₃N (101.19 g/mol, 18.00 ml, 129.85 mmol, 2.0 eq.) and dry AcCN (200.00 ml) was added ethyl nipecotate (157.21 g/mol, 10.10 ml, 65.08 mmol, 1.0 eq.) and BnCl (126.59 g/mol, 8.10 ml, 70.38 mmol, 1.1 eq.). The mixture was refluxed for 3 hours and then removed from heat in order to stir at room

temperature overnight. Solvent was removed *in vacuo*, whereafter 200.00 ml EtOAc was added and extracted with 3 M NaOH (3 x 40.00 ml) and H₂O (1 x 40.00 ml). Solvent was removed *in vacuo* and then purified using column chromatography using the eluent EtOAc: Hexane (1:3). A pure orange oil was collected with a yield of 99 % (15.8281 g), with an R_f value of 0.68 (3:2; EtOAc: Hexane). **¹H NMR (300 MHz, Chloroform-*d*)** δ 7.45 – 7.09 (m, 5H, Ar H's), 4.13 (q, *J* = 7.1 Hz, 2H, C-7), 3.62 – 3.44 (q, 2H, C-9), 3.02 – 2.91 (d, 1H, , C-5), 2.79 – 2.68 (d, 1H, C-5), 2.60 (tt, *J* = 10.1, 3.8 Hz, 1H, C-4), 2.26 (t, *J* = 10.5 Hz, 1H, C-2), 2.07 (td, *J* = 10.8, 3.1 Hz, 1H, C-2), 1.94 (dt, *J* = 12.4, 4.0 Hz, 1H, C-3), 1.74 (dt, *J* = 11.5, 6.1, 3.6 Hz, 1H, C-3), 1.69 – 1.42 (m, 2H, C-1), 1.25 (t, *J* = 7.2 Hz, 3H, C-8). **¹³C NMR (75 MHz, CDCl₃)** δ 174.28 (C-6), 138.40 (C-10), 129.03 (C-11), 128.19 (C-12), 126.97 (C-13), 63.33 (C-9), 60.23 (C-7), 55.46 (C-5), 53.65 (C-2), 41.94 (C-4), 26.99 (C-3), 24.58 (C-1), 14.24 (C-8).

8.3.7. 1-benzyl-*N*-methoxy-*N*-methylpiperidine-3-carboxamide (105)



1.) Propylmagnesium chloride (2 M; 102.84 g/mol, 9.32 ml, 81.20 mmol, 4.0 eq.) in dry ether (40.00 ml) was added dropwise to a mixture of 1-benzyl-nipecotic acid (247.16 g/mol, 5.0147 g, 20.29 mmol, 1.0 eq.) and *N,O*-dimethylhydroxylamine hydrochloride (97.54 g/mol, 3.9582 g, 40.58 mmol, 2.0 eq.) in dry THF (200.00 ml) at -20 °C. The reaction was stirred for 1 hour at -20 °C and then stirred overnight at room temperature. A saturated solution of ammonium chloride (100.00 ml) was then added. The organic layer was collected while the aqueous layer was extracted with ether (2 x 20.00 ml). The organic layers were combined, washed with NaCl (20.00 ml), dried and concentrated *in vacuo*. The reaction was unsuccessful.

2.) Trimethyl aluminium (2 M; 72.09 g/mol, 3.00 ml, 31.29 mmol, 1.5 eq.) was added dropwise to a stirring solution of *N,O*-dimethylhydroxylamine hydrochloride (97.54 g/mol, 3.0173 g, 30.93 mmol, 1.5 eq.) in dry DCM (100.00 ml) at 0 °C. The mixture was stirred at 0 °C for 20 min. After the dropwise addition of 1-benzyl-nipecotic acid (247.16 g/mol, 5.0555 g, 20.45 mmol, 1.0 eq.), the reaction was left to stir for 20 min at 0 °C and left to stir overnight at room temperature. DCM (41.00 ml) was added before adding 0.1 M HCl (4.05 ml) to the mixture and leaving the reaction to stir at 0 °C for 1 hour. Magnesium sulphate (120.37 g/mol, 1.3500 g, 11.22 mmol, 1.8 eq.) was added and left to stir at room temperature for 4 hours. The mixture was filtered and concentrated *in vacuo*. The reaction was unsuccessful.

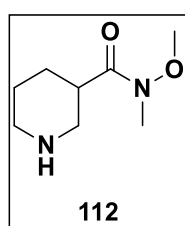
3.) Pyridine (79.10 g/mol, 3.00 ml, 37.24 mmol, 2.2 eq.) was added to a slurry of *N,O*-dimethylhydroxylamine

hydrochloride (97.54 g/mol, 2.1826 g, 22.38 mmol, 1.1 eq.) in dry DCM (41.00 ml) at 0 °C. Dropwise addition of 1-benzyl-nipecotic acid (247.16 g/mol, 4.1054 g, 16.61 mmol, 1.0 eq.), the mixture was then left to stir for 15 min at 0 °C, warmed to room temperature and left to stir for 20 hours. The reaction was then quenched with a saturated solution of NaHCO₃ and left to stir for 40 min. The organic layer was separated and washed with 6 M HCl (50.00 ml) and brine (50.00 ml). The aqueous layer was extracted with DCM (3 x 40.00 ml). The organic layers were combined, dried, filtered and concentrated *in vacuo*. The reaction was unsuccessful.

4.) Pyridine (79.10 g/mol, 1.00 ml, 12.41 mmol, 2.2 eq.) was added to a slurry of *N,O*-dimethylhydroxylamine hydrochloride (97.54 g/mol, 0.5997 g, 6.15 mmol, 1.1 eq.) in dry DCM (15.00 ml) at 0 °C. Dropwise addition of 1-benzylpiperidine-3-carbonyl chloride hydrochloride (237.09 g/mol, 1.3208 g, 5.57 mmol, 1.0 eq.), the mixture was then left to stir for 15 min at 0 °C, warmed to room temperature and left to stir for 4 days. The reaction was then quenched with a saturated solution of NaHCO₃ and left to stir for 40 min. The organic layer was separated and washed with 6 M HCl (50.00 ml) and brine (50.00 ml). The aqueous layer was extracted with DCM (3 x 40.00 ml). The organic layers were combined, dried, filtered and concentrated *in vacuo*. The reaction was unsuccessful.

5.) A mixture of HCl (20 %, 14.15 ml) and ethyl 1-benzylpiperidine-3-carboxylate (247.16 g/mol, 2.0050 g, 8.11 mmol, 1.0 eq.) was refluxed for 4 hours. The reaction was cooled down, and water is blown off to give the carboxylic acid. The solid was then dissolved in thionyl chloride and under inert atmosphere it was stirred at room temperature for 1 hour. Thionyl chloride was removed *in vacuo*, and dry THF was added to azeotrope the acid chloride. Pyridine (79.10 g/mol, 1.44 ml, 17.88 mmol, 2.2 eq.) was added to a slurry of *N,O*-dimethylhydroxylamine hydrochloride (97.54 g/mol, 0.8756 g, 8.98 mmol, 1.1 eq.) in dry THF (16.50 ml) at 0 °C. The acid chloride was then added dropwise, and the mixture was then left to stir for 15 min at 0 °C. The reaction was warmed to room temperature and left to stir for 5 days. The reaction was then quenched with a saturated solution of KHCO₃ and left to stir for 40 min. The organic layer was separated and washed with 6 M HCl (50.00 ml) and brine (50.00 ml). The aqueous layer was extracted with DCM (3 x 40.00 ml). The organic layers were combined, dried, filtered and concentrated *in vacuo*. NMR indicated that the reaction was unsuccessful.

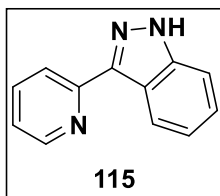
8.3.8. *N*-methoxy-*N*-methylpiperidine-3-carboxamide (112)



Trimethyl aluminium (2 M; 72.09 g/mol, 3.82 ml, 39.85 mmol, 2.0 eq.) was added dropwise to a stirring

solution of *N,O*-dimethylhydroxylamine hydrochloride (97.54 g/mol, 0.7707 g, 7.90 mmol, 2.0 eq.) in dry DCM (25.00 ml) at 0 °C. The mixture was stirred at 0 °C for 20 min. After the dropwise addition of ethyl nipecotate (157.21 g/mol, 0.6007 g, 3.82 mmol, 1.0 eq.), the reaction was left to stir for 20 min at 0 °C and left to stir overnight at room temperature. DCM (41.00 ml) was added before adding 0.1 M HCl (4.05 ml) and leaving the reaction to stir at 0 °C for 1 hour. Magnesium sulphate was added and left to stir at room temperature for 4 hours. The mixture was filtered and concentrated *in vacuo*. The reaction was unsuccessful.

8.3.9. 3-(pyridin-2-yl)-1*H*-indazole (115)



1) A solution of (2-aminophenyl)(pyridine-3-yl) methanone (198.22 g/mol, 0.4308 g, 2.17 mmol, 1.0 eq.) and dry AcCN (6.00 ml) was cooled to 0 °C. Dropwise addition of methanolic hydrochloric acid (68.50 g/mol, 0.80 ml, 2.40 mmol, 1.1 eq.) and then isopentyl nitrite (117.15 g/mol, 0.32 ml, 2.39 mmol, 1.1 eq.). The mixture was then left to stir overnight. THF was added and then filtered, the solids collected were washed with cold THF. The reaction was unsuccessful.

2) A solution of sodium nitrate (84.99 g/mol, 0.1221 g, 1.44 mmol, 1.3 eq.) in H₂O (0.50 ml) was added dropwise to a solution of (2-aminophenyl)(pyridine-3-yl) methanone (198.22 g/mol, 0.2191 g, 1.11 mmol, 1.0 eq.) in 6 M HCl (10.00 ml) and THF (12.00 ml) at -15 °C. The mixture was stirred for 30 min in an ice bath. Calcium chloride (110.98 g/mol, 0.3435 g, 3.10 mmol, 2.8 eq.) in CHCl₃ (2.00 ml) was added dropwise and stirred for 30 min. The mixture was filtered, but no solids were present. The solvent was then removed and dissolved in EtOAc. The mixture was then washed with a saturated sodium bicarbonate solution. The mixture was neutralized with NaOH and extracted using DCM (3 x 20.00 ml). The organic layer was collected, dried, filtered and concentrated *in vacuo*. The reaction was unsuccessful.

3) A mixture of (2-aminophenyl)(pyridine-2-yl) methanone (198.22 g/mol, 0.6762 g, 3.41 mmol, 1.0 eq.) and H₂SO₄ (50 %; 7.00 ml) was cooled to 0 °C, sodium nitrate (84.99 g/mol, 0.3508 g, 4.13 mmol, 1.2 eq.) was then slowly added. The mixture was then left to stir at room temperature for 1 hour. Tin(II)chloride (225.63 g/mol, 2.3167 g, 10.27 mmol, 3.0 eq.) was then added and stirred for 1 hour at 0 °C, and the mixture was then diluted with H₂O. The organic layer was extracted, washed with DCM (3 x 20.00 ml) and brine (1 x 20.00 ml). The reaction was unsuccessful.

4) A mixture of (2-aminophenyl)(pyridine-2-yl)methanone (198.22 g/mol, 0.5014 g, 2.53 mmol, 1.0 eq.) and CHCl₃ (3.32 ml) was cooled to 0 °C. A solution of sodium nitrite (3.6 M; 68.99 g/mol, 0.1935 g, 2.80 mmol, 1.1

eq.) in H₂O (0.77 ml) was then added dropwise and then left to stir for 1 hour at 0 °C. A solution of SnCl₂ (225.63 g/mol, 1.3730 g, 6.09 mmol, 2.4 eq.) in CHCl₃ (1.78 ml) was then added dropwise and left to stir for 2 hours at 0 °C. The reaction was then left to warm to room temperature and extracted with DCM (3 x 20.00 ml) and washed with brine (30.00 ml). The organic layer was dried, filtered and concentrated *in vacuo* to give yellow solids, which was not the desired product.

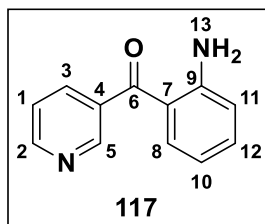
5) A mixture of (2-aminophenyl)(pyridine-2-yl)methanone (198.08 g/mol, 0.2395 g, 1.21 mmol, 1.0 eq.) and NH₂OH·HCl (69.49 g/mol, 0.2650 g, 3.81 mmol, 3.0 eq.) was stirred in a solution of H₂O (0.19 ml) and EtOH (1.02 ml). NaOH (40.00 g/mol, 0.3903 g, 9.76 mmol, 8.0 eq.) was added to the solution under an N-atmosphere. The mixture was then refluxed for 2 hours. The mixture was concentrated *in vacuo*, dissolved in H₂O and extracted with EtOAc (2 x 10.00 ml), dried and concentrated *in vacuo*. The residue was dissolved in DCM (1.10 ml) and left to stir at room temperature for 15 min. The mixture was cooled to 0-5 °C. A mixture of methanesulfonyl chloride (114.55 g/mol, 0.1872 g, 1.63 mmol, 1.3 eq.) in DCM (3.40 ml) was cooled to 0-5 °C and then added dropwise to the starting material flask. Et₃N (101.19 g/mol, 0.34 ml, 2.44 mmol, 2.0 eq.) was added to the flask. The mixture was then left to stir at 0-5 °C overnight. The mixture was purified with column chromatography, but NMR indicated that the reaction was unsuccessful.

6) A mixture of (2-aminophenyl)(pyridine-2-yl)methanone (198.08 g/mol, 0.2132 g, 1.08 mmol, 1.0 eq.) and NH₂OH·HCl (69.49 g/mol, 0.2275 g, 3.27 mmol, 3.0 eq.) in H₂O (0.17 ml) and EtOH (0.91 ml) was added NaOH (0.88 ml) under N-atmosphere at 0 °C. Subsequent to the addition, the mixture was refluxed at 80 °C for 2 hours. The mixture was then concentrated and dissolved in H₂O and extracted with EtOAc (2 x 20.00 ml). The organic layer was dried and concentrated *in vacuo*. The residue was dissolved in DCM (10.00 ml) and Et₃N (101.19 g/mol, 0.30 ml, 2.15 mmol, 2.0 eq.) which was added via a syringe. The reaction mixture was left to stir for 15 min. at room temperature and then cooled to 0-5 °C. Thionyl chloride (118.97 g/mol, 0.2667 g, 2.24 mmol, 1.3 eq.) in DCM (30.00 ml) was cooled to 0-5 °C before being added in a dropwise manner to the reaction mixture. The mixture was left to stir for 1.5 hours. The mixture was purified with column chromatography, but NMR indicated that the reaction was unsuccessful.

7) A mixture of (2-aminophenyl)(pyridine-2-yl)methanone (198.08 g/mol, 0.2149 g, 1.08 mmol, 1.0 eq.) and NH₂OH·HCl (69.49 g/mol, 0.2302 g, 3.31 mmol, 3.0 eq.) was stirred in a solution of H₂O (0.17 ml) and EtOH (0.92 ml). NaOH (40.00 g/mol, 0.3729 g, 9.32 mmol, 8.0 eq.) was added to the solution under an N-atmosphere and left to stir at room temperature for 1 hour. The mixture was then refluxed for 1 hour. The mixture was concentrated *in vacuo*, dissolved in H₂O and extracted with EtOAc (2 x 10.00 ml), dried and concentrated *in vacuo*. The residue was dissolved in DCM (1.10 ml) and then Et₃N (101.19 g/mol, 0.30 ml, 2.15 mmol, 2.0 eq.) was added whereafter the mixture was left to stir at room temperature for 15 min. The mixture was cooled to 0-5 °C. A mixture of tosyl chloride (190.65 g/mol, 0.2746 g, 1.44 mmol, 1.3 eq.) in DCM

(3.02 ml) was cooled to 0-5 °C and then added dropwise to the starting material flask. The mixture was then left to stir at 0-5 °C overnight. The mixture was purified by column chromatography, but NMR indicated that the reaction was unsuccessful.

8.3.10. (2-aminophenyl)(pyridin-3-yl)methanone (**117**)



1) A mixture of 2-aminobenzonitrile (118.14 g/mol, 0.2084 g, 1.76 mmol, 1.0 eq.) and 3-bromopyridine (158.00 g/mol, 0.4763 g, 3.01 mmol, 1.7 eq.) in 6.00 mL dry toluene was kept under Ar atmosphere at -50 °C. n-BuLi (1.6 M; 64.06 g/mol, 2.76 ml in hexanes, 4.40 mmol, 2.5 eq.) was added to the mixture and then left to stir for 1 hour at -50 °C. The solution was then warmed to 0 °C whereafter 3 M HCl (3.00 ml) was added to the solution, keeping the temperature below 10 °C. The organic layer was collected and extracted with 3 M HCl (2 x 3.00 ml). The combined aqueous fractions were basified to pH 10 using a 3 M NaOH solution. The mixture was kept in the fridge overnight. The brown crystals were collected and dried. The impure yield (35 %) to be used with the following reaction products to purify simultaneously and isolate the product. This was not possible due to the next couple of test reactions not being successful.

2) The same procedure was followed as in a, but changing solvent to dry THF. The reaction was unsuccessful.

3) The same procedure was followed as in a, but changing solvent to dry ether. The reaction was unsuccessful.

d) A mixture of 2-aminobenzonitrile (118.14 g/mol, 0.2078 g, 1.76 mmol, 1.0 eq.) and 3-bromopyridine (158.00 g/mol, 0.4763 g, 3.01 mmol, 1.7 eq.) in 6.00 mL dry toluene was kept under Ar atmosphere at -70 °C. n-BuLi (1.6 M; 64.06 g/mol, 2.75 ml in hexanes, 4.40 mmol, 2.5 eq.) was added to the mixture and then left to stir for 1 hour at -70 °C. The solution was then warmed to 0 °C whereafter 3 M HCl (3.00 ml) was added to the solution, keeping the temperature below 10 °C. The organic layer was collected and extracted with 3 M HCl (2 x 3.00 ml). The combined aqueous fractions were basified to pH 10 using a 3 M NaOH solution. The mixture was kept in the fridge overnight. The brown crystals were collected and dried.

4) The same procedure was followed as in (1.), but changing solvent to dry THF. The reaction was unsuccessful.

5) The same procedure was followed as in (1.), but changing solvent to dry ether. The reaction was unsuccessful.

6) A mixture of 2-aminobenzonitrile (118.14 g/mol, 0.2099 g, 1.78 mmol, 1.0 eq.) and 3-bromopyridine

(158.00 g/mol, 0.4783 g, 3.03 mmol, 1.7 eq.) in 5.50 ml dry ether were kept under Ar atmosphere at $-50\text{ }^{\circ}\text{C}$. n-BuLi (1.6 M; 64.06 g/mol, 2.78 ml in hexanes, 4.44 mmol, 2.5 eq.) was added to the mixture and then left to stir overnight at $-50\text{ }^{\circ}\text{C}$. The solution was then warmed to $0\text{ }^{\circ}\text{C}$ whereafter 3 M HCl (3.00 ml) was added to the solution, keeping the temperature below $10\text{ }^{\circ}\text{C}$. The organic layer was collected and extracted with 3 M HCl (2 x 3.00 ml). The combined aqueous fractions were basified to pH 8.53, adding potassium carbonate very slowly. The mixture was kept in the fridge for 3 days. The brown crystals were collected and dried. The product did not form.

7) The same procedure was followed as in (6), but the eq. of n-BuLi added was changed to 3.0. The reaction was unsuccessful.

8) The same procedure was followed as in (6), but the eq. of n-BuLi added was altered to 4.0. The result was unsuccessful.

9) The same procedure was followed as in (6), but the eq. of n-BuLi added was changed to 5.0. The reaction was ineffective.

10) The same procedure was followed as in (6), but the eq. of n-BuLi added was altered to 3.0, and the 3-bromopyridine eq. was increased to 2.0. The reaction time was for 3 hours at $-50\text{ }^{\circ}\text{C}$. The reaction was unsuccessful.

11) The same procedure was followed as in (10), but the eq. of 3-bromopyridine was decreased to 1.8. The result was unsuccessful.

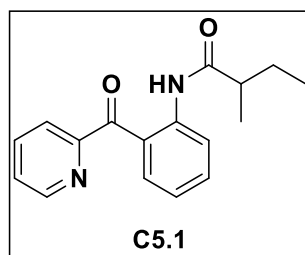
m) A mixture of 2- aminobenzonitrile (118.14 g/mol, 2.1324 g, 18.05 mmol, 1.0 eq.) and 3-bromopyridine (158.00 g/mol, 4.8535 g, 30.72 mmol, 1.7 eq.) in 60.00 ml dry ether were kept under Ar atmosphere at $-50\text{ }^{\circ}\text{C}$. n-BuLi (1.6 M; 64.06 g/mol, 33.84 ml in hexanes, 54.14 mmol, 3.0 eq.) was added to the mixture and then left to stir at $-50\text{ }^{\circ}\text{C}$ for 3 hours and then left to stir for 6 days. The solution was then cooled to $0\text{ }^{\circ}\text{C}$ whereafter 3 M HCl (60.00 ml) was added to the solution, keeping the temperature below $10\text{ }^{\circ}\text{C}$. The organic layer was collected and extracted with 3 M HCl (2 x 30.00 ml). The combined aqueous fractions were basified to pH 10 using a 3 M NaOH solution. The mixture was kept in the fridge overnight. The brown crystals were collected and dried. No desired product was collected.

12) **Batch 1:** A mixture of 2- aminobenzonitrile (118.14 g/mol, 2.2750 g, 19.26 mmol, 1.0 eq.) and 3-bromopyridine (158.00 g/mol, 5.1918 g, 32.86 mmol, 1.7 eq.) in 57.00 mL dry toluene was kept under inert conditions at $-50\text{ }^{\circ}\text{C}$. n-BuLi (1.6 M; 64.06 g/mol, 24.10 mL in hexanes, 38.56 mmol, 2.0 eq.) was added to the mixture and then left to stir 1 hour and 30 min at $-50\text{ }^{\circ}\text{C}$. The solution was then warmed to $0\text{ }^{\circ}\text{C}$ whereafter 3 M HCl (60.00 ml) was added to the solution, keeping the temperature below $10\text{ }^{\circ}\text{C}$. The organic layer was collected and extracted with 3 M HCl (2 x 30.00 ml). The combined aqueous fractions were basified to pH 10 using a 6 M NaOH solution and extracted with DCM, concentrated *in vacuo* and columned with batch 2.

Batch 2: A mixture of 2-aminobenzonitrile (118.14 g/mol, 2.0538 g, 17.38 mmol, 1.0 eq.) and 3-bromopyridine (158.00 g/mol, 4.6800 g, 29.62 mmol, 1.7 eq.) in 55.00 mL dry toluene was kept under inert conditions at $-50\text{ }^{\circ}\text{C}$. n-BuLi (1.6 M; 64.06 g/mol, 22.00 ml in hexanes, 38.20 mmol, 2.0 eq.) was added to the mixture and then left to stir 1 hour and 30 min at $-50\text{ }^{\circ}\text{C}$ and left to stir at room temperature overnight. The solution was then warmed to $0\text{ }^{\circ}\text{C}$ whereafter 3 M HCl (60.00 ml) was added to the solution, keeping the temperature below $10\text{ }^{\circ}\text{C}$. The organic layer was collected and extracted with 3 M HCl (2 x 30.00 ml). The combined aqueous fractions were basified to pH 10 using a 6 M NaOH solution and extracted with DCM, concentrated *in vacuo* and columned with batch 1.

Bath 1 and 2 were combined and columned using EtOAc: Hexane (1:3) in order to collect the pure product. The product was a dark yellow solid with a yield of 10 % (0.7367 g), with an R_f value of 0.26 (1:3; EtOAc: Hexane). $^1\text{H NMR}$ (300 MHz, Chloroform-*d*) δ 8.84 (d, $J = 2.2$ Hz, 1H, C-5), 8.77 – 8.69 (d, 1H, C-2), 7.96 – 7.87 (d, 1H, C-3), 7.40 (t, $J = 5.1$ Hz, 2H, C-1, C-8), 7.28 (td, $J = 7.7, 6.8, 1.6$ Hz, 1H, C-12), 6.73 (d, $J = 8.4$ Hz, 1H, C-10), 6.58 (t, $J = 7.5$ Hz, 1H, C-11), 6.32 (s, 2H, N-13). $^{13}\text{C NMR}$ (75 MHz, CDCl_3) δ 196.54 (C-6), 151.54 (C-2), 151.37 (C-9), 149.81 (C-5), 136.47 (C-3), 135.76 (C-4), 134.93 (C-12), 134.20 (C-8), 123.16 (C-1), 117.34 (C-10), 117.21 (C-11), 115.67 (C-7).

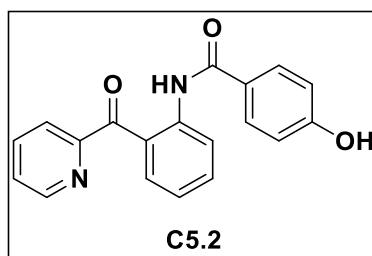
8.3.11. 2-methyl-*N*-(2-picolinoylphenyl)butanamide (C5.1)



A mixture of 2-methylbutanoic acid (102.13 g/mol, 0.2093 g, 2.05 mmol, 1.0 eq.) and EDC-HCl (191.70 g/mol, 0.3820 g, 1.99 mmol, 2.0 eq.) was added to dry DCM and left to stir at room temperature for 2 hours under inert conditions. A solution of (2-aminophenyl)(pyridin-2-yl)methanone (198.08 g/mol, 0.2078 g, 1.05 mmol, 1.0 eq.) in DMAP (122.17 g/mol, 0.1787 g, 1.46 mmol, 1.5 eq.) and dry DCM was added to the first mixture at $0\text{ }^{\circ}\text{C}$ and left to stir for 5 min. The mixture was warmed to room temperature and left to stir overnight. The product is a yellow oil with a yield of 22 % (0.1287 g), with an R_f value of 0.21 (1:3; EtOAc: Hexane). $^1\text{H NMR}$ (300 MHz, Chloroform-*d*) δ 11.22 (s, 1H, N-13), 8.78 (d, $J = 8.5, 1.1$ Hz, 1H, C-4), 8.70 (d, $J = 4.8, 1.3$ Hz, 1H, C-11), 7.95 – 7.81 (dt, 2H, C-1; C-8), 7.76 (dd, $J = 8.0, 1.7$ Hz, 1H, C-3), 7.56 (dt, $J = 8.7, 7.3, 1.7$ Hz, 1H, C-2), 7.47 (dt, $J = 6.9, 4.8, 1.8$ Hz, 1H, C-12), 7.09 – 7.01 (dt, 1H, C-10), 2.40 (m, $J = 6.9$ Hz, 1H, C-15), 1.87 – 1.71 (m, 1H, C-17), 1.56 (m, $J = 14.1, 7.2$ Hz, 1H, C-17), 1.26 (d, $J = 6.9$ Hz, 3H, C-16), 0.96 (t, $J = 7.4$ Hz, 3H, C-18). $^{13}\text{C NMR}$ (75 MHz, CDCl_3) δ 197.36 (C-6), 175.87 (C-14), 156.03 (C-5), 148.73 (C-9), 141.92 (C-4), 137.10 (C-

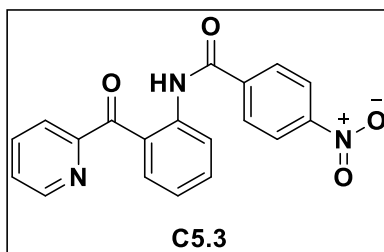
1), 135.10 (C-12), 134.85 (C-8), 125.93 (C-2), 124.51 (C-3), 121.79 (C-10), 121.26 (C-11), 120.94 (C-7), 44.94 (C-15), 27.37 (C-17), 17.32 (C-16), 11.87 (C-18).

8.3.12. 4-hydroxy-*N*-(2-picolinoylphenyl)benzamide (C5.2)

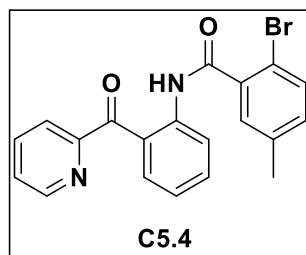


A mixture of 4-hydroxybenzoic acid (138.12 g/mol, 0.1456 g, 1.05 mmol, 1.0 eq.) and EDC-HCl (191.70 g/mol, 0.4090 g, 2.13 mmol, 2.1 eq.) was added to dry DCM and left to stir at room temperature for 2 hours, under inert conditions. A solution of (2-aminophenyl)(pyridin-2-yl)methanone (198.22 g/mol, 0.2064 g, 1.04 mmol, 1.0 eq.) in DMAP (122.17 g/mol, 0.1972 g, 1.61 mmol, 1.0 eq.) and dry DCM was added to the first mixture at 0 °C and left to stir for 5 min. The mixture was warmed to room temperature and left to stir overnight. The reaction was unsuccessful.

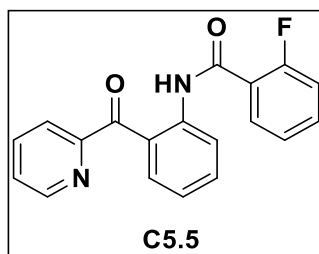
8.3.13. 4-nitro-*N*-(2-picolinoylphenyl)benzamide (C5.3)



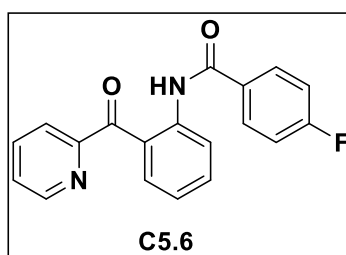
A mixture of 4-nitrobenzoic acid (167.12 g/mol, 0.1779 g, 1.06 mmol, 1.1 eq.) and EDC-HCl (191.70 g/mol, 0.3994 g, 2.08 mmol, 2.0 eq.) was added to dry DCM and left to stir at room temperature for 2 hours, under inert conditions. A solution of (2-aminophenyl)(pyridin-2-yl)methanone (198.08 g/mol, 0.2066 g, 1.04 mmol, 1.0 eq.) in DMAP (122.17 g/mol, 0.1910 g, 1.56 mmol, 1.0 eq.) and dry DCM was added to the first mixture at 0 °C and left to stir for 5 min. The mixture was warmed to room temperature and left to stir overnight. The reaction was unsuccessful.

8.3.14. 2-bromo-5-methyl-*N*-(2-picolinoylphenyl)benzamide (C5.4)

A mixture of 2-bromo-5-methylbenzoic acid (215.04 g/mol, 0.2179 g, 1.01 mmol, 1.0 eq.) and EDC-HCl (191.70 g/mol, 0.3944 g, 2.09 mmol, 2.0 eq.) was added to dry DCM and left to stir at room temperature for 2 hours, under inert conditions. A solution of (2-aminophenyl)(pyridin-2-yl)methanone (198.08 g/mol, 0.2008 g, 1.01 mmol, 1.0 eq.) in DMAP (122.17 g/mol, 0.1929 g, 1.58 mmol, 1.0 eq.) and dry DCM was added to the first mixture at 0 °C and left to stir for 5 min. The mixture was warmed to room temperature and left to stir overnight. The reaction was unsuccessful.

8.3.15. 2-fluoro-*N*-(2-picolinoylphenyl)benzamide (C5.5)

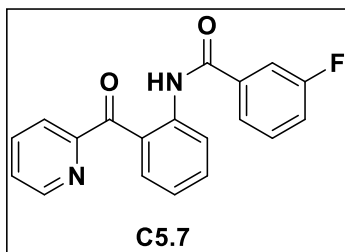
A mixture of 2-fluorobenzoic acid (140.11 g/mol, 0.1450 g, 1.03 mmol, 1.0 eq.) and EDC-HCl (191.70 g/mol, 0.3947 g, 2.06 mmol, 2.0 eq.) was added to dry DCM and left to stir at room temperature for 2 hours, under inert conditions. A solution of (2-aminophenyl)(pyridin-2-yl)methanone (198.08 g/mol, 0.2017 g, 1.02 mmol, 1.0 eq.) in DMAP (122.17 g/mol, 0.1849 g, 1.51 mmol, 1.0 eq.) and dry DCM was added to the first mixture at 0 °C and left to stir for 5 min. The mixture was warmed to room temperature and left to stir overnight. The reaction was unsuccessful.

8.3.16. 4-fluoro-*N*-(2-picolinoylphenyl)benzamide (C5.6)

A mixture of 4-fluorobenzoic acid (140.11 g/mol, 0.1458 g, 1.04 mmol, 1.0 eq.) and EDC-HCl (191.70 g/mol, 0.3927 g, 2.05 mmol, 2.0 eq.) was added to dry DCM and left to stir at room temperature for 2 hours, under

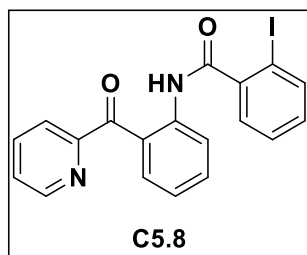
inert conditions. A solution of (2-aminophenyl)(pyridin-2-yl)methanone (198.08 g/mol, 0.2028 g, 1.02 mmol, 1.0 eq.) in DMAP (122.17 g/mol, 0.1912 g, 1.57 mmol, 1.0 eq.) and dry DCM was added to the first mixture at 0 °C and left to stir for 5 min. The mixture was warmed to room temperature and left to stir overnight. The reaction was unsuccessful.

8.3.17. 3-fluoro-*N*-(2-picolinoylphenyl)benzamide (C5.7)

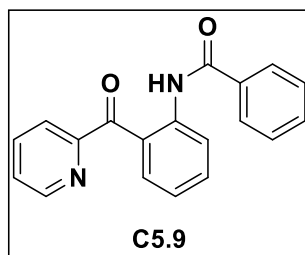


A mixture of 3-fluorobenzoic acid (140.11 g/mol, 0.1482 g, 1.06 mmol, 1.0 eq.) and EDC-HCl (191.70 g/mol, 0.4079 g, 2.14 mmol, 2.0 eq.) was added to dry DCM and left to stir at room temperature for 2 hours, under inert conditions. A solution of (2-aminophenyl)(pyridin-2-yl)methanone (198.08 g/mol, 0.2078 g, 1.05 mmol, 1.0 eq.) in DMAP (122.17 g/mol, 0.1974 g, 1.62 mmol, 1.0 eq.) and dry DCM was added to the first mixture at 0 °C and left to stir for 5 min. The mixture was warmed to room temperature and left to stir overnight. The reaction was unsuccessful.

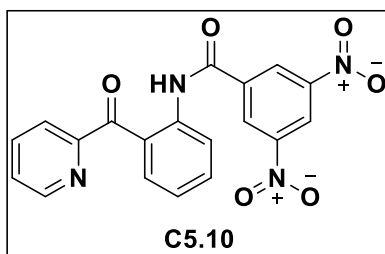
8.3.18. 2-iodo-*N*-(2-picolinoylphenyl)benzamide (C5.8)



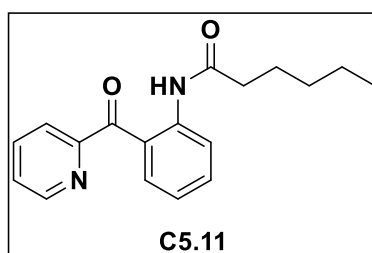
A mixture of 2-iodobenzoic acid (248.02 g/mol, 0.2556 g, 1.03 mmol, 1.0 eq.) and EDC-HCl (191.70 g/mol, 0.3944 g, 2.06 mmol, 2.0 eq.) was added to dry DCM and left to stir at room temperature for 2 hours, under inert conditions. A solution of (2-aminophenyl)(pyridin-2-yl)methanone (198.22 g/mol, 0.2039 g, 1.03 mmol, 1.0 eq.) in DMAP (122.17 g/mol, 0.1871 g, 1.53 mmol, 1.0 eq.) and dry DCM was added to the first mixture at 0 °C and left to stir for 5 min. The mixture was warmed to room temperature and left to stir overnight. The reaction was unsuccessful.

8.3.19. *N*-(2-picolinoylphenyl)benzamide (C5.9)

A mixture of benzoic acid (122.12 g/mol, 0.1294 g, 1.06 mmol, 1.0 eq.) and EDC-HCl (191.70 g/mol, 0.3891 g, 2.03 mmol, 2.0 eq.) was added to dry DCM and left to stir at room temperature for 2 hours, under inert conditions. A solution of (2-aminophenyl)(pyridin-2-yl)methanone (198.22 g/mol, 0.2031 g, 1.02 mmol, 1.0 eq.) in DMAP (122.17 g/mol, 0.1888 g, 1.55 mmol, 1.0 eq.) and dry DCM was added to the first mixture at 0 °C and left to stir for 5 min. The mixture was warmed to room temperature and left to stir overnight. The reaction was unsuccessful.

8.3.20. 3,5-dinitro-*N*-(2-picolinoylphenyl)benzamide (C5.10)

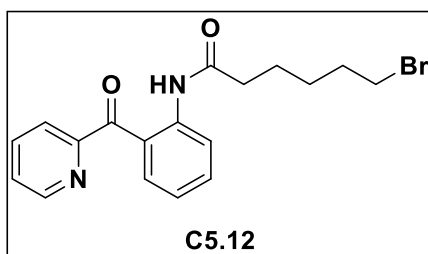
A mixture of 3,5-dinitrobenzoic acid (212.12 g/mol, 0.2190 g, 1.03 mmol, 1.0 eq.) and EDC-HCl (191.70 g/mol, 0.3937 g, 2.05 mmol, 2.0 eq.) was added to dry DCM and left to stir at room temperature for 2 hours, under inert conditions. A solution of (2-aminophenyl)(pyridin-2-yl)methanone (198.08 g/mol, 0.2073 g, 1.03 mmol, 1.0 eq.) in DMAP (122.17 g/mol, 0.1877 g, 1.54 mmol, 1.0 eq.) and dry DCM was added to the first mixture at 0 °C and left to stir for 5 min. The mixture was warmed to room temperature and left to stir overnight. The reaction was unsuccessful.

8.3.21. *N*-(2-picolinoylphenyl)hexanamide (C5.11)

A mixture of hexanoic acid (116.16 g/mol, 0.1200 g, 1.03 mmol, 1.0 eq.) and EDC-HCl (191.70 g/mol, 0.4031

g, 2.10 mmol, 2.0 eq.) was added to dry DCM and left to stir at room temperature for 2 hours under inert conditions. A solution of (2-aminophenyl)(pyridin-2-yl)methanone (198.08 g/mol, 0.2070 g, 1.04 mmol, 1.0 eq.) in DMAP (122.17 g/mol, 0.1961 g, 1.61 mmol, 1.6 eq.) and dry DCM was added to the first mixture at 0 °C and left to stir for 5 min. The mixture was warmed to room temperature and left to stir overnight. The reaction was unsuccessful.

8.3.22. 6-bromo-*N*-(2-picolinoylphenyl)hexanamide (C5.12)

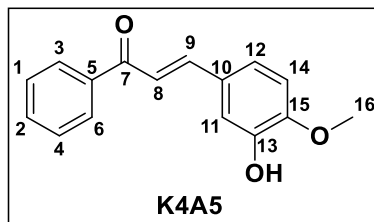


A mixture of 6-bromohexanoic acid (195.05 g/mol, 0.2049 g, 1.05 mmol, 1.0 eq.) and EDC-HCl (191.70 g/mol, 0.4111 g, 2.14 mmol, 2.0 eq.) was added to dry DCM and left to stir at room temperature for 2 hours under inert conditions. A solution of (2-aminophenyl)(pyridin-2-yl)methanone (198.08 g/mol, 0.2069 g, 1.04 mmol, 1.0 eq.) in DMAP (122.17 g/mol, 0.1970 g, 1.61 mmol, 1.6 eq.) and dry DCM was added to the first mixture at 0 °C and left to stir for 5 min. The mixture was warmed to room temperature and left to stir overnight. The reaction was unsuccessful.

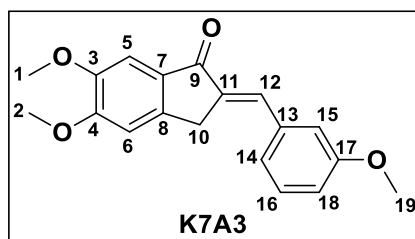
8.4. Experimental details relating to scaffold D

8.4.1. General procedure for the formation of α,β -unsaturated ketones with method 1:

NaOH pellets (3.0 eq.) was added to methanol (30.00 ml) and stirred at room temperature till all the NaOH was dissolved. The aldehyde (1.0 eq.) was added to the solution and then left to stir at room temperature for 10 min. The ketone (1.0 eq.) was added dropwise, keeping the solution's temperature at 0 °C. The solution was then left to stir overnight at room temperature. The solvent was evaporated *in vacuo*, and then extracted using EtOAc (30.00 ml) as 40.00 ml of H₂O was added. The organic layer was combined, dried with Na₂SO₄, concentrated, and purified using column chromatography (1:1; EtOAc: Hexane).

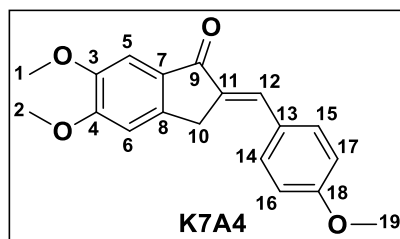
8.4.1.1. (*E*)-3-(3-hydroxy-4-methoxyphenyl)-1-phenylprop-2-en-1-one (K4A5)

NaOH (40.00 g/mol, 0.2722 g, 6.81 mmol, 3.6 eq.), 3-hydroxy-4-methoxybenzaldehyde (152.15 g/mol, 0.2838 g, 1.87 mmol, 1.0 eq.) and acetophenone (120.15 g/mol, 0.22 ml, 1.89 mmol, 1.1 eq.). The reaction was stirred overnight and after no significant amount of product was formed the reaction was refluxed for 3 days. The product collected were dark yellow crystals. Yield 63 % (0.3006 g), R_f value of 0.66 (1:1; EtOAc: Hexane). $^1\text{H NMR}$ (400 MHz, CDCl_3) δ 7.99-8.03 (m, $J = 8.4, 1.4$ Hz, 2H, C-3 and C-6), 7.73 (d, $J = 15.6$ Hz, 1H, C-9), 7.56 – 7.43 (m, 3H, C-1, C-4 and C-8), 7.40 (d, $J = 2.0$ Hz, 1H, C-2), 7.27 (d, $J = 2.1$ Hz, 1H, C-11), 7.09 (dd, $J = 8.4, 2.1$ Hz, 1H, C-14), 6.81 (d, $J = 8.4, 1.2$ Hz, 1H, C-12), 6.22 (s, 1H, C-13-OH), 3.84 (s, 3H, C-16). $^{13}\text{C NMR}$ (101 MHz, CDCl_3) δ 190.65 (C-7), 149.18 (C-15), 146.06 (C-9), 145.07 (C-13), 138.39 (C-5), 132.70 (C-2), 128.61 (C-1, C-4), 128.47 (C-3, C-6), 128.38 (C-10), 122.79 (C-12), 120.06 (C-8), 113.32 (C-11), 110.75 (C-14), 55.99 (C-16). HRMS m/z (ESI) 255.118 ($[\text{M}+\text{H}]^+$ requires 255.102).

8.4.1.2. (*E*)-5,6-dimethoxy-2-(3-methoxybenzylidene)-2,3-dihydro-1*H*-inden-1-one (K7A3)

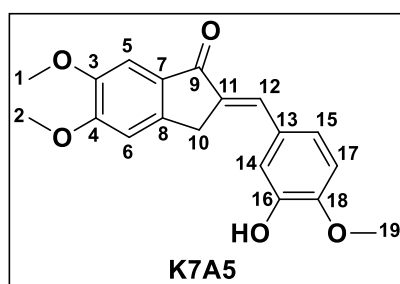
NaOH (40.00 g/mol, 0.5385 g, 13.46 mmol, 3.6 eq.), 3-methoxybenzaldehyde (136.15 g/mol, 0.5113 g, 3.76 mmol, 1.0 eq.) and 5,6-dimethoxyindenone (192.21 g/mol, 0.7225 g, 3.76 mmol, 1.0 eq.). The reaction was stirred overnight at room temperature. The product collected were light yellow-brown crystals. Yield 40 % (0.4649 g), R_f value of 0.25 (1:1; EtOAc: Hexane). $^1\text{H NMR}$ (300 MHz, CDCl_3) δ 7.63 – 7.56 (m, 2H, C-12 and C-16), 7.53 (d, $J = 2.0$ Hz, 1H, C-14), 7.28 (s, 1H, C-5), 6.96 (d, $J = 3.6$ Hz, 2H, C-6 and C-15), 6.94 (s, 1H, C-18), 3.99 (s, 3H, C-1), 3.93 (s, 3H, C-19), 3.88 (d, $J = 2.0$ Hz, 2H, C-10), 3.85 (s, 3H, C-2). $^{13}\text{C NMR}$ (101 MHz, CDCl_3) δ 193.24 (C-9), 160.61 (C-17), 155.19 (C-4), 149.56 (C-3), 144.66 (C-7), 133.13 (C-8), 132.31 (C-12 and C-16), 132.24 (C-11), 131.26 (C-14), 128.33 (C-13), 114.41 (C-15 and C-18), 107.19 (C-6), 105.04 (C-5), 56.27 (C-1), 56.16 (C-2), 55.38 (C-19), 32.17 (C-10). HRMS m/z (ESI) 311.147 ($[\text{M}+\text{H}]^+$ requires 311.128).

8.4.1.3. (*E*)-5,6-dimethoxy-2-(4-methoxybenzylidene)-2,3-dihydro-1*H*-inden-1-one (K7A4)



NaOH (40.00 g/mol, 0.5477 g, 13.69 mmol, 3.8 eq.), 4-anisaldehyde (98 %, 136.15 g/mol, 0.5026 g, 3.62 mmol, 1.0 eq.) and 5,6-dimethoxyindenone (192.21 g/mol, 0.7459 g, 3.88 mmol, 1.1 eq.). The reaction was stirred overnight at room temperature. The product collected were brown crystals. Yield 52 % (0.5883 g), R_f value of 0.24 (1:1; EtOAc: Hexane). $^1\text{H NMR}$ (400 MHz, CDCl_3) δ 7.55 (d, 2H, C-14 and C-15), 7.50 (s, 1H, C-12), 7.27 (s, 1H, C-5), 6.96 – 6.90 (m, 3H, C-6, C-16 and C-17), 3.97 (s, 3H, C-1), 3.91 (s, 3H, C-19), 3.83 (s, 5H, C-2 and C-10). $^{13}\text{C NMR}$ (101 MHz, CDCl_3) δ 193.22 (C-9), 160.57 (C-18), 155.16 (C-4), 149.48 (C-3), 144.68 (C-7), 133.05 (C-8), 132.27 (C-14 and C-15), 132.18 (C-12), 131.12 (C-11), 128.21 (C-13), 114.35 (C-16 and C-17), 107.15 (C-6), 104.91 (C-5), 56.22 (C-1), 56.06 (C-2), 55.33 (C-19), 32.10 (C-10). HRMS m/z (ESI) 311.146 ($[\text{M}-\text{H}]^+$ requires 311.128). The results correspond to previously published results [113].

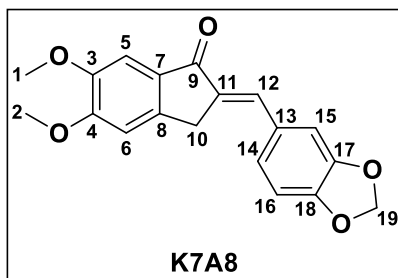
8.4.1.4. (*E*)-2-(3-hydroxy-4-methoxybenzylidene)-5,6-dimethoxy-2,3-dihydro-1*H*-inden-1-one (K7A5)



NaOH (40.00 g/mol, 0.4478 g, 11.20 mmol, 4.1 eq.), 3-hydroxy-4-methoxybenzaldehyde (99 %, 152.15 g/mol, 0.4151 g, 2.70 mmol, 1.0 eq.) and 5,6-dimethoxyindenone (192.21 g/mol, 0.5184 g, 2.70 mmol, 1.0 eq.). The reaction was stirred overnight at room temperature. The novel product was found in the aqueous layer and was blown off overnight where light-yellow crystals were collected. Yield 77 % (0.6790 g), R_f value of 0.13 (1:1; EtOAc: Hexane). $^1\text{H NMR}$ (400 MHz, CDCl_3) δ 7.51 (s, 1H, C-12), 7.34 (s, 1H, C-5), 7.30 (s, 1H, C-14), 7.16 (dd, $J = 8.4, 2.2$ Hz, 1H, C-15), 6.97 (s, 1H, C-6), 6.91 (d, $J = 8.4$ Hz, 1H, C-17), 5.78 (s, 1H, C-16-OH), 3.99 (s, 3H, C-19), 3.94 (dd, $J = 7.0, 1.7$ Hz, 8H, C-1, C-2 and C10). $^{13}\text{C NMR}$ (101 MHz, CDCl_3) δ 193.29 (C-9), 155.26 (C-4), 149.58 (C-18), 147.82 (C-3), 145.78 (C-16), 144.80 (C-7), 133.63 (C-8), 132.41 (C-12), 131.20 (C-11),

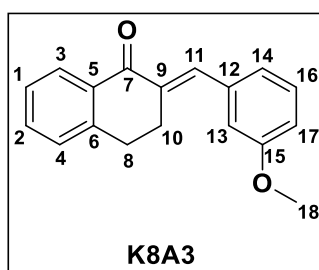
129.19 (C-13), 124.66 (C-15), 115.49 (C-6), 110.71 (C-14), 107.19 (C-17), 105.06 (C-5), 56.28 (C-1), 56.17 (C-2), 56.00 (C-19), 32.15 (C-10). HRMS m/z (ESI) 325.125 ($[M-H]^+$ requires 325.108).

8.4.1.5. (*E*)-2-(benzo[*d*][1,3]dioxol-5-ylmethylene)-5,6-dimethoxy-2,3-dihydro-1*H*-inden-1-one (K7A8)



NaOH (40.00 g/mol, 0.4374 g, 10.94 mmol, 4.2 eq.), piperonal (150.13 g/mol, 0.4006 g, 2.64 mmol, 1.0 eq.) and 5,6-dimethoxyindene (192.21 g/mol, 0.5065 g, 2.63 mmol, 1.0 eq.). The reaction was stirred overnight at room temperature. Addition of water and EtOAc resulted in most of the product to crash out of solution, liquid-liquid extraction of the left-over solution was used to collect the last of the product left over in the organic layer. The product collected were light yellow crystals. Yield 95 % (0.8083 g), R_f value of 0.18 (1:3; EtOAc: Hexane). $^1\text{H NMR}$ (300 MHz, CDCl_3) δ 7.51 (s, 1H, C-12), 7.34 (s, 1H, C-5), 7.18 (s, 2H, C-14 and C-15), 6.98 (s, 1H, C-6), 6.89 (d, $J = 7.8$ Hz, 1H, C-16), 6.05 (s, 2H, C-19), 4.01 (s, 3H, C-1), 3.96 (s, 3H, C-2), 3.91 (s, 2H, C-10). $^{13}\text{C NMR}$ (75 MHz, CDCl_3) δ 193.14 (C-9), 155.24 (C-4), 149.56 (C-17), 148.77 (C-18), 148.23 (C-3), 144.62 (C-7), 133.44 (C-8), 132.37 (C-12), 131.11 (C-11), 129.87 (C-13), 126.69 (C-14), 109.34 (C-6), 108.80 (C-15), 107.14 (C-16), 104.98 (C-5), 101.59 (C-19), 56.20 (C-1), 56.08 (C-2), 32.14 (C-10). HRMS m/z (ESI) 347.110 ($[M+Na]^+$ requires 347.089).

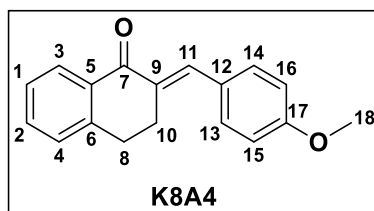
8.4.1.6. (*E*)-2-(3-methoxybenzylidene)-3,4-dihydronaphthalen-1(2*H*)-one (K8A3)



NaOH (40.00 g/mol, 0.5643 g, 14.11 mmol, 4.0 eq.), 3-methoxybenzaldehyde (136.15 g/mol, 0.5106 g, 3.75 mmol, 1.1 eq.) and tetralone (97 %, 146.19 g/mol, 0.5341 g, 3.54 mmol, 1.0 eq.). The reaction was stirred overnight at room temperature. The product collected was a dark brown oil. Yield 98 % (0.9185 g), R_f value of 0.80 (1:1; EtOAc: Hexane). $^1\text{H NMR}$ (400 MHz, CDCl_3) δ 8.09 (d, $J = 7.9$, 1.5 Hz, 1H, C-2), 7.81 (s, 1H, C-11), 7.44 – 7.34 (m, $J = 7.5$, 1.5 Hz, 1H, C-4), 7.26 (dd, 2H, C-1 and C-14), 7.15 (d, $J = 7.6$ Hz, 1H, C-16), 6.96 (d, $J =$

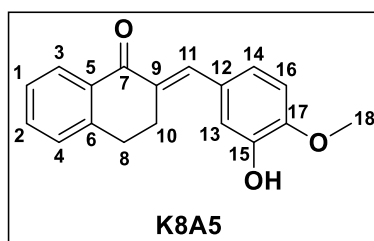
7.7 Hz, 1H, C-3), 6.91 (s, 1H, C-13), 6.83 (dd, $J = 8.3, 2.7$ Hz, 1H, C-17), 3.73 (s, $J = 1.6$ Hz, 3H, C-18), 3.02 (td, $J = 7.8, 3.9$ Hz, 2H, C-10), 2.87 – 2.69 (m, $J = 6.6$ Hz, 2H, C-8) [114]. ^{13}C NMR (101 MHz, CDCl_3) δ 187.55 (C-7), 159.56 (C-15), 143.26 (C-5), 137.11 (C-9), 136.42 (C-11), 135.70 (C-6), 133.43 (C-12), 133.29 (C-2), 129.50 (C-14), 128.26 (C-4), 128.12 (C-3), 126.98 (C-1), 122.26 (C-13), 115.43 (C-17), 114.11 (C-16), 55.19 (C-18), 28.75 (C-8), 27.23 (C-10). HRMS m/z (ESI) 282.279 ($[\text{M}+\text{NH}_4]^+$ requires 282.149).

8.4.1.7. (*E*)-2-(4-methoxybenzylidene)-3,4-dihydronaphthalen-1(2*H*)-one (K8A4)



NaOH (40.00 g/mol, 0.5069 g, 12.67 mmol, 3.3 eq.), *p*-anisaldehyde (98 %, 136.15 g/mol, 0.5389 g, 3.88 mmol, 1.0 eq.) and tetralone (97 %, 146.19 g/mol, 0.5738 g, 3.81 mmol, 1.0 eq.). The reaction was stirred overnight at room temperature. The product collected was dark brown crystals. Yield 91 % (0.9189 g), R_f value of 0.57 (1:3; EtOAc: Hexane). ^1H NMR (400 MHz, CDCl_3) δ 8.11 (d, $J = 7.8, 1.5$ Hz, 1H, C-2), 7.84 (s, 1H, C-11), 7.49 – 7.36 (m, $J = 7.4, 1.5$ Hz, 3H, C-4, C-13 and C-14), 7.35 (m, $J = 7.6, 1.3$ Hz, 1H, C-3), 7.23 (d, 1H, C-1), 6.94 (d, 2H, C-15 and C-16), 3.83 (s, 3H, C-18), 3.15 – 3.10 (m, $J = 6.9, 5.7, 1.8$ Hz, 2H, C-10), 2.93 (t, $J = 7.6, 5.4$ Hz, 2H, C-8). ^{13}C NMR (101 MHz, CDCl_3) δ 187.92 (C-7), 159.99 (C-17), 143.11 (C-5), 136.74 (C-11), 133.65 (C-6), 133.54 (C-9), 133.15 (C-2), 131.80 (C-13 and C-14), 128.39 (C-12), 128.15 (C-3), 128.13 (C-4), 126.99 (C-1), 113.98 (C-15 and C-16), 55.36 (C-18), 28.79 (C-8), 27.24 (C-10). HRMS m/z (ESI) 282.280 ($[\text{M}+\text{NH}_4]^+$ requires 282.149). The results correspond to previously published results [115].

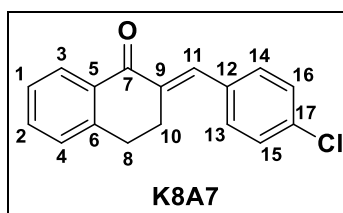
8.4.1.8. (*E*)-2-(3-hydroxy-4-methoxybenzylidene)-3,4-dihydronaphthalen-1(2*H*)-one (K8A5)



NaOH (40.00 g/mol, 0.5731 g, 14.33 mmol, 4.1 eq.), 3-hydroxy-4-methoxybenzaldehyde (99 %, 152.15 g/mol, 0.5322 g, 3.46 mmol, 1.0 eq.) and tetralone (97 %, 146.19 g/mol, 0.5062 g, 3.46 mmol, 1.0 eq.). The reaction was left to stir for 60 hours at room temperature. The novel product collected was dark yellow crystals. Yield 71 % (0.6879 g), R_f value of 0.53 (1:1; EtOAc: Hexane). ^1H NMR (300 MHz, CDCl_3) δ 8.14 (dd, $J = 7.8, 1.5$ Hz,

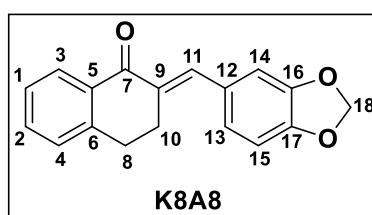
1H, C-2), 7.83 (s, 1H, C-11), 7.55 – 7.46 (m, J = 7.4, 1.5 Hz, 1H, C-4), 7.43 - 7.32 (m, J = 7.6, 1.4 Hz, 1H, C-3), 7.27 (d, 1H, C-1), 7.12 (d, J = 2.1 Hz, 1H, C-13), 7.02 (dd, J = 8.5, 2.1 Hz, 1H, C-14), 6.92 (d, J = 8.3 Hz, 1H, C-16), 5.81 (s, 1H, C-15-OH), 3.95 (s, 3H, C-18), 3.17 (dt, J = 6.9, 5.5, 1.8 Hz, 2H, C-8), 2.96 (t, J = 7.6, 5.4 Hz, 2H, C-10). ¹³C NMR (101 MHz, CDCl₃) δ 187.97 (C-7), 147.16 (C-17), 145.41 (C-15), 143.19 (C-5), 136.82 (C-11), 133.93 (C-6), 133.61 (C-9), 133.18 (C-2), 129.24 (C-12), 128.17 (C-3), 128.13 (C-4), 126.98 (C-1), 123.27 (C-14), 115.90 (C-13), 110.53 (C-16), 56.00 (C-18), 28.77 (C-8), 27.23 (C-10). HRMS m/z (ESI) 279.129 ([M-H]⁺ requires 279.103).

8.4.1.9. (*E*)-2-(4-chlorobenzylidene)-3,4-dihydronaphthalen-1(2*H*)-one (K8A7)



NaOH (40.00 g/mol, 0.5771 g, 14.43 mmol, 4.1 eq.), 4-chlorobenzaldehyde (97 %, 140.57 g/mol, 0.5078 g, 3.50 mmol, 1.0 eq.) and tetralone (97 %, 146.19 g/mol, 0.5280 g, 3.50 mmol, 1.0 eq.). The reaction was stirred overnight at room temperature. The product collected was dark brown crystals. Yield 93 % (0.8788 g), R_f value of 0.83 (1:1; EtOAc: Hexane). ¹H NMR (400 MHz, CDCl₃) δ: 8.12 (d, J = 7.8, 1.4 Hz, 1H, C-2), 7.79 (s, 1H, C-11), 7.52 - 7.45 (m, J = 7.5, 1.5 Hz, 1H, C-3), 7.31 – 7.42 (m, 5H, C-4, and C13-C16), 7.28 - 7.21 (m, J = 7.5 Hz, 1H, C-1), 3.12 – 3.05 (m, J = 6.8, 5.4, 1.8 Hz, 2H, C-10), 2.98 – 2.90 (m, J = 7.5, 5.3 Hz, 2H, C-8). ¹³C NMR (101 MHz, CDCl₃) δ 187.68 (C-7), 143.16 (C-5), 135.98 (C-9), 135.30 (C-11), 134.48 (C-12), 134.27 (C-6), 133.44 (C-2), 133.35 (C-17), 131.16 (C-13 and C-14), 128.74 (C-15 and C-16), 128.28 (C-1), 128.24 (C-3), 127.12 (C-4), 28.78 (C-8), 27.19 (C-10). HRMS m/z (ESI) 267.075 ([M-H]⁺ requires 267.057). The results correspond to previously published results [114].

8.4.1.10. (*E*)-2-(benzo[*d*][1,3]dioxol-5-ylmethylene)-3,4-dihydronaphthalen-1(2*H*)-one (K8A8)



NaOH (40.00 g/mol, 0.5513 g, 13.78 mmol, 3.9 eq.), piperonal (99 %, 150.13 g/mol, 0.5391 g, 3.55 mmol, 1.0 eq.) and tetralone (97 %, 146.19 g/mol, 0.5355 g, 3.55 mmol, 1.0 eq.). The reaction was stirred overnight at

room temperature. Solids precipitated out and no further purification needed. The product collected was light off-yellow crystals. Yield 99 % (0.9861 g), R_f value of 0.59 (1:3; EtOAc: Hexane) whose NMR spectra corresponded to literature [115]. $^1\text{H NMR}$ (400 MHz, CDCl_3) δ 8.12 (dd, $J = 7.7, 1.5$ Hz, 1H, C-2), 7.80 (s, 1H, C-11), 7.57 – 7.45 (m, $J = 7.5, 1.5$ Hz, 1H, C-3), 7.40 – 7.32 (m, $J = 7.6, 1.2$ Hz, 1H, C-4), 7.24 (s, 1H, C-14), 7.01 – 6.94 (m, 2H, C-1 and C-13), 6.87 (d, $J = 8.0$ Hz, 1H, C-15), 6.02 (s, 2H, C-18), 3.17 – 3.10 (m, $J = 6.9, 5.6, 1.8$ Hz, 2H, C-10), 2.99 – 2.90 (m, $J = 7.6, 5.4$ Hz, 2H, C-8). $^{13}\text{C NMR}$ (101 MHz, CDCl_3) δ 187.72 (C-7), 148.06 (C-16), 147.77 (C-17), 143.09 (C-5), 136.70 (C-11), 133.98 (C-6), 133.56 (C-9), 133.20 (C-2), 129.86 (C-12), 128.14 (C-1 and C-4), 127.00 (C-3), 125.10 (C-13), 109.77 (C-14), 108.48 (C-15), 101.42 (C-18), 28.73 (C-8), 27.25 (C-10). HRMS m/z (ESI) 296.259 ($[\text{M}+\text{NH}_4]^+$ requires 296.128). The results correspond to previously published results [115].

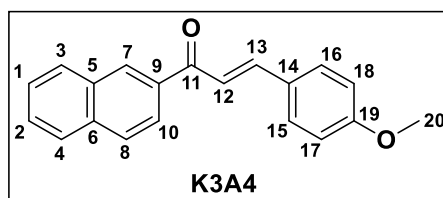
8.4.1.11. Unsuccessful reactions using method 1:

K3A3, K3A4, K3A5, K3A7, K3A8, K4A3, K4A4, K4A7, K4A8, K6A3, K6A4, K6A5, K6A7, K6A8, and K7A7.

8.4.2. General procedure for the formation of α,β -unsaturated ketones with method 2:

Ketone (15.00 mmol) was added to a mixture of EtOH (7.50 ml), NaOH (2 M, 2.00 ml), and water (8.80 ml). A solution of aldehyde (30.30 mmol) and EtOH (30.00 ml) was added dropwise to the mixture and then left to stir overnight. The flask was cooled to room temperature and then cooled on an ice bath for 15 min before filtering the resultant solution. The product was either found as the solids or dissolved in the filtrate.

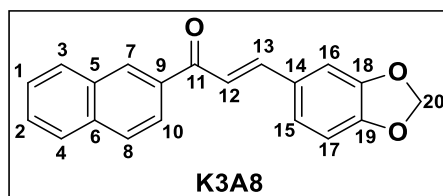
8.4.2.1. (*E*)-3-(4-methoxyphenyl)-1-(naphthalen-2-yl)prop-2-en-1-one (K3A4)



2-acetonaphthone (170.21 g/mol, 0.5553 g, 3.26 mmol, 1.0 eq.) was added to a mixture of EtOH (1.65 ml), NaOH (2 M, 0.50 ml) and water (1.90 ml). A solution of 4-anisaldehyde (98 %, 136.15 g/mol, 0.5001 g, 3.67 mmol, 1.1 eq.) and EtOH (3.70 ml) was added dropwise to the mixture and then left to stir overnight. The flask was cooled to room temperature and then cooled on an ice bath for 15 min before filtering the resultant solution. The filtrate was concentrated *in vacuo* which resulted in light yellow crystals which was recrystallized in warm toluene, which gave a pure product with a 41 % yield (0.3797 g), R_f value of 0.49 (1:3; EtOAc: Hexane). $^1\text{H NMR}$ (300 MHz, CDCl_3) δ 8.54 (s, 1H, C-7), 8.14 (dd, $J = 8.7, 1.8$ Hz, 1H, C-8), 7.98 (d, 1H,

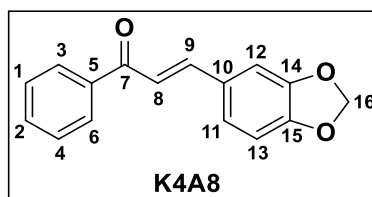
C-10), 7.94 – 7.82 (m, 3H, C-3, C-4 and C-13), 7.66 – 7.50 (m, 5H, C-1, C-2, C-12, C-15 and C-16), 6.93 (d, 2H, C-17 and C-18), 3.81 (s, 3H, C-20). ^{13}C NMR (75 MHz, CDCl_3) δ 190.21 (C-11), 161.72 (C-19), 144.64 (C-13), 135.84 (C-9), 135.59 (C-6), 135.42 (C-5), 134.27 (C-7), 132.61 (C-15), 132.55 (C-16), 130.36 (C-3), 129.80 (C-2), 128.51 (C-8), 127.84 (C-4), 127.68 (C-14), 126.77 (C-1), 124.57 (C-10), 119.68 (C-12), 114.46 (C-17 and C-18), 55.36 (C-20). HRMS m/z (ESI) 289.140 ($[\text{M}+\text{H}]^+$ requires 289.122).

8.4.2.2. (*E*)-3-(benzo[*d*][1,3]dioxol-5-yl)-1-(naphthalen-2-yl)prop-2-en-1-one (K3A8)



2-acetonaphthone (170.21 g/mol, 0.5490 g, 3.23 mmol, 1.0 eq.) was added to a mixture of EtOH (1.60 ml), NaOH (2 M, 0.45 ml) and water (1.90 ml). A solution of piperonal (99 %, 150.13 g/mol, 0.5346 g, 3.56 mmol, 1.1 eq.) and EtOH (3.20 ml) was added dropwise to the mixture and then left to stir overnight. The flask was cooled to room temperature and then cooled on an ice bath for 15 min before filtering the resultant solution. The product precipitated out of solution which was air dried, the resultant fine light-yellow crystals was recrystallized in warm toluene, which gave a pure product with a 41 % yield (0.3977 g), R_f value of 0.49 (1:3; EtOAc: Hexane). ^1H NMR (400 MHz, CDCl_3) δ 8.52 (s, 1H, C-7), 8.08 (dd, $J = 8.5, 1.8$ Hz, 1H, C-8), 7.99 (d, 1H, C-3), 7.91 (dd, $J = 15.6, 8.3$ Hz, 2H, C-4 and C-13), 7.80 (d, $J = 15.5$ Hz, 1H, C-10), 7.63 – 7.53 (m, 3H, C-1, C-2 and C-12), 7.23 (d, $J = 1.8$ Hz, 1H, C-16), 7.16 (dd, $J = 8.0, 1.8$ Hz, 1H, C-15), 6.86 (d, $J = 8.0$ Hz, 1H, C-17), 6.03 (s, 2H, C-20). ^{13}C NMR (101 MHz, CDCl_3) δ 190.37 (C-11), 149.97 (C-18), 148.42 (C-19), 144.80 (C-13), 135.65 (C-5), 135.44 (C-6), 132.55 (C-9), 129.82 (C-7), 129.50 (C-3), 129.38 (C-14), 128.53 (C-2), 128.35 (C-8), 127.80 (C-4), 126.76 (C-1), 125.37 (C-10), 124.44 (C-15), 120.03 (C-12), 108.69 (C-17), 106.70 (C-16), 101.66 (C-20). HRMS m/z (ESI) 325.101 ($[\text{M}+\text{Na}]^+$ requires 325.084).

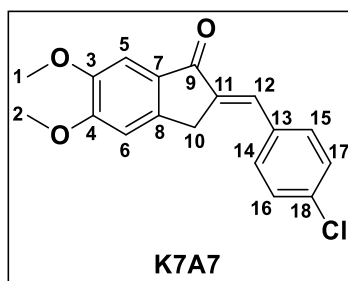
8.4.2.3. (*E*)-3-(benzo[*d*][1,3]dioxol-5-yl)-1-phenylprop-2-en-1-one (K4A8)



Acetophenone (120.15 g/mol, 0.5275 g, 4.39 mmol, 1.0 eq.) was added to a mixture of EtOH (2.20 ml), NaOH (2 M, 0.60 ml) and water (2.60 ml). A solution of piperonal (99 %, 150.13 g/mol, 0.7254 g, 4.83 mmol, 1.1

eq.) and EtOH (4.50 ml) was added dropwise to the mixture and then left to stir overnight. The flask was cooled to room temperature and then cooled on an ice bath for 15 min before filtering the resultant solution. The product precipitated out of solution which was air dried, the resultant fine light-yellow crystals was recrystallized in warm toluene, which gave a pure product with a 47 % yield (0.5257 g), R_f value of 0.52 (1:3; EtOAc: Hexane). ¹H NMR (400 MHz, CDCl₃) δ 8.02 – 7.97 (m, 2H, C-3 and C-6), 7.73 (d, J = 15.6 Hz, 1H, C-9), 7.60 – 7.54 (m, 1H, C-2), 7.52 – 7.46 (m, 2H, C-1 and C-4), 7.37 (d, J = 15.6 Hz, 1H, C-8), 7.17 (d, J = 1.8 Hz, 1H, C-12), 7.12 (d, J = 8.1, 1.7 Hz, 1H, C-11), 6.83 (d, J = 8.0 Hz, 1H, C-13), 6.01 (s, 2H, C-16). ¹³C NMR (101 MHz, CDCl₃) δ 190.66 (C-7), 149.96 (C-15), 148.39 (C-14), 144.88 (C-9), 138.28 (C-5), 132.71 (C-2), 129.26 (C-10), 128.58 (C-1 and C-4), 128.40 (C-3 and C-6), 125.33 (C-11), 119.99 (C-8), 108.64 (C-13), 106.63 (C-12), 101.64 (C-16). HRMS m/z (ESI) 253.101 ([M+H]⁺ requires 253.086). The results correspond to previously published results [116].

8.4.2.4. (*E*)-2-(4-chlorobenzylidene)-5,6-dimethoxy-2,3-dihydro-1*H*-inden-1-one (K7A7)

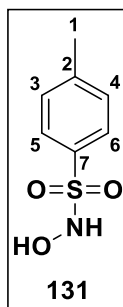


5,6-dimethoxyindanone (192.21 g/mol, 0.6158 g, 3.20 mmol, 1.0 eq.) was added to a mixture of EtOH (1.60 ml), NaOH (2 M, 4.00 ml) and water (2.85 ml). A solution of 4-chlorobenzaldehyde (97 %, 140.56 g/mol, 0.5117 g, 3.53 mmol, 1.1 eq.) and EtOH (30.00 ml) was added dropwise to the mixture and then left to stir overnight. The flask was cooled to room temperature and then cooled on an ice bath for 15 min before filtering the resultant solution. The product precipitated out and was then filtered to collect the light yellow crystals which were recrystallized in warm toluene. The dried pure product had a yield of 39 % (0.3931 g). R_f value of 0.51 (1:1; EtOAc: Hexane) ¹H NMR (400 MHz, CDCl₃) δ 7.43 (d, 2H, C-14 and C-15), 7.36 (s, 1H, C-12), 7.33 (d, 2H, C-16 and C-17), 7.17 (s, 1H, C-5), 6.87 (s, 1H, C-6), 3.95 (s, 3H, C-1), 3.87 (s, 3H, C-2), 3.74 (d, J = 2.4 Hz, 2H, C-5). ¹³C NMR (75 MHz, CDCl₃) δ 192.52 (C-9), 155.37 (C-4), 149.48 (C-3), 144.58 (C-7), 144.58 (C-8), 135.65 (C-13), 135.13 (C-11), 133.77 (C-18), 131.45 (C-12), 130.61 (C-14), 130.55 (C-15), 128.94 (C-16 and C-17), 106.99 (C-5), 104.68 (C-6), 56.10 (C-1), 55.98 (C-2), 31.84 (C-10). HRMS m/z (ESI) 315.098 ([M+H]⁺ requires 315.078).

8.4.2.5. Unsuccessful reactions with Method 2:

K3A5, K4A4, K6A3, K6A4, K6A5, K6A7, and K6A8.

8.4.3. Synthesis of *N*-hydroxy-4-methylbenzenesulfonamide (**131**)



1.) AlO_3 (101.96 g/mol, 0.5322 g, 5.22 mmol, 2.0 eq.) was added to a stirring solution of $\text{NH}_2\text{OH}\cdot\text{HCl}$ (69.49 g/mol, 0.4538 g, 6.53 mmol, 2.5 eq.), MeOH (3.00 ml) and water (2.00 ml). The reaction was then left to stir at room temperature before a solution of TsCl (190.65 g/mol, 0.5073 g, 2.66 mmol, 1.0 eq.) and THF (10.00 ml) was added. More AlO_3 (101.96 g/mol, 0.2662 g, 2.61 mmol, 1.0 eq.) was added to the mixture; after that, it was left to stir overnight. The mixture was filtered, dried with MgSO_4 , and concentrated *in vacuo*. The crystals formed were washed with DCM, where the filtrate was analysed. The solids were then washed with MeOH and filtrate collected and analysed. The analysis of both samples indicated that no product formed.

2.) MgO (40.30 g/mol, 0.2277 g, 5.48 mmol, 2.0 eq.) was added to a stirring solution of $\text{NH}_2\text{OH}\cdot\text{HCl}$ (69.49 g/mol, 0.4921 g, 7.08 mmol, 2.6 eq.), MeOH (3.00 ml) and water (2.00 ml). The reaction was then left to stir at room temperature before a solution of TsCl (98 %, 190.65 g/mol, 0.5459 g, 2.81 mmol, 1.0 eq.) and THF (10.00 ml) was added. More MgO (40.00 g/mol, 0.1146 g, 2.76 mmol, 1.0 eq.) was added to the mixture; after that, it was left to stir overnight. The mixture was concentrated *in vacuo*. DCM was added, resulting in some crystals not dissolving in the solution and collected via vacuum filtration. The crystals were washed with DCM. The crystals were then washed with MeOH, leaving some catalyst behind. The filtrate was concentrated *in vacuo*, but no product was formed.

3.) Cr_2O_3 (151.99 g/mol, 0.8131 g, 5.35 mmol, 2.0 eq.) was added to a stirring solution of $\text{NH}_2\text{OH}\cdot\text{HCl}$ (69.49 g/mol, 0.4635 g, 6.67 mmol, 2.5 eq.), MeOH (3.00 ml) and water (2.00 ml). The reaction was then left to stir at room temperature before a solution of TsCl (98 %, 190.65 g/mol, 0.5192 g, 2.72 mmol, 1.0 eq.) and THF (10.00 ml) was added. More Cr_2O_3 (151.99 g/mol, 0.4064 g, 2.67 mmol, 1.0 eq.) was added to the mixture. After that, it was left to stir overnight. The mixture was concentrated *in vacuo*. DCM was added, resulting in some crystals not dissolving in the solution and collected with vacuum filtration. The crystals were washed with DCM. The crystals were then washed with MeOH, leaving most of the catalyst behind. The filtrate was concentrated *in vacuo*, which gave white crystals as the product, but a green tinge indicated there was still

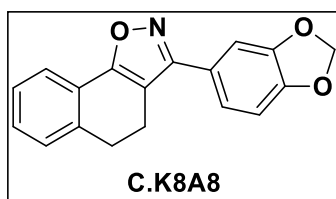
Cr₂O₃ present which results that the impure yield of 66 % was collected as a result, R_f value of 0.57 (1:1; EtOAc: Hexane). ¹H NMR (300 MHz, Methanol-d₄) δ 10.35 (s, 2H, NH and OH), 7.72 (d, 2H, C-5 and C-6), 7.24 (d, J = 7.9 Hz, 2H, C-3 and C-4), 2.38 (s, 3H, C-1). ¹³C NMR (75 MHz, MeOD) δ 144.14 (C-2), 134.23 (C-7), 129.10 (C-3), 129.04 (C-4), 128.31 (C-5), 128.24 (C-6), 20.23 (C-1). HRMS m/z (ESI) 186.128 ([M-H]⁺ requires 186.023).

-Increasing the reaction ten fold resulted in an unsuccessful reaction.

8.4.4. General procedure for the attempted formation of isoxazole ring systems from α,β -unsaturated ketones

TsNHOH (7.0 eq.) was added to a stirring solution of MeOH: H₂O (1.20 ml:0.20 ml), which was stirred until all the TsNHOH was dissolved. K₂CO₃ (5.0 eq.) was added in portions to the stirring mixture, whereafter the α,β -unsaturated ketone (1.0 eq.) in MeOH (0.60 ml) was added dropwise or in small portions when the sample did not dissolve in the MeOH. The mixture was then refluxed for 2 hours, whereafter K₂CO₃ (2.5 eq.) was added and then left to reflux for 2 days. The solvent was removed, and then EtOAc (40.00 ml) was added. The mixture was then extracted with H₂O (2 x 15.00 ml) and brine (15.00 ml). The organic layer was combined, dried, and concentrated *in vacuo*.

8.4.4.1. 3-(benzo[d][1,3]dioxol-5-yl)-4,5-dihydronaphtho[2,1-d]isoxazole (C.K8A8)



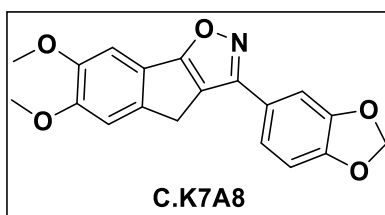
1.) TsNHOH (187.21 g/mol, 0.5457 g, 2.91 mmol, 6.9 eq.) was added to a stirring solution of MeOH: H₂O (2.50 ml: 0.42 ml), which was stirred until all the TsNHOH was dissolved. K₂CO₃ (138.21 g/mol, 0.3469 g, 2.51 mmol, 6.0 eq.) was added in portions to the stirring mixture whereafter (*E*)-2-(benzo[d][1,3]dioxol-5-ylmethylene)-3,4-dihydronaphthalen-1(2*H*)-one (278.31 g/mol, 0.1161 g, 0.42 mmol, 1.0 eq.) in MeOH (0.26 ml) was added dropwise. The mixture was then refluxed overnight after K₂CO₃ (138.21 g/mol, 0.1735 g, 1.26 mmol, 3.0 eq.) was added to the solution. The solvent was removed, and then EtOAc (40.00 ml) was added. The mixture was then extracted with H₂O (2 x 15.00 ml) and brine (15.00 ml). The organic layer was combined, dried, and concentrated *in vacuo*. The reaction was unsuccessful.

2.) TsNHOH (187.21 g/mol, 0.4911 g, 2.62 mmol, 7.1 eq.) was added to a stirring solution of MeOH: H₂O (2.30 ml: 0.37 ml), which was stirred until all the TsNHOH was dissolved. K₂CO₃ (138.21 g/mol, 0.4136 g, 2.99

mmol, 8.1 eq.) was added in portions to the stirring mixture whereafter (*E*)-2-(benzo[*d*][1,3]dioxol-5-ylmethylene)-3,4-dihydronaphthalen-1(2*H*)-one (278.31 g/mol, 0.1039 g, 0.37 mmol, 1.0 eq.) in MeOH (0.26 ml) was added dropwise. The mixture was then refluxed for 5 days after K₂CO₃ (138.21 g/mol, 0.1735 g, 1.26 mmol, 3.0 eq.) was added to the solution. The solvent was removed, and then EtOAc (50.00 ml), 40.00 ml H₂O and 20.00 ml brine were added. To this mixture, 1.0 M HCl was added in a dropwise manner until the aqueous layer turned white. The organic layer was collected, dried, and concentrated *in vacuo*. The reaction was unsuccessful.

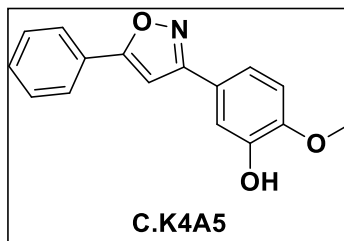
3.) TsNHOH (187.21 g/mol, 0.4941 g, 2.64 mmol, 6.7 eq.) was added to a stirring solution of EtOH: H₂O (2.52 ml: 0.28 ml), which was stirred until all the TsNHOH was dissolved. Concentrated K₂CO₃ (138.21 g/mol, 0.50 ml, 8.79 mmol, 22.5 eq.) was added in portions to the stirring mixture whereafter (*E*)-2-(benzo[*d*][1,3]dioxol-5-ylmethylene)-3,4-dihydronaphthalen-1(2*H*)-one (278.31 g/mol, 0.1083 g, 0.39 mmol, 1.0 eq.) was added in small portions. The mixture was then refluxed at 140 °C for 4 days after K₂CO₃ (138.21 g/mol, 0.30 ml, 5.27 mmol, 3.0 eq.) was added to the solution. The solvent was removed *in vacuo*, and then EtOAc (50.00 ml) was added, H₂O (40.00 ml) and 20.00 ml brine were added to extract the organic layer. To this layer, 1.0 M HCl (20.00 ml) was added in a dropwise manner. The organic layer was then collected, dried, and concentrated *in vacuo*. The reaction was unsuccessful.

8.4.4.2. C.K7A8 3-(benzo[*d*][1,3]dioxol-5-yl)-6,7-dimethoxy-4*H*-indeno[2,1-*d*]isoxazole



TsNHOH (187.21 g/mol, 0.4490 g, 2.40 mmol, 7.1 eq.) was added to a stirring solution of acetonitrile: H₂O (2.52 ml: 0.28 ml), which was stirred until all the TsNHOH was dissolved. Concentrated K₂CO₃ (138.21 g/mol, 0.15 ml, 2.64 mmol, 7.8 eq.) was added to the stirring mixture whereafter 3-(benzo[*d*][1,3]dioxol-5-yl)-6,7-dimethoxy-4*H*-indeno[2,1-*d*]isoxazole (324.33 g/mol, 0.1092 g, 0.34 mmol, 1.0 eq.) was added in small portions. The mixture was then refluxed at 140 °C for 4 days after K₂CO₃ (138.21 g/mol, 0.10 ml, 1.76 mmol, 5.2 eq.) was added to the solution. The solvent was removed *in vacuo*, and then EtOAc (50.00 ml) was added, H₂O (40.00 ml) and 20.00 ml brine were added to extract the organic layer. To this layer, 1.0 M HCl (20.00 ml) was added in a dropwise manner. The organic layer was then collected, dried, and concentrated *in vacuo*. The reaction was unsuccessful.

8.4.4.3. C.K4A5 2-methoxy-5-(5-phenylisoxazol-3-yl)phenol

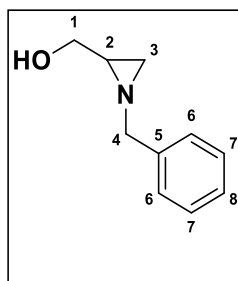


TsNHOH (187.21 g/mol, 0.5481 g, 2.93 mmol, 7.1 eq.) was added to a stirring solution of MeOH: H₂O (2.52 ml: 0.28 ml), which was stirred until all the TsNHOH was dissolved. Concentrated K₂CO₃ (138.21 g/mol, 0.15 ml, 2.64 mmol, 6.4 eq.) was added to the stirring mixture whereafter (*E*)-3-(3-hydroxy-4-methoxyphenyl)-1-phenylprop-2-en-1-one (254.29 g/mol, 0.1052 g, 0.41 mmol, 1.0 eq.) was added in small portions. The mixture was then refluxed at 140 °C for 4 days after K₂CO₃ (138.21 g/mol, 0.10 ml, 1.76 mmol, 4.3 eq.) was added to the solution. The solvent was removed *in vacuo*, and then EtOAc (50.00 ml) was added, H₂O (40.00 ml) and 20.00 ml brine were added to extract the organic layer. To this layer, 1.0 M HCl (20.00 ml) was added in a dropwise manner. The organic layer was then collected, dried, and concentrated *in vacuo*. The reaction was unsuccessful.

8.5. Experimental details relating to other

These experimental methods were conducted during the course of the projects in parallel to the targeted scaffolds as these molecules would have been incorporated in the diversification steps of the different scaffolds.

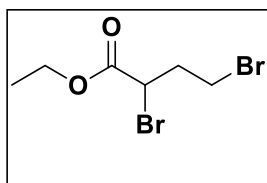
8.5.1. (1-benzylaziridin-2-yl)methanol



To a stirring of dry DCM (40.00 ml) and methyl 1-benzylaziridine-2-carboxylate (191.23 g/mol, 1.9624 g, 10.26 mmol, 1.0 eq.), Red-Al (60 % in CH₃Ph; 202.16 g/mol, 6.67 ml, 20.52 mmol, 2.0 eq.) was added drop wise to the solution at 15 - 20 °C. The mixture was left to stir overnight at room temperature and then quenched with 10 % NaOH solution. The mixture was then diluted with H₂O (80.00 ml) and Na₂SO₄ (30.00 ml). It was left to stir for 45 min. The organic layer was separated and washed with H₂O (3 x 40.00 ml) and

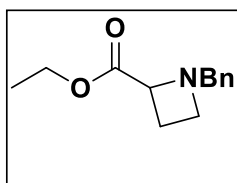
saturated Na_2SO_4 (10 x 40.00 ml). The DCM layer was dried with anhydrous Na_2SO_4 , filtered and evaporated *in vacuo* giving a yield of 74 % (4.7339 g). $^1\text{H NMR}$ (300 MHz, Chloroform-*d*) δ 7.30 – 7.15 (m, 5H, Ar H's), 3.87 (s, 1H, OH), 3.65 (dd, $J = 11.9, 3.2$ Hz, 1H, C-4), 3.45 (d, $J = 13.3$ Hz, 1H, C-4), 3.27 (dd, $J = 12.8, 6.9$ Hz, 2H, C-1), 1.80 – 1.68 (m, 2H, C-2; C-3), 1.38 (d, $J = 6.2$ Hz, 1H, C-3). $^{13}\text{C NMR}$ (75 MHz, CDCl_3) δ 138.72 (C-5), 128.49 (C-6), 128.12 (C-7), 127.27 (C-8), 63.97 (C-1), 62.66 (C-4), 40.91 (C-2), 31.12 (C-3).

8.5.2. Ethyl 2,4-dibromobutanoate



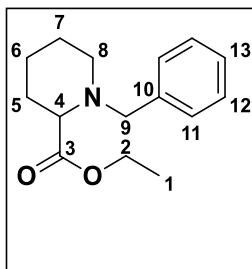
A solution of phosphorous tribromide (270.69 g/mol, 0.20 ml, 3.15 mmol, 0.02 eq.) and γ -butyrolactone (86.09 g/mol, 12.00 ml, 157.51 mmol, 1.0 eq.) was heated to 100 $^\circ\text{C}$ and left to stir for 15 min. Bromine (159.80 g/mol, 8.93 ml, 173.26 mmol, 1.1 eq.) was added dropwise to the solution. The reaction was cooled to room temperature and then cooled to 0 $^\circ\text{C}$. Methanol (60.00 ml) was added, followed by the addition of CHCl_3 until the pH of 1 was reached. The reaction was left to stir at room temperature overnight. Saturated sodium thiosulfate solution was added until the dark red solution turned clear. The aqueous layer was extracted with diethyl ether (3 x 50.00 ml), organic layers were combined, dried using Na_2SO_4 , filtered and evaporated *in vacuo*. The mixture was columned, but the product did not form.

8.5.3. Ethyl 1-benzylazetidino-2-carboxylate



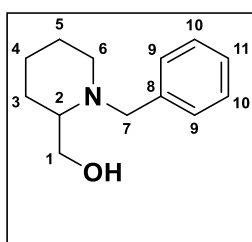
A mixture of ethyl 2,4-dibromobutanoate (271.98 g/mol, 17.4400 g, 64.12 mmol, 1.0 eq.) in methanol (25.00 ml) was added dropwise to a stirring solution of Et_3N (101.19 g/mol, 26.81 ml, 192.36 mmol, 3.0 eq.) in methanol (70.00 ml) at 0 $^\circ\text{C}$. The mixture was left to stir for 15 min. A mixture of benzylamine (107.15 g/mol, 7.35 ml, 67.33 mmol, 1.1 eq.) in methanol (42.00 ml) was then added dropwise and then left to stir for 30 min. The solution was then warmed to room temperature and left to stir overnight. The solvent was removed *in vacuo* and then diluted with diethyl ether (100.00 ml). Solids were removed, and then the organic layer was collected and washed with water (200.00 ml), and the aqueous phase was extracted using diethyl ether (3 x 50.00 ml). The combined organic phase was dried with anhydrous Na_2SO_4 , filtered and then evaporated *in vacuo*. The mixture was columned, but the product did not form.

8.5.4. Ethyl 1-benzylpiperidine-2-carboxylate



Ethyl piperidine-2-carboxylate hydrochloride (193.67 g/mol, 5.0868 g, 26.27 mmol, 1.0 eq.) and BnCl (126.59 g/mol, 3.32 ml, 28.89 mmol, 1.1 eq.) were added to Et₃N (101.19 g/mol, 14.64 ml, 105.04 mmol, 4.0 eq.) in 100.00 ml dry AcCN. The mixture was then refluxed for 3 hours and then removed from heat and left to stir overnight (formed a red/orange solution). Solvent was removed *in vacuo*. A 100.00 ml of EtOAc was added and was then extracted using 3 M NaOH (3 x 40.00 ml) and H₂O (2 x 40.00 ml). Organic layer (orange solution) was dried, filtered and then removed the solvent *in vacuo*. The pure product was a dark yellow oil with a yield of 84 % (5.4398 g). **¹H NMR (300 MHz, Chloroform-*d*)** δ 7.30 – 7.14 (m, 5H, Ar H's), 4.15 (q, *J* = 7.2 Hz, 2H, C-2), 3.74 (d, *J* = 13.3 Hz, 1H, C-9), 3.33 (d, *J* = 13.3 Hz, 1H, C-9), 3.06 (dd, *J* = 7.9, 4.4 Hz, 1H, C-4), 2.88 (dt, *J* = 10.5, 4.7 Hz, 1H, C-8), 2.12 – 1.99 (m, 1H, C-8), 1.87 – 1.66 (m, 2H, C-5), 1.63 – 1.41 (m, 3H, C-6, C-6, C-7), 1.36 – 1.20 (m, 4H, C-7 and C-1). **¹³C NMR (75 MHz, CDCl₃)** δ 173.55 (C-3), 138.19 (C-10), 129.09 (C-11), 128.06 (C-12), 126.95 (C-13), 64.20 (C-4), 60.46 (C-9), 60.10 (C-2), 49.97 (C-8), 29.50 (C-5), 25.27 (C-7), 22.45 (C-6), 14.29 (C-1). HRMS *m/z* (ESI) 248.168 ([M+H]⁺ requires 248.165).

8.5.5. (1-benzylpiperidin-2-yl)methanol

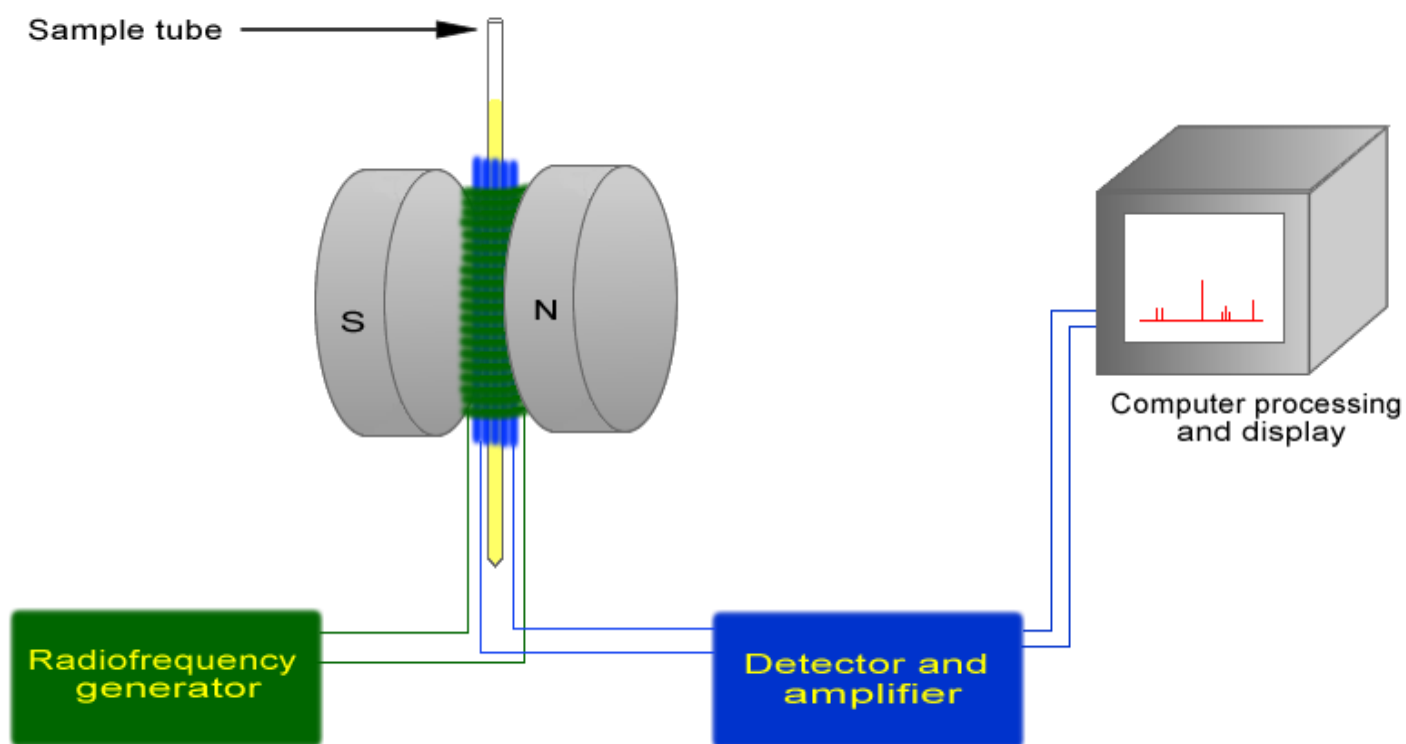


Red-Al (60 % in CH₃Ph; 202.16 g/mol, 5.10 ml, 15.68 mmol, 1.9 eq.) was added drop wise to a stirring solution of dry DCM (30.00 ml) and ethyl 1-benzylpiperidine-2-carboxylate (247.33 g/mol, 2.0680 g, 8.36 mmol, 1.0 eq.) at 15 - 20 °C (solution turned light yellow and then became cloudier). The mixture was left to stir overnight at room temperature. The solution was then quenched with 10 % NaOH. The mixture was then diluted with H₂O (20.00 ml) and saturated Na₂SO₄ (20.00 ml - in order to get rid of the emulsion). The solution was left to stir for 30 min. The organic layer was then separated and washed with H₂O (3 x 20.00 ml) and saturated NaCl (3 x 20.00 ml). The organic layer was dried with anhydrous Na₂SO₄, filtered and then evaporated *in vacuo* to yield the impure product. Which was columned using the eluent EtOAc: Hexane (3:1)

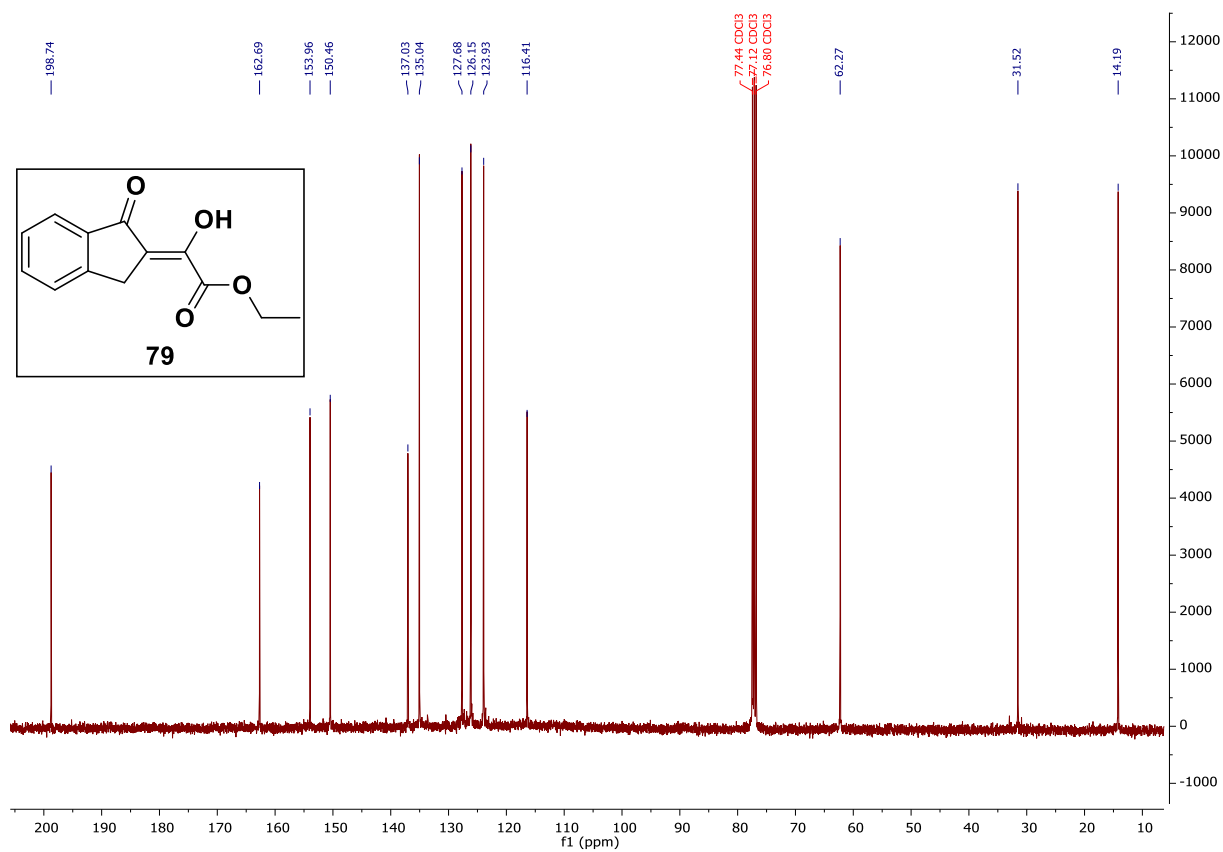
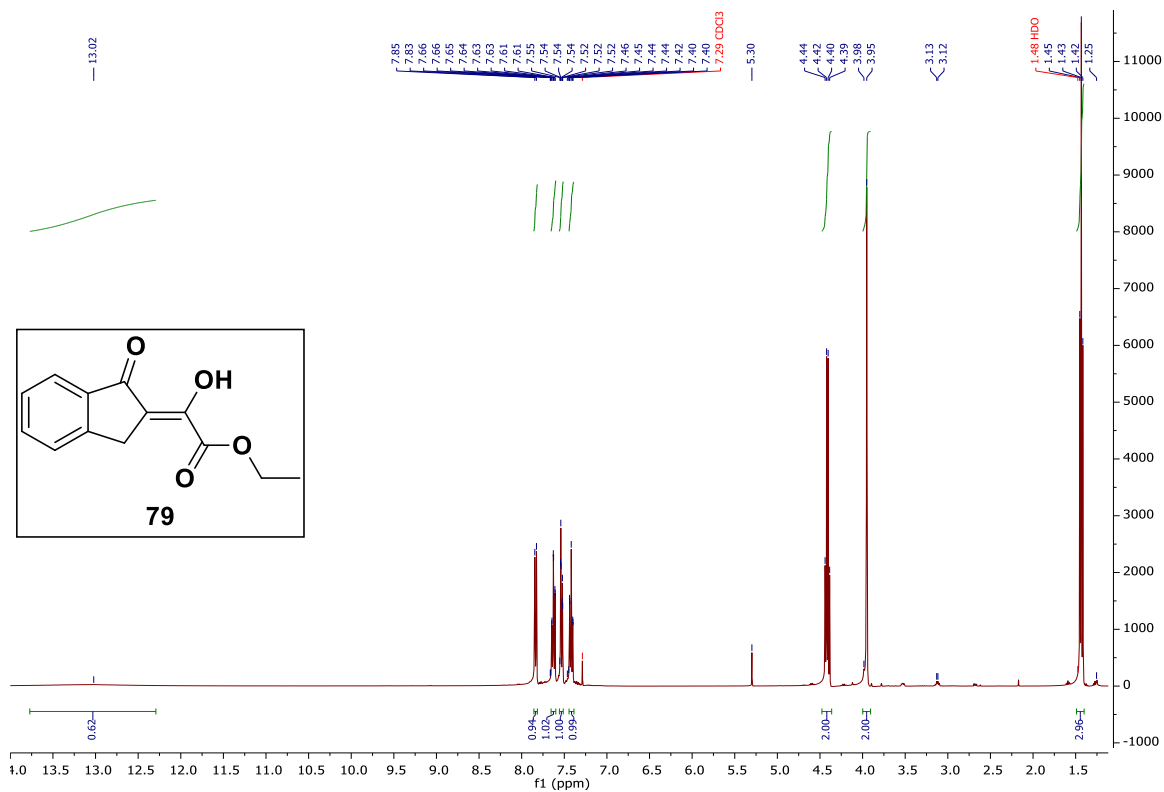
giving the pure product as a light-yellow oil with a yield of 52 % (0.8869 g). **¹H NMR (300 MHz, Chloroform-*d*)** δ 7.44 – 7.15 (m, 5H, Ar H's), 4.09 (d, J = 13.4 Hz, 1H, C-7), 3.86 (dd, J = 10.9, 4.3 Hz, 1H, C-1), 3.76 (s, 1H, C1-OH), 3.57 (dd, J = 10.9, 4.0 Hz, 1H, C-1), 3.36 (d, J = 13.4 Hz, 1H, C-7), 2.92 – 2.81 (m, 1H, C-6), 2.47 (dq, J = 8.1, 4.1 Hz, 1H, C-2), 2.16 (ddd, J = 12.2, 10.0, 3.1 Hz, 1H, C-6), 1.75 – 1.53 (m, 4H, C-3; C-4; C5), 1.39 (ddt, J = 13.5, 10.0, 5.5 Hz, 2H, C-3; C-4). **¹³C NMR (75 MHz, CDCl₃)** δ 136.56 (C-8), 129.55 (C-9), 128.51 (C-10), 127.63 (C-11), 62.21 (C-2), 61.95 (C-1), 57.23 (C-7), 50.93 (C-6), 27.02 (C-3), 23.56 (C-5), 23.01 (C-4). HRMS m/z (ESI) 206.167 ([M-H]⁺ requires) 206.154.

Chapter 9

Experimental Spectrums

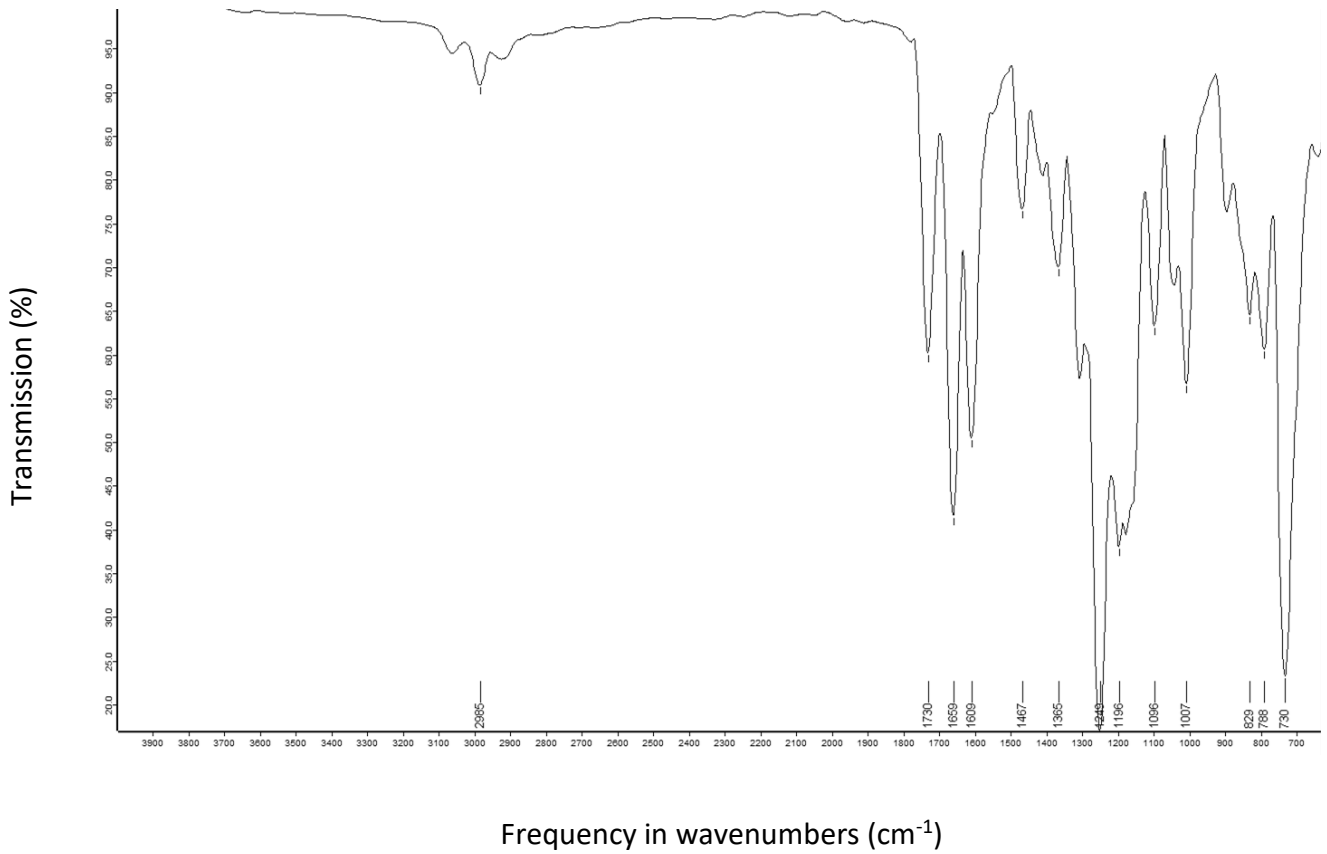
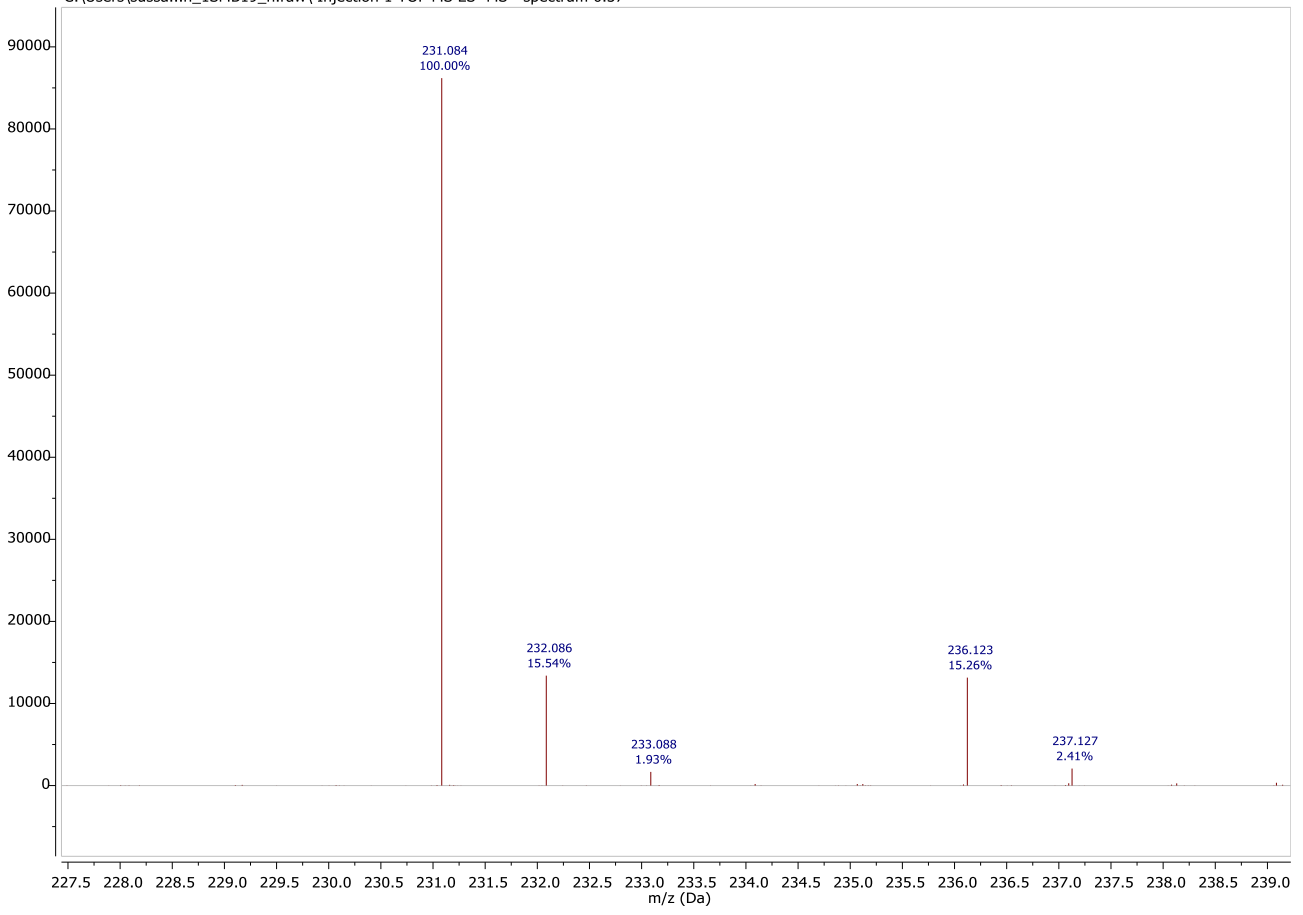


9.1. Experimental details relating to scaffold A and B

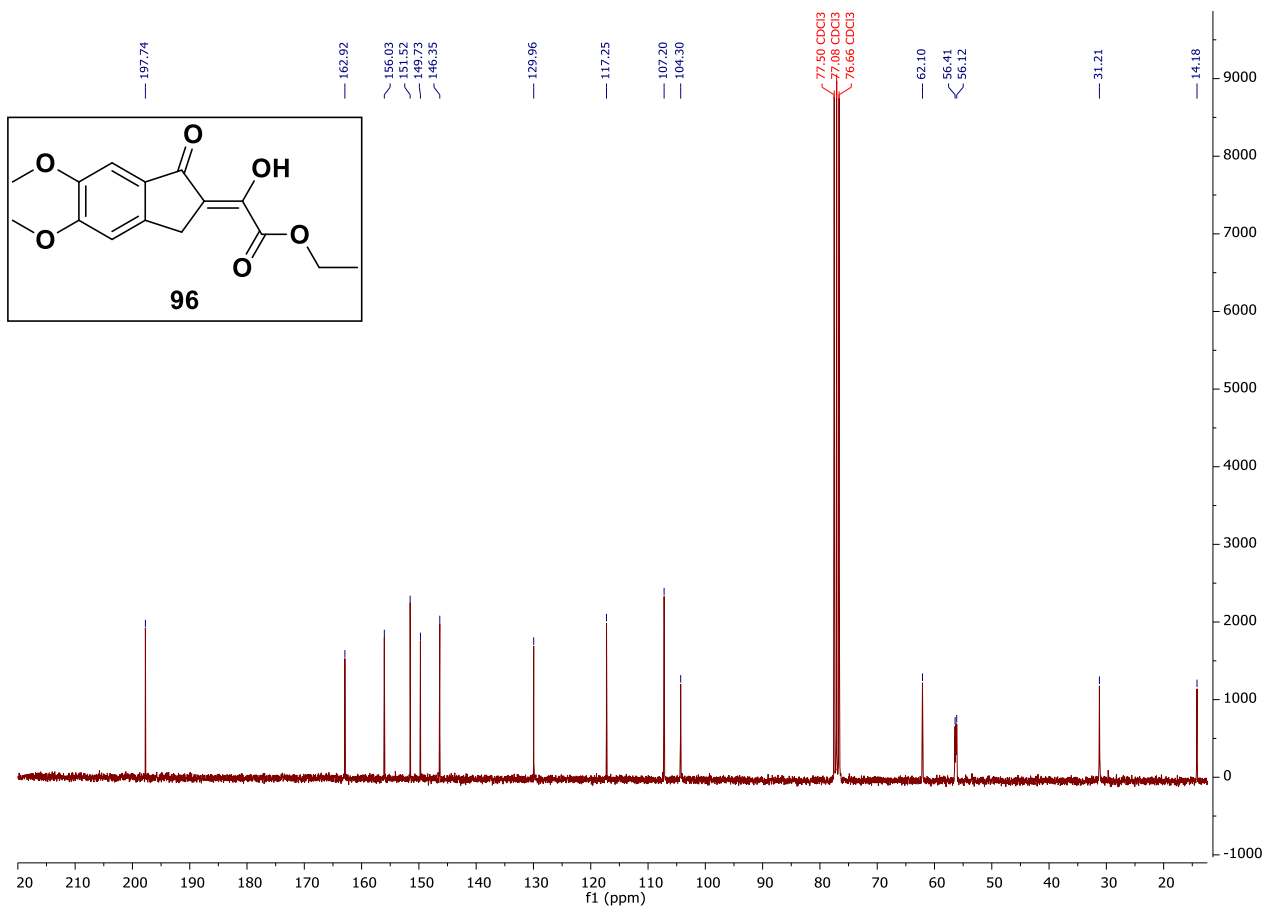
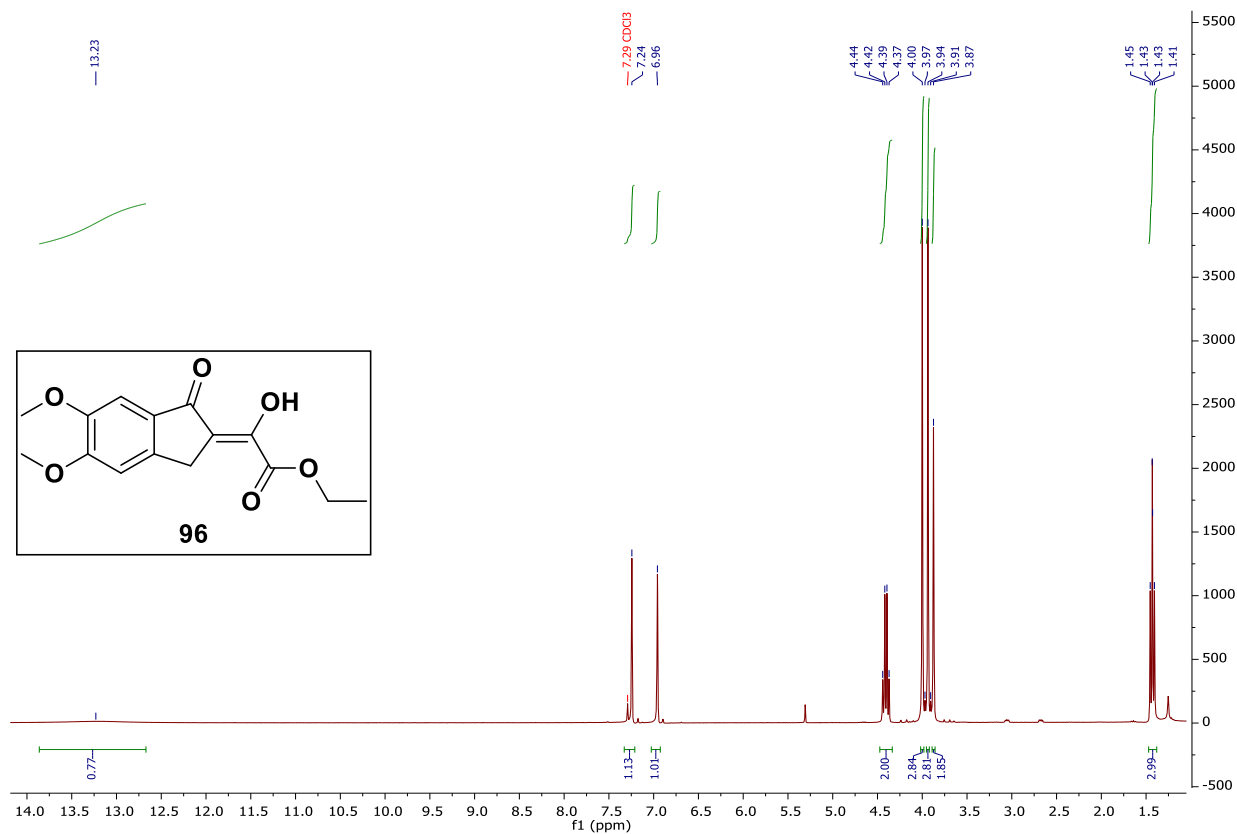
9.1.1. Ethyl (Z)-2-hydroxy-2-(1-oxo-1,3-dihydro-2H-inden-2-ylidene)acetate (**79**)

Chapter 9: Experimental Spectrums

C:\Users\sussa...n_1SMB19_n.raw\ Injection 1 TOF MS ES- MS - spectrum 0.37

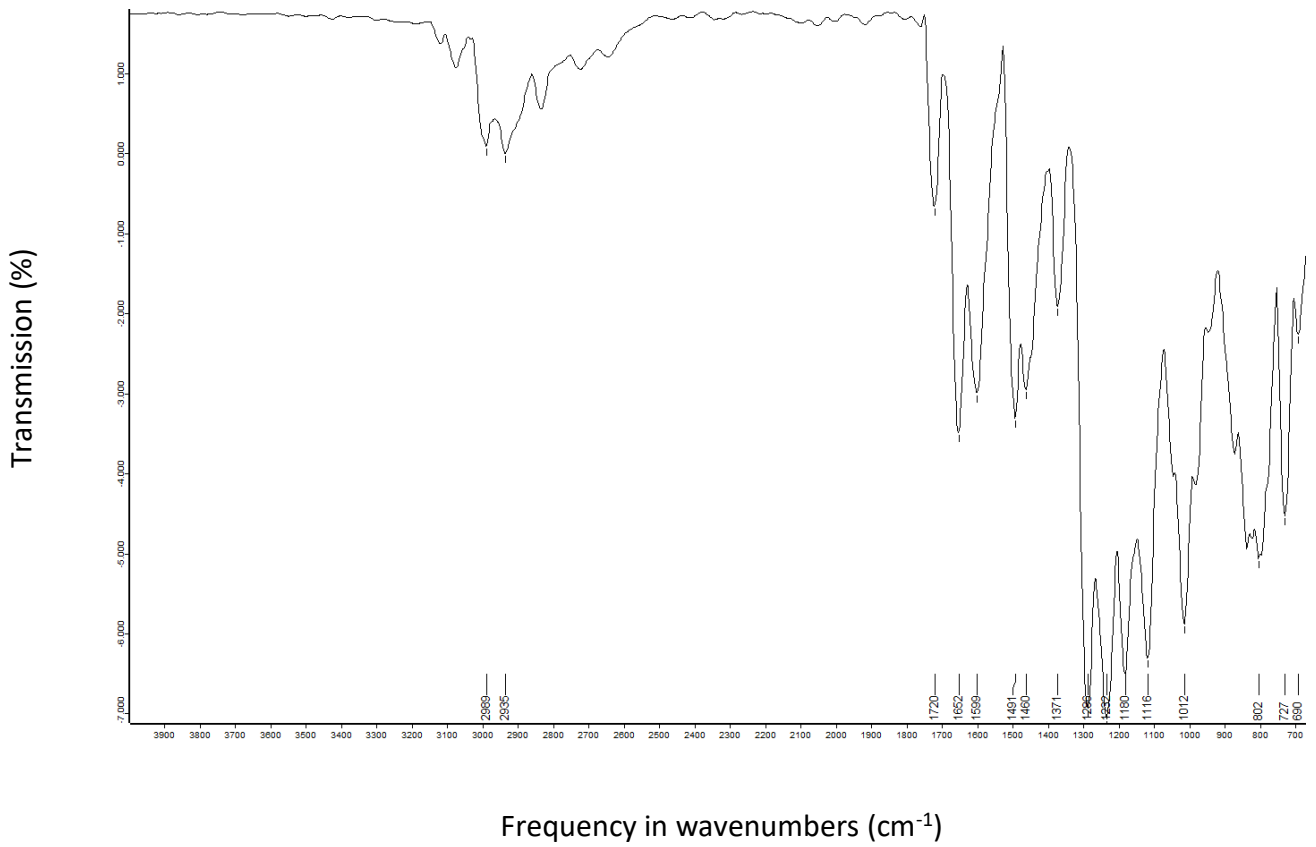
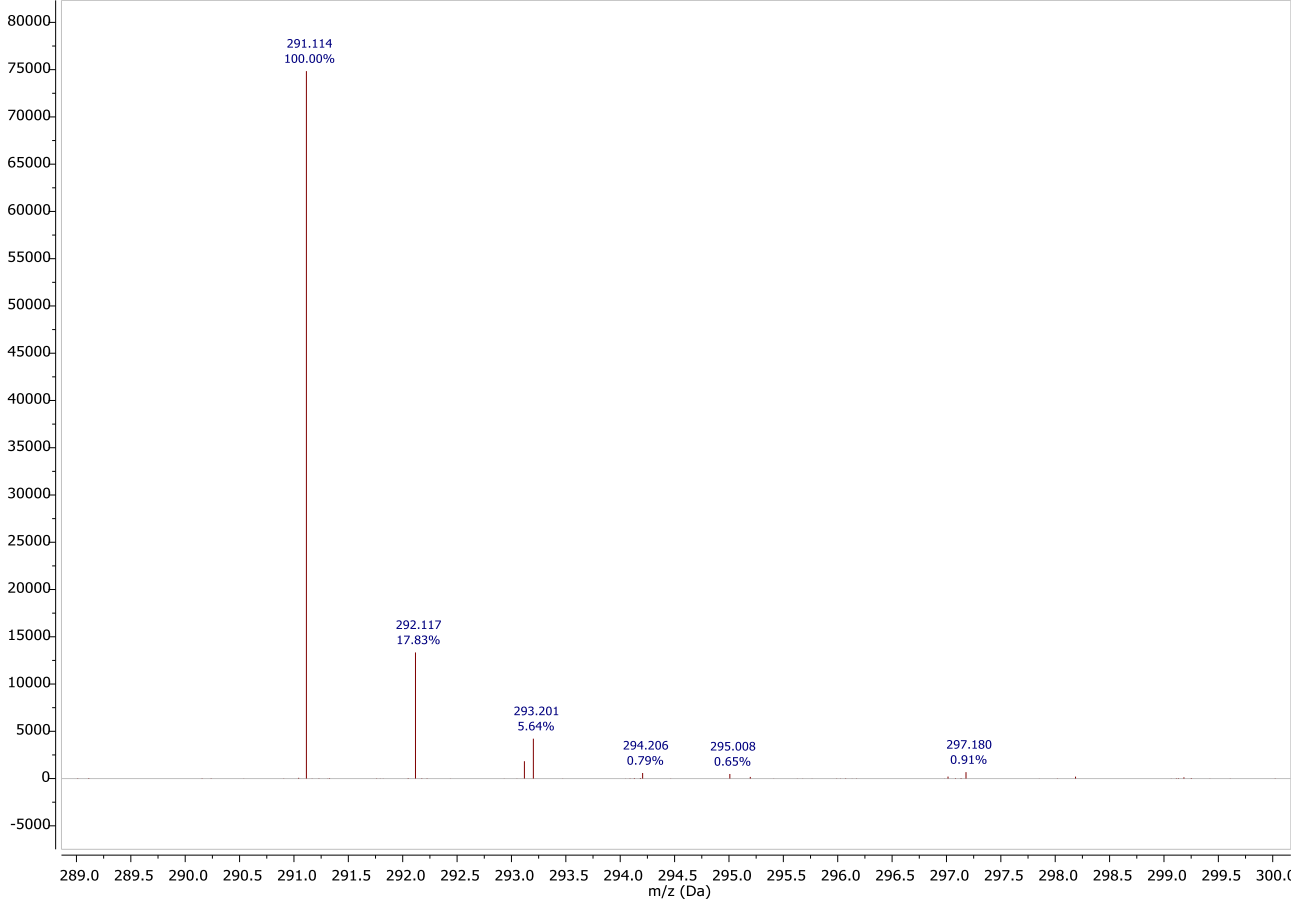


9.1.2. Ethyl (Z)-2-(5,6-dimethoxy-1-oxo-1,3-dihydro-2H-inden-2-ylidene)-2-hydroxyacetate (**96**)

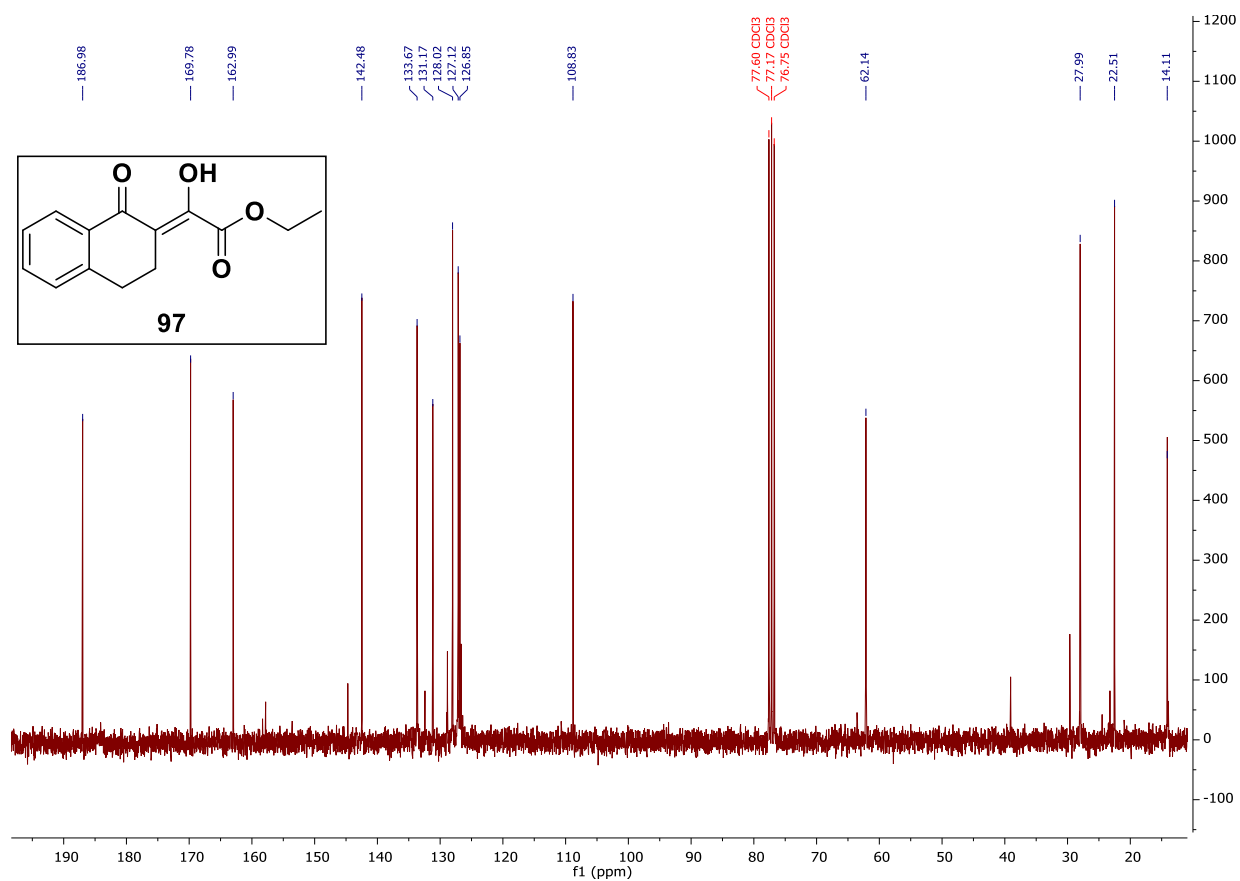
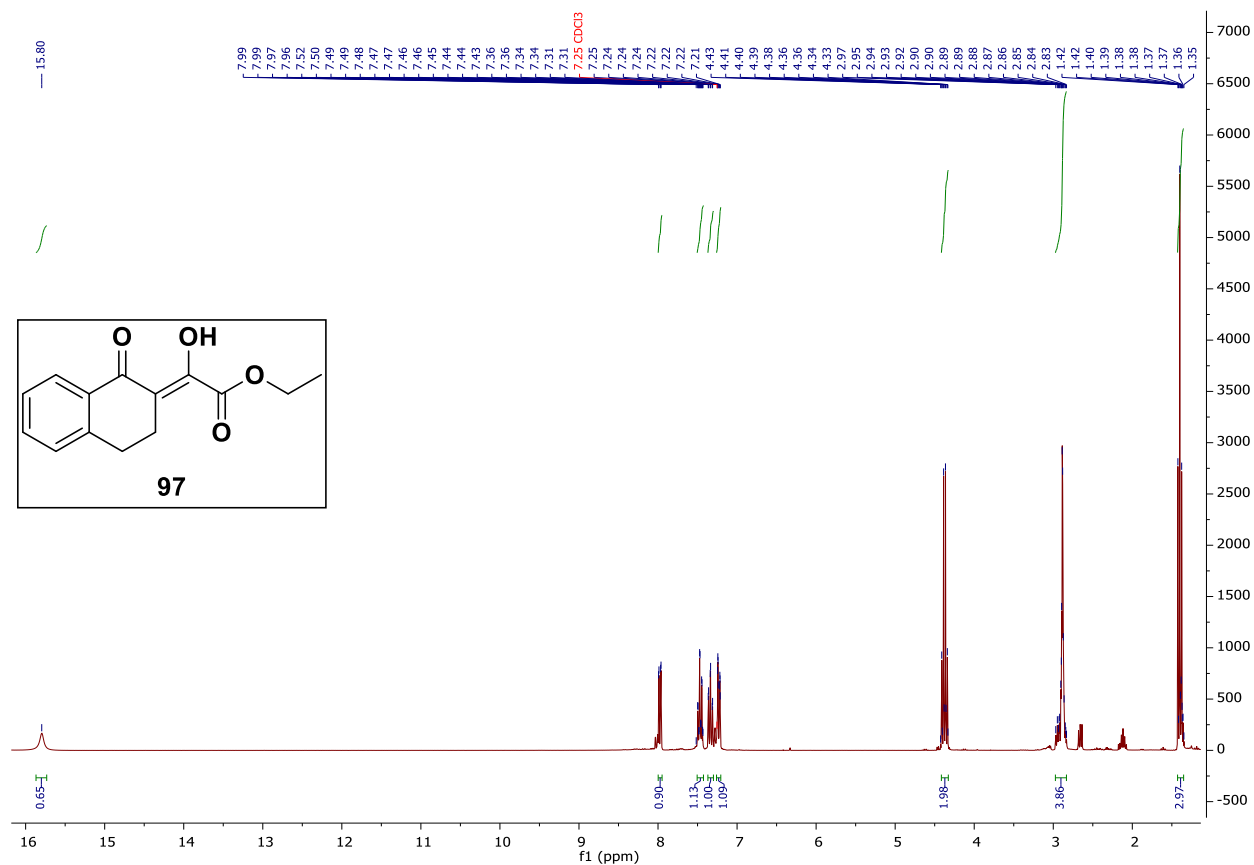


Chapter 9: Experimental Spectrums

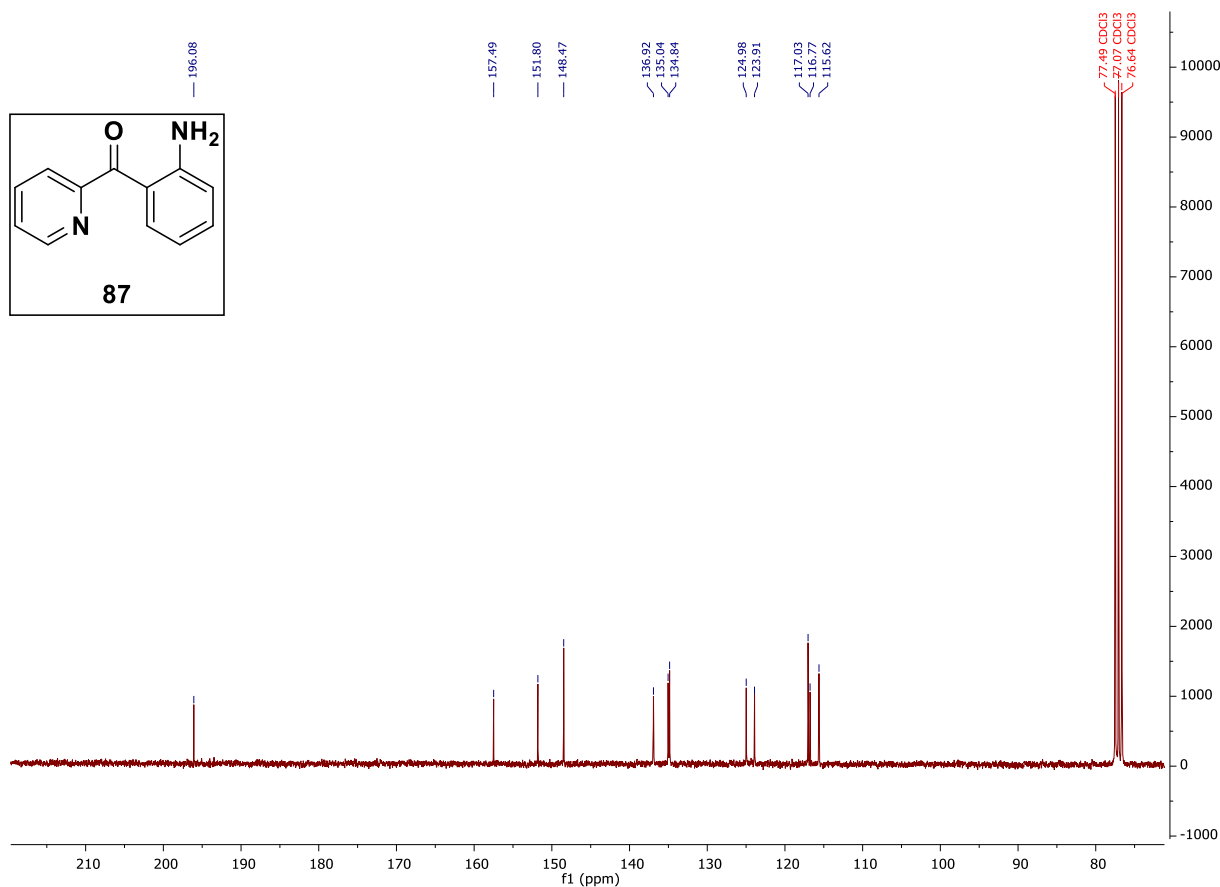
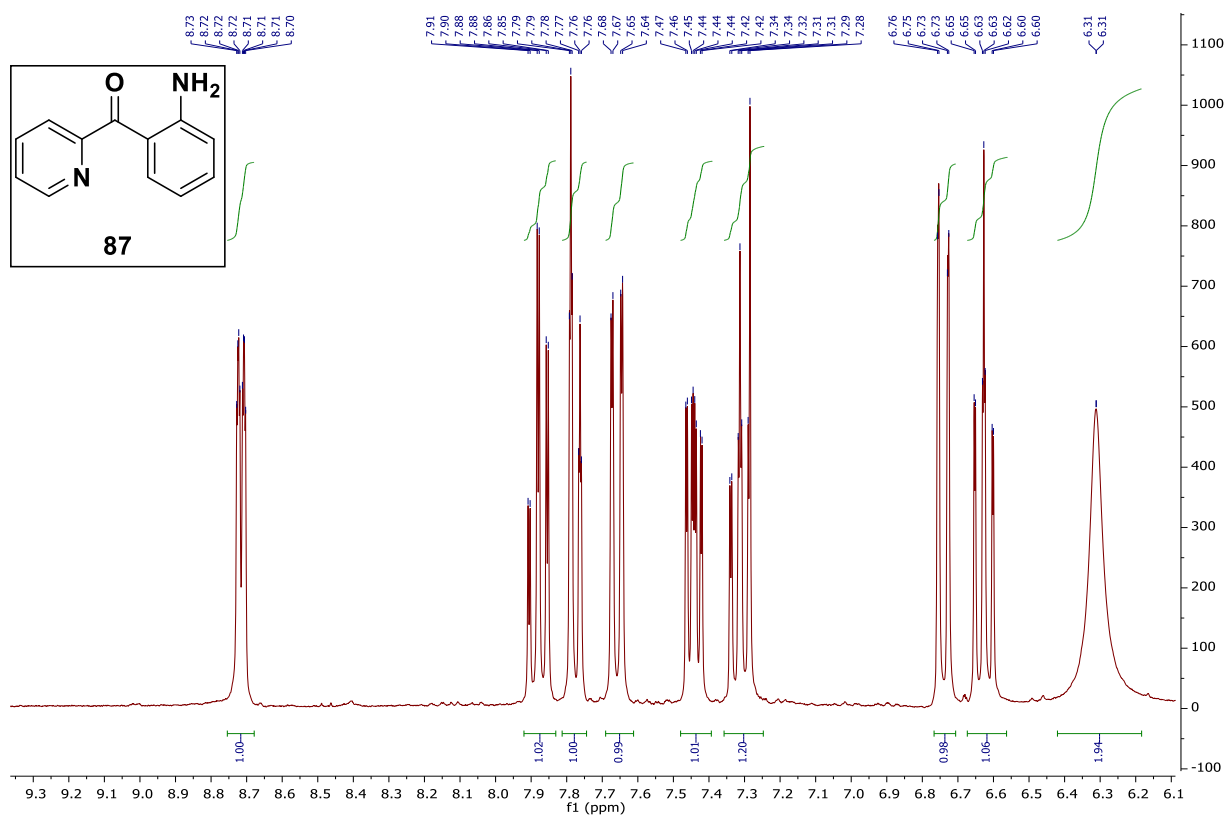
C:\Users\sussa...15MB20_2_n.raw\ Injection 1 TOF MS ES- MS - spectrum 0.40



9.1.3. Ethyl (Z)-2-hydroxy-2-(1-oxo-3,4-dihydronaphthalen-2(1H)-ylidene)acetate (**97**)

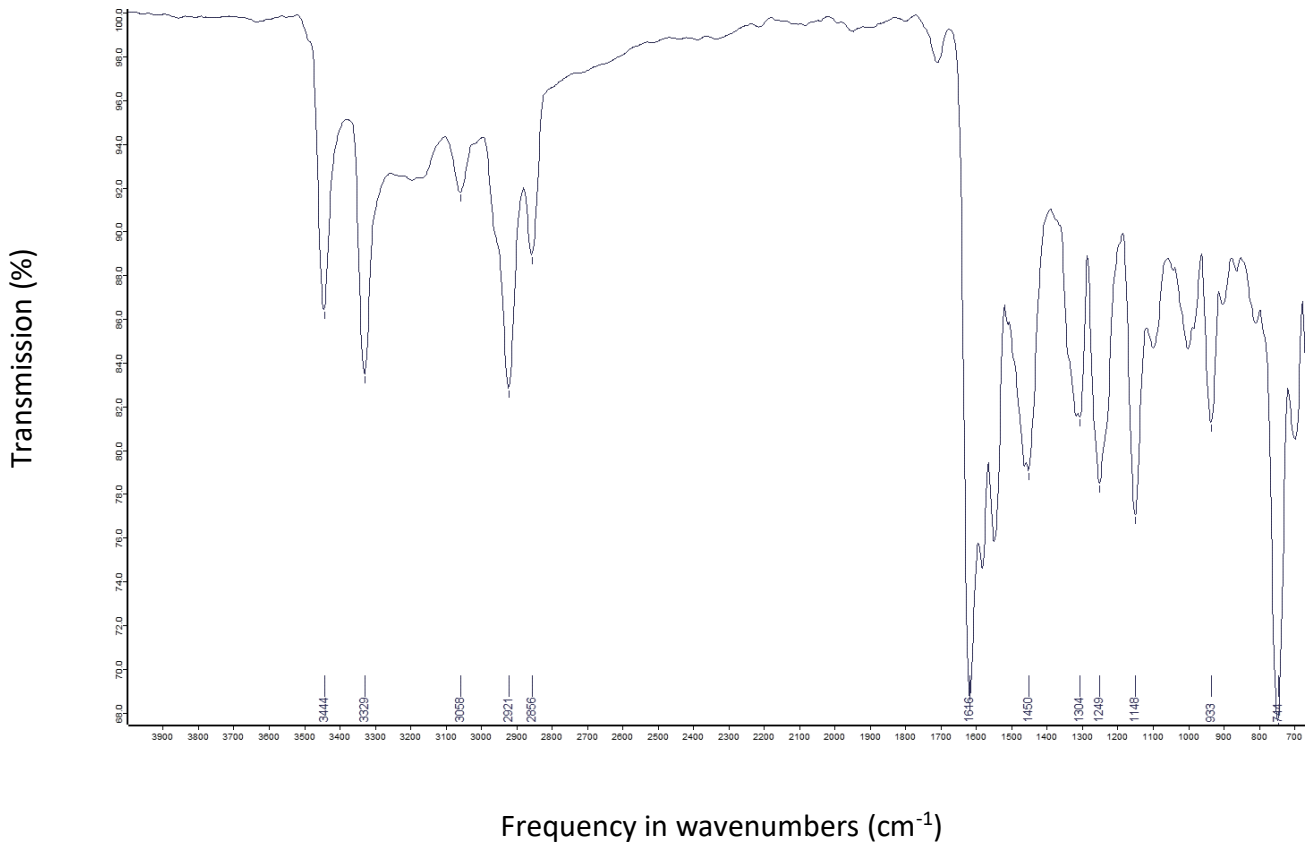
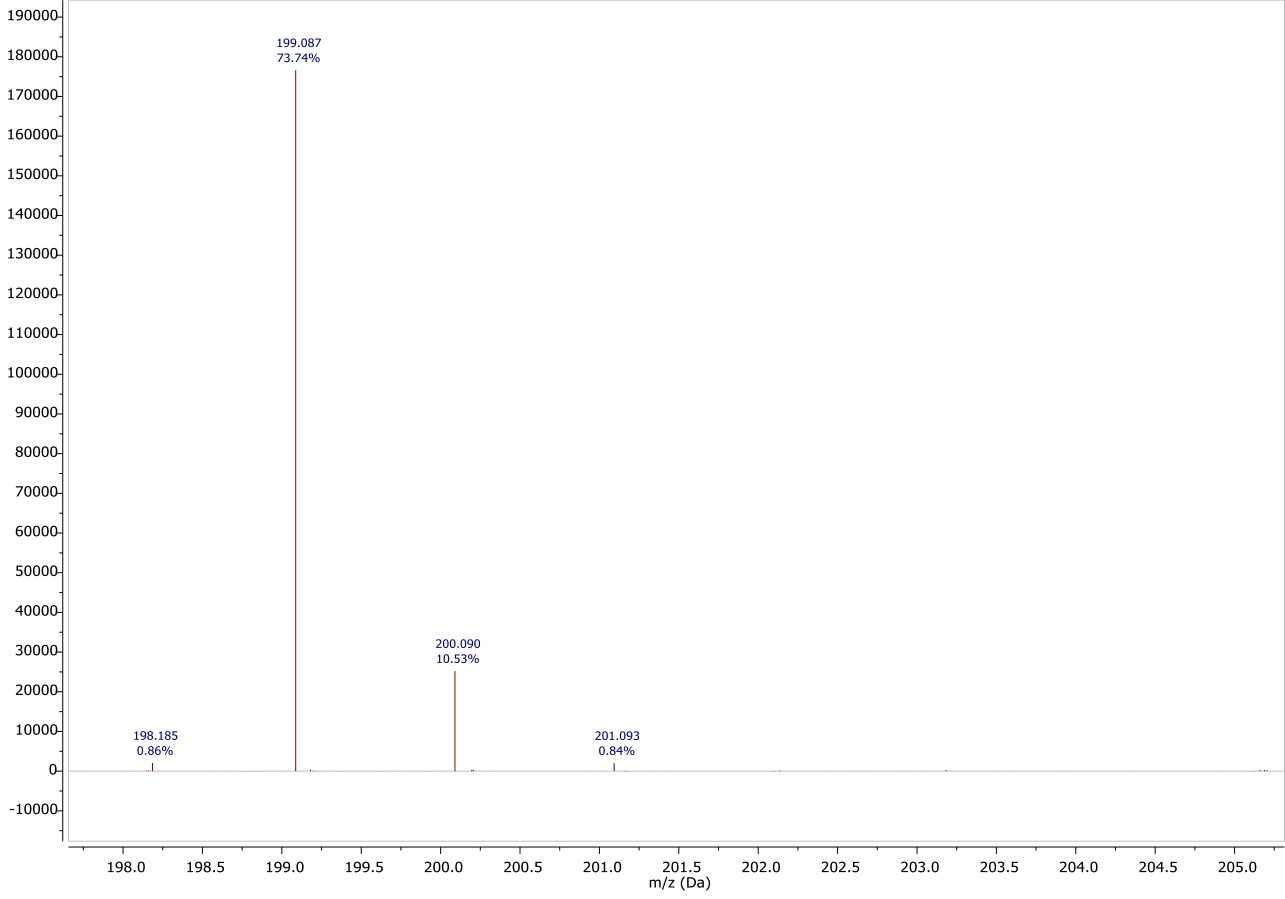


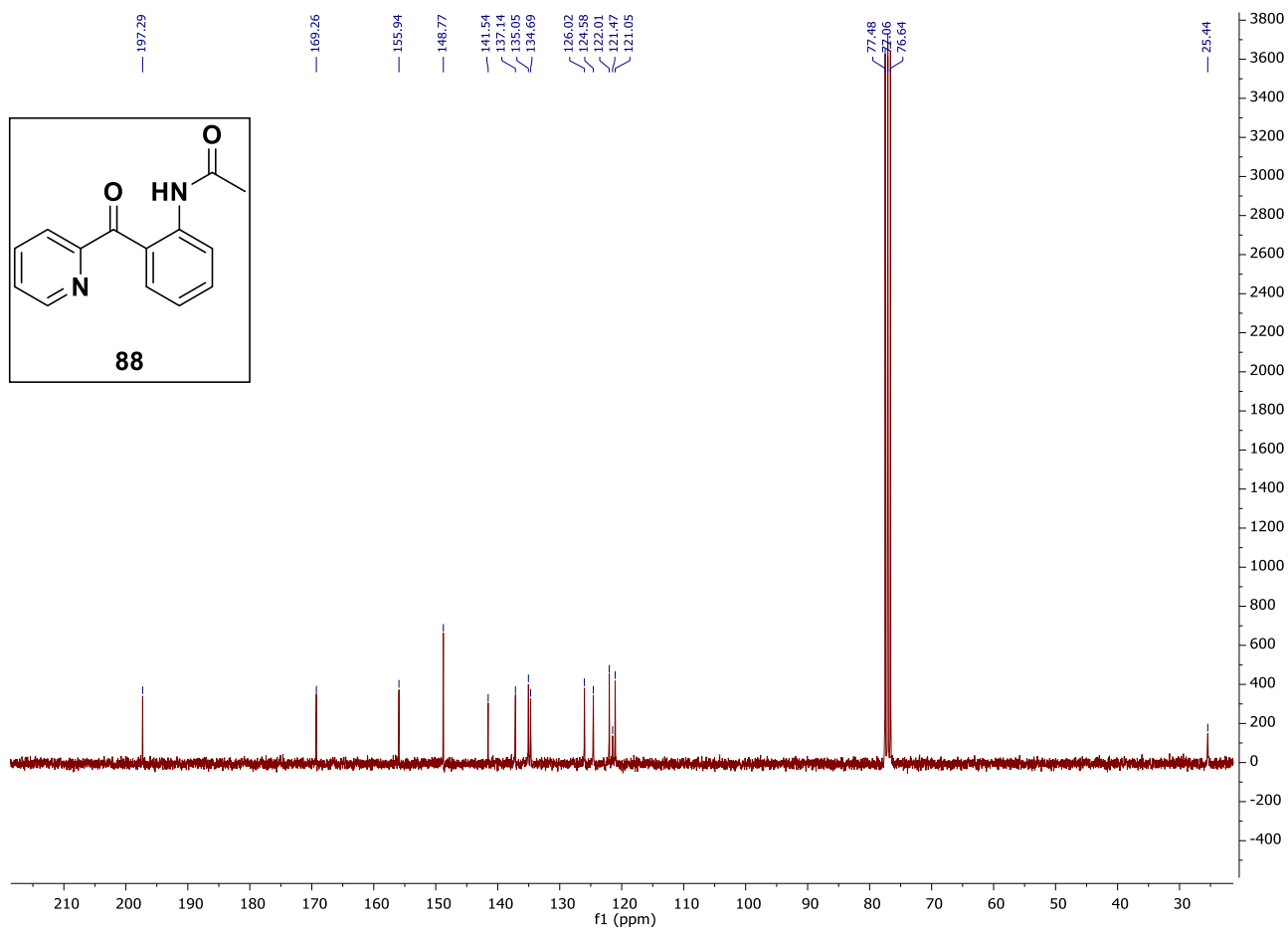
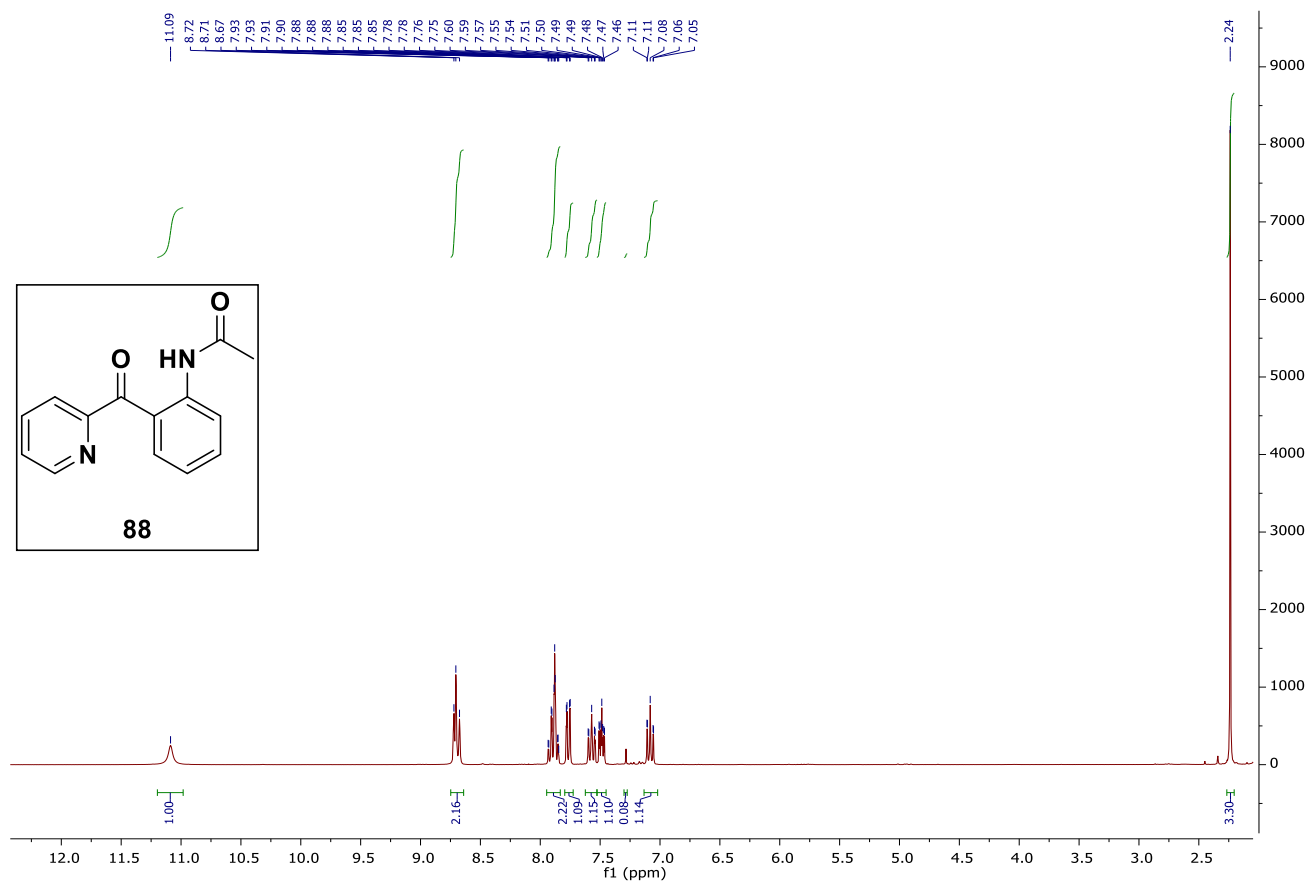
9.2. Experimental details relating to scaffold C

9.2.1. (2-aminophenyl)(pyridin-2-yl)methanone (**87**)

Chapter 9: Experimental Spectrums

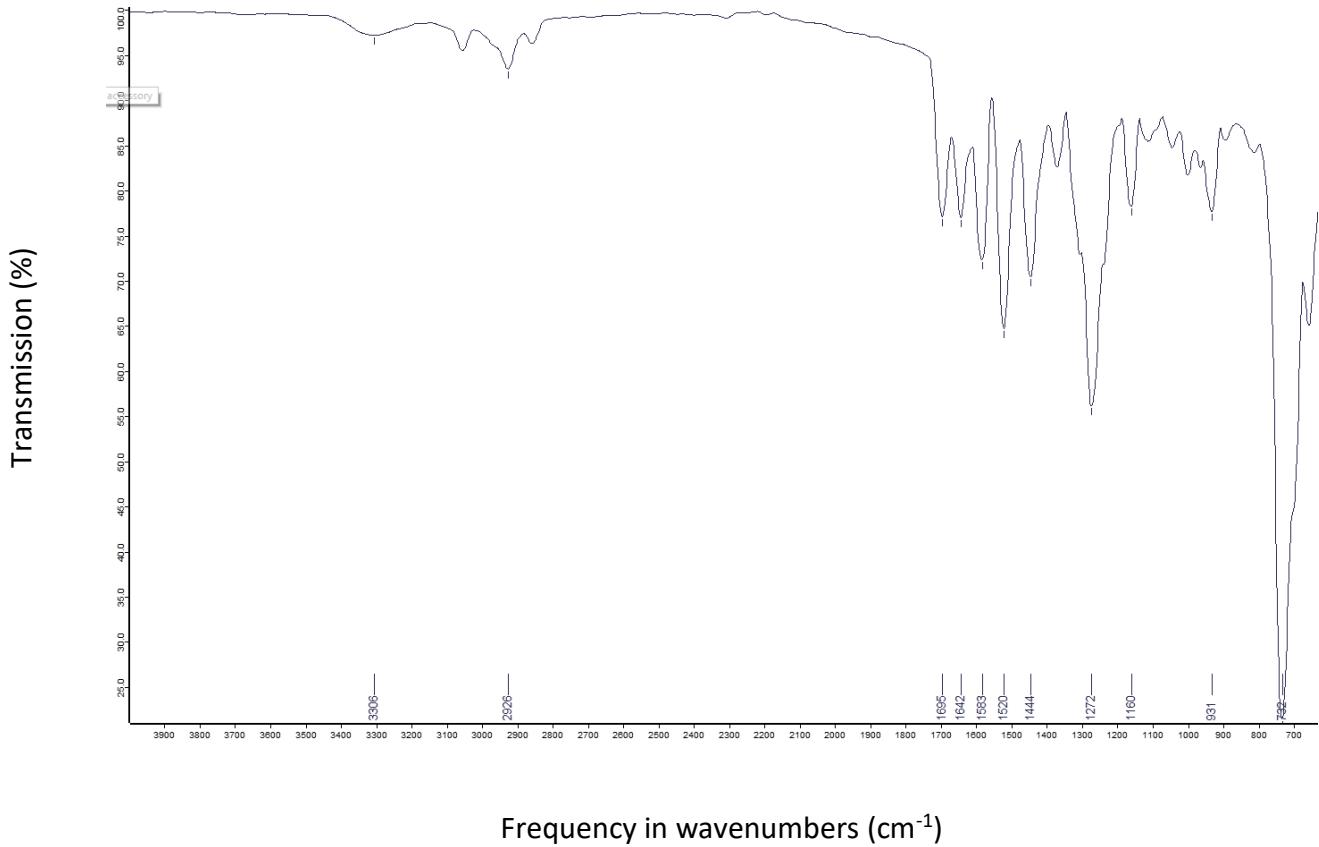
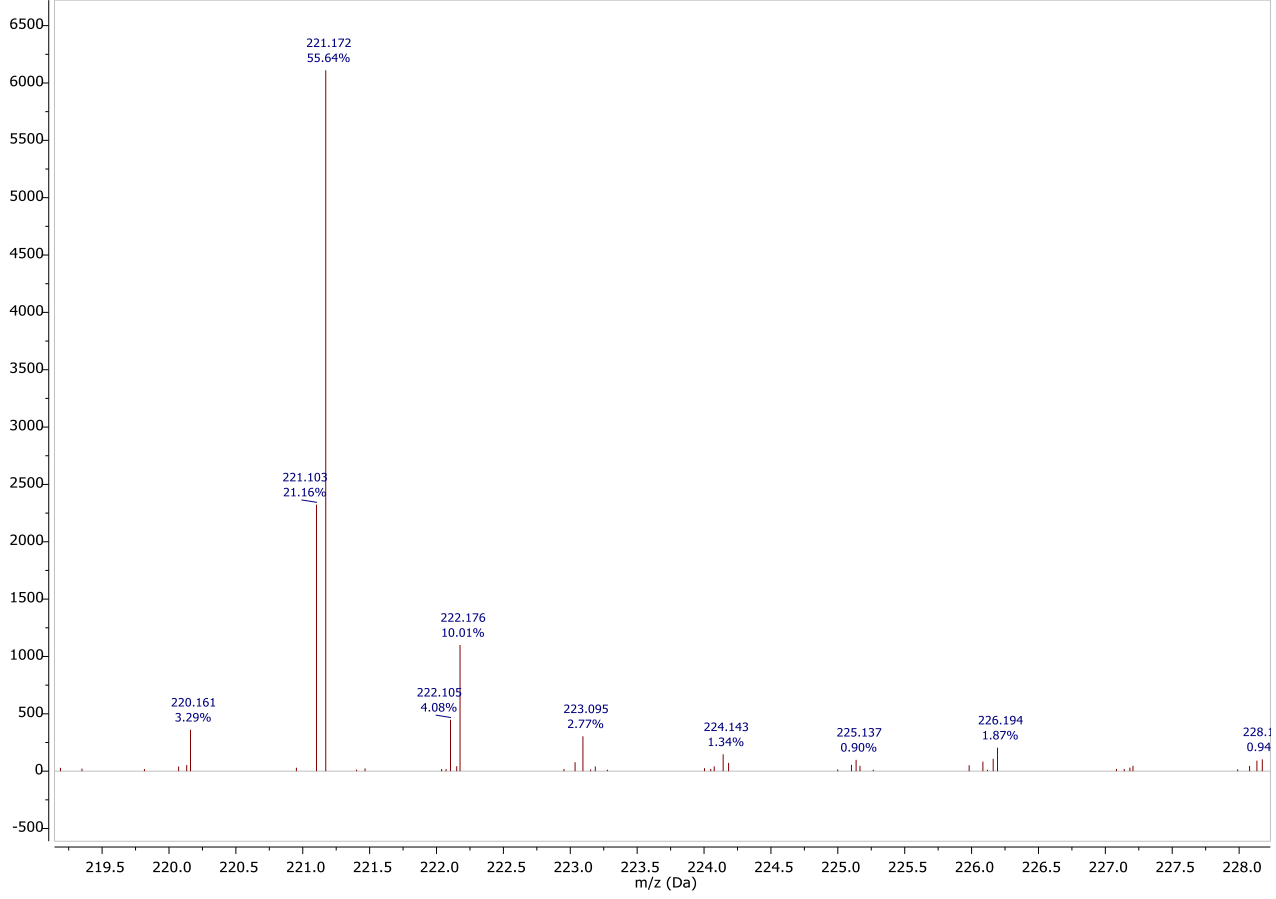
C:\Users\sussa...an_2SMB4_p.raw\ Injection 1 TOF MS ES+ MS + spectrum 0.37

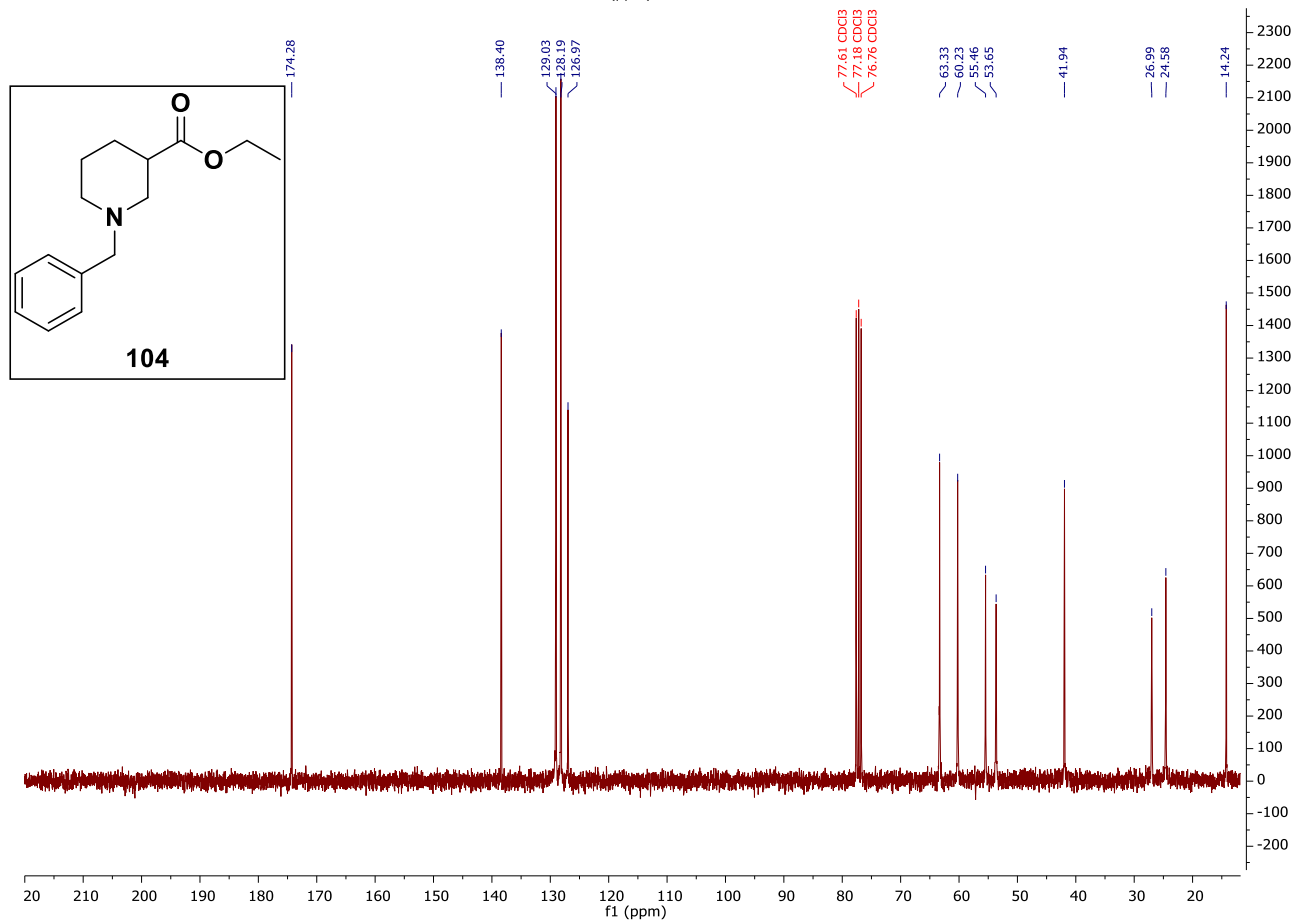
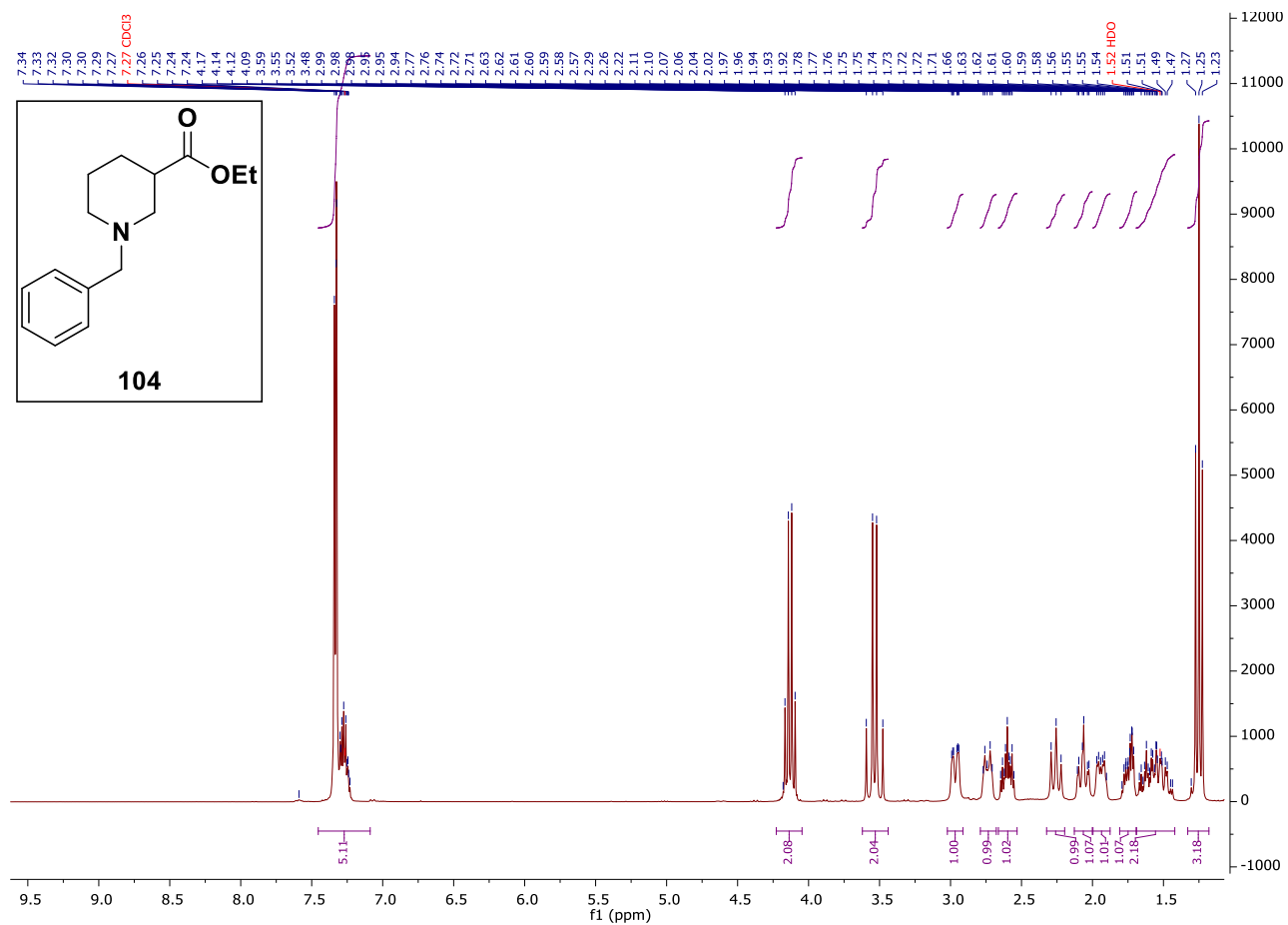


9.2.2. *N*-(2-picolinoylphenyl)acetamide (**88**)

Chapter 9: Experimental Spectrums

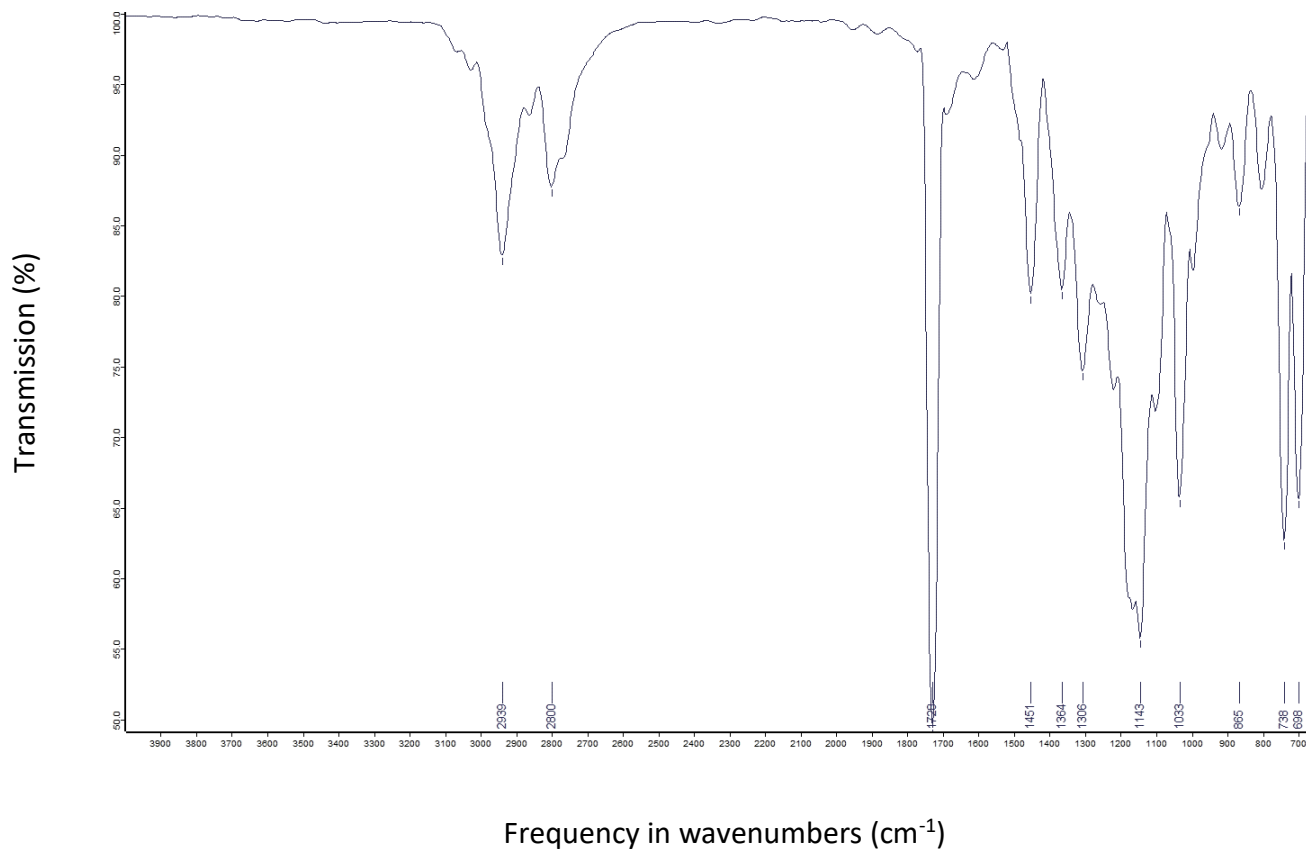
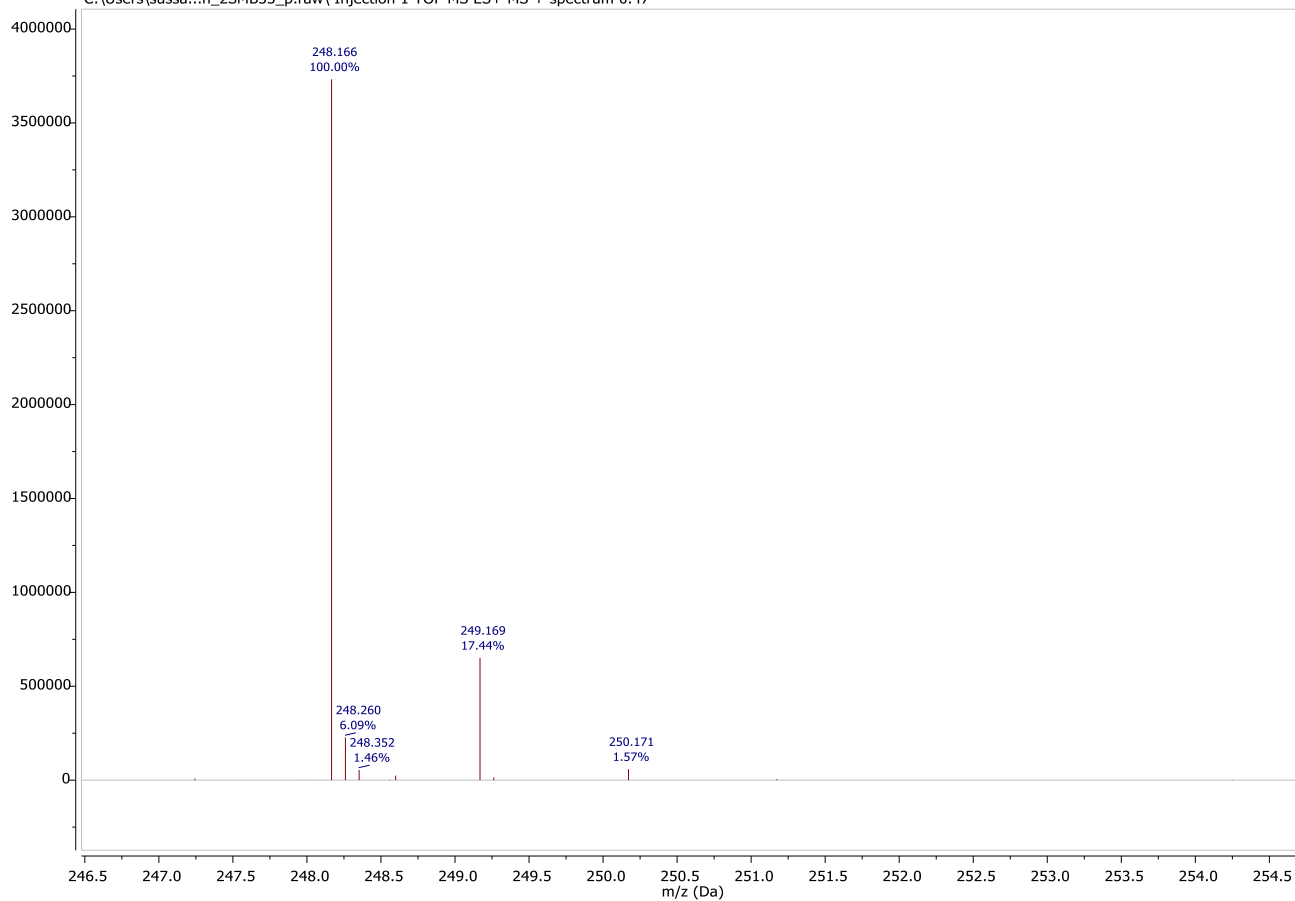
C:\Users\sussa...an_2SMB3_n.raw\ Injection 1 TOF MS ES- MS - spectrum 0.38

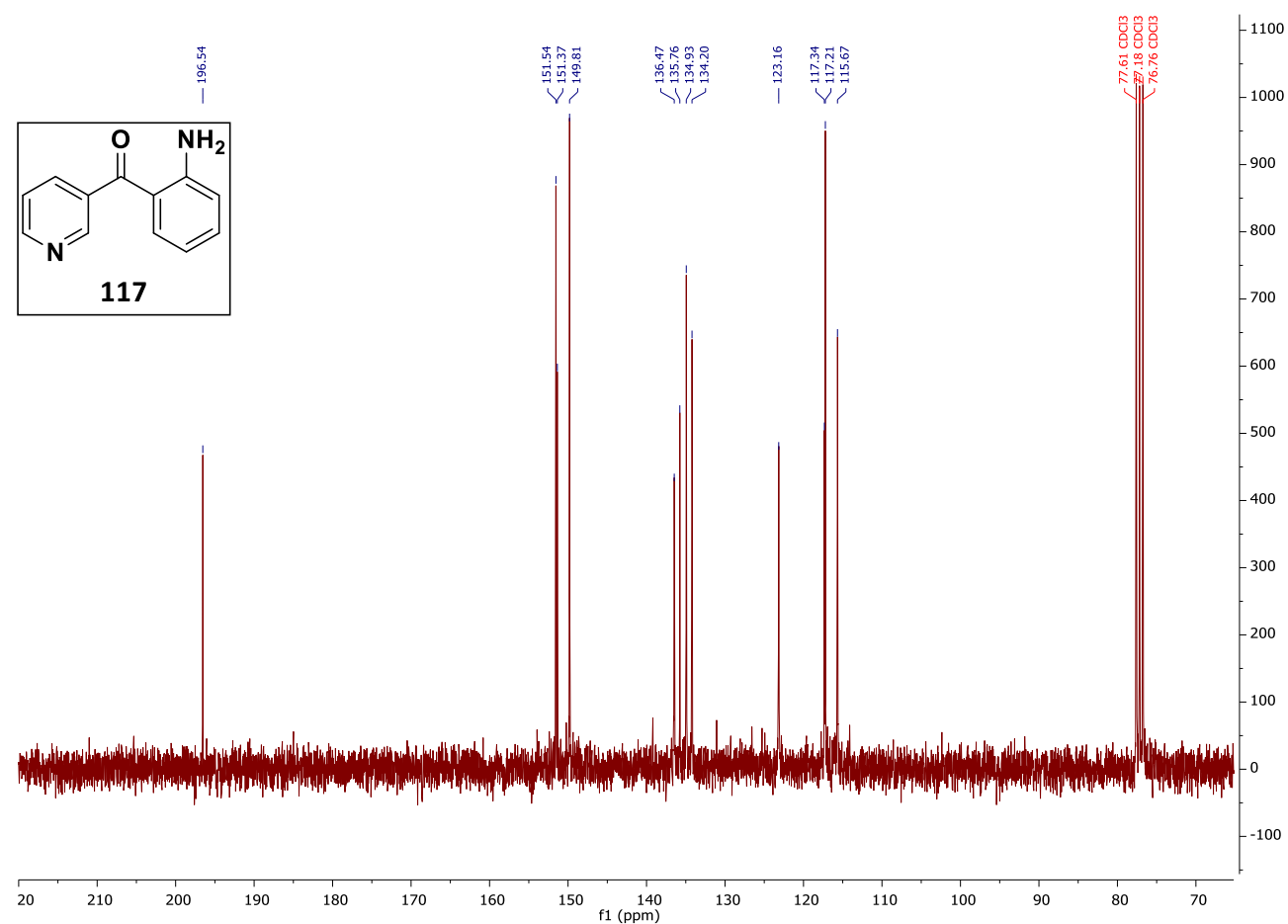
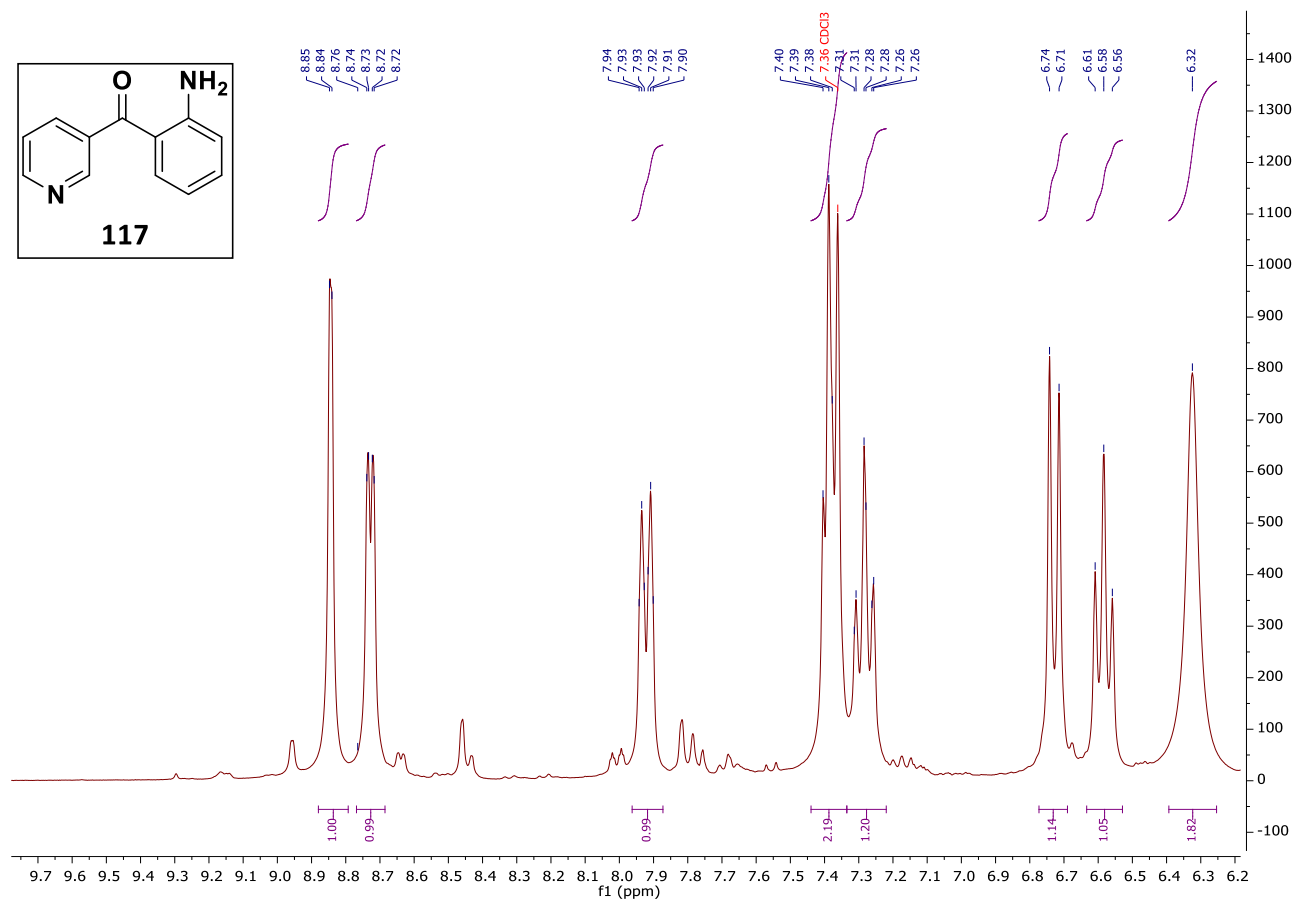


9.2.3. Ethyl 1-benzylpiperidine-3-carboxylate (**104**)

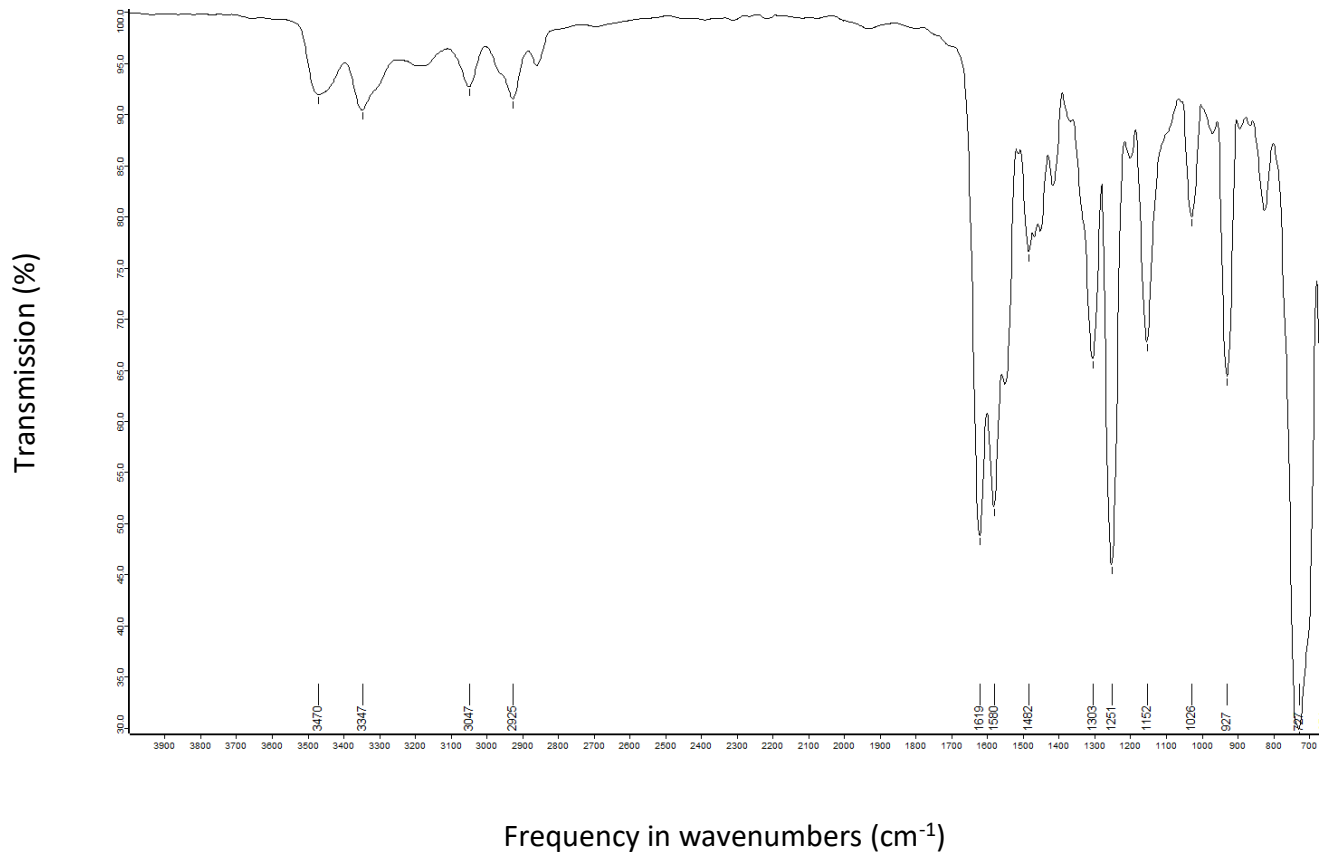
Chapter 9: Experimental Spectrums

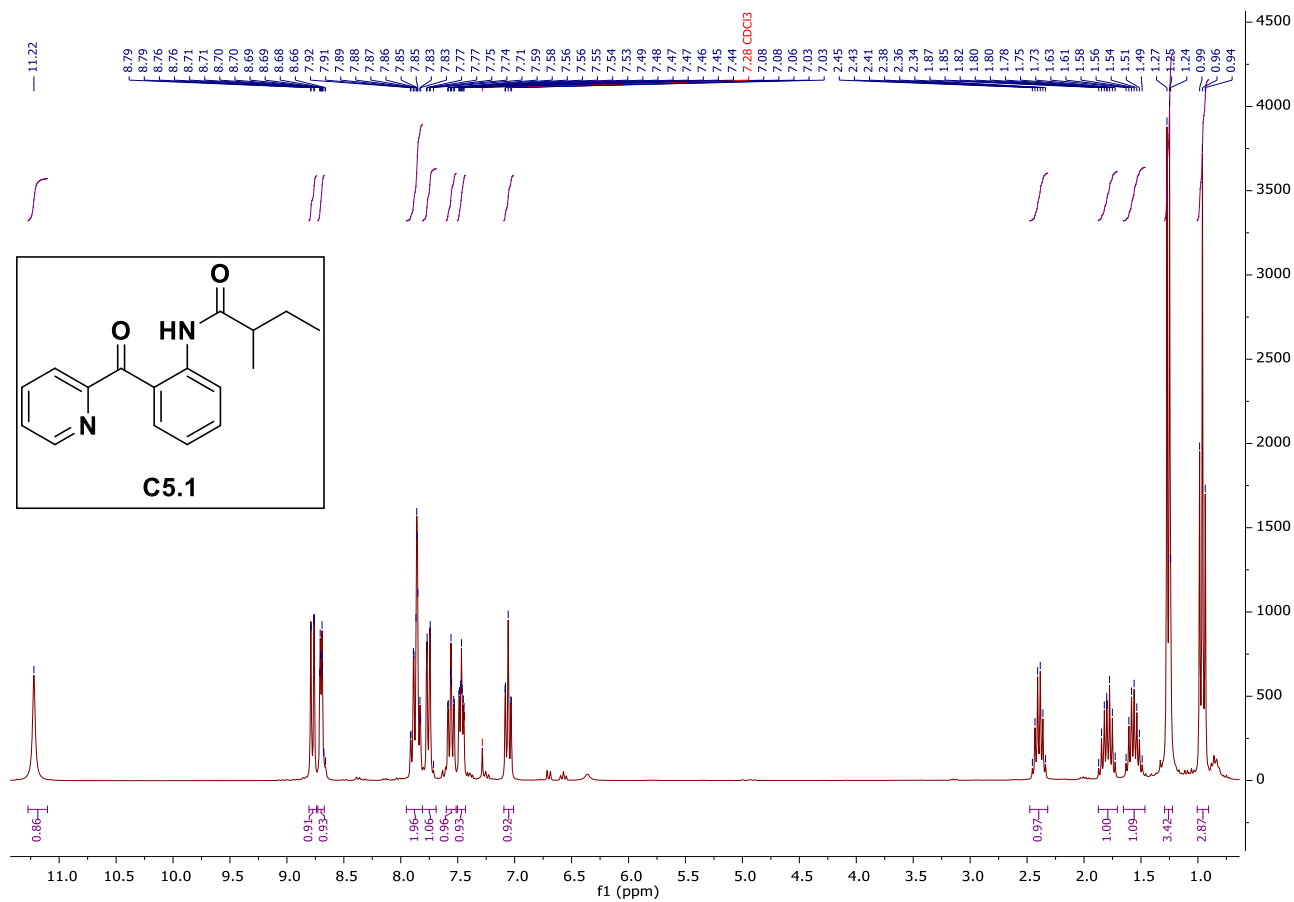
C:\Users\sussa...n_2SMB53_p.raw\ Injection 1 TOF MS ES+ MS + spectrum 0.47



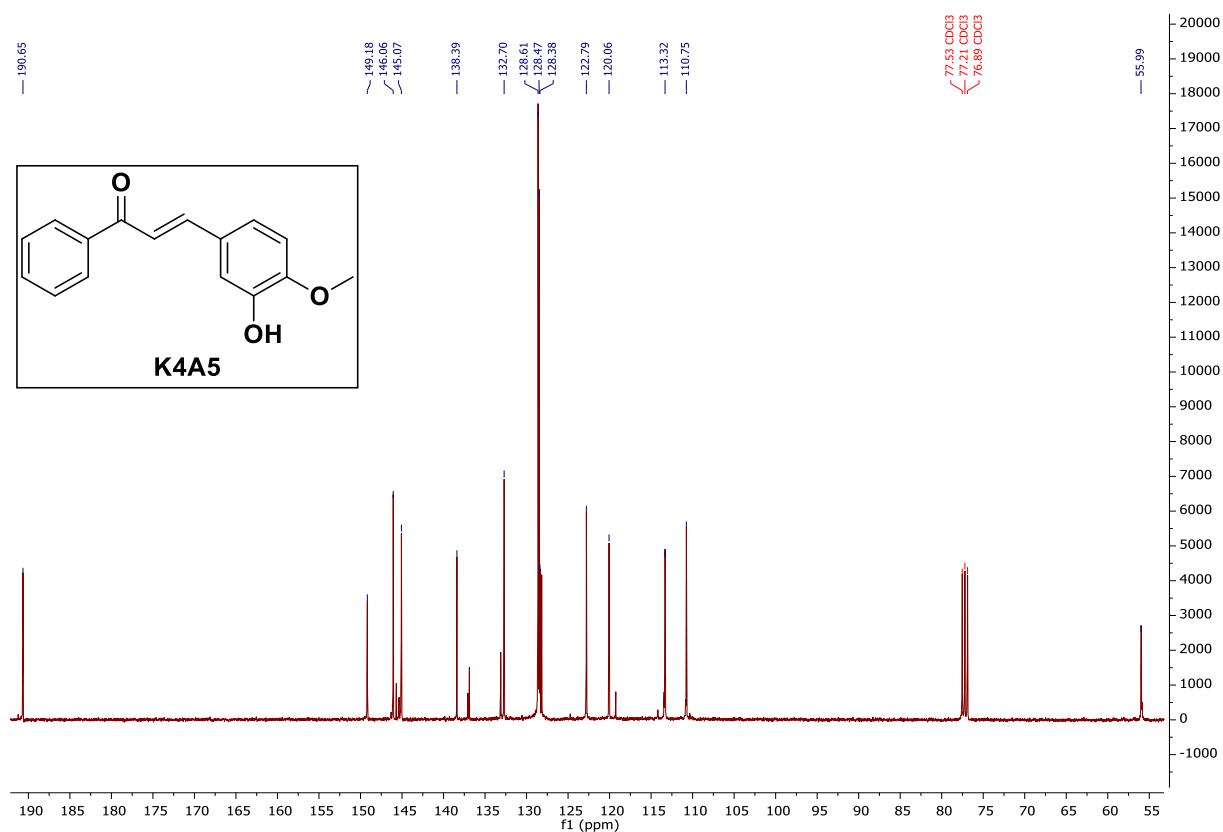
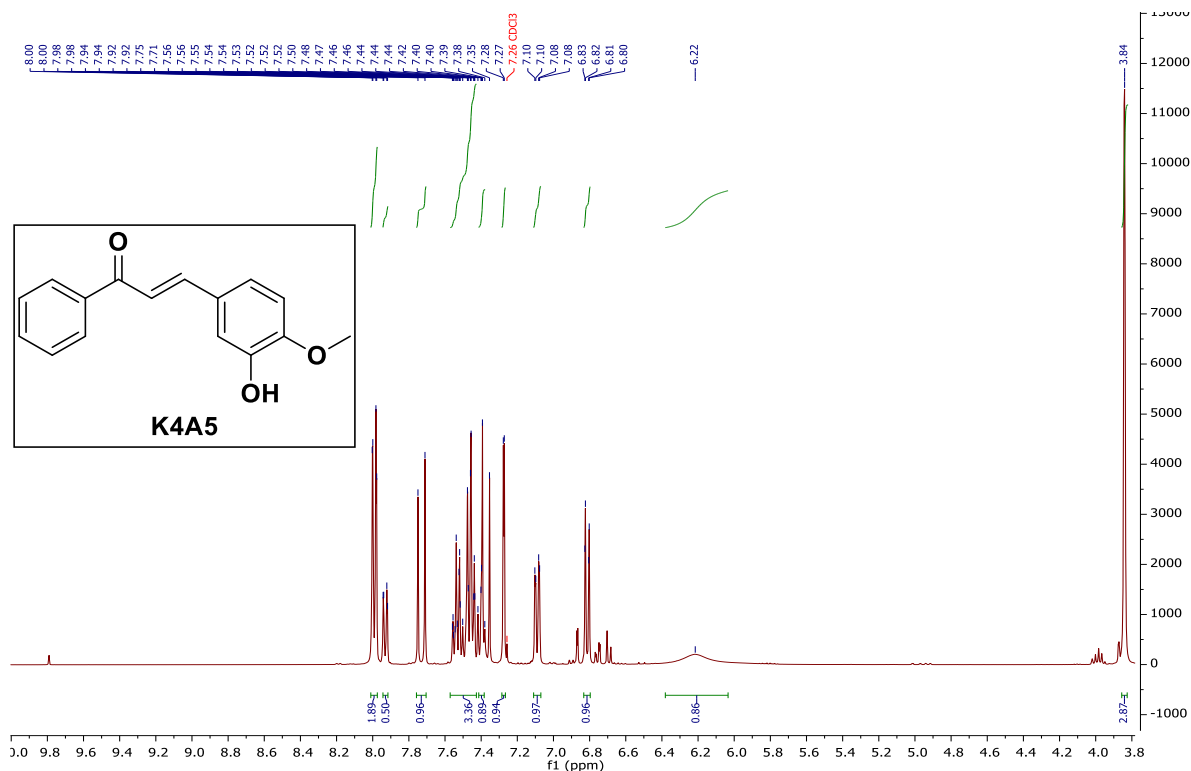
9.2.4. (2-aminophenyl)(pyridin-3-yl)methanone (**117**)

Chapter 9: Experimental Spectrums

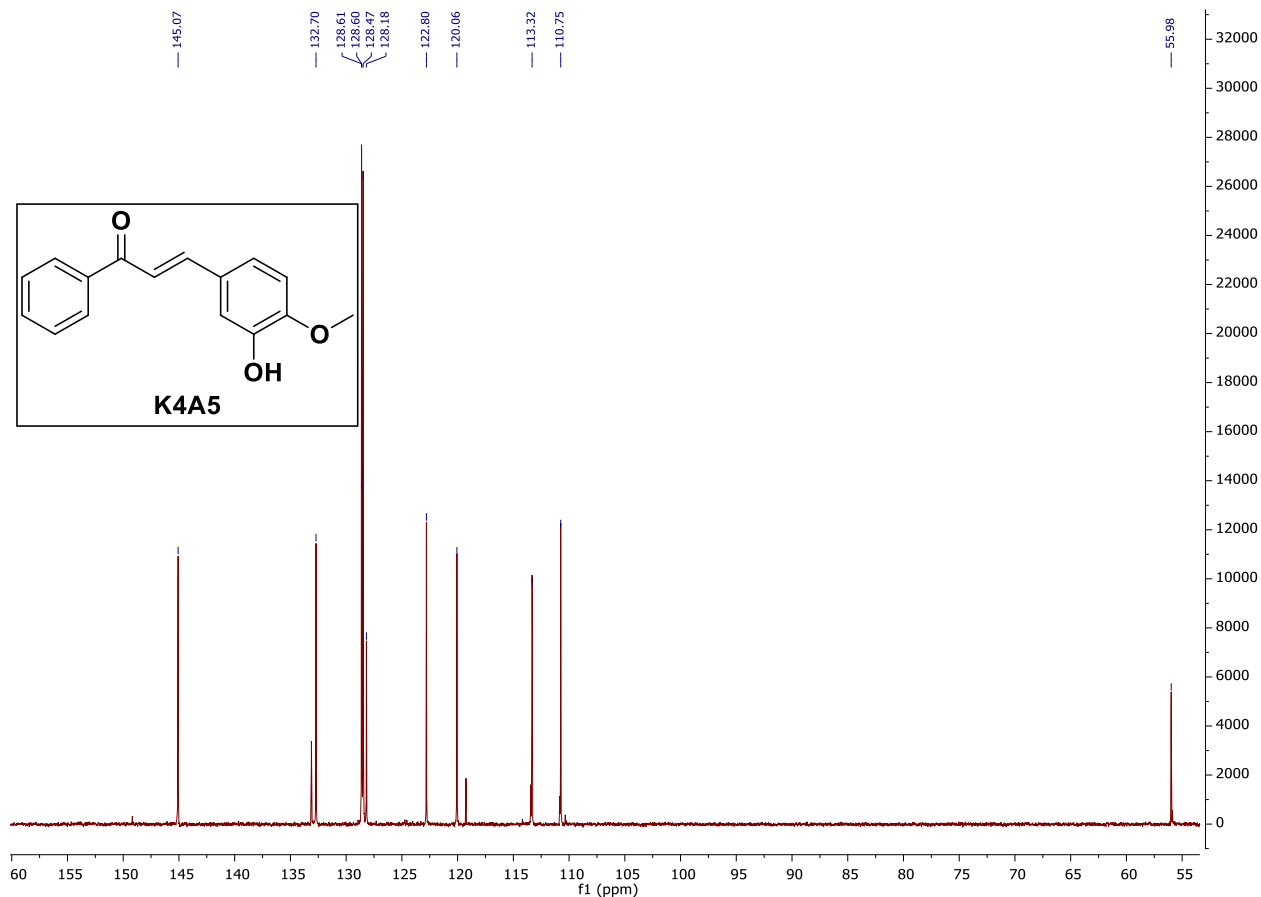


9.2.5. 2-methyl-*N*-(2-picolinoylphenyl)butanamide (C5.1)

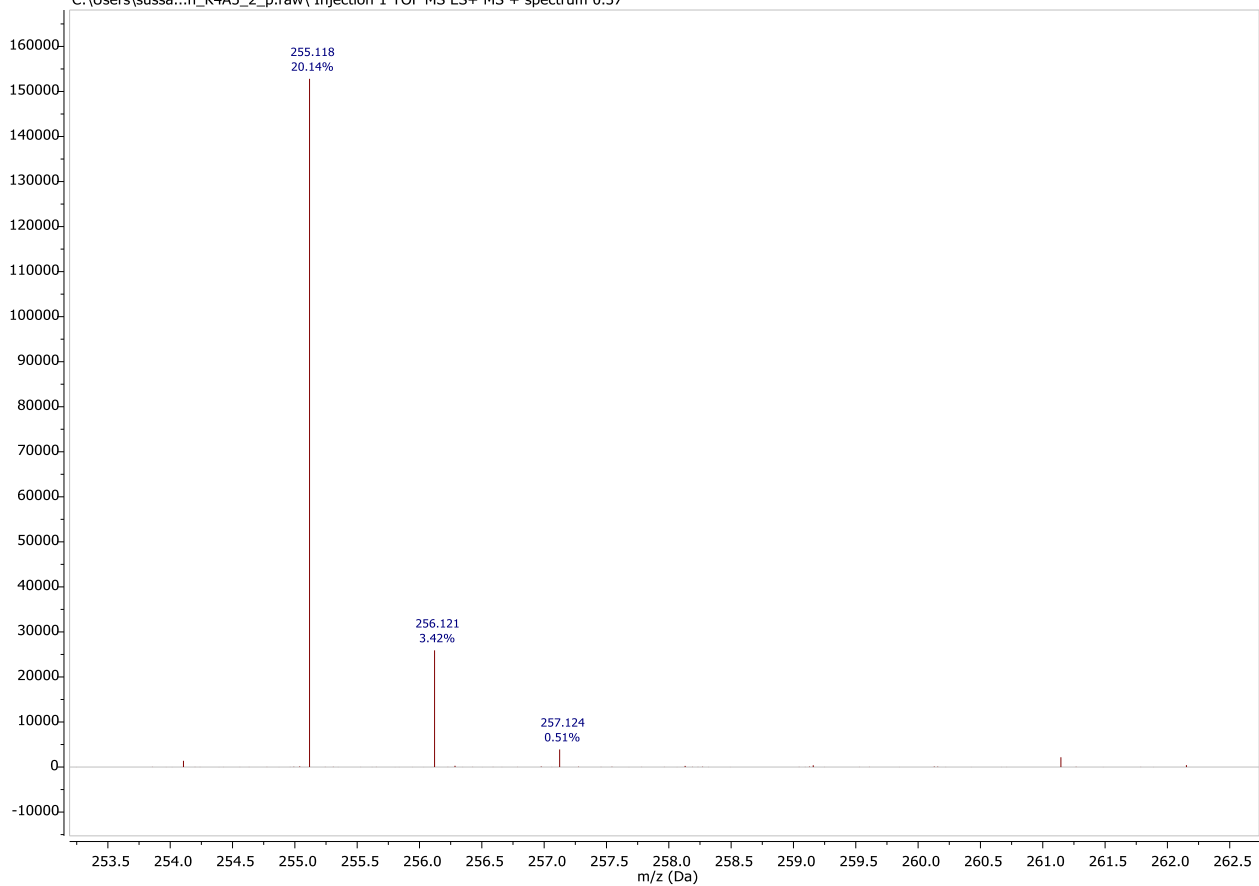
9.3. Experimental details relating to scaffold D

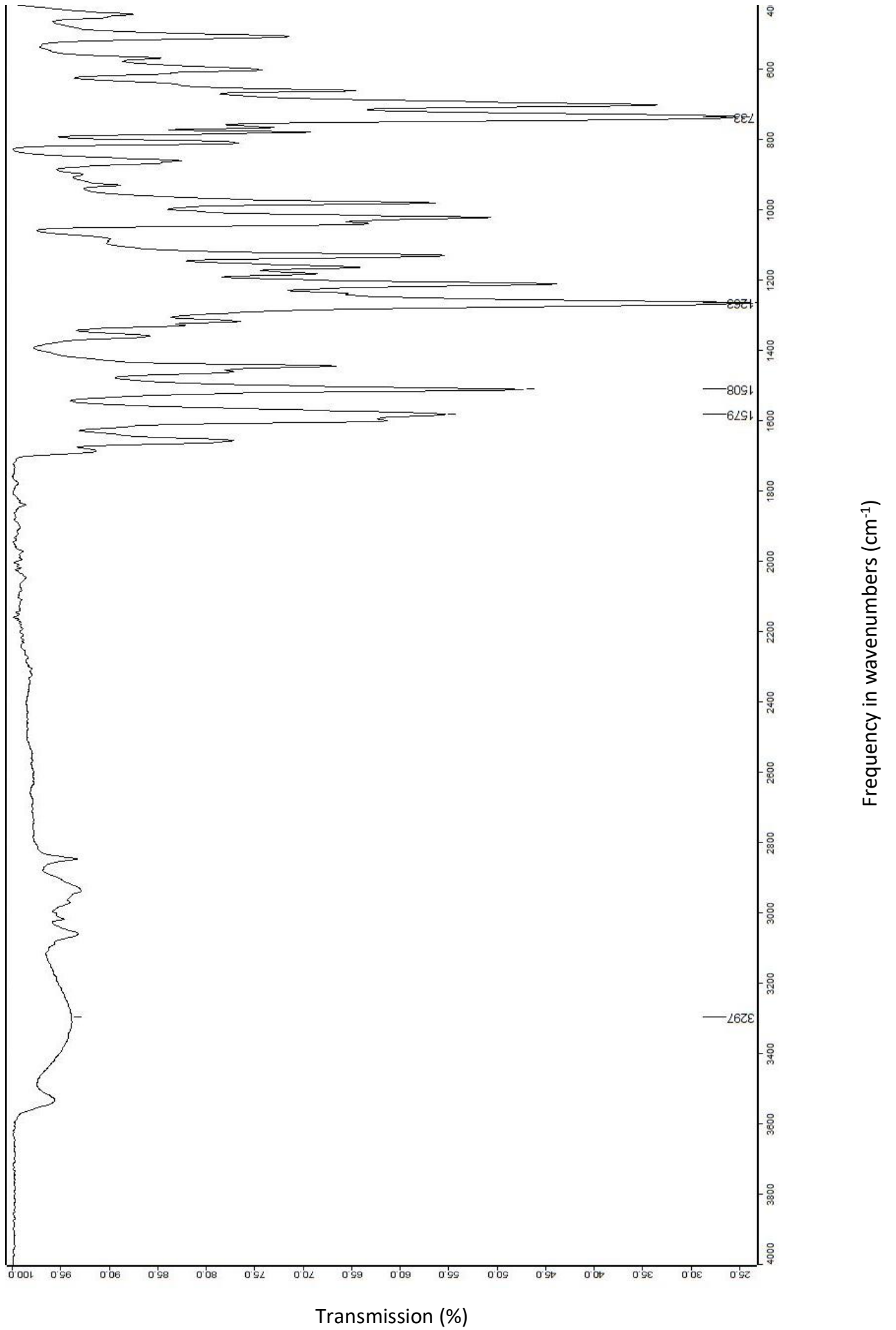
9.3.1. (*E*)-3-(3-hydroxy-4-methoxyphenyl)-1-phenylprop-2-en-1-one
(K4A5)

Chapter 9: Experimental Spectrums

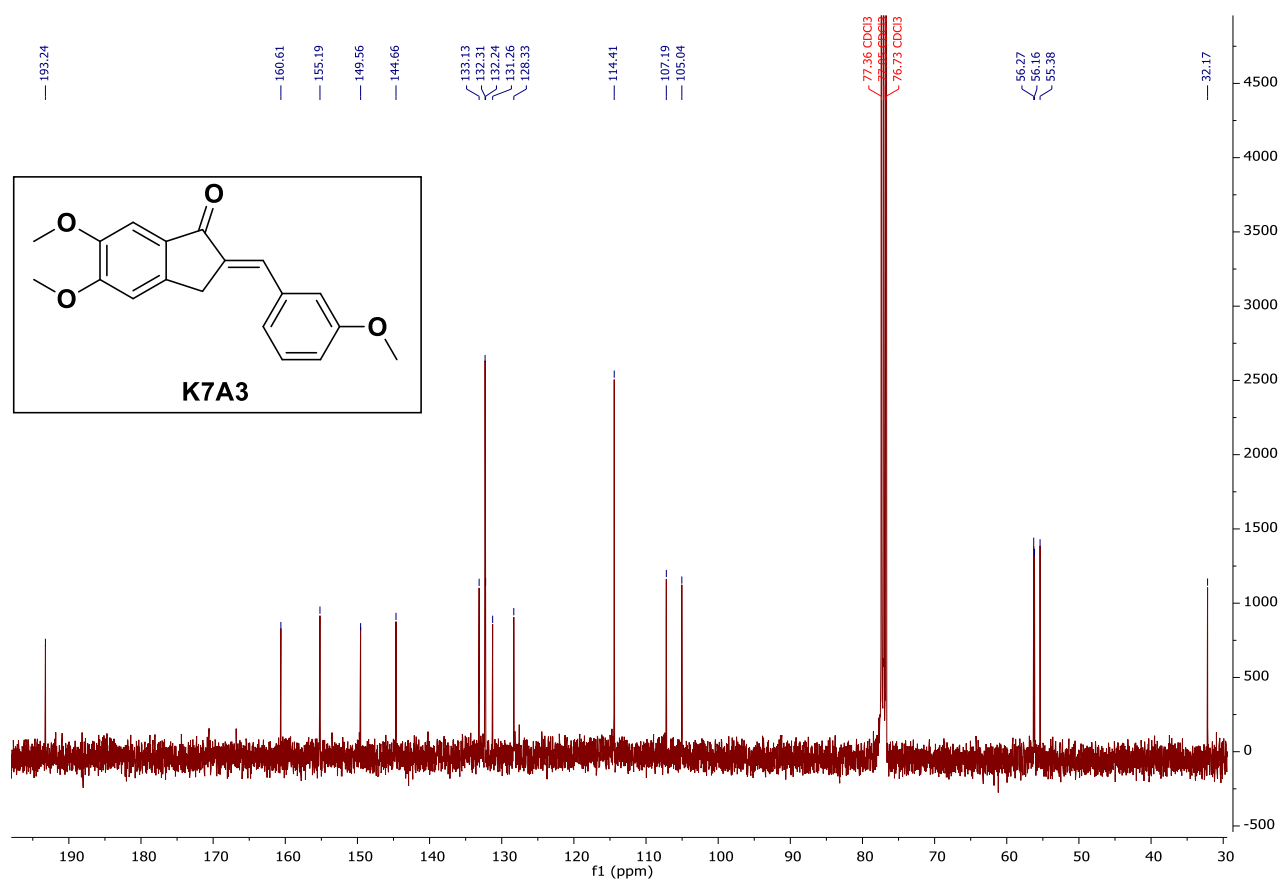
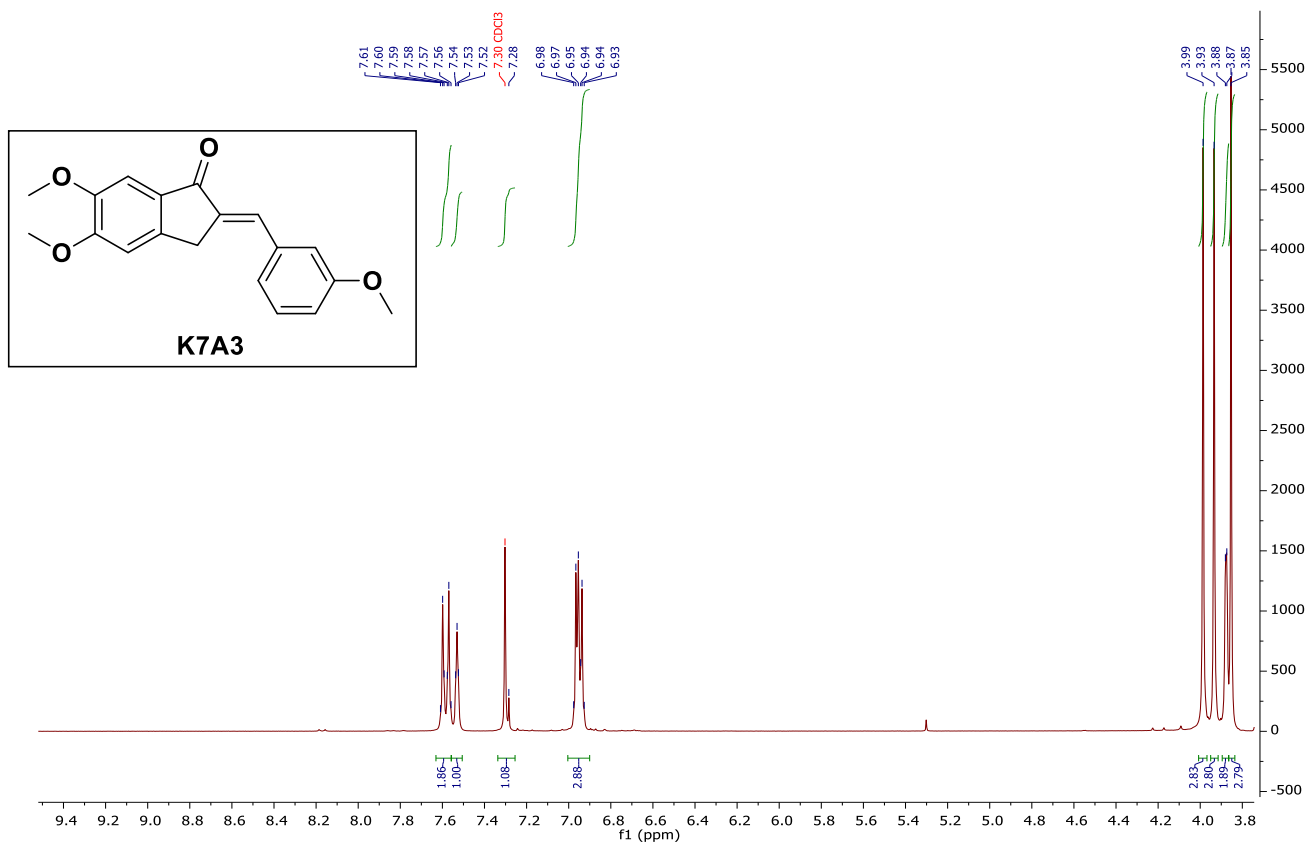


C:\Users\sussa...n_K4A5_2_p.raw\ Injection 1 TOF MS ES+ MS + spectrum 0.37

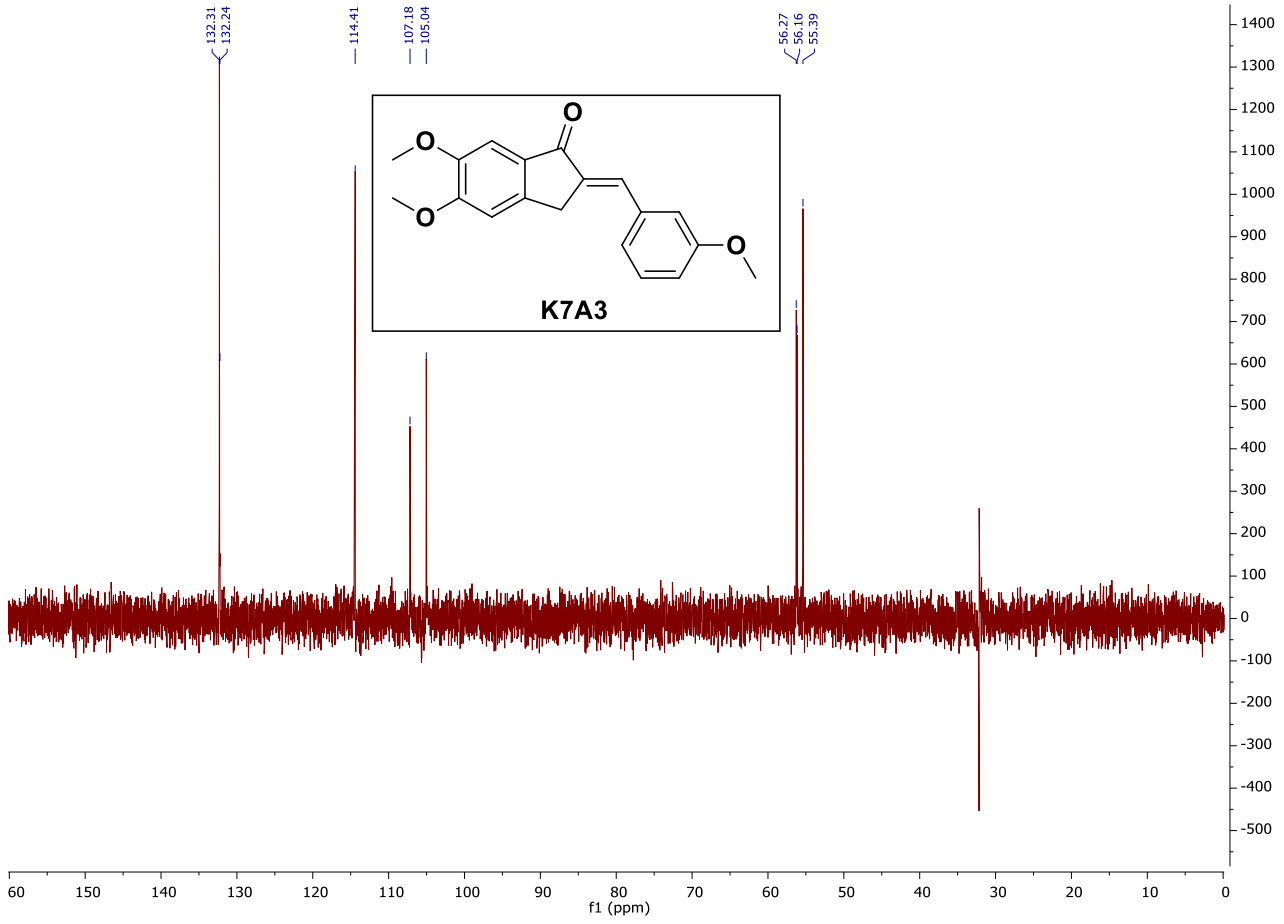




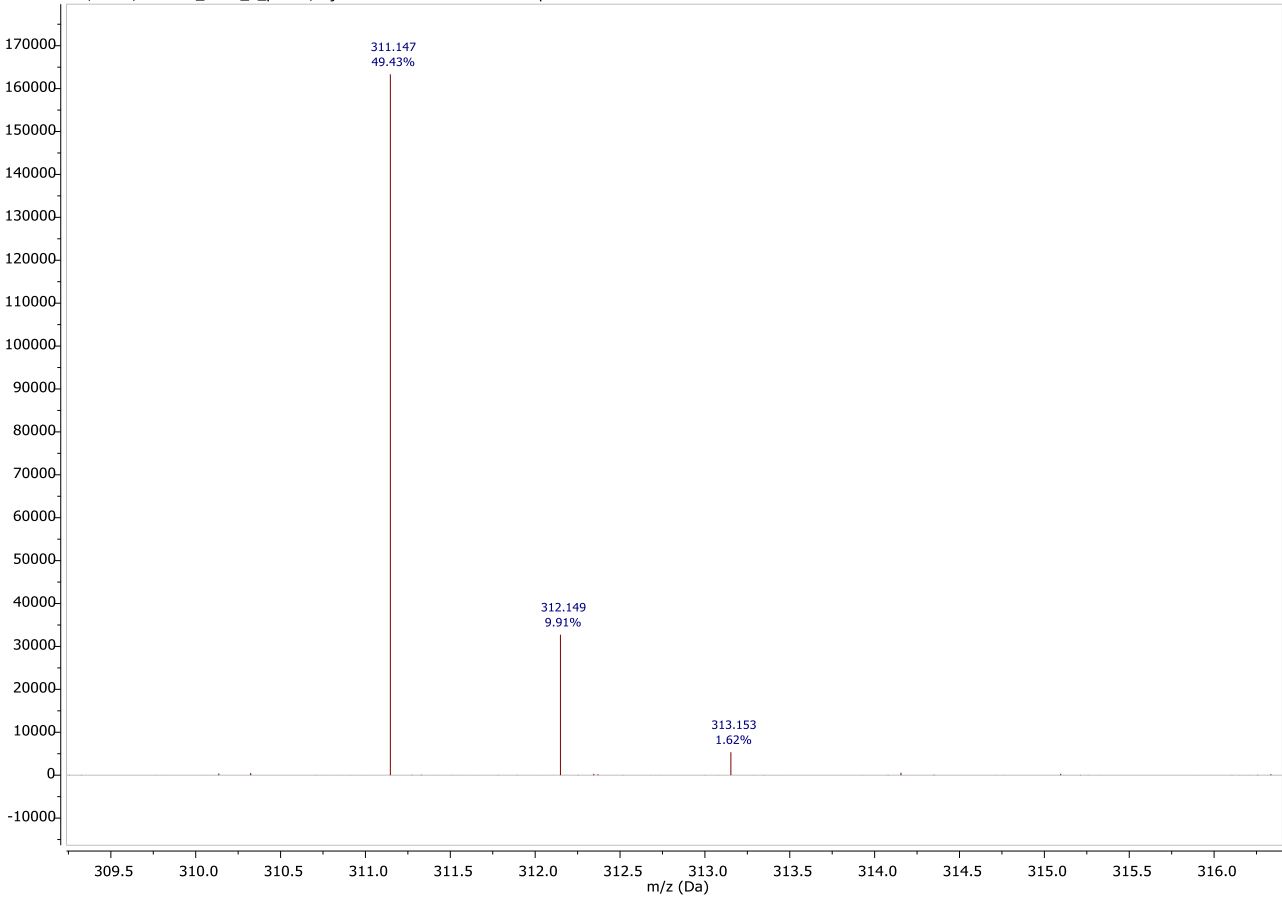
9.3.2. (E)-5,6-dimethoxy-2-(3-methoxybenzylidene)-2,3-dihydro-1H-inden-1-one (K7A3)

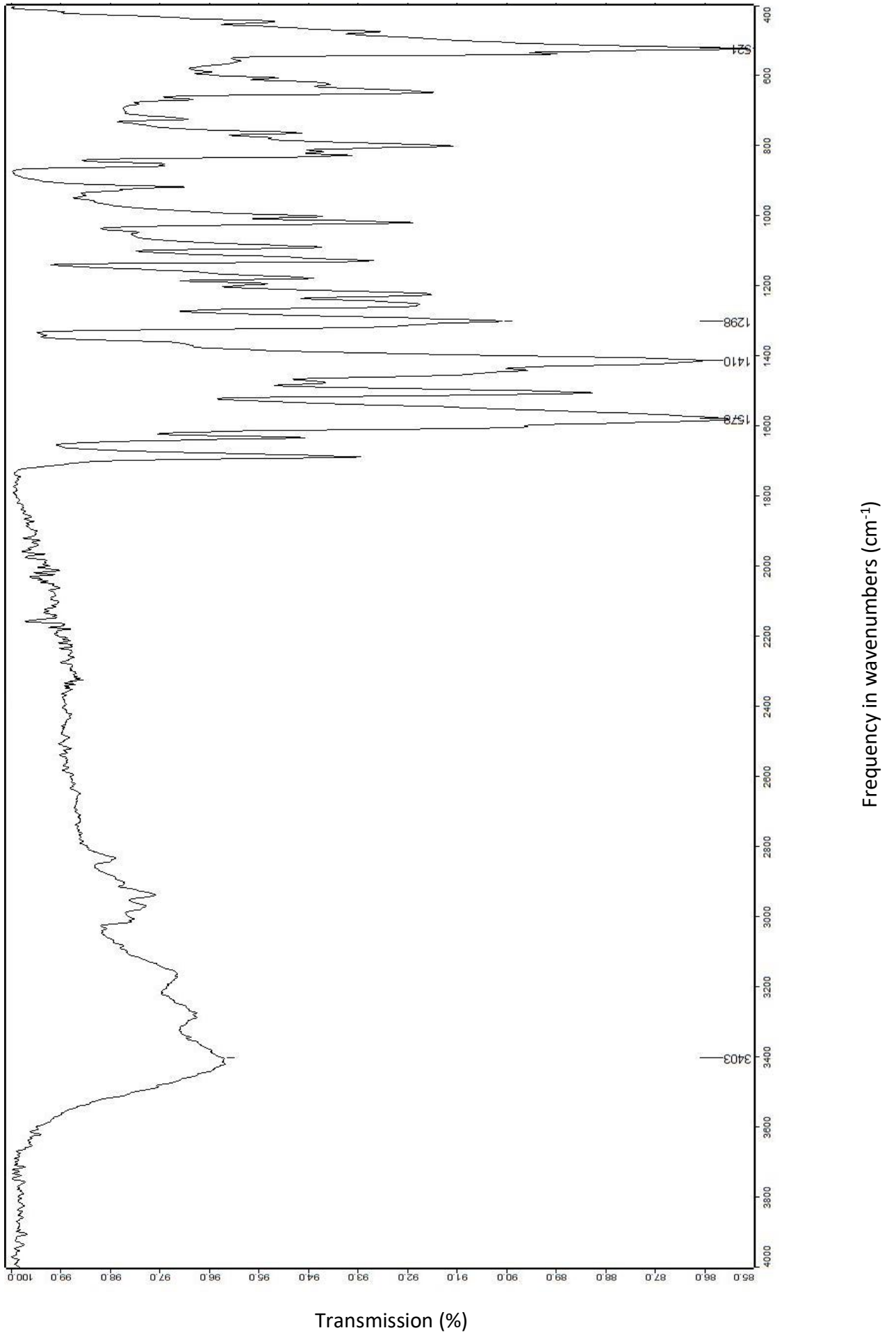


Chapter 9: Experimental Spectra

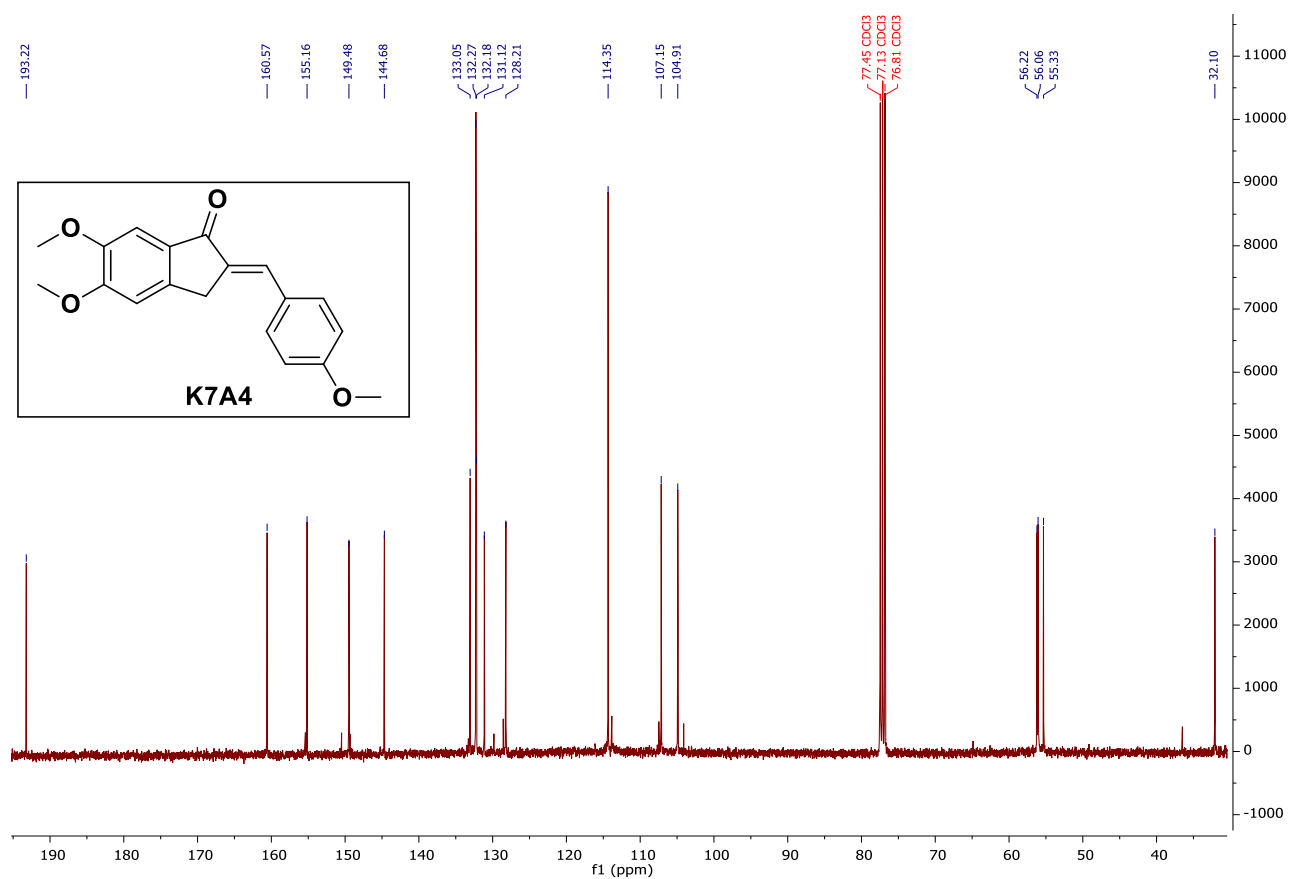
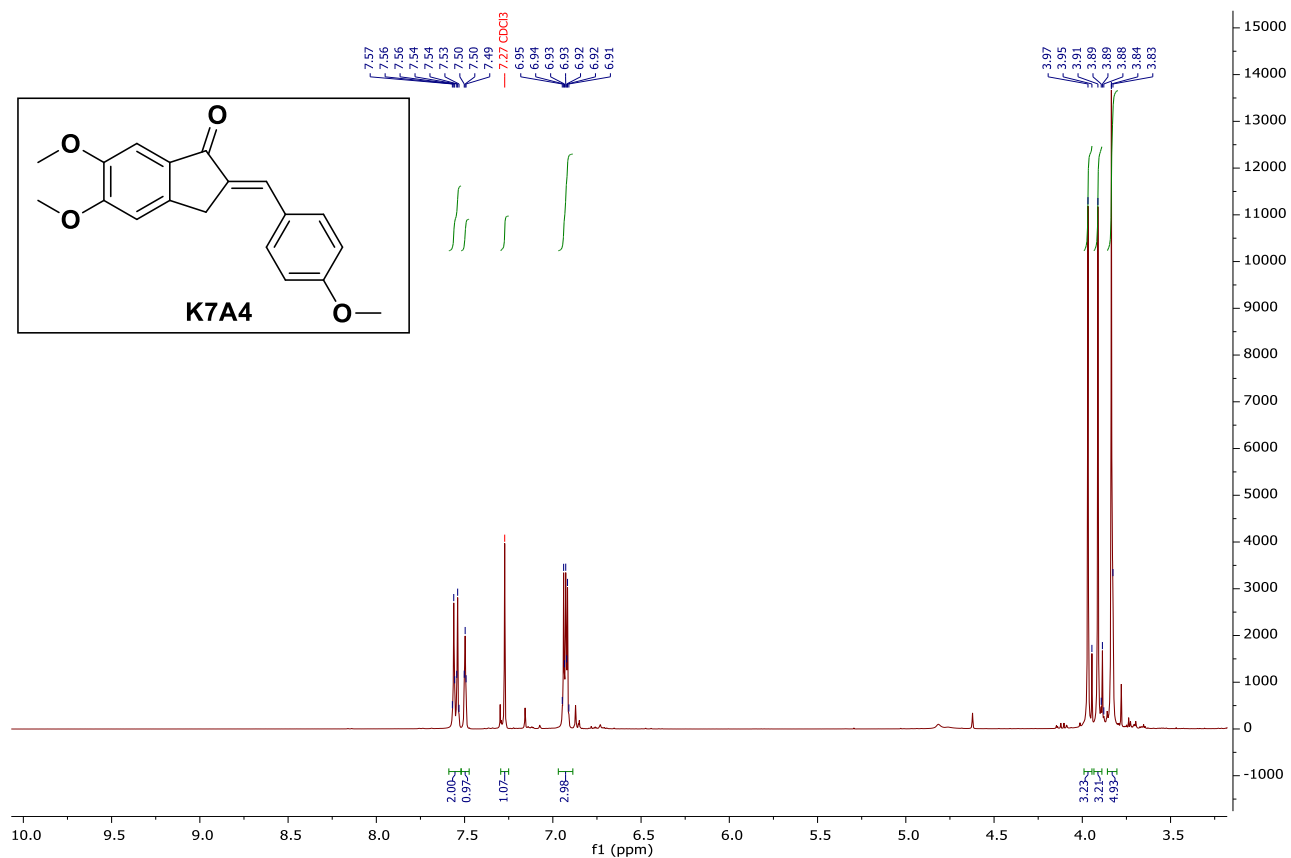


C:\Users\sussa...n_K7A3_2_p.raw\ Injection 1 TOF MS ES+ MS + spectrum 0.39

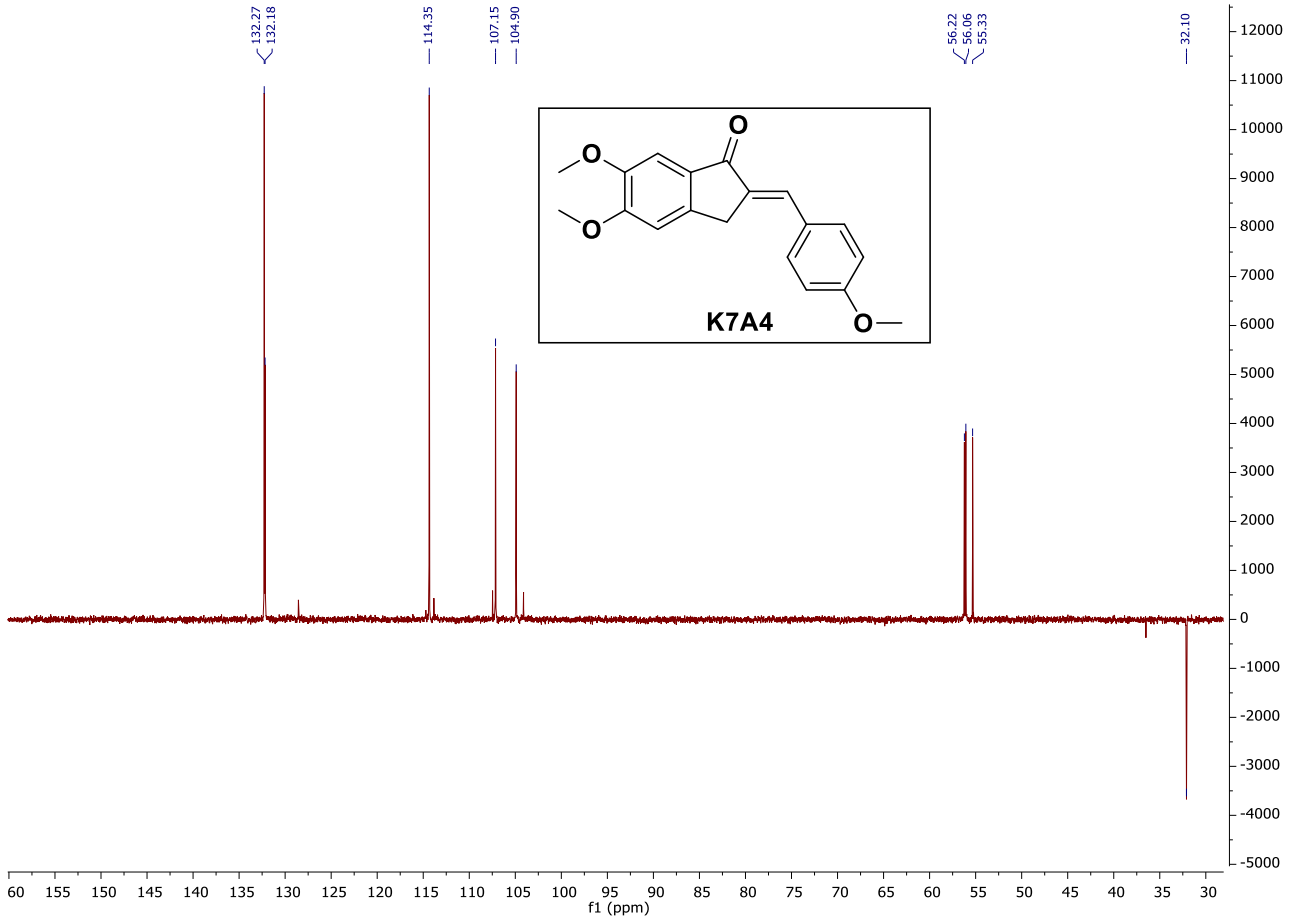




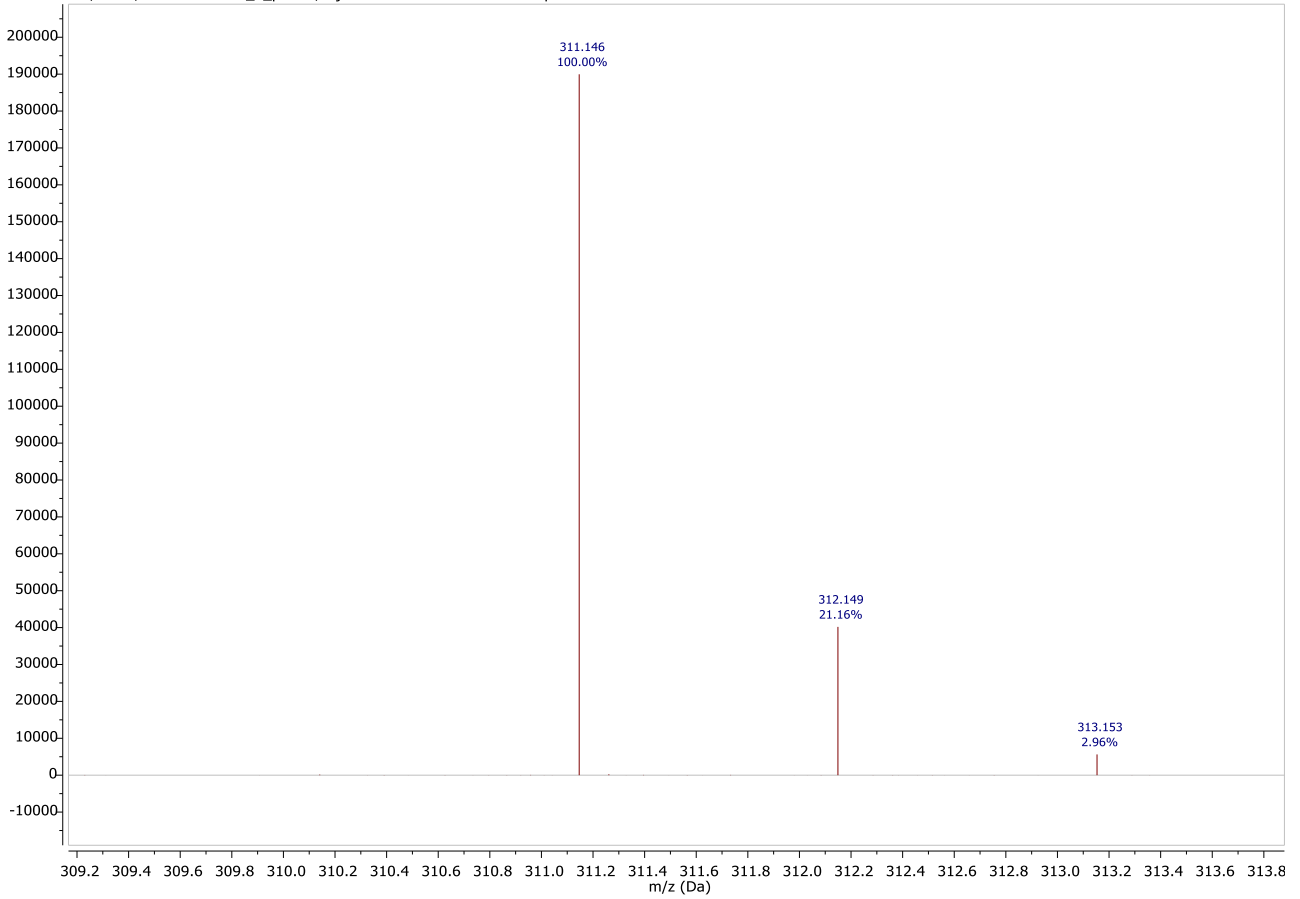
9.3.3. (*E*)-5,6-dimethoxy-2-(4-methoxybenzylidene)-2,3-dihydro-1*H*-inden-1-one (K7A4)

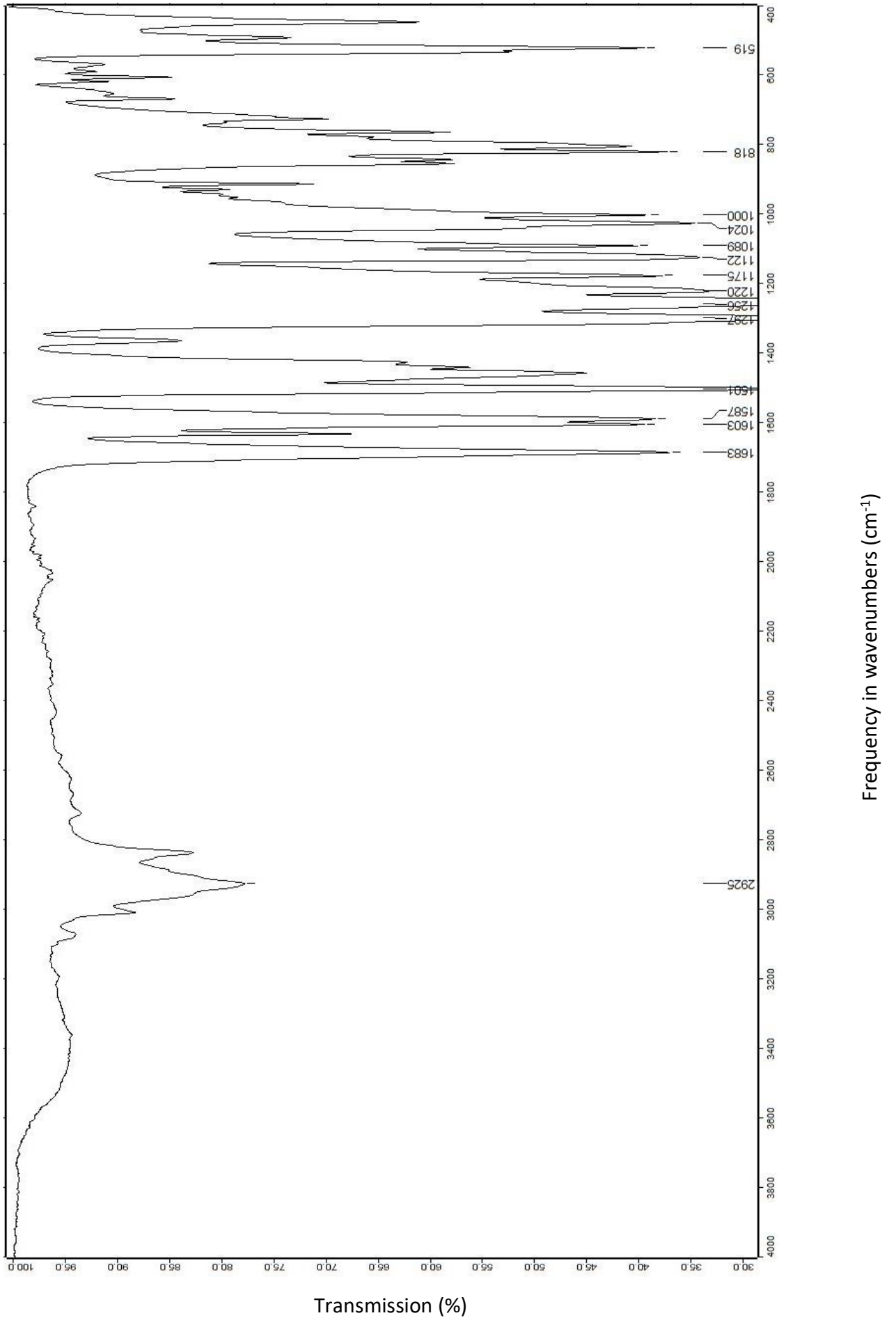


Chapter 9: Experimental Spectrums

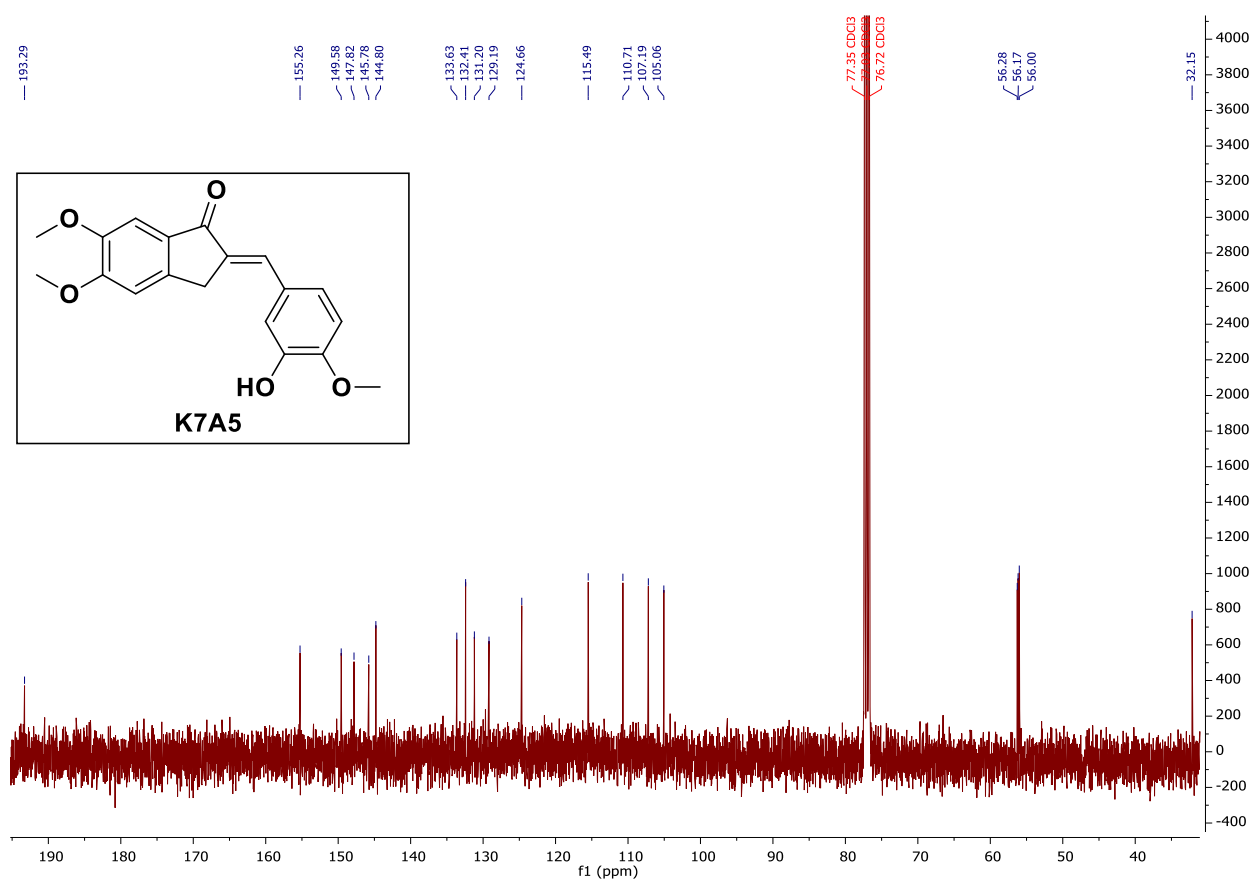
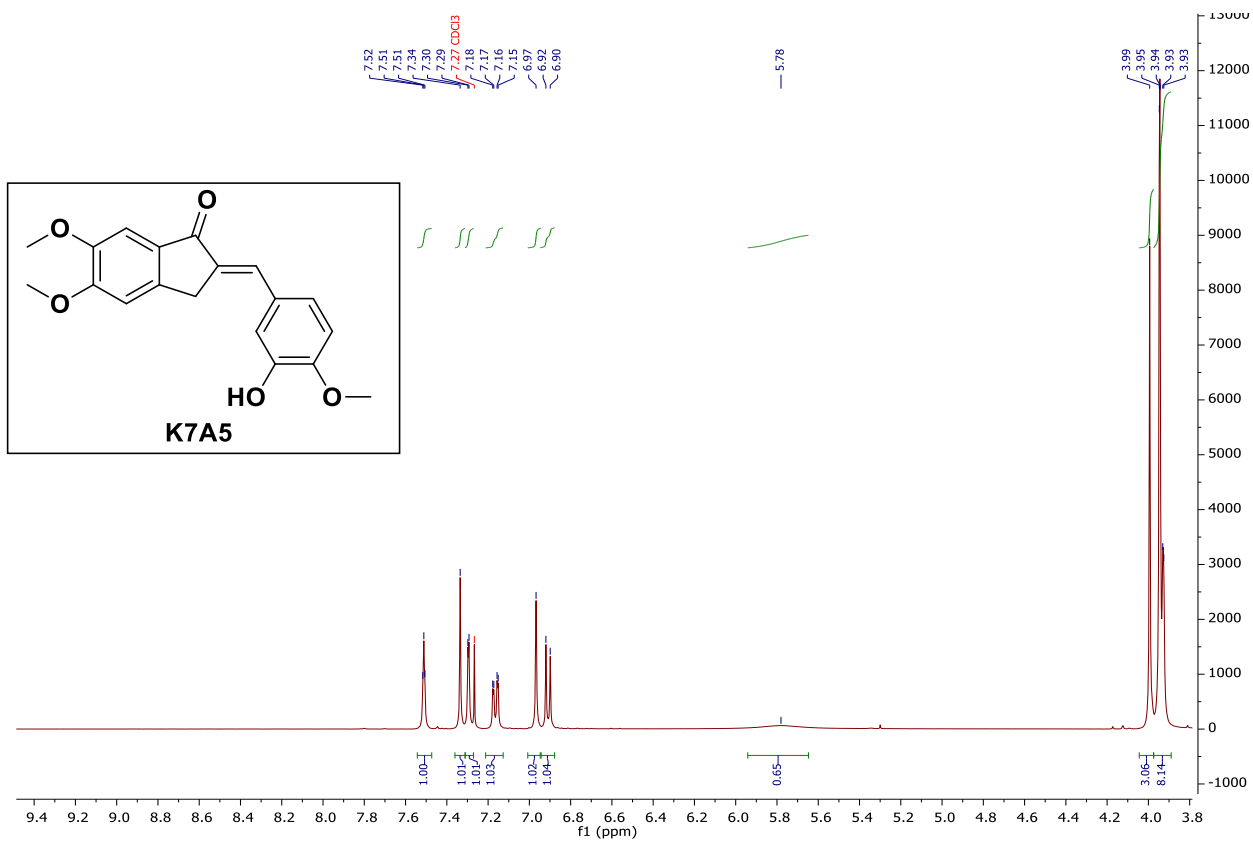


C:\Users\sussa...K7A4MS_2_p.raw\ Injection 1 TOF MS ES+ MS + spectrum 0.38

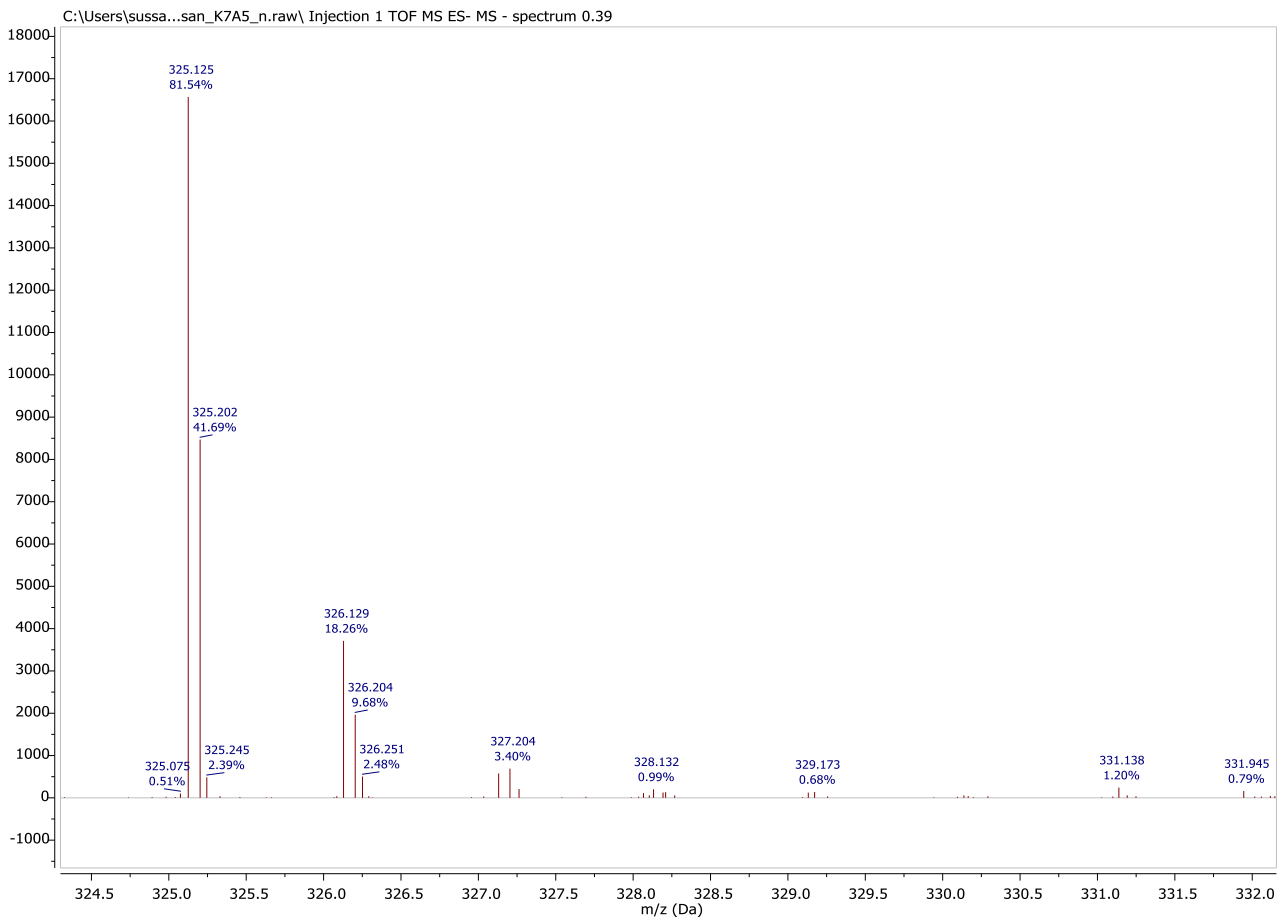
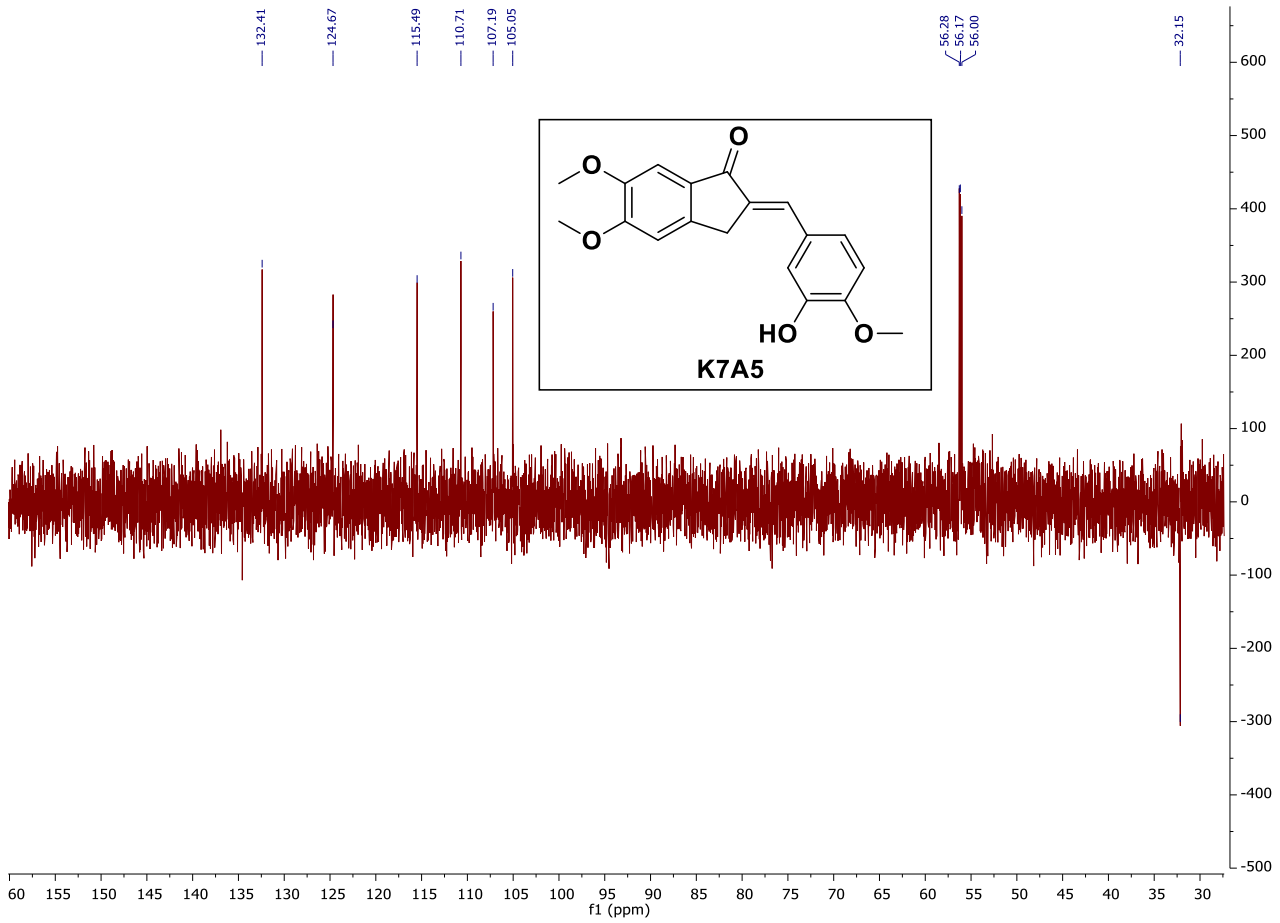


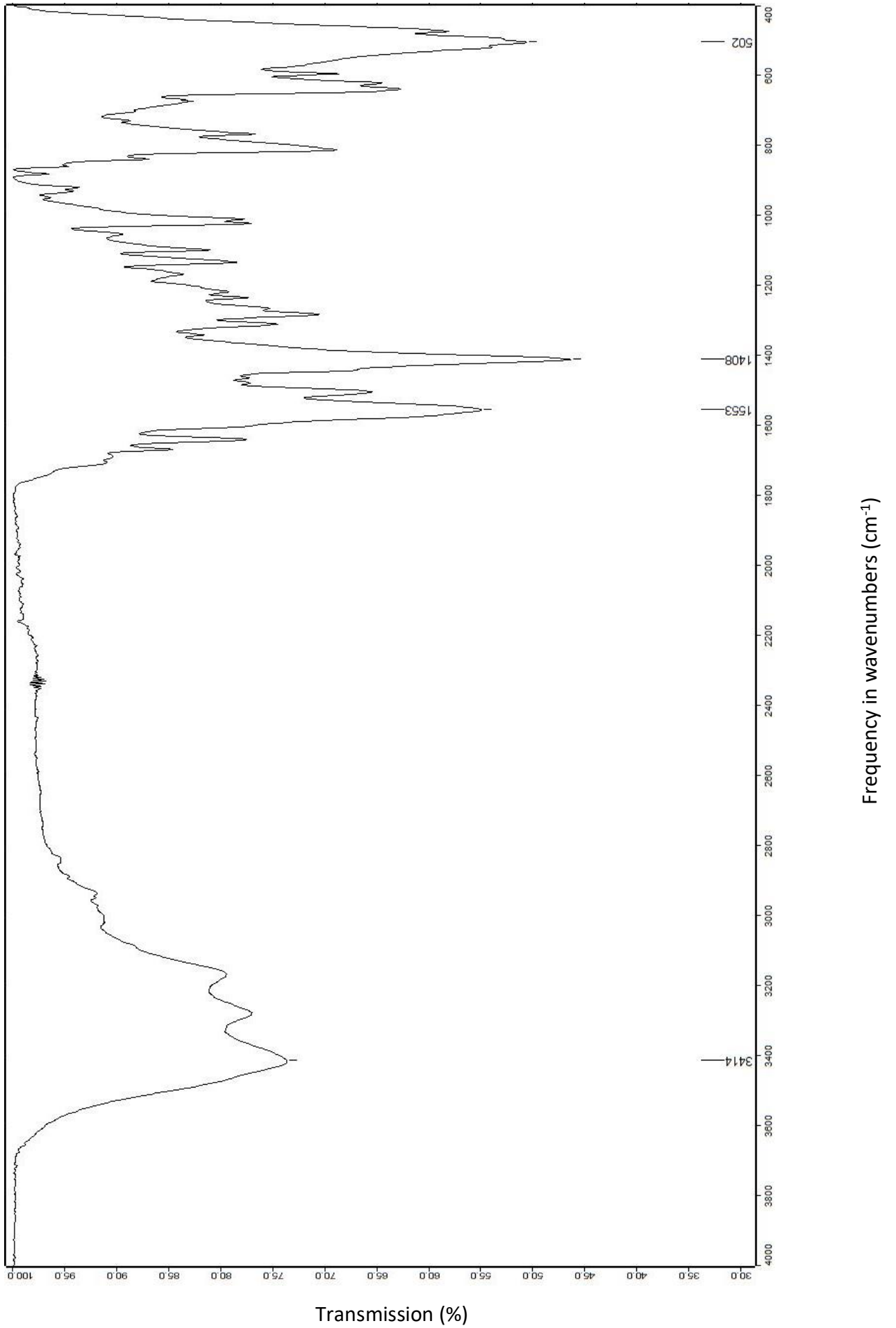


9.3.4. (*E*)-2-(3-hydroxy-4-methoxybenzylidene)-5,6-dimethoxy-2,3-dihydro-1*H*-inden-1-one (K7A5)

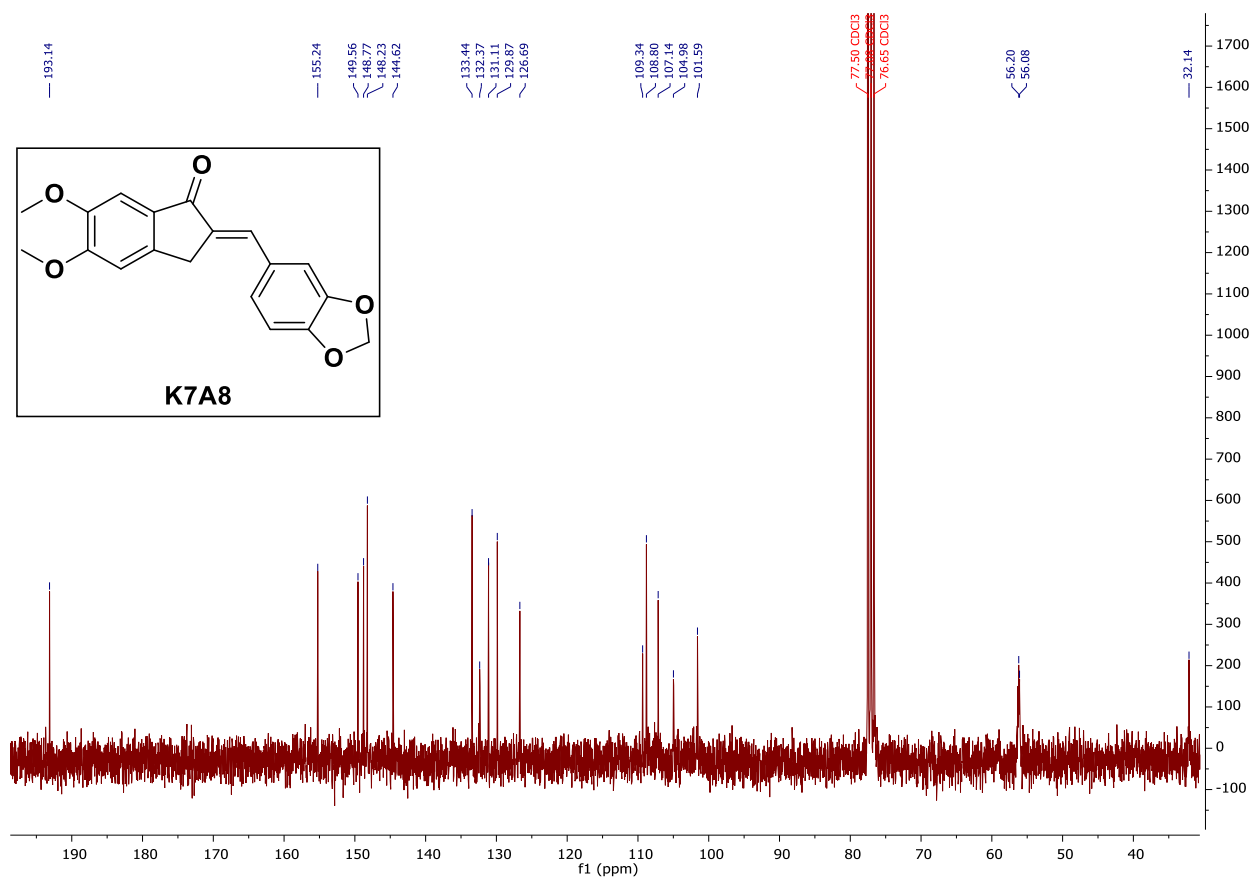
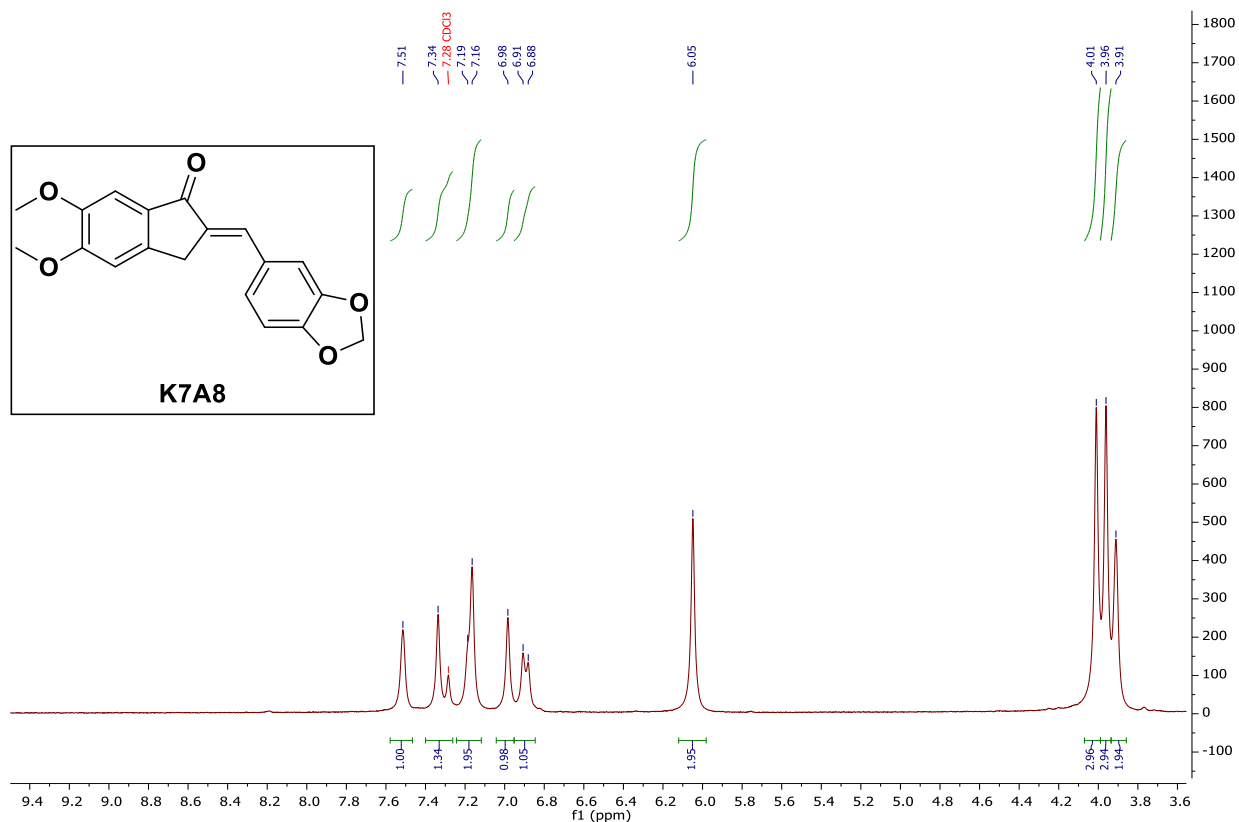


Chapter 9: Experimental Spectrums

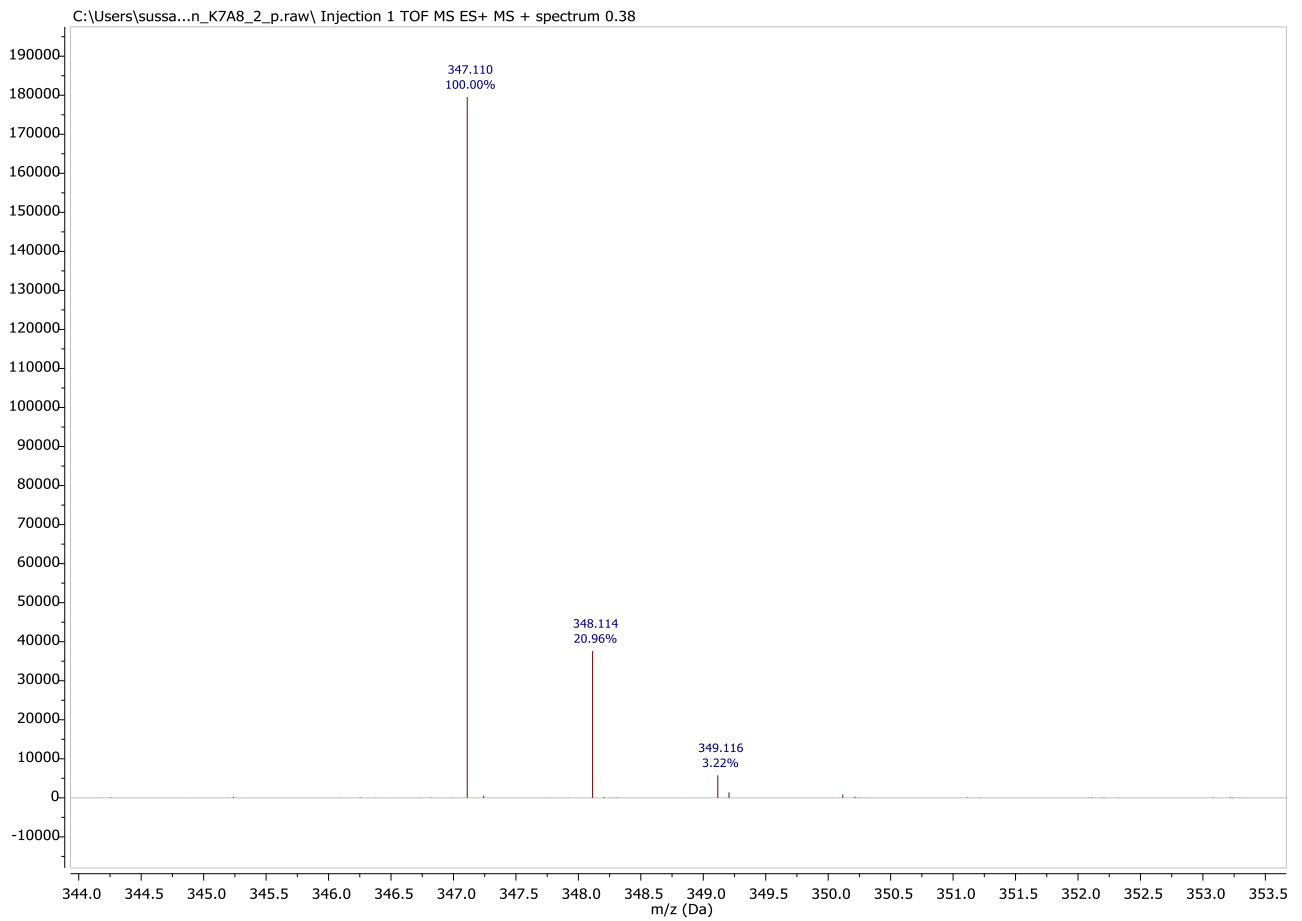
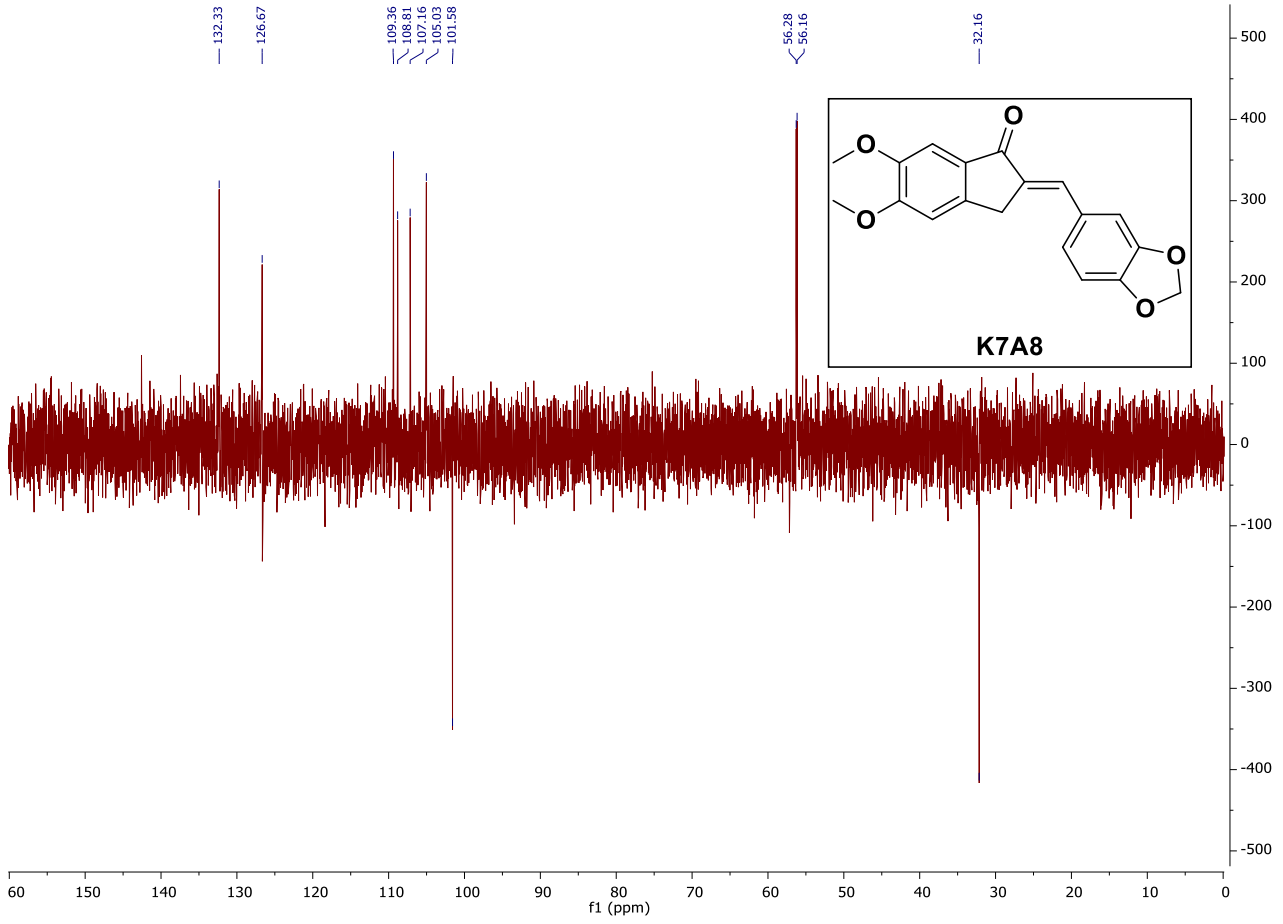


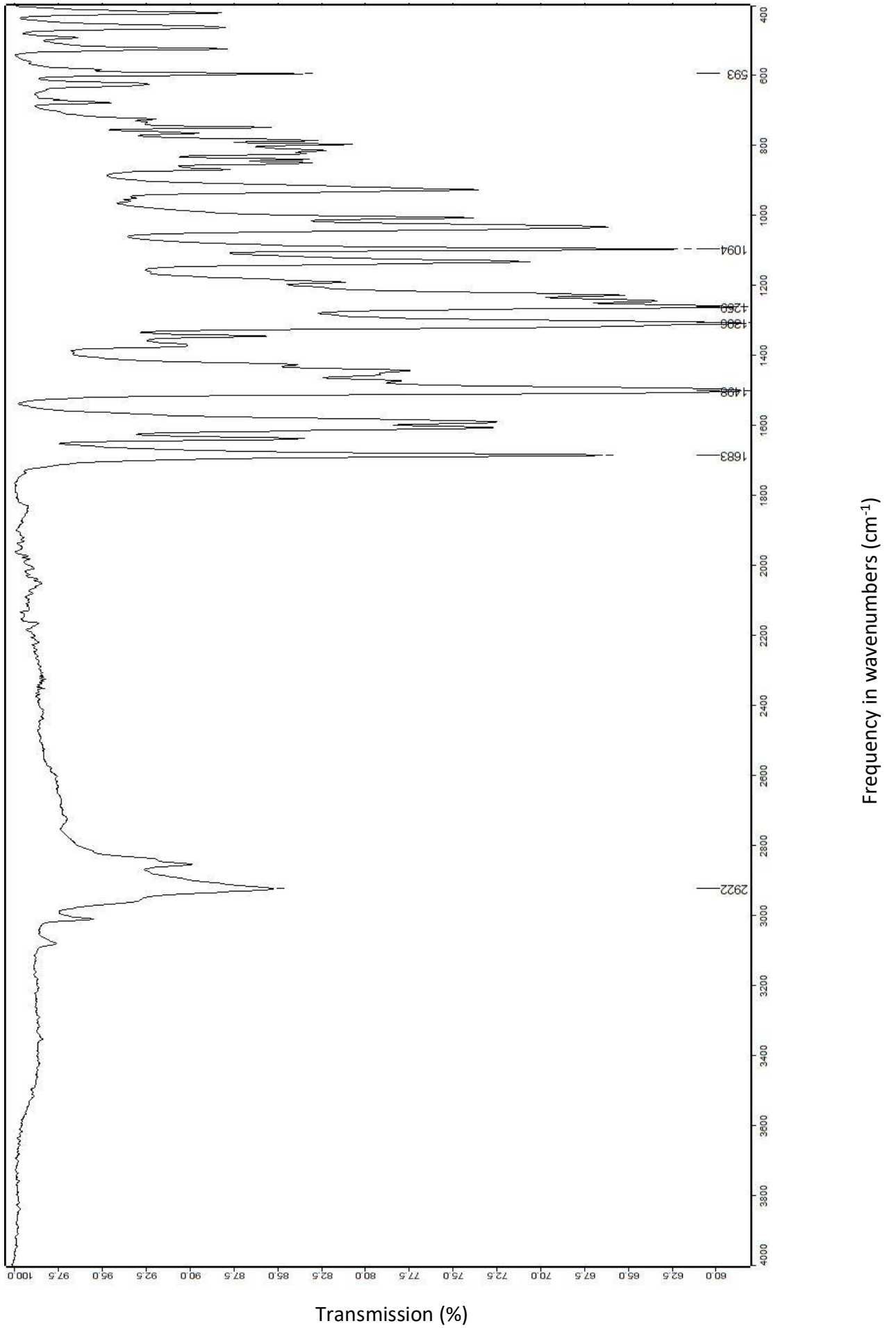


9.3.5. (*E*)-2-(benzo[*d*][1,3]dioxol-5-ylmethylene)-5,6-dimethoxy-2,3-dihydro-1*H*-inden-1-one (K7A8)

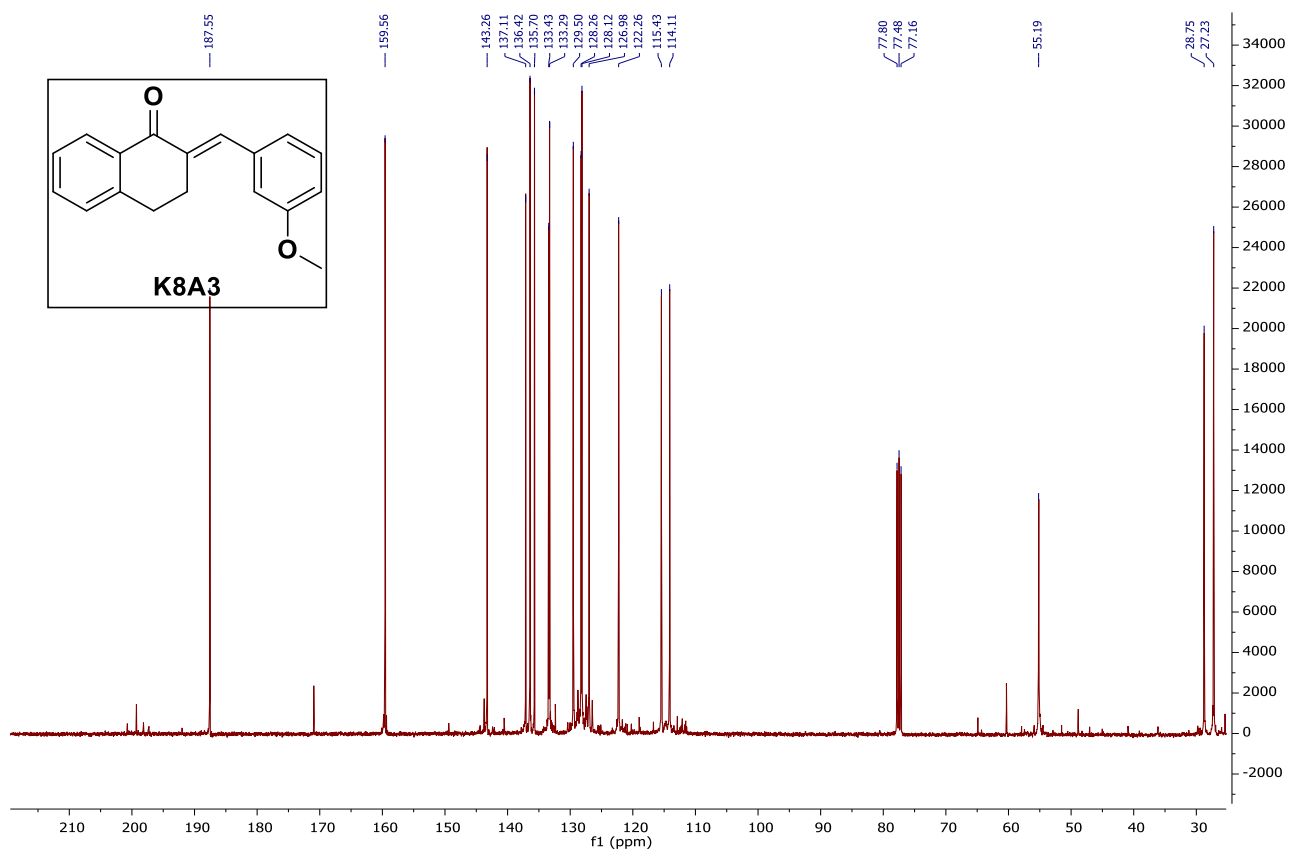
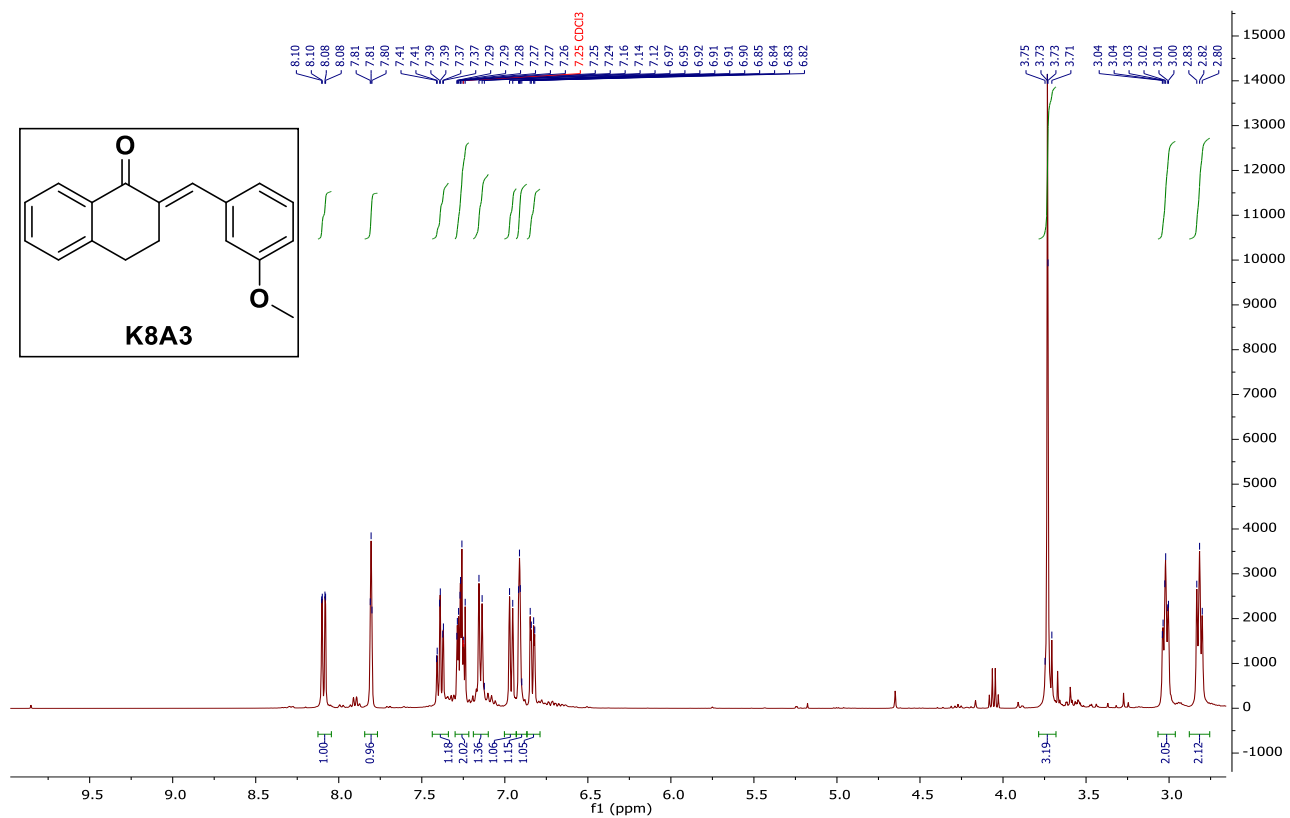


Chapter 9: Experimental Spectrums

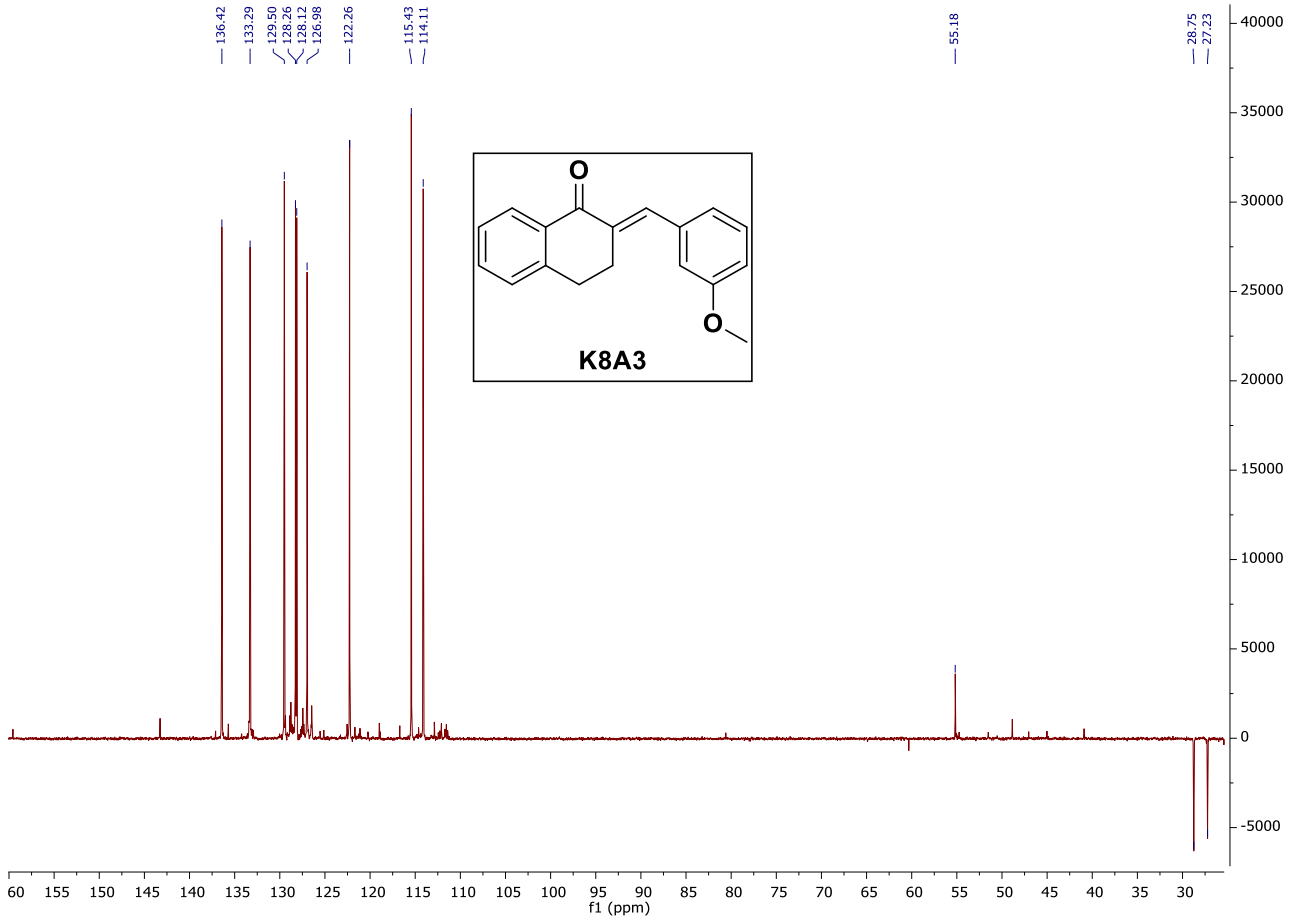




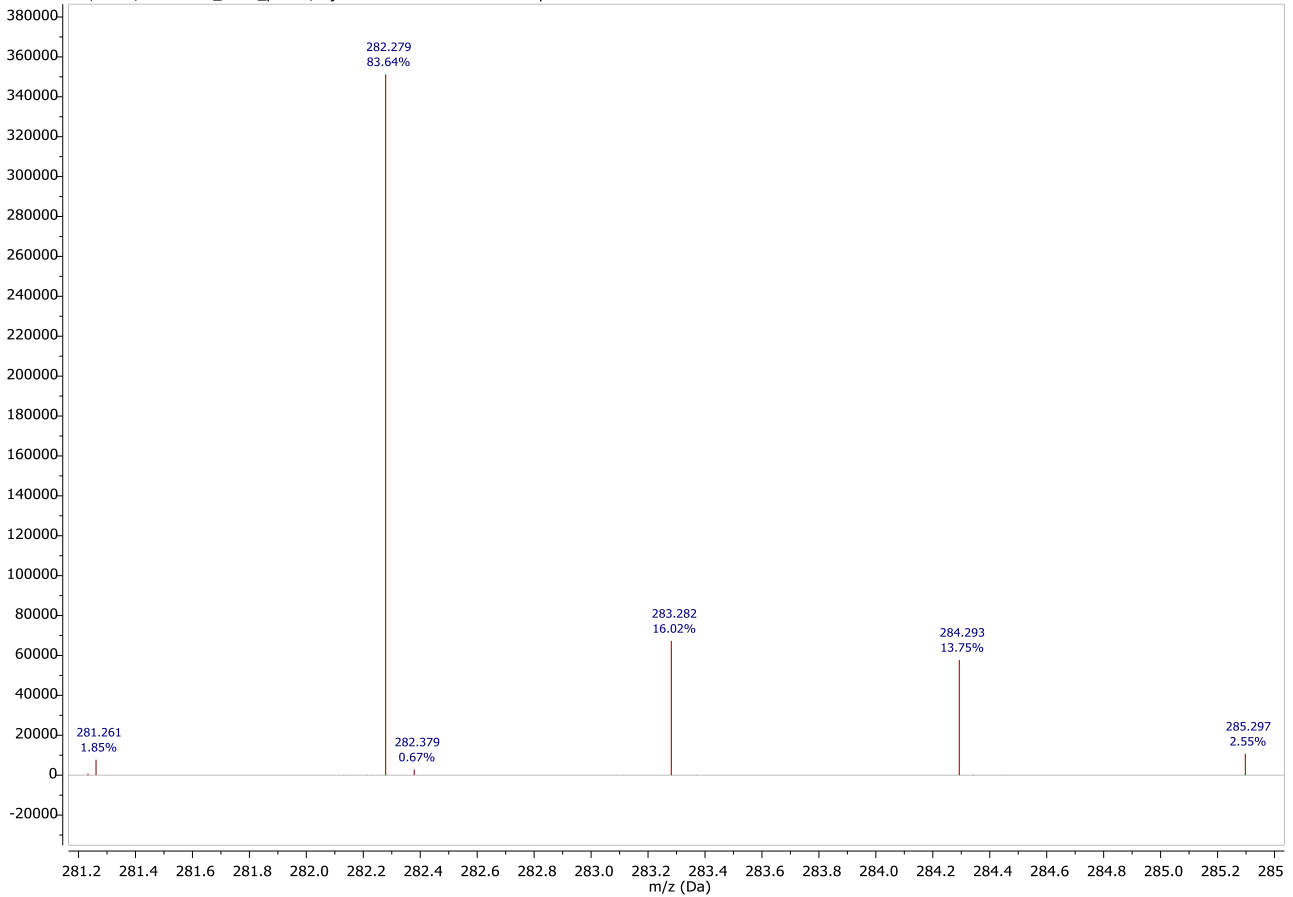
9.3.6. (*E*)-2-(3-methoxybenzylidene)-3,4-dihydronaphthalen-1(2*H*)-one (K8A3)

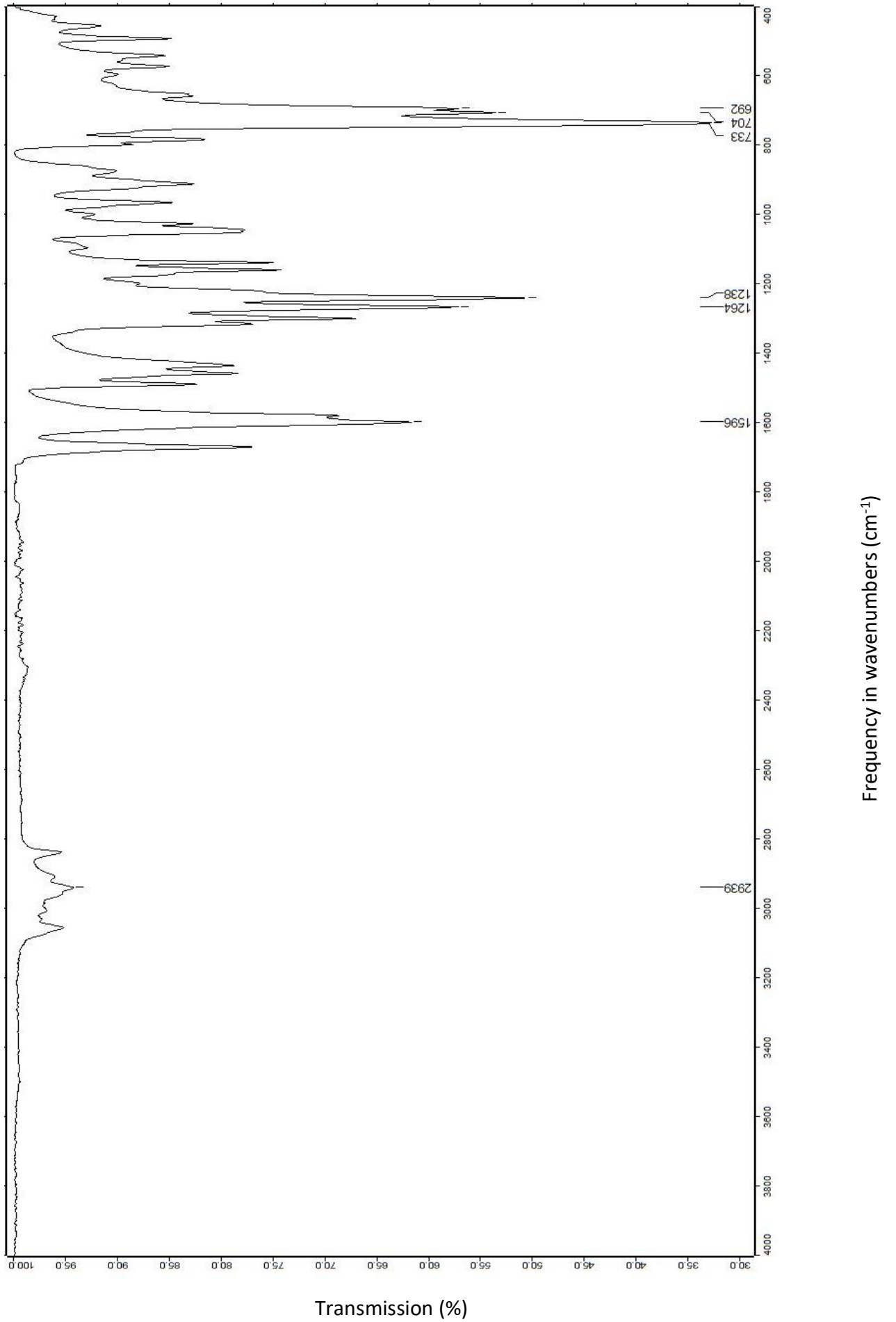


Chapter 9: Experimental Spectrums

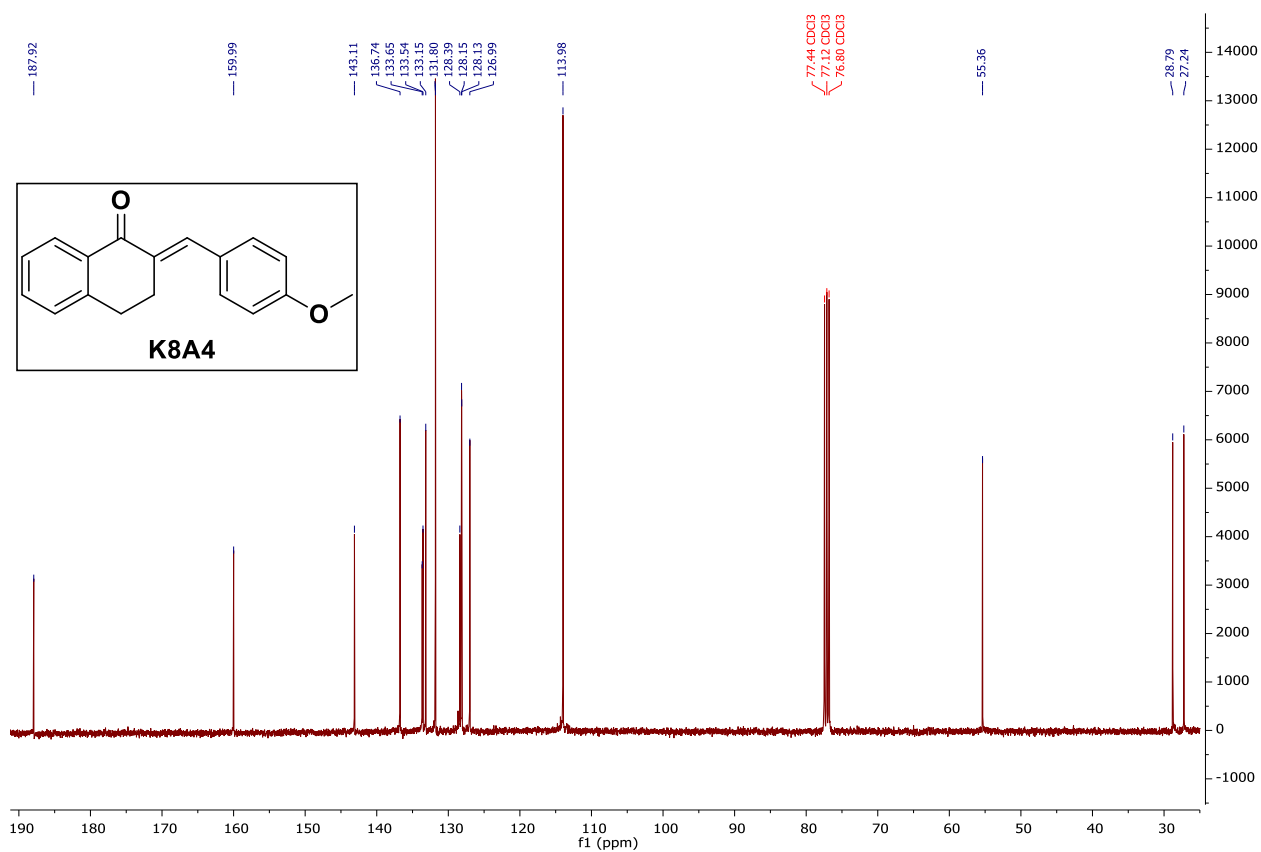
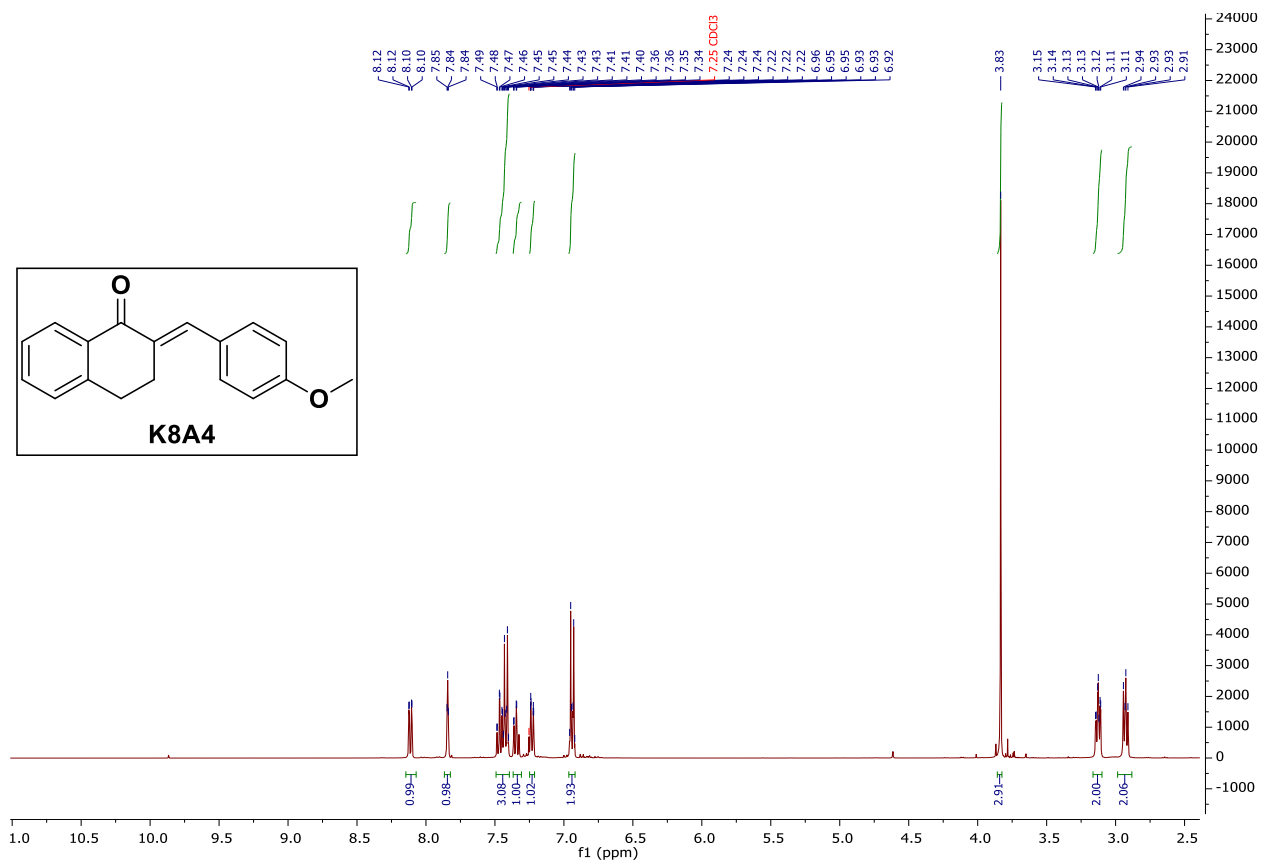


C:\Users\sussa...san_K8A3_p.raw\ Injection 1 TOF MS ES+ MS + spectrum 0.43

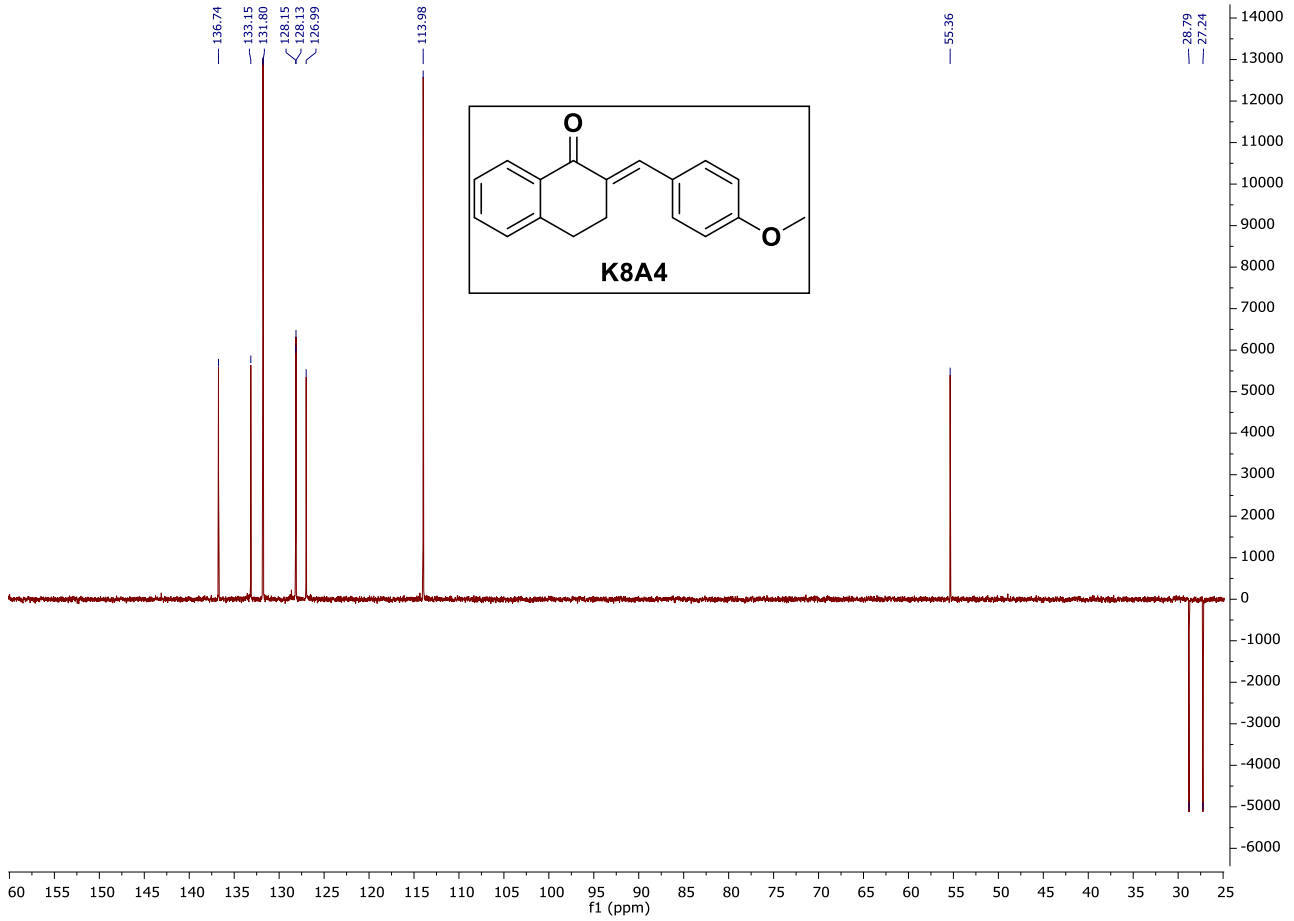




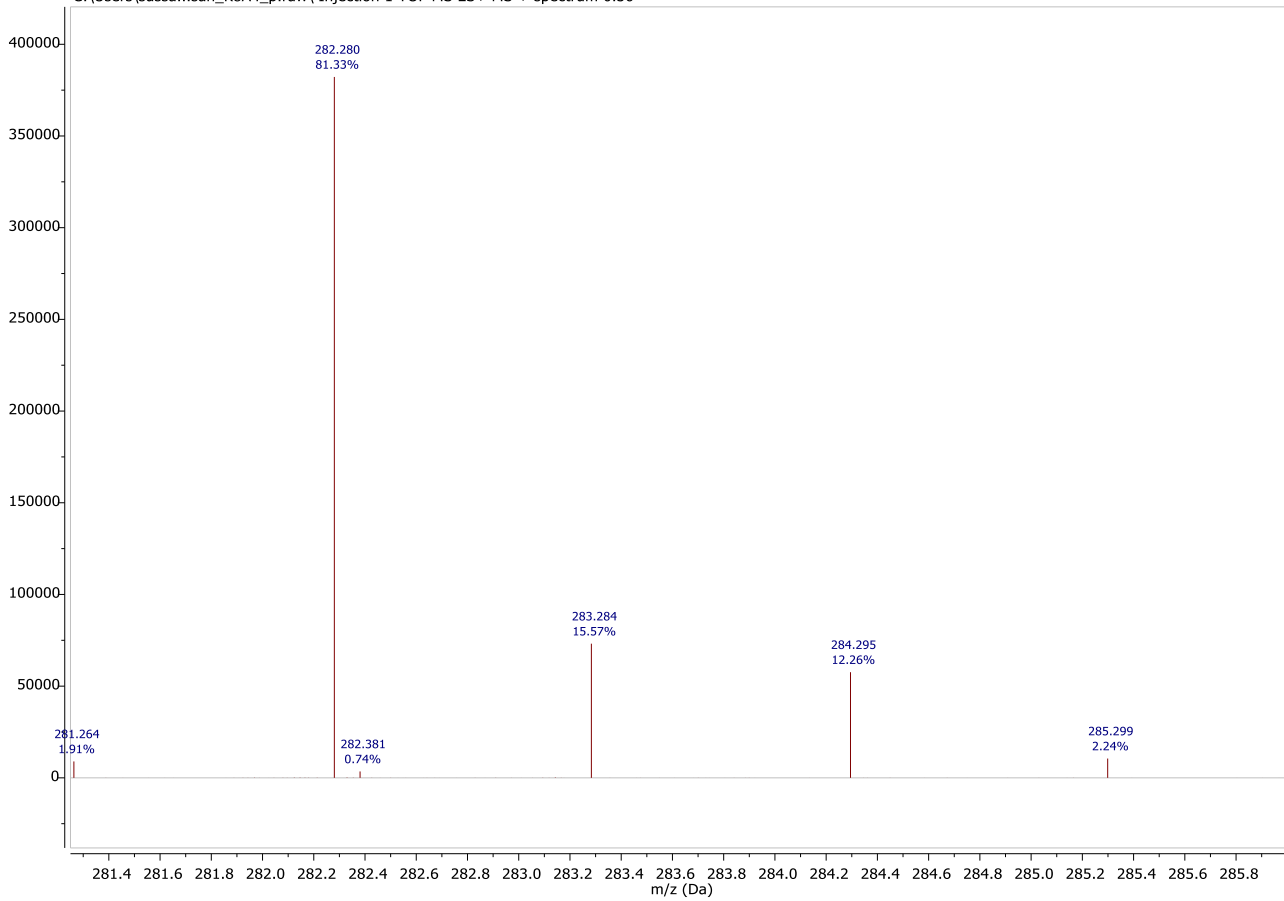
9.3.7. (*E*)-2-(4-methoxybenzylidene)-3,4-dihydronaphthalen-1(2*H*)-one (K8A4)

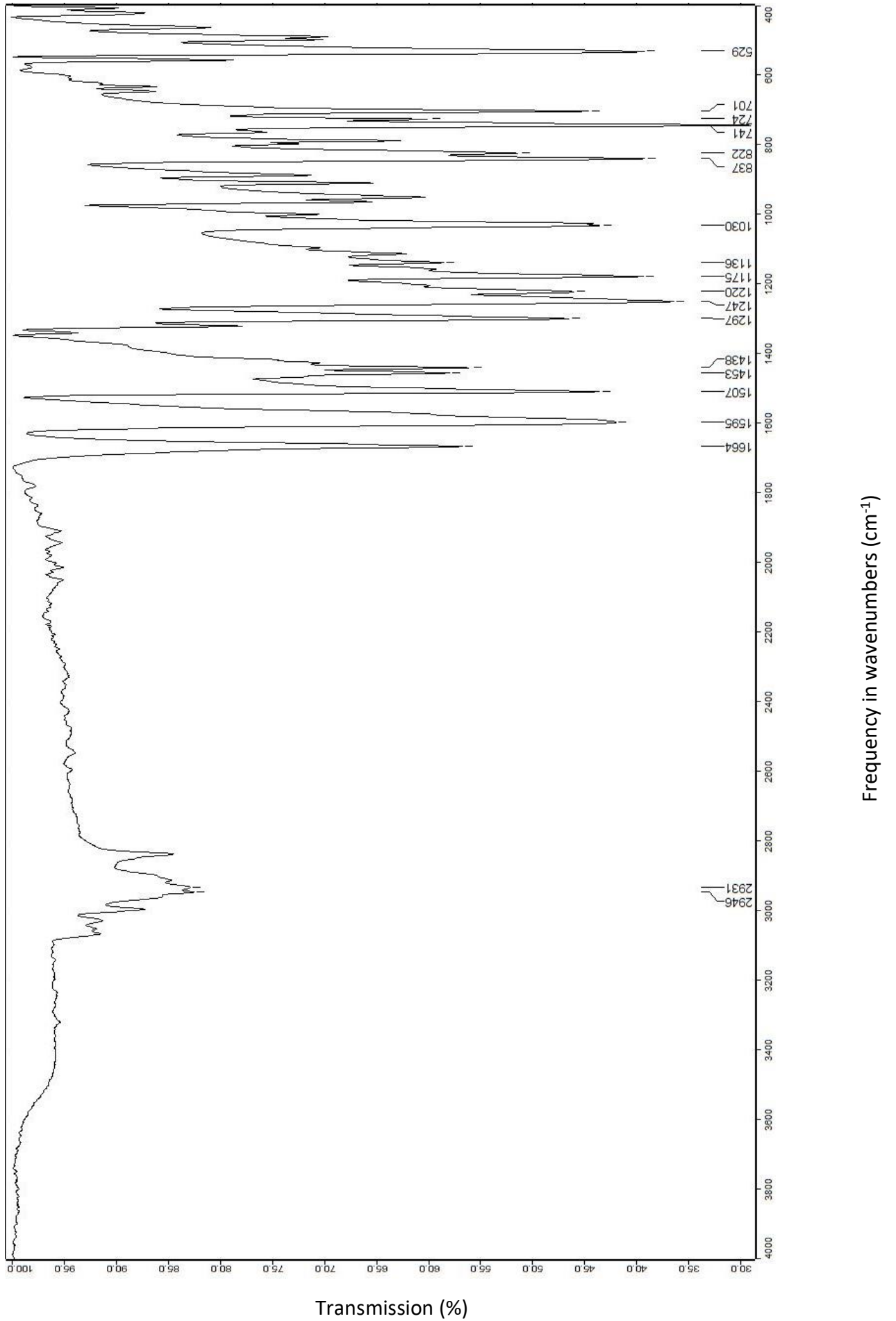


Chapter 9: Experimental Spectra

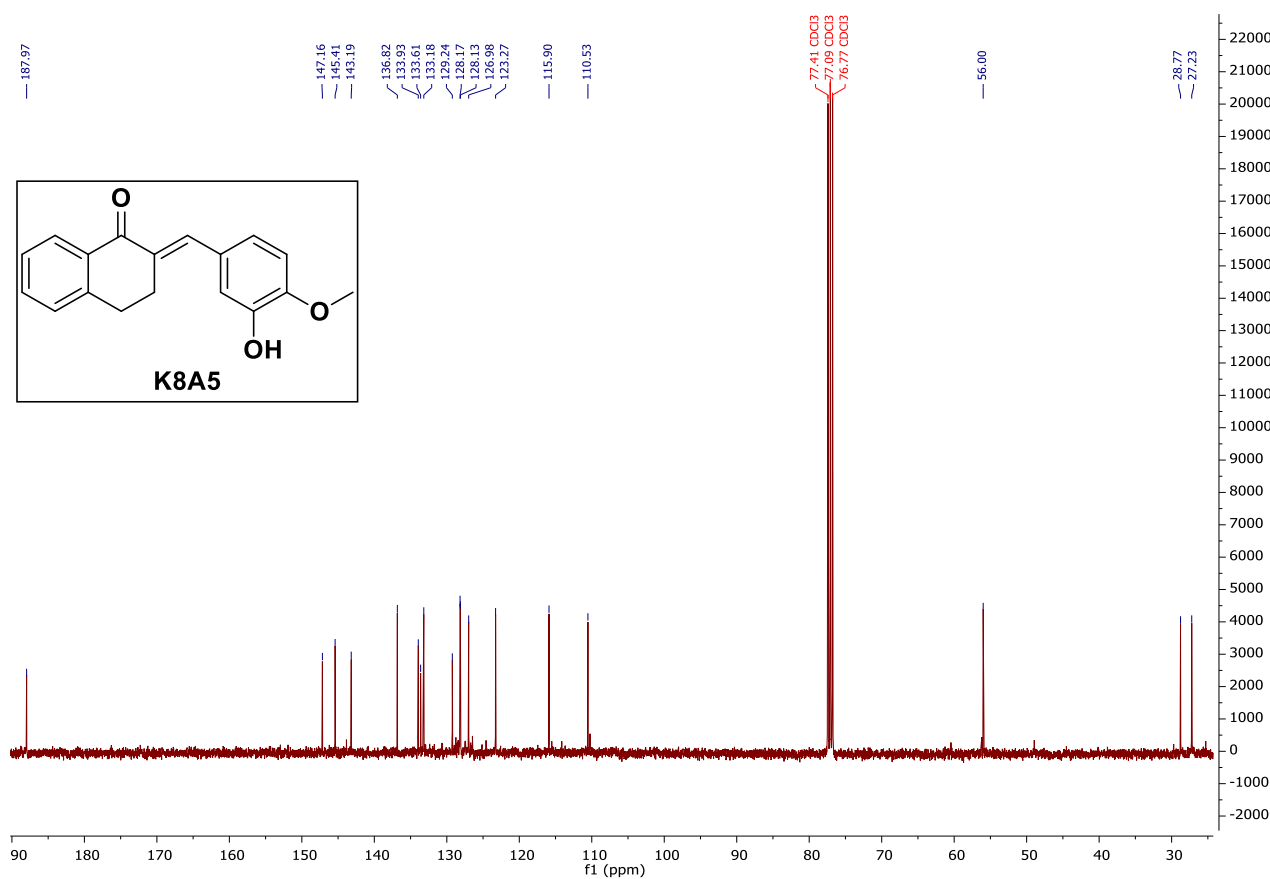
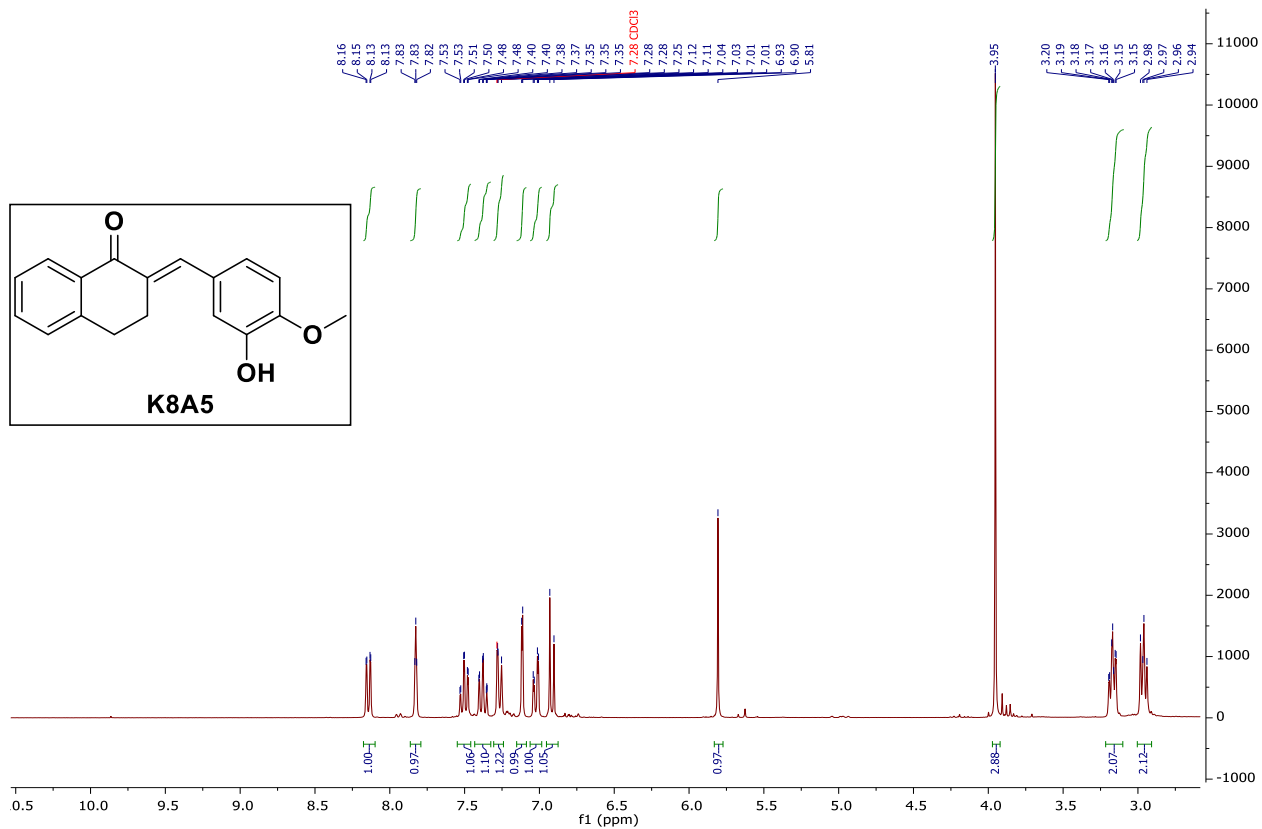


C:\Users\sussa...san_K8A4_p.raw\ Injection 1 TOF MS ES+ MS + spectrum 0.36

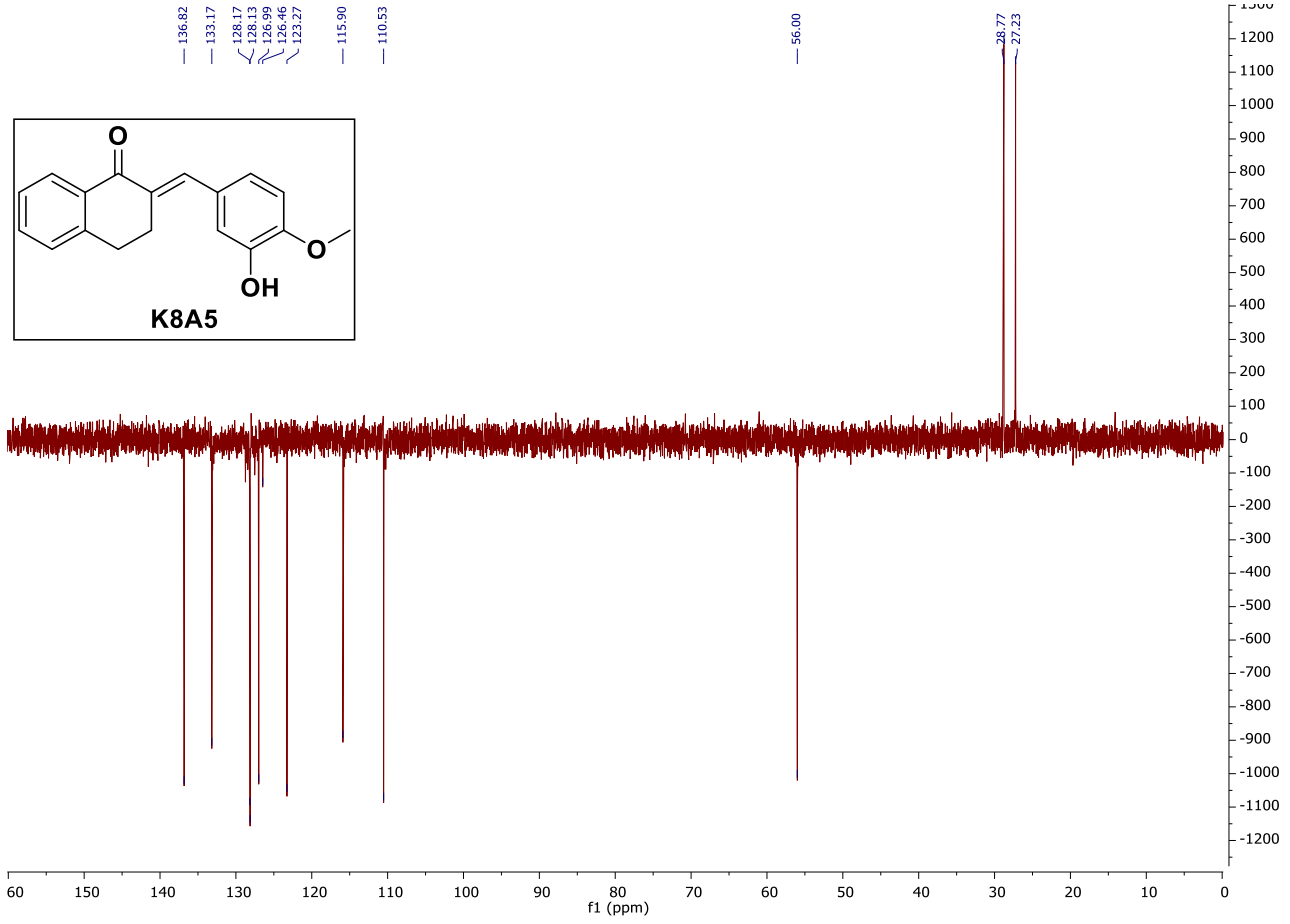




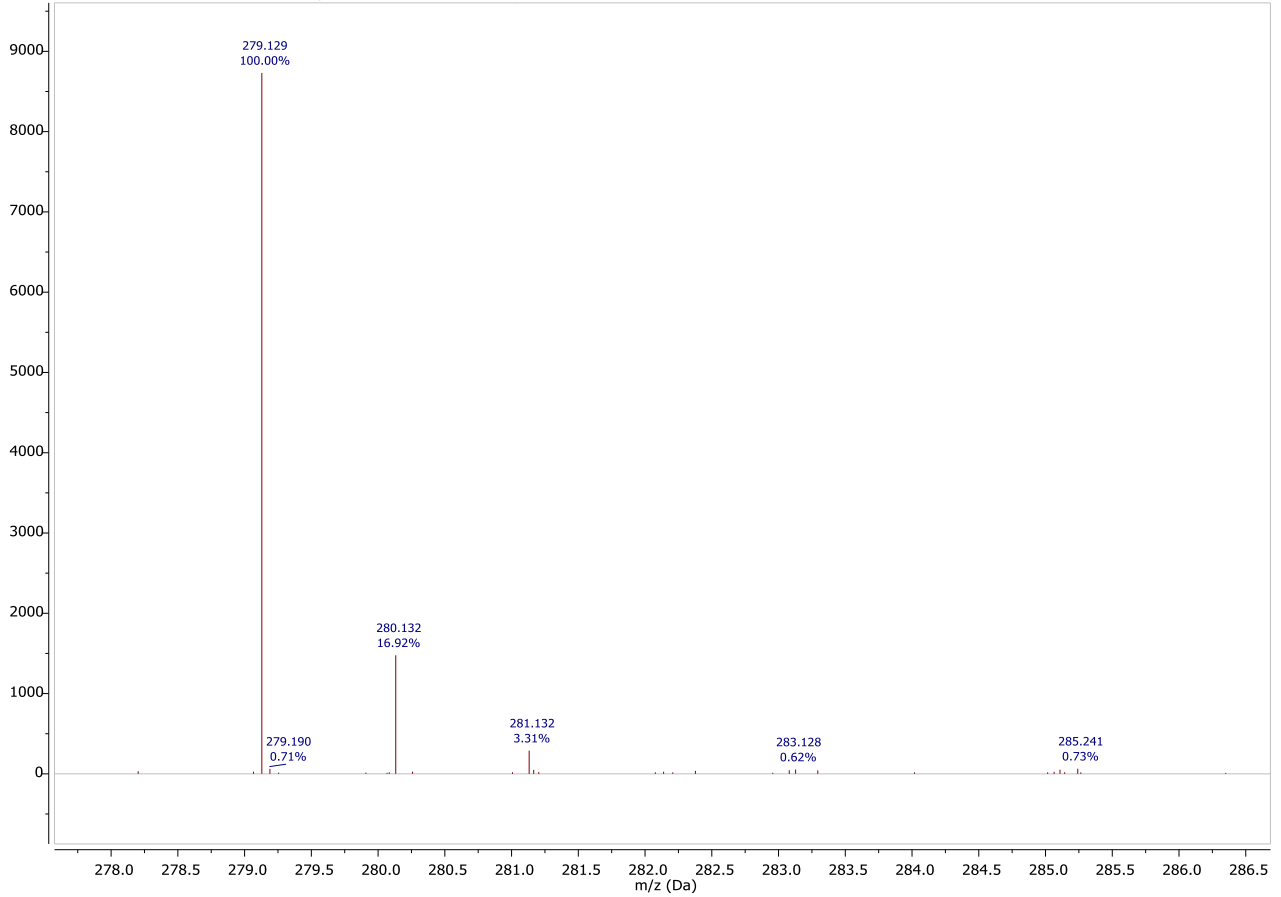
9.3.8. (*E*)-2-(3-hydroxy-4-methoxybenzylidene)-3,4-dihydronaphthalen-1(2*H*)-one (K8A5)

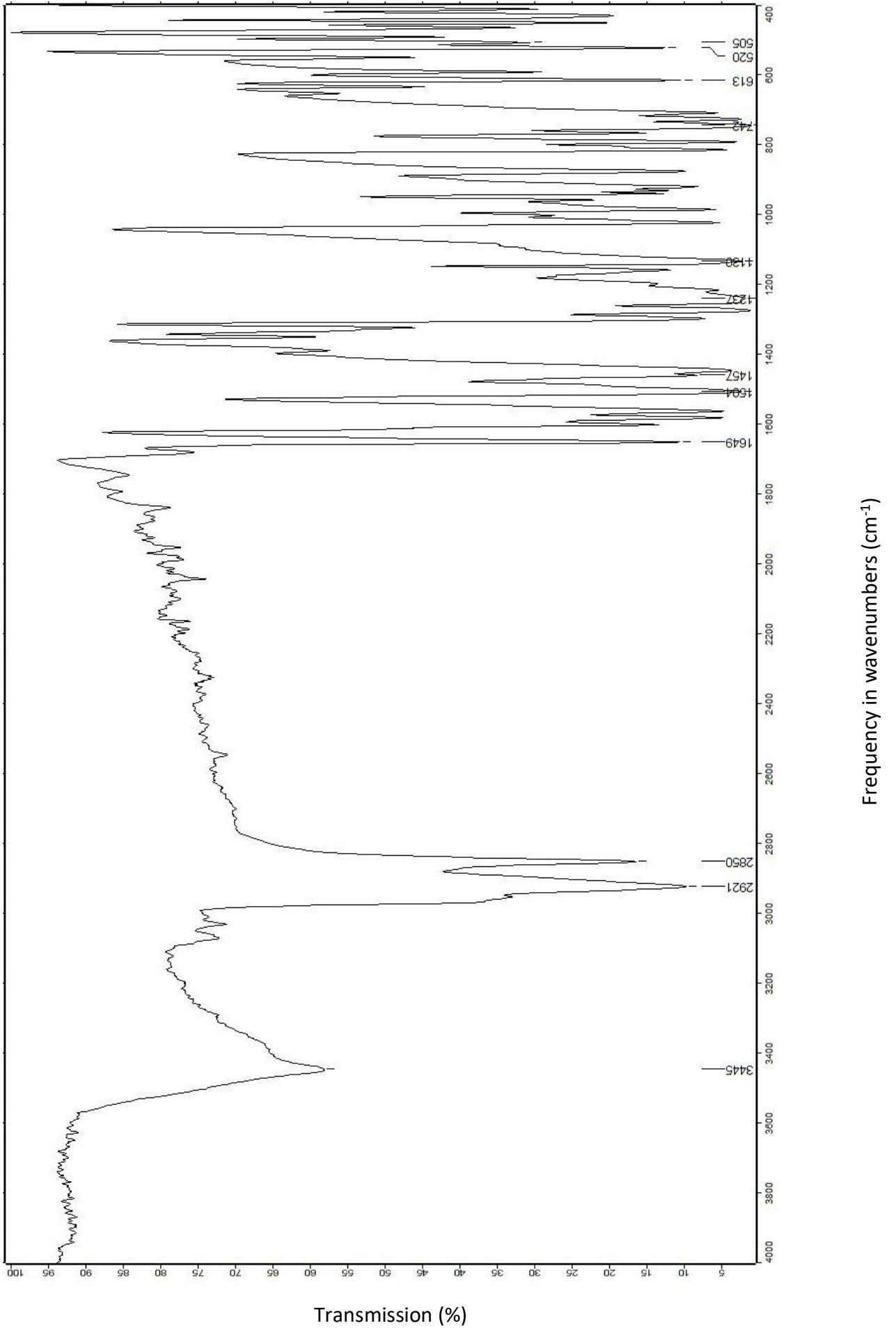


Chapter 9: Experimental Spectrums

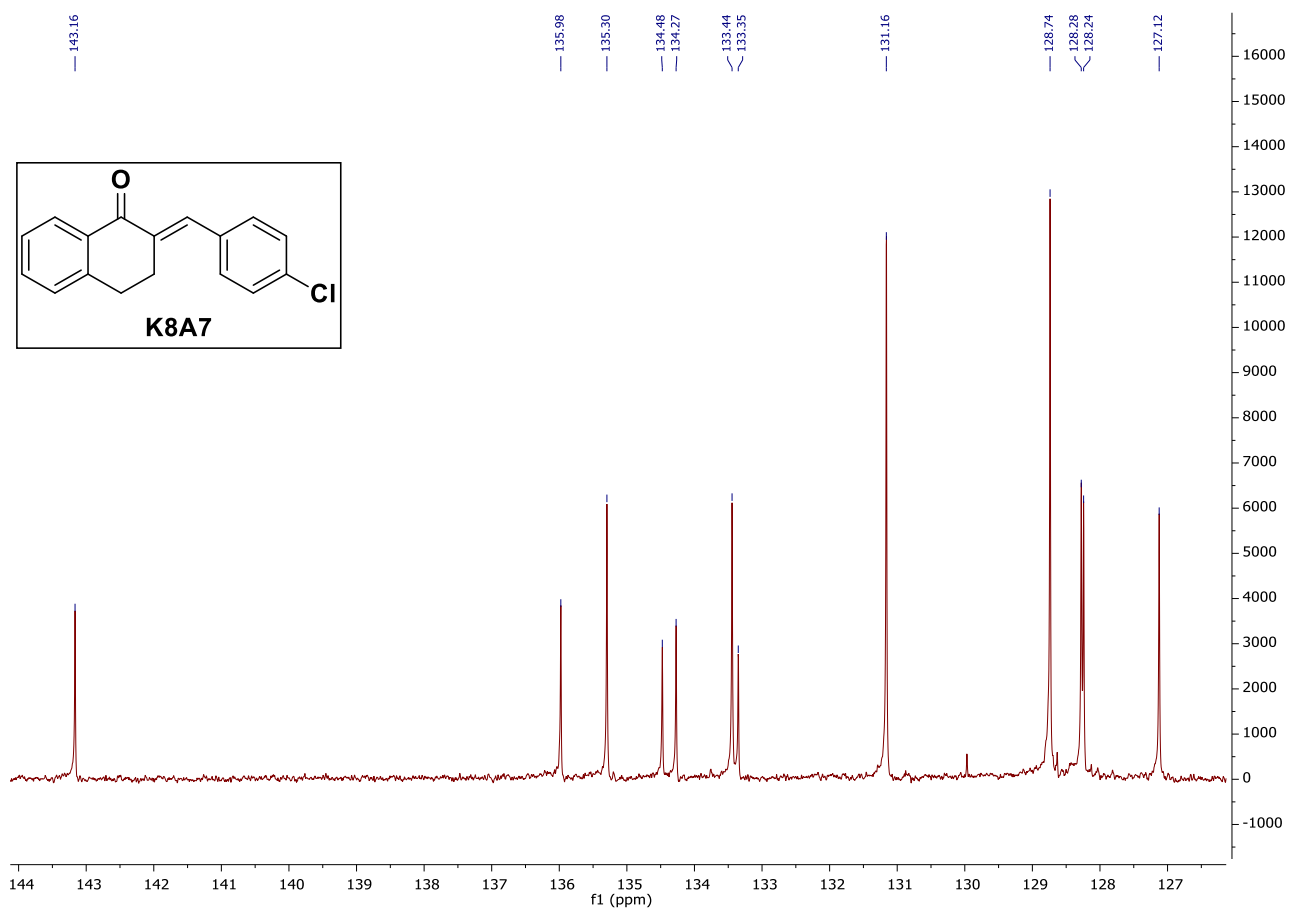
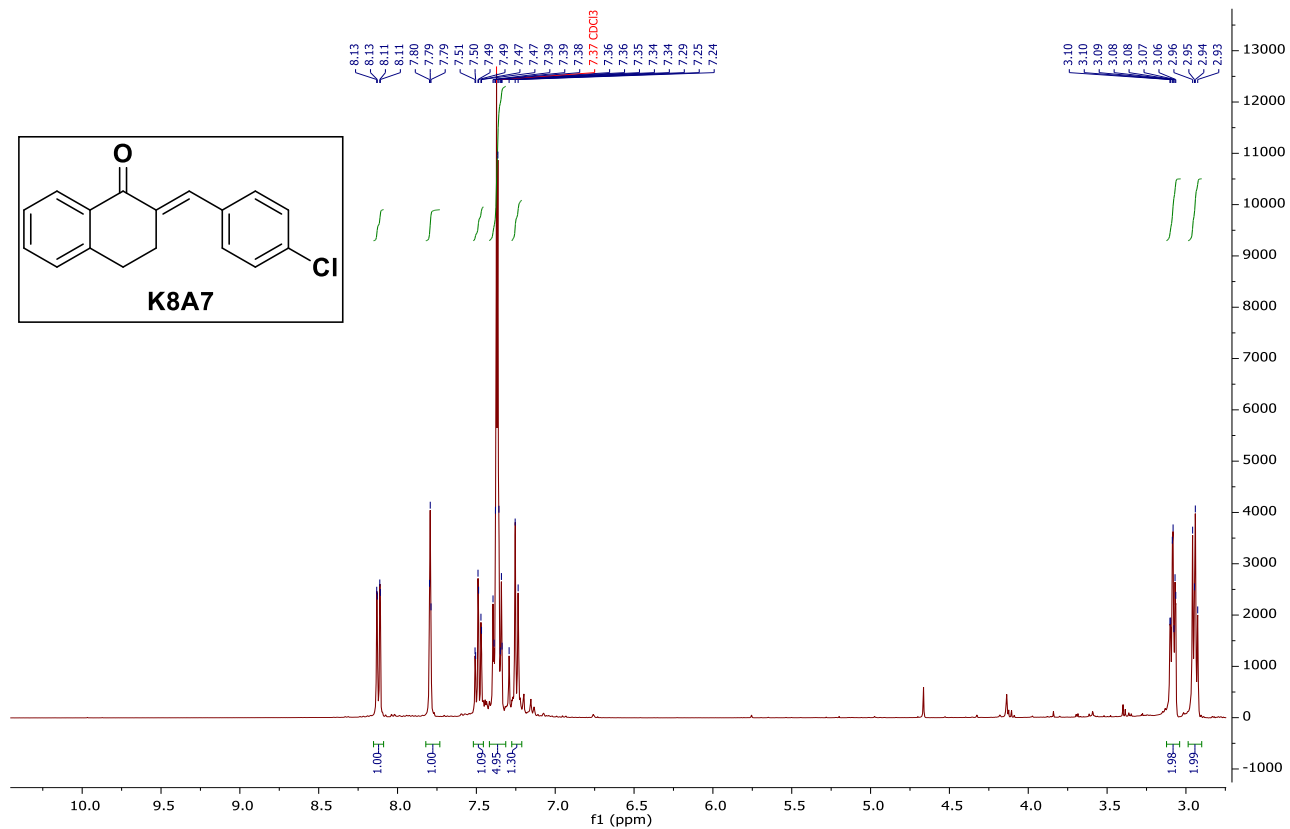


C:\Users\sussa...K8A5_2_P_n.raw\ Injection 1 TOF MS ES- MS - spectrum 0.39

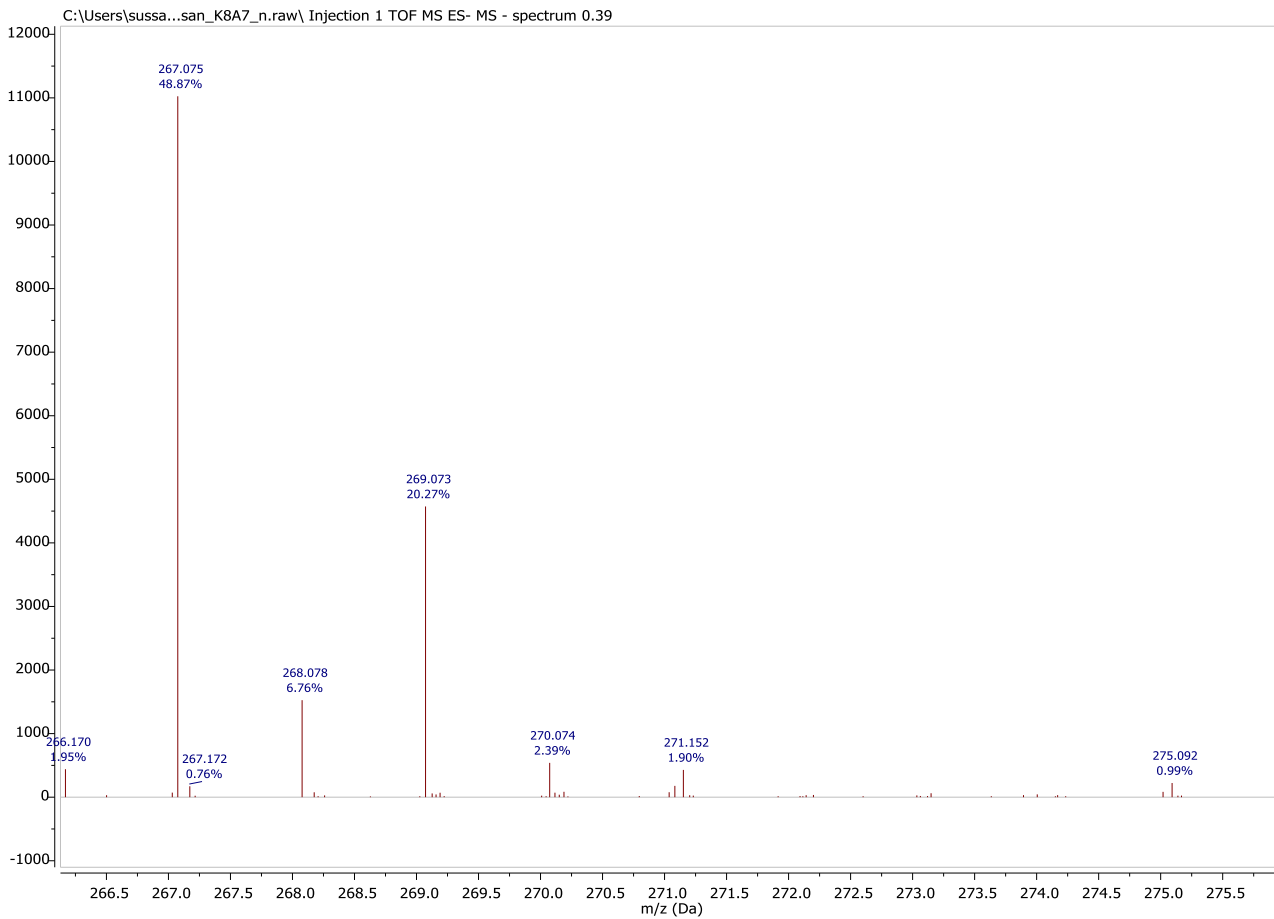
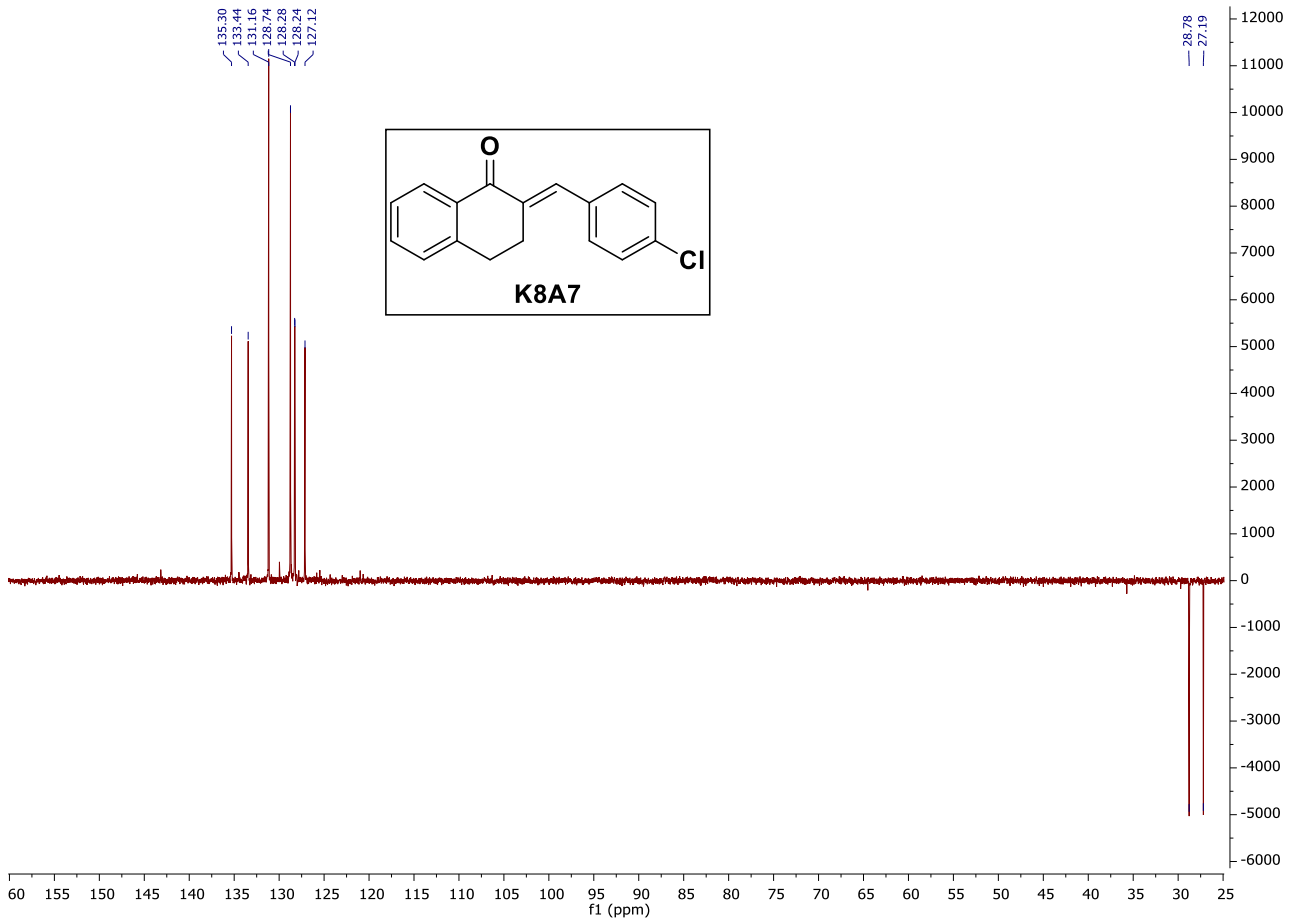


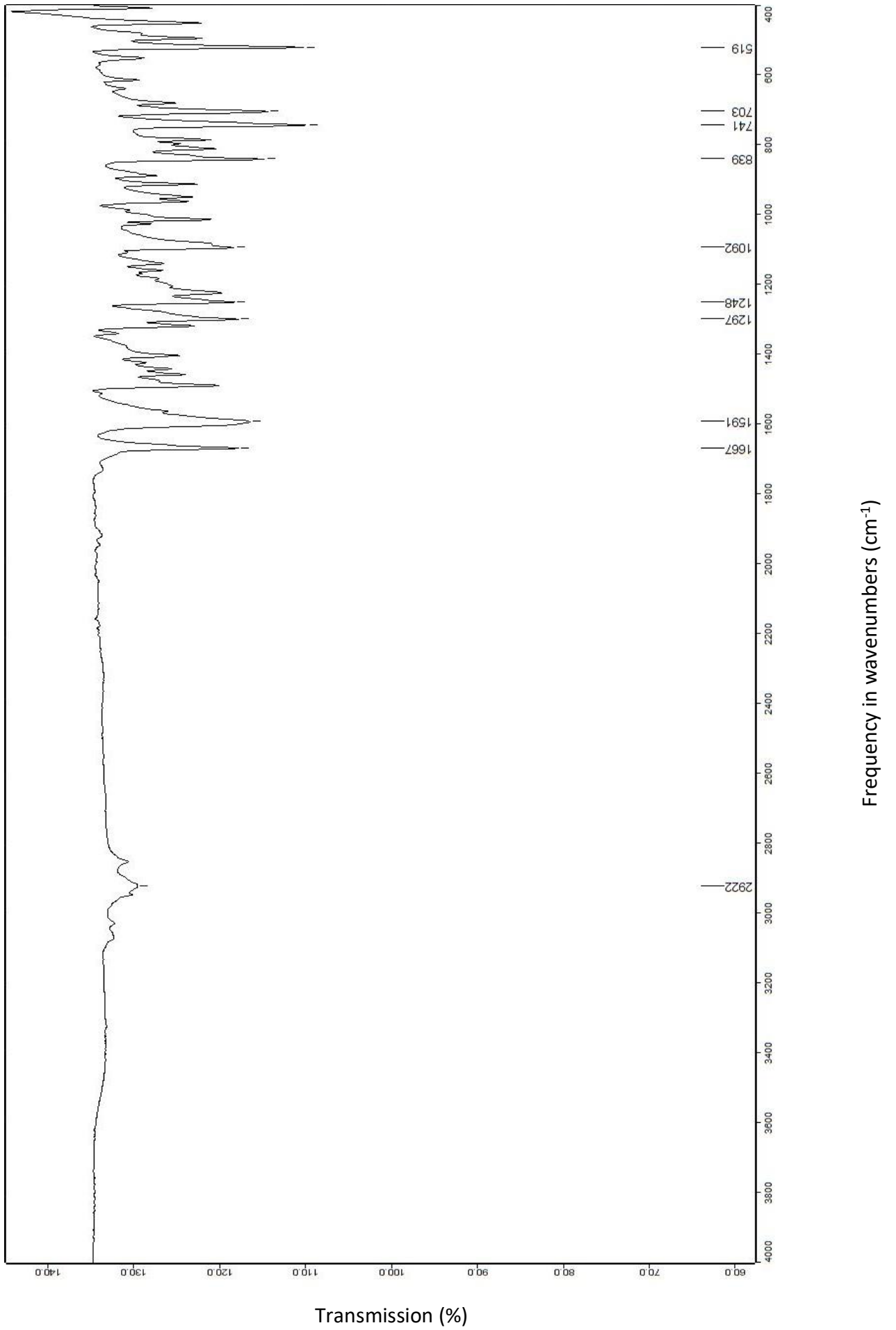


9.3.9. (*E*)-2-(4-chlorobenzylidene)-3,4-dihydronaphthalen-1(2*H*)-one (K8A7)

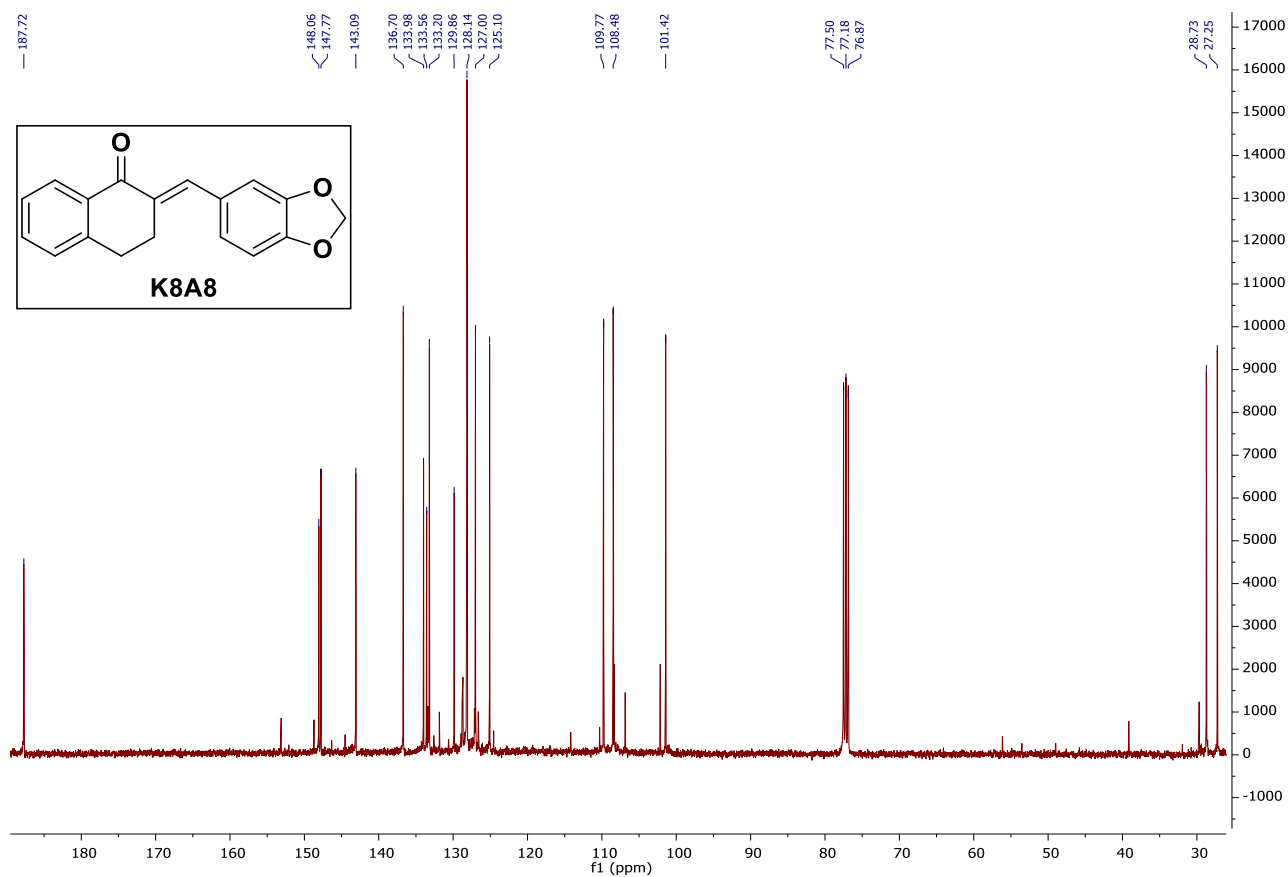
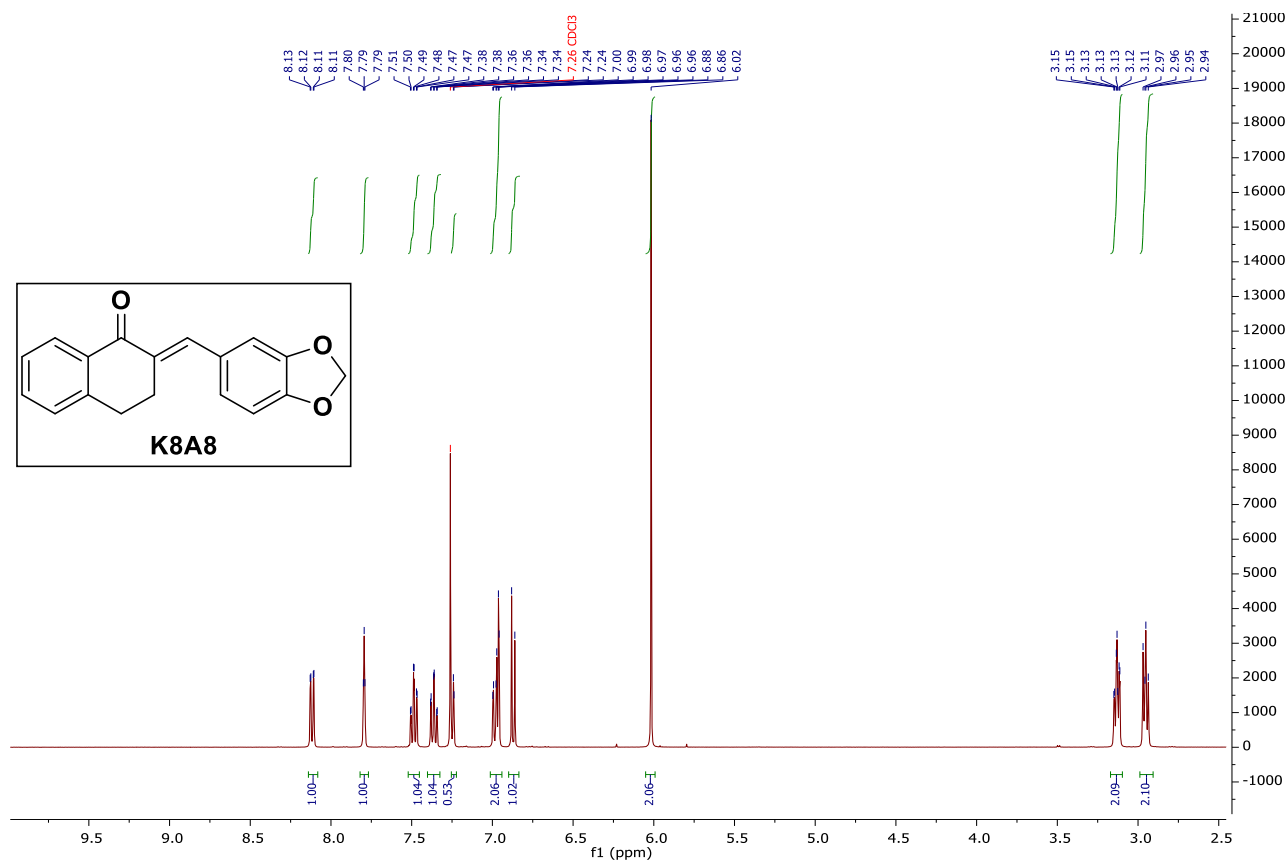


Chapter 9: Experimental Spectrums

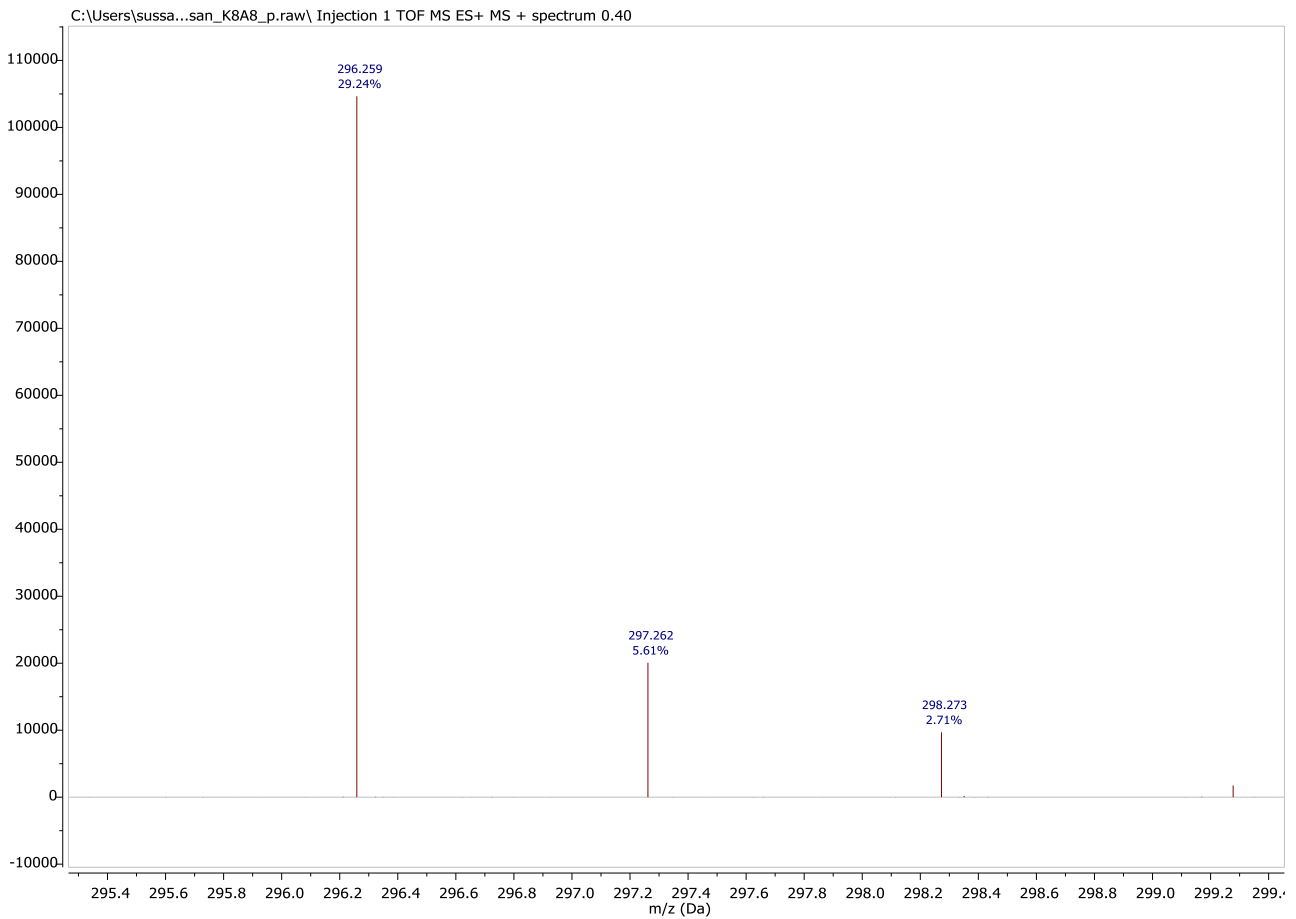
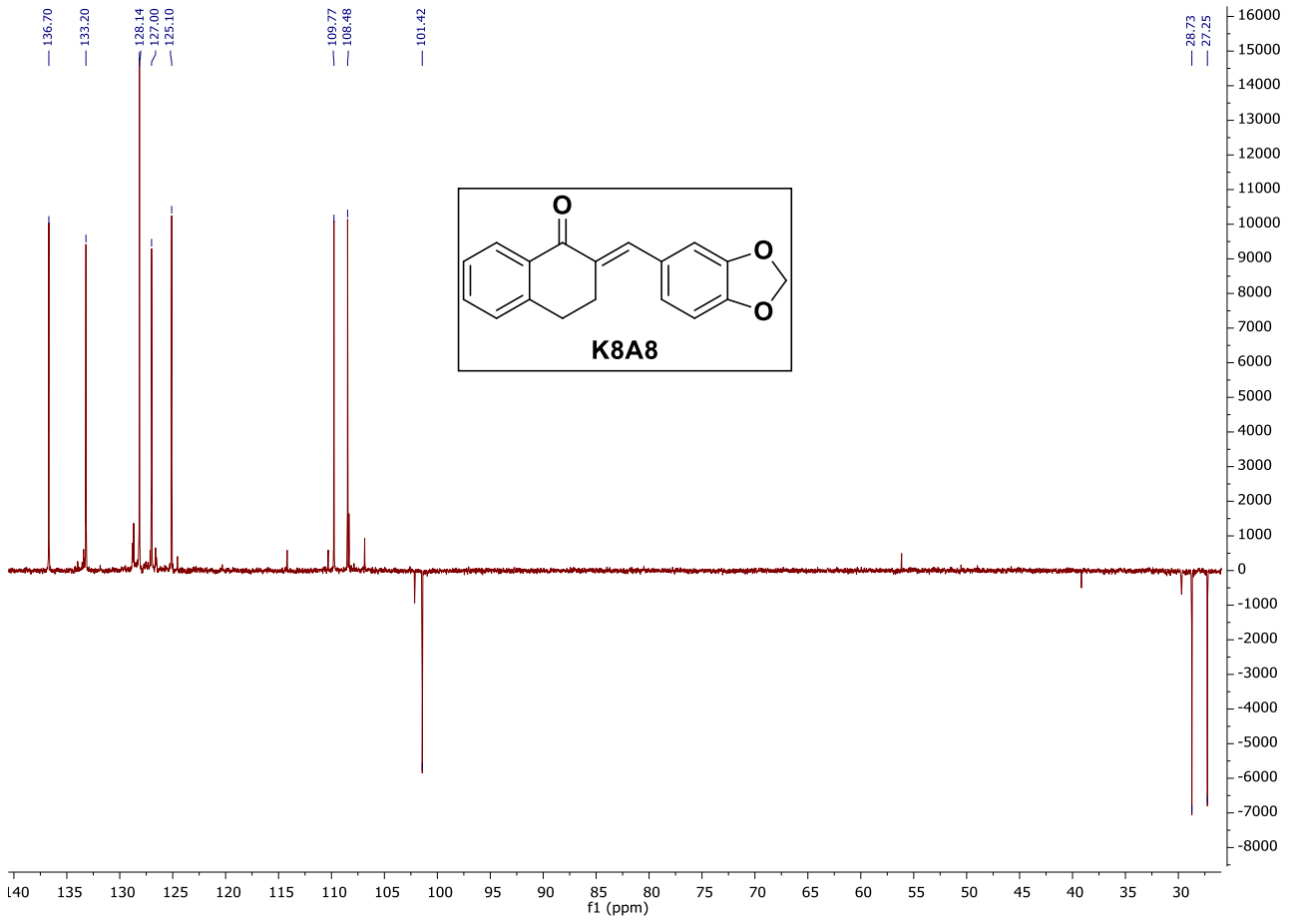


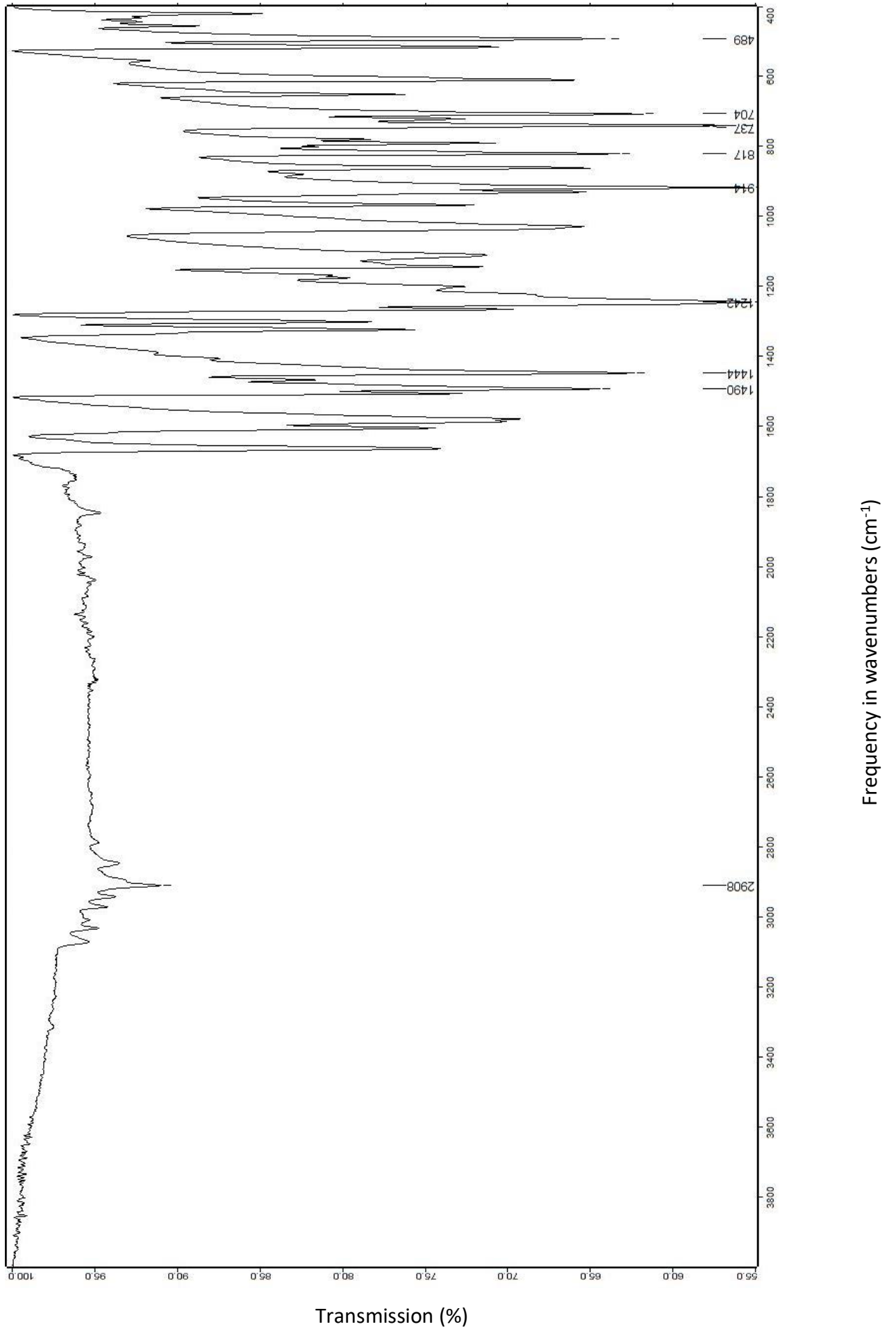


9.3.10. (*E*)-2-(benzo[*d*][1,3]dioxol-5-ylmethylene)-3,4-dihydronaphthalen-1(2*H*)-one (K8A8)

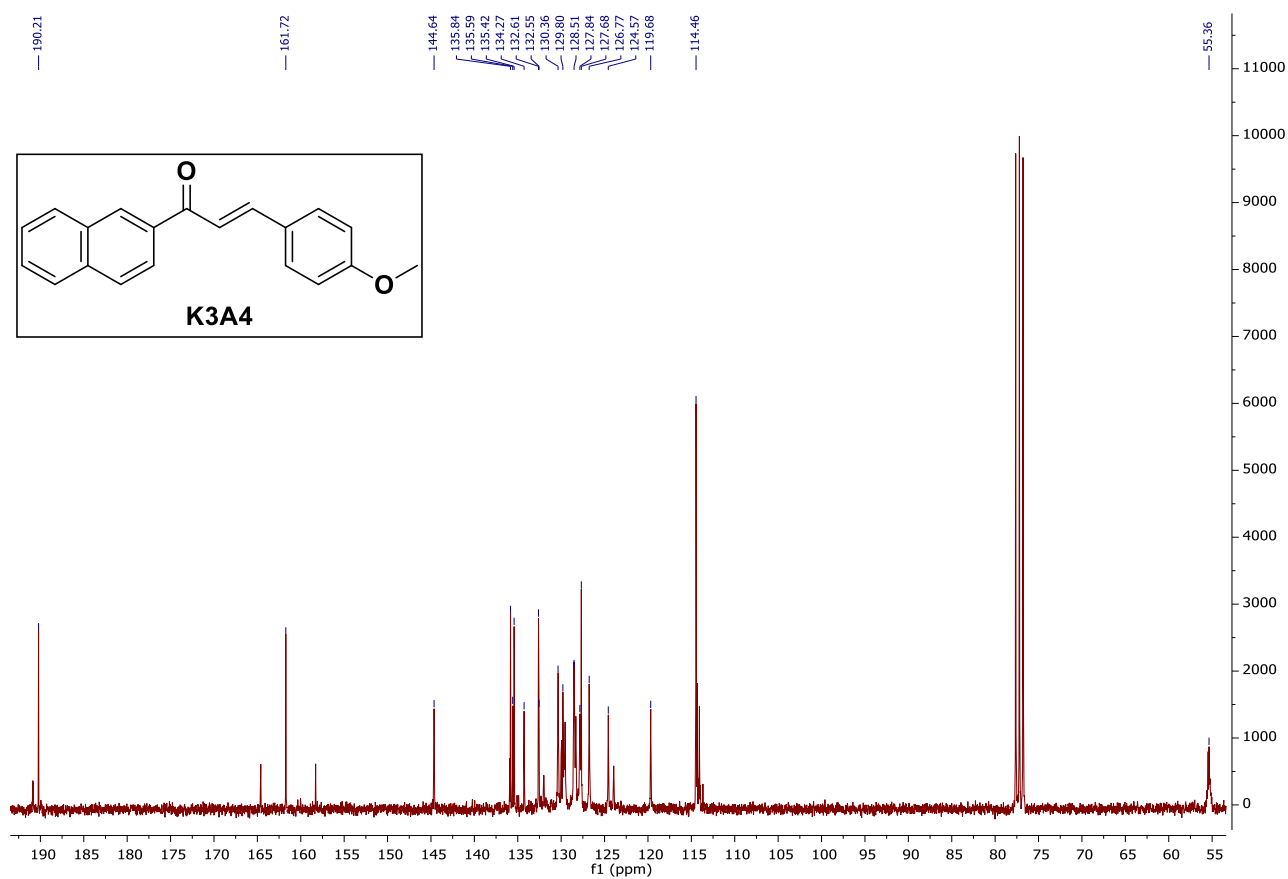
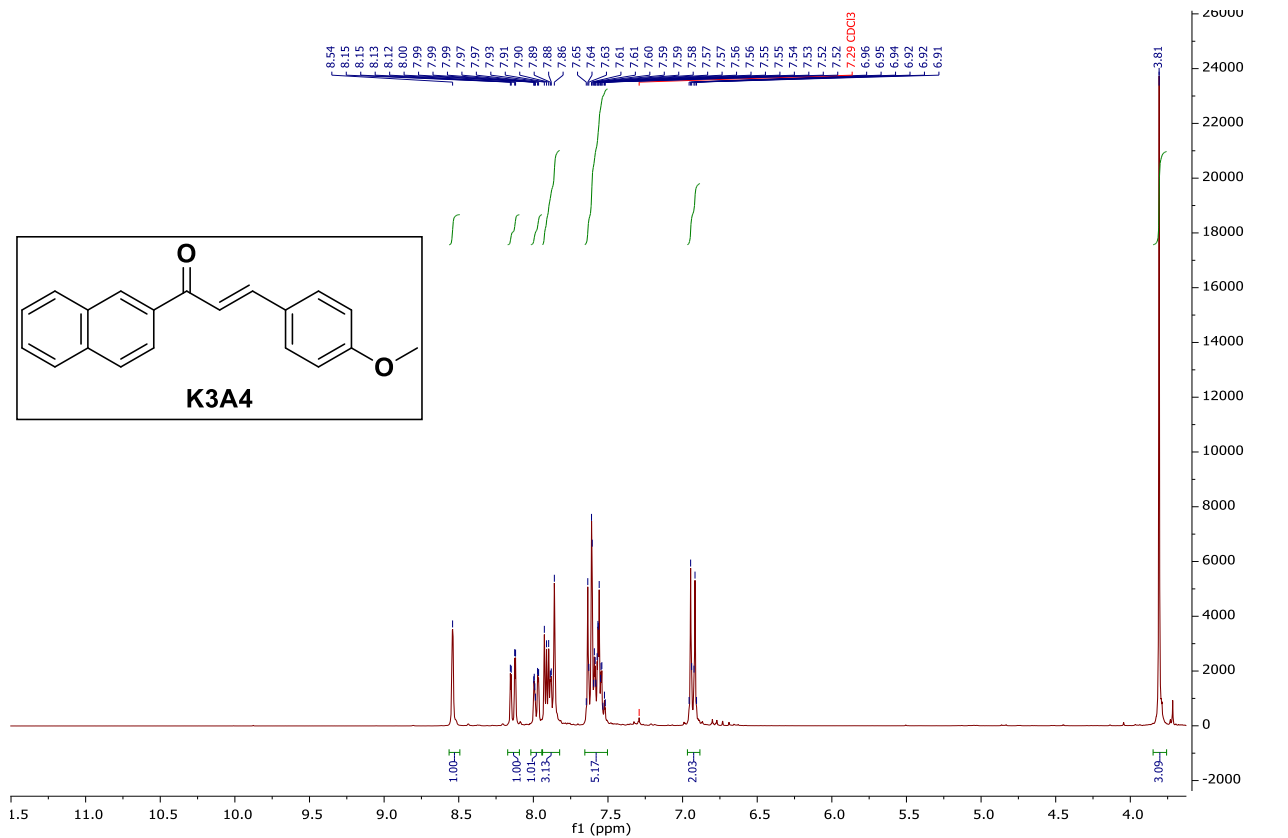


Chapter 9: Experimental Spectrums



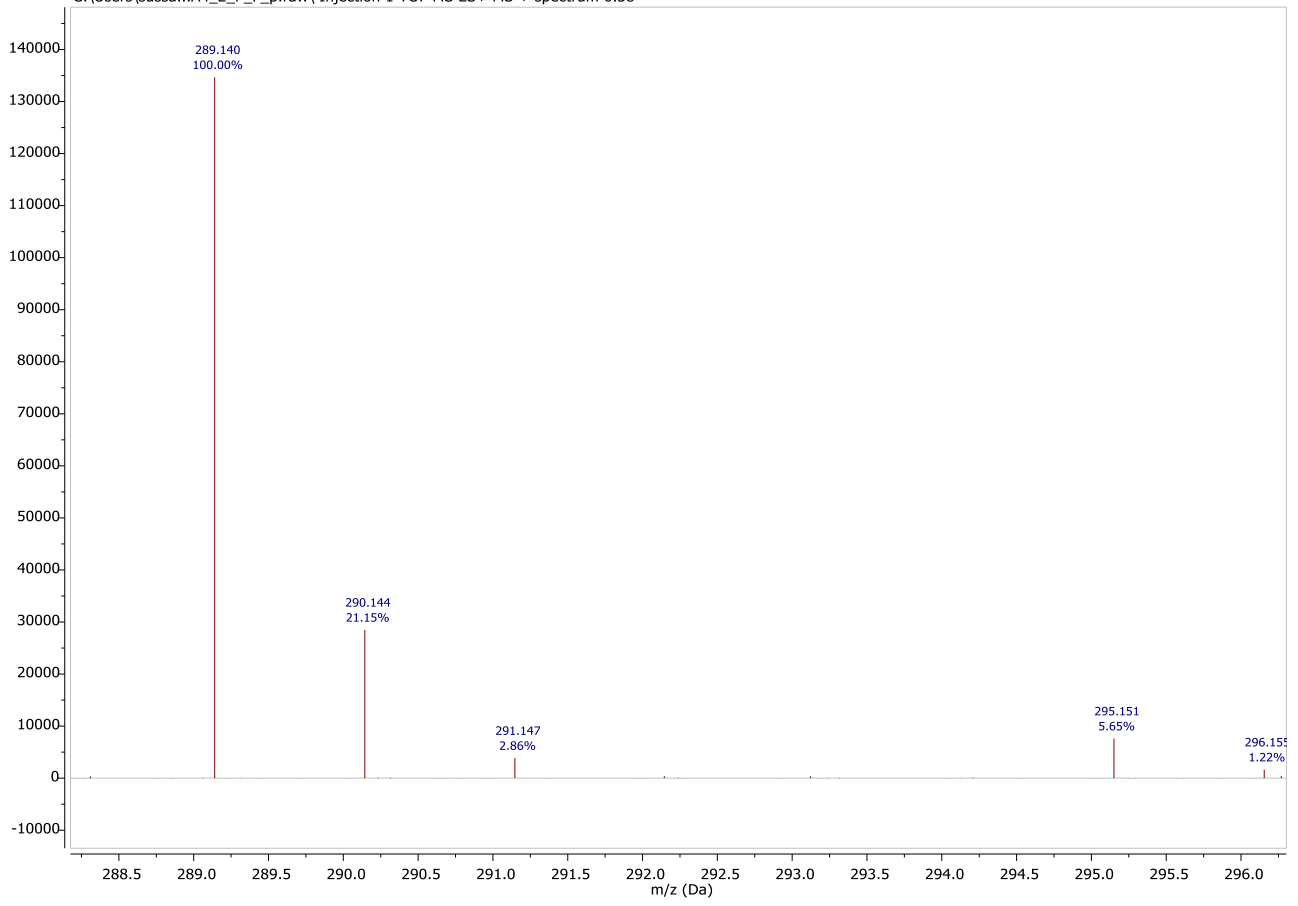


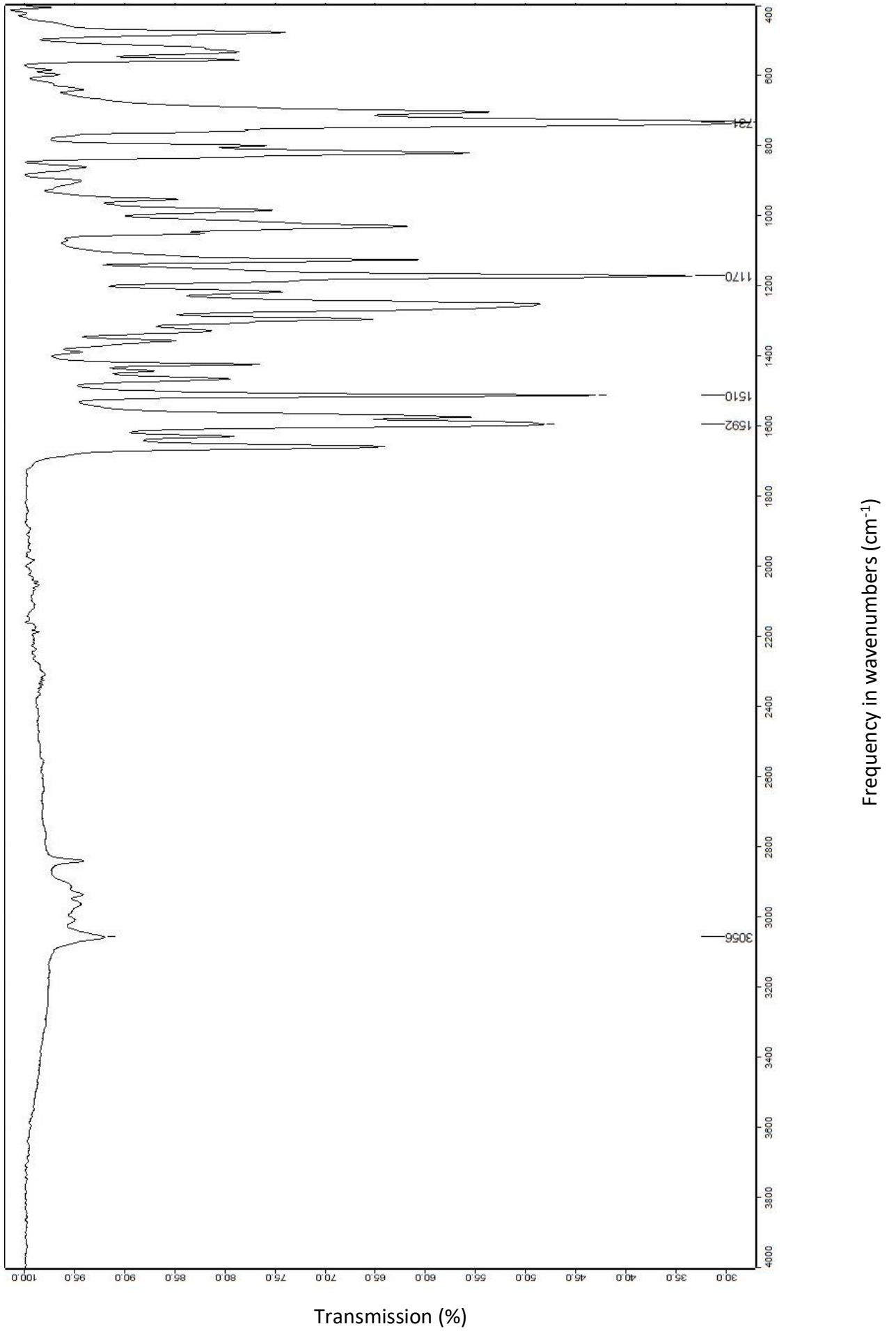
9.3.11. (*E*)-3-(4-methoxyphenyl)-1-(naphthalen-2-yl)prop-2-en-1-one (K3A4)



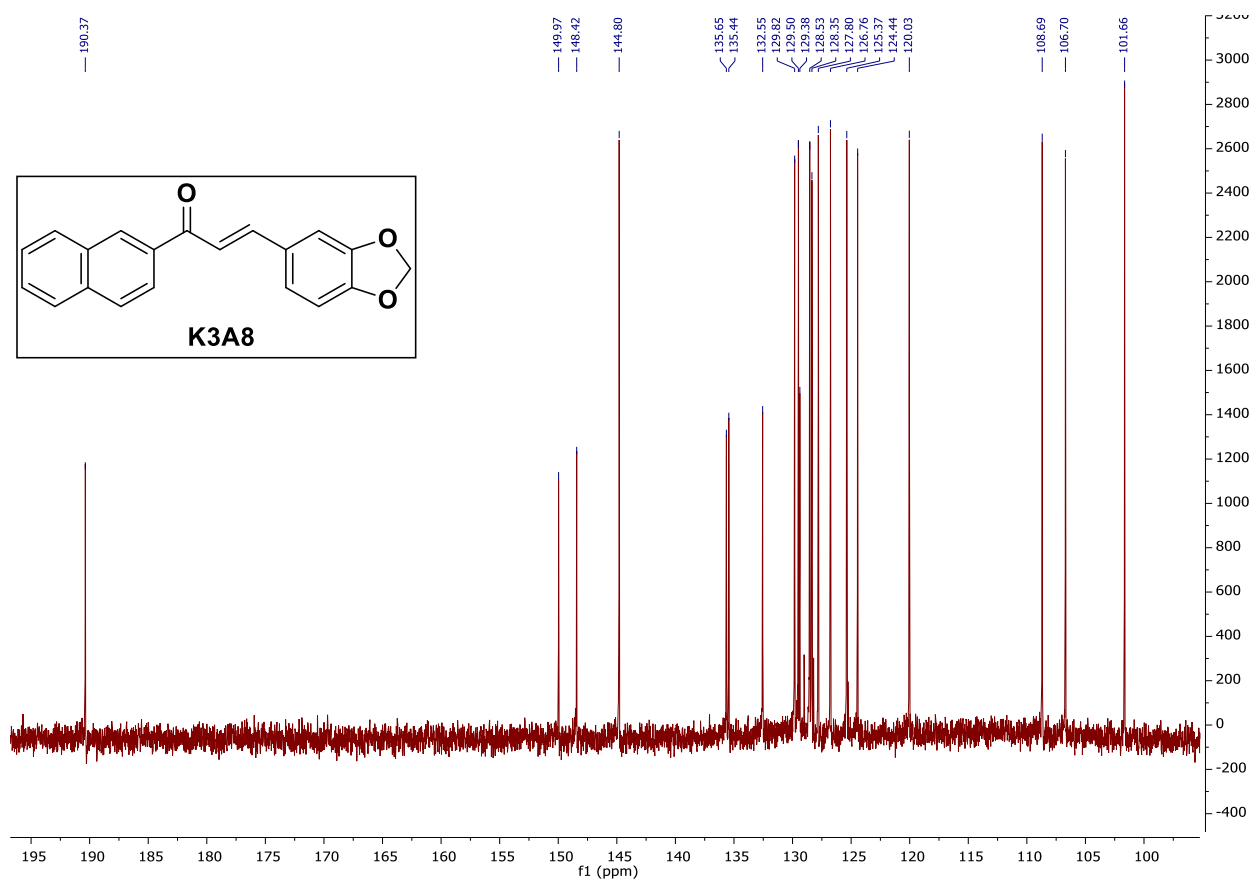
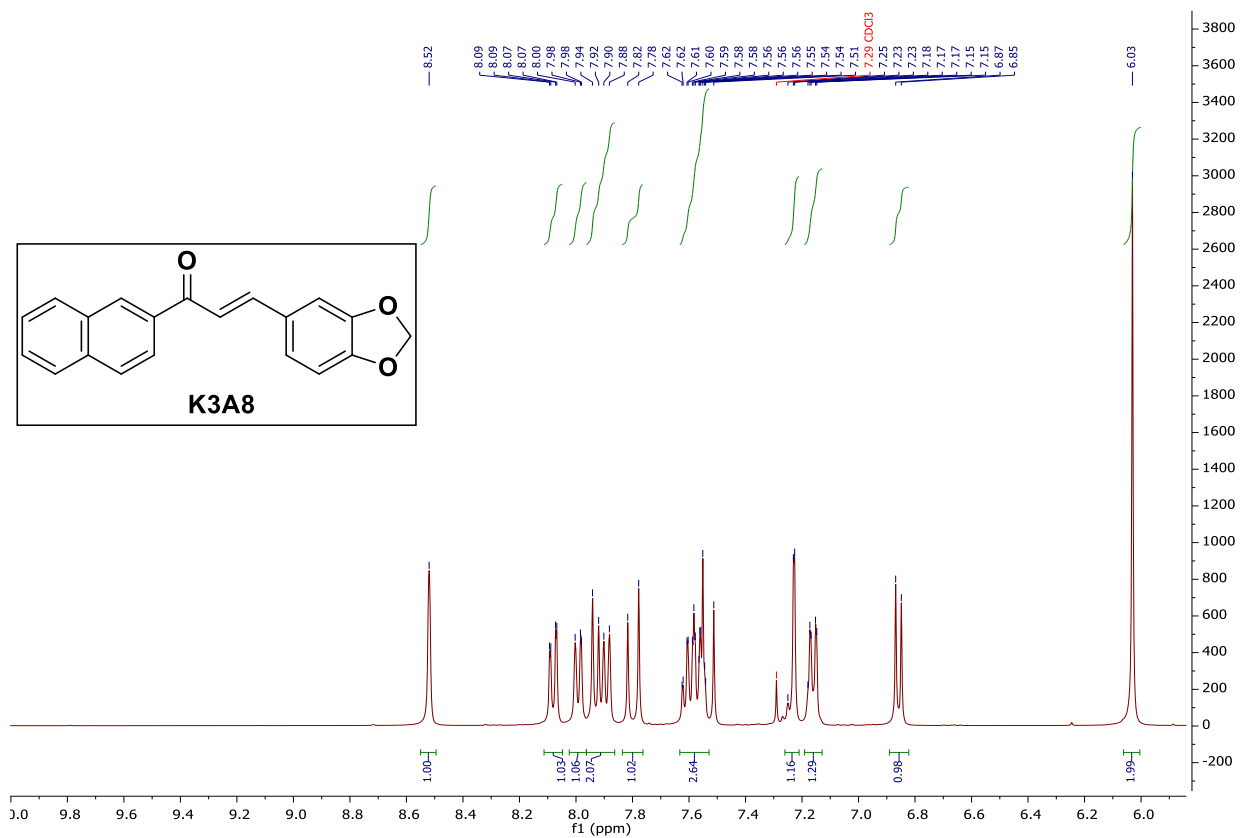
Chapter 9: Experimental Spectrums

C:\Users\sussa...A4_2_P_F_p.raw\ Injection 1 TOF MS ES+ MS + spectrum 0.38

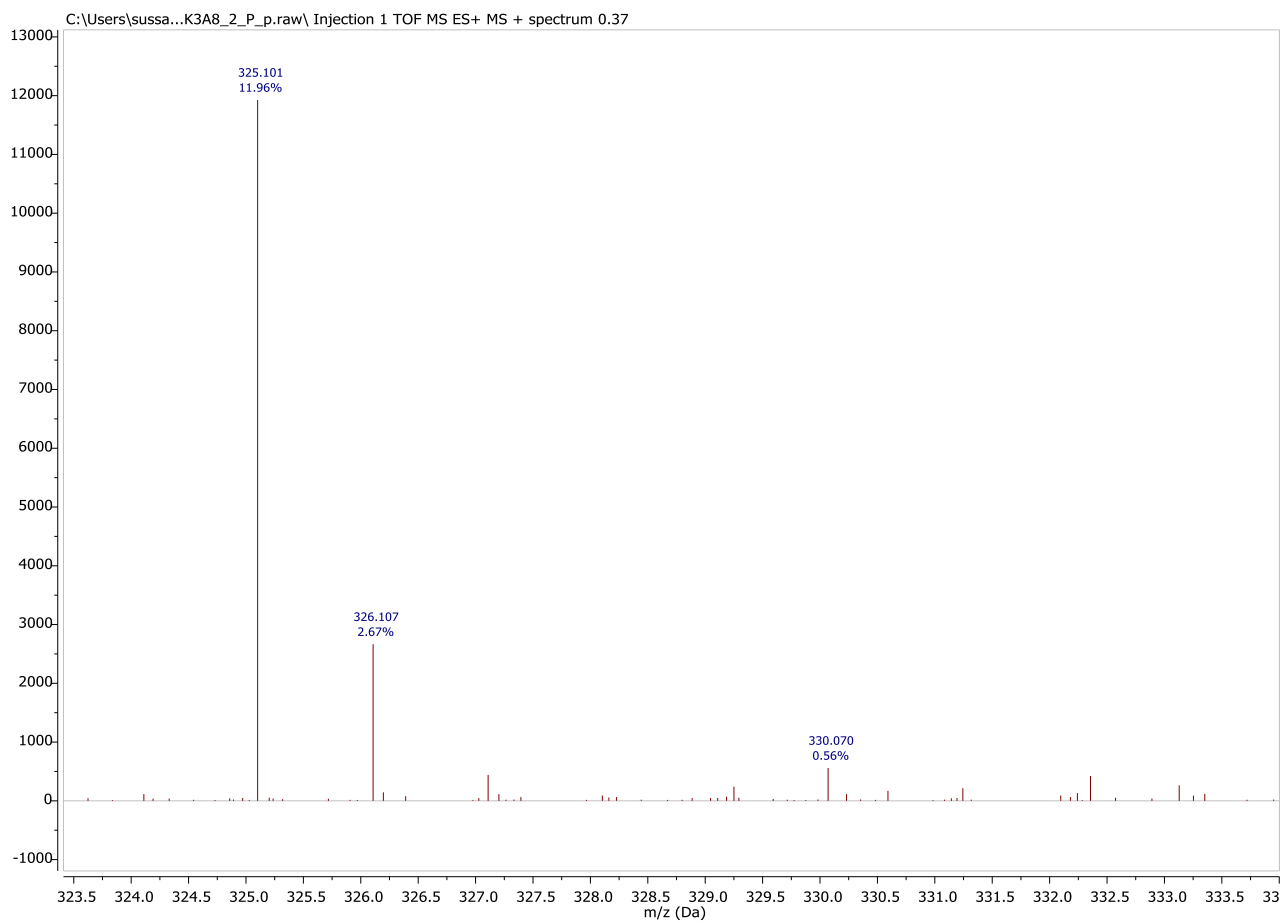
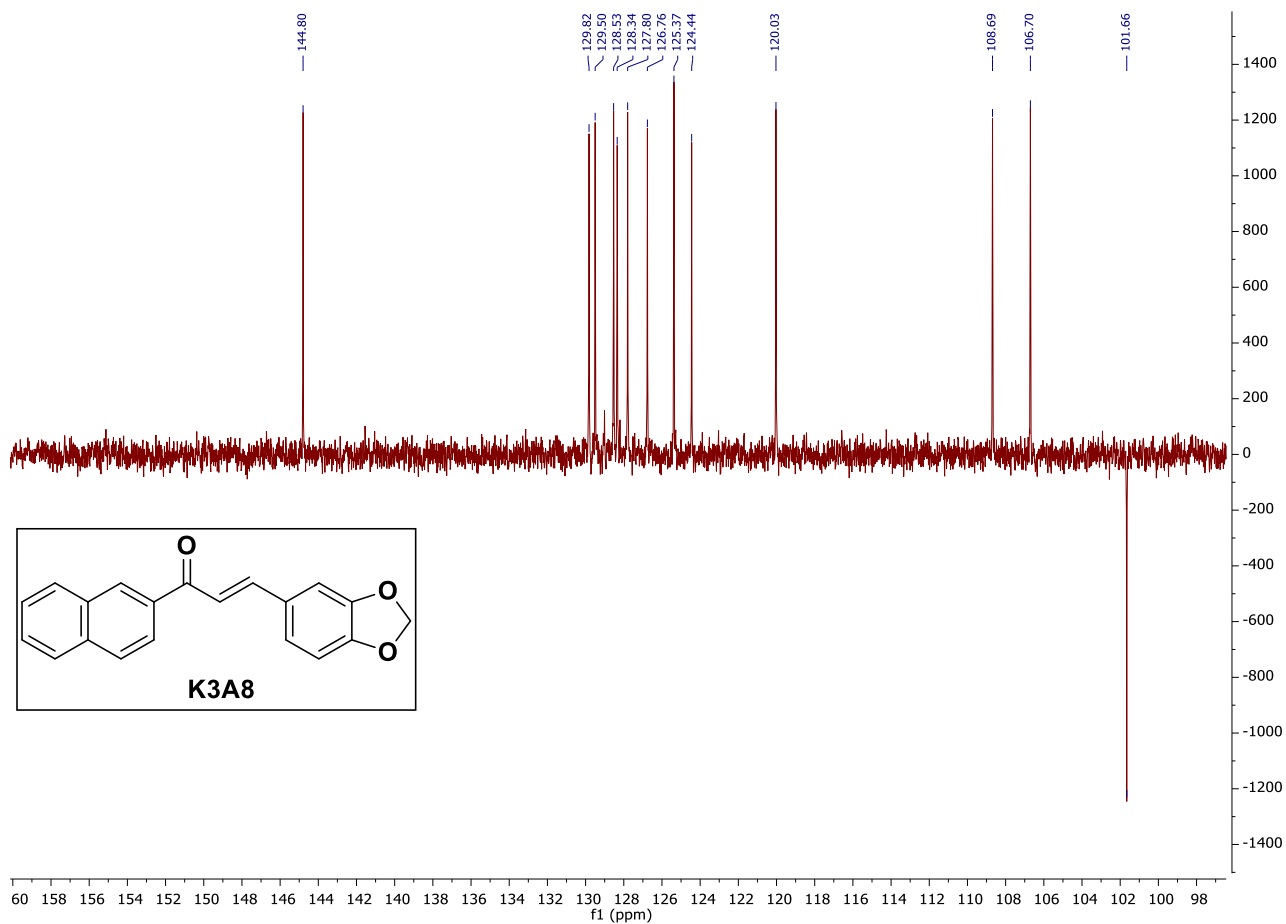


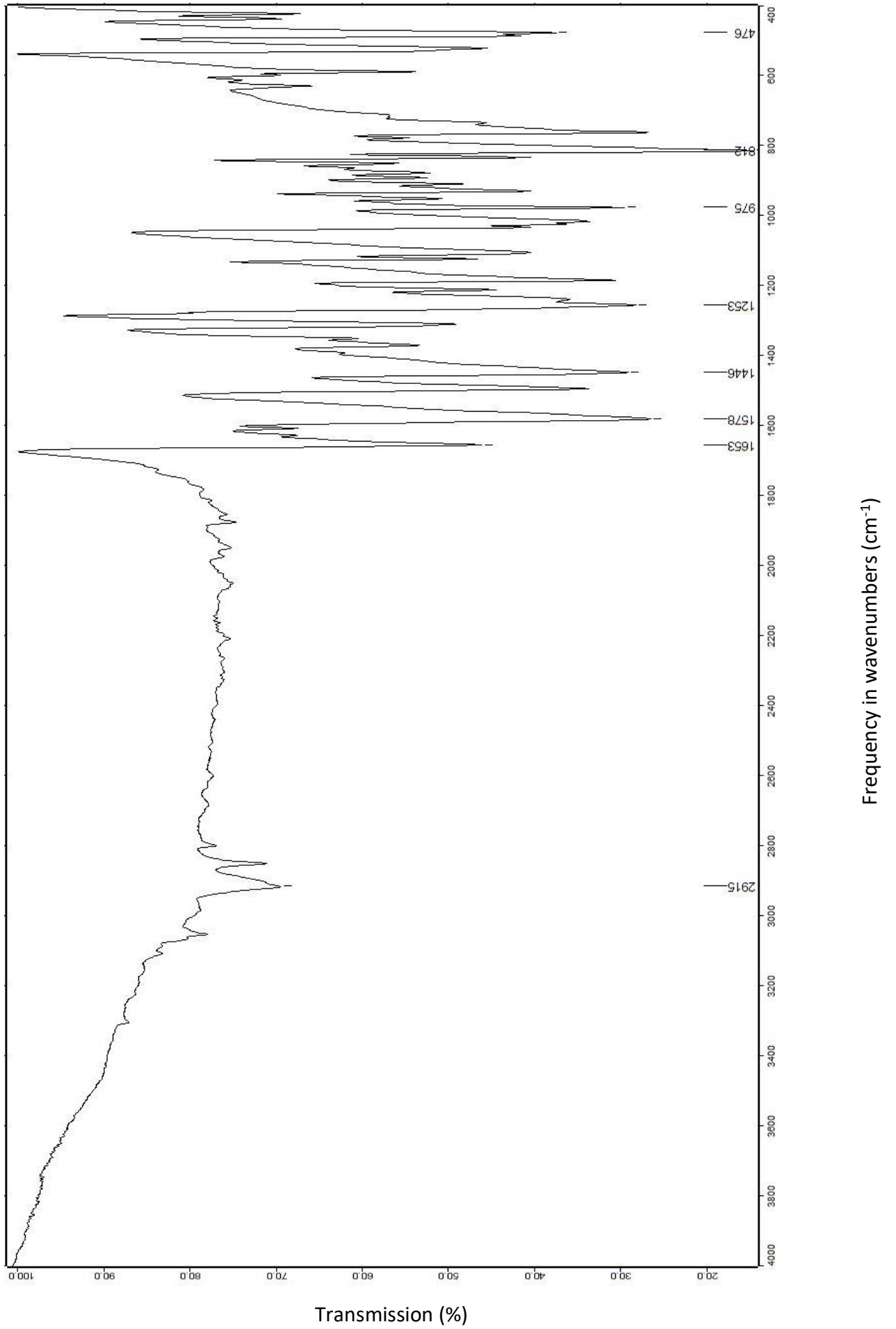


9.3.12. (*E*)-3-(benzo[*d*][1,3]dioxol-5-yl)-1-(naphthalen-2-yl)prop-2-en-1-one (K3A8)

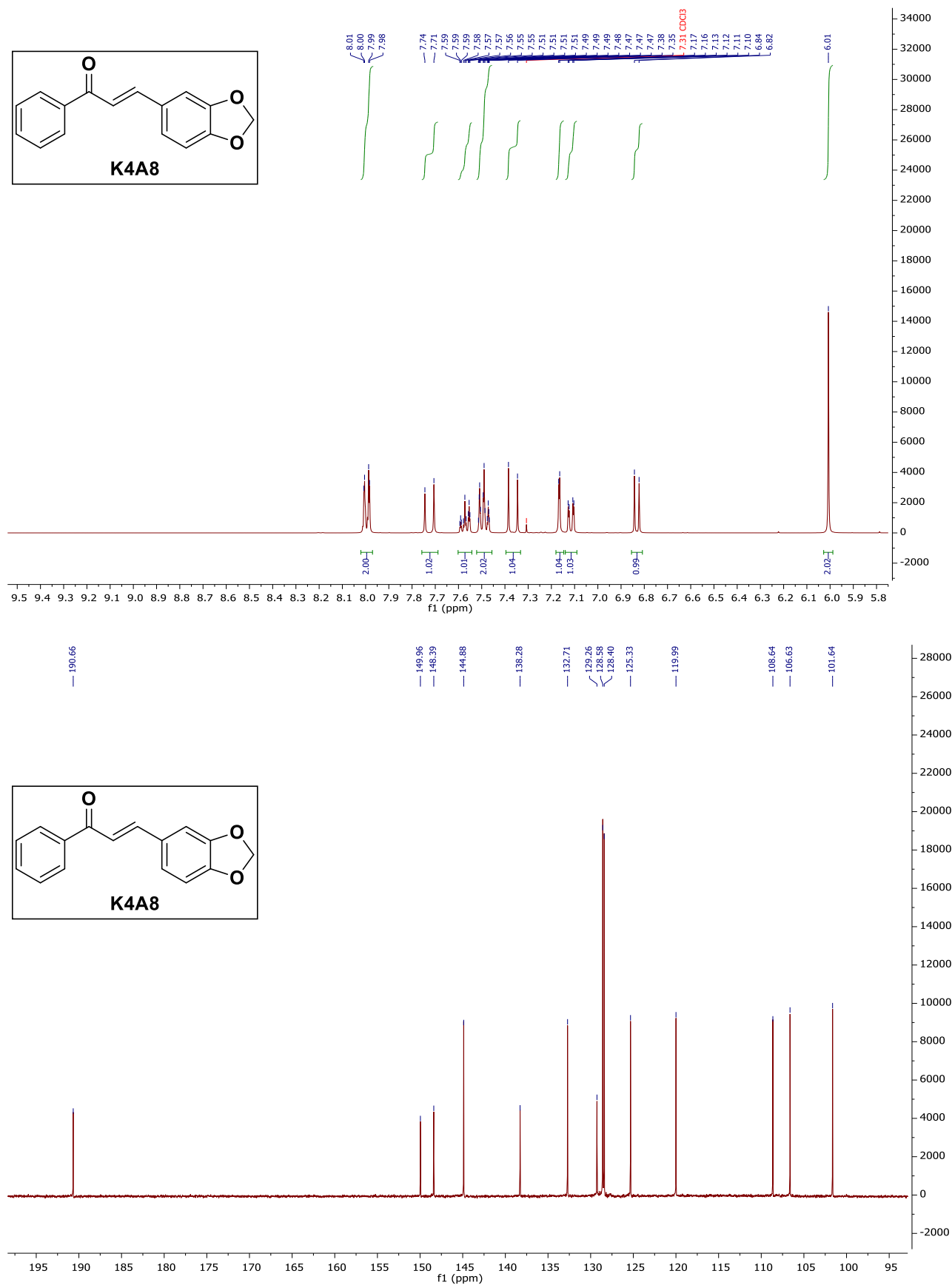


Chapter 9: Experimental Spectra

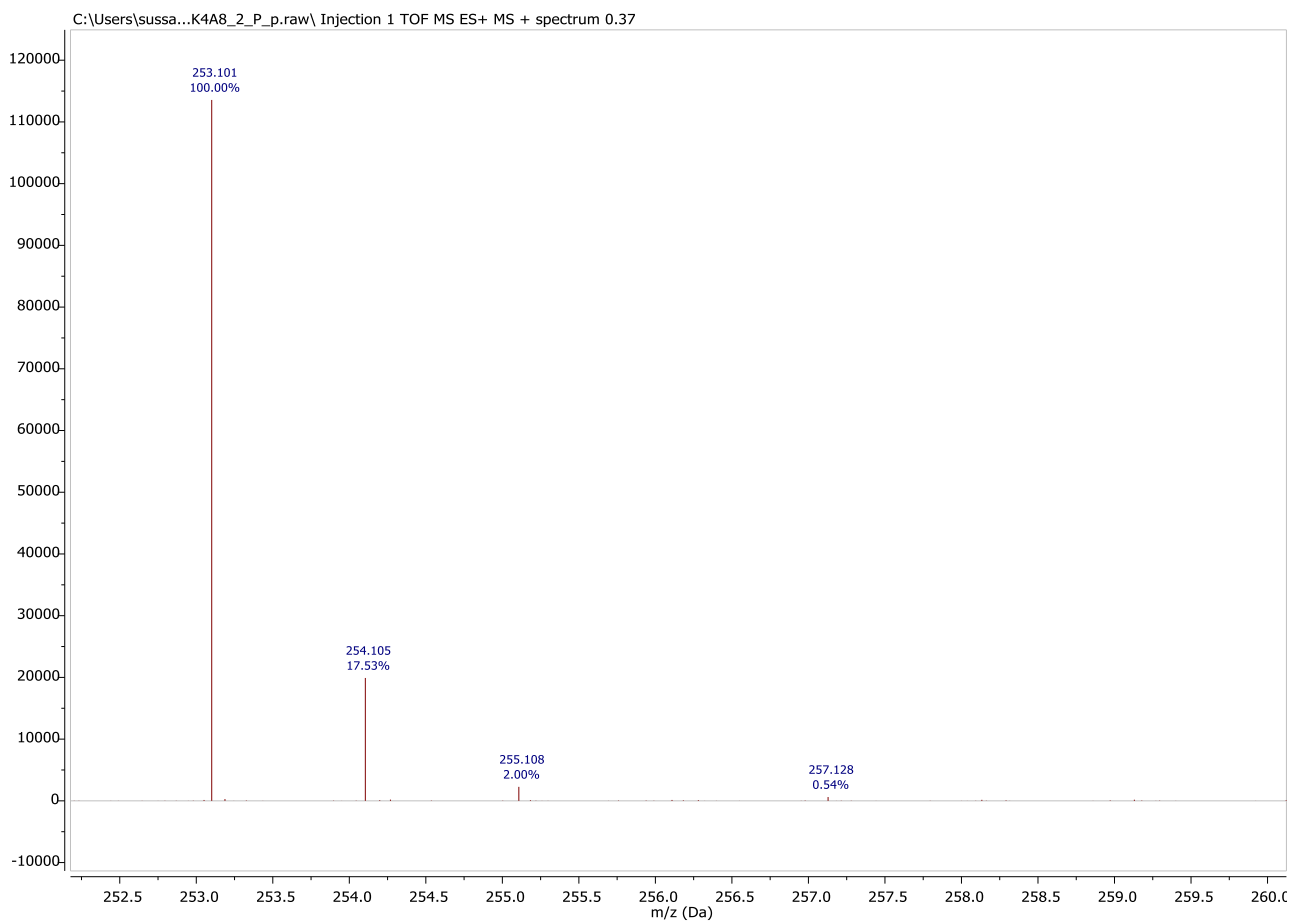
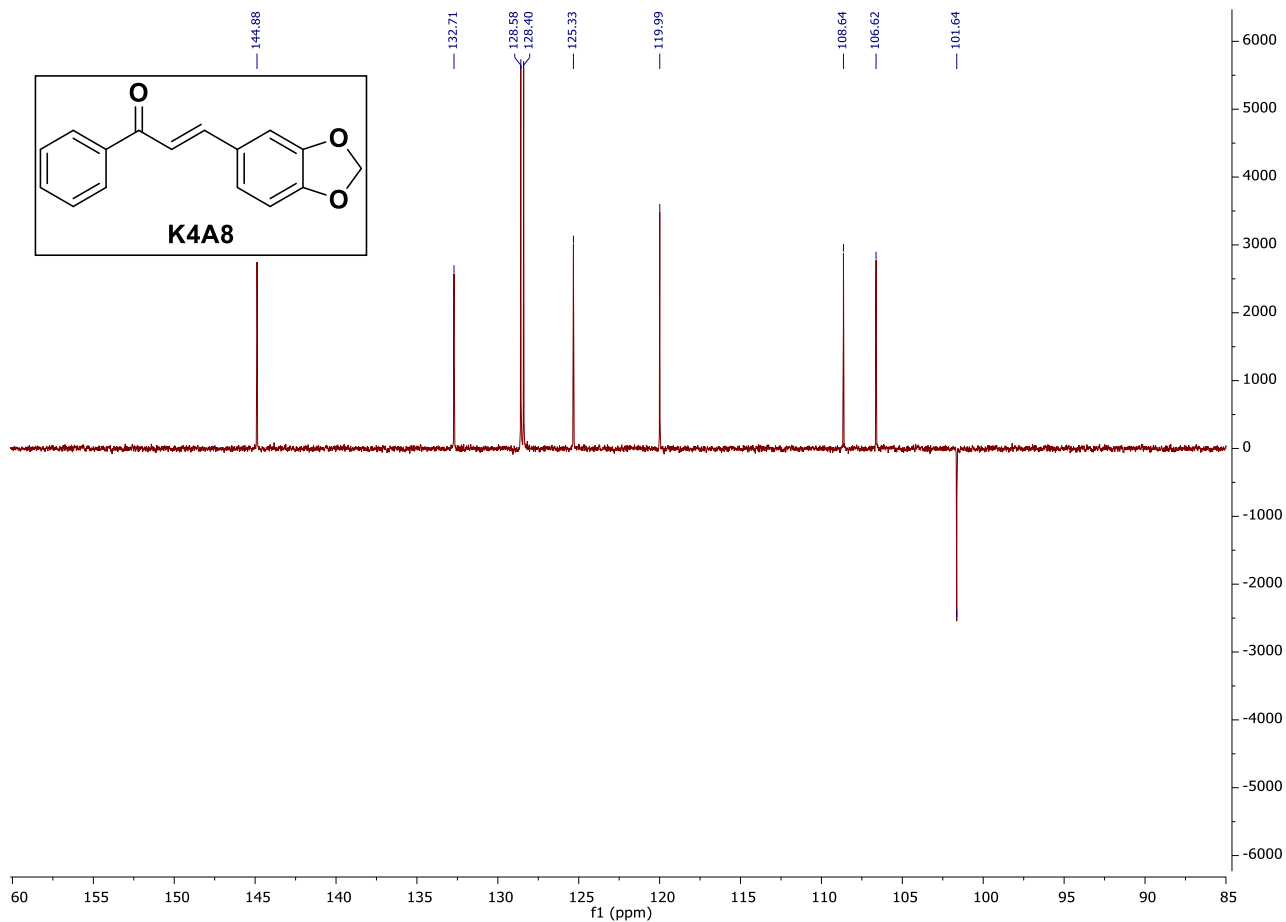


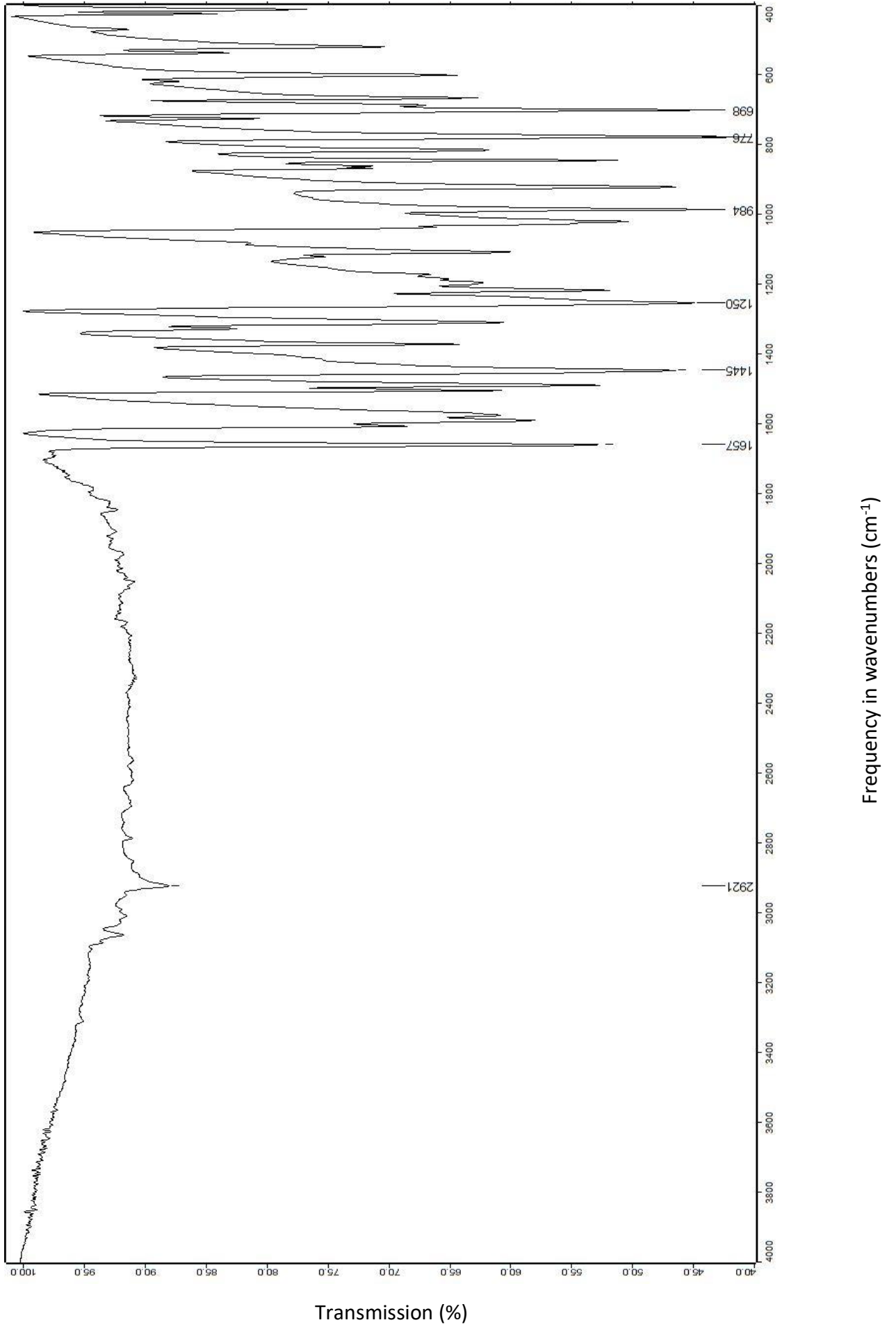


9.3.13. (*E*)-3-(benzo[*d*][1,3]dioxol-5-yl)-1-phenylprop-2-en-1-one (K4A8)

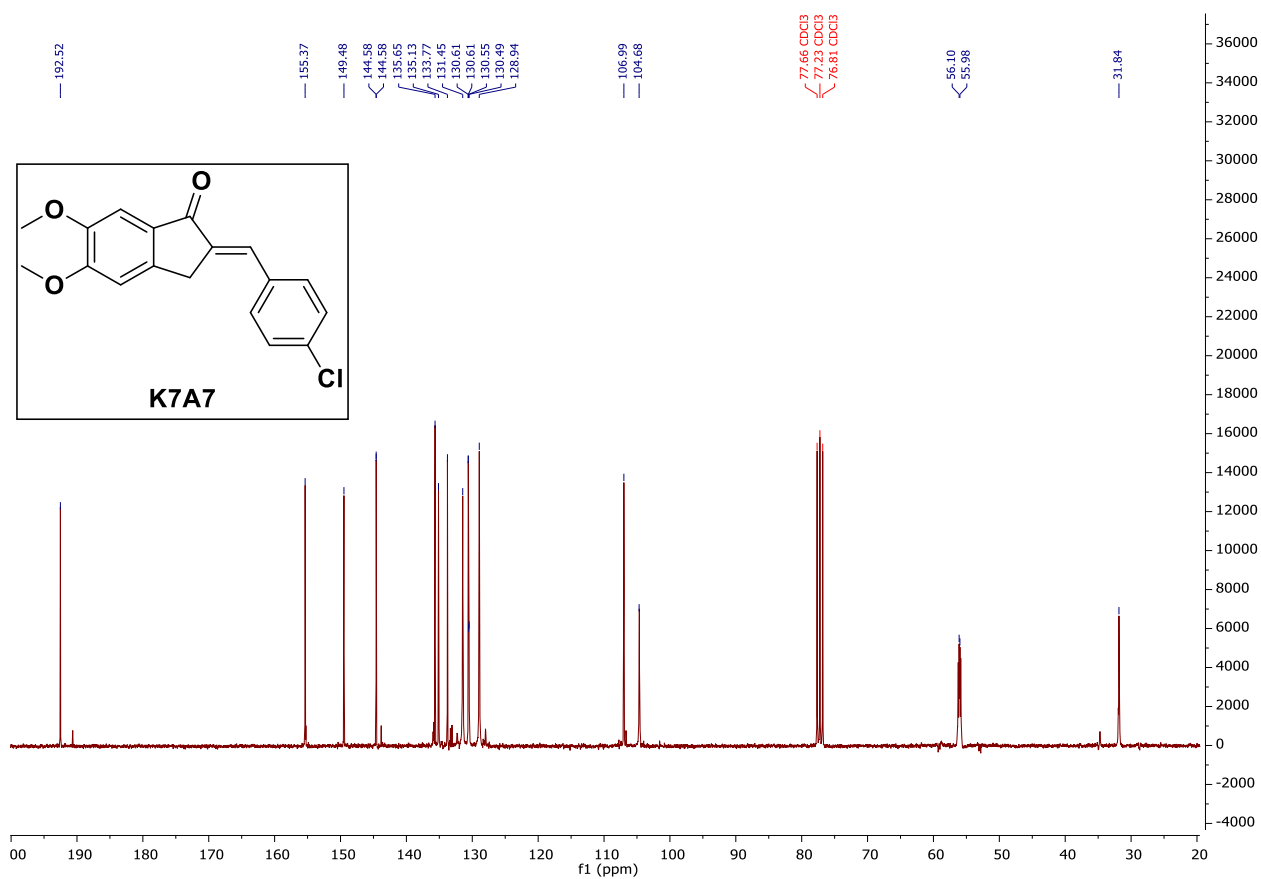
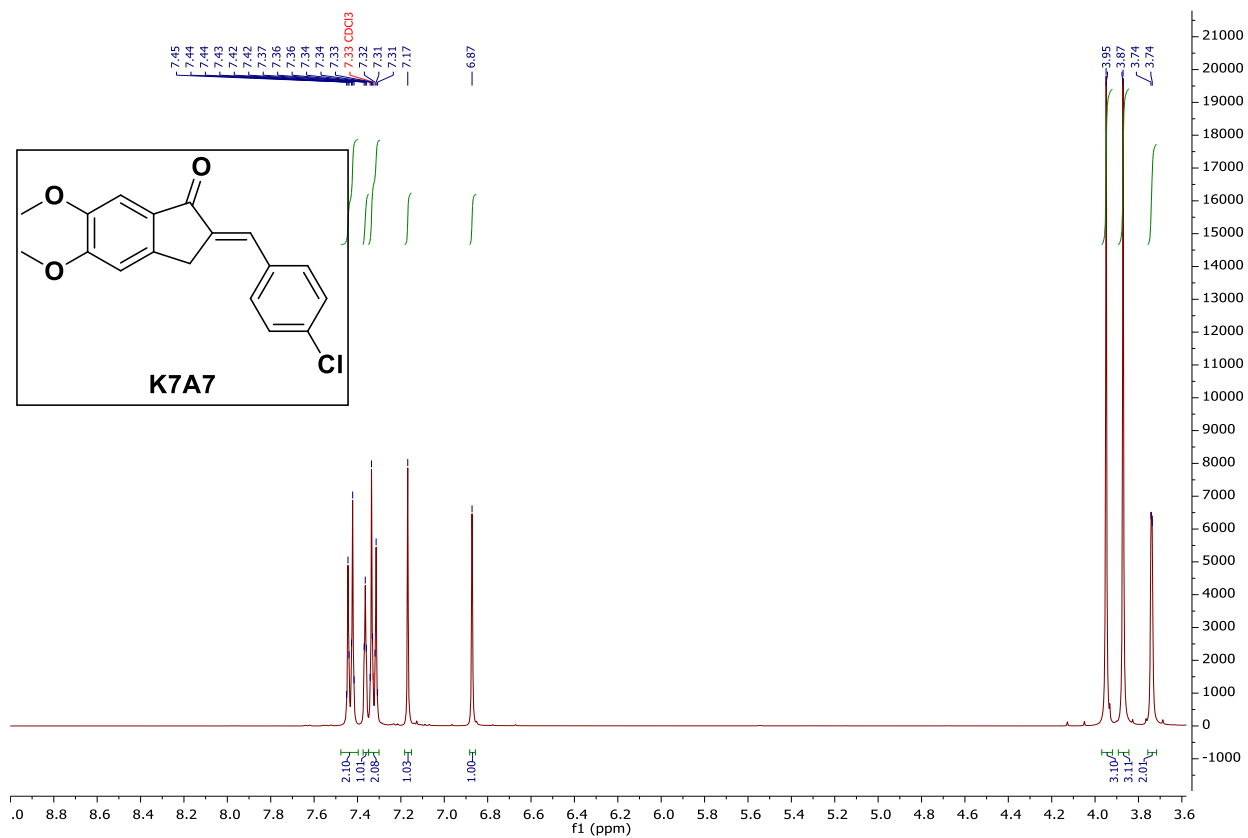


Chapter 9: Experimental Spectrums

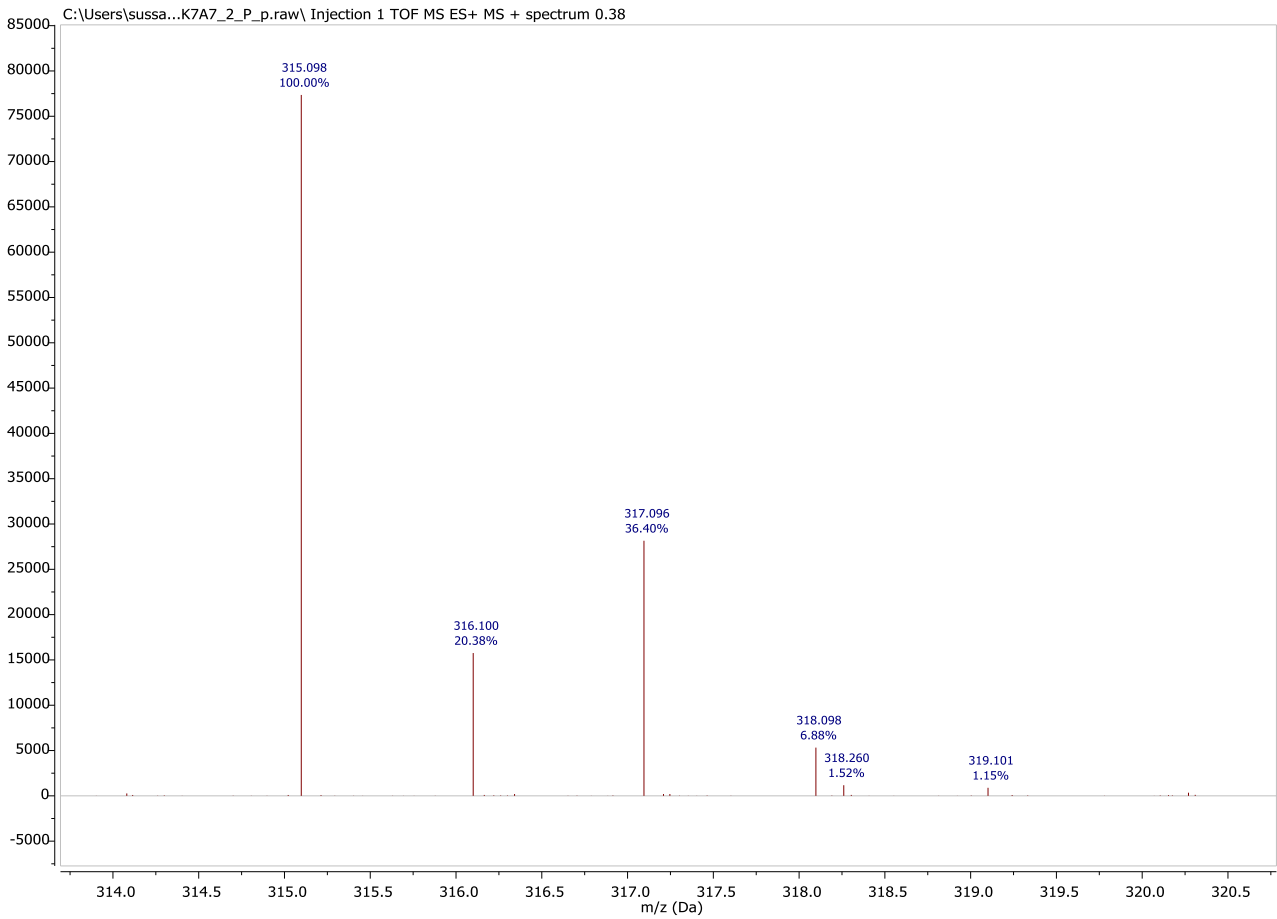
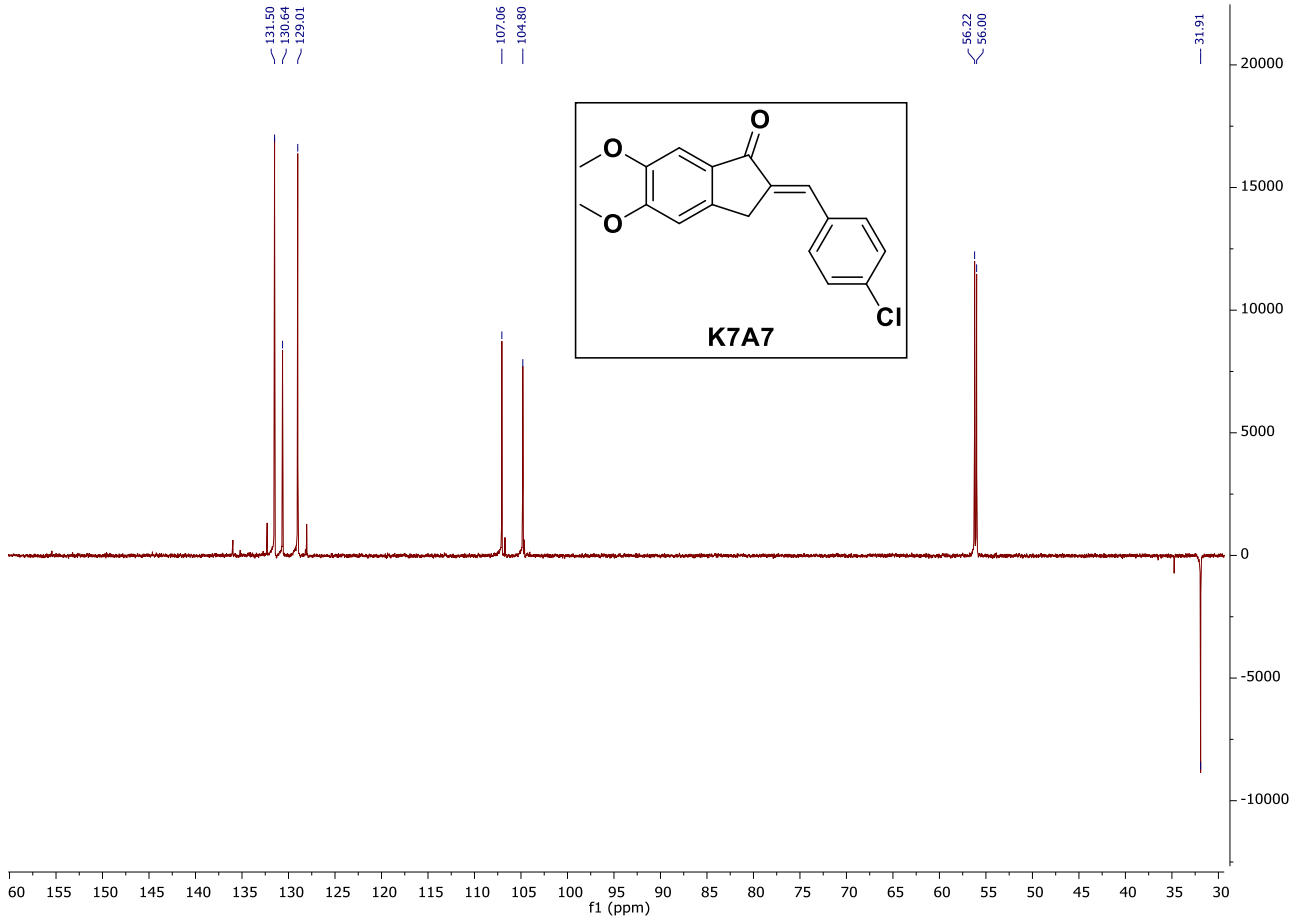


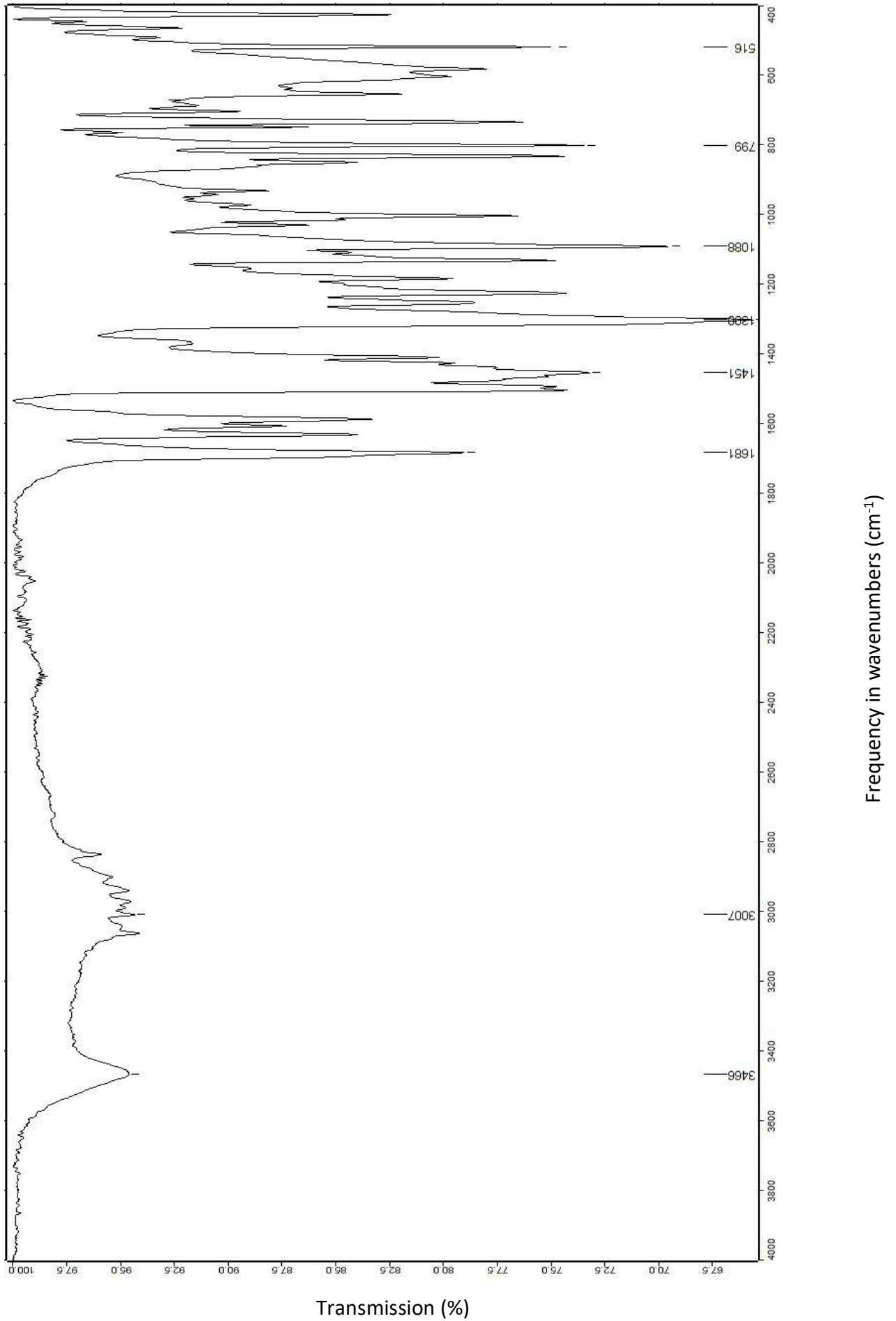


9.3.14. (*E*)-2-(4-chlorobenzylidene)-5,6-dimethoxy-2,3-dihydro-1*H*-inden-1-one (K7A7)



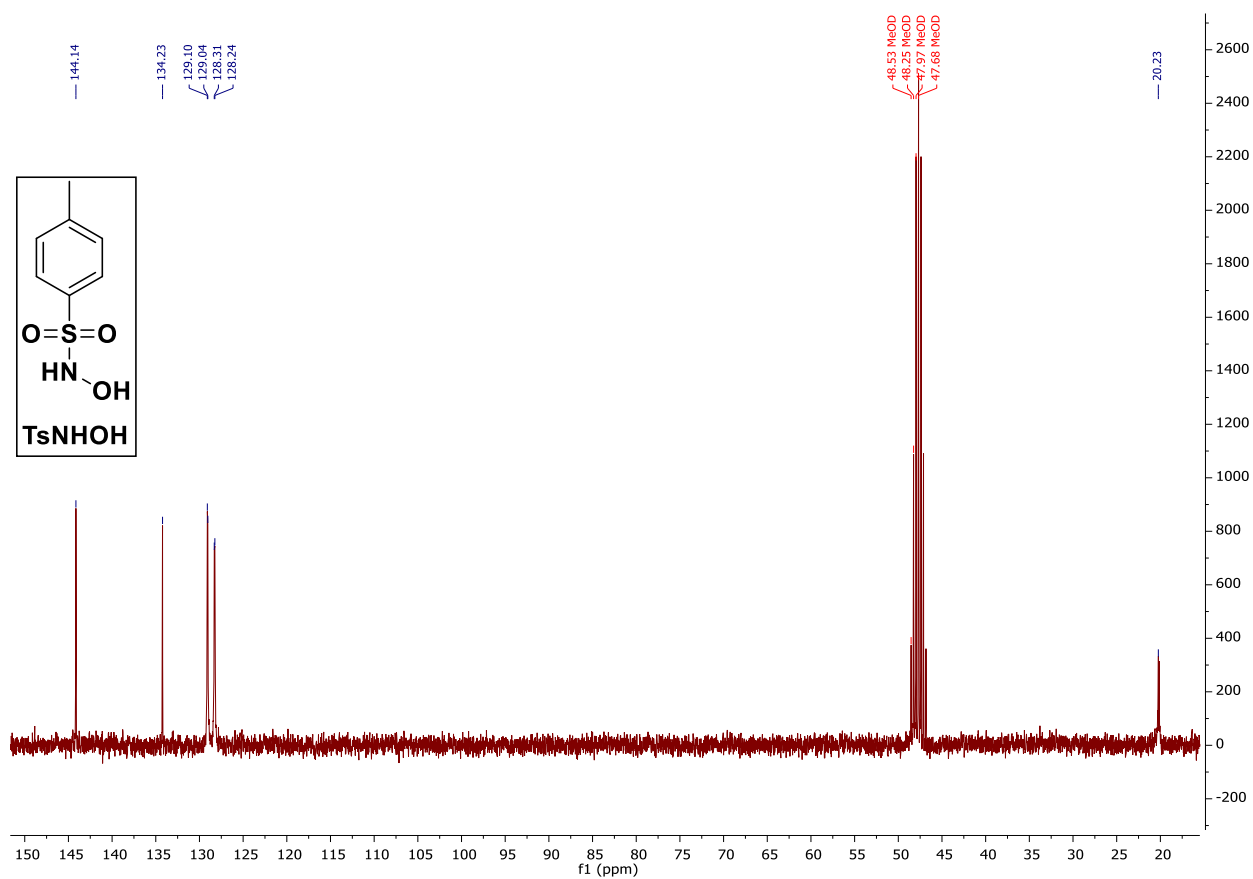
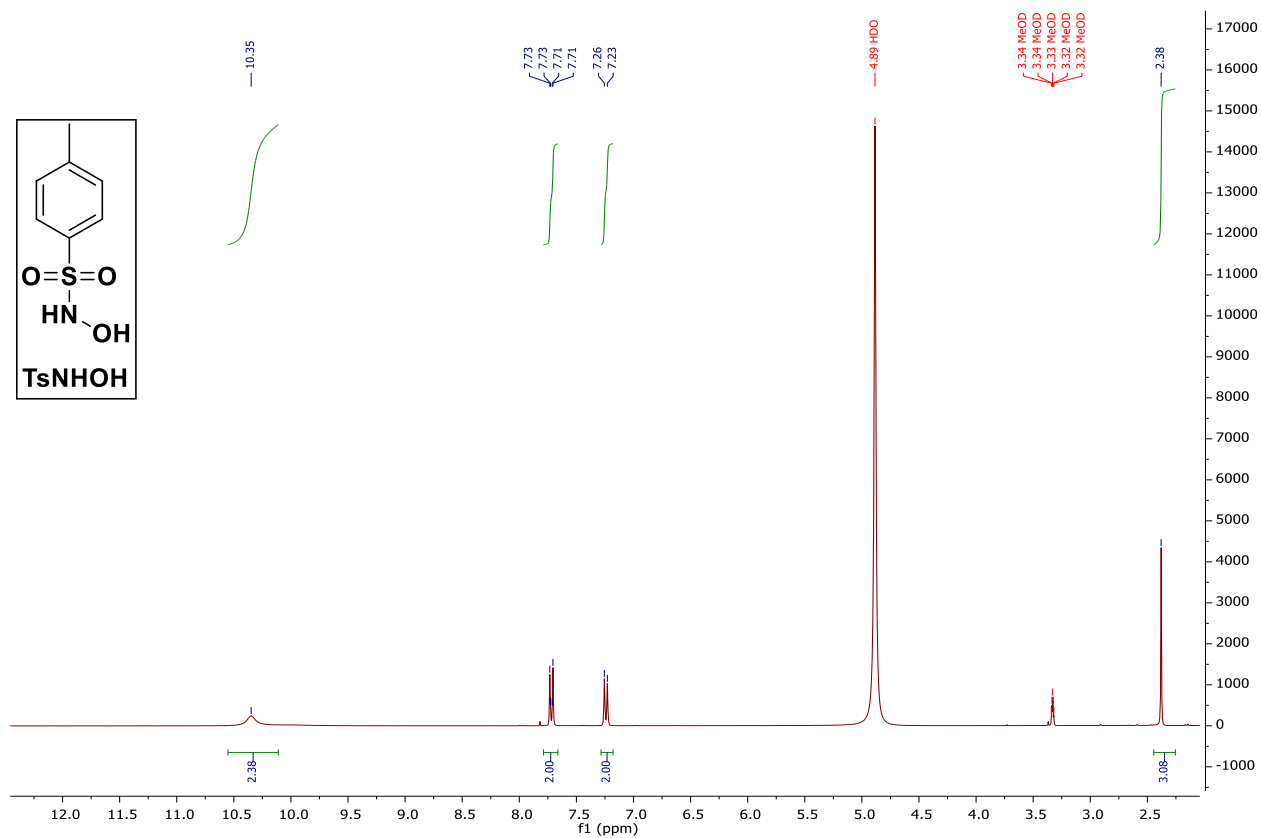
Chapter 9: Experimental Spectra



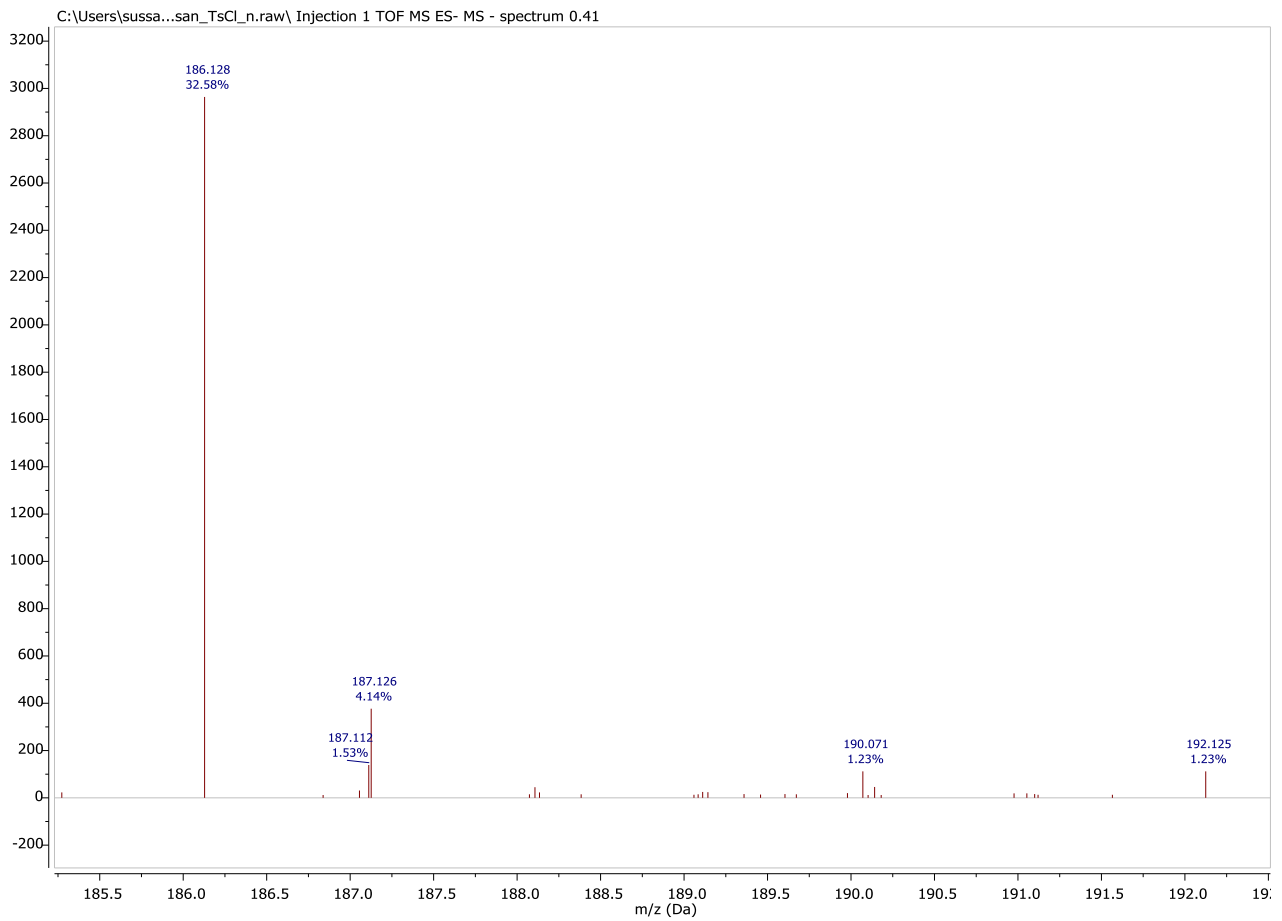
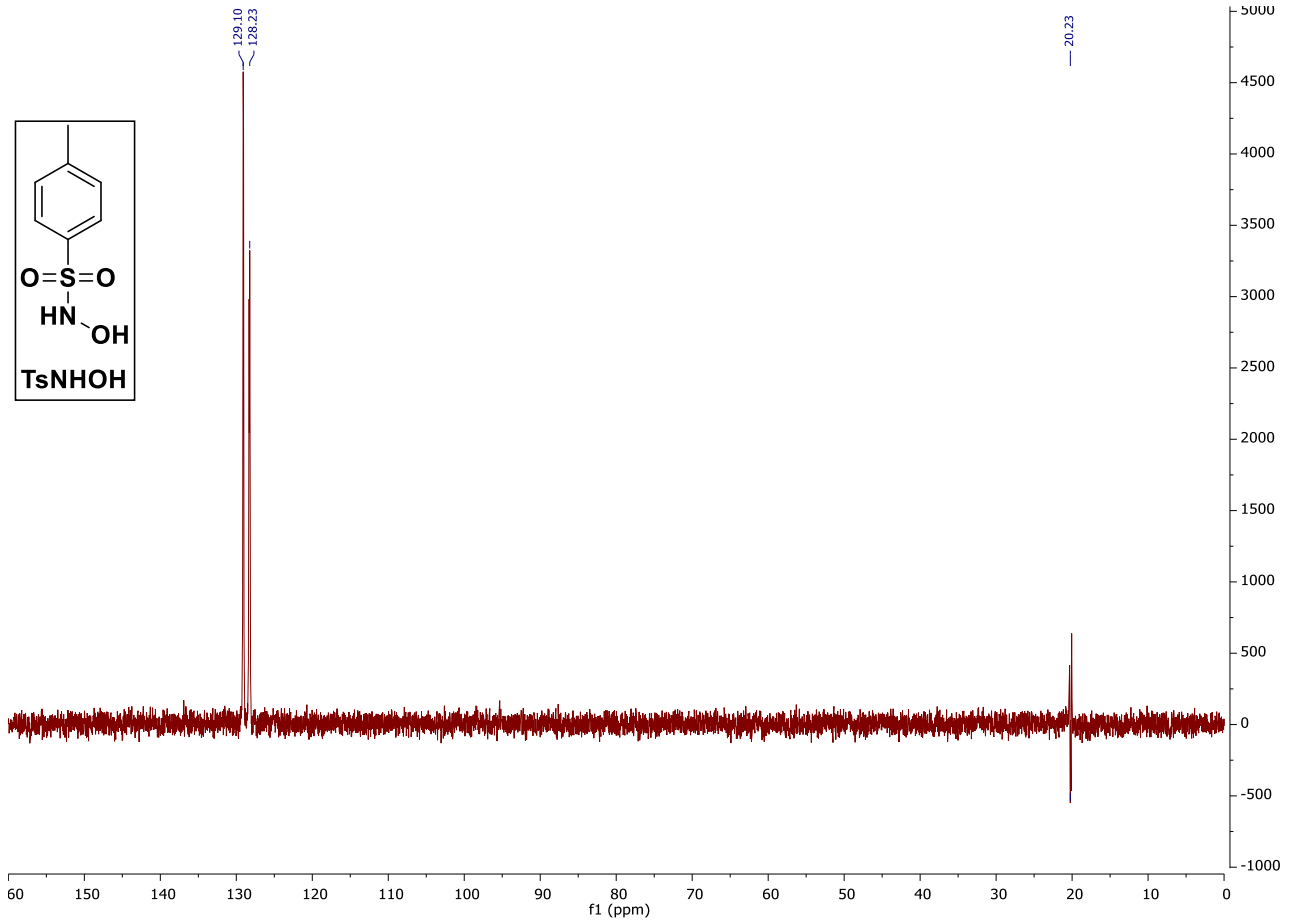


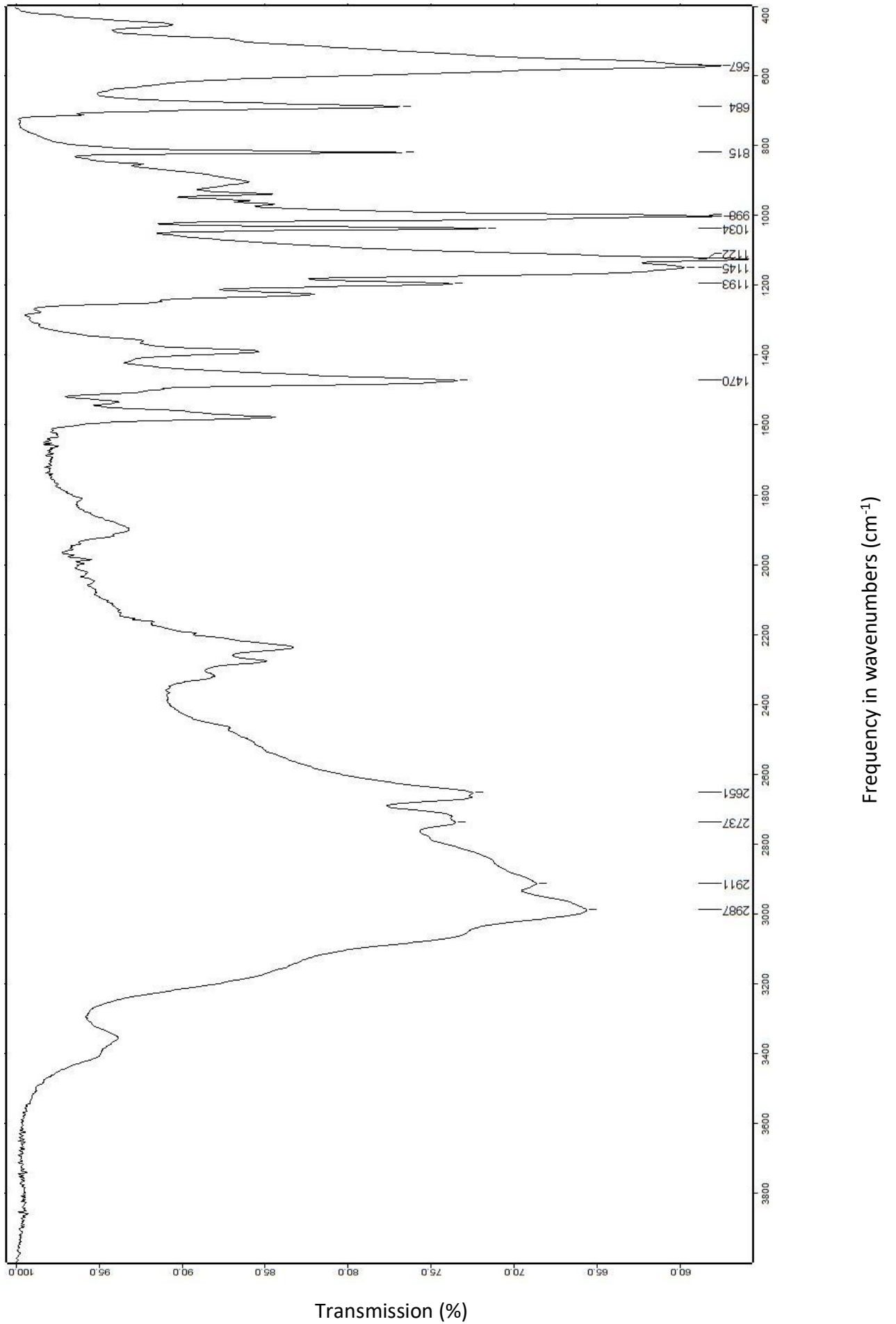
9.3.15. TsNHOH: Synthesis of N-hydroxy-4-methylbenzenesulfonamide

(131)



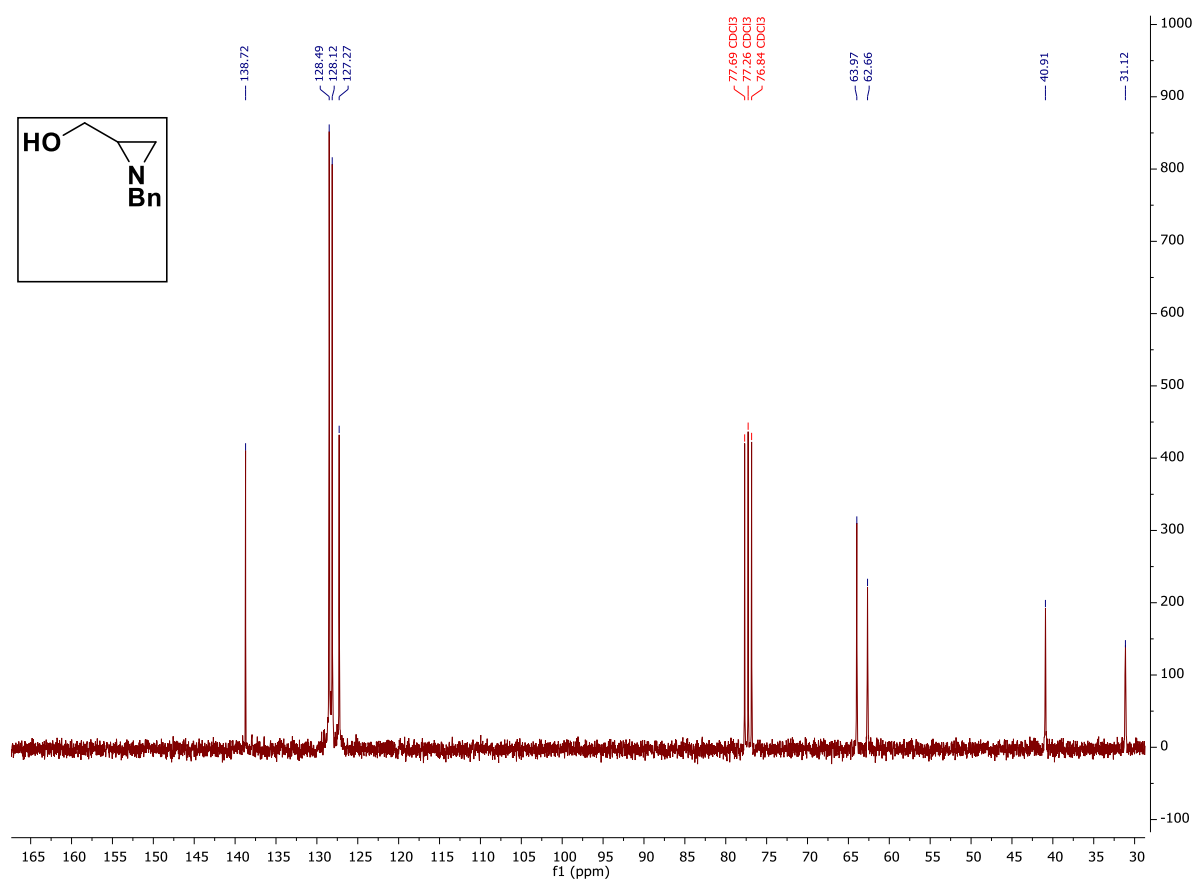
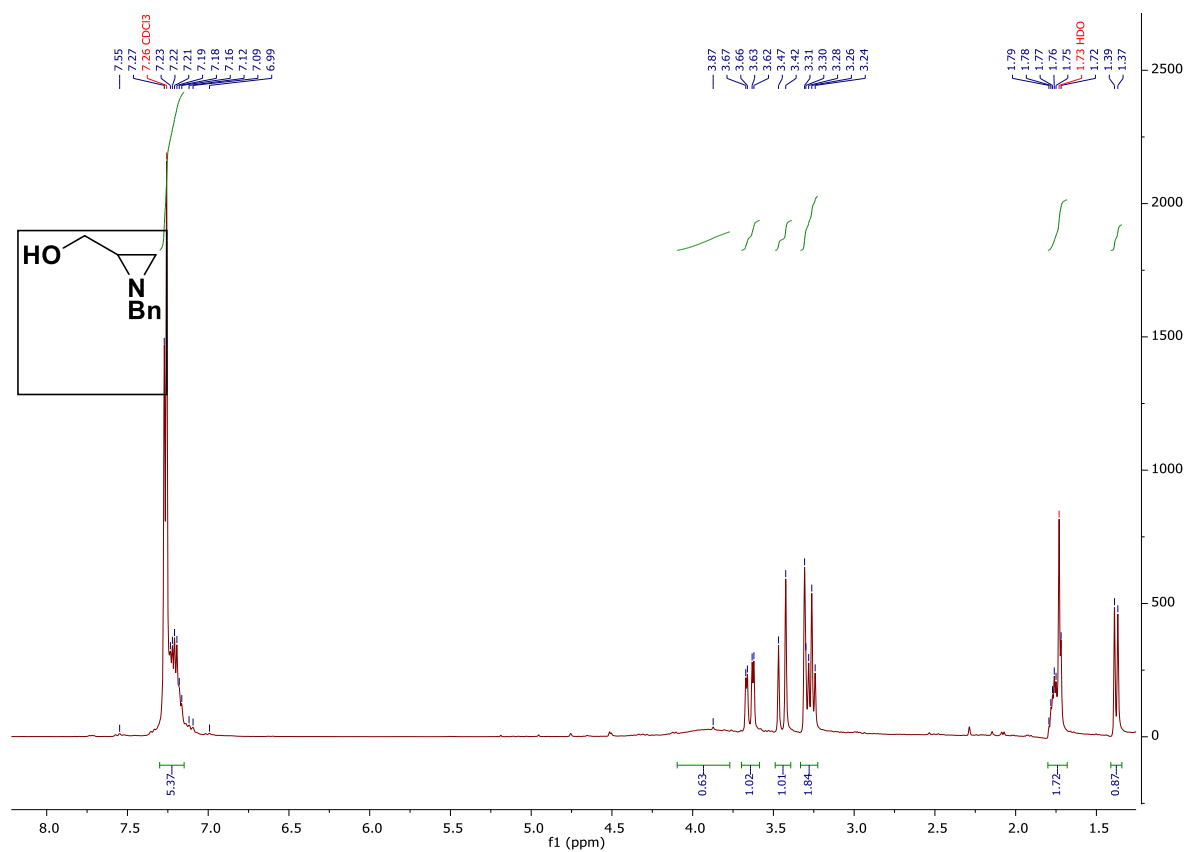
Chapter 9: Experimental Spectrums



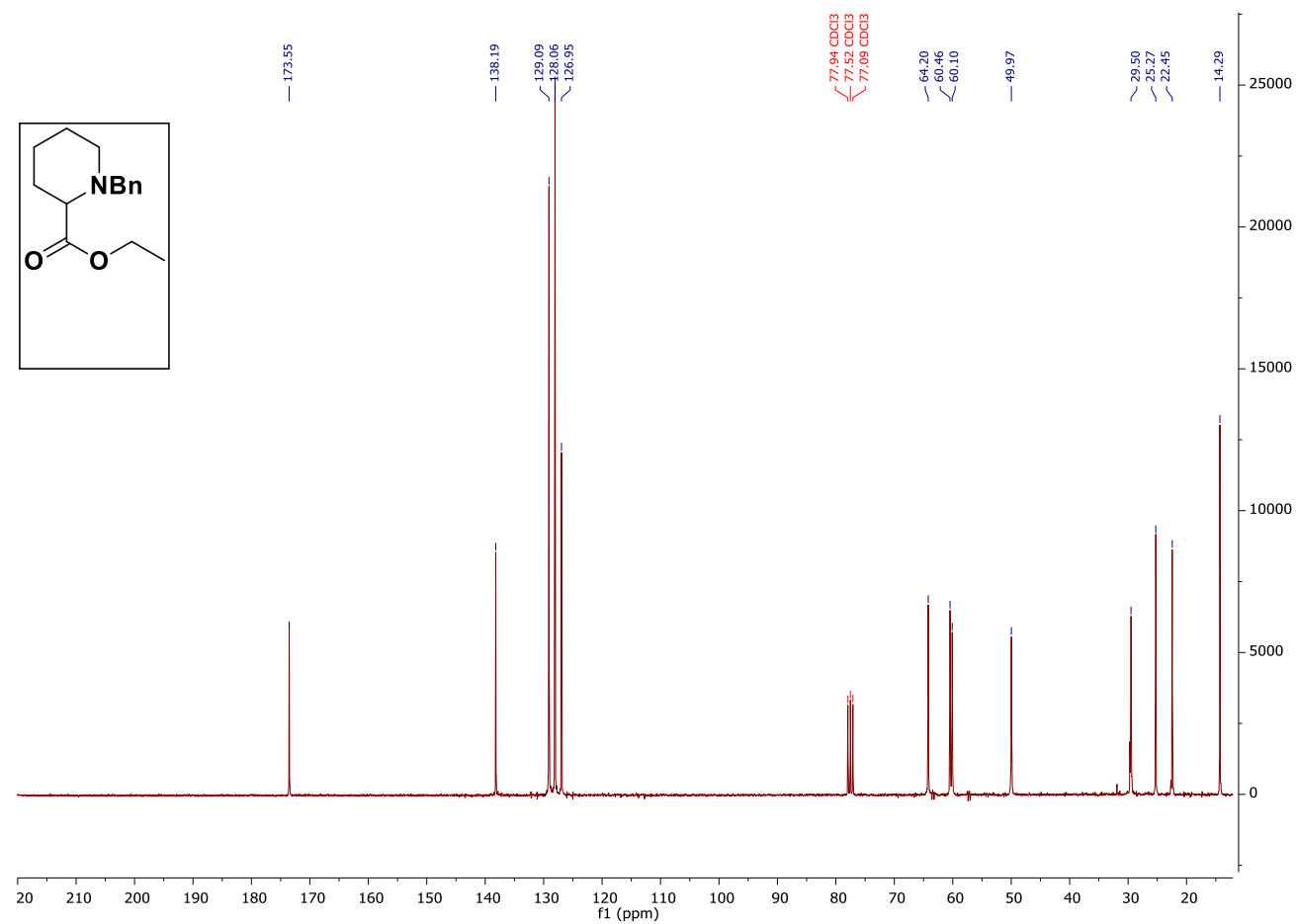
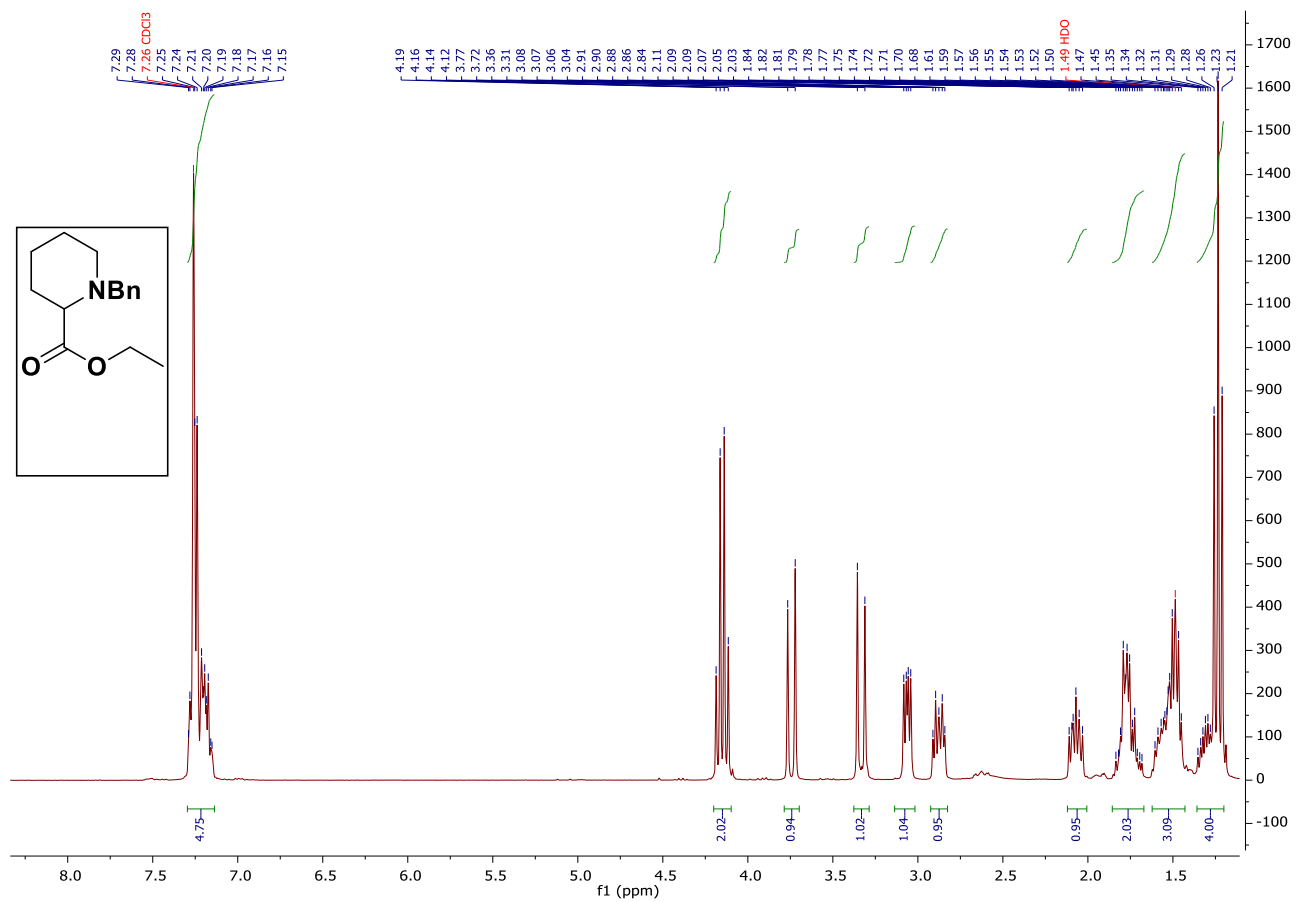


9.4. Experimental details relating to other

9.4.1. (1-benzylaziridin-2-yl)methanol

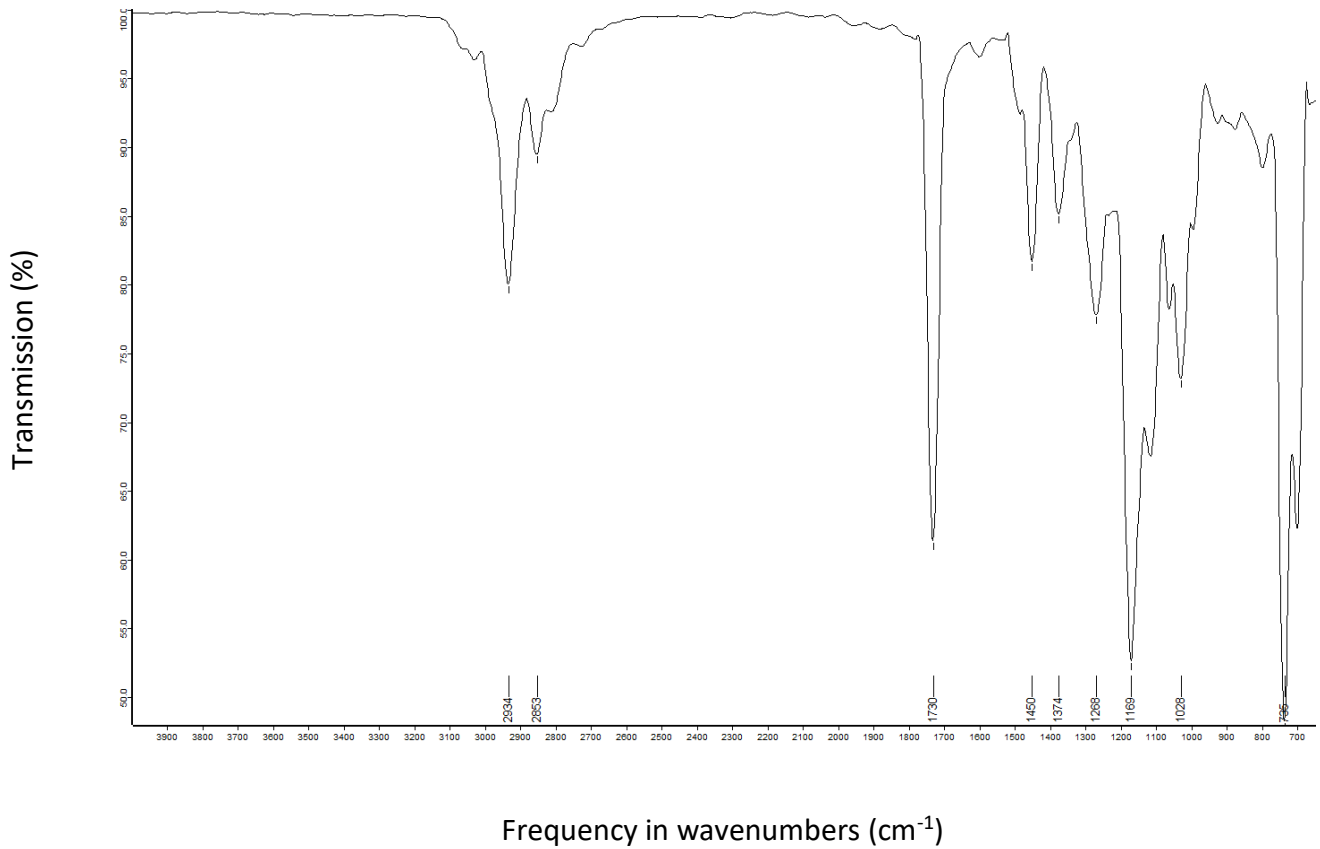
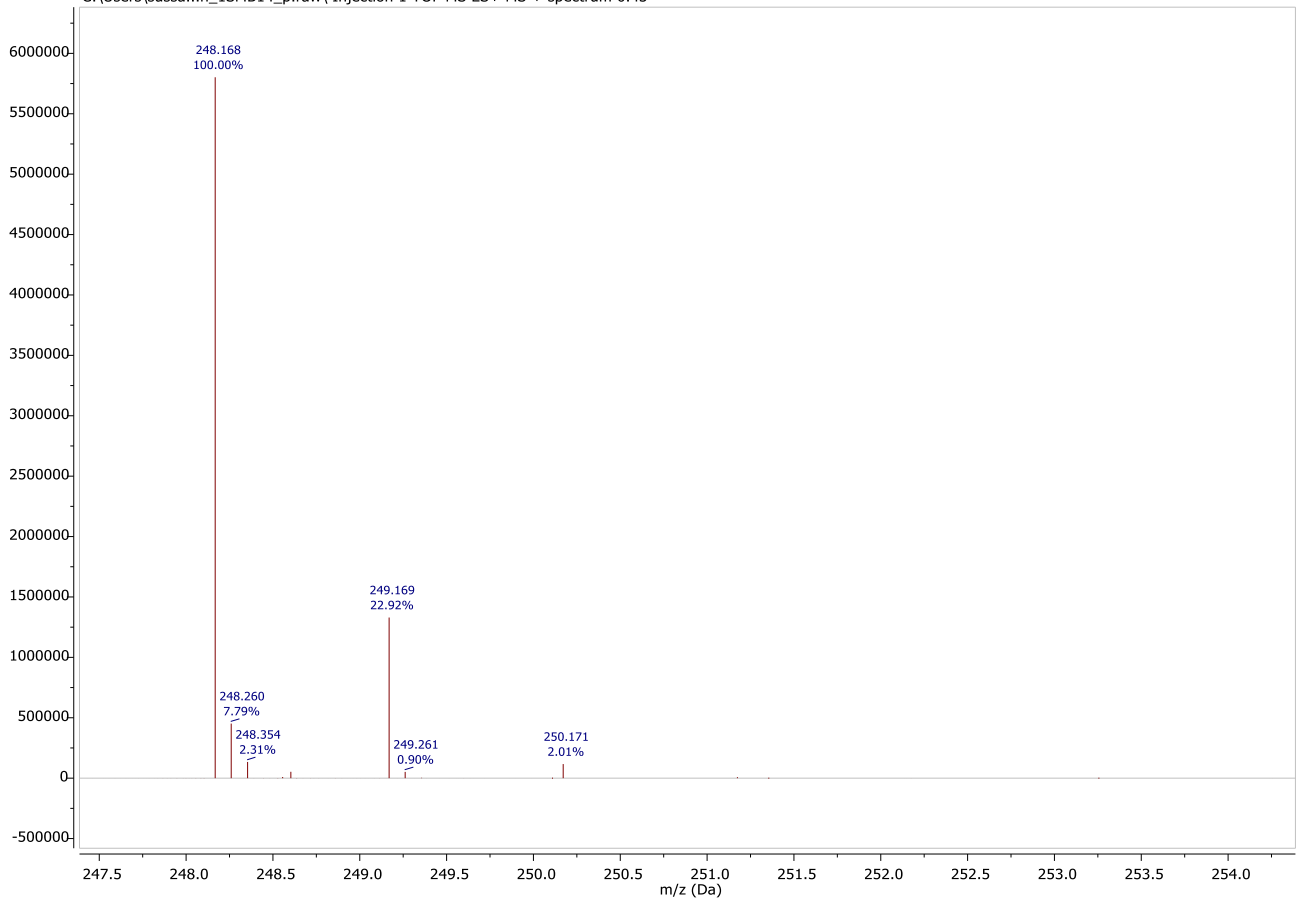


9.4.2. Ethyl 1-benzylpiperidine-2-carboxylate

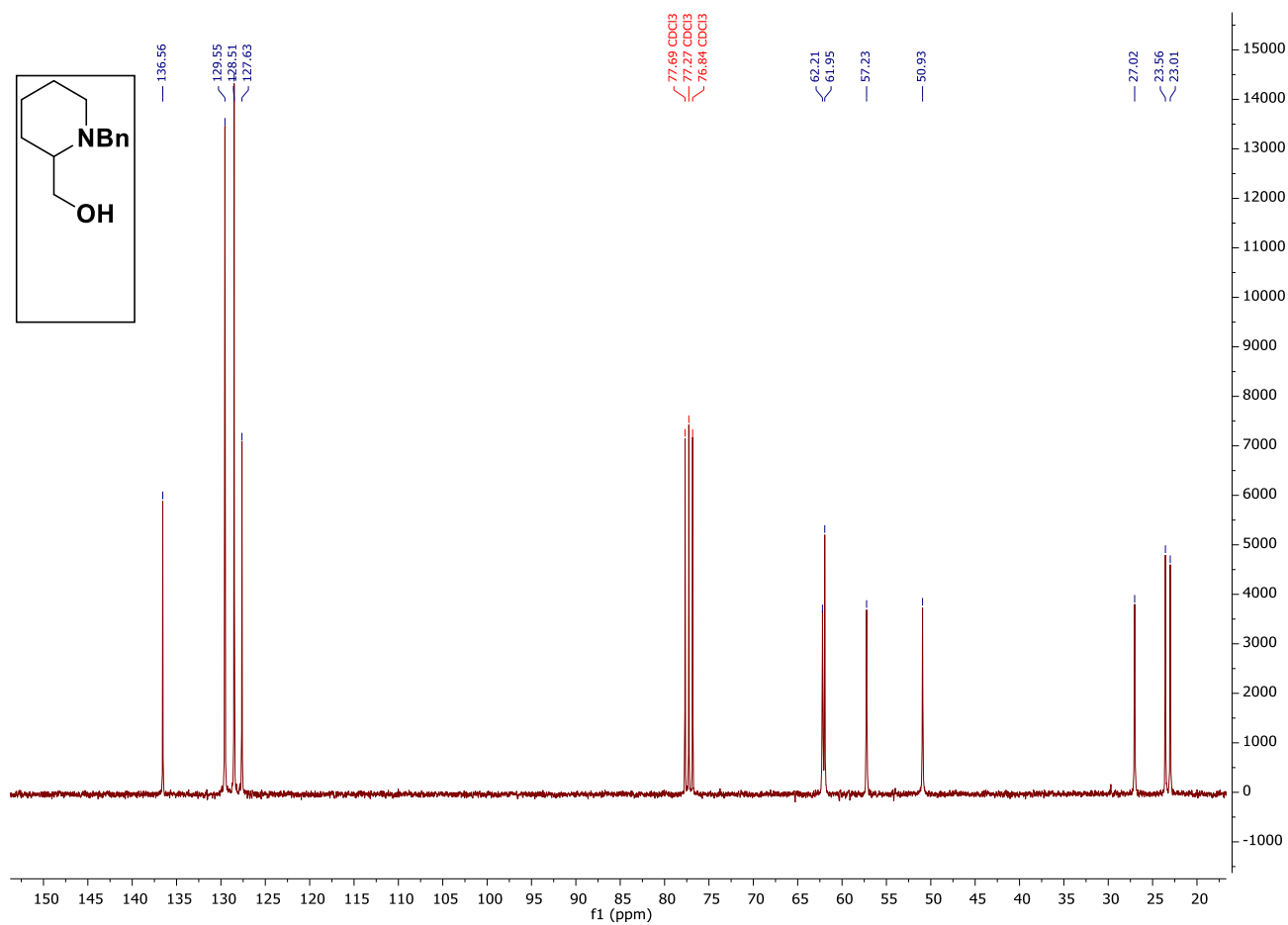
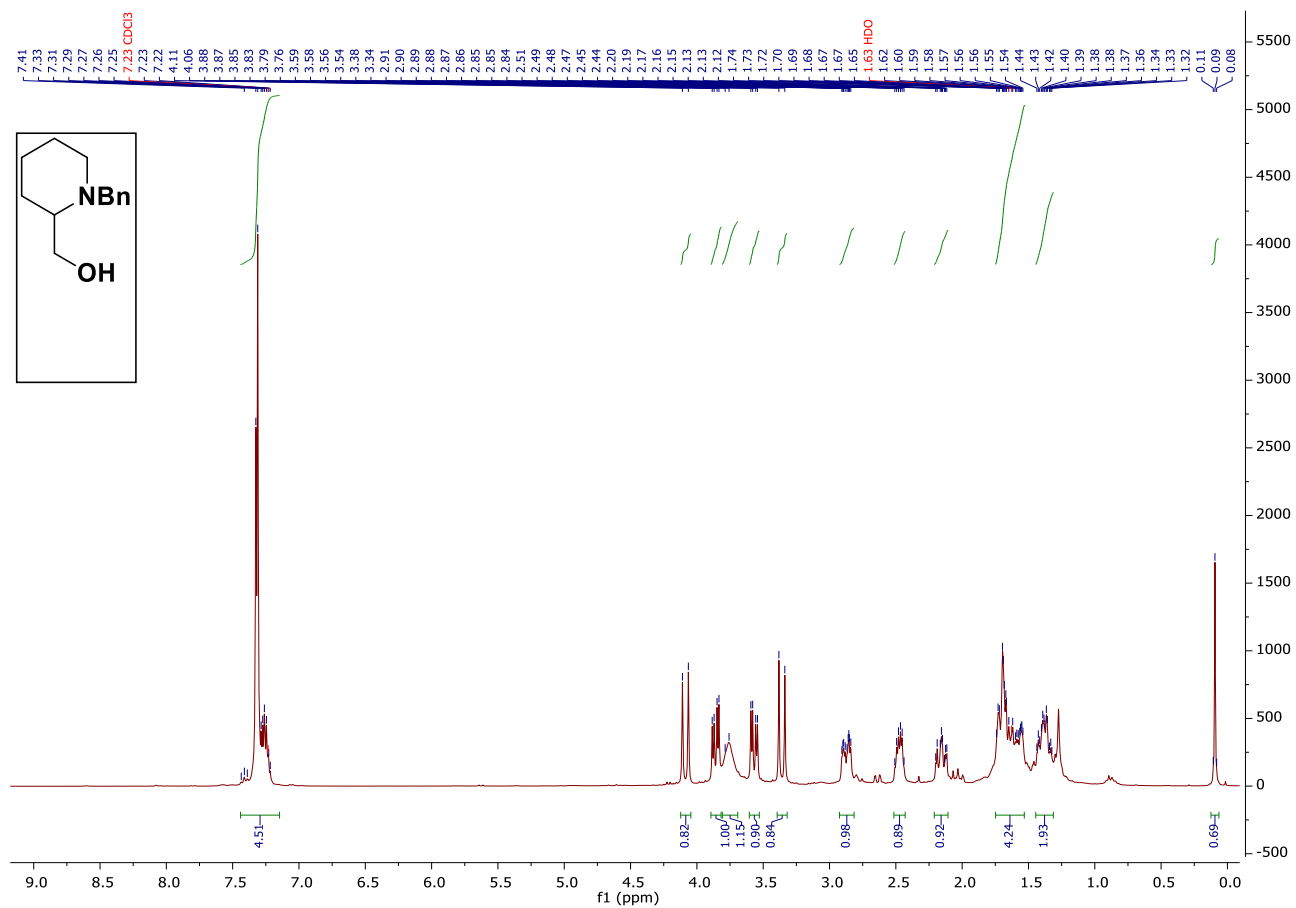


Chapter 9: Experimental Spectrums

C:\Users\sussa...n_15MB14_p.raw\ Injection 1 TOF MS ES+ MS + spectrum 0.43

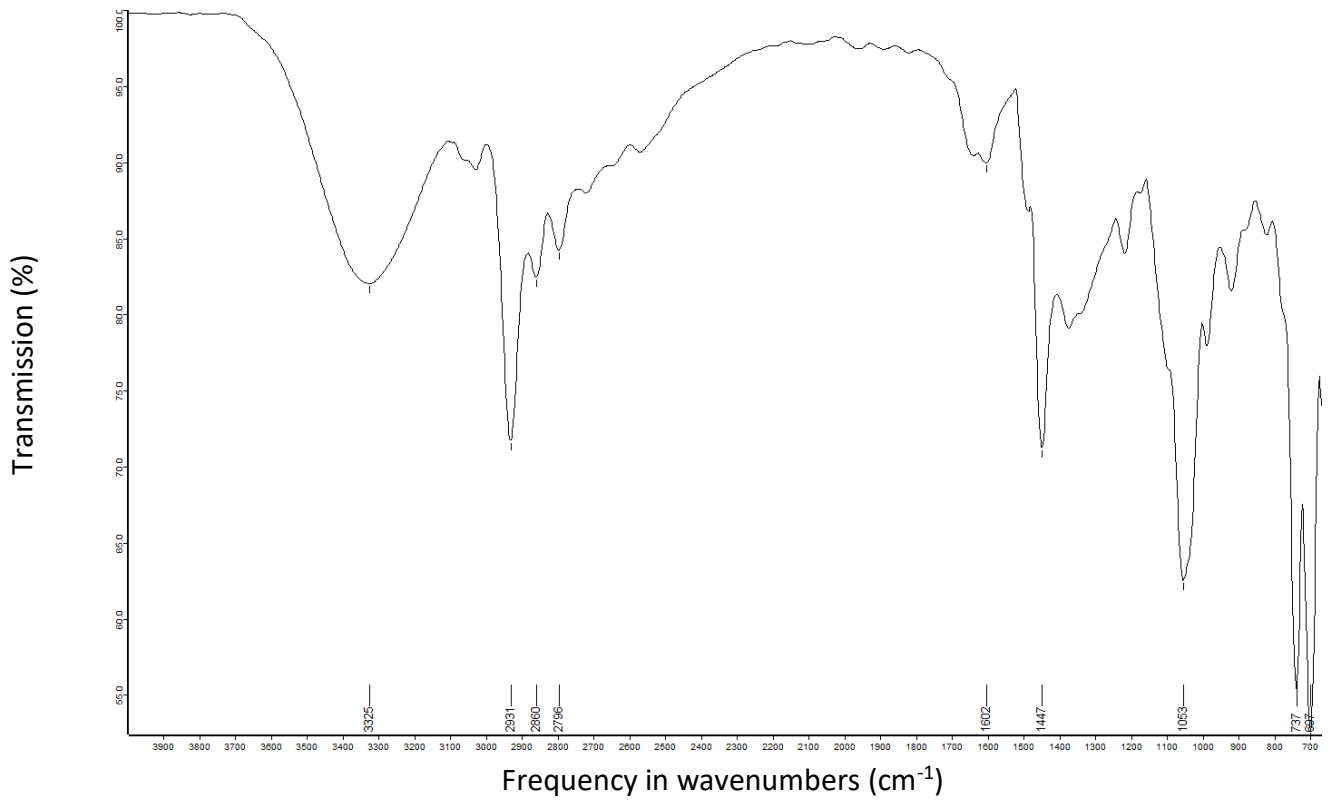
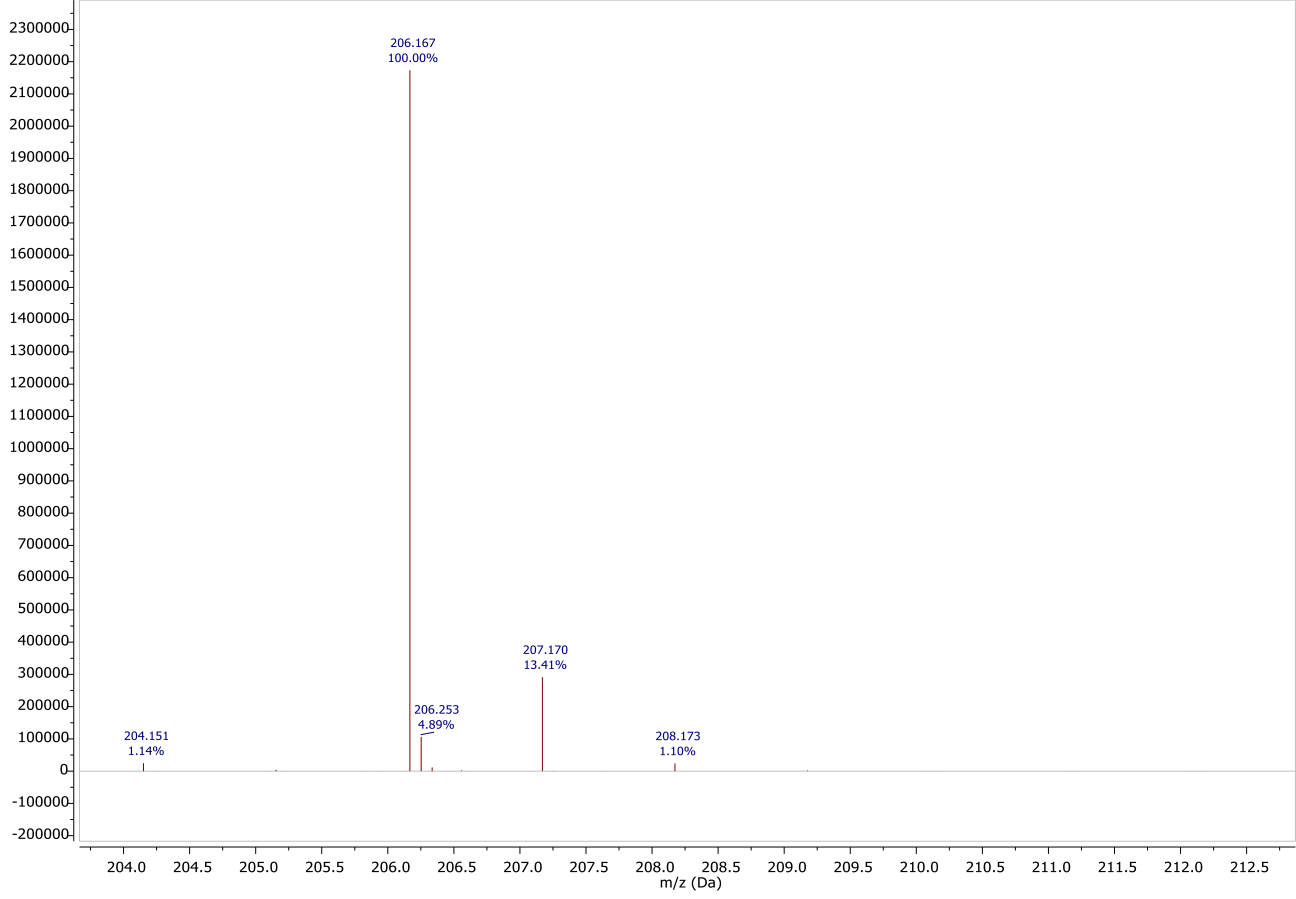


9.4.3. (1-benzylpiperidin-2-yl)methanol



Chapter 9: Experimental Spectra

C:\Users\sussa...1SMB41_2_p.raw\ Injection 1 TOF MS ES+ MS + spectrum 0.56

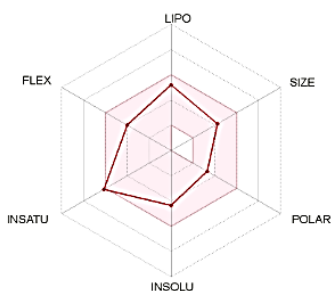
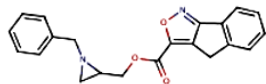


Chapter 10

Appendix I – SwissADME data scaffolds A, B and C



A1.1

SMILES O=C(c1onc2c1Cc1c2cccc1)OCC1CN1Cc1cccc1

Physicochemical Properties

Formula	C21H18N2O3
Molecular weight	346.38 g/mol
Num. heavy atoms	26
Num. arom. heavy atoms	17
Fraction Csp3	0.24
Num. rotatable bonds	6
Num. H-bond acceptors	5
Num. H-bond donors	0
Molar Refractivity	99.83
TPSA	55.34 Å²

Lipophilicity

Log P_{ow} (iLOGP)	3.49
Log P_{ow} (XLOGP3)	3.59
Log P_{ow} (WLOGP)	2.75
Log P_{ow} (MLOGP)	2.75
Log P_{ow} (SILICOS-IT)	3.92
Consensus Log P_{ow}	3.30

Water Solubility	
Log S (ESOL)	-4.34
Solubility	1.59e-02 mg/ml ; 4.60e-05 mol/l
Class	Moderately soluble
Log S (Ali)	-4.44
Solubility	1.26e-02 mg/ml ; 3.64e-05 mol/l
Class	Moderately soluble
Log S (SILICOS-IT)	-6.66
Solubility	7.53e-05 mg/ml ; 2.17e-07 mol/l
Class	Poorly soluble

Pharmacokinetics

GI absorption	High
BBB permeant	Yes
P-gp substrate	No
CYP1A2 inhibitor	Yes
CYP2C19 inhibitor	Yes
CYP2C9 inhibitor	Yes
CYP2D6 inhibitor	Yes
CYP3A4 inhibitor	Yes
Log K_p (skin permeation)	-5.86 cm/s

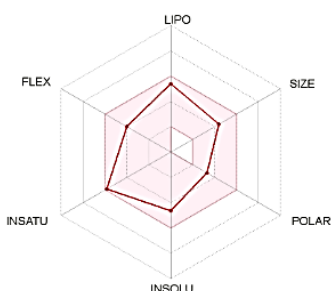
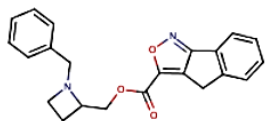
Druglikeness

Lipinski	Yes; 0 violation
Ghose	Yes
Veber	Yes
Egan	Yes
Muegge	Yes
Bioavailability Score	0.55

Medicinal Chemistry

PAINS	0 alert
Brenk	1 alert: Three-membered_heterocycle
Leadlikeness	No; 1 violation: XLOGP3>3.5
Synthetic accessibility	3.97

A1.2

SMILES O=C(c1onc2c1Cc1c2cccc1)OCC1CCN1Cc1cccc1

Physicochemical Properties

Formula	C22H20N2O3
Molecular weight	360.41 g/mol
Num. heavy atoms	27
Num. arom. heavy atoms	17
Fraction Csp3	0.27
Num. rotatable bonds	6
Num. H-bond acceptors	5
Num. H-bond donors	0
Molar Refractivity	104.64
TPSA	55.57 Å²

Lipophilicity

Log P_{ow} (iLOGP)	3.07
Log P_{ow} (XLOGP3)	3.95
Log P_{ow} (WLOGP)	3.14
Log P_{ow} (MLOGP)	2.97
Log P_{ow} (SILICOS-IT)	4.18
Consensus Log P_{ow}	3.46

Water Solubility	
Log S (ESOL)	-4.63
Solubility	8.39e-03 mg/ml ; 2.33e-05 mol/l
Class	Moderately soluble
Log S (Ali)	-4.82
Solubility	5.49e-03 mg/ml ; 1.52e-05 mol/l
Class	Moderately soluble
Log S (SILICOS-IT)	-6.93
Solubility	4.21e-05 mg/ml ; 1.17e-07 mol/l
Class	Poorly soluble

Pharmacokinetics

GI absorption	High
BBB permeant	Yes
P-gp substrate	Yes
CYP1A2 inhibitor	No
CYP2C19 inhibitor	Yes
CYP2C9 inhibitor	Yes
CYP2D6 inhibitor	Yes
CYP3A4 inhibitor	Yes
Log K_p (skin permeation)	-5.69 cm/s

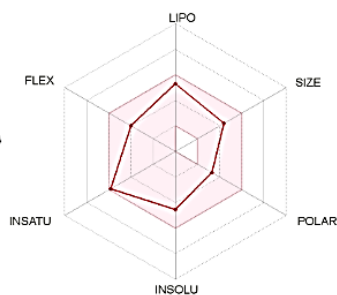
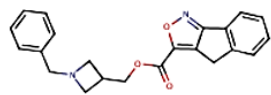
Druglikeness

Lipinski	Yes; 0 violation
Ghose	Yes
Veber	Yes
Egan	Yes
Muegge	Yes
Bioavailability Score	0.55

Medicinal Chemistry

PAINS	0 alert
Brenk	0 alert
Leadlikeness	No; 2 violations: MW>350, XLOGP3>3.5
Synthetic accessibility	4.02

A1.3



SMILES O=C(c1onc2c1Cc1c2cccc1)OCC1CN(C1)Cc1cccc1

Physicochemical Properties

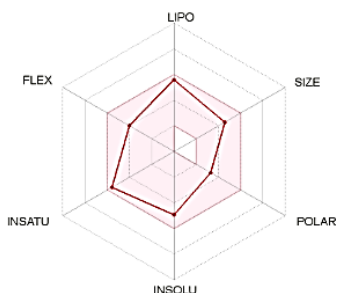
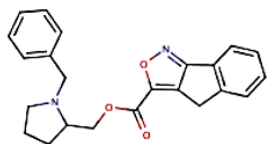
Formula	C22H20N2O3
Molecular weight	360.41 g/mol
Num. heavy atoms	27
Num. arom. heavy atoms	17
Fraction Csp3	0.27
Num. rotatable bonds	6
Num. H-bond acceptors	5
Num. H-bond donors	0
Molar Refractivity	104.64
TPSA	55.57 Å²

Lipophilicity

Log P_{ow} (ILOGP)	3.61
Log P_{ow} (XLOGP3)	3.78
Log P_{ow} (WLOGP)	3.00
Log P_{ow} (MLOGP)	2.97
Log P_{ow} (SILICOS-IT)	4.18
Consensus Log P_{ow}	3.51

Water Solubility	
Log S (ESOL)	-4.53
Solubility	1.07e-02 mg/ml ; 2.98e-05 mol/l
Class	Moderately soluble
Log S (Ali)	-4.64
Solubility	8.24e-03 mg/ml ; 2.29e-05 mol/l
Class	Moderately soluble
Log S (SILICOS-IT)	-6.93
Solubility	4.21e-05 mg/ml ; 1.17e-07 mol/l
Class	Poorly soluble
Pharmacokinetics	
GI absorption	High
BBB permeant	Yes
P-gp substrate	Yes
CYP1A2 inhibitor	No
CYP2C19 inhibitor	Yes
CYP2C9 inhibitor	Yes
CYP2D6 inhibitor	Yes
CYP3A4 inhibitor	Yes
Log K_p (skin permeation)	-5.81 cm/s
Druglikeness	
Lipinski	Yes; 0 violation
Ghose	Yes
Veber	Yes
Egan	Yes
Muegge	Yes
Bioavailability Score	0.55
Medicinal Chemistry	
PAINS	0 alert
Brenk	0 alert
Leadlikeness	No; 2 violations: MW>350, XLOGP3>3.5
Synthetic accessibility	4.07

A1.4



SMILES O=C(c1onc2c1Cc1c2cccc1)OCC1CCCN1Cc1cccc1

Physicochemical Properties

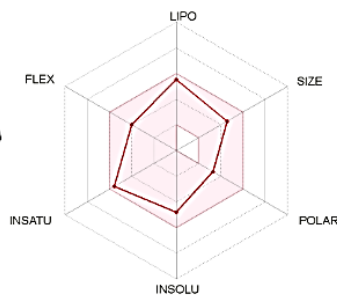
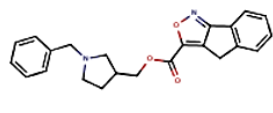
Formula	C23H22N2O3
Molecular weight	374.43 g/mol
Num. heavy atoms	28
Num. arom. heavy atoms	17
Fraction Csp3	0.30
Num. rotatable bonds	6
Num. H-bond acceptors	5
Num. H-bond donors	0
Molar Refractivity	109.45
TPSA	55.57 Å²

Lipophilicity

Log P_{ow} (ILOGP)	3.87
Log P_{ow} (XLOGP3)	4.30
Log P_{ow} (WLOGP)	3.53
Log P_{ow} (MLOGP)	3.19
Log P_{ow} (SILICOS-IT)	4.41
Consensus Log P_{ow}	3.86

Water Solubility	
Log S (ESOL)	-4.92
Solubility	4.46e-03 mg/ml ; 1.19e-05 mol/l
Class	Moderately soluble
Log S (Ali)	-5.18
Solubility	2.47e-03 mg/ml ; 6.60e-06 mol/l
Class	Moderately soluble
Log S (SILICOS-IT)	-7.20
Solubility	2.36e-05 mg/ml ; 6.30e-08 mol/l
Class	Poorly soluble
Pharmacokinetics	
GI absorption	High
BBB permeant	Yes
P-gp substrate	Yes
CYP1A2 inhibitor	No
CYP2C19 inhibitor	Yes
CYP2C9 inhibitor	Yes
CYP2D6 inhibitor	Yes
CYP3A4 inhibitor	Yes
Log K_p (skin permeation)	-5.53 cm/s
Druglikeness	
Lipinski	Yes; 0 violation
Ghose	Yes
Veber	Yes
Egan	Yes
Muegge	Yes
Bioavailability Score	0.55
Medicinal Chemistry	
PAINS	0 alert
Brenk	0 alert
Leadlikeness	No; 2 violations: MW>350, XLOGP3>3.5
Synthetic accessibility	4.12

A1.5



SMILES O=C(c1onc2c1Cc1c2cccc1)OCC1CCN(C1)Cc1ccccc1

Physicochemical Properties

Formula	C23H22N2O3
Molecular weight	374.43 g/mol
Num. heavy atoms	28
Num. arom. heavy atoms	17
Fraction Csp3	0.30
Num. rotatable bonds	6
Num. H-bond acceptors	5
Num. H-bond donors	0
Molar Refractivity	109.45
TPSA	55.57 Å²

Lipophilicity

Log $P_{o/w}$ (iLOGP)	3.75
Log $P_{o/w}$ (XLOGP3)	4.14
Log $P_{o/w}$ (WLOGP)	3.39
Log $P_{o/w}$ (MLOGP)	3.19
Log $P_{o/w}$ (SILICOS-IT)	4.41
Consensus Log $P_{o/w}$	3.78

Water Solubility	
Log S (ESOL)	-4.82
Solubility	5.63e-03 mg/ml ; 1.50e-05 mol/l
Class	Moderately soluble
Log S (Ali)	-5.01
Solubility	3.62e-03 mg/ml ; 9.68e-06 mol/l
Class	Moderately soluble
Log S (SILICOS-IT)	-7.20
Solubility	2.36e-05 mg/ml ; 6.30e-08 mol/l
Class	Poorly soluble

Pharmacokinetics

GI absorption	High
BBB permeant	Yes
P-gp substrate	Yes
CYP1A2 inhibitor	No
CYP2C19 inhibitor	Yes
CYP2C9 inhibitor	Yes
CYP2D6 inhibitor	Yes
CYP3A4 inhibitor	Yes
Log K_p (skin permeation)	-5.64 cm/s

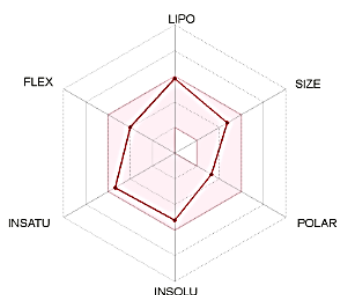
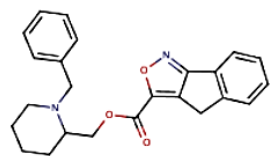
Druglikeness

Lipinski	Yes; 0 violation
Ghose	Yes
Weber	Yes
Egan	Yes
Muegge	Yes
Bioavailability Score	0.55

Medicinal Chemistry

PAINS	0 alert
Brenk	0 alert
Leadlikeness	No; 2 violations: MW>350, XLOGP3>3.5
Synthetic accessibility	4.17

A1.6



SMILES O=C(c1onc2c1Cc1c2cccc1)OCC1CCCCN1Cc1ccccc1

Physicochemical Properties

Formula	C24H24N2O3
Molecular weight	388.46 g/mol
Num. heavy atoms	29
Num. arom. heavy atoms	17
Fraction Csp3	0.33
Num. rotatable bonds	6
Num. H-bond acceptors	5
Num. H-bond donors	0
Molar Refractivity	114.26
TPSA	55.57 Å²

Lipophilicity

Log $P_{o/w}$ (iLOGP)	3.66
Log $P_{o/w}$ (XLOGP3)	4.66
Log $P_{o/w}$ (WLOGP)	3.92
Log $P_{o/w}$ (MLOGP)	3.40
Log $P_{o/w}$ (SILICOS-IT)	4.64
Consensus Log $P_{o/w}$	4.06

Water Solubility	
Log S (ESOL)	-5.22
Solubility	2.33e-03 mg/ml ; 6.00e-06 mol/l
Class	Moderately soluble
Log S (Ali)	-5.55
Solubility	1.09e-03 mg/ml ; 2.79e-06 mol/l
Class	Moderately soluble
Log S (SILICOS-IT)	-7.47
Solubility	1.32e-05 mg/ml ; 3.40e-08 mol/l
Class	Poorly soluble

Pharmacokinetics

GI absorption	High
BBB permeant	Yes
P-gp substrate	Yes
CYP1A2 inhibitor	No
CYP2C19 inhibitor	Yes
CYP2C9 inhibitor	Yes
CYP2D6 inhibitor	Yes
CYP3A4 inhibitor	Yes
Log K_p (skin permeation)	-5.36 cm/s

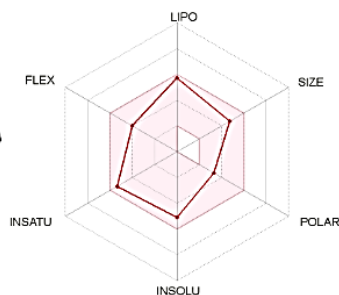
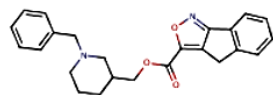
Druglikeness

Lipinski	Yes; 0 violation
Ghose	Yes
Weber	Yes
Egan	Yes
Muegge	Yes
Bioavailability Score	0.55

Medicinal Chemistry

PAINS	0 alert
Brenk	0 alert
Leadlikeness	No; 2 violations: MW>350, XLOGP3>3.5
Synthetic accessibility	4.23

A1.7



SMILES O=C(c1onc2c1Cc1c2cccc1)OCC1CCCN(C1)Cc1cccc1

Physicochemical Properties

Formula	C24H24N2O3
Molecular weight	388.46 g/mol
Num. heavy atoms	29
Num. arom. heavy atoms	17
Fraction Csp3	0.33
Num. rotatable bonds	6
Num. H-bond acceptors	5
Num. H-bond donors	0
Molar Refractivity	114.26
TPSA	55.57 Å²

Lipophilicity

Log $P_{o/w}$ (iLOGP)	3.88
Log $P_{o/w}$ (XLOGP3)	4.49
Log $P_{o/w}$ (WLOGP)	3.78
Log $P_{o/w}$ (MLOGP)	3.40
Log $P_{o/w}$ (SILICOS-IT)	4.64
Consensus Log $P_{o/w}$	4.04

Water Solubility	
Log S (ESOL)	-5.11
Solubility	2.98e-03 mg/ml ; 7.67e-06 mol/l
Class	Moderately soluble
Log S (Ali)	-5.38
Solubility	1.63e-03 mg/ml ; 4.19e-06 mol/l
Class	Moderately soluble
Log S (SILICOS-IT)	-7.47
Solubility	1.32e-05 mg/ml ; 3.40e-08 mol/l
Class	Poorly soluble

Pharmacokinetics

GI absorption	High
BBB permeant	Yes
P-gp substrate	Yes
CYP1A2 inhibitor	No
CYP2C19 inhibitor	Yes
CYP2C9 inhibitor	Yes
CYP2D6 inhibitor	Yes
CYP3A4 inhibitor	Yes
Log K_p (skin permeation)	-5.48 cm/s

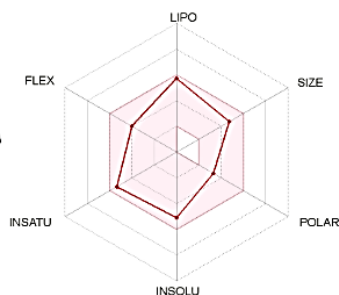
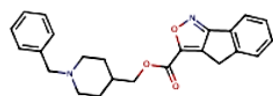
Druglikeness

Lipinski	Yes; 0 violation
Ghose	Yes
Veber	Yes
Egan	Yes
Muegge	Yes
Bioavailability Score	0.55

Medicinal Chemistry

PAINS	0 alert
Brenk	0 alert
Leadlikeness	No; 2 violations: MW>350, XLOGP3>3.5
Synthetic accessibility	4.25

A1.8



SMILES O=C(c1onc2c1Cc1c2cccc1)OCC1CCN(CC1)Cc1cccc1

Physicochemical Properties

Formula	C24H24N2O3
Molecular weight	388.46 g/mol
Num. heavy atoms	29
Num. arom. heavy atoms	17
Fraction Csp3	0.33
Num. rotatable bonds	6
Num. H-bond acceptors	5
Num. H-bond donors	0
Molar Refractivity	114.26
TPSA	55.57 Å²

Lipophilicity

Log $P_{o/w}$ (iLOGP)	3.93
Log $P_{o/w}$ (XLOGP3)	4.49
Log $P_{o/w}$ (WLOGP)	3.78
Log $P_{o/w}$ (MLOGP)	3.40
Log $P_{o/w}$ (SILICOS-IT)	4.64
Consensus Log $P_{o/w}$	4.05

Water Solubility	
Log S (ESOL)	-5.11
Solubility	2.98e-03 mg/ml ; 7.67e-06 mol/l
Class	Moderately soluble
Log S (Ali)	-5.38
Solubility	1.63e-03 mg/ml ; 4.19e-06 mol/l
Class	Moderately soluble
Log S (SILICOS-IT)	-7.47
Solubility	1.32e-05 mg/ml ; 3.40e-08 mol/l
Class	Poorly soluble

Pharmacokinetics

GI absorption	High
BBB permeant	Yes
P-gp substrate	Yes
CYP1A2 inhibitor	No
CYP2C19 inhibitor	Yes
CYP2C9 inhibitor	Yes
CYP2D6 inhibitor	Yes
CYP3A4 inhibitor	Yes
Log K_p (skin permeation)	-5.48 cm/s

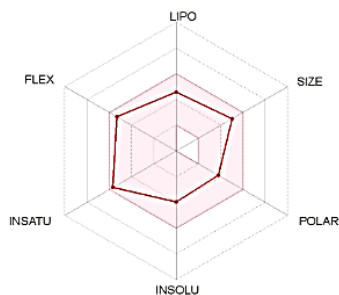
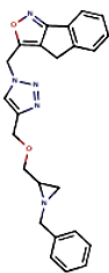
Druglikeness

Lipinski	Yes; 0 violation
Ghose	Yes
Veber	Yes
Egan	Yes
Muegge	Yes
Bioavailability Score	0.55

Medicinal Chemistry

PAINS	0 alert
Brenk	0 alert
Leadlikeness	No; 2 violations: MW>350, XLOGP3>3.5
Synthetic accessibility	4.23

B1.1



SMILES c1ccc(cc1)CN1CC1COCc1nnn(c1)Cc1onc2c1Cc1c2cccc1

Physicochemical Properties

Formula	C24H23N5O2
Molecular weight	413.47 g/mol
Num. heavy atoms	31
Num. arom. heavy atoms	22
Fraction Csp3	0.29
Num. rotatable bonds	8
Num. H-bond acceptors	6
Num. H-bond donors	0
Molar Refractivity	118.74
TPSA	68.98 Å²

Lipophilicity

Log $P_{o/w}$ (ILOGP)	3.71
Log $P_{o/w}$ (XLOGP3)	2.49
Log $P_{o/w}$ (WLOGP)	2.60
Log $P_{o/w}$ (MLOGP)	2.22
Log $P_{o/w}$ (SILICOS-IT)	3.66
Consensus Log $P_{o/w}$	2.94

Water Solubility

Log S (ESOL)	-3.97
Solubility	4.44e-02 mg/ml ; 1.07e-04 mol/l
Class	Soluble
Log S (Ali)	-3.58
Solubility	1.08e-01 mg/ml ; 2.61e-04 mol/l
Class	Soluble
Log S (SILICOS-IT)	-7.63
Solubility	9.74e-06 mg/ml ; 2.36e-08 mol/l
Class	Poorly soluble

Pharmacokinetics

GI absorption	High
BBB permeant	Yes
P-gp substrate	Yes
CYP1A2 inhibitor	No
CYP2C19 inhibitor	Yes
CYP2C9 inhibitor	Yes
CYP2D6 inhibitor	Yes
CYP3A4 inhibitor	Yes
Log K_p (skin permeation)	-7.05 cm/s

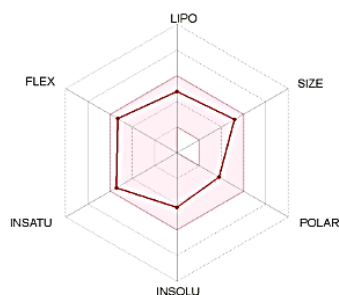
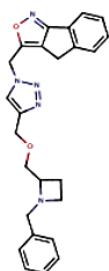
Druglikeness

Lipinski	Yes; 0 violation
Ghose	Yes
Veber	Yes
Egan	Yes
Muegge	Yes
Bioavailability Score	0.55

Medicinal Chemistry

PAINS	0 alert
Brenk	1 alert: Three-membered_heterocycle
Leadlikeness	No; 2 violations: MW>350, Rotors>7
Synthetic accessibility	4.36

B1.2



SMILES c1ccc(cc1)CN1CCC1COCc1nnn(c1)Cc1onc2c1Cc1c2cccc1

Physicochemical Properties

Formula	C25H25N5O2
Molecular weight	427.50 g/mol
Num. heavy atoms	32
Num. arom. heavy atoms	22
Fraction Csp3	0.32
Num. rotatable bonds	8
Num. H-bond acceptors	6
Num. H-bond donors	0
Molar Refractivity	123.55
TPSA	69.21 Å²

Lipophilicity

Log $P_{o/w}$ (ILOGP)	3.67
Log $P_{o/w}$ (XLOGP3)	2.84
Log $P_{o/w}$ (WLOGP)	2.99
Log $P_{o/w}$ (MLOGP)	2.43
Log $P_{o/w}$ (SILICOS-IT)	3.90
Consensus Log $P_{o/w}$	3.17

Water Solubility

Log S (ESOL)	-4.26
Solubility	2.35e-02 mg/ml ; 5.49e-05 mol/l
Class	Moderately soluble
Log S (Ali)	-3.95
Solubility	4.78e-02 mg/ml ; 1.12e-04 mol/l
Class	Soluble
Log S (SILICOS-IT)	-7.89
Solubility	5.46e-06 mg/ml ; 1.28e-08 mol/l
Class	Poorly soluble

Pharmacokinetics

GI absorption	High
BBB permeant	Yes
P-gp substrate	Yes
CYP1A2 inhibitor	No
CYP2C19 inhibitor	Yes
CYP2C9 inhibitor	Yes
CYP2D6 inhibitor	Yes
CYP3A4 inhibitor	Yes
Log K_p (skin permeation)	-6.89 cm/s

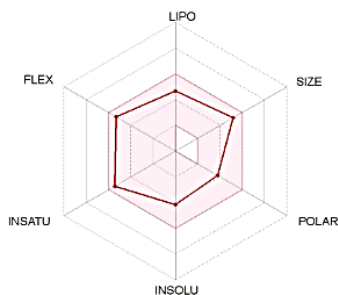
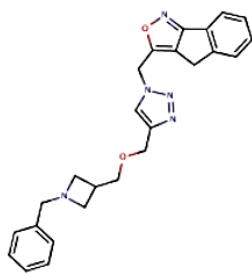
Druglikeness

Lipinski	Yes; 0 violation
Ghose	Yes
Veber	Yes
Egan	Yes
Muegge	Yes
Bioavailability Score	0.55

Medicinal Chemistry

PAINS	0 alert
Brenk	0 alert
Leadlikeness	No; 2 violations: MW>350, Rotors>7
Synthetic accessibility	4.47

B1.3



SMILES c1ccc(cc1)CN1CC(C1)COCc1nnn(c1)Cc1onc2c1Cc1c2cccc1

Physicochemical Properties

Formula	C25H25N5O2
Molecular weight	427.50 g/mol
Num. heavy atoms	32
Num. arom. heavy atoms	22
Fraction Csp3	0.32
Num. rotatable bonds	8
Num. H-bond acceptors	6
Num. H-bond donors	0
Molar Refractivity	123.55
TPSA	69.21 Å²

Lipophilicity

Log $P_{o/w}$ (ILOGP)	3.53
Log $P_{o/w}$ (XLOGP3)	2.68
Log $P_{o/w}$ (WLOGP)	2.85
Log $P_{o/w}$ (MLOGP)	2.43
Log $P_{o/w}$ (SILICOS-IT)	3.90
Consensus Log $P_{o/w}$	3.08

Water Solubility

Log S (ESOL)	-4.16
Solubility	2.96e-02 mg/ml ; 6.92e-05 mol/l
Class	Moderately soluble
Log S (Ali)	-3.79
Solubility	7.00e-02 mg/ml ; 1.64e-04 mol/l
Class	Soluble
Log S (SILICOS-IT)	-7.89
Solubility	5.46e-06 mg/ml ; 1.28e-08 mol/l
Class	Poorly soluble

Pharmacokinetics

GI absorption	High
BBB permeant	Yes
P-gp substrate	Yes
CYP1A2 inhibitor	No
CYP2C19 inhibitor	Yes
CYP2C9 inhibitor	Yes
CYP2D6 inhibitor	Yes
CYP3A4 inhibitor	Yes
Log K_p (skin permeation)	-7.00 cm/s

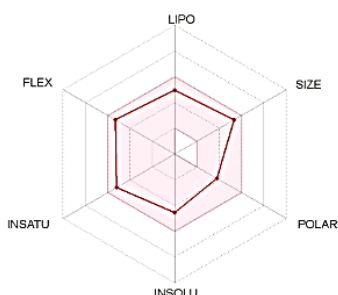
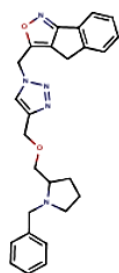
Druglikeness

Lipinski	Yes; 0 violation
Ghose	Yes
Weber	Yes
Egan	Yes
Muegge	Yes
Bioavailability Score	0.55

Medicinal Chemistry

PAINS	0 alert
Brenk	0 alert
Leadlikeness	No; 2 violations: MW>350, Rotors>7
Synthetic accessibility	4.46

B1.4



SMILES c1ccc(cc1)CN1CCCC1COCc1nnn(c1)Cc1onc2c1Cc1c2cccc1

Physicochemical Properties

Formula	C26H27N5O2
Molecular weight	441.52 g/mol
Num. heavy atoms	33
Num. arom. heavy atoms	22
Fraction Csp3	0.35
Num. rotatable bonds	8
Num. H-bond acceptors	6
Num. H-bond donors	0
Molar Refractivity	128.36
TPSA	69.21 Å²

Lipophilicity

Log $P_{o/w}$ (ILOGP)	4.23
Log $P_{o/w}$ (XLOGP3)	3.20
Log $P_{o/w}$ (WLOGP)	3.38
Log $P_{o/w}$ (MLOGP)	2.63
Log $P_{o/w}$ (SILICOS-IT)	4.13
Consensus Log $P_{o/w}$	3.51

Water Solubility

Log S (ESOL)	-4.56
Solubility	1.22e-02 mg/ml ; 2.76e-05 mol/l
Class	Moderately soluble
Log S (Ali)	-4.33
Solubility	2.09e-02 mg/ml ; 4.73e-05 mol/l
Class	Moderately soluble
Log S (SILICOS-IT)	-8.16
Solubility	3.05e-06 mg/ml ; 6.92e-09 mol/l
Class	Poorly soluble

Pharmacokinetics

GI absorption	High
BBB permeant	Yes
P-gp substrate	Yes
CYP1A2 inhibitor	No
CYP2C19 inhibitor	No
CYP2C9 inhibitor	Yes
CYP2D6 inhibitor	Yes
CYP3A4 inhibitor	Yes
Log K_p (skin permeation)	-6.72 cm/s

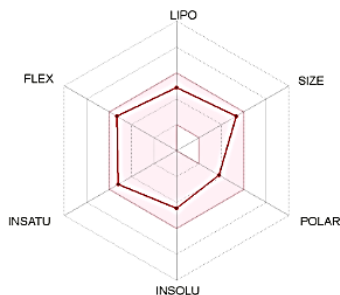
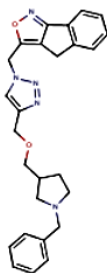
Druglikeness

Lipinski	Yes; 0 violation
Ghose	Yes
Weber	Yes
Egan	Yes
Muegge	Yes
Bioavailability Score	0.55

Medicinal Chemistry

PAINS	0 alert
Brenk	0 alert
Leadlikeness	No; 2 violations: MW>350, Rotors>7
Synthetic accessibility	4.57

B1.5



SMILES c1ccc(cc1)CN1CCC(C1)COCc1nnn(c1)Cc1onc2c1Cc1c2cccc1

Physicochemical Properties

Formula	C26H27N5O2
Molecular weight	441.52 g/mol
Num. heavy atoms	33
Num. arom. heavy atoms	22
Fraction Csp3	0.35
Num. rotatable bonds	8
Num. H-bond acceptors	6
Num. H-bond donors	0
Molar Refractivity	128.36
TPSA	69.21 Å²

Lipophilicity

Log $P_{o/w}$ (iLOGP)	3.87
Log $P_{o/w}$ (XLOGP3)	3.03
Log $P_{o/w}$ (WLOGP)	3.24
Log $P_{o/w}$ (MLOGP)	2.63
Log $P_{o/w}$ (SILICOS-IT)	4.13
Consensus Log $P_{o/w}$	3.38

Water Solubility	
Log S (ESOL)	-4.45
Solubility	1.56e-02 mg/ml ; 3.53e-05 mol/l
Class	Moderately soluble
Log S (Ali)	-4.15
Solubility	3.13e-02 mg/ml ; 7.10e-05 mol/l
Class	Moderately soluble
Log S (SILICOS-IT)	-8.16
Solubility	3.05e-06 mg/ml ; 6.92e-09 mol/l
Class	Poorly soluble

Pharmacokinetics

GI absorption	High
BBB permeant	Yes
P-gp substrate	Yes
CYP1A2 inhibitor	No
CYP2C19 inhibitor	Yes
CYP2C9 inhibitor	Yes
CYP2D6 inhibitor	Yes
CYP3A4 inhibitor	Yes
Log K_p (skin permeation)	-6.84 cm/s

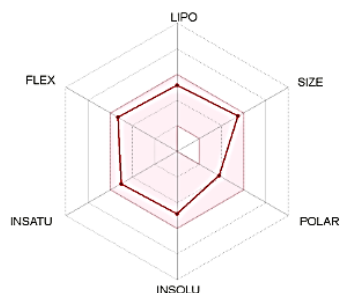
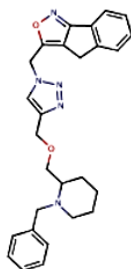
Druglikeness

Lipinski	Yes; 0 violation
Ghose	Yes
Weber	Yes
Egan	Yes
Muegge	Yes
Bioavailability Score	0.55

Medicinal Chemistry

PAINS	0 alert
Brenk	0 alert
Leadlikeness	No; 2 violations: MW>350, Rotors>7
Synthetic accessibility	4.60

B1.6



SMILES c1ccc(cc1)CN1CCCCC1COCc1nnn(c1)Cc1onc2c1Cc1c2cccc1

Physicochemical Properties

Formula	C27H29N5O2
Molecular weight	455.55 g/mol
Num. heavy atoms	34
Num. arom. heavy atoms	22
Fraction Csp3	0.37
Num. rotatable bonds	8
Num. H-bond acceptors	6
Num. H-bond donors	0
Molar Refractivity	133.16
TPSA	69.21 Å²

Lipophilicity

Log $P_{o/w}$ (iLOGP)	4.31
Log $P_{o/w}$ (XLOGP3)	3.56
Log $P_{o/w}$ (WLOGP)	3.77
Log $P_{o/w}$ (MLOGP)	2.83
Log $P_{o/w}$ (SILICOS-IT)	4.37
Consensus Log $P_{o/w}$	3.77

Water Solubility	
Log S (ESOL)	-4.86
Solubility	6.32e-03 mg/ml ; 1.39e-05 mol/l
Class	Moderately soluble
Log S (Ali)	-4.70
Solubility	9.11e-03 mg/ml ; 2.00e-05 mol/l
Class	Moderately soluble
Log S (SILICOS-IT)	-8.43
Solubility	1.71e-06 mg/ml ; 3.76e-09 mol/l
Class	Poorly soluble

Pharmacokinetics

GI absorption	High
BBB permeant	Yes
P-gp substrate	Yes
CYP1A2 inhibitor	No
CYP2C19 inhibitor	No
CYP2C9 inhibitor	Yes
CYP2D6 inhibitor	Yes
CYP3A4 inhibitor	Yes
Log K_p (skin permeation)	-6.55 cm/s

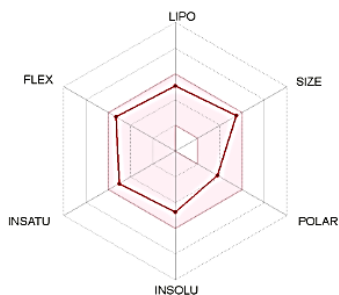
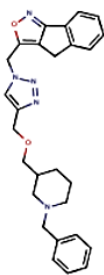
Druglikeness

Lipinski	Yes; 0 violation
Ghose	No; 1 violation: MR>130
Weber	Yes
Egan	Yes
Muegge	Yes
Bioavailability Score	0.55

Medicinal Chemistry

PAINS	0 alert
Brenk	0 alert
Leadlikeness	No; 3 violations: MW>350, Rotors>7, XLOGP3>3.5
Synthetic accessibility	4.68

B1.7



SMILES c1ccc(cc1)CN1CCCC(C1)COCc1nnn(c1)Cc1onc2c1Cc1c2cccc1

Physicochemical Properties

Formula	C27H29N5O2
Molecular weight	455.55 g/mol
Num. heavy atoms	34
Num. arom. heavy atoms	22
Fraction Csp3	0.37
Num. rotatable bonds	8
Num. H-bond acceptors	6
Num. H-bond donors	0
Molar Refractivity	133.16
TPSA [?]	69.21 Å²

Lipophilicity

Log P_{ow} (ILOGP) [?]	4.00
Log P_{ow} (XLOGP3) [?]	3.39
Log P_{ow} (WLOGP) [?]	3.63
Log P_{ow} (MLOGP) [?]	2.83
Log P_{ow} (SILICOS-IT) [?]	4.37
Consensus Log P_{ow} [?]	3.64

Water Solubility	
Log S (ESOL) [?]	-4.75
Solubility	8.08e-03 mg/ml ; 1.77e-05 mol/l
Class [?]	Moderately soluble
Log S (Ali) [?]	-4.52
Solubility	1.37e-02 mg/ml ; 3.00e-05 mol/l
Class [?]	Moderately soluble
Log S (SILICOS-IT) [?]	-8.43
Solubility	1.71e-06 mg/ml ; 3.76e-09 mol/l
Class [?]	Poorly soluble

Pharmacokinetics

GI absorption [?]	High
BBB permeant [?]	Yes
P-gp substrate [?]	Yes
CYP1A2 inhibitor [?]	No
CYP2C19 inhibitor [?]	No
CYP2C9 inhibitor [?]	Yes
CYP2D6 inhibitor [?]	Yes
CYP3A4 inhibitor [?]	Yes
Log K_p (skin permeation) [?]	-6.67 cm/s

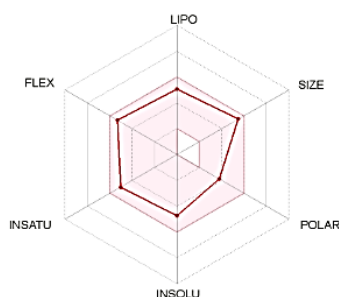
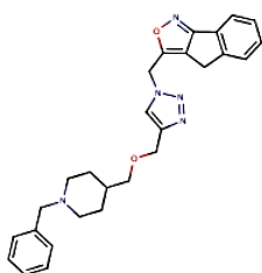
Druglikeness

Lipinski [?]	Yes; 0 violation
Ghose [?]	No; 1 violation: MR>130
Veber [?]	Yes
Egan [?]	Yes
Muegge [?]	Yes
Bioavailability Score [?]	0.55

Medicinal Chemistry

PAINS [?]	0 alert
Brenk [?]	0 alert
Leadlikeness [?]	No; 2 violations: MW>350, Rotors>7
Synthetic accessibility [?]	4.70

B1.8



SMILES c1ccc(cc1)CN1CCC(CC1)COCc1nnn(c1)Cc1onc2c1Cc1c2cccc1

Physicochemical Properties

Formula	C27H29N5O2
Molecular weight	455.55 g/mol
Num. heavy atoms	34
Num. arom. heavy atoms	22
Fraction Csp3	0.37
Num. rotatable bonds	8
Num. H-bond acceptors	6
Num. H-bond donors	0
Molar Refractivity	133.16
TPSA [?]	69.21 Å²

Lipophilicity

Log P_{ow} (ILOGP) [?]	4.51
Log P_{ow} (XLOGP3) [?]	3.39
Log P_{ow} (WLOGP) [?]	3.63
Log P_{ow} (MLOGP) [?]	2.83
Log P_{ow} (SILICOS-IT) [?]	4.37
Consensus Log P_{ow} [?]	3.74

Water Solubility	
Log S (ESOL) [?]	-4.75
Solubility	8.08e-03 mg/ml ; 1.77e-05 mol/l
Class [?]	Moderately soluble
Log S (Ali) [?]	-4.52
Solubility	1.37e-02 mg/ml ; 3.00e-05 mol/l
Class [?]	Moderately soluble
Log S (SILICOS-IT) [?]	-8.43
Solubility	1.71e-06 mg/ml ; 3.76e-09 mol/l
Class [?]	Poorly soluble

Pharmacokinetics

GI absorption [?]	High
BBB permeant [?]	Yes
P-gp substrate [?]	Yes
CYP1A2 inhibitor [?]	No
CYP2C19 inhibitor [?]	No
CYP2C9 inhibitor [?]	Yes
CYP2D6 inhibitor [?]	Yes
CYP3A4 inhibitor [?]	Yes
Log K_p (skin permeation) [?]	-6.67 cm/s

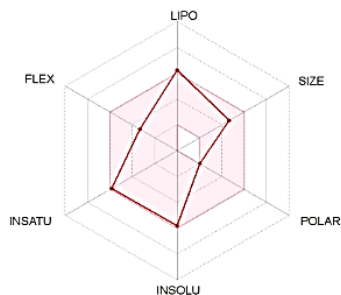
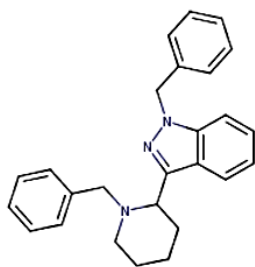
Druglikeness

Lipinski [?]	Yes; 0 violation
Ghose [?]	No; 1 violation: MR>130
Veber [?]	Yes
Egan [?]	Yes
Muegge [?]	Yes
Bioavailability Score [?]	0.55

Medicinal Chemistry

PAINS [?]	0 alert
Brenk [?]	0 alert
Leadlikeness [?]	No; 2 violations: MW>350, Rotors>7
Synthetic accessibility [?]	4.69

C1.1



SMILES c1ccc(cc1)CN1CCCCC1c1nn(c2c1cccc2)Cc1ccccc1

Physicochemical Properties

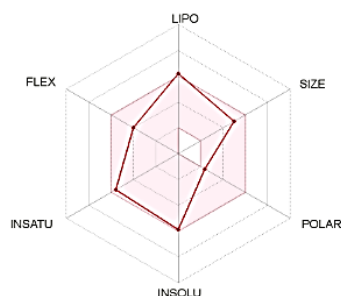
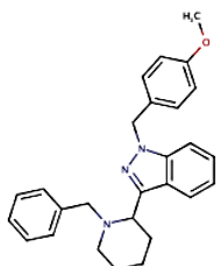
Formula	C ₂₆ H ₂₇ N ₃
Molecular weight	381.51 g/mol
Num. heavy atoms	29
Num. arom. heavy atoms	21
Fraction Csp ³	0.27
Num. rotatable bonds	5
Num. H-bond acceptors	2
Num. H-bond donors	0
Molar Refractivity	123.67
TPSA	21.06 Å ²

Lipophilicity

Log <i>P</i> _{ow} (iLOGP)	3.63
Log <i>P</i> _{ow} (XLOGP3)	5.41
Log <i>P</i> _{ow} (WLOGP)	4.95
Log <i>P</i> _{ow} (MLOGP)	4.57
Log <i>P</i> _{ow} (SILICOS-IT)	4.88
Consensus Log <i>P</i> _{ow}	4.69

Water Solubility	
Log S (ESOL)	-5.82
Solubility	5.78e-04 mg/ml ; 1.52e-06 mol/l
Class	Moderately soluble
Log S (Ali)	-5.61
Solubility	9.42e-04 mg/ml ; 2.47e-06 mol/l
Class	Moderately soluble
Log S (SILICOS-IT)	-8.36
Solubility	1.67e-06 mg/ml ; 4.37e-09 mol/l
Class	Poorly soluble
Pharmacokinetics	
GI absorption	High
BBB permeant	Yes
P-gp substrate	Yes
CYP1A2 inhibitor	Yes
CYP2C19 inhibitor	No
CYP2C9 inhibitor	Yes
CYP2D6 inhibitor	Yes
CYP3A4 inhibitor	Yes
Log <i>K</i> _p (skin permeation)	-4.79 cm/s
Druglikeness	
Lipinski	Yes; 1 violation: MLOGP>4.15
Ghose	Yes
Veber	Yes
Egan	Yes
Muegge	No; 1 violation: XLOGP3>5
Bioavailability Score	0.55
Medicinal Chemistry	
PAINS	0 alert
Brenk	0 alert
Leadlikeness	No; 2 violations: MW>350, XLOGP3>3.5
Synthetic accessibility	3.63

C1.2



SMILES COc1ccc(cc1)Cn1nc(c2c1cccc2)C1CCCCN1Cc1ccccc1

Physicochemical Properties

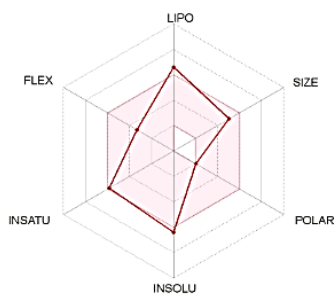
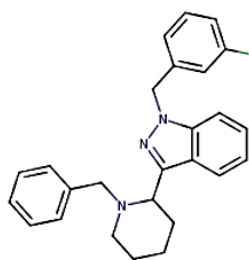
Formula	C ₂₇ H ₂₉ N ₃ O
Molecular weight	411.54 g/mol
Num. heavy atoms	31
Num. arom. heavy atoms	21
Fraction Csp ³	0.30
Num. rotatable bonds	6
Num. H-bond acceptors	3
Num. H-bond donors	0
Molar Refractivity	130.16
TPSA	30.29 Å ²

Lipophilicity

Log <i>P</i> _{ow} (iLOGP)	4.30
Log <i>P</i> _{ow} (XLOGP3)	5.38
Log <i>P</i> _{ow} (WLOGP)	4.96
Log <i>P</i> _{ow} (MLOGP)	4.19
Log <i>P</i> _{ow} (SILICOS-IT)	4.93
Consensus Log <i>P</i> _{ow}	4.75

Water Solubility	
Log S (ESOL)	-5.89
Solubility	5.35e-04 mg/ml ; 1.30e-06 mol/l
Class	Moderately soluble
Log S (Ali)	-5.77
Solubility	6.99e-04 mg/ml ; 1.70e-06 mol/l
Class	Moderately soluble
Log S (SILICOS-IT)	-8.46
Solubility	1.42e-06 mg/ml ; 3.45e-09 mol/l
Class	Poorly soluble
Pharmacokinetics	
GI absorption	High
BBB permeant	Yes
P-gp substrate	Yes
CYP1A2 inhibitor	Yes
CYP2C19 inhibitor	No
CYP2C9 inhibitor	Yes
CYP2D6 inhibitor	Yes
CYP3A4 inhibitor	Yes
Log <i>K</i> _p (skin permeation)	-4.99 cm/s
Druglikeness	
Lipinski	Yes; 1 violation: MLOGP>4.15
Ghose	No; 1 violation: MR>130
Veber	Yes
Egan	Yes
Muegge	No; 1 violation: XLOGP3>5
Bioavailability Score	0.55
Medicinal Chemistry	
PAINS	0 alert
Brenk	0 alert
Leadlikeness	No; 2 violations: MW>350, XLOGP3>3.5
Synthetic accessibility	3.76

C1.3

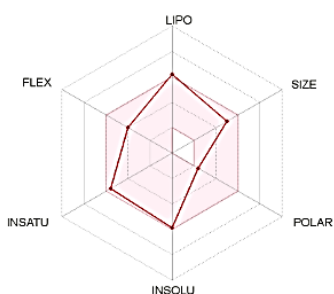
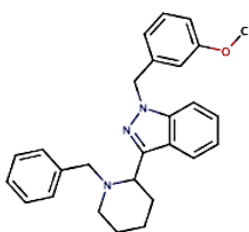


SMILES Clc1cccc(c1)Cn1nc(c2c1cccc2)C1CCCN1Cc1ccccc1

Physicochemical Properties	
Formula	C ₂₆ H ₂₆ ClN ₃
Molecular weight	415.96 g/mol
Num. heavy atoms	30
Num. arom. heavy atoms	21
Fraction Csp ³	0.27
Num. rotatable bonds	5
Num. H-bond acceptors	2
Num. H-bond donors	0
Molar Refractivity	128.68
TPSA	21.06 Å ²
Lipophilicity	
Log P _{ow} (iLOGP)	3.50
Log P _{ow} (XLOGP3)	6.04
Log P _{ow} (WLOGP)	5.61
Log P _{ow} (MLOGP)	5.04
Log P _{ow} (SILICOS-IT)	5.51
Consensus Log P _{ow}	5.14

Water Solubility	
Log S (ESOL)	-6.41
Solubility	1.61e-04 mg/ml ; 3.87e-07 mol/l
Class	Poorly soluble
Log S (Ali)	-6.26
Solubility	2.28e-04 mg/ml ; 5.48e-07 mol/l
Class	Poorly soluble
Log S (SILICOS-IT)	-8.95
Solubility	4.71e-07 mg/ml ; 1.13e-09 mol/l
Class	Poorly soluble
Pharmacokinetics	
GI absorption	High
BBB permeant	Yes
P-gp substrate	Yes
CYP1A2 inhibitor	Yes
CYP2C19 inhibitor	No
CYP2C9 inhibitor	Yes
CYP2D6 inhibitor	Yes
CYP3A4 inhibitor	Yes
Log K _p (skin permeation)	-4.55 cm/s
Druglikeness	
Lipinski	Yes; 1 violation: MLOGP>4.15
Ghose	No; 1 violation: WLOGP>5.6
Weber	Yes
Egan	Yes
Muegge	No; 1 violation: XLOGP3>5
Bioavailability Score	0.55
Medicinal Chemistry	
PAINS	0 alert
Brenk	0 alert
Leadlikeness	No; 2 violations: MW>350, XLOGP3>3.5
Synthetic accessibility	3.69

C1.4

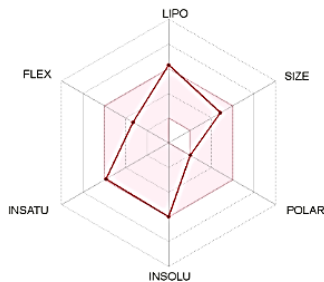
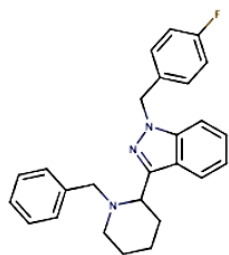


SMILES COc1cccc(c1)Cn1nc(c2c1cccc2)C1CCCCN1Cc1ccccc1

Physicochemical Properties	
Formula	C ₂₇ H ₂₉ N ₃ O
Molecular weight	411.54 g/mol
Num. heavy atoms	31
Num. arom. heavy atoms	21
Fraction Csp ³	0.30
Num. rotatable bonds	6
Num. H-bond acceptors	3
Num. H-bond donors	0
Molar Refractivity	130.16
TPSA	30.29 Å ²
Lipophilicity	
Log P _{ow} (iLOGP)	4.34
Log P _{ow} (XLOGP3)	5.38
Log P _{ow} (WLOGP)	4.96
Log P _{ow} (MLOGP)	4.19
Log P _{ow} (SILICOS-IT)	4.93
Consensus Log P _{ow}	4.76

Water Solubility	
Log S (ESOL)	-5.89
Solubility	5.35e-04 mg/ml ; 1.30e-06 mol/l
Class	Moderately soluble
Log S (Ali)	-5.77
Solubility	6.99e-04 mg/ml ; 1.70e-06 mol/l
Class	Moderately soluble
Log S (SILICOS-IT)	-8.46
Solubility	1.42e-06 mg/ml ; 3.45e-09 mol/l
Class	Poorly soluble
Pharmacokinetics	
GI absorption	High
BBB permeant	Yes
P-gp substrate	Yes
CYP1A2 inhibitor	Yes
CYP2C19 inhibitor	No
CYP2C9 inhibitor	Yes
CYP2D6 inhibitor	Yes
CYP3A4 inhibitor	Yes
Log K _p (skin permeation)	-4.99 cm/s
Druglikeness	
Lipinski	Yes; 1 violation: MLOGP>4.15
Ghose	No; 1 violation: MR>130
Weber	Yes
Egan	Yes
Muegge	No; 1 violation: XLOGP3>5
Bioavailability Score	0.55
Medicinal Chemistry	
PAINS	0 alert
Brenk	0 alert
Leadlikeness	No; 2 violations: MW>350, XLOGP3>3.5
Synthetic accessibility	3.83

C1.5



SMILES Fc1ccc(cc1)Cn1nc(c2c1cccc2)C1CCCCN1Cc1ccccc1

Physicochemical Properties

Formula	C26H26FN3
Molecular weight	399.50 g/mol
Num. heavy atoms	30
Num. arom. heavy atoms	21
Fraction Csp3	0.27
Num. rotatable bonds	5
Num. H-bond acceptors	3
Num. H-bond donors	0
Molar Refractivity	123.62
TPSA	21.06 Å ²

Lipophilicity

Log P_{ow} (iLOGP)	3.49
Log P_{ow} (XLOGP3)	5.51
Log P_{ow} (WLOGP)	5.51
Log P_{ow} (MLOGP)	4.94
Log P_{ow} (SILICOS-IT)	5.29
Consensus Log P_{ow}	4.95

Water Solubility	
Log S (ESOL)	-5.98
Solubility	4.22e-04 mg/ml ; 1.06e-06 mol/l
Class	Moderately soluble
Log S (Ali)	-5.71
Solubility	7.77e-04 mg/ml ; 1.94e-06 mol/l
Class	Moderately soluble
Log S (SILICOS-IT)	-8.62
Solubility	9.50e-07 mg/ml ; 2.38e-09 mol/l
Class	Poorly soluble

Pharmacokinetics

GI absorption	High
BBB permeant	Yes
P-gp substrate	Yes
CYP1A2 inhibitor	Yes
CYP2C19 inhibitor	No
CYP2C9 inhibitor	Yes
CYP2D6 inhibitor	Yes
CYP3A4 inhibitor	Yes
Log K_p (skin permeation)	-4.82 cm/s

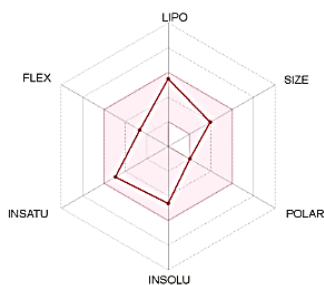
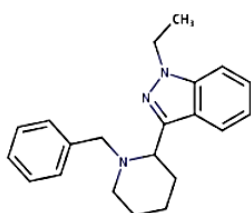
Druglikeness

Lipinski	Yes; 1 violation: MLOGP>4.15
Ghose	Yes
Veber	Yes
Egan	Yes
Muegge	No; 1 violation: XLOGP3>5
Bioavailability Score	0.55

Medicinal Chemistry

PAINS	0 alert
Brenk	0 alert
Leadlikeness	No; 2 violations: MW>350, XLOGP3>3.5
Synthetic accessibility	3.67

C1.6



SMILES CCn1nc(c2c1cccc2)C1CCCCN1Cc1ccccc1

Physicochemical Properties

Formula	C21H25N3
Molecular weight	319.44 g/mol
Num. heavy atoms	24
Num. arom. heavy atoms	15
Fraction Csp3	0.38
Num. rotatable bonds	4
Num. H-bond acceptors	2
Num. H-bond donors	0
Molar Refractivity	103.99
TPSA	21.06 Å ²

Lipophilicity

Log P_{ow} (iLOGP)	3.21
Log P_{ow} (XLOGP3)	4.12
Log P_{ow} (WLOGP)	3.93
Log P_{ow} (MLOGP)	3.73
Log P_{ow} (SILICOS-IT)	3.85
Consensus Log P_{ow}	3.77

Water Solubility	
Log S (ESOL)	-4.61
Solubility	7.76e-03 mg/ml ; 2.43e-05 mol/l
Class	Moderately soluble
Log S (Ali)	-4.27
Solubility	1.72e-02 mg/ml ; 5.39e-05 mol/l
Class	Moderately soluble
Log S (SILICOS-IT)	-6.27
Solubility	1.71e-04 mg/ml ; 5.35e-07 mol/l
Class	Poorly soluble

Pharmacokinetics

GI absorption	High
BBB permeant	Yes
P-gp substrate	Yes
CYP1A2 inhibitor	Yes
CYP2C19 inhibitor	No
CYP2C9 inhibitor	Yes
CYP2D6 inhibitor	Yes
CYP3A4 inhibitor	Yes
Log K_p (skin permeation)	-5.32 cm/s

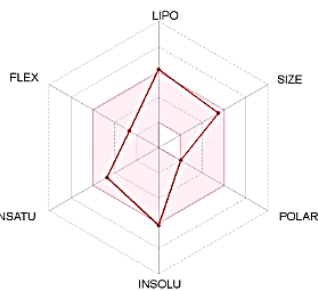
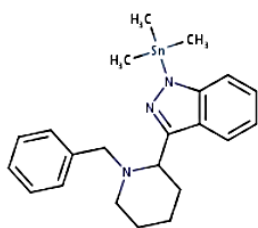
Druglikeness

Lipinski	Yes; 0 violation
Ghose	Yes
Veber	Yes
Egan	Yes
Muegge	Yes
Bioavailability Score	0.55

Medicinal Chemistry

PAINS	0 alert
Brenk	0 alert
Leadlikeness	No; 1 violation: XLOGP3>3.5
Synthetic accessibility	3.28

C1.7



SMILES C[Sn](n1nc(c2c1cccc2)C1CCCCN1Cc1cccc1)(C)C

Physicochemical Properties

Formula	C22H29N3Sn
Molecular weight	454.19 g/mol
Num. heavy atoms	26
Num. arom. heavy atoms	15
Fraction Csp3	0.41
Num. rotatable bonds	4
Num. H-bond acceptors	2
Num. H-bond donors	0
Molar Refractivity	116.66
TPSA [?]	21.06 Å ²

Lipophilicity

Log $P_{o/w}$ (iLOGP) [?]	0.00
Log $P_{o/w}$ (XLOGP3) [?]	5.34
Log $P_{o/w}$ (WLOGP) [?]	4.59
Log $P_{o/w}$ (MLOGP) [?]	3.95
Log $P_{o/w}$ (SILICOS-IT) [?]	3.31
Consensus Log $P_{o/w}$ [?]	3.44

Water Solubility

Log S (ESOL) [?]	-6.18
Solubility	2.98e-04 mg/ml ; 6.56e-07 mol/l
Class [?]	Poorly soluble
Log S (Ali) [?]	-5.53
Solubility	1.33e-03 mg/ml ; 2.92e-06 mol/l
Class [?]	Moderately soluble
Log S (SILICOS-IT) [?]	-6.95
Solubility	5.10e-05 mg/ml ; 1.12e-07 mol/l
Class [?]	Poorly soluble

Pharmacokinetics

GI absorption [?]	High
BBB permeant [?]	Yes
P-gp substrate [?]	Yes
CYP1A2 inhibitor [?]	Yes
CYP2C19 inhibitor [?]	No
CYP2C9 inhibitor [?]	No
CYP2D6 inhibitor [?]	Yes
CYP3A4 inhibitor [?]	Yes
Log K_p (skin permeation) [?]	-5.28 cm/s

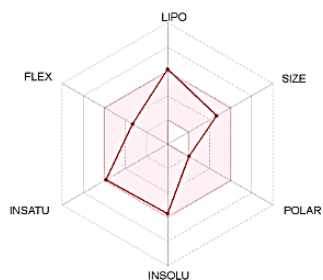
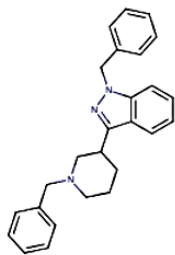
Druglikeness

Lipinski [?]	Yes; 0 violation
Ghose [?]	Yes
Veber [?]	Yes
Egan [?]	Yes
Muegge [?]	No; 1 violation: XLOGP3>5
Bioavailability Score [?]	0.55

Medicinal Chemistry

PAINS [?]	0 alert
Brenk [?]	0 alert
Leadlikeness [?]	No; 2 violations: MW>350, XLOGP3>3.5
Synthetic accessibility [?]	4.04

C2.1



SMILES c1ccc(cc1)CN1CCCC(C1)c1nn(c2c1cccc2)Cc1ccccc1

Physicochemical Properties

Formula	C26H27N3
Molecular weight	381.51 g/mol
Num. heavy atoms	29
Num. arom. heavy atoms	21
Fraction Csp3	0.27
Num. rotatable bonds	5
Num. H-bond acceptors	2
Num. H-bond donors	0
Molar Refractivity	123.67
TPSA	21.06 Å²

Lipophilicity

Log P_{ow} (iLOGP)	4.12
Log P_{ow} (XLOGP3)	5.27
Log P_{ow} (WLOGP)	4.93
Log P_{ow} (MLOGP)	4.57
Log P_{ow} (SILICOS-IT)	4.88
Consensus Log P_{ow}	4.75

Water Solubility	
Log S (ESOL)	-5.73
Solubility	7.08e-04 mg/ml ; 1.86e-06 mol/l
Class	Moderately soluble
Log S (Ali)	-5.46
Solubility	1.32e-03 mg/ml ; 3.45e-06 mol/l
Class	Moderately soluble
Log S (SILICOS-IT)	-8.36
Solubility	1.67e-06 mg/ml ; 4.37e-09 mol/l
Class	Poorly soluble

Pharmacokinetics

GI absorption	High
BBB permeant	Yes
P-gp substrate	Yes
CYP1A2 inhibitor	Yes
CYP2C19 inhibitor	No
CYP2C9 inhibitor	Yes
CYP2D6 inhibitor	Yes
CYP3A4 inhibitor	Yes
Log K_p (skin permeation)	-4.89 cm/s

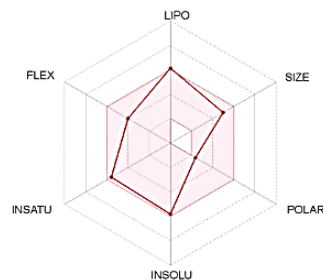
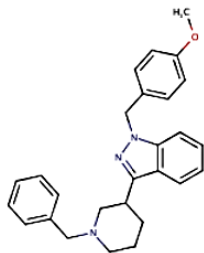
Druglikeness

Lipinski	Yes; 1 violation: MLOGP>4.15
Ghose	Yes
Veber	Yes
Egan	Yes
Muegge	No; 1 violation: XLOGP3>5
Bioavailability Score	0.55

Medicinal Chemistry

PAINS	0 alert
Brenk	0 alert
Leadlikeness	No; 2 violations: MW>350, XLOGP3>3.5
Synthetic accessibility	3.62

C2.2



SMILES COc1ccc(cc1)Cn1nc(c2c1cccc2)C1CCCN(C1)Cc1ccccc1

Physicochemical Properties

Formula	C27H29N3O
Molecular weight	411.54 g/mol
Num. heavy atoms	31
Num. arom. heavy atoms	21
Fraction Csp3	0.30
Num. rotatable bonds	6
Num. H-bond acceptors	3
Num. H-bond donors	0
Molar Refractivity	130.16
TPSA	30.29 Å²

Lipophilicity

Log P_{ow} (iLOGP)	4.28
Log P_{ow} (XLOGP3)	5.24
Log P_{ow} (WLOGP)	4.94
Log P_{ow} (MLOGP)	4.19
Log P_{ow} (SILICOS-IT)	4.93
Consensus Log P_{ow}	4.71

Water Solubility	
Log S (ESOL)	-5.80
Solubility	6.55e-04 mg/ml ; 1.59e-06 mol/l
Class	Moderately soluble
Log S (Ali)	-5.62
Solubility	9.76e-04 mg/ml ; 2.37e-06 mol/l
Class	Moderately soluble
Log S (SILICOS-IT)	-8.46
Solubility	1.42e-06 mg/ml ; 3.45e-09 mol/l
Class	Poorly soluble

Pharmacokinetics

GI absorption	High
BBB permeant	Yes
P-gp substrate	Yes
CYP1A2 inhibitor	Yes
CYP2C19 inhibitor	No
CYP2C9 inhibitor	Yes
CYP2D6 inhibitor	Yes
CYP3A4 inhibitor	Yes
Log K_p (skin permeation)	-5.09 cm/s

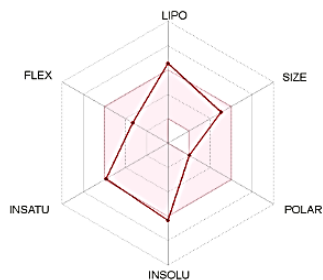
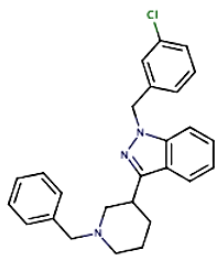
Druglikeness

Lipinski	Yes; 1 violation: MLOGP>4.15
Ghose	No; 1 violation: MR>130
Veber	Yes
Egan	Yes
Muegge	No; 1 violation: XLOGP3>5
Bioavailability Score	0.55

Medicinal Chemistry

PAINS	0 alert
Brenk	0 alert
Leadlikeness	No; 2 violations: MW>350, XLOGP3>3.5
Synthetic accessibility	3.76

C2.3



SMILES Clc1cccc(c1)Cn1nc(c2c1cccc2)C1CCCN(C1)Cc1ccccc1

Physicochemical Properties

Formula	C26H26ClN3
Molecular weight	415.96 g/mol
Num. heavy atoms	30
Num. arom. heavy atoms	21
Fraction Csp3	0.27
Num. rotatable bonds	5
Num. H-bond acceptors	2
Num. H-bond donors	0
Molar Refractivity	128.68
TPSA	21.06 Å²

Lipophilicity

Log $P_{o/w}$ (ILOGP)	4.12
Log $P_{o/w}$ (XLOGP3)	5.90
Log $P_{o/w}$ (WLOGP)	5.58
Log $P_{o/w}$ (MLOGP)	5.04
Log $P_{o/w}$ (SILICOS-IT)	5.51
Consensus Log $P_{o/w}$	5.23

Water Solubility

Log S (ESOL)	-6.32
Solubility	1.97e-04 mg/ml ; 4.74e-07 mol/l
Class	Poorly soluble
Log S (Ali)	-6.12
Solubility	3.19e-04 mg/ml ; 7.66e-07 mol/l
Class	Poorly soluble
Log S (SILICOS-IT)	-8.95
Solubility	4.71e-07 mg/ml ; 1.13e-09 mol/l
Class	Poorly soluble

Pharmacokinetics

GI absorption	High
BBB permeant	Yes
P-gp substrate	Yes
CYP1A2 inhibitor	Yes
CYP2C19 inhibitor	No
CYP2C9 inhibitor	Yes
CYP2D6 inhibitor	Yes
CYP3A4 inhibitor	Yes
Log K_p (skin permeation)	-4.65 cm/s

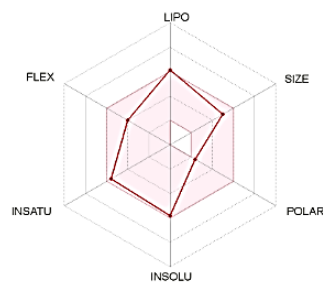
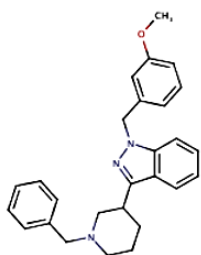
Druglikeness

Lipinski	Yes; 1 violation: MLOGP>4.15
Ghose	Yes
Weber	Yes
Egan	Yes
Muegge	No; 1 violation: XLOGP3>5
Bioavailability Score	0.55

Medicinal Chemistry

PAINS	0 alert
Brenk	0 alert
Leadlikeness	No; 2 violations: MW>350, XLOGP3>3.5
Synthetic accessibility	3.68

C2.4



SMILES COc1cccc(c1)Cn1nc(c2c1cccc2)C1CCCN(C1)Cc1ccccc1

Physicochemical Properties

Formula	C27H29N3O
Molecular weight	411.54 g/mol
Num. heavy atoms	31
Num. arom. heavy atoms	21
Fraction Csp3	0.30
Num. rotatable bonds	6
Num. H-bond acceptors	3
Num. H-bond donors	0
Molar Refractivity	130.16
TPSA	30.29 Å²

Lipophilicity

Log $P_{o/w}$ (ILOGP)	4.02
Log $P_{o/w}$ (XLOGP3)	5.24
Log $P_{o/w}$ (WLOGP)	4.94
Log $P_{o/w}$ (MLOGP)	4.19
Log $P_{o/w}$ (SILICOS-IT)	4.93
Consensus Log $P_{o/w}$	4.66

Water Solubility

Log S (ESOL)	-5.80
Solubility	6.55e-04 mg/ml ; 1.59e-06 mol/l
Class	Moderately soluble
Log S (Ali)	-5.62
Solubility	9.76e-04 mg/ml ; 2.37e-06 mol/l
Class	Moderately soluble
Log S (SILICOS-IT)	-8.46
Solubility	1.42e-06 mg/ml ; 3.45e-09 mol/l
Class	Poorly soluble

Pharmacokinetics

GI absorption	High
BBB permeant	Yes
P-gp substrate	Yes
CYP1A2 inhibitor	Yes
CYP2C19 inhibitor	No
CYP2C9 inhibitor	Yes
CYP2D6 inhibitor	Yes
CYP3A4 inhibitor	Yes
Log K_p (skin permeation)	-5.09 cm/s

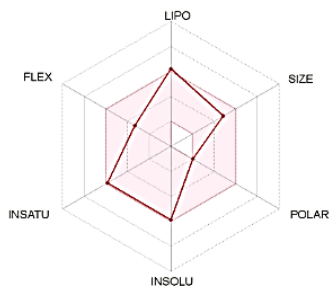
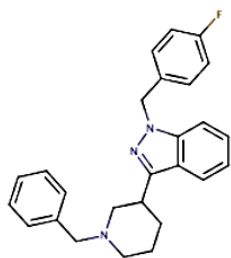
Druglikeness

Lipinski	Yes; 1 violation: MLOGP>4.15
Ghose	No; 1 violation: MR>130
Weber	Yes
Egan	Yes
Muegge	No; 1 violation: XLOGP3>5
Bioavailability Score	0.55

Medicinal Chemistry

PAINS	0 alert
Brenk	0 alert
Leadlikeness	No; 2 violations: MW>350, XLOGP3>3.5
Synthetic accessibility	3.82

C2.5

SMILES Fc1ccc(cc1)Cn1nc(c2c1cccc2)C1CCCN(C1)Cc1ccccc1

Physicochemical Properties

Formula	C ₂₆ H ₂₆ FN ₃
Molecular weight	399.50 g/mol
Num. heavy atoms	30
Num. arom. heavy atoms	21
Fraction Csp ³	0.27
Num. rotatable bonds	5
Num. H-bond acceptors	3
Num. H-bond donors	0
Molar Refractivity	123.62
TPSA	21.06 Å ²

Lipophilicity

Log <i>P</i> _{0/w} (iLOGP)	4.07
Log <i>P</i> _{0/w} (XLOGP3)	5.37
Log <i>P</i> _{0/w} (WLOGP)	5.49
Log <i>P</i> _{0/w} (MLOGP)	4.94
Log <i>P</i> _{0/w} (SILICOS-IT)	5.29
Consensus Log <i>P</i> _{0/w}	5.03

Water Solubility	
Log S (ESOL)	-5.89
Solubility	5.17e-04 mg/ml ; 1.29e-06 mol/l
Class	Moderately soluble
Log S (All)	-5.57
Solubility	1.09e-03 mg/ml ; 2.72e-06 mol/l
Class	Moderately soluble
Log S (SILICOS-IT)	-8.62
Solubility	9.50e-07 mg/ml ; 2.38e-09 mol/l
Class	Poorly soluble

Pharmacokinetics

GI absorption	High
BBB permeant	Yes
P-gp substrate	Yes
CYP1A2 inhibitor	Yes
CYP2C19 inhibitor	No
CYP2C9 inhibitor	Yes
CYP2D6 inhibitor	Yes
CYP3A4 inhibitor	Yes
Log <i>K</i> _p (skin permeation)	-4.92 cm/s

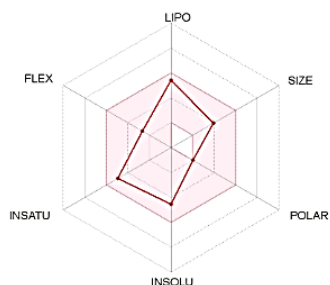
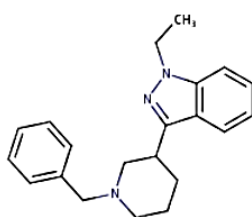
Druglikeness

Lipinski	Yes; 1 violation: MLOGP>4.15
Ghose	Yes
Veber	Yes
Egan	Yes
Muegge	No; 1 violation: XLOGP3>5
Bioavailability Score	0.55

Medicinal Chemistry

PAINS	0 alert
Brenk	0 alert
Leadlikeness	No; 2 violations: MW>350, XLOGP3>3.5
Synthetic accessibility	3.65

C2.6

SMILES CCn1nc(c2c1cccc2)C1CCCN(C1)Cc1ccccc1

Physicochemical Properties

Formula	C ₂₁ H ₂₅ N ₃
Molecular weight	319.44 g/mol
Num. heavy atoms	24
Num. arom. heavy atoms	15
Fraction Csp ³	0.38
Num. rotatable bonds	4
Num. H-bond acceptors	2
Num. H-bond donors	0
Molar Refractivity	103.99
TPSA	21.06 Å ²

Lipophilicity

Log <i>P</i> _{0/w} (iLOGP)	3.64
Log <i>P</i> _{0/w} (XLOGP3)	3.98
Log <i>P</i> _{0/w} (WLOGP)	3.90
Log <i>P</i> _{0/w} (MLOGP)	3.73
Log <i>P</i> _{0/w} (SILICOS-IT)	3.85
Consensus Log <i>P</i> _{0/w}	3.82

Water Solubility	
Log S (ESOL)	-4.53
Solubility	9.50e-03 mg/ml ; 2.98e-05 mol/l
Class	Moderately soluble
Log S (All)	-4.12
Solubility	2.40e-02 mg/ml ; 7.52e-05 mol/l
Class	Moderately soluble
Log S (SILICOS-IT)	-6.27
Solubility	1.71e-04 mg/ml ; 5.35e-07 mol/l
Class	Poorly soluble

Pharmacokinetics

GI absorption	High
BBB permeant	Yes
P-gp substrate	Yes
CYP1A2 inhibitor	Yes
CYP2C19 inhibitor	No
CYP2C9 inhibitor	Yes
CYP2D6 inhibitor	Yes
CYP3A4 inhibitor	Yes
Log <i>K</i> _p (skin permeation)	-5.42 cm/s

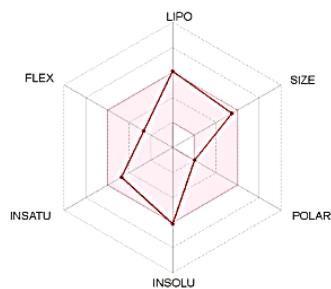
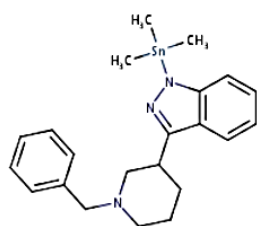
Druglikeness

Lipinski	Yes; 0 violation
Ghose	Yes
Veber	Yes
Egan	Yes
Muegge	Yes
Bioavailability Score	0.55

Medicinal Chemistry

PAINS	0 alert
Brenk	0 alert
Leadlikeness	No; 1 violation: XLOGP3>3.5
Synthetic accessibility	3.27

C2.7



SMILES C[Sn](n1nc(c2c1cccc2)C1CCCN(C1)Cc1cccc1)(C)C

Physicochemical Properties

Formula	C22H29N3Sn
Molecular weight	454.19 g/mol
Num. heavy atoms	26
Num. arom. heavy atoms	15
Fraction Csp3	0.41
Num. rotatable bonds	4
Num. H-bond acceptors	2
Num. H-bond donors	0
Molar Refractivity	116.66
TPSA	21.06 Å ²

Lipophilicity

Log $P_{0/w}$ (iLOGP)	0.00
Log $P_{0/w}$ (XLOGP3)	5.20
Log $P_{0/w}$ (WLOGP)	4.57
Log $P_{0/w}$ (MLOGP)	3.95
Log $P_{0/w}$ (SILICOS-IT)	3.31
Consensus Log $P_{0/w}$	3.41

Water Solubility

Log S (ESOL)	-6.09
Solubility	3.65e-04 mg/ml ; 8.04e-07 mol/l
Class	Poorly soluble
Log S (Ali)	-5.39
Solubility	1.85e-03 mg/ml ; 4.08e-06 mol/l
Class	Moderately soluble
Log S (SILICOS-IT)	-6.95
Solubility	5.10e-05 mg/ml ; 1.12e-07 mol/l
Class	Poorly soluble

Pharmacokinetics

GI absorption	High
BBB permeant	Yes
P-gp substrate	Yes
CYP1A2 inhibitor	Yes
CYP2C19 inhibitor	No
CYP2C9 inhibitor	No
CYP2D6 inhibitor	Yes
CYP3A4 inhibitor	Yes
Log K_p (skin permeation)	-5.38 cm/s

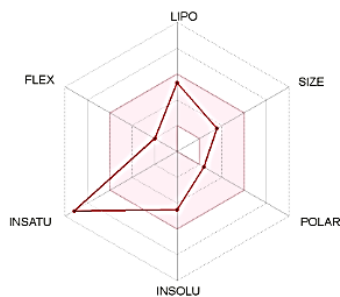
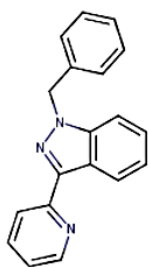
Druglikeness

Lipinski	Yes; 0 violation
Ghose	Yes
Veber	Yes
Egan	Yes
Muegge	No; 1 violation: XLOGP3>5
Bioavailability Score	0.55

Medicinal Chemistry

PAINS	0 alert
Brenk	0 alert
Leadlikeness	No; 2 violations: MW>350, XLOGP3>3.5
Synthetic accessibility	4.02

C3.1

SMILES c1ccc(cc1)Cn1nc(c2c1cccc2)c1ccccn1

Physicochemical Properties

Formula	C19H15N3
Molecular weight	285.34 g/mol
Num. heavy atoms	22
Num. arom. heavy atoms	21
Fraction Csp3	0.05
Num. rotatable bonds	3
Num. H-bond acceptors	2
Num. H-bond donors	0
Molar Refractivity	88.71
TPSA [?]	30.71 Å ²

Lipophilicity

Log P_{ow} (ILOGP) [?]	3.00
Log P_{ow} (XLOGP3) [?]	3.79
Log P_{ow} (WLOGP) [?]	4.15
Log P_{ow} (MLOGP) [?]	3.06
Log P_{ow} (SILICOS-IT) [?]	3.85
Consensus Log P_{ow} [?]	3.57

Water Solubility	
Log S (ESOL) [?]	-4.51
Solubility	8.92e-03 mg/ml ; 3.12e-05 mol/l
Class [?]	Moderately soluble
Log S (Ali) [?]	-4.13
Solubility	2.12e-02 mg/ml ; 7.43e-05 mol/l
Class [?]	Moderately soluble
Log S (SILICOS-IT) [?]	-7.15
Solubility	2.03e-05 mg/ml ; 7.13e-08 mol/l
Class [?]	Poorly soluble

Pharmacokinetics

GI absorption [?]	High
BBB permeant [?]	Yes
P-gp substrate [?]	Yes
CYP1A2 inhibitor [?]	Yes
CYP2C19 inhibitor [?]	Yes
CYP2C9 inhibitor [?]	Yes
CYP2D6 inhibitor [?]	Yes
CYP3A4 inhibitor [?]	Yes
Log K_p (skin permeation) [?]	-5.35 cm/s

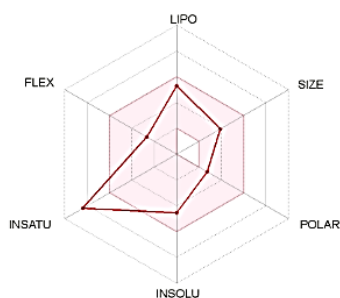
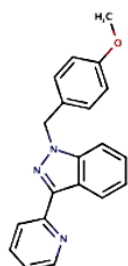
Druglikeness

Lipinski [?]	Yes; 0 violation
Ghose [?]	Yes
Weber [?]	Yes
Egan [?]	Yes
Muegge [?]	Yes
Bioavailability Score [?]	0.55

Medicinal Chemistry

PAINS [?]	0 alert
Brenk [?]	0 alert
Leadlikeness [?]	No; 1 violation: XLOGP3>3.5
Synthetic accessibility [?]	2.60

C3.2

SMILES COC1ccc(cc1)Cn1nc(c2c1cccc2)c1ccccn1

Physicochemical Properties

Formula	C20H17N3O
Molecular weight	315.37 g/mol
Num. heavy atoms	24
Num. arom. heavy atoms	21
Fraction Csp3	0.10
Num. rotatable bonds	4
Num. H-bond acceptors	3
Num. H-bond donors	0
Molar Refractivity	95.20
TPSA [?]	39.94 Å ²

Lipophilicity

Log P_{ow} (ILOGP) [?]	3.23
Log P_{ow} (XLOGP3) [?]	3.76
Log P_{ow} (WLOGP) [?]	4.16
Log P_{ow} (MLOGP) [?]	2.70
Log P_{ow} (SILICOS-IT) [?]	3.86
Consensus Log P_{ow} [?]	3.54

Water Solubility	
Log S (ESOL) [?]	-4.55
Solubility	8.94e-03 mg/ml ; 2.83e-05 mol/l
Class [?]	Moderately soluble
Log S (Ali) [?]	-4.29
Solubility	1.61e-02 mg/ml ; 5.11e-05 mol/l
Class [?]	Moderately soluble
Log S (SILICOS-IT) [?]	-7.26
Solubility	1.73e-05 mg/ml ; 5.48e-08 mol/l
Class [?]	Poorly soluble

Pharmacokinetics

GI absorption [?]	High
BBB permeant [?]	Yes
P-gp substrate [?]	Yes
CYP1A2 inhibitor [?]	Yes
CYP2C19 inhibitor [?]	Yes
CYP2C9 inhibitor [?]	Yes
CYP2D6 inhibitor [?]	Yes
CYP3A4 inhibitor [?]	Yes
Log K_p (skin permeation) [?]	-5.55 cm/s

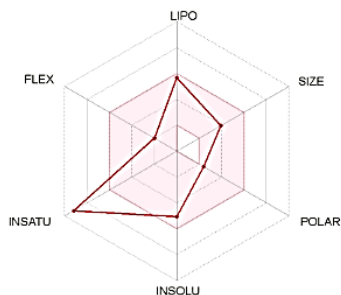
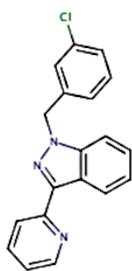
Druglikeness

Lipinski [?]	Yes; 0 violation
Ghose [?]	Yes
Weber [?]	Yes
Egan [?]	Yes
Muegge [?]	Yes
Bioavailability Score [?]	0.55

Medicinal Chemistry

PAINS [?]	0 alert
Brenk [?]	0 alert
Leadlikeness [?]	No; 1 violation: XLOGP3>3.5
Synthetic accessibility [?]	2.72

C3.3



SMILES Clc1ccc(c1)Cn1nc(c2c1cccc2)c1cccn1

Physicochemical Properties

Formula	C19H14ClN3
Molecular weight	319.79 g/mol
Num. heavy atoms	23
Num. arom. heavy atoms	21
Fraction Csp3	0.05
Num. rotatable bonds	3
Num. H-bond acceptors	2
Num. H-bond donors	0
Molar Refractivity	93.72
TPSA [?]	30.71 Å²

Lipophilicity

Log $P_{o/w}$ (ILOGP) [?]	2.80
Log $P_{o/w}$ (XLOGP3) [?]	4.42
Log $P_{o/w}$ (WLOGP) [?]	4.80
Log $P_{o/w}$ (MLOGP) [?]	3.56
Log $P_{o/w}$ (SILICOS-IT) [?]	4.46
Consensus Log $P_{o/w}$ [?]	4.01

Water Solubility	
Log S (ESOL) [?]	-5.08
Solubility	2.63e-03 mg/ml ; 8.22e-06 mol/l
Class [?]	Moderately soluble
Log S (Ali) [?]	-4.78
Solubility	5.27e-03 mg/ml ; 1.65e-05 mol/l
Class [?]	Moderately soluble
Log S (SILICOS-IT) [?]	-7.75
Solubility	5.73e-06 mg/ml ; 1.79e-08 mol/l
Class [?]	Poorly soluble

Pharmacokinetics

GI absorption [?]	High
BBB permeant [?]	Yes
P-gp substrate [?]	Yes
CYP1A2 inhibitor [?]	Yes
CYP2C19 inhibitor [?]	Yes
CYP2C9 inhibitor [?]	Yes
CYP2D6 inhibitor [?]	Yes
CYP3A4 inhibitor [?]	Yes
Log K_p (skin permeation) [?]	-5.11 cm/s

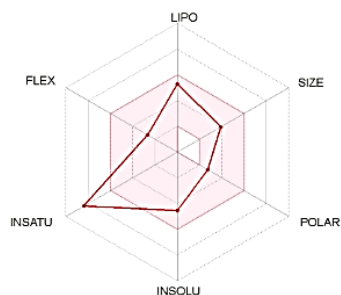
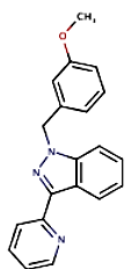
Druglikeness

Lipinski [?]	Yes; 0 violation
Ghose [?]	Yes
Veber [?]	Yes
Egan [?]	Yes
Muegge [?]	Yes
Bioavailability Score [?]	0.55

Medicinal Chemistry

PAINS [?]	0 alert
Brenk [?]	0 alert
Leadlikeness [?]	No; 1 violation: XLOGP3>3.5
Synthetic accessibility [?]	2.65

C3.4



SMILES COc1ccc(c1)Cn1nc(c2c1cccc2)c1cccn1

Physicochemical Properties

Formula	C20H17N3O
Molecular weight	315.37 g/mol
Num. heavy atoms	24
Num. arom. heavy atoms	21
Fraction Csp3	0.10
Num. rotatable bonds	4
Num. H-bond acceptors	3
Num. H-bond donors	0
Molar Refractivity	95.20
TPSA [?]	39.94 Å²

Lipophilicity

Log $P_{o/w}$ (ILOGP) [?]	3.29
Log $P_{o/w}$ (XLOGP3) [?]	3.76
Log $P_{o/w}$ (WLOGP) [?]	4.16
Log $P_{o/w}$ (MLOGP) [?]	2.70
Log $P_{o/w}$ (SILICOS-IT) [?]	3.86
Consensus Log $P_{o/w}$ [?]	3.55

Water Solubility	
Log S (ESOL) [?]	-4.55
Solubility	8.94e-03 mg/ml ; 2.83e-05 mol/l
Class [?]	Moderately soluble
Log S (Ali) [?]	-4.29
Solubility	1.61e-02 mg/ml ; 5.11e-05 mol/l
Class [?]	Moderately soluble
Log S (SILICOS-IT) [?]	-7.26
Solubility	1.73e-05 mg/ml ; 5.48e-08 mol/l
Class [?]	Poorly soluble

Pharmacokinetics

GI absorption [?]	High
BBB permeant [?]	Yes
P-gp substrate [?]	Yes
CYP1A2 inhibitor [?]	Yes
CYP2C19 inhibitor [?]	Yes
CYP2C9 inhibitor [?]	Yes
CYP2D6 inhibitor [?]	Yes
CYP3A4 inhibitor [?]	Yes
Log K_p (skin permeation) [?]	-5.55 cm/s

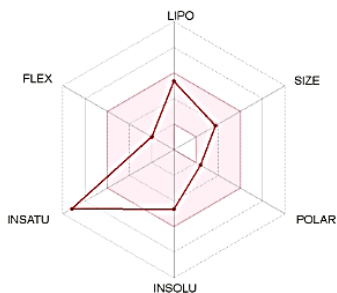
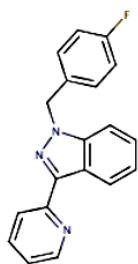
Druglikeness

Lipinski [?]	Yes; 0 violation
Ghose [?]	Yes
Veber [?]	Yes
Egan [?]	Yes
Muegge [?]	Yes
Bioavailability Score [?]	0.55

Medicinal Chemistry

PAINS [?]	0 alert
Brenk [?]	0 alert
Leadlikeness [?]	No; 1 violation: XLOGP3>3.5
Synthetic accessibility [?]	2.77

C3.5

SMILES Fc1ccc(cc1)Cn1nc(c2c1cccc2)c1cccn1

Physicochemical Properties

Formula	C19H14FN3
Molecular weight	303.33 g/mol
Num. heavy atoms	23
Num. arom. heavy atoms	21
Fraction Csp3	0.05
Num. rotatable bonds	3
Num. H-bond acceptors	3
Num. H-bond donors	0
Molar Refractivity	88.67
TPSA [?]	30.71 Å ²

Lipophilicity

Log P_{ow} (iLOGP) [?]	2.59
Log P_{ow} (XLOGP3) [?]	3.89
Log P_{ow} (WLOGP) [?]	4.71
Log P_{ow} (MLOGP) [?]	3.44
Log P_{ow} (SILICOS-IT) [?]	4.25
Consensus Log P_{ow} [?]	3.77

Water Solubility	
Log S (ESOL) [?]	-4.65
Solubility	6.81e-03 mg/ml ; 2.24e-05 mol/l
Class [?]	Moderately soluble
Log S (All) [?]	-4.23
Solubility	1.77e-02 mg/ml ; 5.85e-05 mol/l
Class [?]	Moderately soluble
Log S (SILICOS-IT) [?]	-7.42
Solubility	1.16e-05 mg/ml ; 3.81e-08 mol/l
Class [?]	Poorly soluble

Pharmacokinetics

GI absorption [?]	High
BBB permeant [?]	Yes
P-gp substrate [?]	Yes
CYP1A2 inhibitor [?]	Yes
CYP2C19 inhibitor [?]	Yes
CYP2C9 inhibitor [?]	No
CYP2D6 inhibitor [?]	Yes
CYP3A4 inhibitor [?]	Yes
Log K_p (skin permeation) [?]	-5.39 cm/s

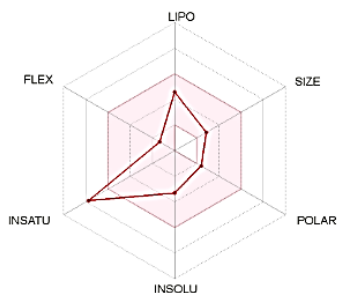
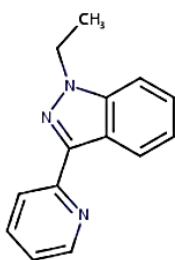
Druglikeness

Lipinski [?]	Yes; 0 violation
Ghose [?]	Yes
Veber [?]	Yes
Egan [?]	Yes
Muegge [?]	Yes
Bioavailability Score [?]	0.55

Medicinal Chemistry

PAINS [?]	0 alert
Brenk [?]	0 alert
Leadlikeness [?]	No; 1 violation: XLOGP3>3.5
Synthetic accessibility [?]	2.60

C3.6

SMILES CCn1nc(c2c1cccc2)c1cccn1

Physicochemical Properties

Formula	C14H13N3
Molecular weight	223.27 g/mol
Num. heavy atoms	17
Num. arom. heavy atoms	15
Fraction Csp3	0.14
Num. rotatable bonds	2
Num. H-bond acceptors	2
Num. H-bond donors	0
Molar Refractivity	69.03
TPSA [?]	30.71 Å ²

Lipophilicity

Log P_{ow} (iLOGP) [?]	2.58
Log P_{ow} (XLOGP3) [?]	2.50
Log P_{ow} (WLOGP) [?]	3.12
Log P_{ow} (MLOGP) [?]	2.06
Log P_{ow} (SILICOS-IT) [?]	2.81
Consensus Log P_{ow} [?]	2.61

Water Solubility	
Log S (ESOL) [?]	-3.32
Solubility	1.07e-01 mg/ml ; 4.78e-04 mol/l
Class [?]	Soluble
Log S (All) [?]	-2.79
Solubility	3.62e-01 mg/ml ; 1.62e-03 mol/l
Class [?]	Soluble
Log S (SILICOS-IT) [?]	-5.03
Solubility	2.09e-03 mg/ml ; 9.35e-06 mol/l
Class [?]	Moderately soluble

Pharmacokinetics

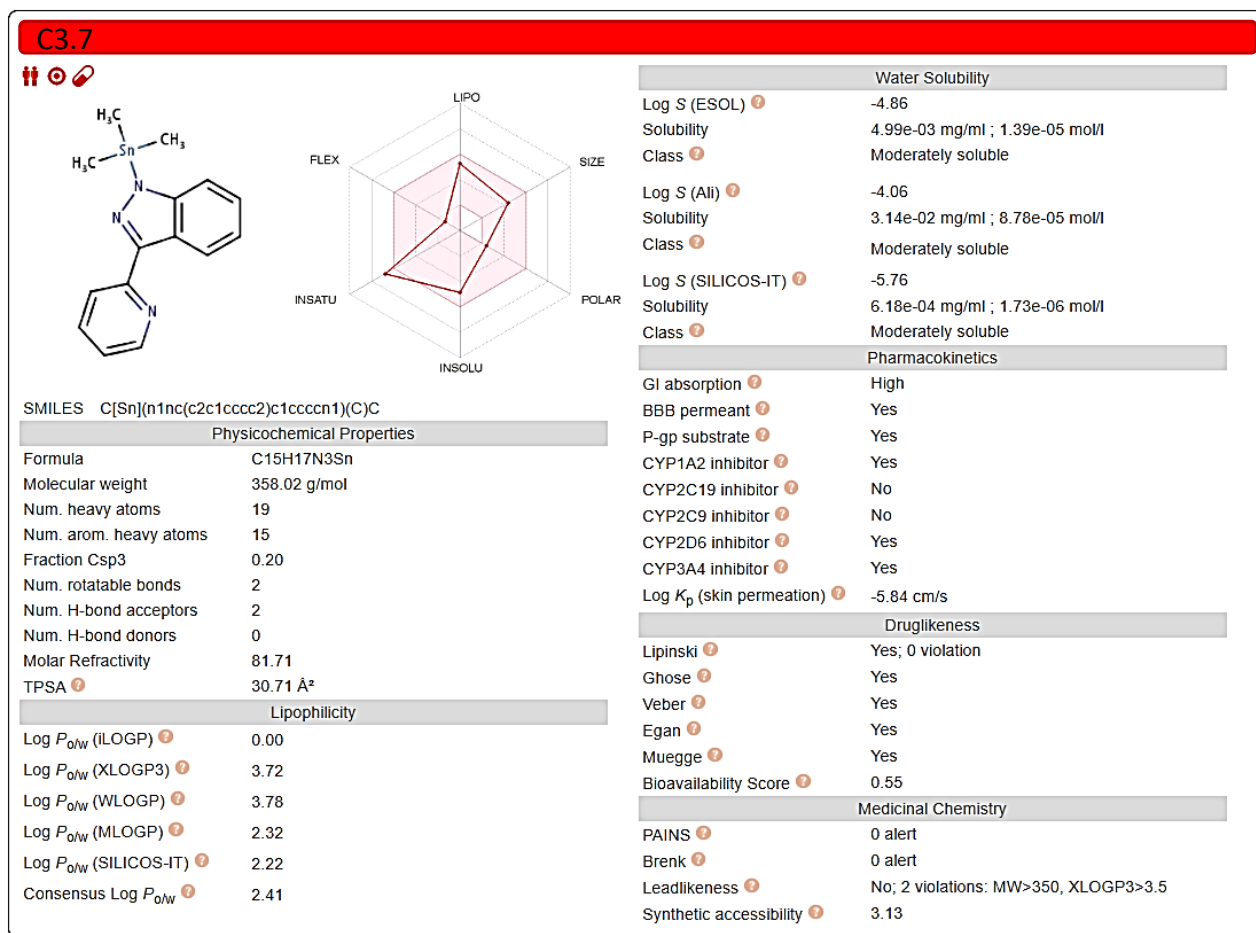
GI absorption [?]	High
BBB permeant [?]	Yes
P-gp substrate [?]	Yes
CYP1A2 inhibitor [?]	Yes
CYP2C19 inhibitor [?]	Yes
CYP2C9 inhibitor [?]	No
CYP2D6 inhibitor [?]	Yes
CYP3A4 inhibitor [?]	Yes
Log K_p (skin permeation) [?]	-5.89 cm/s

Druglikeness

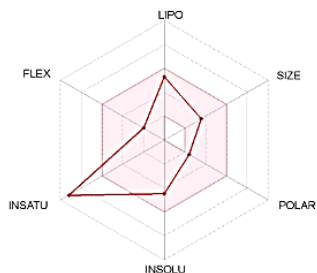
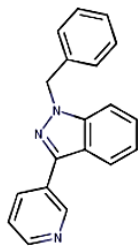
Lipinski [?]	Yes; 0 violation
Ghose [?]	Yes
Veber [?]	Yes
Egan [?]	Yes
Muegge [?]	Yes
Bioavailability Score [?]	0.55

Medicinal Chemistry

PAINS [?]	0 alert
Brenk [?]	0 alert
Leadlikeness [?]	No; 1 violation: MW<250
Synthetic accessibility [?]	2.28



C4.1

SMILES c1ccc(cc1)Cn1nc(c2c1cccc2)c1cccnc1

Physicochemical Properties

Formula	C19H15N3
Molecular weight	285.34 g/mol
Num. heavy atoms	22
Num. arom. heavy atoms	21
Fraction Csp3	0.05
Num. rotatable bonds	3
Num. H-bond acceptors	2
Num. H-bond donors	0
Molar Refractivity	88.71
TPSA	30.71 Å²

Lipophilicity

Log P_{ow} (iLOGP)	2.81
Log P_{ow} (XLOGP3)	3.76
Log P_{ow} (WLOGP)	4.15
Log P_{ow} (MLOGP)	3.06
Log P_{ow} (SILICOS-IT)	3.85
Consensus Log P_{ow}	3.53

Water Solubility	
Log S (ESOL)	-4.49
Solubility	9.31e-03 mg/ml ; 3.26e-05 mol/l
Class	Moderately soluble
Log S (Ali)	-4.10
Solubility	2.28e-02 mg/ml ; 7.98e-05 mol/l
Class	Moderately soluble
Log S (SILICOS-IT)	-7.15
Solubility	2.03e-05 mg/ml ; 7.13e-08 mol/l
Class	Poorly soluble

Pharmacokinetics

GI absorption	High
BBB permeant	Yes
P-gp substrate	Yes
CYP1A2 inhibitor	Yes
CYP2C19 inhibitor	Yes
CYP2C9 inhibitor	Yes
CYP2D6 inhibitor	Yes
CYP3A4 inhibitor	Yes
Log K_p (skin permeation)	-5.37 cm/s

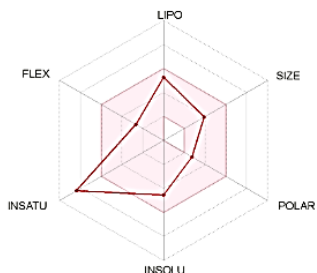
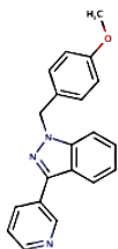
Druglikeness

Lipinski	Yes; 0 violation
Ghose	Yes
Veber	Yes
Egan	Yes
Muegge	Yes
Bioavailability Score	0.55

Medicinal Chemistry

PAINS	0 alert
Brenk	0 alert
Leadlikeness	No; 1 violation: XLOGP3>3.5
Synthetic accessibility	2.61

C4.2

SMILES COC1ccc(cc1)Cn1nc(c2c1cccc2)c1cccnc1

Physicochemical Properties

Formula	C20H17N3O
Molecular weight	315.37 g/mol
Num. heavy atoms	24
Num. arom. heavy atoms	21
Fraction Csp3	0.10
Num. rotatable bonds	4
Num. H-bond acceptors	3
Num. H-bond donors	0
Molar Refractivity	95.20
TPSA	39.94 Å²

Lipophilicity

Log P_{ow} (iLOGP)	3.00
Log P_{ow} (XLOGP3)	3.73
Log P_{ow} (WLOGP)	4.16
Log P_{ow} (MLOGP)	2.70
Log P_{ow} (SILICOS-IT)	3.86
Consensus Log P_{ow}	3.49

Water Solubility	
Log S (ESOL)	-4.53
Solubility	9.34e-03 mg/ml ; 2.96e-05 mol/l
Class	Moderately soluble
Log S (Ali)	-4.26
Solubility	1.73e-02 mg/ml ; 5.49e-05 mol/l
Class	Moderately soluble
Log S (SILICOS-IT)	-7.26
Solubility	1.73e-05 mg/ml ; 5.48e-08 mol/l
Class	Poorly soluble

Pharmacokinetics

GI absorption	High
BBB permeant	Yes
P-gp substrate	Yes
CYP1A2 inhibitor	Yes
CYP2C19 inhibitor	Yes
CYP2C9 inhibitor	Yes
CYP2D6 inhibitor	Yes
CYP3A4 inhibitor	Yes
Log K_p (skin permeation)	-5.58 cm/s

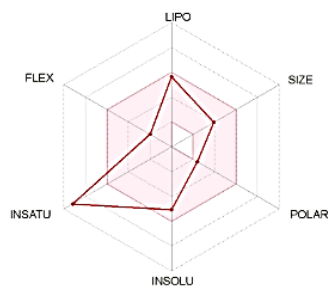
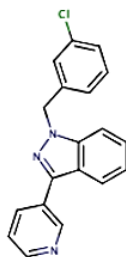
Druglikeness

Lipinski	Yes; 0 violation
Ghose	Yes
Veber	Yes
Egan	Yes
Muegge	Yes
Bioavailability Score	0.55

Medicinal Chemistry

PAINS	0 alert
Brenk	0 alert
Leadlikeness	No; 1 violation: XLOGP3>3.5
Synthetic accessibility	2.73

C4.3

SMILES Clc1cccc(c1)Cn1nc(c2c1cccc2)c1ccnc1

Physicochemical Properties

Formula	C19H14ClN3
Molecular weight	319.79 g/mol
Num. heavy atoms	23
Num. arom. heavy atoms	21
Fraction Csp3	0.05
Num. rotatable bonds	3
Num. H-bond acceptors	2
Num. H-bond donors	0
Molar Refractivity	93.72
TPSA [?]	30.71 Å ²

Lipophilicity

Log $P_{o/w}$ (iLOGP) [?]	2.95
Log $P_{o/w}$ (XLOGP3) [?]	4.39
Log $P_{o/w}$ (WLOGP) [?]	4.80
Log $P_{o/w}$ (MLOGP) [?]	3.56
Log $P_{o/w}$ (SILICOS-IT) [?]	4.46
Consensus Log $P_{o/w}$ [?]	4.03

Water Solubility	
Log S (ESOL) [?]	-5.07
Solubility	2.75e-03 mg/ml ; 8.59e-06 mol/l
Class [?]	Moderately soluble
Log S (Ali) [?]	-4.75
Solubility	5.67e-03 mg/ml ; 1.77e-05 mol/l
Class [?]	Moderately soluble
Log S (SILICOS-IT) [?]	-7.75
Solubility	5.73e-06 mg/ml ; 1.79e-08 mol/l
Class [?]	Poorly soluble

Pharmacokinetics

GI absorption [?]	High
BBB permeant [?]	Yes
P-gp substrate [?]	Yes
CYP1A2 inhibitor [?]	Yes
CYP2C19 inhibitor [?]	Yes
CYP2C9 inhibitor [?]	Yes
CYP2D6 inhibitor [?]	Yes
CYP3A4 inhibitor [?]	Yes
Log K_p (skin permeation) [?]	-5.13 cm/s

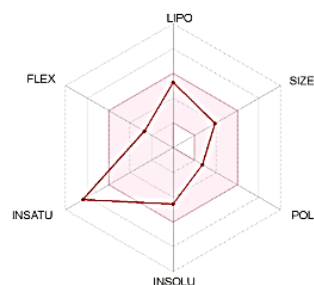
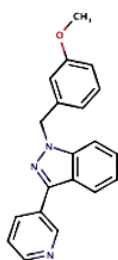
Druglikeness

Lipinski [?]	Yes; 0 violation
Ghose [?]	Yes
Veber [?]	Yes
Egan [?]	Yes
Muegge [?]	Yes
Bioavailability Score [?]	0.55

Medicinal Chemistry

PAINS [?]	0 alert
Brenk [?]	0 alert
Leadlikeness [?]	No; 1 violation: XLOGP3>3.5
Synthetic accessibility [?]	2.66

C4.4

SMILES COc1cccc(c1)Cn1nc(c2c1cccc2)c1ccnc1

Physicochemical Properties

Formula	C20H17N3O
Molecular weight	315.37 g/mol
Num. heavy atoms	24
Num. arom. heavy atoms	21
Fraction Csp3	0.10
Num. rotatable bonds	4
Num. H-bond acceptors	3
Num. H-bond donors	0
Molar Refractivity	95.20
TPSA [?]	39.94 Å ²

Lipophilicity

Log $P_{o/w}$ (iLOGP) [?]	3.16
Log $P_{o/w}$ (XLOGP3) [?]	3.73
Log $P_{o/w}$ (WLOGP) [?]	4.16
Log $P_{o/w}$ (MLOGP) [?]	2.70
Log $P_{o/w}$ (SILICOS-IT) [?]	3.86
Consensus Log $P_{o/w}$ [?]	3.52

Water Solubility	
Log S (ESOL) [?]	-4.53
Solubility	9.34e-03 mg/ml ; 2.96e-05 mol/l
Class [?]	Moderately soluble
Log S (Ali) [?]	-4.26
Solubility	1.73e-02 mg/ml ; 5.49e-05 mol/l
Class [?]	Moderately soluble
Log S (SILICOS-IT) [?]	-7.26
Solubility	1.73e-05 mg/ml ; 5.48e-08 mol/l
Class [?]	Poorly soluble

Pharmacokinetics

GI absorption [?]	High
BBB permeant [?]	Yes
P-gp substrate [?]	Yes
CYP1A2 inhibitor [?]	Yes
CYP2C19 inhibitor [?]	Yes
CYP2C9 inhibitor [?]	Yes
CYP2D6 inhibitor [?]	Yes
CYP3A4 inhibitor [?]	Yes
Log K_p (skin permeation) [?]	-5.58 cm/s

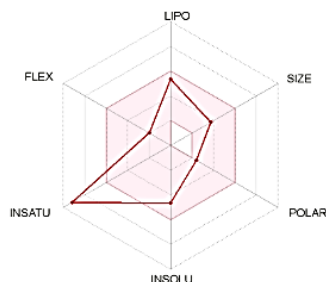
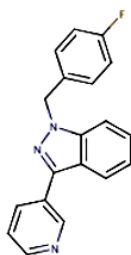
Druglikeness

Lipinski [?]	Yes; 0 violation
Ghose [?]	Yes
Veber [?]	Yes
Egan [?]	Yes
Muegge [?]	Yes
Bioavailability Score [?]	0.55

Medicinal Chemistry

PAINS [?]	0 alert
Brenk [?]	0 alert
Leadlikeness [?]	No; 1 violation: XLOGP3>3.5
Synthetic accessibility [?]	2.78

C4.5

SMILES Fc1ccc(cc1)Cn1nc(c2c1cccc2)c1cccn1

Physicochemical Properties

Formula	C19H14FN3
Molecular weight	303.33 g/mol
Num. heavy atoms	23
Num. arom. heavy atoms	21
Fraction Csp3	0.05
Num. rotatable bonds	3
Num. H-bond acceptors	3
Num. H-bond donors	0
Molar Refractivity	88.67
TPSA [?]	30.71 Å ²

Lipophilicity

Log $P_{o/w}$ (iLOGP) [?]	2.84
Log $P_{o/w}$ (XLOGP3) [?]	3.86
Log $P_{o/w}$ (WLOGP) [?]	4.71
Log $P_{o/w}$ (MLOGP) [?]	3.44
Log $P_{o/w}$ (SILICOS-IT) [?]	4.25
Consensus Log $P_{o/w}$ [?]	3.82

Water Solubility

Log S (ESOL) [?]	-4.63
Solubility	7.11e-03 mg/ml ; 2.34e-05 mol/l
Class [?]	Moderately soluble
Log S (Ali) [?]	-4.20
Solubility	1.91e-02 mg/ml ; 6.29e-05 mol/l
Class [?]	Moderately soluble
Log S (SILICOS-IT) [?]	-7.42
Solubility	1.16e-05 mg/ml ; 3.81e-08 mol/l
Class [?]	Poorly soluble

Pharmacokinetics

GI absorption [?]	High
BBB permeant [?]	Yes
P-gp substrate [?]	Yes
CYP1A2 inhibitor [?]	Yes
CYP2C19 inhibitor [?]	Yes
CYP2C9 inhibitor [?]	No
CYP2D6 inhibitor [?]	Yes
CYP3A4 inhibitor [?]	Yes
Log K_p (skin permeation) [?]	-5.41 cm/s

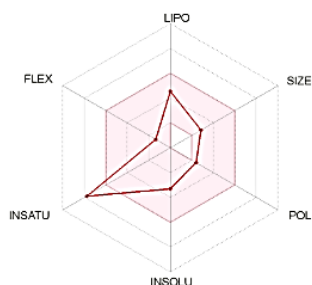
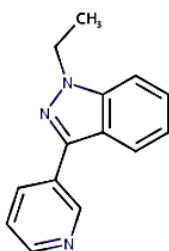
Druglikeness

Lipinski [?]	Yes; 0 violation
Ghose [?]	Yes
Veber [?]	Yes
Egan [?]	Yes
Muegge [?]	Yes
Bioavailability Score [?]	0.55

Medicinal Chemistry

PAINS [?]	0 alert
Brenk [?]	0 alert
Leadlikeness [?]	No; 1 violation: XLOGP3>3.5
Synthetic accessibility [?]	2.61

C4.6

SMILES CCn1nc(c2c1cccc2)c1cccn1

Physicochemical Properties

Formula	C14H13N3
Molecular weight	223.27 g/mol
Num. heavy atoms	17
Num. arom. heavy atoms	15
Fraction Csp3	0.14
Num. rotatable bonds	2
Num. H-bond acceptors	2
Num. H-bond donors	0
Molar Refractivity	69.03
TPSA [?]	30.71 Å ²

Lipophilicity

Log $P_{o/w}$ (iLOGP) [?]	2.33
Log $P_{o/w}$ (XLOGP3) [?]	2.46
Log $P_{o/w}$ (WLOGP) [?]	3.12
Log $P_{o/w}$ (MLOGP) [?]	2.06
Log $P_{o/w}$ (SILICOS-IT) [?]	2.81
Consensus Log $P_{o/w}$ [?]	2.56

Water Solubility

Log S (ESOL) [?]	-3.30
Solubility	1.13e-01 mg/ml ; 5.07e-04 mol/l
Class [?]	Soluble
Log S (Ali) [?]	-2.75
Solubility	3.98e-01 mg/ml ; 1.78e-03 mol/l
Class [?]	Soluble
Log S (SILICOS-IT) [?]	-5.03
Solubility	2.09e-03 mg/ml ; 9.35e-06 mol/l
Class [?]	Moderately soluble

Pharmacokinetics

GI absorption [?]	High
BBB permeant [?]	Yes
P-gp substrate [?]	Yes
CYP1A2 inhibitor [?]	Yes
CYP2C19 inhibitor [?]	Yes
CYP2C9 inhibitor [?]	No
CYP2D6 inhibitor [?]	Yes
CYP3A4 inhibitor [?]	Yes
Log K_p (skin permeation) [?]	-5.92 cm/s

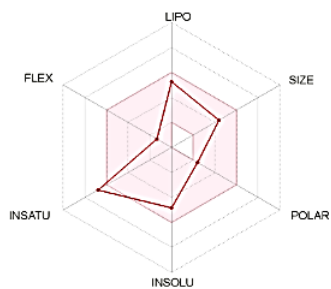
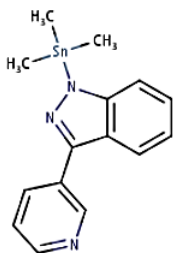
Druglikeness

Lipinski [?]	Yes; 0 violation
Ghose [?]	Yes
Veber [?]	Yes
Egan [?]	Yes
Muegge [?]	Yes
Bioavailability Score [?]	0.55

Medicinal Chemistry

PAINS [?]	0 alert
Brenk [?]	0 alert
Leadlikeness [?]	No; 1 violation: MW<250
Synthetic accessibility [?]	2.29

C4.7

SMILES C[Sn](n1nc(c2c1cccc2)c1cccnc1)(C)C

Physicochemical Properties

Formula	C15H17N3Sn
Molecular weight	358.02 g/mol
Num. heavy atoms	19
Num. arom. heavy atoms	15
Fraction Csp3	0.20
Num. rotatable bonds	2
Num. H-bond acceptors	2
Num. H-bond donors	0
Molar Refractivity	81.71
TPSA [?]	30.71 Å ²

Lipophilicity

Log $P_{o/w}$ (iLOGP) [?]	0.00
Log $P_{o/w}$ (XLOGP3) [?]	3.69
Log $P_{o/w}$ (WLOGP) [?]	3.78
Log $P_{o/w}$ (MLOGP) [?]	2.32
Log $P_{o/w}$ (SILICOS-IT) [?]	2.22
Consensus Log $P_{o/w}$ [?]	2.40

Water Solubility

Log S (ESOL) [?]	-4.84
Solubility	5.22e-03 mg/ml ; 1.46e-05 mol/l
Class [?]	Moderately soluble
Log S (All) [?]	-4.03
Solubility	3.38e-02 mg/ml ; 9.44e-05 mol/l
Class [?]	Moderately soluble
Log S (SILICOS-IT) [?]	-5.76
Solubility	6.18e-04 mg/ml ; 1.73e-06 mol/l
Class [?]	Moderately soluble

Pharmacokinetics

GI absorption [?]	High
BBB permeant [?]	Yes
P-gp substrate [?]	Yes
CYP1A2 inhibitor [?]	Yes
CYP2C19 inhibitor [?]	No
CYP2C9 inhibitor [?]	No
CYP2D6 inhibitor [?]	Yes
CYP3A4 inhibitor [?]	Yes
Log K_p (skin permeation) [?]	-5.86 cm/s

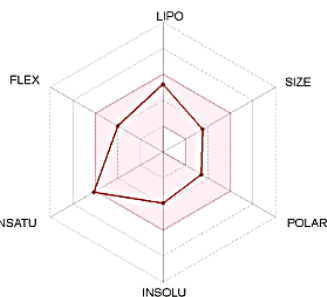
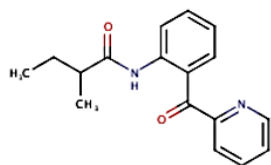
Druglikeness

Lipinski [?]	Yes; 0 violation
Ghose [?]	Yes
Veber [?]	Yes
Egan [?]	Yes
Muegge [?]	Yes
Bioavailability Score [?]	0.55

Medicinal Chemistry

PAINS [?]	0 alert
Brenk [?]	0 alert
Leadlikeness [?]	No; 2 violations: MW>350, XLOGP3>3.5
Synthetic accessibility [?]	3.10

C5.1

SMILES CCC(C(=O)Nc1ccccc1C(=O)c1ccccc1)C

Physicochemical Properties

Formula	C17H18N2O2
Molecular weight	282.34 g/mol
Num. heavy atoms	21
Num. arom. heavy atoms	12
Fraction Csp3	0.24
Num. rotatable bonds	6
Num. H-bond acceptors	3
Num. H-bond donors	1
Molar Refractivity	82.85
TPSA	59.06 Å²

Lipophilicity

Log $P_{o/w}$ (ILOGP)	2.65
Log $P_{o/w}$ (XLOGP3)	3.66
Log $P_{o/w}$ (WLOGP)	3.11
Log $P_{o/w}$ (MLOGP)	1.56
Log $P_{o/w}$ (SILICOS-IT)	3.40
Consensus Log $P_{o/w}$	2.88

Water Solubility

Log S (ESOL)	-3.92
Solubility	3.37e-02 mg/ml ; 1.19e-04 mol/l
Class	Soluble
Log S (Ali)	-4.59
Solubility	7.27e-03 mg/ml ; 2.57e-05 mol/l
Class	Moderately soluble
Log S (SILICOS-IT)	-5.71
Solubility	5.44e-04 mg/ml ; 1.93e-06 mol/l
Class	Moderately soluble

Pharmacokinetics

GI absorption	High
BBB permeant	Yes
P-gp substrate	No
CYP1A2 inhibitor	Yes
CYP2C19 inhibitor	Yes
CYP2C9 inhibitor	Yes
CYP2D6 inhibitor	Yes
CYP3A4 inhibitor	No
Log K_p (skin permeation)	-5.42 cm/s

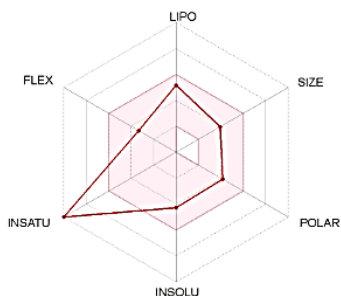
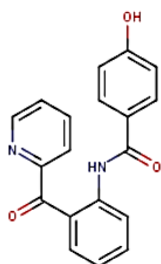
Druglikeness

Lipinski	Yes; 0 violation
Ghose	Yes
Veber	Yes
Egan	Yes
Muegge	Yes
Bioavailability Score	0.55

Medicinal Chemistry

PAINS	0 alert
Brenk	0 alert
Leadlikeness	No; 1 violation: XLOGP3>3.5
Synthetic accessibility	2.69

C5.2

SMILES Oc1ccc(cc1)C(=O)Nc1ccccc1C(=O)c1ccccc1

Physicochemical Properties

Formula	C19H14N2O3
Molecular weight	318.33 g/mol
Num. heavy atoms	24
Num. arom. heavy atoms	18
Fraction Csp3	0.00
Num. rotatable bonds	5
Num. H-bond acceptors	4
Num. H-bond donors	2
Molar Refractivity	90.35
TPSA	79.29 Å²

Lipophilicity

Log $P_{o/w}$ (ILOGP)	2.13
Log $P_{o/w}$ (XLOGP3)	3.56
Log $P_{o/w}$ (WLOGP)	3.08
Log $P_{o/w}$ (MLOGP)	1.51
Log $P_{o/w}$ (SILICOS-IT)	3.06
Consensus Log $P_{o/w}$	2.67

Water Solubility

Log S (ESOL)	-4.28
Solubility	1.67e-02 mg/ml ; 5.23e-05 mol/l
Class	Moderately soluble
Log S (Ali)	-4.91
Solubility	3.91e-03 mg/ml ; 1.23e-05 mol/l
Class	Moderately soluble
Log S (SILICOS-IT)	-6.41
Solubility	1.23e-04 mg/ml ; 3.86e-07 mol/l
Class	Poorly soluble

Pharmacokinetics

GI absorption	High
BBB permeant	No
P-gp substrate	No
CYP1A2 inhibitor	Yes
CYP2C19 inhibitor	Yes
CYP2C9 inhibitor	Yes
CYP2D6 inhibitor	Yes
CYP3A4 inhibitor	Yes
Log K_p (skin permeation)	-5.71 cm/s

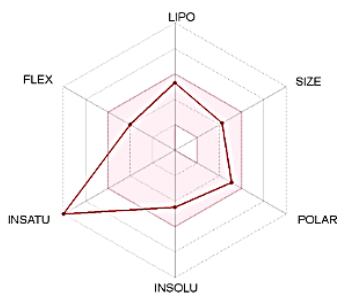
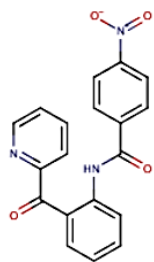
Druglikeness

Lipinski	Yes; 0 violation
Ghose	Yes
Veber	Yes
Egan	Yes
Muegge	Yes
Bioavailability Score	0.55

Medicinal Chemistry

PAINS	0 alert
Brenk	0 alert
Leadlikeness	No; 1 violation: XLOGP3>3.5
Synthetic accessibility	2.23

C5.3



SMILES O=C(c1ccc(cc1)[N+](=O)[O-])Nc1cccc1C(=O)c1cccn1

Physicochemical Properties

Formula	C19H13N3O4
Molecular weight	347.32 g/mol
Num. heavy atoms	26
Num. arom. heavy atoms	18
Fraction Csp3	0.00
Num. rotatable bonds	6
Num. H-bond acceptors	5
Num. H-bond donors	1
Molar Refractivity	97.15
TPSA [?]	104.88 Å ²

Lipophilicity

Log $P_{o/w}$ (iLOGP) [?]	2.36
Log $P_{o/w}$ (XLOGP3) [?]	3.74
Log $P_{o/w}$ (WLOGP) [?]	3.28
Log $P_{o/w}$ (MLOGP) [?]	1.92
Log $P_{o/w}$ (SILICOS-IT) [?]	1.37
Consensus Log $P_{o/w}$ [?]	2.54

Water Solubility	
Log S (ESOL) [?]	-4.47
Solubility	1.19e-02 mg/ml ; 3.42e-05 mol/l
Class [?]	Moderately soluble
Log S (Alli) [?]	-5.63
Solubility	8.05e-04 mg/ml ; 2.32e-06 mol/l
Class [?]	Moderately soluble
Log S (SILICOS-IT) [?]	-6.35
Solubility	1.55e-04 mg/ml ; 4.47e-07 mol/l
Class [?]	Poorly soluble

Pharmacokinetics

GI absorption [?]	High
BBB permeant [?]	No
P-gp substrate [?]	No
CYP1A2 inhibitor [?]	Yes
CYP2C19 inhibitor [?]	Yes
CYP2C9 inhibitor [?]	Yes
CYP2D6 inhibitor [?]	No
CYP3A4 inhibitor [?]	No
Log K_p (skin permeation) [?]	-5.76 cm/s

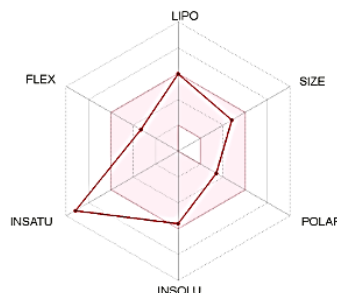
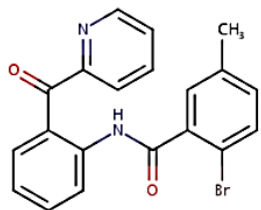
Druglikeness

Lipinski [?]	Yes; 0 violation
Ghose [?]	Yes
Veber [?]	Yes
Egan [?]	Yes
Muegge [?]	Yes
Bioavailability Score [?]	0.55

Medicinal Chemistry

PAINS [?]	0 alert
Brenk [?]	2 alerts: nitro_group, oxygen-nitrogen_single_bond [?]
Leadlikeness [?]	No; 1 violation: XLOGP3>3.5
Synthetic accessibility [?]	2.49

C5.4



SMILES Cc1ccc(c(c1)C(=O)Nc1cccc1C(=O)c1cccn1)Br

Physicochemical Properties

Formula	C20H15BrN2O2
Molecular weight	395.25 g/mol
Num. heavy atoms	25
Num. arom. heavy atoms	18
Fraction Csp3	0.05
Num. rotatable bonds	5
Num. H-bond acceptors	3
Num. H-bond donors	1
Molar Refractivity	100.99
TPSA [?]	59.06 Å ²

Lipophilicity

Log $P_{o/w}$ (iLOGP) [?]	3.28
Log $P_{o/w}$ (XLOGP3) [?]	4.97
Log $P_{o/w}$ (WLOGP) [?]	4.45
Log $P_{o/w}$ (MLOGP) [?]	2.90
Log $P_{o/w}$ (SILICOS-IT) [?]	4.73
Consensus Log $P_{o/w}$ [?]	4.06

Water Solubility	
Log S (ESOL) [?]	-5.62
Solubility	9.38e-04 mg/ml ; 2.37e-06 mol/l
Class [?]	Moderately soluble
Log S (Alli) [?]	-5.95
Solubility	4.45e-04 mg/ml ; 1.13e-06 mol/l
Class [?]	Moderately soluble
Log S (SILICOS-IT) [?]	-8.17
Solubility	2.65e-06 mg/ml ; 6.71e-09 mol/l
Class [?]	Poorly soluble

Pharmacokinetics

GI absorption [?]	High
BBB permeant [?]	Yes
P-gp substrate [?]	No
CYP1A2 inhibitor [?]	Yes
CYP2C19 inhibitor [?]	Yes
CYP2C9 inhibitor [?]	Yes
CYP2D6 inhibitor [?]	No
CYP3A4 inhibitor [?]	Yes
Log K_p (skin permeation) [?]	-5.18 cm/s

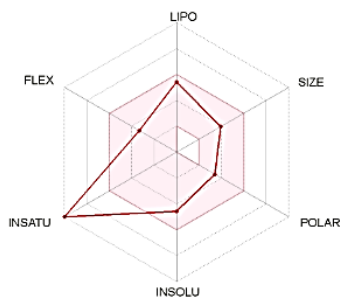
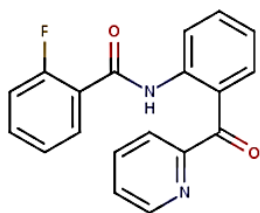
Druglikeness

Lipinski [?]	Yes; 0 violation
Ghose [?]	Yes
Veber [?]	Yes
Egan [?]	Yes
Muegge [?]	Yes
Bioavailability Score [?]	0.55

Medicinal Chemistry

PAINS [?]	0 alert
Brenk [?]	0 alert
Leadlikeness [?]	No; 2 violations: MW>350, XLOGP3>3.5
Synthetic accessibility [?]	2.49

C5.5



SMILES O=C(c1cccc1F)Nc1cccc1C(=O)c1ccccn1

Physicochemical Properties

Formula	C ₁₉ H ₁₃ FN ₂ O ₂
Molecular weight	320.32 g/mol
Num. heavy atoms	24
Num. arom. heavy atoms	18
Fraction Csp ³	0.00
Num. rotatable bonds	5
Num. H-bond acceptors	4
Num. H-bond donors	1
Molar Refractivity	88.28
TPSA	59.06 Å ²

Lipophilicity

Log <i>P</i> _{ow} (iLOGP)	2.41
Log <i>P</i> _{ow} (XLOGP3)	4.01
Log <i>P</i> _{ow} (WLOGP)	3.93
Log <i>P</i> _{ow} (MLOGP)	2.45
Log <i>P</i> _{ow} (SILICOS-IT)	3.96
Consensus Log <i>P</i> _{ow}	3.35

Water Solubility	
Log S (ESOL)	-4.58
Solubility	8.48e-03 mg/ml ; 2.65e-05 mol/l
Class	Moderately soluble
Log S (Ali)	-4.95
Solubility	3.57e-03 mg/ml ; 1.12e-05 mol/l
Class	Moderately soluble
Log S (SILICOS-IT)	-7.27
Solubility	1.74e-05 mg/ml ; 5.42e-08 mol/l
Class	Poorly soluble

Pharmacokinetics

GI absorption	High
BBB permeant	Yes
P-gp substrate	No
CYP1A2 inhibitor	Yes
CYP2C19 inhibitor	Yes
CYP2C9 inhibitor	Yes
CYP2D6 inhibitor	Yes
CYP3A4 inhibitor	Yes
Log <i>K</i> _p (skin permeation)	-5.41 cm/s

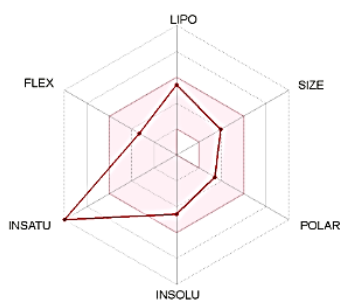
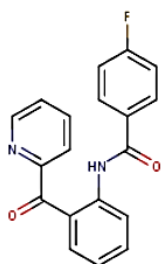
Druglikeness

Lipinski	Yes; 0 violation
Ghose	Yes
Veber	Yes
Egan	Yes
Muegge	Yes
Bioavailability Score	0.55

Medicinal Chemistry

PAINS	0 alert
Brenk	0 alert
Leadlikeness	No; 1 violation: XLOGP3>3.5
Synthetic accessibility	2.37

C5.6



SMILES Fc1ccc(cc1)C(=O)Nc1cccc1C(=O)c1ccccn1

Physicochemical Properties

Formula	C ₁₉ H ₁₃ FN ₂ O ₂
Molecular weight	320.32 g/mol
Num. heavy atoms	24
Num. arom. heavy atoms	18
Fraction Csp ³	0.00
Num. rotatable bonds	5
Num. H-bond acceptors	4
Num. H-bond donors	1
Molar Refractivity	88.28
TPSA	59.06 Å ²

Lipophilicity

Log <i>P</i> _{ow} (iLOGP)	2.28
Log <i>P</i> _{ow} (XLOGP3)	4.01
Log <i>P</i> _{ow} (WLOGP)	3.93
Log <i>P</i> _{ow} (MLOGP)	2.45
Log <i>P</i> _{ow} (SILICOS-IT)	3.96
Consensus Log <i>P</i> _{ow}	3.33

Water Solubility	
Log S (ESOL)	-4.58
Solubility	8.48e-03 mg/ml ; 2.65e-05 mol/l
Class	Moderately soluble
Log S (Ali)	-4.95
Solubility	3.57e-03 mg/ml ; 1.12e-05 mol/l
Class	Moderately soluble
Log S (SILICOS-IT)	-7.27
Solubility	1.74e-05 mg/ml ; 5.42e-08 mol/l
Class	Poorly soluble

Pharmacokinetics

GI absorption	High
BBB permeant	Yes
P-gp substrate	No
CYP1A2 inhibitor	Yes
CYP2C19 inhibitor	Yes
CYP2C9 inhibitor	Yes
CYP2D6 inhibitor	Yes
CYP3A4 inhibitor	Yes
Log <i>K</i> _p (skin permeation)	-5.41 cm/s

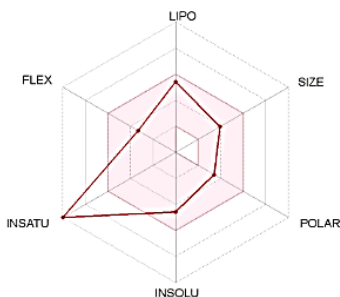
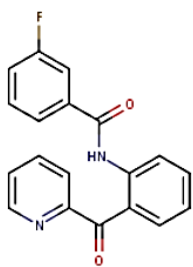
Druglikeness

Lipinski	Yes; 0 violation
Ghose	Yes
Veber	Yes
Egan	Yes
Muegge	Yes
Bioavailability Score	0.55

Medicinal Chemistry

PAINS	0 alert
Brenk	0 alert
Leadlikeness	No; 1 violation: XLOGP3>3.5
Synthetic accessibility	2.29

C5.7



SMILES Fc1cccc(c1)C(=O)Nc1cccc1C(=O)c1cccn1

Physicochemical Properties

Formula	C19H13FN2O2
Molecular weight	320.32 g/mol
Num. heavy atoms	24
Num. arom. heavy atoms	18
Fraction Csp3	0.00
Num. rotatable bonds	5
Num. H-bond acceptors	4
Num. H-bond donors	1
Molar Refractivity	88.28
TPSA	59.06 Å²

Lipophilicity

Log P_{ow} (ILOGP)	2.97
Log P_{ow} (XLOGP3)	4.01
Log P_{ow} (WLOGP)	3.93
Log P_{ow} (MLOGP)	2.45
Log P_{ow} (SILICOS-IT)	3.96
Consensus Log P_{ow}	3.47

Water Solubility	
Log S (ESOL)	-4.58
Solubility	8.48e-03 mg/ml ; 2.65e-05 mol/l
Class	Moderately soluble
Log S (Ali)	-4.95
Solubility	3.57e-03 mg/ml ; 1.12e-05 mol/l
Class	Moderately soluble
Log S (SILICOS-IT)	-7.27
Solubility	1.74e-05 mg/ml ; 5.42e-08 mol/l
Class	Poorly soluble

Pharmacokinetics

GI absorption	High
BBB permeant	Yes
P-gp substrate	No
CYP1A2 inhibitor	Yes
CYP2C19 inhibitor	Yes
CYP2C9 inhibitor	Yes
CYP2D6 inhibitor	Yes
CYP3A4 inhibitor	Yes
Log K_p (skin permeation)	-5.41 cm/s

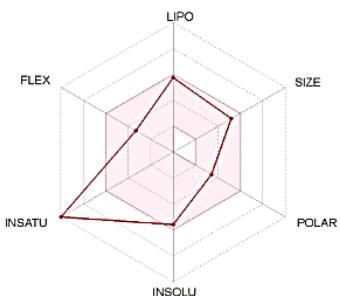
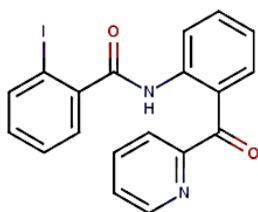
Druglikeness

Lipinski	Yes; 0 violation
Ghose	Yes
Veber	Yes
Egan	Yes
Muegge	Yes
Bioavailability Score	0.55

Medicinal Chemistry

PAINS	0 alert
Brenk	0 alert
Leadlikeness	No; 1 violation: XLOGP3>3.5
Synthetic accessibility	2.29

C5.8



SMILES O=C(c1cccc1I)Nc1cccc1C(=O)c1cccn1

Physicochemical Properties

Formula	C19H13IN2O2
Molecular weight	428.22 g/mol
Num. heavy atoms	24
Num. arom. heavy atoms	18
Fraction Csp3	0.00
Num. rotatable bonds	5
Num. H-bond acceptors	3
Num. H-bond donors	1
Molar Refractivity	101.04
TPSA	59.06 Å²

Lipophilicity

Log P_{ow} (ILOGP)	3.03
Log P_{ow} (XLOGP3)	4.56
Log P_{ow} (WLOGP)	3.98
Log P_{ow} (MLOGP)	2.79
Log P_{ow} (SILICOS-IT)	4.50
Consensus Log P_{ow}	3.77

Water Solubility	
Log S (ESOL)	-5.59
Solubility	1.09e-03 mg/ml ; 2.55e-06 mol/l
Class	Moderately soluble
Log S (Ali)	-5.52
Solubility	1.28e-03 mg/ml ; 3.00e-06 mol/l
Class	Moderately soluble
Log S (SILICOS-IT)	-7.85
Solubility	5.99e-06 mg/ml ; 1.40e-08 mol/l
Class	Poorly soluble

Pharmacokinetics

GI absorption	High
BBB permeant	Yes
P-gp substrate	No
CYP1A2 inhibitor	Yes
CYP2C19 inhibitor	Yes
CYP2C9 inhibitor	Yes
CYP2D6 inhibitor	Yes
CYP3A4 inhibitor	Yes
Log K_p (skin permeation)	-5.67 cm/s

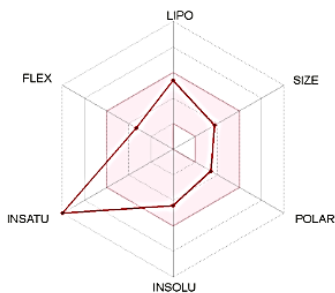
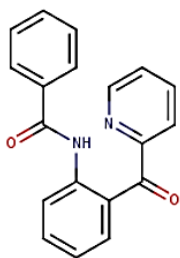
Druglikeness

Lipinski	Yes; 0 violation
Ghose	Yes
Veber	Yes
Egan	Yes
Muegge	Yes
Bioavailability Score	0.55

Medicinal Chemistry

PAINS	0 alert
Brenk	1 alert: iodine
Leadlikeness	No; 2 violations: MW>350, XLOGP3>3.5
Synthetic accessibility	2.47

C5.9

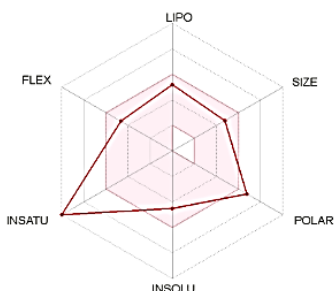
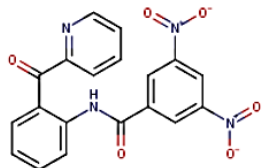


SMILES O=C(c1ccccc1)Nc1cccc1C(=O)c1ccccc1

Physicochemical Properties	
Formula	C ₁₉ H ₁₄ N ₂ O ₂
Molecular weight	302.33 g/mol
Num. heavy atoms	23
Num. arom. heavy atoms	18
Fraction Csp ³	0.00
Num. rotatable bonds	5
Num. H-bond acceptors	3
Num. H-bond donors	1
Molar Refractivity	88.33
TPSA	59.06 Å ²
Lipophilicity	
Log P _{ow} (ILOGP)	2.15
Log P _{ow} (XLOGP3)	3.91
Log P _{ow} (WLOGP)	3.37
Log P _{ow} (MLOGP)	2.07
Log P _{ow} (SILICOS-IT)	3.55
Consensus Log P _{ow}	3.01

Water Solubility	
Log S (ESOL)	-4.43
Solubility	1.13e-02 mg/ml ; 3.74e-05 mol/l
Class	Moderately soluble
Log S (All)	-4.85
Solubility	4.28e-03 mg/ml ; 1.42e-05 mol/l
Class	Moderately soluble
Log S (SILICOS-IT)	-7.00
Solubility	3.05e-05 mg/ml ; 1.01e-07 mol/l
Class	Poorly soluble
Pharmacokinetics	
GI absorption	High
BBB permeant	Yes
P-gp substrate	No
CYP1A2 inhibitor	Yes
CYP2C19 inhibitor	Yes
CYP2C9 inhibitor	Yes
CYP2D6 inhibitor	Yes
CYP3A4 inhibitor	Yes
Log K _p (skin permeation)	-5.37 cm/s
Druglikeness	
Lipinski	Yes; 0 violation
Ghose	Yes
Veber	Yes
Egan	Yes
Muegge	Yes
Bioavailability Score	0.55
Medicinal Chemistry	
PAINS	0 alert
Brenk	0 alert
Leadlikeness	No; 1 violation: XLOGP3>3.5
Synthetic accessibility	2.22

C5.10

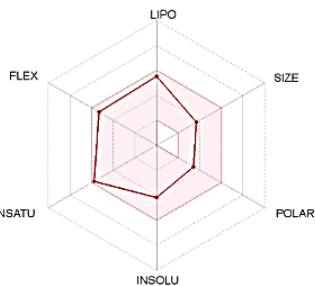
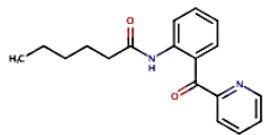


SMILES O=C(c1cc(ccc1)[N+](=O)[O-])[N+](=O)[O-]Nc1cccc1C(=O)c1ccccc1

Physicochemical Properties	
Formula	C ₁₉ H ₁₂ N ₄ O ₆
Molecular weight	392.32 g/mol
Num. heavy atoms	29
Num. arom. heavy atoms	18
Fraction Csp ³	0.00
Num. rotatable bonds	7
Num. H-bond acceptors	7
Num. H-bond donors	1
Molar Refractivity	105.97
TPSA	150.70 Å ²
Lipophilicity	
Log P _{ow} (ILOGP)	1.84
Log P _{ow} (XLOGP3)	3.57
Log P _{ow} (WLOGP)	3.19
Log P _{ow} (MLOGP)	1.07
Log P _{ow} (SILICOS-IT)	-0.78
Consensus Log P _{ow}	1.78

Water Solubility	
Log S (ESOL)	-4.52
Solubility	1.19e-02 mg/ml ; 3.03e-05 mol/l
Class	Moderately soluble
Log S (All)	-6.42
Solubility	1.49e-04 mg/ml ; 3.80e-07 mol/l
Class	Poorly soluble
Log S (SILICOS-IT)	-5.70
Solubility	7.90e-04 mg/ml ; 2.01e-06 mol/l
Class	Moderately soluble
Pharmacokinetics	
GI absorption	Low
BBB permeant	No
P-gp substrate	No
CYP1A2 inhibitor	No
CYP2C19 inhibitor	Yes
CYP2C9 inhibitor	Yes
CYP2D6 inhibitor	No
CYP3A4 inhibitor	Yes
Log K _p (skin permeation)	-6.16 cm/s
Druglikeness	
Lipinski	Yes; 0 violation
Ghose	Yes
Veber	No; 1 violation: TPSA>140
Egan	No; 1 violation: TPSA>131.6
Muegge	No; 1 violation: TPSA>150
Bioavailability Score	0.55
Medicinal Chemistry	
PAINS	0 alert
Brenk	2 alerts: nitro_group, oxygen-nitrogen_single_bond
Leadlikeness	No; 2 violations: MW>350, XLOGP3>3.5
Synthetic accessibility	2.83

C5.11

SMILES CCCCC(=O)Nc1cccc1C(=O)c1cccc1

Physicochemical Properties

Formula	C18H20N2O2
Molecular weight	296.36 g/mol
Num. heavy atoms	22
Num. arom. heavy atoms	12
Fraction Csp3	0.28
Num. rotatable bonds	8
Num. H-bond acceptors	3
Num. H-bond donors	1
Molar Refractivity	87.65
TPSA	59.06 Å ²

Lipophilicity

Log $P_{o/w}$ (iLOGP)	2.74
Log $P_{o/w}$ (XLOGP3)	4.17
Log $P_{o/w}$ (WLOGP)	3.64
Log $P_{o/w}$ (MLOGP)	1.79
Log $P_{o/w}$ (SILICOS-IT)	3.97
Consensus Log $P_{o/w}$	3.26

Water Solubility	
Log S (ESOL)	-4.18
Solubility	1.96e-02 mg/ml ; 6.60e-05 mol/l
Class	Moderately soluble
Log S (All)	-5.12
Solubility	2.26e-03 mg/ml ; 7.61e-06 mol/l
Class	Moderately soluble
Log S (SILICOS-IT)	-6.49
Solubility	9.63e-05 mg/ml ; 3.25e-07 mol/l
Class	Poorly soluble

Pharmacokinetics	
GI absorption	High
BBB permeant	Yes
P-gp substrate	No
CYP1A2 inhibitor	Yes
CYP2C19 inhibitor	Yes
CYP2C9 inhibitor	Yes
CYP2D6 inhibitor	Yes
CYP3A4 inhibitor	Yes
Log K_p (skin permeation)	-5.15 cm/s

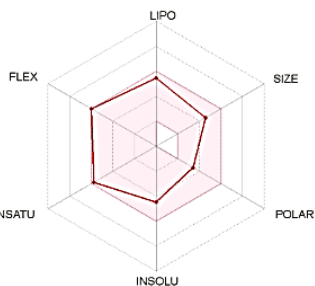
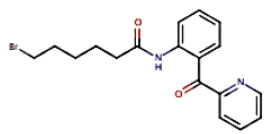
Druglikeness

Lipinski	Yes; 0 violation
Ghose	Yes
Veber	Yes
Egan	Yes
Muegge	Yes
Bioavailability Score	0.55

Medicinal Chemistry

PAINS	0 alert
Brenk	0 alert
Leadlikeness	No; 2 violations: Rotors>7, XLOGP3>3.5
Synthetic accessibility	2.36

C5.12

SMILES BrCCCCC(=O)Nc1cccc1C(=O)c1cccc1

Physicochemical Properties

Formula	C18H19BrN2O2
Molecular weight	375.26 g/mol
Num. heavy atoms	23
Num. arom. heavy atoms	12
Fraction Csp3	0.28
Num. rotatable bonds	9
Num. H-bond acceptors	3
Num. H-bond donors	1
Molar Refractivity	95.52
TPSA	59.06 Å ²

Lipophilicity

Log $P_{o/w}$ (iLOGP)	3.12
Log $P_{o/w}$ (XLOGP3)	4.02
Log $P_{o/w}$ (WLOGP)	4.02
Log $P_{o/w}$ (MLOGP)	2.14
Log $P_{o/w}$ (SILICOS-IT)	4.52
Consensus Log $P_{o/w}$	3.56

Water Solubility	
Log S (ESOL)	-4.49
Solubility	1.21e-02 mg/ml ; 3.23e-05 mol/l
Class	Moderately soluble
Log S (All)	-4.96
Solubility	4.09e-03 mg/ml ; 1.09e-05 mol/l
Class	Moderately soluble
Log S (SILICOS-IT)	-7.31
Solubility	1.84e-05 mg/ml ; 4.91e-08 mol/l
Class	Poorly soluble

Pharmacokinetics	
GI absorption	High
BBB permeant	Yes
P-gp substrate	No
CYP1A2 inhibitor	Yes
CYP2C19 inhibitor	Yes
CYP2C9 inhibitor	Yes
CYP2D6 inhibitor	Yes
CYP3A4 inhibitor	Yes
Log K_p (skin permeation)	-5.73 cm/s

Druglikeness

Lipinski	Yes; 0 violation
Ghose	Yes
Veber	Yes
Egan	Yes
Muegge	Yes
Bioavailability Score	0.55

Medicinal Chemistry

PAINS	0 alert
Brenk	1 alert: alkyl_halide
Leadlikeness	No; 3 violations: MW>350, Rotors>7, XLOGP3>3.5
Synthetic accessibility	2.57

Chapter 11

References



1. B.J. Harmer and M. Orrell, *What is meaningful activity for people with dementia living in care homes? A comparison of the views of older people with dementia, staff and family carers*. *Aging & Mental Health*, 2008. **12**(5): p. 548 - 558.
2. Z. Liu, A. Zhang, H. Sun, Y. Han, L. Konga, and X. Wang, *Two decades of new drug discovery and development for Alzheimer's disease*. *Royal Society of Chemistry Advances*, 2017. **7**(10): p. 6046-6058.
3. D.H. Small and R. Cappai, *Alois Alzheimer and alzheimer's disease: a centennial perspective*. *Journal of Neurochemistry*, 2006. **99**: p. 708-710.
4. Foundation, B. *Understanding your disease*. Quick facts about alzheimer's disease 2019 [cited 2020 11]; Available from: <https://www.brightfocus.org/alzheimers/information>.
5. B.M. McGleenon, K.B. Dynan, and A.P. Passmore, *Acetylcholinesterase inhibitors in alzheimer's disease*. *British Journal of Clinical Pharmacology*, 1999.
6. H. Sugimoto, Y.Y., Y. Limura, and Y. Kawakami, *Donepezil hydrochloride (E2020) and other acetylcholinesterase inhibitors*. *Current Medicinal Chemistry*, 2000. **7**: p. 303-338.
7. N.R. Sims, D.M.B., S.J. Allen, C.C.T. Smith, D. Neary, T.D.J. Thomas, and A.N. Davison, *Presynaptic cholinergic dysfunction in patients with dementia*. *Journal of Neurochemistry*, 1983. **40**(2): p. 503-508.
8. Bachurin, S.O., *Medicinal chemistry approaches for the treatment and prevention of alzheimer's disease*. *Medicinal Research Reviews*, 2003. **23**: p. 48-88.
9. P.T. Francis, A. Nordberg, and S.E. Arnold, *A preclinical view of cholinesterase inhibitors in neuroprotection: do they provide more than symptomatic benefits in alzheimer's disease?* *Trends in Pharmacological Sciences*, 2005. **26**(2): p. 54-61.
10. Ellison, J.M., *The history of alzheimer's disease*. Brightfocus Foundation, 2018.
11. M.B. Graeber, S.K., R. Egensperger, R.B. Banati, U. Muller, K. Bise, P. Hoff, H.J. Moller, K. Fujisawa, and P. Mehraein, *Rediscovery of the case described by Alois Alzheimer in 1911: historical, histological and molecular genetic analysis*. *Neurogenetics*, 1997. **1**(1): p. 73-80.
12. Ellison, J.M. *Alzheimer's birthday: celebrating the legacy of a great physician and researcher*. 2016 [cited 2020 11]; Available from: <https://www.brightfocus.org/alzheimers/article/alzheimers-birthday-celebrating-legacy-great-physician-and-researcher>.
13. D. Selkoe and J. Hardy, *The amyloid hypothesis of alzheimer's disease at 25 years*. *EMBO Molecular Medicine*, 2016. **8**(6): p. 595-608.
14. R.J. Bateman, C.X., T.L.S. Benzinger, A.M. Fagan, A. Goate, N.C. Fox, D.S. Marcus, N.J. Cairns, X. Xie, T.M. Blazey, D.M. Holtzman, A. Santacruz, V. Buckles, A. Oliver, K. Moulder, P.S. Aisen, B. Ghetti, W.E. Klunk, E. McDade, R.N. Martins, C.L. Masters, R. Mayeux, J.M. Ringman, M.N. Rossor, P.R. Schofield, R.A. Sperling, S. Salloway, J.C. Morris, *Clinical and biomarker changes in dominantly inherited alzheimer's disease*. *The New England Journal of Medicine*, 2012. **367**(9): p. 795-802.
15. Schneider, L.S., *Chapter 2 - Issues in design and conduct of clinical trials for cognitive-enhancing drugs*, in *Animal and Translational Models For CNS Drug Discovery*. 2008, University of Southern California, Los Angeles. p. 21-76.
16. C.J. Camp and K.S. Judge, *Chapter 20 - Cognitive assessment in late stage dementia*, in *Handbook of assessment in clinical gerontology*. 2010. p. 531-555.
17. Molloy, D.W., *Standardised mini-mental state examination (SMMSE) - guidelines for administration and scoring instructions*. 2014, Independent Hospital Pricing Authority. p. 1-11.
18. G. McKhann, D.D., M. Folstein, R. Katzman, D. Price, E.M. Stadlan, *Clinical diagnosis of alzheimer's disease: report of the NINCDS-ADRDA work group under the auspices of department of health and human services task force on alzheimer's disease*. *Neurology*, 1984. **34**: p. 939-944.
19. S.D. Santia, M.J.d.L., H. Rusinek, A. Convita, C.Y. Tarshisha, A. Rochea, W.H. Tsuic, E. Kandila, M. Boppanaa, K. Daisleya, G.J. Wangd, D. Schlyere, J. Fowler, *Hippocampal formation glucose metabolism and volume losses in MCI and AD*. *Neurobiology of Aging*, 2001. **22**: p. 529-539.
20. Leung, K. *[18F] Fluoro-2-deoxy-2-D-glucose*. 2005; January 12 2005:[1-8]. Available from: https://www.ncbi.nlm.nih.gov/books/NBK23335/pdf/Bookshelf_NBK23335.pdf.
21. S. Minoshima, N.L.F., A.A.F. Sima, K.A. Frey, R.L. Albin, D.E. Kuhl, *Alzheimer's disease versus dementia with lewy bodies: cerebral metabolic distinction with autopsy confirmation*. *Annals of Neurology: Official Journal of the American Neurological Association and the Child Neurology Society*, 2001. **50**(3): p. 3-8.
22. P.T. Francis, A.M.P., M. Snape, G.K. Wilcock, *The cholinergic hypothesis of alzheimer's disease: a review of progress*. *Journal of Neurology, Neurosurgery & Psychiatry*, 1999. **66**: p. 137-147.

23. M.B. Colovic, D.Z.K., T.D. Lazarevic-Pasti, A.M. Bondzic, V.M. Vasic, *Acetylcholinesterase inhibitors: pharmacology and toxicology*. Current Neuropharmacology, 2013. **11**: p. 315-335.
24. Cummings, J.L., *Cholinesterase inhibitors: a new class of psychotropic compounds*. American Journal of Psychiatry, 2000. **157**: p. 4-15.
25. E. Perry, M.W., J. Grace, R. Perry, *Acetylcholine in mind a neurotransmitter correlate of consciousness*. Trends In Neurosciences, 1999. **22**: p. 273-280.
26. Weinstock, M., *The pharmacotherapy of Alzheimer's disease based on the cholinergic hypothesis: an update*. Neurodegeneration, 1995. **4**(4): p. 349-356.
27. Cottage, M.L. *How the brain changes during alzheimer's disease*. 2015 15/11/2020 [cited 2020 11]; Available from: <http://memorylanecottage.com/about-alzheimers-and-dementia/how-the-brain-changes-during-alzheimers-disease/>.
28. Yakel, J.L., *Cholinergic receptors: functional role of nicotinic ACh receptors in brain circuits and disease*. Pflügers Archiv-European Journal of Physiology, 2013. **465**(4): p. 441-450.
29. D. Voet and J.G. Voet, *Biochemistry fourth edition*. John Wiley & sons. inc.
30. G.G. Glenner and C.W. Wong, *Alzheimer's disease initial report of the purification and characterization of a novel cerebrovascular amyloid protein*. Biochemical and Biophysical Research Communications, 1984. **120**(3): p. 885-890.
31. Foundation, B. *Amyloid plaques and neurofibrillary tangles*. 2015 [cited 2020 11]; Available from: <https://www.brightfocus.org/alzheimers-disease/infographic/amyloid-plaques-and-neurofibrillary-tangles>.
32. C.J. Pike, A.J. Walencewicz-Wasserman, J. Kosmoski, D.H. Cribbs, C.G. Glabe, and C.W. Cotman, *Structure-activity analyses of β -amyloid peptides: contributions of the 625–35 region to aggregation and neurotoxicity*. Journal of Neurochemistry, 1995. **64**(1).
33. P.A. Adlard, R.A. Cherny, D.I. Finkelstein, E. Gautier, E. Robb, M. Cortes, I. Volitakis, X. Liu, J.P. Smith, K. Perez, K. Laughton, Q.X. Li, S.A. Charman, J.A. Nicolazzo, S. Wilkins, K. Deleva, T. Lynch, G. Kok, C.W. Ritchie, R.E. Tanzi, R. Cappai, C.L. Masters, K.J. Barnham, and A.I. Bush, *Rapid restoration of cognition in alzheimer's transgenic mice with 8-hydroxy quinoline analogs is associated with decreased interstitial A β* . Neuron, 2008. **59**(1): p. 43-55.
34. P.A. Adlard, A. Sedjahtera, L. Gunawan, L. Bray, D. Hare, J. Lear, P. Doble, A.I. Bush, D.I. Finkelstein, and R.A. Cherny, *A novel approach to rapidly prevent age-related cognitive decline*. Aging Cell, 2013. **13**(2): p. 351.
35. L. Lannfelt, K. Blennow, H. Zetterberg, S. Batsman, D. Ames, J. Harrison, C.L. Masters, S. Targum, A.I. Bush, R. Murdoch, J. Wilson, and C.W. Ritchie, *Safety, efficacy, and biomarker findings of PBT2 in targeting abeta as a modifying therapy for alzheimer's disease: a phase IIa, double-blind, randomised, placebo-controlled trial*. The Lancet Neurology, 2008. **7**(9): p. 779-786.
36. G.B. Freeman, J.C. Lin, J. Pons, and N.M. Raha, *39-week toxicity and toxicokinetic study of ponezumab (PF-04360365) in cynomolgus monkeys with 12-week recovery period*. Journal of Alzheimer's Disease, 2012. **28**(3): p. 531.
37. I. Miyoshi, Y. Fujimoto, M. Yamada, S. Abe, Q. Zhao, C. Cronenberger, K. Togo, T. Ishibashi, M.M. Bednar, J.W. Kupiec, and B. Binneman, *Safety and pharmacokinetics of PF-04360365 following a single-dose intravenous infusion in Japanese subjects with mild-to-moderate alzheimer's disease: a multicenter, randomized, double-blind, placebo-controlled, dose-escalation study*. International Journal of Clinical Pharmacology and Therapeutics, 2013. **51**(12): p. 911.
38. K.R. Brunden, J.Q. Trojanowski, and V.M.Y. Lee, *Advances in tau-focused drug discovery for Alzheimer's disease and related tauopathies*. Nature Reviews Drug discovery, 2009. **8**(10): p. 783-793.
39. K. Iqbal, A.D.C. Alonso, S. Chen, M.O. Chohan, E. El-Akkad, C-X. Gong, S. Khatoon, B. Li, F. Liu, A. Rahman, H. Tanimukai, and I. Grundke-Iqbal, *Tau pathology in Alzheimer disease and other tauopathies*. Biochimica et Biophysica Acta - Molecular Basis of Disease, 2005: p. 198-210.
40. C.L. Masters, G. Simms, N.A. Weinman, G. Multhaup, B.L. McDonald, and K. Beyreuther, *Amyloid plaque core protein in Alzheimer disease and down syndrome*. Proceedings of the National Academy of Sciences, 1985. **82**: p. 4254-4249.
41. M. Pickhardt, Z. Gazova, M. von Bergen, I. Khlistunova, Y. Wang, A. Hascher, E. Mandelkow, J. Biernat, and E. Mandelkow, *Anthraquinones inhibit tau aggregation and dissolve Alzheimer's paired helical filaments in vitro and in cells*. Journal of Biological Chemistry, 2005. **280**(5): p. 3628-3635.

42. U. Escher, E. Giladi, I.R. Dunay, S. Bereswill, I. Gozes, and M.M. Heimesaat, *Anti-inflammatory effects of the octapeptide NAP in human microbiota-associated mice suffering from subacute ileitis*. *European Journal of Microbiology and Immunology*, 2018. **8**(2): p. 34-40.
43. T. Kramer, B. Schmidt, and F.L. Monte, *Small-molecule inhibitors of GSK-3: structural insights and their application to Alzheimer's disease models*. *International Journal of Alzheimer's Disease*, 2012: p. 32.
44. G. Armagan, A. Keser, C. Atalayin, and T. Dagci, *Tideglusib protects neural stem cells against NMDA receptor overactivation*. *Pharmacological Reports*, 2015. **67**(5): p. 823-831.
45. C.J. Phiel, C.A. Wilson, V.M. Lee, and P.S. Klein, *GSK-3 α regulates production of Alzheimer's disease amyloid- β peptides*. *Nature*, 2003. **22**: p. 435-439.
46. P. Anand and B. Singh, *A review on cholinesterase inhibitors for alzheimer's disease*. *Archives of Pharmacal Research*, 2013. **36**: p. 375-399.
47. P. Zatta, D. Drago, S. Bolognin, and S.L. Sensi, *Alzheimer's disease, metal ions and metal homeostatic therapy*. *Trends in Pharmacological Sciences*, 2009. **30**(7).
48. L.M. Sayre, P.I.M., M.A. Smith, G. Perry, *Metal ions and oxidative protein modification in neurological disease*. *Annali dell'Istituto Superiore di Sanità*, 2005. **41**: p. 143-165.
49. Ashley, I.B., *The metallobiology of Alzheimer's disease*. *Trends in Neurosciences*, 2003. **26**(4): p. 207-214.
50. Andersen, J.K., *Oxidative stress in neurodegeneration: cause or consequence?* *Nature Medicine*, 2004. **10 Suppl**: p. S18-25.
51. A.I. Bush and R.E. Tanzi, *Therapeutics for Alzheimer's disease based on the metal hypothesis*. *Neurotherapeutics*, 2008. **5**: p. 421-432.
52. Butterfield, D.A., *Amyloid β -peptide (1-42)-induced oxidative stress and neurotoxicity: implications for neurodegeneration in Alzheimer's disease brain*. *Free Radical Research*, 2002. **36**(12): p. 1307-13.
53. T. Grune, T. Reinheckel, and K.J. Davies, *Degradation of oxidized proteins in mammalian cells*. *The FASEB Journal*, 1997.
54. Tabet, N., *Acetylcholinesterase inhibitors for alzheimer's disease: anti-inflammatories in acetylcholine clothing!* *Age and Ageing*, 2006.
55. R.G. Cutler, J.K., K. Storie, W.A. Pedersen, A. Tammara, K. Hatanpaa, J.C. Troncoso, M.P. Mattson, *Involvement of oxidative stress-induced abnormalities in ceramide and cholesterol metabolism in brain aging and alzheimer's disease*. *Proceedings of the National Academy of Sciences*, 2004. **101**(7): p. 2070-2075.
56. Castegna, A., V. Thongboonkerd, J.B. Klein, B. Lynn, W.R. Markesbery, and D.A. Butterfield, *Proteomic identification of nitrated proteins in Alzheimer's disease brain*. *Journal of Neurochemistry*, 2003. **85**(6): p. 1394-401.
57. H. Akiyama, S.B., S. Barnum, B. Bradt, J. Bauer, G.M. Cole, N.R. Cooper, P. Eikelenboom, M. Emmerling, B.L. Fiebich, C.E. Finch, S. Frautschy, W.S.T. Griffin, H. Hampel, M. Hull, G. Landreth, L. Lue, R. Mrak, I.R. Mackenzie, P.L. McGeer, M.K. O'Banion, J. Pachter, G. Pasinetti, C. Plata-Salaman, J. Rogers, R. Rydel, Y. Shen, W. Streit, R. Strohmeyer, I. Tooyoma, F.L. Van Muiswinkel, R. Veerhuis, D. Walker, S. Webster, B. Wegrzyniak, G. Wenk, T. Wyss-Coray, *Inflammation and Alzheimer's disease*. *Neurobiology of Aging*, 2000(21): p. 3.
58. M.E. Bamberger, G.E.L., *Inflammation, apoptosis and Alzheimer's disease*. *The Neuroscientist*, 2002. **8**(3): p. 2-8.
59. H.D. Venters, Q.T., Q. Liu, R.W. Vanhoy, R. Dantzer, K.W. Kelley, *A new mechanism of neurodegeneration: A proinflammatory cytokine inhibits receptor signaling by a survival peptide*. *Proceedings of the National Academy of Sciences*, 1999. **96**: p. 9879-9884.
60. L.J. Thal, S.H. Ferris, L. Kirby, G.A. Block, C.R. Lines, E. Yuen, C. Assaid, M.L. Nessly, B.A. Norman, C.C. Baranak, and S.A. Reines, *A randomized, double-blind, study of rofecoxib in patients with mild cognitive impairment*. *Neuropsychopharmacology* 2005. **30**: p. 1204-1215.
61. D. Olivares, V.K. Deshpande, Y. Shi, D.K. Lahiri, N.H. Greig, J.T. Rogers, and X. Huang, *N-methyl-D-aspartate (NMDA) receptor antagonists and memantine treatment for Alzheimer's disease, vascular dementia and parkinson's disease*. *Current Alzheimer Research*, 2012. **9**(6): p. 746-758.
62. W. Danysz, C.G.P., *The NMDA receptor antagonist memantine as a symptomatological and neuroprotective treatment for Alzheimer's disease: preclinical evidence*. *International Journal of Geriatric Psychiatry*, 2003. **18**: p. 23-32.
63. G. Johnson and S.W. Moore, *The peripheral anionic site of acetylcholinesterase: structure, functions and potential role in rational drug design*. *Current Pharmaceutical Design*, 2006. **12**: p. 217-225.

64. R.M. Lane, M. Kivipelto, and N.H. Greig, *Acetylcholinesterase and its inhibition in Alzheimer disease*. *Clinical Neuropharmacology*, 2004. **27**(3): p. 1-9.
65. Association, A.s. *FDA-approved drugs for Alzheimer's disease*. 2017 [cited 2020 11]; Available from: <https://www.alz.org/media/documents/fda-approved-treatments-alzheimers-ts.pdf>.
66. B. Borroni, F. Colciaghi, L. Pastorino, C. Pettenati, E. Cottini, L. Rozzini, R. Monastero, G.L. Lenzi, F. Cattabeni, M.D. Luca, and A. Padovani, *Amyloid precursor protein in platelets of patients with Alzheimer disease*. *Archives of Neurology*, 2001. **58**: p. 442-446.
67. M. Nanri, J. Yamamoto, H. Miyake, and H. Watanabe, *Protective effect of GTS-21, a novel nicotinic receptor agonist, on delayed neuronal death induced by ischemia in gerbils*. *The Japanese Journal of Pharmacology*, 1998. **76**: p. 23-29.
68. D.G. van Greunen, W. Cordier, M. Nell, C. van der Westhuyzen, V. Steenkamp, and D.L.R. J. Panayides, *Targeting Alzheimer's disease by investigating previously unexplored chemical space surrounding the cholinesterase inhibitor donepezil*. *European Journal of Medicinal Chemistry*, 2016: p. 1-20.
69. D.G van Greunen, C.J. van der Westhuizen, W. Cordier, M. Nell, A. Stander, V. Steenkamp, J. Panayides, and D.L. Riley, *Novel N-benzylpiperidine carboxamide derivatives as potential cholinesterase inhibitors for the treatment of alzheimer's disease*. *European Journal of Medicinal Chemistry*, 2019. **179**: p. 680-693.
70. W.F. Maragos, J.T. Greenamyre, J.B. Penney, and A.B. Young, *Glutamate dysfunction in Alzheimer's disease: an hypothesis*. *Trends in Neurosciences*, 1987. **10**: p. 65-68.
71. W. Danyasz, C.G. Parsons, J. Kornhuber, W.J. Schmidt, and G. Quack, *Aminoadamantanes as NMDA receptor antagonists and antiparkinsonian agents preclinical studies*. *Neuroscience & Biobehavioral Reviews*, 1997. **21**(4): p. 455-468.
72. T.M. Acker, A. Khatri, K.M. Vance, C. Slabber, J. Bacsá, J.P. Snyder, S.F. Traynelis, and D.C. Liotta, *Structure-activity relationships and pharmacophore model of a noncompetitive pyrazoline containing class of GluN2C/GluN2D selective antagonists*. *Journal of Medicinal Chemistry*, 2013. **56**: p. 6434-6456.
73. T.M. Acker, H.Y., K.B. Hansen, K.M. Vance, K.K. Ogden, H.S. Jensen, P.B. Burger, P. Mullasseril, J.P. Snyder, D.C. Liotta, S.F. Traynelis, *Mechanism for noncompetitive inhibition by novel GluN2C/D N-methyl-D-aspartate receptor subunit-selective modulators*. *Molecular Pharmacology*, 2011. **80**(5): p. 782-795.
74. A. Villalobos, J.F. Blake, C.K. Biggers, T.W. Butler, D.S. Chapin, Y.L. Chen, J.L. Ives, S.B. Jones, D.R. Liston, A.A. Nagel, D.M. Nason, J.A. Nielsen, I.A. Shalaby, and W.F. White, *Novel benzisoxazole derivatives as potent and selective inhibitors of acetylcholinesterase*. *Journal of Medicinal Chemistry*, 1994. **37**(17): p. 2721-2733.
75. A. Villalobos, T.W. Butler, D.S. Chapin, Y.L. Chen, S.B. DeMattos, J.L. Ives, S.B. Jones, D.R. Liston, A.A. Nagel, D.M. Nason, J.A. Nielsen, A.D. Ramirez, I.A. Shalaby, and W.F. White, *5,7-dihydro-3-[2-[1-(phenylmethyl)-4-piperidinyl]ethyl]-6H-pyrrolo[3,2-f]-1,2-benzisoxazol-6-one: a potent and centrally-selective inhibitor of acetylcholinesterase with an improved margin of safety*. *Journal of medicinal chemistry*, 1995. **38**(15): p. 2802-2807.
76. Gitay Kryger, I.S., Joel L Sussman, *Structure of acetylcholinesterase complexed with E2020 (Aricept): implications for the design of new anti-Alzheimer drugs*. *Science Direct*, 1999. **7**(3): p. 297-307.
77. press, S., *QikProp 3.5*, ed. U. manual. 2012: Schrödinger.
78. Lipinski, C.A., *Lead- and drug-like compounds: the rule-of-five revolution*. *Drug Discovery Today: Technologies*, 2004. **1**(4): p. 337 - 340.
79. A.K. Ghose, T.H., R.L. Hudkins, B.D. Dorsey, J.P. Mallamo, *Knowledge-based, central nervous system (CNS) lead selection and lead optimization for CNS drug discovery*. *ACS Chemical Neuroscience* 2012. **3**(1): p. 50-68.
80. Y.J. Chae, H.J. Lee, J.H. Jeon, I. Kim, J. Choi, K. Sung, and S.J. Hahn, *Effects of donepezil on hERG potassium channels*. *Brain Research*, 2015: p. 77-85.
81. A. Daina, O. Michielin, and V. Zoete, *SwissADME: a free web tool to evaluate pharmacokinetics, druglikeness and medicinal chemistry friendliness of small molecules*. *Scientific Reports*, 2017.
82. K.B. Lipkowitz and D.B. Boyd, *Reviews in Computational Chemistry 6*. Wiley-VCH. **11**(1): p. 242.
83. P. Ertl, B. Rohde, and P. Selzer, *Fast calculation of molecular polar surface area as a sum of fragment-based contributions and its application to the prediction of drug transport properties*. *Journal of Medicinal Chemistry*, 2000. **43**(20): p. 3714-3717.
84. G. Gilardi and G.D. Nardo, *Heme iron centers in cytochrome P450: Structure and catalytic activity*. *Rendiconti Lincei*, 2016. **28**: p. 159-167.
85. Guengerich, F.P., *Cytochrome P450 and chemical toxicology*. *Chemical Research in Toxicology*, 2008. **21**: p. 70-83.

86. A.E. Rettie and J.P. Jones, *Clinical and toxicological relevance of CYP2C9: drug-drug interactions and pharmacogenetics*. Annual Review of Pharmacology and Toxicology, 2005. **45**: p. 477-494.
87. S.E. Rau, J.R. Bend, J.M.O. Arnold, L.T. Tran, J.D. Spence, and D.G. Bailey, *Grapefruit juice-terfenadine single-dose interaction: magnitude, mechanism, and relevance*. Clinical Pharmacology & Therapeutics, 1995. **61**(4): p. 401-409.
88. N.R. Dunn, G.L. Pearce, and S.A.W. Shakir, *Adverse effects associated with the use of donepezil in general practice in England*. Journal of Psychopharmacology, 2000. **14**(4): p. 406-408.
89. Hunt, D.I., *The Claisen condensation. Chapter 21: Ester Enolates*. University of Calgary.
90. Jean-Mario Mussinu, S.R., Antonio C. Mule, Amedeo Pau, Mauro A. M. Carai, Giovanni Loriga, Gabriele Murineddu, and Ge' rard A. Pinna, *Tricyclic Pyrazoles. Part 1: Synthesis and biological evaluation of novel 1,4-dihydroindeno[1,2-c]pyrazol-based ligands for CB1 and CB2 cannabinoid receptors*. Pergamon Bioorganic & Medicinal Chemistry, 2003. **11**: p. 251-263.
91. S. Rosenberg, S. M. Silver, J. M. Sayer, and W.P. Jencks, *Evidence for two concurrent mechanisms and a kinetically significant proton transfer process in acid-catalyzed O-methyloxime formation*. Journal of the American Chemical Society, 1974. **96**(26): p. 7986-7998.
92. V. Andrzejak, G.G.M., M. Body-Malapel, J.E. Bakali, M. Djouina, N. Renault, P. Chavatte, P. Desreumaux, D.M. Lambert, R. Millet, *New FAAH inhibitors based on 3-carboxamido-5-aryl-isoxazole scaffold that protect against experimental colitis*. Bioorganic & Medicinal Chemistry, 2011. **19**: p. 3777-3786.
93. R.P. Clausen, P. Naur, A.S. Kristensen, J.R. Greenwood, M. Strange, H. Brauner-Osborne, A.A. Jensen, A.S.T. Nielsen, U. Geneser, L.M. Ringgaard, B. Nielsen, D.S. Pickering, L. Brehm, M. Gajhede, P. Krogsgaard-Larsen, and J.S. Kastrop, *The glutamate receptor GluR5 agonist (S)-2-amino-3-(3-hydroxy-7,8-dihydro-6H-cyclohepta[d]isoxazol-4-yl)propionic acid and the 8-methyl analogue: synthesis, molecular pharmacology, and biostructural characterization*. Journal of medicinal chemistry, 2009. **52**: p. 4911-4922.
94. Pushpak Mizar, A.L., Mohammad El-Sherbini, Umar Farid, Michael Brown, and a.T.W. Florence Malmedy, *Enantioselective diamination with novel chiral hypervalent iodine catalysts*. Chemistry (Weinheim an der Bergstrasse, Germany), 2014. **20**(32): p. 9910.
95. W.E. Parham and C.K. Bradsher, *Aromatic organolithium reagents bearing electrophilic groups. Preparation by halogen-lithium exchange*. Accounts of Chemical Research, 1982. **15**(10): p. 300-305.
96. Smith, J.G., *Organic Chemistry third edition*. Vol. 3. McGraw-Hill.
97. P.V. Joshi, A.A. Sayed, A. RaviKumar, V.G. Puranik, and S.S. Zinjarde, *4-Phenyl quinoline derivatives as potential serotonin receptor ligands with antiproliferative activity*. European Journal of Medicinal Chemistry, 2017. **136**: p. 246-258.
98. M.N. Javed, S.M., I.A. Hashmi, A. Bari, S.G. Musharraf, F.I. Ali, *Newly designed pyridine and piperidine based Ionic Liquids: Aggregation behavior in ESI-MS and catalytic activity in CC bond formation reactions*. Journal of Molecular Liquids, 2018. **272**: p. 84-91.
99. A.A. Zaki, M. Hagar, and N.R.E. Radwan, *Synthesis and optical properties of new alkylated pyridinium halides*. Optik, 2017. **139**: p. 95-103.
100. Nahm, S. and S.M. Weinreb, *N-methoxy-N-methylamides as effective acylating agents*. Tetrahedron Letters, 1981. **22**(39): p. 3815 - 3818.
101. Portal, O.C. *Weinreb ketone synthesis*. [cited 2020 11]; Available from: <https://www.organic-chemistry.org/namedreactions/weinreb-ketone-synthesis.shtm>.
102. Padwa, A., S.F. Hornbuckle, G.E. Fryxell, and P.D. Stull, *Reactivity patterns in the rhodium carbenoid induced tandem cyclization-cycloaddition reaction*. The Journal Of Organic Chemistry, 1988. **54**(4): p. 817 - 822.
103. M. Iwakubo, A. Takami, Y. Okada, T. Kawata, Y. Tagami, H. Ohashi, M. Sato, T. Sugiyama, K. Fukushima, and H. Iijima, *Design and synthesis of Rho kinase inhibitors (II)*. Bioorganic & Medicinal Chemistry, 2007. **15**: p. 350-364.
104. C.C. Tjin, R.F. Wissner, H. Jamali, A. Schepartz, and J.A. Ellman, *Synthesis and biological evaluation of an indazole-based selective protein arginine deiminase 4 (PAD4) inhibitor*. American Chemical Society Medicinal Chemistry Letters, 2018. **9**: p. 1013-1018.
105. C. Zhang, F. Li, Y. Yu, A. Huang, P. He, M. Lei, J. Wang, L. Huang, Z. Liu, J. Liu, and Y. Wei, *Design, synthesis and evaluation of a series of novel benzocyclobutene derivatives as general anesthetics*. Journal of Medicinal Chemistry, 2017. **60**: p. 3618-3625.
106. Ashenhurst, J., *Reactions of diazonium salts: sandmeyer and related reactions*. Master Organic Chemistry, 2019.

107. S. Tang, J. He, Y. Sun, L. He, and X. She, *Efficient and regioselective one-pot synthesis of 3-substituted and 3,5-disubstituted isoxazoles*. *Organic Letters*, 2009. **11**(17): p. 3982-3985.
108. P. Siengalewicz, J. Mulzer, and U. Rinner, *Comprehensive organic synthesis II*. Heteroatom Manipulation. Vol. 6. 2014. 355-410.
109. A. Rania, S. Jaina, R. Kumarb, and A. Kumar, *1,5-bis-(2-hydroxyphenyl)pent-1,4-diene-3-one: a lead compound for the development of broad-spectrum antibacterial agents*. *South African Journal of Chemistry*, 2010. **63**: p. 31-35.
110. K.L. Lahtchev, D.I.B., St.P. Parushev, V.M. Ubiyvovk, A.A. Sibirny, *Antifungal activity of chalcones: A mechanistic study using various yeast strains*. Elsevier, 2008. **43**: p. 2220-2228.
111. X. Zhang, J.K., P. Niu, J. Wu, W. Yu, J. Chang, *I₂-mediated oxidative C–N bond formation for metal-free one-pot synthesis of di-, tri-, and tetrasubstituted pyrazoles from α,β -unsaturated aldehydes/ketones and hydrazines*. *The Journal Of Organic Chemistry*, 2014. **79**: p. 10170-10178.
112. S. Tang, J. He, Y. Sun, L. He, and X. She, *Efficient and regioselective synthesis of 5-hydroxy-2-isoxazolines: versatile synthons for isoxazoles, β -lactams, and γ -amino alcohols*. *The Journal Of Organic Chemistry*, 2010. **75**: p. 1961-1966.
113. S. Mozaffarnia, F.P., E. Payami, H. Karami, S. Soltani, M-R. Rashidi, and R. Teimuri-Mofrad, *Design, synthesis and biological assessment of novel 2-(4-alkoxybenzylidene)-2,3-dihydro-5,6-dimethoxy-1H-inden-1-one derivatives as hAChE and hBuChE enzyme inhibitors*. *ChemPubSoc Chemistry Select*, 2019. **4**: p. 9376 - 9380.
114. Mustafa Ceylan, U.M.K., Necibe Canan Usta, Belma Gürbüzlü, Yusuf Temel, Saleh H. Alwasel, Ilhami Gülçin, *Synthesis, carbonic anhydrase I and II isoenzymes inhibition properties, and antibacterial activities of novel tetralone-based 1,4-benzothiazepine derivatives*. *Journal of Biochemical Molecular Toxicology*, 2016. **0**: p. 1-11.
115. Motahar Sk, A.K., Jagadish Das and Debasis Banerjee, *A simple iron-catalyst for alkenylation of ketones using primary alcohols*. *Molecules*, 2020: p. `1-14.
116. M. Rueping, T.B., H. Baars and E. Sugiono, *Continuous-flow hydration–condensation reaction: Synthesis of α,β -unsaturated ketones from alkynes and aldehydes by using a heterogeneous solid acid catalyst*. *Beilstein Journal of Organic Chemistry*, 2011. **7**: p. 1680-1687.